

Advanced Structured Materials

Konstantin Naumenko
Holm Altenbach

Modeling High Temperature Materials Behavior for Structural Analysis

Part I: Continuum Mechanics
Foundations and Constitutive Models

 Springer

Advanced Structured Materials

Volume 28

Series editors

Andreas Öchsner, Southport Queensland, Australia

Lucas F.M. da Silva, Porto, Portugal

Holm Altenbach, Magdeburg, Germany

More information about this series at <http://www.springer.com/series/8611>

Konstantin Naumenko · Holm Altenbach

Modeling High Temperature Materials Behavior for Structural Analysis

Part I: Continuum Mechanics Foundations
and Constitutive Models

 Springer

Konstantin Naumenko
Institute of Mechanics
Otto-von-Guericke University Magdeburg
Magdeburg
Germany

Holm Altenbach
Institute of Mechanics
Otto-von-Guericke University Magdeburg
Magdeburg
Germany

ISSN 1869-8433
Advanced Structured Materials
ISBN 978-3-319-31627-7
DOI 10.1007/978-3-319-31629-1

ISSN 1869-8441 (electronic)
ISBN 978-3-319-31629-1 (eBook)

Library of Congress Control Number: 2016933798

© Springer International Publishing Switzerland 2016

This work is subject to copyright. All rights are reserved by the Publisher, whether the whole or part of the material is concerned, specifically the rights of translation, reprinting, reuse of illustrations, recitation, broadcasting, reproduction on microfilms or in any other physical way, and transmission or information storage and retrieval, electronic adaptation, computer software, or by similar or dissimilar methodology now known or hereafter developed.

The use of general descriptive names, registered names, trademarks, service marks, etc. in this publication does not imply, even in the absence of a specific statement, that such names are exempt from the relevant protective laws and regulations and therefore free for general use.

The publisher, the authors and the editors are safe to assume that the advice and information in this book are believed to be true and accurate at the date of publication. Neither the publisher nor the authors or the editors give a warranty, express or implied, with respect to the material contained herein or for any errors or omissions that may have been made.

Printed on acid-free paper

This Springer imprint is published by Springer Nature
The registered company is Springer International Publishing AG Switzerland

Preface

Many engineering structures are subjected to high temperature environment and mechanical loadings over a long period of time. Examples include components of power plants, chemical refineries, and heat engines. Design procedures and residual life assessments for pipework systems, rotors, turbine blades, etc., require to take into account inelastic deformation and damage processes. The aim of “modeling materials behavior at high temperature for structural analysis” is the development of methods to simulate and analyze time-dependent changes of stress and strain states in engineering structures up to the critical stage of rupture.

The scope of this book is related to the fields “creep mechanics” (Betten 2008; Hyde et al. 2013; Naumenko and Altenbach 2007; Odqvist 1981), “continuum creep and damage mechanics” (Hayhurst 2001; Murakami 2012), “mechanics of high-temperature plasticity” (Ilshner 1973) or in a broader sense to “behavior of materials and structures at high temperature.” The objectives are the formulation of constitutive equations describing the mechanical behavior of structural materials under multi-axial stress states; the application of structural mechanics models of beams, plates, shells, and three-dimensional solids; and the utilization of solution procedures of nonlinear initial-boundary value problems. They have become traditional since the pioneering texts written in the 1950s by Prager (1959) and in the 1960s by Odqvist and Hult (1962), Hult (1966), and Rabotnov (1969), among others. These classical books provide a first collection of solutions to plasticity and creep problems for elementary structures such as rods, beams, and circular plates based on simple constitutive models like the Norton-Bailey equation. The results illustrate the basic features of inelastic behavior of materials and structures: time-dependent deformations, relaxation and redistribution of stresses, and creep buckling. Furthermore, the introduction of internal or hidden state variables to characterize processes accompanying inelastic deformation has been established. The monographs by Penny and Marriott (1995) (first edition in 1971) and Viswanathan (1989) concentrate on robust methods and empirical relationships, which are useful for the design procedures. The monographs by Kraus (1980), Malinin (1981), and Boyle and Spence (1983), published in the 1980s introduce

new constitutive models with hardening/recovery and damage variables and initiate the use of advanced numerical methods for structural analysis. The monographs published by Lemaitre and Chaboche (1990) (3rd French edition Lemaitre et al. 2009) and Skrzypek and Ganczarski (1998) in 1990s designate the framework of continuum thermodynamics to derive constitutive models, present the advanced techniques for testing materials under multi-axial non-proportional loading conditions, and overview the developments of continuum damage mechanics. Recent monographs (Besson et al. 2009; Kassner and Pérez-Prado 2004; Yagi et al. 2004; François et al. 2012a, b) and collections of papers (Altenbach and Kruch 2013; Altenbach and Brüning 2015; Altenbach et al. 2015) present constitutive models at different length scales, and provide new methods of homogenization and localization with interlinks to materials science and physics.

Creep problems in materials and structures are widely discussed at various conferences and in scientific papers. The International Union of Theoretical and Applied Mechanics (IUTAM) organizes once in every ten years the symposium “Creep in Structures”: 1960—Stanford (Hoff 1962), 1970—Gothenburg (Hult 1972), 1980—Leicester (Ponter and Hayhurst 1981), 1990—Cracow (Zyczkowski 1991), and 2000—Nagoya (Murakami and Ohno 2001). The aim of these symposia was to establish new and fundamental topics on creep and bring together scientists and engineers from fundamental research and applications. The proceedings show developments in modeling and understanding creep phenomena starting from the physical and microstructural aspects of creep and creep-damage up to the structural design procedures. The IUTAM symposium “Advanced Materials Modelling for Structures,” held in Paris during April 23–27, 2012, was a continuation and a new version of the previous IUTAM symposia “Creep in Structures” with a focus on new materials and on generalized and unified models of inelastic deformation (Altenbach and Kruch 2013). Materials science foundations of high-temperature plasticity including deformation and damage mechanisms, materials design for high-temperature applications, experimental data on creep and plasticity as well as constitutive models are discussed in International Conferences of Creep and Fracture of Engineering Materials and Structures (CREEP), first organized in 1981 and held from 1981 to 1993 in Swansea on a triennial basis. Since 1993 this conference has been held in London (1995), Irvine (1997), Tsukuba (1999), Swansea (2001), Pittsburgh (2005), Bad Berneck (2008), Kyoto (2012), and Toulouse (2015). The European Creep Collaborative Committee (ECCC) organized the International Conference on Creep and Fracture in High Temperature Components: 2005 in London, 2009 in Zurich, and 2014 in Rome.

During the past decade many advances and new results in the field of high-temperature inelasticity were presented at conference proceedings and in scientific papers. Examples include: the interlinks with materials science in formulation of constitutive equations to consider different deformation and damage mechanisms over a wide range of stresses and temperature; the application of tensor-valued state variables to account for stress state effects and deformation/damage-induced anisotropy; the assessment of models for beams, plates, and shells in structural analysis considering inelastic deformation and damage; the development and verification of

material subroutines for use in general-purpose finite element codes; the application of the finite element method to the inelastic analysis of engineering structures under complex thermo-mechanical loading profiles; the consideration of processing conditions, such as welding or induction bending of pipes, and their influence on the subsequent behavior in structures.

The objective of this book is to review some of the classical and recently proposed approaches to modeling of high-temperature inelasticity of materials for structural analysis as well as to extend the collection of available solutions of inelastic problems by new, more sophisticated examples.

In Chap. 1 we discuss the basic features of the inelastic behavior of materials and structures and present an overview of various experimental and theoretical approaches to modeling of inelastic behavior. Typical material responses for various loading paths are presented and classified. Microstructural features and microstructural changes in the course of inelastic deformation at high temperature are discussed. Furthermore, the state of the art on material modeling and structural analysis in the inelastic range at high temperature is presented.

Chapter 2 gives a short introduction to the basics of Continuum Mechanics in one dimension. Here we consider a rod subjected to uniaxial stress state to illustrate the main ideas of continuum mechanics in a simple, transparent manner. Motion, deformation, conservation of mass, balance of momentum, balance of energy, entropy inequality, and the dissipation inequality are introduced and some consequences for material modeling are presented.

Chapter 3 collects elementary constitutive models that describe material behavior under uniaxial stress state. Constitutive equations for elasto-plasticity as well as evolution equations to characterize hardening, softening, aging, and damage processes are presented.

Chapter 4 gives an introduction to the basics of three-dimensional Continuum Mechanics. Equations describing kinematics motion, deformation as well as balance laws are now extended to the three-dimensional case. The consequences for material modeling are discussed.

Chapter 5 is devoted to constitutive modeling of materials subjected to multi-axial stress states. To analyze material behavior under complex thermo-mechanical loading a combined model for thermo(visco)elasto-plasticity considering hardening, softening, damage, and other processes is required. The idea of this chapter is to introduce basic ingredients, useful for the formulation of such unified material models. They include heat transfer modeling, modeling of elasto-plastic deformations, hardening and softening rules as well as aging and damage evolution equations. To formulate a constitutive model for a multi-axial stress state several assumptions must be introduced. Appropriate stress and deformation measures must be considered to capture complex local loadings. Constitutive and evolution equations must be defined such that invariance requirements with respect to the choice of reference frame, laws of continuum thermodynamics, and other principles are fulfilled. To specialize the constitutive equation, results of basic tests of the material behavior, such as tensile test, creep test, relaxation test, etc., should be systematically analyzed. On the other hand, basic features of materials microstructure in the reference state and

after a course of inelastic deformation process should be established. Microstructural analysis and appropriate assumptions with regard to symmetries of microstructure would essentially reduce the identification effort. Different types of material symmetries and appropriate forms of constitutive laws are discussed.

Chapter 6 deals with the application of constitutive models to the description of inelastic behavior of several structural materials. Basic approaches to calibrate constitutive models against experimental data of high-temperature material behavior are discussed. Constitutive models of isotropic high-temperature plasticity of several alloys including identified response functions and material parameters are introduced. Two examples of initially anisotropic materials including a forged aluminum alloy and a multi-pass weld metal are presented.

Appendices A and B are a summary of the direct tensor notation and basic tensor operations used throughout the text. This notation has the advantage of a clear, compact, and coordinate free representation of constitutive models and initial-boundary value problems. The theory of anisotropic tensor functions and invariants is discussed in detail. Approaches to derive basic sets of functionally independent invariants for vectors and second rank tensors for the given symmetry group is presented. The invariants are found as integrals of a generic partial differential equation (basic equation for invariants).

Several chapters of this book have grown out of our lectures and lecture notes on fundamentals of continuum mechanics, mechanics of materials, and finite element modeling for graduate level students and Ph.D. students held at the Martin-Luther-Universität Halle-Wittenberg, Otto-von-Guericke-Universität Magdeburg, Fraunhofer Institut für Werkstoffmechanik, Politecnico Milano, Nagoya University, Politechnika Lubelska and National Technical University “Kharkiv Polytechnical Institute.” Many results presented originate from scientific and academic exchange projects. We wish to acknowledge financial support from the German Research Foundation (DFG), German Academic Exchange Service (DAAD), the State Saxony-Anhalt, and European Commission (ERASMUS). This book is partly based on the *Habilitation* thesis of the first author (Naumenko 2006) and the book *Modeling of Creep for Structural Analysis* (Naumenko and Altenbach 2007). The extensions are made with regard to the description of the inelastic behavior in a unified manner to include creep, rate-dependent plasticity, hardening/recovery, softening, aging, and damage. New examples are included to illustrate structural behavior under complex, thermo-mechanical loadings.

We acknowledge Professors J. Betten, O.T. Bruhns, E. Gariboldi, T. Hyde, R. Kienzler, Z.L. Kowalewski, E. Krempl, O.K. Morachowski, N. Ohno, J. Skrzypek, and P.A. Zhilin for many fruitful discussions which stimulated our research in mechanics of inelastic material behavior. For the careful reading of the manuscript we thank Mr. Helal Chowdhury. We thank Dr. Christoph Baumann from Springer Publisher for the assistance and support during the preparation of the book.

References

- Altenbach H, Brünig M (eds) (2015) Inelastic behavior of materials and structures under monotonic and cyclic loading. In: *Advanced structured materials*, vol 57. Springer, Heidelberg
- Altenbach H, Kruch S (eds) (2013) *Advanced materials modelling for structures*, *Advanced structured materials*, vol 19. Springer, Heidelberg
- Altenbach H, Matsuda T, Okumura D (eds) (2015) From creep damage mechanics to homogenization methods: a liber amicorum to celebrate the birthday of Nobutada Ohno, *Advanced structured materials*, vol 64. Springer, Heidelberg
- Besson J, Blétry M, Cailletaud G, Chaboche J, Forest S (2009) *Non-linear mechanics of materials. solid mechanics and its applications*, Springer, Netherlands
- Betten J (2008) *Creep mechanics*, 3rd edn. Springer, Berlin
- Boyle JT, Spence J (1983) *Stress analysis for creep*. Butterworth, London
- François D, Pineau A, Zaoui A (2012a) *Mechanical behaviour of materials: Volume I: Micro- and macroscopic constitutive behaviour*, vol 191. Springer Science & Business Media
- François D, Pineau A, Zaoui A (2012b) *Mechanical behaviour of materials: Volume II: Fracture mechanics and damage*, vol 191. Springer Science & Business Media
- Hayhurst DR (2001) Computational continuum damage mechanics: its use in the prediction of creep fracture in structures—past, present and future. In: Murakami S, Ohno N (eds) *IUTAM Symposium on creep in structures*, Kluwer, Dordrecht, pp 175–188
- Hoff N (ed) (1962) *Creep in structures*. Springer, Berlin
- Hult J (ed) (1972) *Creep in structures*. Springer, Berlin, Heidelberg, New York
- Hult JA (1966) *Creep in engineering structures*. Blaisdell Publishing Company, Waltham
- Hyde T, Sun W, Hyde C (2013) *Applied creep mechanics*. McGraw-Hill Education
- Ilschner B (1973) *Hochtemperatur-Plastizität*. Springer, Berlin, Heidelberg, New York
- Kassner ME, Pérez-Prado MT (2004) *Fundamentals of creep in metals and alloys*. Elsevier, Amsterdam
- Kraus H (1980) *Creep analysis*. John Wiley & Sons, New York
- Lemaitre J, Chaboche JL (1990) *Mechanics of solid materials*. Cambridge University Press, Cambridge
- Lemaitre J, Chaboche J, Benallal A, Desmorat R (2009) *Mécanique des matériaux solides*, 3rd edn. The Addison-Wesley Series in the engineering sciences: mechanics and thermodynamics, Dunod, Paris
- Malinin NN (1981) Raschet na polzuchest' konstrukcionnykh elementov (Creep calculations of structural elements, in Russia). Mashinostroenie, Moskva
- Murakami S (2012) *Continuum damage mechanics: a continuum mechanics approach to the analysis of damage and fracture*. *Solid mechanics and its applications*, Springer
- Murakami S, Ohno N (eds) (2001) *IUTAM Symposium on creep in structures*. Kluwer, Dordrecht
- Naumenko K (2006) *Modeling of high-temperature creep for structural analysis applications*. Habilitationsschrift, Mathematisch-Naturwissenschaftlich-Technische Fakultät, Martin-Luther-Universität Halle-Wittenberg
- Naumenko K, Altenbach H (2007) *Modelling of creep for structural analysis*. Springer, Berlin.
- Odqvist FKG (1981) Historical survey of the development of creep mechanics from its beginnings in the last century to 1970. In: Ponter ARS, Hayhurst DR (eds) *Creep in Structures*, Springer, Berlin, pp 1–12
- Odqvist FKG, Hult J (1962) *Kriechfestigkeit metallischer Werkstoffe*. Springer, Berlin u.a.
- Penny RK, Marriott DL (1995) *Design for creep*. Chapman & Hall, London
- Ponter ARS, Hayhurst DR (eds) (1981) *Creep in structures*. Springer, Berlin
- Prager W (1959) *An introduction to plasticity*. Addison-Wesley Publishing Company
- Rabotnov YN (1969) *Creep problems in structural members*. North-Holland, Amsterdam
- Skrzypiek J, Ganczarski A (1998) *Modelling of material damage and failure of structures. foundation of engineering mechanics*, Springer, Berlin

- Viswanathan R (1989) Damage mechanisms and life assessment of high temperature components. ASM international
- Yagi K, Merckling G, Kern TU, Irie H, Warlimont H (2004) Creep properties of heat resistant steels and superalloys. Landolt-Börnstein—Group VIII Advanced materials and technologies: numerical data and functional relationships in science and technology. Springer, Berlin
- Zyczkowski M (ed) (1991) Creep in structures. Springer, Berlin, Heidelberg

Contents

1 Introduction	1
1.1 High-Temperature Inelasticity in Structural Materials	2
1.1.1 Uni-axial Stress State	2
1.1.2 Multi-axial Effects	22
1.2 High-Temperature Inelasticity in Structures	30
1.2.1 Examples for Creep in Structures	30
1.2.2 Examples for Thermo-mechanical Cycling	39
1.3 Microstructural Features and Length Scale Effects	52
1.4 Temporal Scale Effects	59
1.5 Modeling Approaches and Objectives	60
1.5.1 Modeling Approaches	60
1.5.2 Objectives, Modeling Requirements, and Steps for Structural Analysis	66
References	68
2 Continuum Mechanics in One Dimension	79
2.1 Motion, Derivatives, and Deformation	80
2.2 Conservation of Mass	83
2.3 Balance of Momentum	83
2.4 Balance of Energy	85
2.5 Entropy Inequality	87
2.6 Dissipation Inequality, Free Energy, and Stress	88
References	90
3 Elementary Uni-axial Constitutive Models	91
3.1 Heat Transfer	91
3.2 Thermo-elasticity	94
3.3 Non-linear Viscosity, Viscoplasticity, and Rigid Plasticity	96
3.4 Elasto-plasticity	99
3.5 Hardening, Softening, and Ageing	106
3.5.1 Strain Hardening	106
3.5.2 Kinematic Hardening	110

- 3.5.3 Phase Mixture Models for Hardening and Softening 115
- 3.5.4 Ageing. 120
- 3.6 Damage 123
 - 3.6.1 Kachanov-Rabotnov Model. 124
 - 3.6.2 Continuum Damage Mechanics. 131
- References 136
- 4 Three-Dimensional Continuum Mechanics. 141**
 - 4.1 Motion, Derivatives and Deformation. 142
 - 4.1.1 Motion and Derivatives 142
 - 4.1.2 Deformation Gradient and Strain Tensors 144
 - 4.1.3 Velocity Gradient, Deformation Rate,
and Spin Tensors. 150
 - 4.2 Conservation of Mass. 159
 - 4.3 Balance of Momentum 159
 - 4.3.1 Stress Vector 159
 - 4.3.2 Integral Form 160
 - 4.3.3 Stress Tensor and Cauchy Formula 161
 - 4.3.4 Local Forms 164
 - 4.4 Balance of Angular Momentum. 165
 - 4.5 Balance of Energy 166
 - 4.6 Entropy and Dissipation Inequalities. 168
 - References 170
- 5 Constitutive Models 173**
 - 5.1 Heat Transfer 174
 - 5.2 Material and Physical Symmetries 176
 - 5.3 Thermo-elasticity 179
 - 5.3.1 Preliminary Remarks 179
 - 5.3.2 Isotropic Materials. 182
 - 5.3.3 Anisotropic Materials. 184
 - 5.3.4 Linear Elasticity 187
 - 5.4 Non-linear Viscosity, Viscoplasticity, and Rigid Plasticity. 190
 - 5.4.1 Preliminary Remarks 190
 - 5.4.2 Isotropic Materials. 198
 - 5.4.3 Initially Anisotropic Materials. 205
 - 5.4.4 Functions of Stress and Temperature 223
 - 5.5 Elasto-plasticity 227
 - 5.5.1 Multiplicative Decomposition of Deformation
Gradient. 228
 - 5.5.2 Small Strains 236
 - 5.6 Hardening and Softening Rules 238
 - 5.6.1 Time and Strain Hardening. 240
 - 5.6.2 Kinematic Hardening 242
 - 5.6.3 Phase Mixture Models for Hardening and Softening 250

- 5.7 Damage Processes and Damage Mechanics 254
 - 5.7.1 Scalar-Valued Damage Variables 254
 - 5.7.2 Damage-Induced Anisotropy 266
- References 272
- 6 Examples of Constitutive Equations for Various Materials 283**
 - 6.1 Basic Approaches of Identification 283
 - 6.2 Isotropic Materials 285
 - 6.2.1 Type 316 Steel 285
 - 6.2.2 Steel 13CrMo4-5 286
 - 6.2.3 Steel X20CrMoV12-1 287
 - 6.2.4 Aluminium Alloy BS 1472 299
 - 6.3 Initially Anisotropic Materials 302
 - 6.3.1 Forged Al-Cu-Mg-Si Alloy 303
 - 6.3.2 Multi-pass Weld Metal 308
 - References 318
- Appendix A: Basic Operations of Tensor Algebra 323**
- Appendix B: Elements of Tensor Analysis 343**
- Index 365**

Chapter 1

Introduction

The objective of this chapter is to give an overview of experimental and theoretical approaches to analyze the behavior of materials and structures subjected to mechanical loading and “high-temperature” environment. The definition of “high-temperature materials” and “high-temperature structures” can be related to the value of the homologous temperature, that is T/T_m , where T is the absolute temperature and T_m is the melting point of the considered material. Materials that can be efficiently used within the temperature range $0.3 < T/T_m < 0.7$ are called high-temperature materials. Examples include heat resistant steels, nickel-bases alloys, age-hardened aluminum alloys, cast iron materials and metal matrix composites. Structures that operate in the same temperature range over a long period of time are called high-temperature structures. Examples include turbine blades, turbine housings, rotors, turbochargers, steam pipework, microelectronics components, etc. This book deals with high-temperature material behavior with the emphasis on modeling, analysis and design of structures.

Despite the structural analysis one has often to analyze hot deformation processes. Examples include friction stir welding and hot forming. Here materials are subjected to higher temperatures but still below the melting point, usually in the range $0.7 < T/T_m < 0.9$. The material behaviors under the condition of long-term high-temperature service and hot working operations appear to be closely related, since they share similar temperature properties and thermally activated deformation mechanisms. However, materials under hot working conditions are subjected to much higher strain rates and strains.

In this chapter we are going to discuss basic features of the inelastic behavior of materials and structures at high temperatures. Typical responses for various loading paths are presented and classified. Microstructural features and microstructural changes in the course of inelastic deformation at high temperature are discussed. Furthermore the state of the art on material modeling and structural analysis in the inelastic range at high temperature is presented.

1.1 High-Temperature Inelasticity in Structural Materials

Material behavior can be examined with different experimental observations, for example, macroscopic and microscopic. The engineering approach is related to the analysis of stress and strain states in structures and mostly based on the standard mechanical tests. In this section we discuss basic features of inelastic material behavior according to published results of material testing under uni-axial and multi-axial stress states.

1.1.1 *Uni-axial Stress State*

Uni-axial stress state is usually realized in experiments like tension tests, creep tests, relaxation tests, low cycle fatigue tests, etc. In Sect. 1.1.1.1 basic experimental features are discussed.

1.1.1.1 **Tensile Behavior**

Uni-axial tensile tests are basic experiments of the material behavior evaluation. A standard tension specimen is subjected to the uniform elongation with a constant rate. From the measured force and the given elongation the stress and the strain are computed. Figure 1.1 shows a sketch of a typical stress-strain diagram for a steel at room temperature. Many materials exhibit a linear stress-strain relationship up to a yield point, Fig. 1.1a. The linear portion of the curve is the elastic region and the slope is the modulus of elasticity or Young's modulus. After the loading and subsequent unloading within the elastic range the specimen takes the original length. The loading and unloading paths coincide, and the work done to deform the specimen is stored as the elastic energy. Beyond the yield point the strain increases for almost constant stress, Fig. 1.1b. Here the material is undergoing a rearrangement of microstructure, such that atoms are being moved to new equilibrium positions. In crystalline materials the plastic flow is explained by motion of dislocations—line defects of the crystal structure. Within the hardening regime the stress-strain curve goes up such that the material supports the additional increasing load, Fig. 1.1c. The hardening is usually explained as an increasing resistance against the plastic flow in the course of deformation. For example, the plastic straining generates dislocations. With the increase in dislocation density, the dislocation movement becomes more difficult. Another example is the micro-stress fields generated during the plastic flow, as a result of heterogeneous deformation on the micro-scale. Several microstructural zones, for example slip planes or grains with certain crystallographic orientations, exhibit higher levels of inelastic strain rate. The remaining part of microstructure behaves more or less elastically. This leads to changes of micro-stress states and to

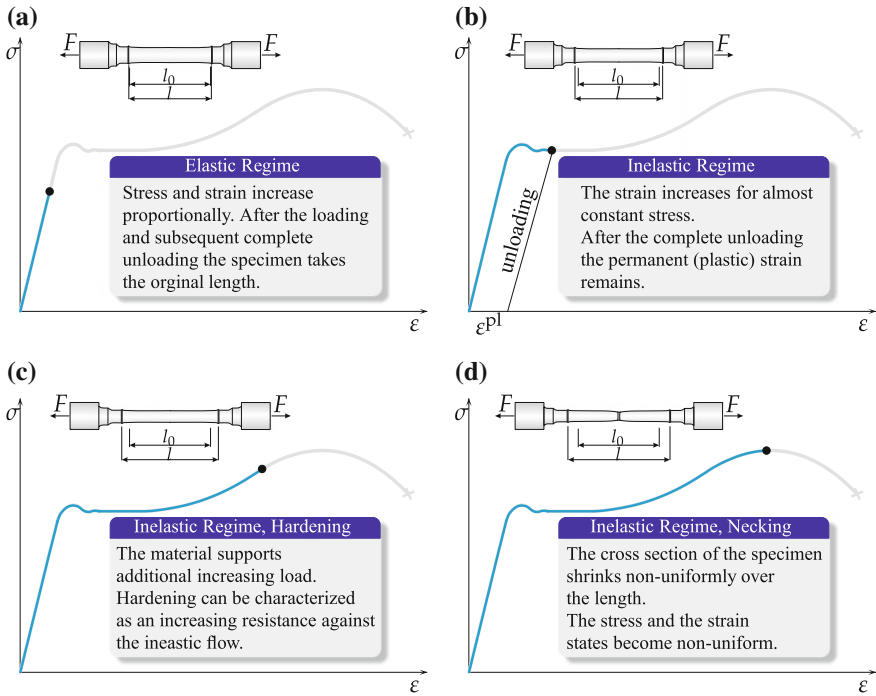
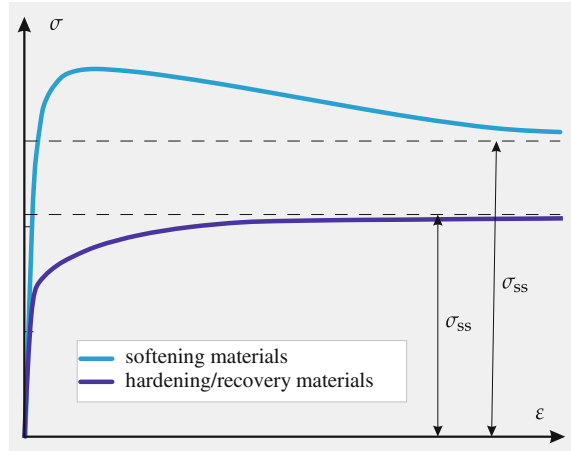


Fig. 1.1 Stress-strain diagram at room temperature. **a** Elastic regime, **b** inelastic regime, **c** inelastic regime with hardening, **d** inelastic regime with necking

formation of residual stresses upon unloading. Residual micro-stress fields affect the overall deformation rate and provide an additional hardening.

In the course of deformation the cross section of the specimen shrinks, starting from the Poisson effect in the elastic regime. For many materials the inelastic deformation does not produce an essential change in volume, such that the uniform change in the cross section can be easily related to the elongation. As deformation proceeds, the geometric instability causes strain to localize in a small region until the final stage of rupture. This phenomenon is called necking, Fig. 1.1d. Within the inelastic regime an essential part of the work done to deform the material dissipates (usually as heat). After the removing the force the specimen does not return to its original shape—after the elastic springback the permanent plastic strain remains. From a stress-strain diagram several material characteristics, important for design of structures, can be identified. They include the Young’s modulus E , the yield limit σ_y and the ultimate tensile strength σ_u . The yield limit is often not well defined from the shape of the stress-strain curve. Instead of yield point the upper and the lower yield points as well as an offset yield point $R_{p0.2}$ are usually introduced. The latter is the stress value, for which the permanent plastic strain is 0.2 %.

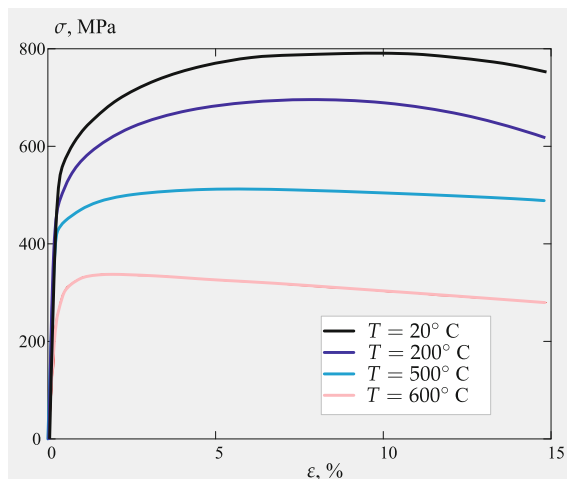
Fig. 1.2 Stress-strain diagrams for materials with hardening and softening at high temperature



Tension tests are often performed at elevated temperature. The standard specimen is uniformly heated up to a certain temperature, usually in the range $T = (0.3-0.7)T_m$ and then subjected to elongation, to examine material properties for high-temperature applications. Let us discuss basic features of hot deformation observed from tensile tests. Figure 1.2 shows schematically stress-strain diagrams obtained at high temperature. Here the yield point cannot be defined, the $R_{p0.2}$ stress is used instead in most cases. Hardening is usually accompanied by recovery. For example the increase of dislocation density with inelastic straining—a hardening phenomenon—is accompanied by annihilation of dislocations—a recovery phenomenon observed at high temperature. Internal stresses, being generated due to heterogeneous inelastic deformation, get relaxed as a result of microstructure rearrangements at high temperature—for example diffusion of vacancies. Therefore, the stress-strain diagram of several materials shows a well-defined horizontal shape, the so-called saturation or steady-state flow regime, for which the hardening and recovery processes are in equilibrium. An important material characteristic is the steady-state (saturated) stress level σ_{ss} , Fig. 1.2. Examples for hardening/recovery materials include pure metals, solid solution alloys with a relatively low initial density of dislocations and 300-series austenitic steels. Experimental data for 304 and 316 steels are presented in Gorash et al. (2012), Kawai (1989), among others.

Many materials contain relatively high dislocation density at the initial (virgin) state after the processing. Examples include 9–12% Cr ferritic steels, where a high density of dislocations is induced after martensitic transformation. For these materials the inelastic deformation is accompanied by the recovery of dislocation substructures such as coarsening of subgrains (Blum 2008). The stress-strain curve shows a descending (softening) branch, Fig. 1.2. Experimental data for 9–12% Cr steels are presented in Naumenko et al. (2011a), Röttger (1997), Yaguchi and Takahashi (2005), among others.

Fig. 1.3 Stress-strain diagrams for X20CrMoV12-1 steel under strain rate $\dot{\epsilon} = 2.63 \cdot 10^{-4} \text{ s}^{-1}$ and different temperature levels, after Röttger (1997)



Material properties like Young's modulus and yield limit as well as, hardening, recovery and softening processes strongly depend on the temperature level. As an example, Fig. 1.3 shows stress-strain diagrams for 12% Cr steel X20CrMoV12-1 steel for different values of the absolute temperature (Röttger 1997). At room temperature the material shows a typical tensile behavior with the elastic range followed by hardening and necking regimes up to final fracture. In contrast, at 600 °C after a relatively short hardening range the stress strain curve shows a clear descending branch. This softening regime is observed for small strains (lower than 2 %) and is related to coarsening of dislocation substructures.

Inelastic response depends on the rate of the applied loading. For many materials the rate dependence becomes essential for high temperatures, i.e. for $T/T_m > 0.3$. As an example, Fig. 1.4 shows stress-strain curves for modified 9Cr-1Mo steel at 550 °C and different strain rates (Yaguchi and Takahashi 2005). Increase of the strain rate leads to an increase in the saturation stress value. The corresponding dependency of σ_{ss} on $\dot{\epsilon}$ is called strain rate sensitivity of the tensile response and is an important characteristic for design and analysis of structures and processes.

1.1.1.2 Creep and Relaxation

The uni-axial creep test is another experiment to examine material behavior at high temperature. A standard cylindrical tension specimen is heated up to the temperature $T = (0.3-0.5)T_m$ and loaded by a tensile force F . The value of the normal stress in the specimen σ is usually less than the yield point σ_y or offset yield point $R_{p0.2}$ of the material at the given temperature. The instantaneous material response is therefore elastic. The load and the temperature are kept constant during the test and the axial engineering strain ϵ is plotted versus time t . A typical creep curve for a metal is schematically shown in Fig. 1.5. The instantaneous response can be characterized by

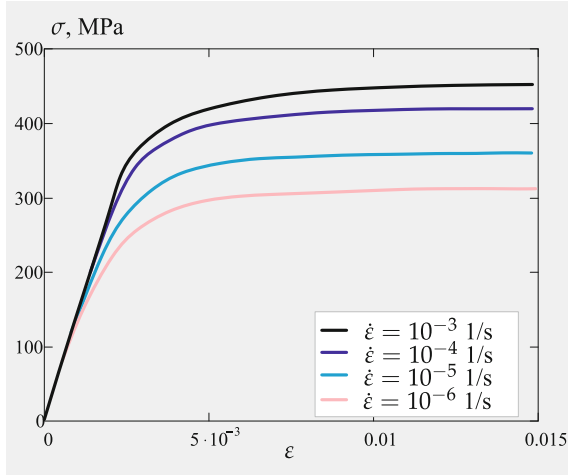


Fig. 1.4 Stress-strain diagrams for modified 9Cr-1Mo steel at $T = 550\text{ }^{\circ}\text{C}$ and different strain rates, after Yaguchi and Takahashi (2005)

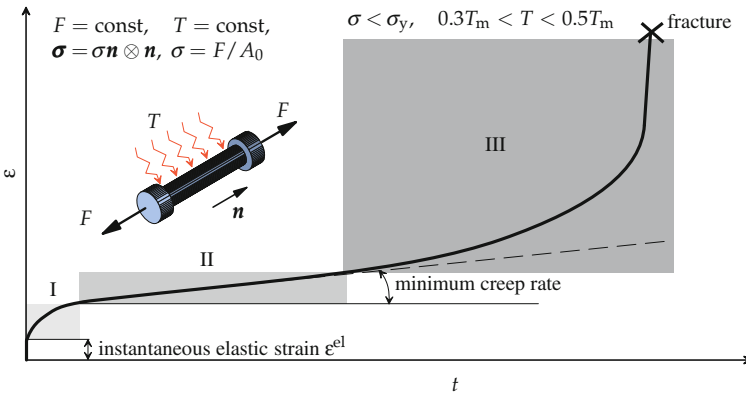


Fig. 1.5 Strain versus time curve under constant load F and temperature T . *I* Primary creep, *II* secondary creep, *III* tertiary creep

the strain value ϵ^{el} . The time-dependent response is the slow increase of the strain ϵ with a variable rate. Following da Andrade (1910), three stages can be considered in a typical creep curve: the first stage (primary or reduced creep), the second stage (secondary or stationary creep) and the third stage (tertiary or accelerated creep). During the primary creep stage the creep rate decreases to a certain value (minimum creep rate). The secondary stage is characterized by the approximately constant creep rate. During the tertiary stage the strain rate increases. At the end of the tertiary stage creep rupture of the specimen occurs. A number of properties, important for design of structures, can be deduced from the uni-axial creep curve. These are the duration of the stages, the value of minimum creep rate, the time to fracture and the strain value before fracture.

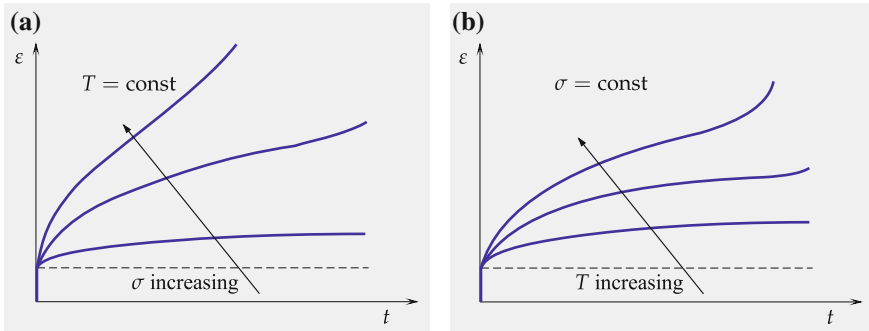


Fig. 1.6 Influence of stress and temperature on the creep behavior. **a** Stress dependence, **b** temperature dependence

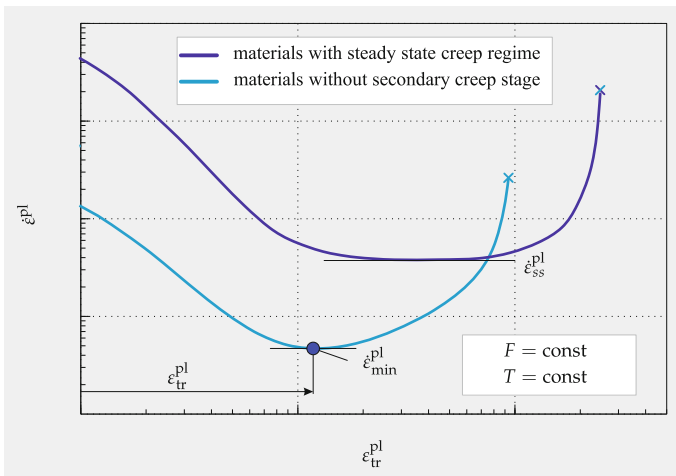


Fig. 1.7 Creep rate versus creep strain curves with and without steady state creep regime

The shape of the creep curve, the duration of the creep stages the creep rate and the time to fracture depend strongly on the stress and temperature values, Fig. 1.6. For the analysis of creep behavior it is convenient to introduce the inelastic (creep) strain ϵ^{pl} as the difference between the measured strain ϵ and the calculated elastic strain $\epsilon^{el} = \sigma/E$, where E is the Young’s modulus. From the original strain versus time curve the creep rates can be computed and plotted as a functions of creep strain and/or time. Two examples of creep rate versus creep strain curves are presented schematically in Fig. 1.7. For several materials, for example pure metals, the classical creep with three creep stages are observed. Here the creep rate is nearly constant over a certain range of creep strain values. The secondary creep stage is characterized by the steady state creep rate $\dot{\epsilon}_{ss}^{pl}$, Fig. 1.7. For a range of temperatures and stress levels an important deformation regime is the dislocation creep. Here the deformation is

controlled by the movement of mobile dislocations (Ilschner 1973; Blum 2001; Frost and Ashby 1982). The creep rate is related to the velocity of mobile dislocations. The dislocation velocity decreases with increasing overall dislocation density (Blum 2001). The creep deformation produces dislocations and the creep rate is expected to decrease with an increase in dislocation density. On the other hand, annihilation of dislocations at high temperature, for example due to diffusion of vacancies takes place leading to a decrease (recovery) of dislocation density. In a steady state creep regime the dislocation density does not change, that is, the rate of production and the rate of annihilation are the same (Blum 2001). For many structural materials, for example advanced heat resistant steel, a pronounced secondary creep stage is not observable. The creep rate decreases at the beginning of the creep process, attains the minimum value at a certain value of the transition strain ε_{tr}^{pl} and immediately increases after that. The corresponding characteristic is the minimum creep rate $\dot{\varepsilon}_{min}^{pl}$, Fig. 1.7.

The dependencies of creep rate on stress and temperature are of primary interest to an engineer in designing some structure or machine. In order to obtain mechanical properties of the material, series of creep tests are usually performed for different stress and temperature values. From the resulting families of creep curves one can obtain the minimum creep rate versus stress curve, the minimum creep rate versus temperature curve, the creep rate versus time curve and the stress versus time to fracture curve (long term strength curve). The ranges of stress and temperature should be specified according to the ranges expected in the structure during the service.

Figure 1.8a illustrates experimental data for minimum creep rate as a function of stress for steel 316 for the temperature 600 °C (Rieth et al. 2004). To generate reliable data for the minimum (secondary) creep rate for the stress values less than 100 MPa creep tests with the long duration (approx. 10 years) are required. The data for this range of moderate and low stress levels are of interest for the analysis of power plant components operating in high-temperature range over long period of time. Special uni-axial specimen with an increased gauge length were designed in Rieth et al. (2004) to improve the resolution of creep strain measurements for low stress levels. In Kloc and Sklenička (1997), Kloc and Sklenička (2004), Kloc et al. (2001) the testing facilities and experimental data for a 9% Cr steel are presented. Creep tests for the stress levels below 20 MPa were performed by the use of helical springs while for the stress levels over approx. 100 MPa standard uni-axial specimen were applied. Figure 1.8b shows the experimental data for the temperature 600 °C. Examples for minimum creep rate versus stress curves for various materials can be found in Altenbach et al. (2008a), Boyle and Spence (1983), Hyde et al. (2013), Ilschner (1973), Kassner and Pérez-Prado (2004), Kraus (1980), Malinin (1981), Odqvist and Hult (1962), Odqvist (1974), Penny and Marriott (1995) and many papers related to the experimental analysis of creep, e.g. Altenbach et al. (2013), Gariboldi and Casaro (2007), El-Magd et al. (1996), Hyde et al. (1997), Hyde et al. (1999), Kimura et al. (2009), Naumenko et al. (2009), Längler et al. (2014). To discuss basic features of tertiary creep consider a sketch of the creep rate versus creep strain curves usually observed for 9–12% Cr steels, Fig. 1.9. Experimental creep curves are published in Kimura et al. (2009), Naumenko et al. (2011a), Straub (1995). The secondary or

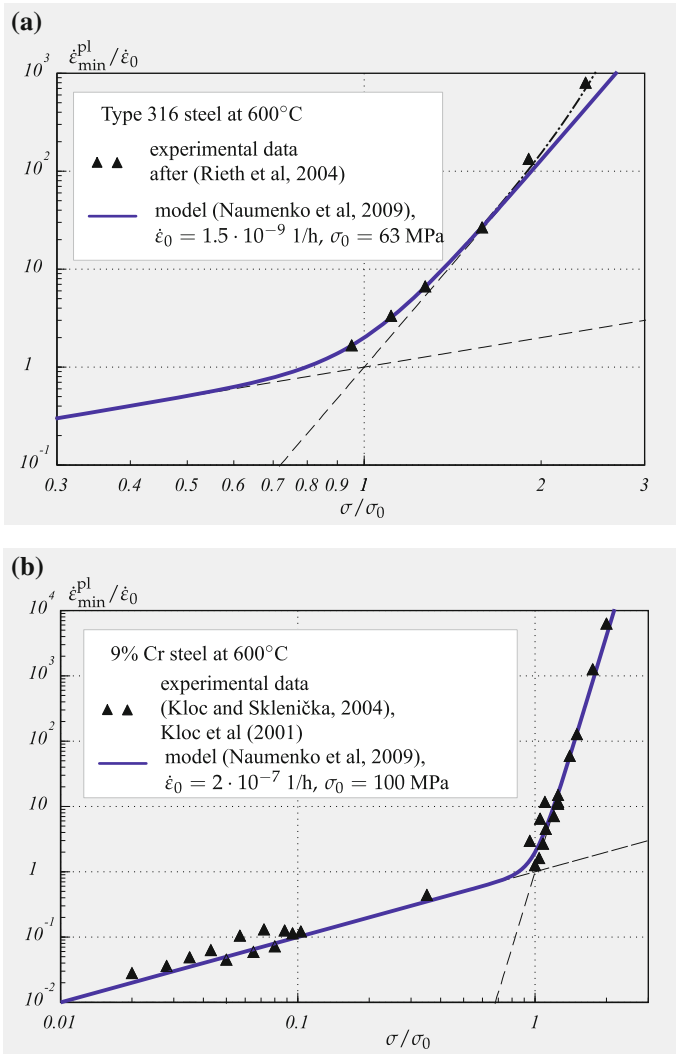


Fig. 1.8 Normalized minimum creep rate versus normalized stress. **a** Type 316 steel at 600°C, **b** 9% Cr steel at 600°C

the steady state creep stage is usually not observable. The creep strain at which the transition from primary to the tertiary creep takes place is dependent on the stress level. The tertiary creep rate is primarily controlled by the softening processes. Two important examples are the coarsening of the subgrain microstructure and coarsening of carbide precipitates (Abe 2009; Blum 2008; Dyson and McLean 1998; Straub 1995). An additional factor is the cross-section shrinkage of the specimen as a result of essential creep deformation. As the force is kept constant during the test the cross section reduction leads to an increase in the true stress value. The

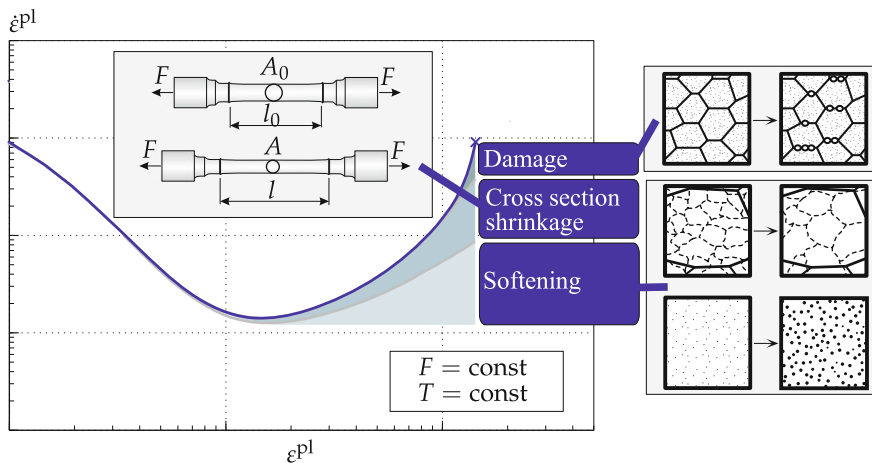


Fig. 1.9 Mechanisms of tertiary creep in advanced steel

essential non-linearity of the creep rate with respect to the true stress leads to an additional acceleration of creep. The final stage of the creep curve is affected by damage processes. The principal damage mechanism is the formation and growth of cavities on grain boundaries, subgrain boundaries or carbides. This mechanism of creep cavitation is common for many polycrystalline materials. Processes including softening, damage and cross-section shrinkage are more or less dominant depending on the stress level and temperature. To explain the influence of these mechanisms let us consider a typical long term strength (creep rupture strength) curve, Fig. 1.10. Here the value of the applied engineering stress is plotted as a function of creep life t_* deduced from uni-axial creep tests. For high stress values the fracture mode is ductile and the uni-axial specimen necks down after a certain time as a result of excessive deformation. For lower stress values the necking is still observed, but the slope of the curve decreases. The origin of this decrease is the microstructure degradation like coarsening of subgrains or coarsening of precipitates. Within the transition range the fracture mode is of the mixed type. Here the nucleation and growth of cavities and microcracks may have an influence on the creep process. The curve changes the slope from the ductile to the brittle regime. For low stresses the brittle damage and fracture modes are usually observed. Experimental creep rupture strength curves are collected in Yagi et al. (2004) for many high temperature materials.

Figure 1.11 illustrates various forms of time-dependent material behavior including creep, Fig. 1.11a, creep, Fig. 1.11b, and stress relaxation, Fig. 1.11c. Creep recovery is usually observed, when after a certain period of time the load is spontaneously removed, Fig. 1.11b. After unloading the strain drops about the value ϵ^{el} (recovery of the elastic strain). Then the strain slowly decreases down the permanent (irrecoverable) value ϵ^{pm} , whereas ϵ^{rec} is the recovered inelastic strain. A typical stress relaxation curve is shown in Fig. 1.11c. Stress relaxation is observed when the strain is held constant in time ($\epsilon = \text{const}$). A uni-axial specimen is instantaneously deformed

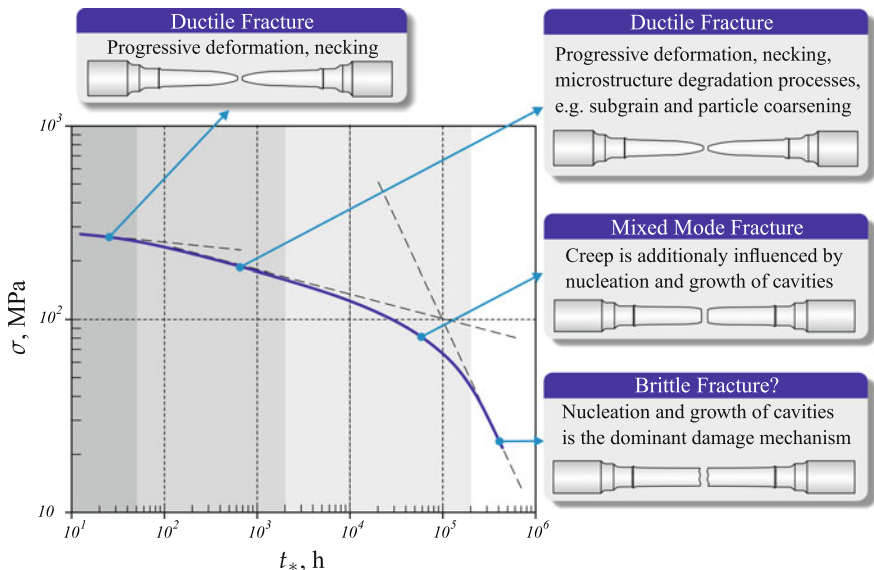


Fig. 1.10 Sketch for a long term strength curve for advanced heat resistant steel (Naumenko and Kostenko 2009)

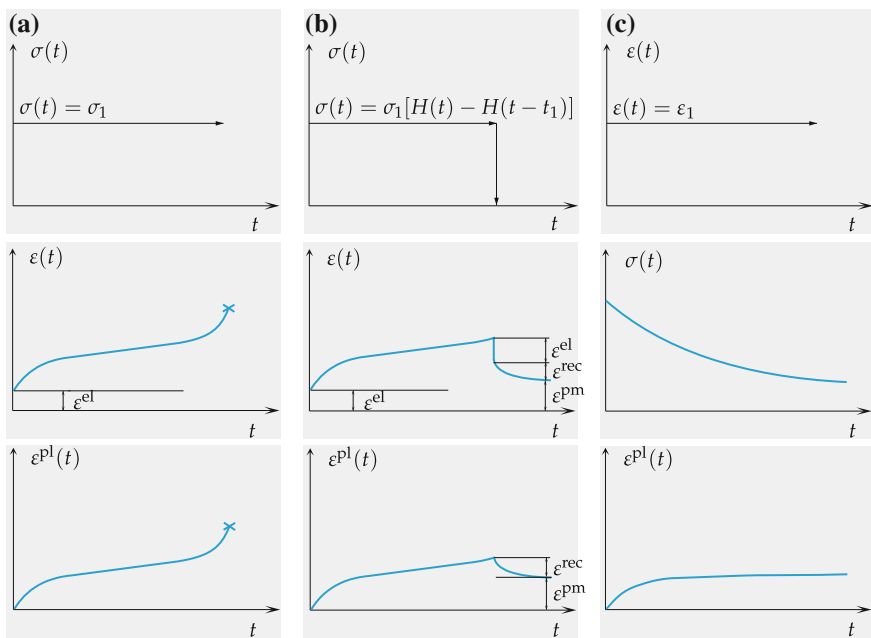


Fig. 1.11 Different forms of time-dependent stress-strain behavior under constant temperature. **a** Creep at constant stress, **b** creep recovery ($H(t)$ denotes the Heaviside function), **c** stress relaxation

to the strain value $\varepsilon^{el} = \sigma/E$, where E is the Young's modulus. During the test the load is continuously decreased in such a way that the initial strain remains constant. A threshold of the initial stress (strain) exists below which the relaxation is not observable.

In the case of relaxation it is usually assumed, e.g. Malinin (1981), Stouffer and Dame (1996), that the total zero strain rate is the sum of the elastic and the creep strain rates

$$\dot{\varepsilon} = \frac{\dot{\sigma}}{E} + \dot{\varepsilon}^{pl} = 0 \quad (1.1.1)$$

With this assumption the creep strain increases with a decaying rate during the relaxation test, Fig. 1.11c. According to Eq. (1.1.1) the stress rate in the course of relaxation can be computed from data concerning creep rates. As the stress level decreases accurate creep data for low and moderate stress levels are required to predict stress relaxation (Altenbach et al. 2008b).

Creep behavior is highly sensitive to the type of material processing (e.g. plastic forming, heat treatment). As an example, let us illustrate the effect of spontaneous plastic pre-strain on the subsequent creep behavior, Fig. 1.12. The creep curve shown by solid line is obtained under the constant stress σ_0 . The dotted lines present the second and the third creep curves after spontaneous loading to the stresses σ_1 and $\sigma_2 > \sigma_1$ leading to small plastic strains ε_1^{pl} and $\varepsilon_2^{pl} > \varepsilon_1^{pl}$, respectively, and subsequent unloading to the stress σ_0 . The creep rate after the loading in the inelastic range is significantly lower compared to the creep rate of the "virgin" material. The effect of

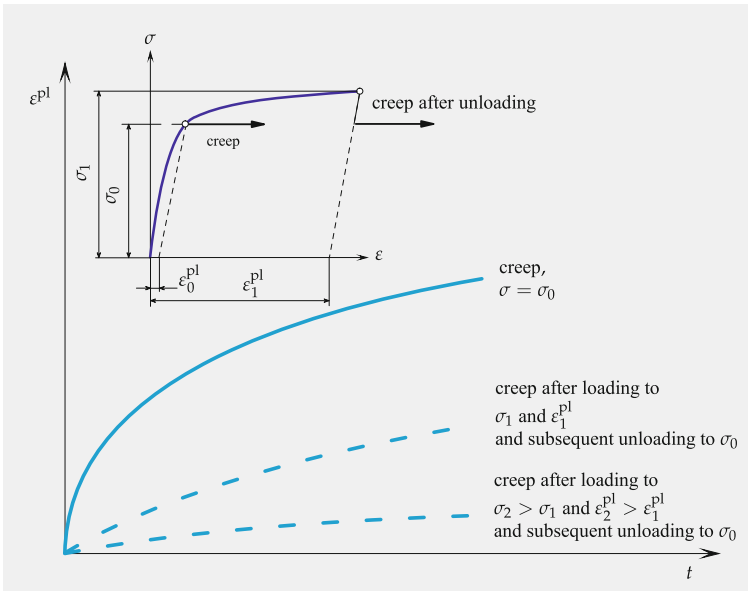


Fig. 1.12 Effect of initial plastic strain on creep behavior, after Kawai (1989)

reduction in creep rate becomes stronger with the increase of the prior plastic strain. Effects of this type are sometimes called “plasticity-creep” or “creep-plasticity” interactions, e.g. Inoue (1988), Krausz and Krausz (1996), Krempl (1999), Miller (1987).

Many materials exhibit anisotropic creep behavior. Examples are: directionally solidified nickel-based superalloys, e.g. Winstone (1998), fiber reinforced materials, e.g. Robinson et al. (2003a, b), deep drawing sheets, e.g. Betten (1976), Betten (2001), forgings (Naumenko and Gariboldi 2014; Gariboldi et al. 2016) and multi-pass weld metals (Hyde et al. 2003a). In these cases series of uni-axial creep tests for specific loading directions are performed in order to establish the material behavior. The number of the required tests and the corresponding loading directions are dictated according to the assumed symmetries of the material microstructure.

1.1.1.3 Creep Under Varying Load and Cyclic Creep

To investigate transient creep effects tests under non-stationary loading under constant high temperature are performed. Creep curves under stepwise loading are presented in Faruque et al. (1996), Malinin (1981), for example. The creep test starts under a certain value of the load. After reaching steady-state creep the load is rapidly increased or decreased and kept constant over a period of time (hold time). Such tests are useful to analyze hardening, recovery and softening processes after the rapid changes of loading. Figure 1.13 shows experimental data from creep test under compressive stress changes published in Straub (1995). During the test the specimen was initially subjected to the constant compressive true stress with the value of 196 MPa. After a certain hold time the stress was rapidly reduced to the value of 150 MPa. Several hold and loading/unloading phases were performed. As Fig. 1.13 shows the first unloading was performed after the reaching the tertiary creep stage. For the loading with the constant compressive true stress the main mechanism for accelerated creep is the softening process, associated with coarsening of subgrain structure (Straub 1995). One additional feature influenced by the softening is observed for variable loading conditions. After the stress decrease the creep rate remains lower, while after the stress increase it becomes higher than the corresponding creep rate under the constant stress level, Fig. 1.13.

Components are often subjected to cyclic loading at high temperature. To analyze the structural behavior material tests for cyclic force or displacement controls are required. Periodically varied force causes cyclic creep response. The applied periodic stress can be characterized by the amplitude σ_a , the period τ_c and the mean stress σ_m . The following stress ratios are used to indicate the kind of cyclic loading

$$\hat{A} = \frac{\sigma_a}{\sigma_m}, \quad R = \frac{\sigma_{\max}}{\sigma_{\min}}, \quad (1.1.2)$$

where $\sigma_{\max} = \sigma_m + \sigma_a$ and $\sigma_{\min} = \sigma_m - \sigma_a$. Two cases of the periodic loading are presented in Fig. 1.14a, b. Let us assume that the value of the maximum stress

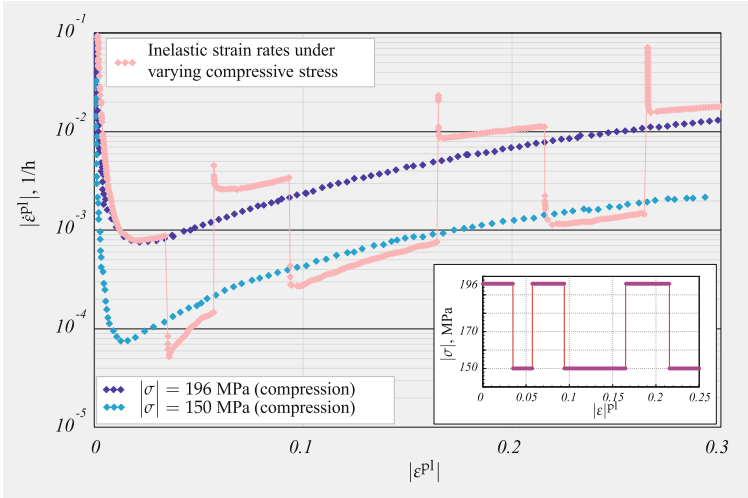


Fig. 1.13 Normalized creep rate versus creep strain for X20CrMoV 12-1 steel at $T = 600\text{ }^{\circ}\text{C}$ and variable compressive stress, after Straub (1995)

σ_{\max} is lower than the yield point (yield offset) of the material at the testing temperature. Creep behavior for the case of periodic loading with hold time is schematically illustrated in Fig. 1.14c. Here the mean stress σ_m , the amplitude σ_a , the rate of loading/unloading and the hold time influence the creep response. The case of harmonic loading is shown in Fig. 1.14b. Such loading is important in those engineering applications, where technological or operational conditions (non-stationary flow, combustion, acoustic action, etc.) cause the development of forced vibrations. The harmonic stress variation can be described as follows

$$\sigma = \sigma_m(1 + \hat{A} \sin \Omega t), \quad \Omega = \frac{2\pi}{\tau_c} = 2\pi, \quad (1.1.3)$$

Creep behavior under harmonic loading (1.1.3) with frequencies $f > 1 \dots 2$ Hz has been studied in Bernhardt and Hanemann (1938), Taira (1962), Taira and Koterazawa (1962). For this cyclic loading condition primary, secondary and tertiary stages can be observed similarly to the static case, Fig. 1.14d. Furthermore, the shape of the cyclic creep curve is geometrically similar to the static one caused by the stress $\sigma = \sigma_m$, but the creep rate is rather higher and the time to fracture is essentially smaller. It was found that creep under fast cyclic loading is not sensitive to the frequency of stress variation, e.g. Taira and Ohtani (1986). In contrast, the stress cycle asymmetry parameter \hat{A} has significant influence on the creep rate. For a number of investigated materials a material property \hat{A}_* has been found which is termed as the critical value of the stress cycle asymmetry parameter. For $\hat{A} < \hat{A}_*$ the high cyclic creep process is similar to the static one with increased creep rate and decreased time to fracture. For $\hat{A} > \hat{A}_*$ such a behavior is not observable, and fracture takes place

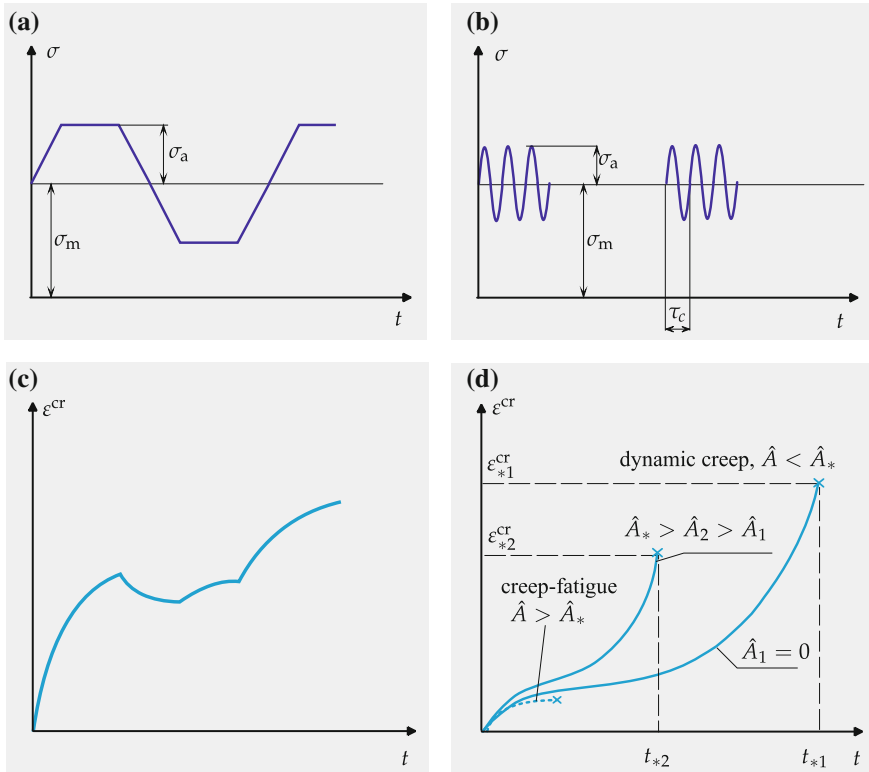


Fig. 1.14 Types of loading and corresponding cyclic creep curves. **a** Cyclic loading with hold time, **b** harmonic loading with high frequency, **c** creep response for cyclic loading with hold time, **d** different responses for loading with high frequency

as a consequence of creep-fatigue interaction. Following Lazan (1949), Rabotnov (1969), Taira and Ohtani (1986), the processes of high-frequency cyclic creep are classified as: dynamic creep for $\hat{A} < \hat{A}_*$ and high cyclic creep for $\hat{A} > \hat{A}_*$. Creep curves for both cases are schematically presented in Fig. 1.14d.

The cycle by cycle accumulation of inelastic strain under the applied cyclic force is called ratchetting. Experimental data show that the ratchetting deformation depends on the mean stress, the stress ratio as well as on the loading rate and hold time (Altenbach et al. 2013; Ohno et al. 1998; Ohno 1998). For advanced 9–12 % Cr steels anomalous ratchetting behavior is documented—in cyclic force controlled tests with zero mean force progressive deformation in the tensile direction is observed (Yaguchi and Takahashi 2005; Röttger 1997; Bunch and McEvily 1987).

1.1.1.4 Low Cycle Fatigue, Creep Fatigue, and Thermo-Mechanical Fatigue

Figure 1.15a shows basic parameters of the strain controlled low cycle fatigue (LCF) test. The loading is characterized by the strain amplitude ε_a , strain range $\Delta\varepsilon = 2\varepsilon_a$, and the mean strain ε_m . Similarly to the stress controlled tests the following ratios can be introduced

$$\hat{A}_\varepsilon = \frac{\varepsilon_a}{\varepsilon_m}, \quad R_\varepsilon = \frac{\varepsilon_{\max}}{\varepsilon_{\min}}, \quad (1.1.4)$$

where $\varepsilon_{\max} = \varepsilon_m + \varepsilon_a$ and $\varepsilon_{\min} = \varepsilon_m - \varepsilon_a$. During the test the stress as a function of time is recorded. The basic stress response parameters are the stress amplitude σ_a and the mean stress σ_m . From a hysteresis loop for a certain loading cycle, Fig. 1.15b one may also compute the elastic strain range $\Delta\varepsilon^{\text{el}}$ and the plastic strain range $\Delta\varepsilon^{\text{pl}}$. Typical stress responses obtained from LCF tests with $R_\varepsilon = -1$ are schematically shown in Fig. 1.16. Here the stress amplitude is presented as a function of the cycle number. For a class of materials, for example 300-series austenitic steels, the cyclic hardening followed by the stabilized response is observed. The stress amplitude increases over a number of cycles (cyclic hardening stage), attains a steady-state value (stabilized response stage) and decreases rapidly at the final stage of fatigue failure. On contrary, many materials, for example 9–12% Cr steels, exhibit cyclic softening, that is the decrease of the stress amplitude starting from the first loading cycles over the whole fatigue life. Figure 1.17 shows the dependence of stress amplitudes on the number of cycles for X 20 CrMoV 12 1 steel $T = 530^\circ\text{C}$ and different strain amplitudes. Strain controlled tests with $R_\varepsilon = -1$ and the loading frequency $f = 5\text{ Hz}$ were performed by Röttger (1997). The cyclic softening regime is clearly observed. The number of cycles to fatigue failure decreases with an increase of the strain amplitude. In strain controlled fatigue tests with $R_\varepsilon = -1$ at low homologous temperature the strain amplitude is the important loading input parameter that determines the fatigue life. Strain amplitude versus cycles to failure diagrams are widely used to characterize fatigue strength of materials.

Fatigue damage evolution is a sequence of several microstructural events. The total fatigue life can be separated into the stage of macrocrack initiation and the stage of macrocrack growth until reaching the critical crack length and final failure. The first initiation stage can include processes of increase in dislocation density, formation of dislocation substructures, localization of inelastic strain along persistent slip bands, surface relief evolution, formation and early growth stage of surface microcracks (Mughrabi 2009; Polák 2003). This early stage is mostly controlled by the non-homogeneous cycle by cycle inelastic deformation. The accumulation of irreversible slip steps on the surface leads to the surface roughening, with sites of local stress concentrations at which microcracks can form (Mughrabi 2009). Short cracks usually grow by the sliding mode (mode II in the sense of fracture mechanics). Progressively, after crossing several grains the main crack propagates, usually in the plane orthogonal to the loading axis.

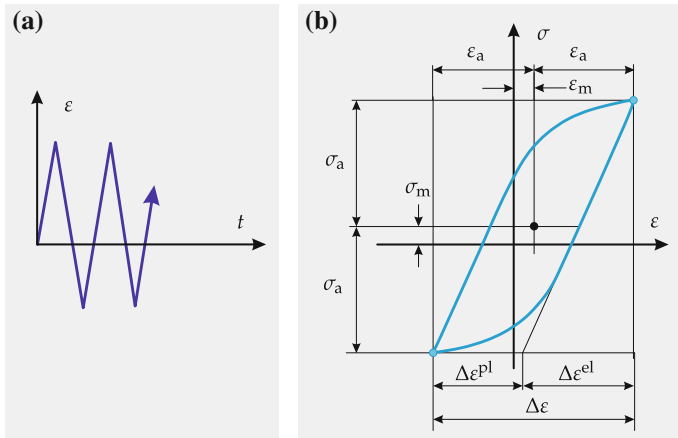


Fig. 1.15 Loading and stress response parameters in LCF regime. **a** Triangular strain waveform, **b** hysteresis loop

Fig. 1.16 Stress amplitude versus number of cycles curves with different cyclic regimes for $R_\epsilon = -1$

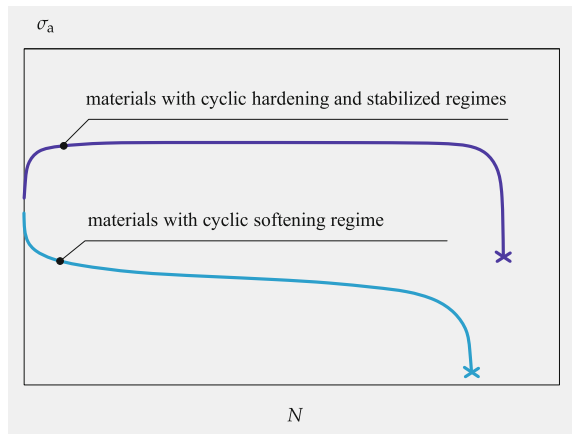
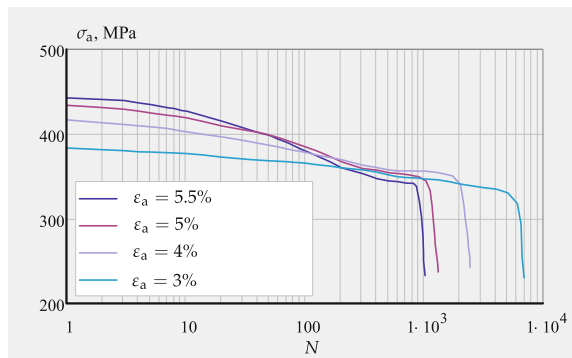


Fig. 1.17 Stress amplitude versus number of cycles for X20CrMoV12-1 steel at $T = 530\text{ }^\circ\text{C}$, $R_\epsilon = -1$ and different strain amplitudes, after Röttger (1997)



The inelastic response at high temperature depends essentially on the rate of loading, cp. Sect. 1.1.1.1. For static and cyclic tests under low strain rates creep regime becomes essential. Decrease in the strain rate by keeping the total strain range fixed leads to an increase in the inelastic strain range and the dissipated work within the cycle. Fatigue life usually decreases with a decrease of the strain rate (loading frequency) for constant strain range, e.g. Skelton (2003).

Test performed under cyclic strain with hold times at high temperature are usually performed to examine creep-fatigue (relaxation-fatigue) behavior. Figure 1.18a provides a sketch of a cyclic strain control with hold phases under tension and compression. The stress response over time, Fig. 1.18b and the hysteresis loop, Fig. 1.18c illustrate the stress relaxation regimes during hold phases. Various controls of creep-fatigue tests can be applied to analyze material behavior. Examples include cycles with tension-compression holds, Fig. 1.18, cycles with tensile holds, cycles with compressive holds, etc. Tensile and compressive holds with the same duration have usually different influence on the creep-fatigue life for many materials. For example 9–12% Cr steels compressive hold phases more detrimental than tensile ones, in the sense that the fatigue life is more severely reduced under compressive holds than under tensile holds (Aktaa and Petersen 2009; Fournier et al. 2008). This effect might be surprising as one expects creep damage evolution under tension rather

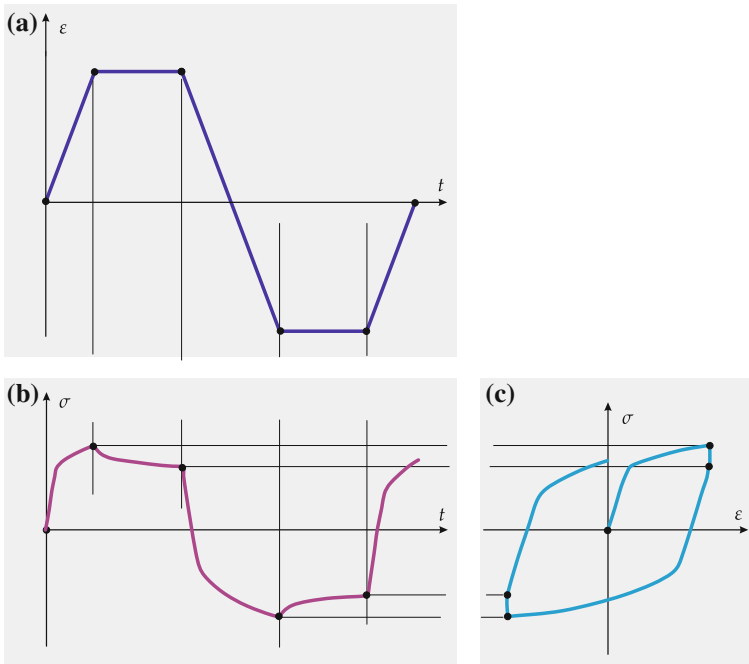


Fig. 1.18 Low cycle fatigue with hold time. **a** Loading, **b** stress response, **c** hysteresis loop

than under compression hold phases. However, analysis of the deformation process and changes in the hysteresis loop from cycle to cycle as a result of softening and relaxation provide explanation as how the fatigue life is affected by tensile and/or compressive holds. Tensile holds reduce tensile stress peaks in the cycle as observed for a half of the fatigue life. Therefore, cycling with compressive holds lead to higher peaks in tensile stress if compared to loading with tensile holds. Assuming that tensile peaks promote fatigue damage from cycle to cycle, the shortening of fatigue life can be explained (Aktaa and Petersen 2009).

Many components operate under changing temperature environment and mechanical loading over a long period. Critical positions may be subjected to fatigue damage due to thermal transients and/or creep damage during exposure at high temperature. Generally, the structural integrity of a component is ensured through reliable design, precise manufacturing, definition of allowable operational modes, and timely inspection. However, permanently changing economic situations and environmental conditions require more flexible operation modes in service, e.g. daily start-up and shut-down and/or increase of steam pressure and temperature. An important step in the life-time assessment is to analyze material behavior for service-type loading and temperature profiles. To this end an inelastic structural analysis that takes into account both the slow changes in the stress and strain states during hold (running) phases and transient behavior during start-ups and shut-downs is required. Hysteresis loops obtained from structural analysis of results of real components provide an input to generate service-type thermo-mechanical fatigue (TMF) loading profiles for laboratory testing of materials. For example, strain and temperature variations on the surface of real components were used for TMF testing of uni-axial specimens in Cui et al. (2009), Holdsworth et al. (2007). Examples for analysis of structures subjected to thermal cycling will be presented in Sect. 1.2.2.

Figure 1.19 illustrates schematically strain and temperature profiles and the stress response over one cycle of TMF loading. Experimental data for such strain and temperature controls are presented in Cui et al. (2009), Kostenko et al. (2013), Cui and Wang (2014) for uni-axial specimens from 10% Cr steel and in Samir et al. (2005) for cruciform specimens from 1% Cr steel under biaxial loading. Following the classification by Berger et al. (2008) the loading profile presented in Fig. 1.19 corresponds to the hot start situation. Further examples include cold and warm start profiles with higher differences in the maximum and minimum absolute temperatures within the cycles (Holdsworth et al. 2007).

In Längler et al. (2014), Nagode et al. (2011a, b) results of TMF tests for a D5S cast iron material are discussed. A series of in-phase TMF tests with the temperature variation within the range from 230 to 680 °C were performed. Figure 1.20 illustrates the strain and the temperature variations within one cycle of loading with the duration of 600 s. TMF tests were performed for two different loading profiles. The first one called direct is presented in Fig. 1.20. The second one has the same temperature control but the direction of the strain path is reversed, that is the specimen is subjected to the compressive strain with the same magnitude. Temperature induced axial thermal strain is measured prior to the start of cycle sequence in strain control mode to enable

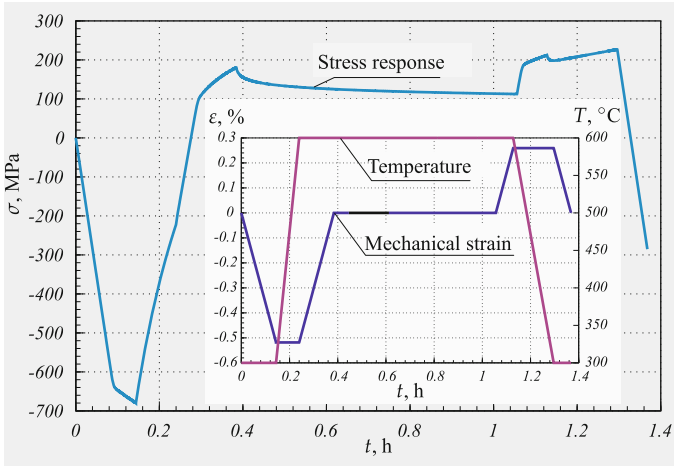


Fig. 1.19 Loading profiles and stress response for one cycle of TMF loading, after Naumenko et al. (2011b)

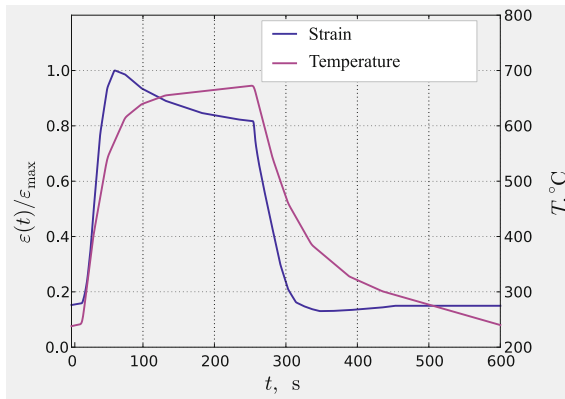


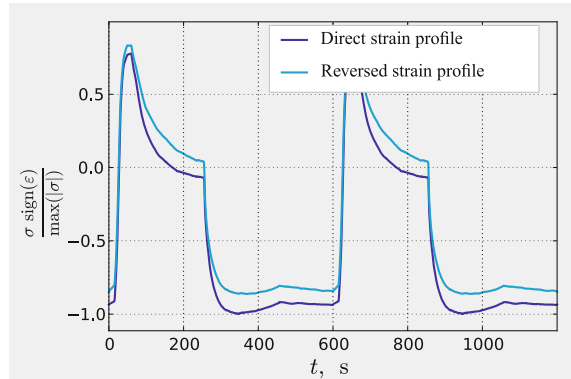
Fig. 1.20 Loading profile for one cycle of TMF loading for D5S cast iron material, after Längler et al. (2014)

thermal strain compensation. Total and thermal strains as well as stress responses were recorded in the course of cyclic loading up to failure of specimens.

Figure 1.21 shows normalized stress responses in a stabilized loading cycle for both the direct and reversed loading profiles. The slight difference in stress response under tension and compression may be caused by asymmetric slip, hardening, damage and other processes, e.g. Naumenko and Altenbach (2007).

Lifetime of specimens or components under TMF loading conditions is limited by fatigue damage, creep damage, environmental damage or in many cases by complex interaction of different damage mechanisms. In Holdsworth et al. (2007) results of uni-axial TMF tests for 1CrMoV forged steel under service-type loading condi-

Fig. 1.21 Stress response for a stabilized cycle of TMF loading for D5S cast iron material, after Längler et al. (2014)



tions are discussed. Specimens were subjected to three heat profiles with the same maximum temperature but different temperatures at the beginning and the end of the cycles. All three types of tests were conducted under the same mechanical strain control that corresponds to the start-up situation. Post test inspection has been employed to characterize the associated damage mechanisms. It was observed that the increase of the temperature difference within the cycle leads to reduction in cycles to crack initiation endurance. Two dominant types of damage are usually observed in TMF tests of the considered low-alloy steel. Fatigue damage develops as a relatively uniform distribution of short transgranular cracks at the surface along and around the gauge section. Creep damage evolution is the nucleation and coalescence of cavities at grain boundaries and propagation of intergranular cracks across the specimen section. In tests with low difference between the minimum and the maximum temperatures in a cycle fatigue-dominated damage evolution was observed. Surface fatigue cracks were initiated and a main crack propagated towards the cross section of the specimen, where creep cavitation was also observed. Damage development in tests with moderate difference in temperature levels was creep dominated. At the end of test there was a high intensity of relatively fine intergranular microcracks in the gauge section. In tests with high temperature differences, the extent of surface oxidation and spallation was high due to the high thermal transient and the rate of metal removal at the surface appeared to be greater than the rate of crack development.

Several elementary rules are available to estimate the LCF life based on the loading characteristics within the cycle. An example is the Coffin-Manson equation (Coffin 1954; Manson 1953) that relates the plastic strain amplitude within a cycle with the number of cycles to fatigue failure. More advanced rules were developed to account for strain rate and hold time dependencies under isothermal loading conditions. They use data from stress-strain loops within a characteristic cycle, for example, the steady state stress and/or strain rate values at the end of the hold phase, strain range, the dissipated mechanical work together with experimental data, for example creep strength and fatigue endurance. For reviews we refer to Viswanathan (1989), Penny and Mariott (1995); Berger et al. (2008). These approaches are mostly applicable to

situations, where stabilized stress-strain behavior after a certain number of loading cycles is expected. For materials with cyclic softening the shape of the stress-strain loop changes continuously from cycle to cycle such that the whole deformation process should be analyzed.

Alternatively, advanced constitutive equations for inelastic deformation and kinetic laws for hardening/recovery, softening and damage can be developed to capture the whole cycle by cycle material behavior (Aktaa and Petersen 2009; Chaboche 2008; Kostenko et al. 2013). Development of kinetic laws for interaction of different damage mechanisms and efficient numerical methods to solve kinetic equations over many loading cycles are still challenging problems.

1.1.2 Multi-axial Effects

Experimental data obtained from uni-axial tests allow us to establish basic features of inelastic behavior and to find relations between strain rate, stress, temperature and time. However, most structural members are subjected to multi-axial stress conditions. In order to analyze the influence of the stress state on the material behavior, multi-axial tests are required.

Various techniques have been developed to test materials under multi-axial loading conditions. Examples are: thin-walled tubes subjected to axial force and torque, e.g. Kowalewski (1995), Kawai (1989), two- and three-dimensional cruciform specimens subjected to axial forces, e.g. Sakane and Hosokawa (2001), Sakane and Tokura (2002), Samir et al. (2005), circumferentially notched specimens subjected to axial force, e.g. Hyde et al. (1996), Perrin and Hayhurst (1994), Simon (2007), Cui et al. (2009) and three-dimensional component-like test pieces (Colombo et al. 2008).

Figure 1.22 shows a thin-walled tube under the axial force and torque with the magnitudes F and M , respectively. Let r_m be the mean radius of the cross section, h the wall thickness and L the gauge length. With the local cylindrical basis \mathbf{e}_r , \mathbf{e}_φ and \mathbf{k} , as shown in Fig. 1.22, the stress state can be characterized by the following tensor

$$\boldsymbol{\sigma} = \sigma \mathbf{k} \otimes \mathbf{k} + \tau (\mathbf{e}_\varphi \otimes \mathbf{k} + \mathbf{k} \otimes \mathbf{e}_\varphi), \quad \sigma = \frac{F}{2\pi r_m h}, \quad \tau = \frac{M}{2\pi r_m^2 h} \quad (1.1.5)$$

The deviatoric part of the stress tensor is¹

$$\mathbf{s} = \sigma \left(\mathbf{k} \otimes \mathbf{k} - \frac{1}{3} \mathbf{I} \right) + \tau (\mathbf{e}_\varphi \otimes \mathbf{k} + \mathbf{k} \otimes \mathbf{e}_\varphi), \quad (1.1.6)$$

where \mathbf{I} is the second rank unit tensor, see Sect. A.4. One possible stress measure which can be used to compare different multi-axial tests is the von Mises equivalent stress σ_{vM} which is defined as follows

¹Basic rules of the direct tensor calculus are presented in Sect. A.4.

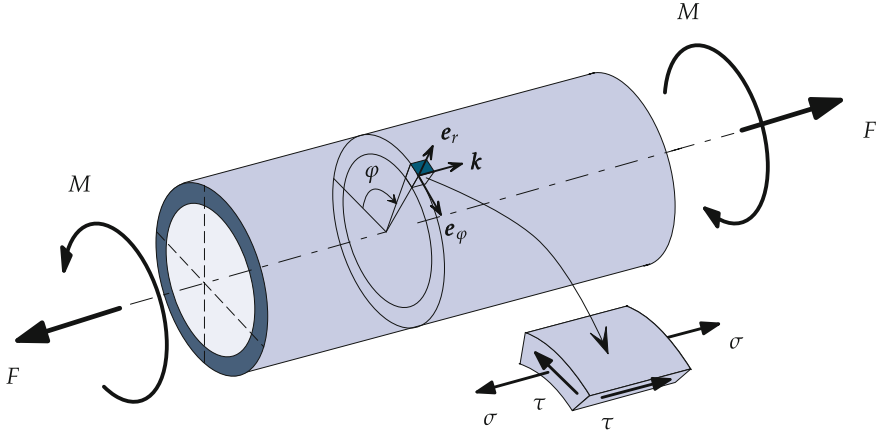


Fig. 1.22 Thin-walled tube for multi-axial creep tests

$$\sigma_{\text{VM}} = \sqrt{\frac{3}{2} \mathbf{s} \cdot \mathbf{s}} = \sqrt{\sigma^2 + 3\tau^2}$$

From the measured elongation ΔL and the angle of twist ϕ_T the axial strain ε_L and the shear strain γ can be computed

$$\varepsilon_L = \frac{\Delta L}{L}, \quad \gamma = \frac{r_m \phi_T}{L}$$

Assuming that the material behavior is isotropic, the strain state in a tube can be characterized by the following tensor

$$\boldsymbol{\varepsilon} = \varepsilon_L \mathbf{k} \otimes \mathbf{k} + \varepsilon_Q (\mathbf{I} - \mathbf{k} \otimes \mathbf{k}) + \frac{1}{2} \gamma (\mathbf{e}_\varphi \otimes \mathbf{k} + \mathbf{k} \otimes \mathbf{e}_\varphi),$$

where $\varepsilon_Q = \Delta r_m / r_m$ is the transverse normal strain.

In what follows let us limit to the stress controlled tests and analyze creep behavior under multi-axial stress states. The inelastic (creep) strain tensor is defined as the difference between the strain tensor $\boldsymbol{\varepsilon}$ which includes the measurable quantities and the tensor of initial elastic strains which can be calculated from Hooke's law. As a result we obtain

$$\begin{aligned} \boldsymbol{\varepsilon}^{\text{pl}} = & \left(\varepsilon_L + 2\varepsilon_Q - \frac{1-2\nu}{E} \sigma \right) \frac{1}{3} \mathbf{I} + \left(\varepsilon_L - \varepsilon_Q - \frac{(1+\nu)}{E} \sigma \right) \left(\mathbf{k} \otimes \mathbf{k} - \frac{1}{3} \mathbf{I} \right) \\ & + \frac{1}{2} \left(\gamma - \frac{2(1+\nu)}{E} \tau \right) (\mathbf{k} \otimes \mathbf{e}_\varphi + \mathbf{e}_\varphi \otimes \mathbf{k}), \end{aligned} \quad (1.1.7)$$

where ν is the Poisson's ratio. The basic assumption related to the multi-axial creep behavior is the volume constancy during the creep deformation, e.g. Odqvist (1974),

Odqvist and Hult (1962). In this case the following relations should be satisfied

$$\text{tr } \boldsymbol{\varepsilon} = \text{tr } \boldsymbol{\varepsilon}^{\text{el}} \Rightarrow \varepsilon_{\text{L}} + 2\varepsilon_{\text{Q}} = \frac{1 - 2\nu}{E} \sigma$$

From (1.1.7) it follows

$$\boldsymbol{\varepsilon}^{\text{pl}} = \frac{3}{2} \left(\varepsilon_{\text{L}} - \frac{1}{E} \sigma \right) \left(\mathbf{k} \otimes \mathbf{k} - \frac{1}{3} \mathbf{I} \right) + \frac{1}{2} \left(\gamma - \frac{2(1 + \nu)}{E} \tau \right) (\mathbf{k} \otimes \mathbf{e}_{\varphi} + \mathbf{e}_{\varphi} \otimes \mathbf{k})$$

Under the condition of stationary loading the creep rate tensor is

$$\dot{\boldsymbol{\varepsilon}} = \dot{\boldsymbol{\varepsilon}}^{\text{pl}} = \frac{3}{2} \dot{\varepsilon}_{\text{L}} \left(\mathbf{k} \otimes \mathbf{k} - \frac{1}{3} \mathbf{I} \right) + \frac{1}{2} \dot{\gamma} (\mathbf{k} \otimes \mathbf{e}_{\varphi} + \mathbf{e}_{\varphi} \otimes \mathbf{k}) \quad (1.1.8)$$

The von Mises equivalent creep rate is defined by

$$\dot{\varepsilon}_{\text{VM}} = \sqrt{\frac{2}{3} \dot{\boldsymbol{\varepsilon}} \cdot \dot{\boldsymbol{\varepsilon}}} = \sqrt{\dot{\varepsilon}_{\text{L}}^2 + \frac{1}{3} \dot{\gamma}^2}$$

The results of creep tests on tubes are usually presented as: strains ε_{L} and γ versus time curves, e.g. Hayhurst and Leckie (1990), Inoue (1988), Kawai (1989), creep strains

$$\varepsilon_{\text{L}}^{\text{cr}} = \varepsilon_{\text{L}} - \frac{\sigma}{E}, \quad \gamma^{\text{cr}} = \gamma - \frac{2(1 + \nu)}{E} \tau$$

versus time curves, e.g. Murakami and Sanomura (1985), Penkalla et al. (1988), Ohno et al. (1990), von Mises equivalent creep strain

$$\varepsilon_{\text{VM}}^{\text{pl}} = \sqrt{\frac{2}{3} \boldsymbol{\varepsilon}^{\text{pl}} \cdot \boldsymbol{\varepsilon}^{\text{pl}}} = \sqrt{(\varepsilon_{\text{L}}^{\text{pl}})^2 + \frac{1}{3} (\gamma^{\text{pl}})^2}$$

versus time curves, e.g. Kowalewski (1995), Kowalewski (2001), and the so-called specific dissipation work

$$q(\bar{t}) = \int_0^{\bar{t}} \dot{\boldsymbol{\varepsilon}} \cdot \mathbf{s} \, dt = \int_0^{\bar{t}} (\dot{\varepsilon}_{\text{L}} \sigma + \dot{\gamma} \tau) dt$$

versus time curves (Sosnin 1974; Sosnin et al. 1986).

Figure 1.23 illustrates typical results of creep testing under constant von Mises stress σ_{VM} . Sketches of creep curves are presented for the case of tension under the normal stress $\sigma = \sigma_{\text{VM}}$ and torsion under the shear stress $\tau = \sigma_{\text{VM}}/\sqrt{3}$. For many structural materials the kind of the stress state (e.g. tension or torsion) has negligible influence on the primary and secondary creep behavior. However, this is not the case for the tertiary creep and the long term strength. Tubular specimen subjected

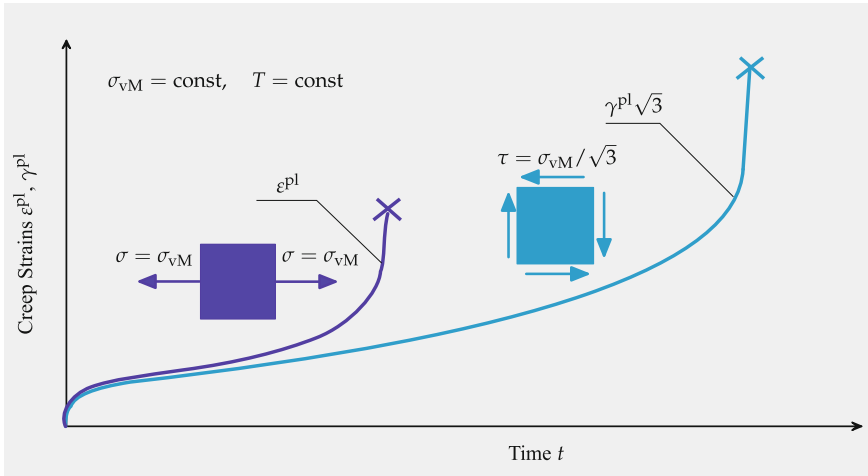


Fig. 1.23 Stress state effect of tertiary creep

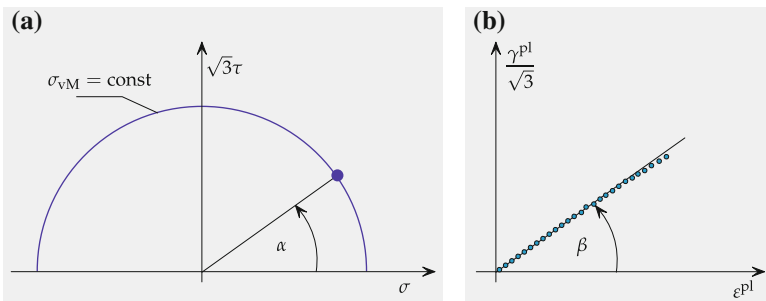


Fig. 1.24 Creep response under combined tension-torsion loading. **a** Plane stress state, **b** strain trajectory

to tension usually exhibit much shorter lifetime and lower ductility if compared to the case of pure torsion. This stress state effect has been observed for copper in Kowalewski (1995) and for austenitic steels in Niu et al. (2002), Trivaudey and Delobelle (1993), for example.

Tests under combined tension-torsion loading are useful to formulate and to verify constitutive models. Figure 1.24a shows the plot of the equation

$$\sigma^2 + 3\tau^2 = \sigma_{VM}^2 = \text{const}$$

with respect to coordinates σ and $\sqrt{3}\tau$. Different stress states leading to the same fixed value of the von Mises stress can be conveniently characterized by the angle α (stress state angle). The corresponding values for the normal and the shear stress

can be then calculated as follows

$$\sigma = \sigma_{\text{VM}} \cos \alpha, \quad \tau = \sigma_{\text{VM}} \frac{\sin \alpha}{\sqrt{3}}$$

For example, $\alpha = 0$ corresponds to the case of tension and $\alpha = \pi/2$ to the case of torsion. $0 < \alpha < \pi/2$ characterizes the combined loading case. The loading conditions realized in creep tests can be classified as follows

- (a) stationary σ_{VM} and α ,
- (b) time-varying (e.g. stepwise or cyclic) σ_{VM} under fixed α ,
- (c) time-varying α under fixed σ_{VM} and
- (d) both σ_{VM} and α are time-varying.

The loading cases (a) and (b) are called simple or proportional loadings, while the cases (c) and (d) are classified as non-proportional loadings. The results of creep tests under the combined loading can be conveniently presented as $\gamma^{\text{cr}}/\sqrt{3}$ versus ε^{cr} curves (so-called strain trajectories), e.g. Murakami and Sanomura (1985), Nikitenko (1984). A sketch of such a curve for the loading case (a) is presented in Fig. 1.24b. For many metals and alloys the direction of the strain trajectory characterized by the angle β , Fig. 1.24b, coincides with the direction of the applied stress state characterized by the angle α . Experimental data are discussed in Murakami and Sanomura (1985), Nikitenko (1984), Oytana et al. (1982). According to this one can assume that the creep rate tensor is coaxial and collinear with the stress deviator, i.e. $\dot{\varepsilon} = \lambda \mathbf{s}$. Taking into account Eqs. (1.1.6) and (1.1.8) the following relations can be obtained

$$\frac{3}{2} \dot{\varepsilon}_{\text{L}} = \lambda \sigma, \quad \frac{1}{2} \dot{\gamma} = \lambda \tau \quad \Rightarrow \quad \frac{\dot{\varepsilon}_{\text{L}}}{\dot{\gamma}/\sqrt{3}} = \frac{\sigma}{\sqrt{3}\tau}$$

For many materials, experimental results show that the above relations are well satisfied, e.g. Hayhurst and Leckie (1990), Murakami and Sanomura (1985), Nikitenko (1984), Oytana et al. (1982).

Non-coincidence of the strain-trajectory and the stress state angles indicates the anisotropy of inelastic behavior and/or dependency of the inelastic strain rate on the kind of the stress state. Anisotropic creep may be caused either by the initial anisotropy of the material microstructure as a result of material processing or by the anisotropy induced in the course of inelastic deformation. Examples for tension-torsion creep of initially anisotropic materials are presented for a directionally solidified nickel-based superalloy in Ohno and Takeuchi (1994) and for a fiber-reinforced material in Robinson et al. (2003a, b).

The trajectories of creep strains presented in Kawai (1989) for austenitic steel tubes demonstrate that initial small plastic pre-strain causes the stress state dependence of subsequent creep behavior. Figure 1.25 provides a sketch of experimental results discussed in Kawai (1989). Here the creep curve of the “virgin” material recorded after the uni-axial loading up to σ_0 is compared with creep curves obtained after the uni-axial loading to σ_1 and subsequent multi-axial loadings with $\sigma_{\text{VM}} = \sigma_0$.

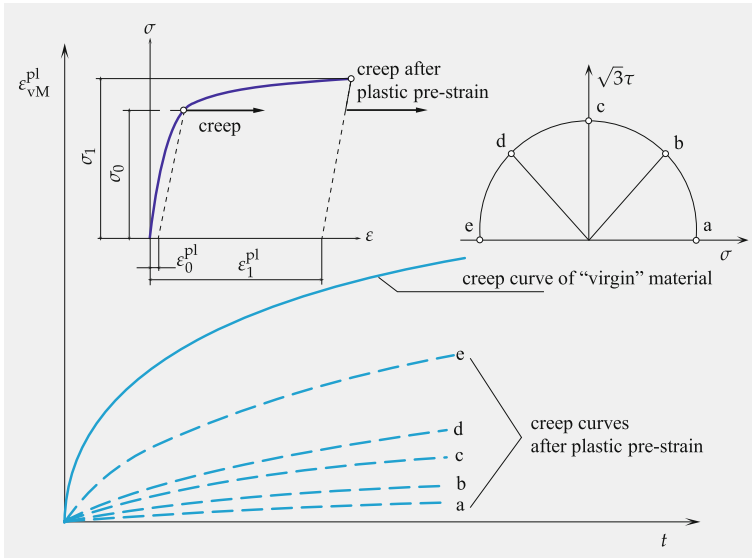


Fig. 1.25 Effect of initial tensile plastic strain on subsequent creep behavior under combined tension and torsion, after Kawai (1989)

Different creep curves under tension, compression, torsion as well as combined tension-torsion and compression-torsion are obtained. This stress state effect of creep is related to the anisotropic hardening induced during the plastic pre-strain. Creep curves illustrating different behavior under tensile and compressive loadings are presented for several alloys in El-Magd and Nicolini (1999), Lucas and Pelloux (1981), Stouffer and Dame (1996), Zolocheskij (1988) and for ceramics in Pintschovius et al. (1989).

The origins of induced anisotropy for polycrystals may be related to hardening due to directed residual stress state in grains, crystallographic texture, formation and growth of cavities and microcracks on grain boundaries. For short fiber reinforced polymers fibers may change the orientation state as a result of creeping flow of the matrix material (Altenbach et al. 2003, 2007). Several methods exist to detect deformation and/or damage induced anisotropy. For example, one may interrupt the test after a certain creep exposure, cut specimen in different directions and perform subsequent creep tests to establish the effect of the induced anisotropy. Such tests are discussed in Betten et al. (1995), El-Magd et al. (1996). Another approach is to subject the specimen to the non-proportional loading with varying principal directions, or in other words to rotate the loading with respect to the material without interrupting the test. To illustrate this consider the stress state (1.1.5) for combined tension (compression) and torsion. The stress tensor σ can also be given in the spectral form as follows

$$\sigma = \sigma_I \mathbf{n}_I \otimes \mathbf{n}_I + \sigma_{III} \mathbf{n}_{III} \otimes \mathbf{n}_{III},$$

where

$$\sigma_I = \frac{\sigma + \sqrt{\sigma^2 + 4\tau^2}}{2}, \quad \sigma_{III} = \frac{\sigma - \sqrt{\sigma^2 + 4\tau^2}}{2}$$

are principal stress values and the unit vectors

$$\mathbf{n}_I = \cos \vartheta \mathbf{k} + \sin \vartheta \mathbf{e}_\varphi, \quad \mathbf{n}_{III} = \sin \vartheta \mathbf{k} - \cos \vartheta \mathbf{e}_\varphi, \quad \tan \vartheta = \frac{\tau}{\sigma_I}$$

define the principal directions. Figure 1.26 illustrates the stress state for the combined tension (compression) and torsion. The stress tensor can be defined with respect to the axial and circumferential directions, Fig. 1.26a as well as principal directions, Fig. 1.26b. By changing the values of σ and/or τ during the test, the angle ϑ can be manipulated. Results of creep tests under non-proportional loading with changing principal directions are published by Trampczynski et al. (1981) and Murakami and Sanomura (1985). Tubular copper specimens were subjected to combined tension and torsion with varying loading amplitudes of σ and τ , correspondingly, Fig. 1.27a. The reversal of torque at time t_1 leads to the change of the angle θ characterizing the first principal direction of the stress tensor. As the absolute value of the shear stress remains the same, the value of the von Mises equivalent stress is not affected by the reversal. Therefore, one expects no changes in creep responses if the material is isotropic. In Murakami and Sanomura (1985) creep responses after shear stress reversals leading to different values of the angle ϑ are systematically analyzed. A sketch of a typical creep response is presented in Fig. 1.27b. Normal and shear creep strain versus time curves for stationary stress values as well as corresponding creep curves after the reversal of shear stress are given. As a result of shear stress reversal two effects can be recognized. After the shear stress reversal both the rate of the normal strain and the rate of the shear strain are significantly affected. This indicates on the anisotropic nature of hardening, induced during the first loading phase before the reversal. Furthermore, the creep life of the specimen after the shear stress reversal is significantly longer than the corresponding life under the stationary loading. This effect can be explained by the anisotropic damage evolution. The principal creep damage mechanism in copper is the nucleation, growth and coalescence of cavities at grain boundaries. The cavitation is found to take place mainly on those grain boundaries, which are orthogonal to the first principal direction of the stress tensor. After the shear stress reversal, former cavities stop to grow and new cavities nucleate and grow on new grain boundaries closely orthogonal to the rotated first principal direction. Cavitated grain boundaries before and after the stress reversal are shown schematically in Fig. 1.27b.

Examples discussed in this section are limited to force (torque) controlled tests. Engineering structures may be subjected to varying external loadings and thermal environment resulting in local non-proportional changes in stress and strain states. Stress and/or strain controlled tests on cruciform specimen with various bi-axial loading and temperature profiles are presented in Zhang et al. (2007), Berger et al. (2008), Wang et al. (2014), Cui et al. (2013).

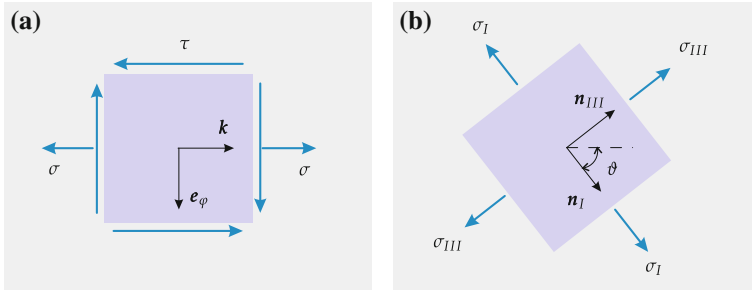


Fig. 1.26 Stress state for combined tension and torsion. **a** Normal and shear stress components, **b** principal stresses and principal directions

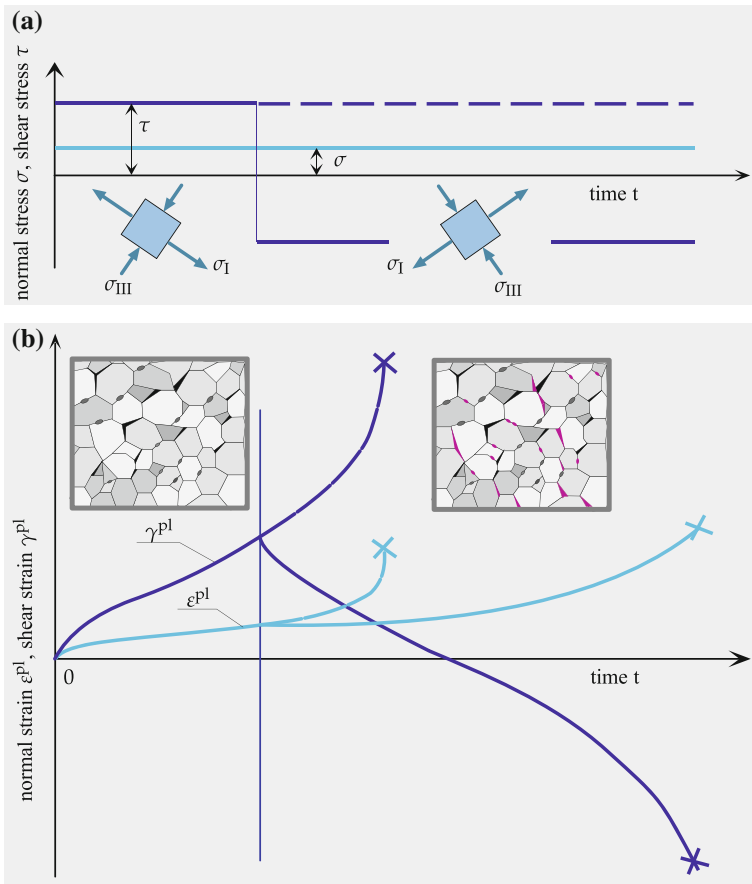


Fig. 1.27 Creep tests at combined tension and torsion. **a** Loading history, **b** creep responses, after Murakami and Sanomura (1985)

1.2 High-Temperature Inelasticity in Structures

Analysis of the structural behavior at high temperature is crucial for understanding time-dependent changes in stress and strain states as a result of constant or variable external loading. Local increase of strains, relaxation and redistribution of stresses are examples for such changes. For adequate experimental analysis of the material behavior a specimen should be subjected to realistic stress, strain and temperature profiles. Such local profiles can be generated by heat transfer and structural analysis of a component. The aim of this section is to present simulation results for several structures. Academic examples from elementary engineering mechanics are selected to illustrate basic features of structural behavior at high temperature. Furthermore examples for real high-temperature components are presented.

1.2.1 Examples for Creep in Structures

Creep in structures is a variety of time-dependent changes of strain and stress states including progressive deformations, relaxation and redistribution of stresses and local reduction of the material strength as a result of softening and damage. In this section basic features of creep in structures are discussed based on two examples for a beam and a steam transfer line.

1.2.1.1 Beam

Let us consider a beam with a rectangular cross section. We assume that the beam is heated up to a certain temperature, clamped at the ends and subjected to the uniformly distributed lateral load q as shown in Fig. 1.28a. The loading is moderate leading to spontaneous elastic deformation of the beam. Let the maximum deflection of the beam in the reference “elastic” state be w_0 and the maximum bending stress be σ_0 . The maximum deflection and the maximum normal stress (bending stress) in the reference state can be computed according to the elementary beam theory as follows

$$w_{\max_0} = \frac{ql^4}{384EI}, \quad \sigma_{\max_0} = \frac{ql^2h}{24I}, \quad I = \frac{bh^3}{12}$$

Furthermore, let us assume that creep curves of the material under uni-axial tension and compression are as sketched in Fig. 1.28b. Here the time to fracture of a uni-axial specimen loaded by the tensile stress with the magnitude σ_0 (the magnitude of maximum reference bending stress in the beam) is specified by t_f . The tertiary creep stage is stress state dependent, i.e. for the same stress magnitudes in tension and compression the creep rate value under tension is much higher than the corresponding

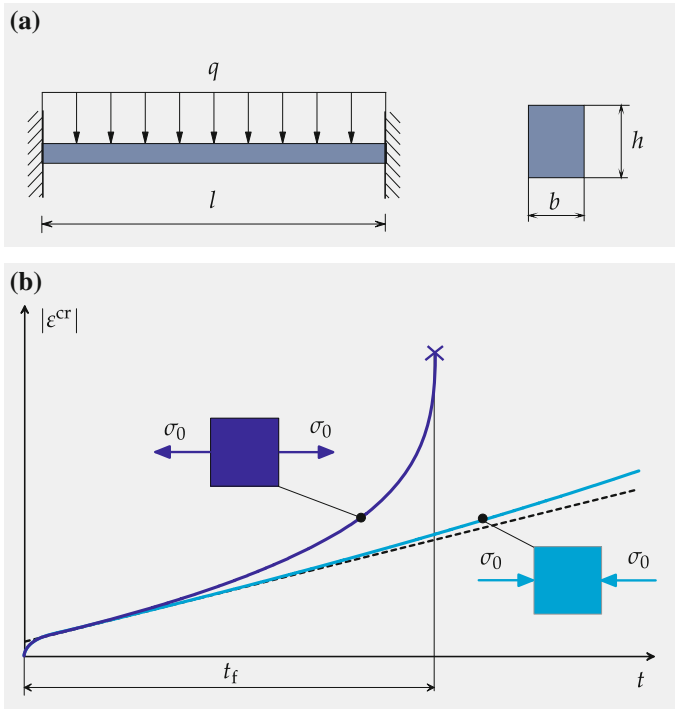


Fig. 1.28 Uniformly loaded clamped beam. **a** Geometry and loading, **b** sketch of the assumed creep curves under tension and compression

absolute value under compression. The dotted line in Fig. 1.28b shows the idealized creep curve having only the stress state independent secondary stage.

Creep processes in a beam under the constant load q and the assumed material behavior are the progressive deformation which may be characterized by the maximum deflection versus time curve, Fig. 1.29a, the relaxation of the bending stresses, Fig. 1.29b, and the stress redistributions, Fig. 1.30. The results illustrated in Figs. 1.29 and 1.30 are obtained from the finite element analysis (Naumenko 2000). Here let us discuss some basic features of creep in the case of the non-homogeneous stress and strain states. First let us explain origins of the simultaneous increase of deformations and the relaxation of stresses. For this purpose we assume that the beam deforms in such a manner that every cross section behaves like a rigid plane, i.e. it may only translate and rotate about the axis which is orthogonal to the plane of bending. Furthermore, we assume that mechanical interactions between the cross sections are only due to forces and moments. The above assumptions are the basis of various theories of beams. Let us note that the results presented in Figs. 1.29 and 1.30 are obtained without these assumptions. However, one may show that they are well satisfied (Naumenko 2000; Altenbach and Naumenko 2002).

Fig. 1.29 Creep of a uniformly loaded clamped beam. **a** Normalized maximum deflection versus normalized time, **b** normalized maximum bending stress versus time

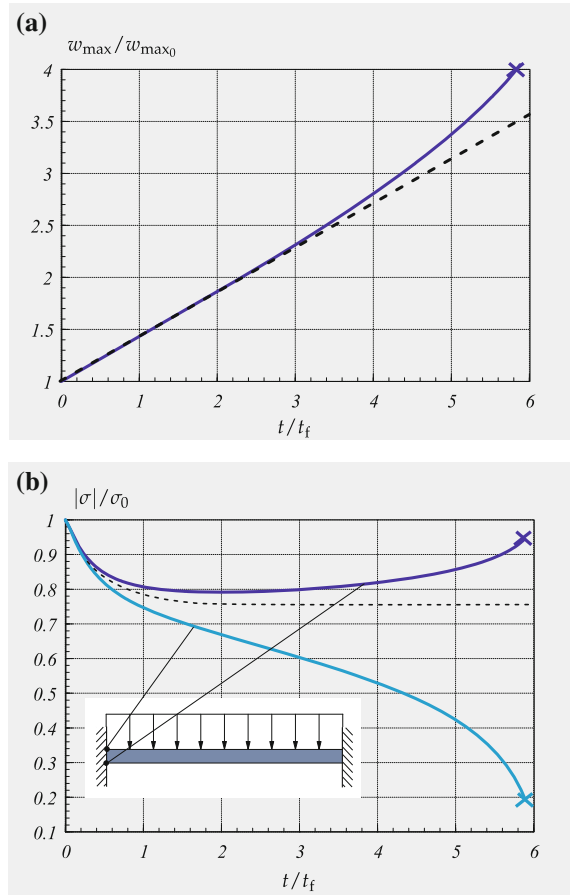


Figure 1.31a is a sketch of the elastic deformation of the beam in the reference state. In Fig. 1.31b the clamped edges are replaced by the pin supports and the moments M_0 . These moments must be applied in order to fix the zero cross section rotations at the ends. As a result of creep, the deformations of the beam increase in time. If the moments M_0 are kept constant then, after a period of time the beam would have a deformed shape as sketched in Fig. 1.31c. In this case the angles of cross section rotations at the ends increase in time. In order to keep the zero cross section rotations the moments must be relaxed, Fig. 1.31d. If the material behaves as shown in Fig. 1.28b by the dotted line, a steady state exists, for which the moments do not depend on time and the deflection increases with a constant rate. The steady-state solutions for the maximum deflection and bending stress are presented in Fig. 1.29 by dotted lines. The rate of maximum deflection, the maximum bending moment and the maximum bending stress in the steady state can be estimated according to the elementary beam theory (Boyle and Spence 1983; Malinin 1981; Odqvist 1974).

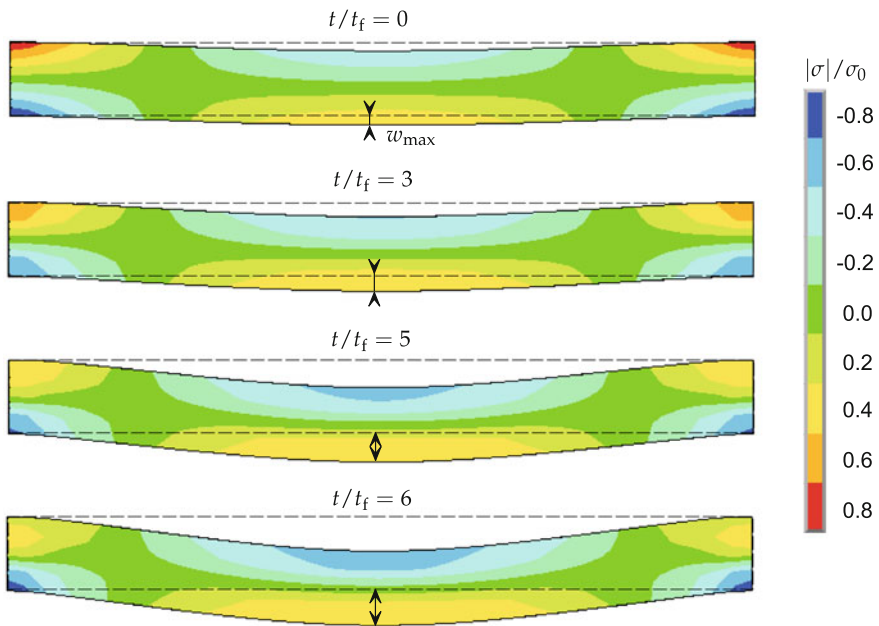


Fig. 1.30 Distributions of the normalized bending stress at different time steps

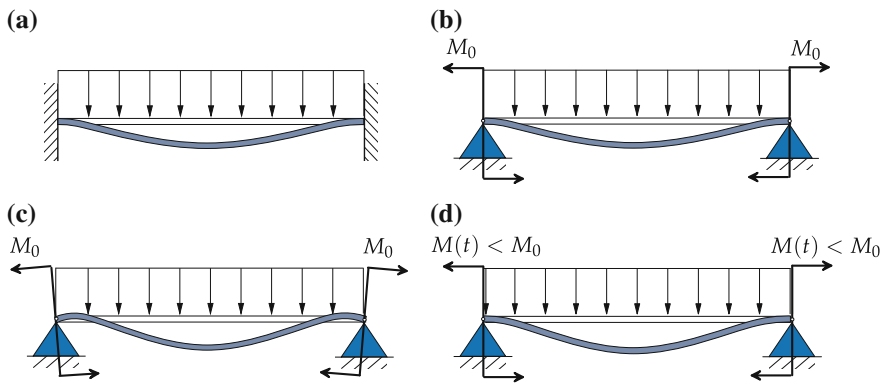


Fig. 1.31 Relaxation of bending moments in clamped edges. **a** Deformed elastic beam in the reference state, **b** equivalent elastic beam with simple supports and edge moments, **c** “crept” beam under constant edge moments, **d** “crept” beam under relaxed edge moments

The next feature is the redistribution of bending moments during the creep process. The origin can be explained based on equilibrium conditions. As an example let us formulate the equilibrium condition for the moments considering a half of the beam

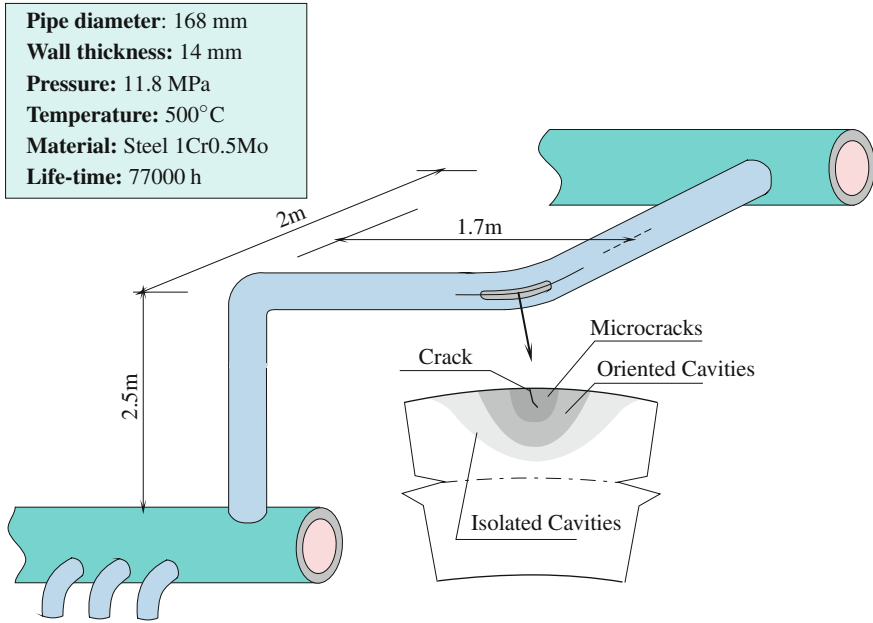


Fig. 1.32 Creep failure in a steam transfer line, after Le May et al. (1994)

$$M(t) + M_m(t) = \frac{ql^2}{8} \Rightarrow \dot{M}_m = -\dot{M},$$

where $M(t)$ is the edge bending moment, Fig. 1.31c, and $M_m(t)$ is the bending moment in the middle cross section. The moment M relaxes down as a consequence of creep process. The above equilibrium condition states that the moment M_m increases. The rate of increase is equal to the rate of relaxation.

Similar considerations explain the redistribution of bending stresses. For the sake of brevity assume that the beam is simply supported, i.e. $M(t) = M_0 = 0$. In this statically determined case the bending moments in all cross sections remain constant during the creep process. However, the stresses in the points of cross sections redistribute essentially. The outer tensile and compressive layers exhibit the highest creep rates due to the maximum stress values in the reference state. Therefore they exhibit the highest relaxation rates at the beginning of the creep process. The redistribution of stresses over the cross section is enhanced by the essential non-linearity of the creep rate with respect to the stress magnitude. Steady state creep solutions for bending stresses are discussed in Boyle and Spence (1983), Malinin (1981), Odqvist (1974).

Results presented in Fig. 1.30 show that the distributions of absolute values of the bending stresses are non-symmetrical with respect to the beam centerline. This is the consequence of the assumed stress state dependent tertiary creep behavior,

Fig. 1.28. Tensile layers of the beam cross section “creep” with higher rates compared to compressive layers.

Creep fracture originates in outer tensile layers of the clamped cross sections (Altenbach et al. 2000b; Naumenko 2000). These layers exhibit, however, the lowest values of stresses at the final stage of creep process, Figs. 1.29b and 1.30. This result can be explained by material damage processes (e.g. grain boundary cavitation and ageing of microstructure) accompanying creep deformation. These processes develop over time with the rates determined not only by the reference stress values but also by the complete loading history. A damaged material has lower ultimate stress compared to the virgin one. Outer tensile layers of the clamped cross sections are places with the highest “damage grade”.

The above discussed features of creep are common for many structures operating under high-temperature conditions. Examples are structural components of power plants, chemical refineries or heat engines, e.g. Gooch (2003). Design of pipework systems, rotors, turbine blades, etc. requires the consideration of creep. Creep processes may cause excessive deformations, damage, buckling, crack initiation and growth.

Different types of creep failure are documented in the literature. Examples of critical structural members include pipe bends (Le May et al. 1994), welds (Shibli 2002), turbine blade root fixings (Gooch 2003), etc. The possibilities to analyze a structural prototype in the laboratory are limited by the long duration of tests and related costs. Furthermore, examinations of creep and damage states in a structure during the service (e.g. replicas) can be only made at specific outer surface positions and after certain periods of time. The modeling of creep processes in structures is therefore an essential contribution to optimal design and residual life assessment. Furthermore it contributes to understanding and analysis of time-dependent deformations, stress redistributions and damage growth under given temperature and loading conditions.

1.2.1.2 Steam Transfer Line

An example for a steam transfer line between a header and a desuperheater of a boiler is presented in Le May et al. (1994). The pipeline from steel 1Cr0.5Mo (13CrMo4-5) had operated under the temperature in the range 500–550 °C and the internal pressure 11.8 MPa. After a service life of 77,000 h rupture occurred along the outer radius of a pipe bend. Metallographic analysis of a section cut from the bend close to the main crack has shown typical creep damage due to microvoids and microcracks on grain boundaries, Fig. 1.32.

Several incidents of pipe bend failures in different power plants are reported in Hald (1998). Inspection techniques were developed to examine the state of creep damage during the service. However, as noted in Le May et al. (1994) any inspection must be conducted at exactly the critical position, or the presence of damage may not be detected. Many investigations have addressed the analysis of mechanical behavior of pressurized curved tubes. Results of studies on elastic and elasto-plastic

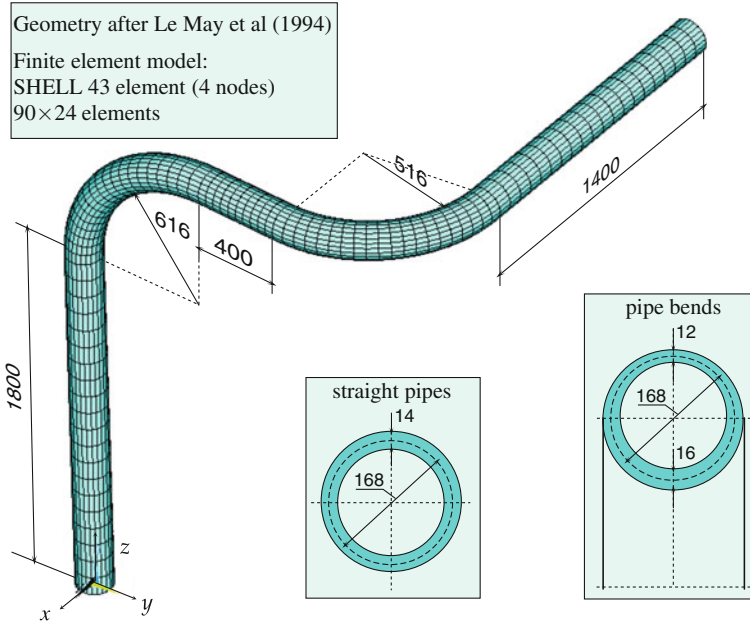


Fig. 1.33 Pipeline: geometry and finite element mesh

deformation and stability are reviewed in Bielski and Skrzypek (1989), Libai and Simmonds (1998). Creep and damage processes in curved tubes were discussed in Altenbach et al. (2001), Boyle and Spence (1983), Hyde et al. (2002). These studies were concerned with the analysis of a single pipe bend subjected to special loading conditions, i.e. in-plane bending moments and internal pressure. In the following example we analyze the behavior of pipe bends in a real spatial pipeline. Figure 1.33 shows the reference geometry of the structure which includes three straight pipe segments (I, III and V) and two pipe bends (II and IV). The lengths of the pipe segments, the mean diameter of the cross section and the wall thickness correspond to the data given in Le May et al. (1994). In addition, we take into account the non-uniformity of the wall thickness in the pipe bends as a result of processing by induction bending. The flanges of the pipeline are clamped. The internal pressure $p = 11.8$ MPa and the temperature $T = 550$ °C are assumed to be constant. The following constitutive model for the creep-damage process is applied

$$\begin{aligned}
 \dot{\boldsymbol{\varepsilon}}^{\text{pl}} &= \frac{3}{2} f_1(\sigma_{\text{vM}}) g_1(\omega) \frac{\mathbf{s}}{\sigma_{\text{vM}}}, \quad \dot{\omega} = f_2(\sigma_{\text{eq}}) g_2(\omega), \\
 \boldsymbol{\varepsilon}^{\text{pl}}|_{t=0} &= \mathbf{0}, \quad \omega|_{t=0} = 0, \quad 0 \leq \omega \leq \omega_*, \\
 \mathbf{s} &= \boldsymbol{\sigma} - \frac{1}{3} \text{tr} \boldsymbol{\sigma} \mathbf{I}, \quad \sigma_{\text{vM}} = \sqrt{\frac{3}{2} \mathbf{s} \cdot \mathbf{s}}
 \end{aligned} \tag{1.2.9}$$

Here $\boldsymbol{\varepsilon}^{\text{pl}}$ is the creep strain tensor, $\boldsymbol{\sigma}$ is the stress tensor, ω is the scalar valued damage parameter and $\sigma_{\text{eq}}^\omega$ is the damage equivalent stress. The response functions f_1 , f_2 , g_1 ,

and g_2 as well as the material constants are taken from Segle et al. (1996) for steel 1Cr0.5Mo at 550 °C as follows

$$\begin{aligned}
 f_1(\sigma) &= a\sigma^n, & g_1(\omega) &= 1 - \zeta + \zeta(1 - \omega)^{-n}, \\
 f_2(\sigma) &= b\sigma^k, & g_2(\omega) &= (1 - \omega)^{-l}, \\
 a &= 1.94 \cdot 10^{-15} \text{ MPa}^{-n}/\text{h}, & b &= 3.302 \cdot 10^{-13} \text{ MPa}^{-k}/\text{h}, \\
 n &= 4.354, & k &= 3.955, & l &= 1.423, & \zeta &= 0.393, & \omega_* &= 0.74
 \end{aligned}
 \tag{1.2.10}$$

The damage equivalent stress is assumed in the form

$$\sigma_{\text{eq}} = \alpha \frac{\sigma_I + |\sigma_I|}{2} + (1 - \alpha)\sigma_{\text{vM}},$$

where σ_I is the first principal stress and $\alpha = 0.43$. The elastic material constants are $E = 1.6 \cdot 10^5 \text{ MPa}$ and $\nu = 0.3$. Figure 1.34 illustrates the deformed shape and the distribution of the magnitude of the displacement vector in the reference state.

Figure 1.35a shows the distribution of the von Mises equivalent stress in the reference state. From the results we may conclude that both the pipe bends are subjected to complex spatial loading and deformation conditions as a result of internal pressure and uniform heating. In addition, the values of the von Mises equivalent stress in three points of the pipe bend IV are plotted as functions of time. According to the results the creep process of the pipeline may be divided into three stages. During the first

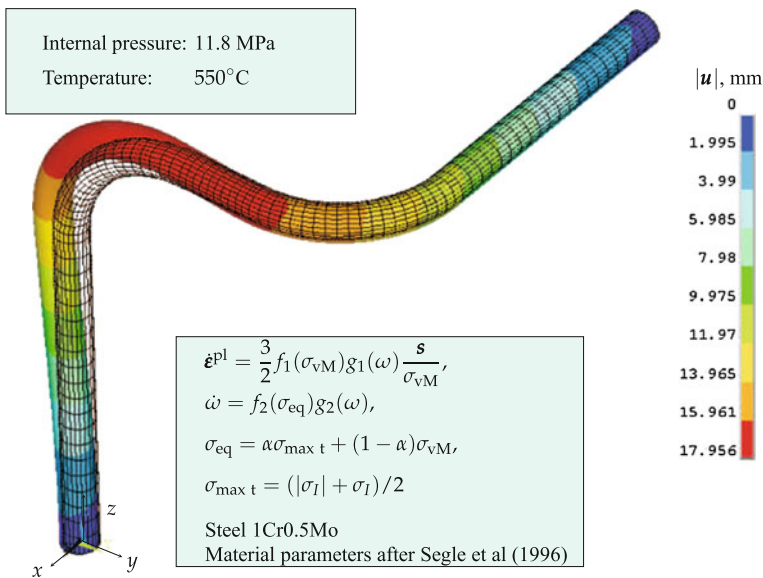


Fig. 1.34 Deformed shape and magnitude of the displacement vector in the reference elastic state

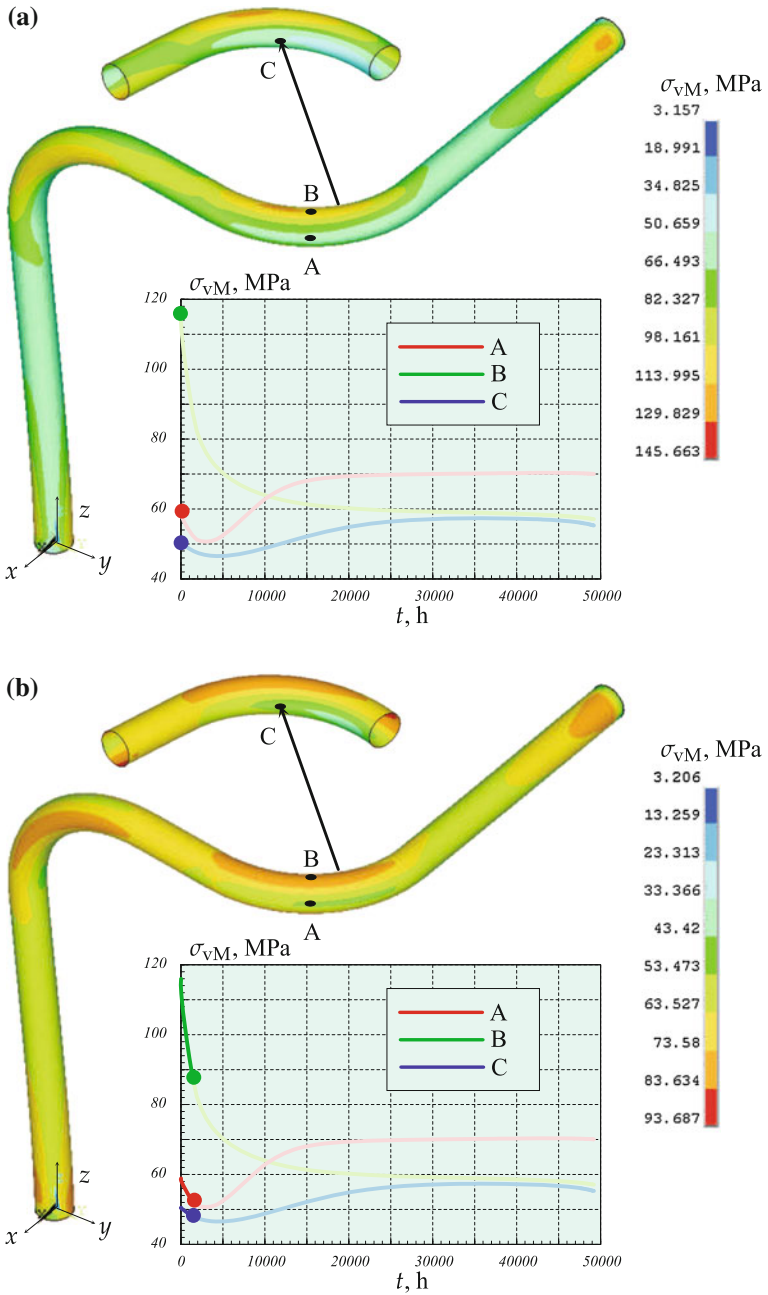


Fig. 1.35 Distribution of the von Mises equivalent stress and corresponding time variations in three points of the pipe bend. **a** Reference elastic state, **b** $t = 2000$ h

stage (approximately 50% of the total life) significant stress redistributions occur leading to quite different stress state in the pipeline (cp. Figs. 1.35 and 1.36). The second stage (approximately 45% of the total life) is characterized by slow changes in the stress state. In the final stage (approximately 5% of the total life) we observe additional stress redistributions, Fig. 1.36b. The distribution of damage parameter at the final time step is shown in Fig. 1.37. According to the results the critical position of possible creep failure is the point *A* of the pipe bend IV. This result agrees well with the data presented in Le May et al. (1994), where the creep failure has been detected at the same position. The processes of time dependent deformation, stress relaxation and redistribution have been illustrated in the literature based on different examples for beams, plates and shells (Altenbach et al. 1997, 2000b, 2001, 2002, 2004; Altenbach and Naumenko 1997). One feature of the example considered here is that the final creep stage is not only the result of the local material deterioration but is additionally governed by the flattening (ovalisation) of the pipe bend cross section.

Let us note that some parameters of the reference pipe bend geometries were not given in Le May et al. (1994) and have been assumed in the presented calculation. Many additional details of geometry including the initial out of roundness of the cross section, inhomogeneous material properties as a result of processing, shutdowns and startups during the service, are not included in the presented model. The influence of hot bending on the subsequent creep behavior in advanced high-chromium steel is discussed in Sklenička et al. (2015). The utilized material model (1.2.9) does not take into account primary creep. Tertiary creep is described by the single damage parameter and the corresponding kinetic equation does not distinguish between processes leading to the accelerated creep, for example coarsening of precipitates and cavitation. Therefore the obtained numerical result for the failure time (49,000 h) “slightly” differs from the value 77,000 h given in Le May et al. (1994). Nevertheless, the results demonstrate the ability of the modeling to represent basic features of the creep process in a structure and to predict critical zones of possible creep failure.

1.2.2 *Examples for Thermo-mechanical Cycling*

Engineering structures are often subjected to non-stationary and non-uniform thermal environment, for example during start-up and shut-down phases. The aim of this section is to present examples illustrating local changes in stress and strain states as a result of thermo-mechanical cycles.

1.2.2.1 **Two-Bar System**

To discuss basic features of the thermo-mechanical cyclic loading let us consider two pipes, rigidly connected as shown in Fig. 1.38a. For the sake of simplicity assume that the diameter of each pipe is much less than the length, such that the stress state is

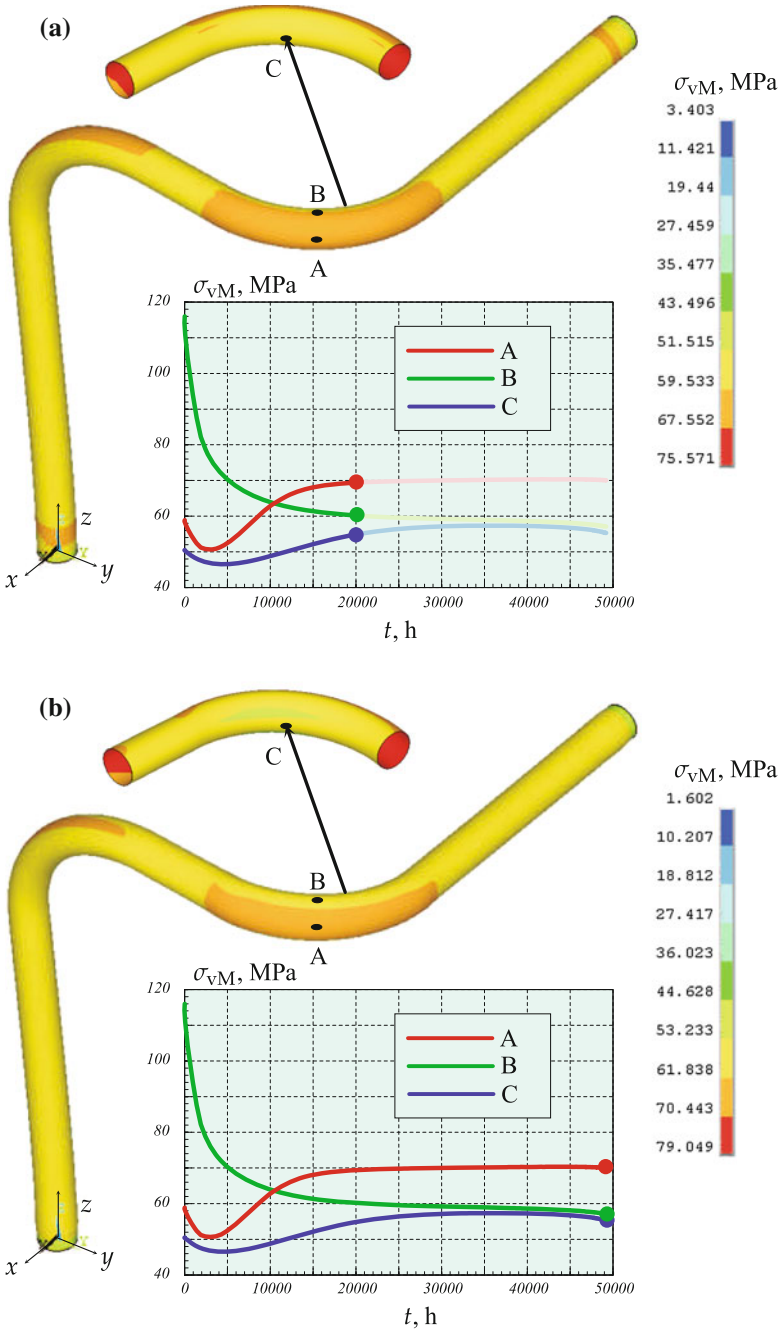


Fig. 1.36 Distribution of the von Mises equivalent stress and corresponding time variations in three points of the pipe bend. **a** $t = 20,000$ h, **b** last time step

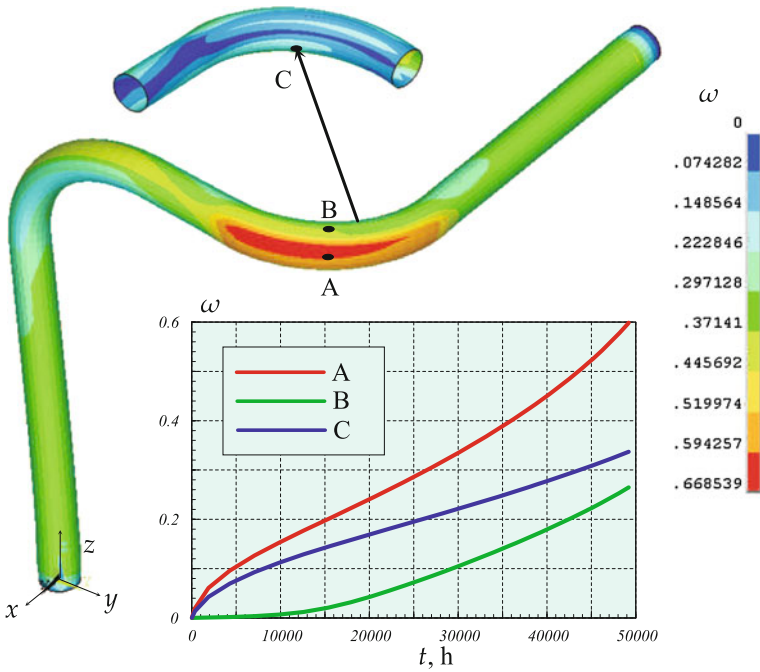


Fig. 1.37 Distribution of the damage parameter at the last time step and corresponding time variations

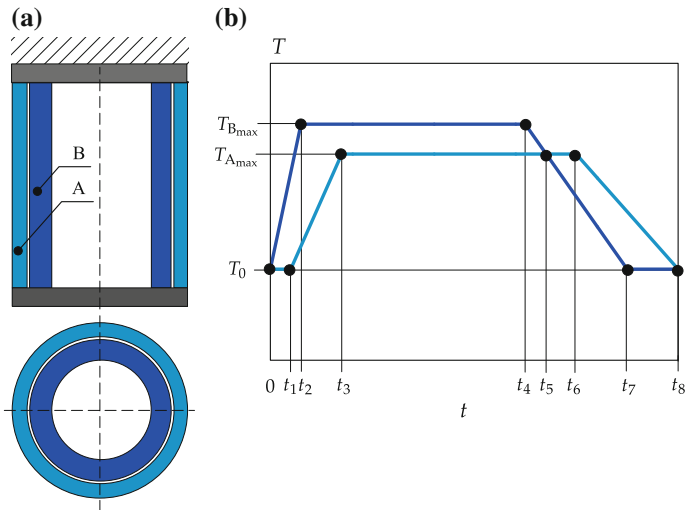


Fig. 1.38 Two bar system. **a** Geometry, **b** temperature profiles

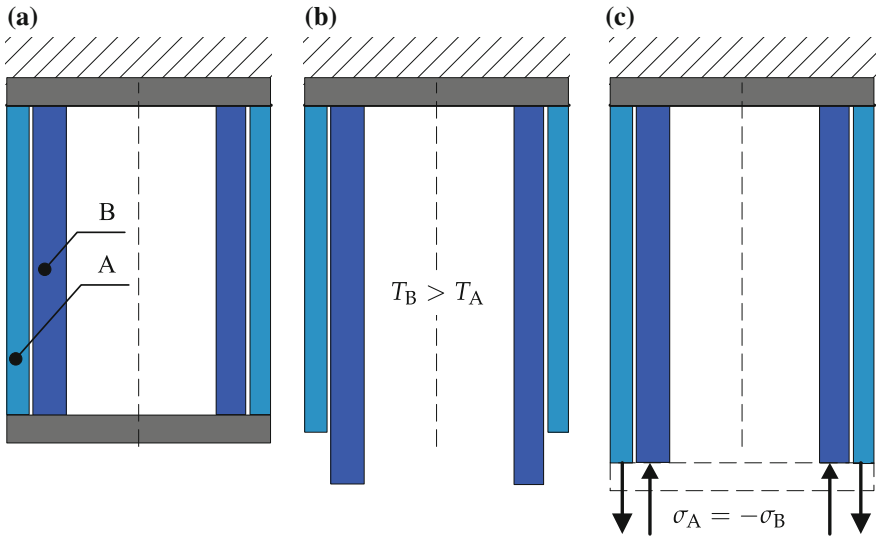


Fig. 1.39 Stress state in a two bar system during heat-up stage. **a** Reference state, **b** free thermal expansion during heat-up with $T_B > T_A$, **c** stresses (compressive for a and tensile for b) required to keep elongations the same

uni-axial and a two-bar model can be used to analyze the structural behavior. Furthermore, assume that the pipes have the same cross section area and are made from the same material. First assume that the pipes are uniformly heated such that $\Delta T_A = \Delta T_B$, where $\Delta T_A = T_A - T_0$, $\Delta T_B = T_B - T_0$. T_A and T_B are absolute temperatures in the actual state and T_0 is the reference temperature. As a result of such a uniform heating the two-bar system will freely expand without stresses since the materials and cross section areas are the same. Now assume that the temperatures of the pipes are different such that $T_B > T_A$. Such a temperature difference may arise during the heat-up stage as a result of hot steam flow through the pipe B . The non-uniform temperature state will cause the non-uniform stress state in the system such that the pipe B will be subjected to compression while the pipe A to tension. To illustrate this remove the rigid connection as shown in Fig. 1.39b. Due to the assumed difference in temperatures, the pipe B is longer than the pipe A in the actual state as a result of thermal expansion. To keep the elongation of the pipes the same, or in other words, to provide the strain compatibility of the structure the forces must be applied, as shown in Fig. 1.39c—the compressive force to the pipe B and tensile force to the bar A . This elementary example explains why the heated surface of a component is usually subjected to compressive stress state.

To illustrate changes in a stress state during a thermal cycle, consider an idealized temperature profile as shown in Fig. 1.38b. Assume that the temperature of the pipe B rapidly increases from T_0 up to $T_{B_{\max}}$ over a time interval $0 - t_2$. As the heat flows towards the pipe A the temperature T_A increases with a delay over the time

interval $t_1 - t_2$. The greatest difference in temperatures is observed at the time point t_2 . This is sometimes called “upshock” (Skelton 2003), the pipe B is subjected to the compression with the maximum stress magnitude. During the time interval $t_2 - t_3$ the temperature difference between the pipes decreases while the absolute temperature of the pipe A increases. The time interval $t_3 - t_4$ is the steady operation period. The time interval $t_4 - t_7$ is the cool-down stage, the steam temperature and the temperature of the pipe B decrease. During the time interval $t_5 - t_7$ the temperature difference increases again. However, the temperature of the pipe B is now lower than the temperature of the pipe A. During this “downshock” stage the pipe B is subjected to tension with the maximum stress value at the time point t_7 .

Let us analyze stress and strain states in the pipes during the whole thermal cycle. For the sake of brevity assume that the Young’s modulus E and the thermal expansion coefficient α_T are constant within the temperature interval $T_0 - T_{B_{\max}}$. In general, the material properties are functions of the absolute temperature. However, the temperature dependence of E and α_T is usually much weaker in comparison to the temperature dependence of the inelastic strain rates. Let N_A and N_B be the internal forces in the bars. The obvious equilibrium condition for the forces yields $N_A = -N_B$. Since the cross section areas are assumed the same the relation between the stresses is $\sigma_A = -\sigma_B$. The constitutive equations for the bars can be formulated as follows

$$\varepsilon_A = \frac{\sigma_A}{E} + \varepsilon_A^{\text{pl}} + \alpha_T \Delta T_A, \quad \varepsilon_B = \frac{\sigma_B}{E} + \varepsilon_B^{\text{pl}} + \alpha_T \Delta T_B, \quad (1.2.11)$$

where $\varepsilon_A^{\text{pl}}$ and $\varepsilon_B^{\text{pl}}$ are plastic strain components in the bars A and B, respectively. The compatibility condition is $\varepsilon_A = \varepsilon_B = \varepsilon$. Subtracting Eqs. (1.2.11)₂ from (1.2.11)₁ provides the stress in the bar B

$$\sigma_B = \frac{E}{2} \left(\varepsilon_A^{\text{pl}} - \varepsilon_B^{\text{pl}} \right) + \frac{E\alpha_T}{2} (T_A - T_B) \quad (1.2.12)$$

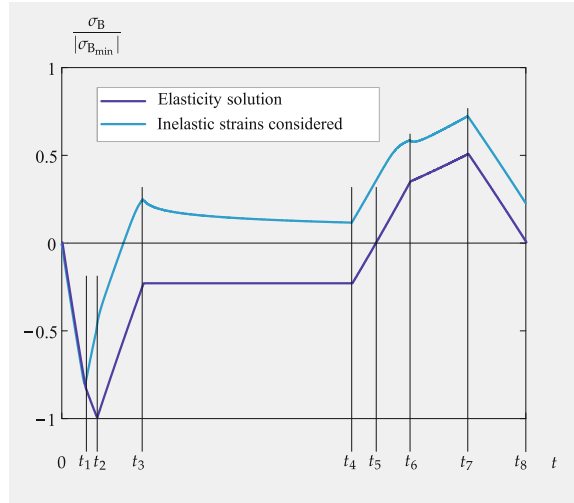
If the inelastic strains are negligible, then the stress in the bar B is related to the difference in absolute temperatures between the bars A and B. As a result the bar B is subjected to compression during warm-up stage and tension during the cool-down stage. After the adding Eqs. (1.2.11) the mean strain of the bar system can be computed

$$\varepsilon = \frac{1}{2} \left(\varepsilon_A^{\text{pl}} + \varepsilon_B^{\text{pl}} \right) + \frac{\alpha_T}{2} (\Delta T_A + \Delta T_B) \quad (1.2.13)$$

Figure 1.40 shows the stress in the pipe B as a function of time. The results are normalized with the minimum stress value during the warm-up stage computed as follows

$$\sigma_{B_{\min}} = \frac{E\alpha_T}{2} [T_A(t_2) - T_B(t_2)]$$

Fig. 1.40 Normalized stress in the pipe B versus time



Two stress peaks are observed—the compressive one during the warm up stage with the maximum temperature difference $T_B - T_A$ at the time point t_2 and the tensile peak during the cool-down stage with the minimum temperature difference at the time point t_7 . To analyze the inelastic response a constitutive model is required that is able to reflect the material behavior during the relatively fast start-up and shut-down stages and the slow regime during the stationary operation. Unified models of inelastic deformation were developed and utilized to capture both plasticity and creep deformation mechanisms under both rapid and slow loadings at high temperatures (Chaboche 2008). A challenging problem is to describe complex interaction of damage processes including the cyclic fatigue damage accumulation and slow creep damage evolution. To simplify the analysis of structures it is suggested to distinguish between different thermo-mechanical loading profiles such as cold starts, warm starts and hot starts (Berger et al. 2008). Figure 1.40 illustrates qualitatively the stress variation for a hot start loading cycle. During the time period $0 - t_1$ the stress distributions based on elasticity solution and the inelastic response coincide. With the increase of absolute temperature and in the stress magnitude compressive inelastic strain starts to accumulate. This leads to the decrease in the stress level for the inelastic solution and the residual tensile stress at the beginning of the stationary stage. This tensile stress relaxes down as a result of creep processes during the stationary operation period. During the cool-down stage an additional tensile inelastic strain accumulation has to be taken into account.

1.2.2.2 Rotor with a Groove

Variations in stress and strain states presented in Sect. 1.2.2.1 for a two-bar system are typical for many components subjected to variable thermal environment. Examples include turbine rotors (Naumenko et al. 2011b; Kostenko et al. 2013; Holdsworth et al. 2007; Colombo et al. 2008), turbocharger casings (Laengler et al. 2010; Nagode et al. 2011a), and many other structures.

In what follows we present results of the thermo-mechanical analysis for a turbine rotor. Figure 1.41 shows a sketch of geometry and the steam temperature profile on the surface of the rotor. To compute the temperature field in the rotor transient heat transfer analysis is performed. The temperature distributions are applied for the subsequent mechanical analysis using a constitutive model for inelastic material behavior. To illustrate the local loading changes over the whole cycle, appropriate values of stresses and strains are presented. Further examples including the analysis of the rotor with a first blade stage groove are presented in Kostenko et al. (2013).

Figure 1.41 shows the time variation of the steam temperature on the surface of the rotor. The maximum steam temperature T_2 in the notched area is increased from

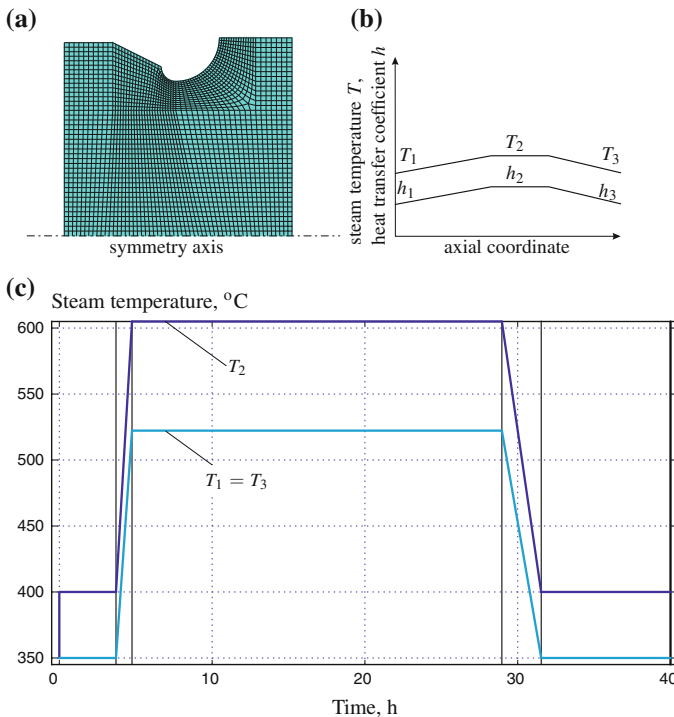


Fig. 1.41 Geometry of a rotor and steam temperature profile. **a** Finite element model, **b** qualitative distribution of steam temperature and heat transfer coefficient along the axial coordinate, **c** steam temperature at different positions of the surface versus time, after Naumenko et al. (2011b)

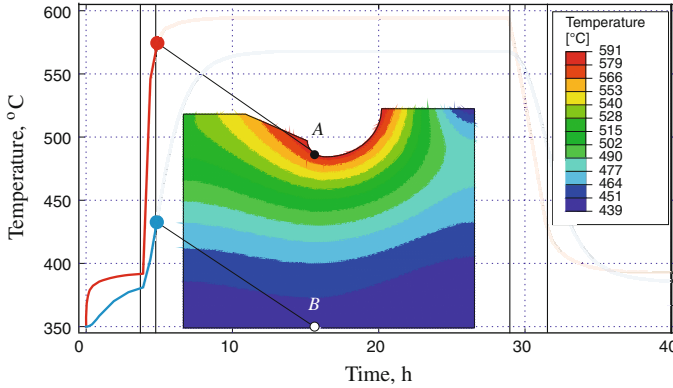


Fig. 1.42 Temperature distribution in a rotor during warm-up at $t = 4.5$ h, after Naumenko et al. (2011b)

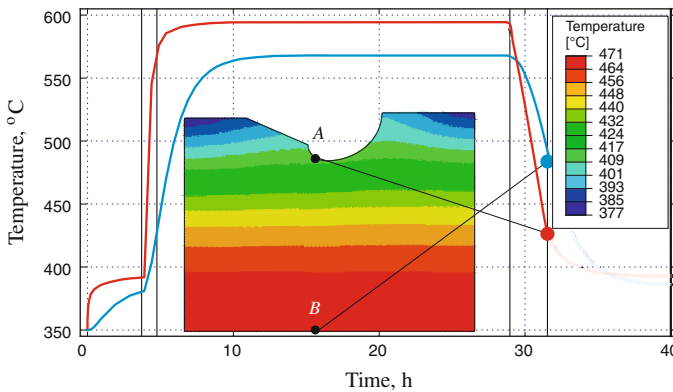


Fig. 1.43 Temperature distribution in a rotor during cool-down at $t = 32$ h, after Naumenko et al. (2011b)

400 to 600 °C, kept at 600 °C and decreased down 400 °C (Fig. 1.41). The changes in the steam parameters during warm-up and cool-down stages are taken into account by the timely varying heat transfer coefficients h_i .

The results of the heat transfer analysis are presented in Figs. 1.42 and 1.43, where the temperature distributions and time variations of the temperature in two points A and B of the rotor are given as functions of time. At $t = 4.5$ h during the warm-up stage the greatest difference between the temperatures at A and B can be observed (Fig. 1.42). During hold time (steady running stage) this difference decreases and attains a constant value of approximately 25 °C (Fig. 1.43). During the cool-down stage the temperature difference decreases such that the temperature of the surface point A becomes lower that the temperature of the core point B (Fig. 1.43). The maximum absolute value of this difference is observed at $t = 32$ h during the

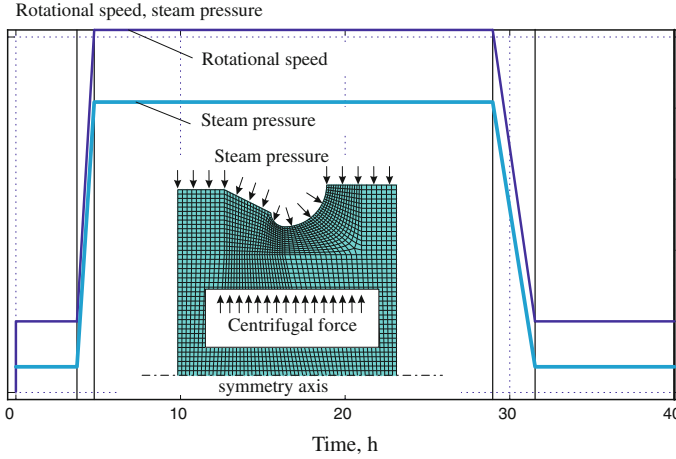


Fig. 1.44 Geometry of a rotor and qualitative profiles of mechanical loadings, after Naumenko et al. (2011b)

cool-down stage (Fig. 1.43). At the end of the cycle the temperature attains the steady-state. The obtained temperature field as well as primary loads (steam pressure on the surface of the rotor and the centrifugal force), Fig. 1.44 are applied for the subsequent structural analysis. To this end the constitutive equation for inelastic material behavior of a high-chromium steel is developed and utilized (Naumenko et al. 2011a, b). Figure 1.45a illustrates time variations of the mechanical strain tensor $\tilde{\boldsymbol{\varepsilon}} = \boldsymbol{\varepsilon} - \alpha_T \Delta T \mathbf{I}$ in the point A of the surface, where α_T is the coefficient of thermal expansion. $\boldsymbol{\varepsilon}$ is the total strain tensor and \mathbf{I} is the second rank unit tensor. The corresponding time variation of the stress state is presented in Fig. 1.45b. Both the stress and the strain tensors are presented with respect to the triad of unit orthogonal vectors \mathbf{n} , \mathbf{t} and \mathbf{e}_φ . Let us note that the normal \mathbf{n} , the tangential \mathbf{t} and the circumferential \mathbf{e}_φ directions on the surface are the principal directions of both the stress and the strain tensors. The corresponding components of stress and mechanical strain including the normal σ_{nn} , $\tilde{\varepsilon}_{nn}$, the tangential σ_{tt} , $\tilde{\varepsilon}_{tt}$ and the circumferential $\sigma_{\varphi\varphi}$, $\tilde{\varepsilon}_{\varphi\varphi}$ ones are the principal values. The normal strain component in A can be computed from Hooke's law as follows

$$\tilde{\varepsilon}_{nn} = \frac{1}{3K} \text{tr } \boldsymbol{\sigma} - (\tilde{\varepsilon}_{tt} + \tilde{\varepsilon}_{\varphi\varphi})$$

The normal stress component is determined as $\sigma_{nn} = -p$, where p is the steam pressure. Based on time variations of $\tilde{\varepsilon}_{tt}$, $\tilde{\varepsilon}_{\varphi\varphi}$, σ_{tt} and $\sigma_{\varphi\varphi}$ one may recognize the local compression during warm-up with the maximum at $t = 4.5$ h, the creep range characterized by an increase in strain, the stress relaxation during the steady running and the local tensile regime during cool-down with the peak at $t = 32$ h.

Figure 1.46a shows the normalized tangential components as functions of time. The corresponding hysteresis loop is shown in Fig. 1.46b. The part I–II of the loop

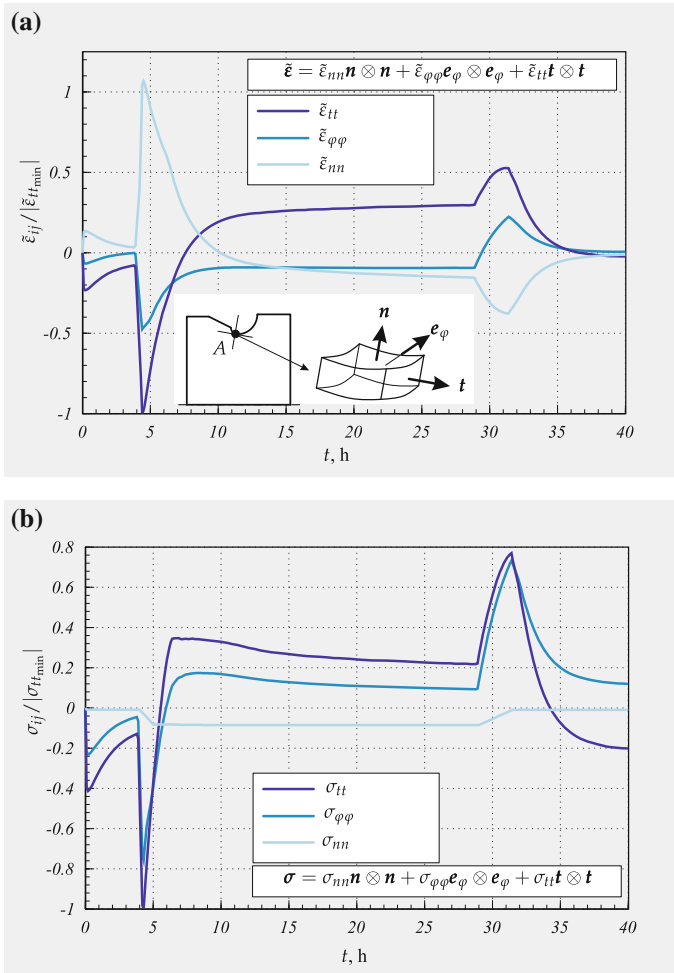


Fig. 1.45 Local loading versus time at point A. **a** Mechanical strain tensor, **b** stress tensor, after Naumenko et al. (2011b)

is the response during the warm-up stage with the increasing temperature difference between the surface and the core point of the rotor. Here the tangential stress and strain decrease down the minimum (negative) values. The part II–III corresponds to the warm up stage with the decreasing temperature difference. At point III the tensile stress and the compressive mechanical strain are observed. This is primarily due to the residual stress accumulated during the warm-up stage. Similar response is usually observed in uni-axial TMF tests, Fig. 1.19, where after unloading from the compressive to the zero strain the stress remains tensile. Experimental data for such TMF responses are presented in Cui et al. (2009), Cui and Wang (2014). The part III–IV corresponds to the steady running stage with a slow increase in the

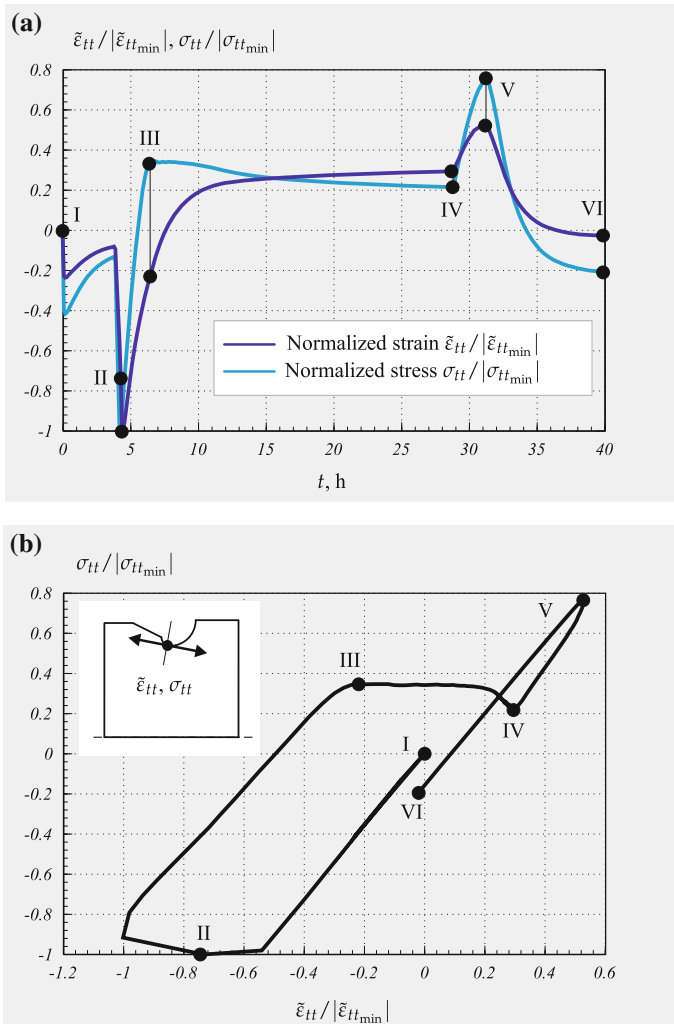


Fig. 1.46 Local loading at point A during first cycle. **a** Tangential stress and tangential mechanical strain versus time, **b** tangential stress versus tangential mechanical strain, after Naumenko et al. (2011b)

strain and decrease in the stress (creep regime). The part IV–V is the tensile regime during the cool-down stage with a decreasing temperature difference. The part V–VI characterizes the cool-down and hold time stages with a low temperature gradient.

Figure 1.47a shows the hysteresis loops for the components of the mechanical strain tensor. One can observe that the local loading path is non-proportional. Note that only the principal values of the strain tensor are non-proportionally changing during the cycle while the corresponding principal directions \mathbf{n} , \mathbf{t} and \mathbf{e}_φ are fixed.

Fig. 1.47 Local loading profiles at point A. **a** Strain paths, **b** hysteresis loops, after Naumenko et al. (2011b)

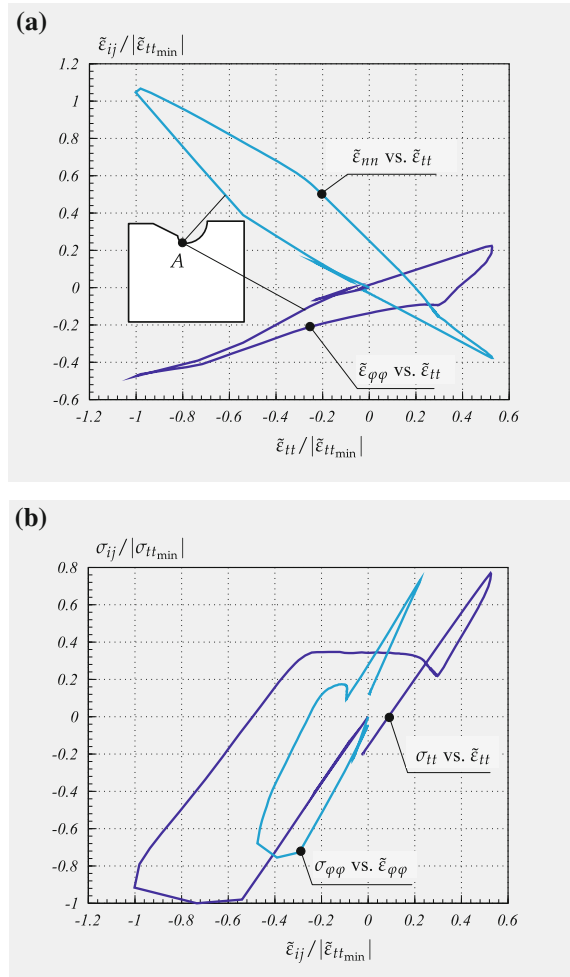


Figure 1.47b shows two hysteresis loops for tangential and circumferential components of stress and strain tensors. To evaluate the mechanical work dissipated through the cycle the circumferential components are essential and cannot be ignored.

Figure 1.48a shows time variations of the tangential strain and stress components over several start-up, steady running and shut-down sequences with the same temperature and external loading profiles. The corresponding stress-strain loops are presented in Fig. 1.48b. The shape of the loops remains approximately the same over many cycles, but the loops shift along both the stress and the strain axes towards the compressive state.

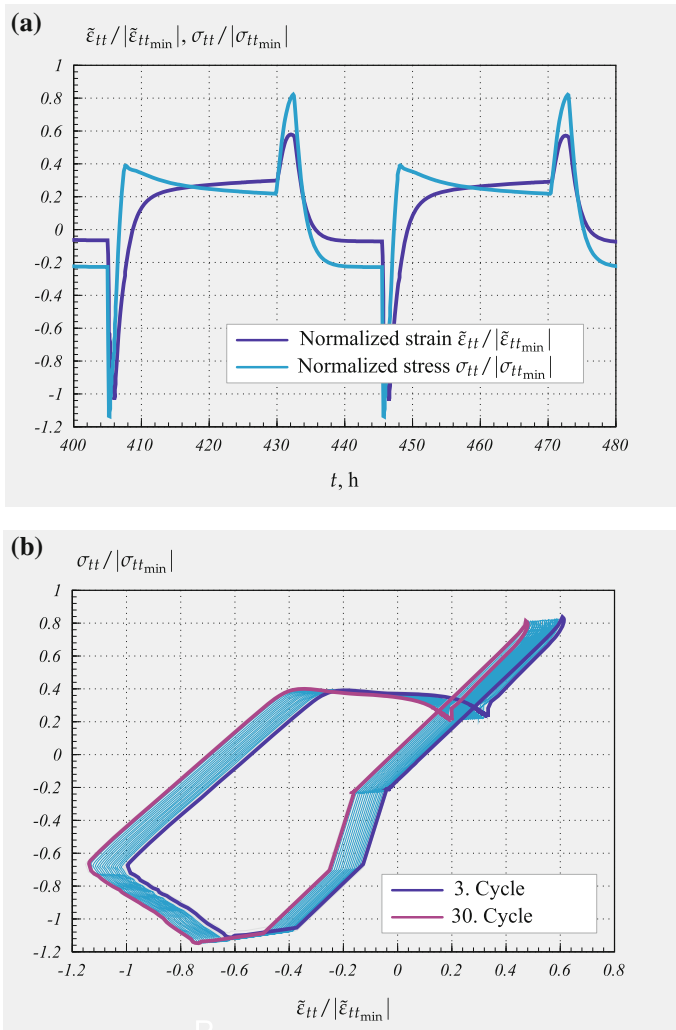


Fig. 1.48 Local loading at point A during several cycles. **a** Tangential stress and tangential mechanical strain versus time, **b** tangential stress versus tangential mechanical strain, after Naumenko et al. (2011b)

The aim of this section was to analyze inelastic behavior in components under non-isothermal loading profiles at high temperature. To generate the local multi-axial stress-strain loops over one or several cycles under realistic external loading conditions a constitutive model is required. The constitutive model must reflect basic features of deformation behavior in structural materials at high temperature including hardening/recovery, softening, ratcheting and other processes for both stress and strain controlled loading paths. The hysteresis loops obtained from

the structural analysis qualitatively agree with the test results for cruciform and notched specimens under TMF loading (Cui et al. 2009; Samir et al. 2005). Structural analysis and laboratory testing provide an important input for the fatigue life estimations. The stress and strain states during the steady running stage correspond to the typical creep regime. Estimation of creep damage and creep life in a structure under stationary loading and temperature must be provided by the constitutive model. Although unified constitutive models discussed in the literature, e.g. Chaboche (2008), Naumenko et al. (2011b), are able to reflect local deformation behavior and creep damage, surface induced fatigue damage processes, e.g. formation of micro-extrusions, oxidation effects and growth of micro-cracks are currently not accounted for. Based on generated multi-axial TMF loops and related material testing, further investigations to elaborate driving force(s) and kinetics for fatigue damage processes should be performed.

1.3 Microstructural Features and Length Scale Effects

Macroscopic inelastic properties of materials are strongly affected by microstructure. Limiting to the analysis of high temperature inelastic behavior and crystalline materials let us discuss basic microstructural features. For polycrystals the mean grain size is found to influence the macroscopic response. For low homologous temperatures and for a certain range of the mean grain size, the grain boundary strengthening (Hall-Petch) effect (Hall 1951; Petch 1953) is usually observed. The lattice structure of adjacent grains differs in orientation. An additional energy is required to change directions of moving dislocations. Impeding the dislocation movement through grain boundaries will hinder the onset of plasticity and hence increase the yield strength of the material. The decrease of mean grain size by an appropriate material processing leads to an increase in the yield strength. Based on the experimental data the following relation can be established (see, for example, Roesler et al. 2007)

$$\sigma_y = \sigma_0 + \frac{k}{\sqrt{d}},$$

where σ_0 and k are constants and d is the mean grain size.

In contrary, several mechanisms may operate leading to the weakening effect of grain boundaries, if the material is loaded at elevated temperature. For moderate stress levels and temperatures over $0.5 T_m$ diffusion of vacancies may control the deformation process. Different theories of diffusion creep provide the following relationship between the inelastic strain rate and the mean grain size

$$\dot{\epsilon}^{pl} \sim \frac{1}{d^k}$$

The exponent k takes the value 2 according to the theory of lattice diffusion as discussed by Nabarro (1948, 2002) and Herring (1950) and 3 according to the theory of grain boundary diffusion as proposed by Coble (1963). An additional mechanism leading to the weakening effect of grain boundaries is the grain boundary sliding. Experimental works devoted to the analysis of grain boundary sliding are reviewed in Nabarro and de Villiers (1995), Nørbygaard (2002), Langdon (2006). An elementary model of creep considering both the deformation of grains and sliding of grain boundaries can be based on the mixture rule (Ilshner 1973). Here the total strain is a sum of strains due to grain interiors and grain boundaries weighted by the corresponding volume fractions. Materials with smaller grains exhibit higher volume fractions of grain boundaries and consequently have more essential contribution of grain boundary sliding to the overall deformation. Again the grain boundary sliding is one of the mechanisms leading to the weakening effect of grain boundaries. To establish the influence of mean grain size on the overall creep rate several additional effects should be considered.

Stress concentrations in the regions of grain intersections lead to the non-uniform creep deformation along grain boundaries. Furthermore, the effect of grain boundary deformation depends essentially on the stress level. For lower stress values grain boundary sliding and diffusion of vacancies have an essential influence on the deformation while for high stresses levels grain the deformation is primarily controlled by glide processes inside the grains. For many polycrystalline materials the dominant creep damage mechanism is the formation, growth and coalescence of cavities on grain boundaries orthogonal to the stress axis. This kind of damage leads again to the weakening effect of grain boundaries. Therefore, one may expect that a material with finer grains would exhibit a shorter lifetime. Summing up, the grain boundaries may have hardening and/or weakening influence on the inelastic deformation and lifetime depending on the loading and temperature levels. Therefore the optimal grain size for a given material depends on the conditions under which it is to be used (Nabarro and de Villiers 1995). The overlapping of several deformation and damage mechanisms makes it difficult to derive a relationship between the deformation rate and the grain size. Recently simulations of three-dimensional polycrystalline aggregates were performed illustrating several deformation and damage mechanisms like grain boundary sliding and cavitation as they influence the overall behavior (Ozhoga-Maslovskaja et al. 2015).

Apart from grains there are several microstructural features at lower length scales that affect inelastic deformation. Examples include cells and subgrains, that are dislocation substructures formed as a result of clustering of uniformly distributed dislocations (Raj et al. 1996). Cells consist of broad diffused walls containing dislocation tangles while boundaries of subgrains are narrow and formed by dislocation networks. Cell walls and subgrain boundaries separate the crystal into the regions with slightly different crystallographic orientations. Subgrain boundaries have larger misorientation than cell walls. Cells and subgrains may form in the course of inelastic deformation process for materials with relatively low dislocation density. At the

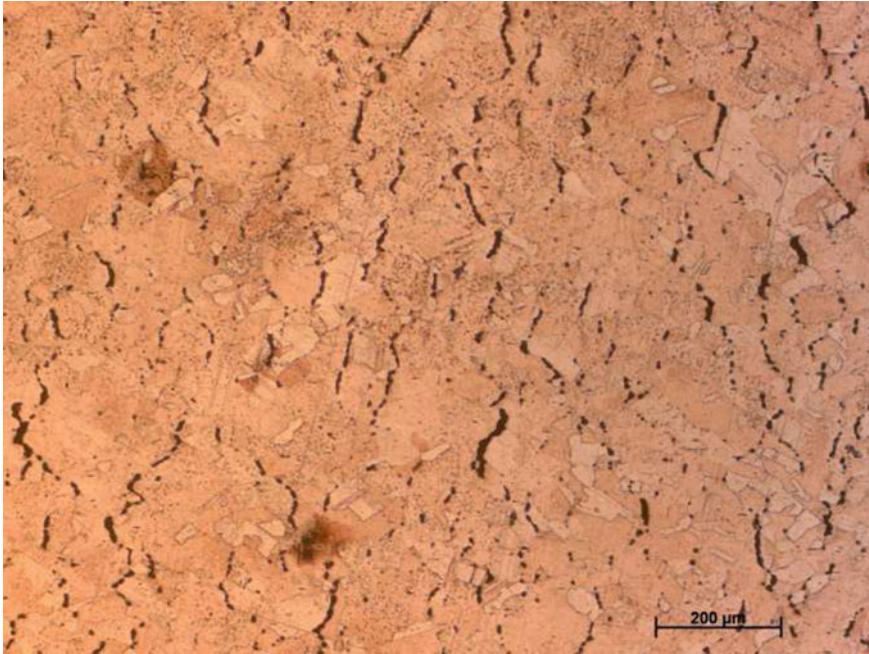


Fig. 1.49 Micrograph of copper specimen tested 20h under constant stress of 10 MPa (stress direction horizontal) and temperature level of 550°C (Ozhoga-Maslovskaja 2014)

macroscale the formation of substructures is observed as hardening, for example the decrease in the creep rate during the primary creep. Many high temperature materials, for example high-chromium steels possess fine subgrain structure. Lower mean subgrain size provides lower inelastic strain rate and higher creep resistance. To describe this mean subgrain size effect composite (phase mixture) model can be applied. Here a composite with two constituents having different initial dislocation densities and as a result different inelastic properties is assumed (Raj et al. 1996; Blum 2001, 2008). The inelastic soft constituent is the zone of cell or subgrain interiors with relatively low dislocation density. The inelastic hard regions include cell or subgrain boundaries with high dislocation density. The deformation process in such a composite is accompanied by a stress redistribution between the constituents—the stress level in the inelastic hard regions increases while the stress level within the inelastic soft regions increases. Lower size of subgrains leads to higher volume fraction of the hard regions and as a result to the lower overall deformation rate. The subgrain microstructure is not stable and subgrain coarsening usually takes place where the average size increases while the number of subgrains decreases. This leads to the overall softening under stationary or cyclic loadings (Fournier et al. 2011; Kimura et al. 2006; Qin et al. 2003).

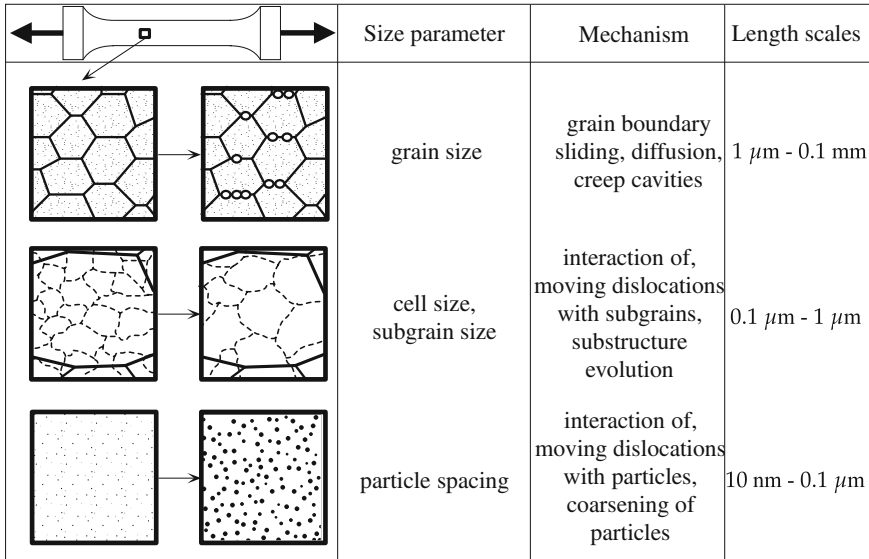
Additional strengthening mechanisms for high temperature materials are precipitation and dispersion hardening. For example heat-resistant steels usually contain

several kinds of precipitate particles in the matrix and at grain boundaries including carbonitrides and intermetallic compounds (Abe 2008). An important role in strengthening of aluminium alloys for high temperature applications plays the θ' phase, in the form of rod-like precipitates aligned along the (001) crystallographic directions of the α -Al matrix (Naumenko and Gariboldi 2014). Dispersed fine precipitates are obstacles for mobile dislocations. Several mechanisms for interaction between mobile dislocations and particles are reviewed in Ilshner (1973), Kassner and Pérez-Prado (2004), Roesler et al. (2007) among others. Both theoretical and experimental results show that the inelastic strain rate primarily depends on the mean spacing between particles. The mean particle spacing can also be related to the mean particle size. As an example let us consider regular arrangement of spheres with the diameter d , spacing between centers l , the volume fraction η_p and the number of particles N_p in a unit volume. In this case the following relation can be derived

$$l = \frac{1}{N_p^{1/3}} = \frac{\pi}{6} \frac{d}{\eta_p^{1/3}},$$

Experimental data suggest that strength of alloys is determined by spacing and diameter of precipitates. The greatest impedance to dislocation motion and hence the maximum potential for strengthening will occur when an alloy contains precipitates that are large enough to resist shearing by dislocations and too finely spaced to be bypassed by moving dislocations (Polmear 2004). Furthermore precipitates stabilize dislocations in the matrix and subgrain boundaries. This enhances strain hardening, for example primary creep. To capture these phenomena kinetic equations for dislocation density are developed, see, for example, Estrin (1996), Naumenko and Gariboldi (2014). One feature of the proposed constitutive and evolution equations is the dependence of the inelastic strain rate as well as rate of change of hardening variables on size parameters, such as mean spacing (or mean diameter) of precipitates (Estrin 1996; Roesler et al. 2007). At high temperature the microstructure of precipitates is not stable and evolves over time as a result of diffusion processes. Coarsening of precipitates in steels (Abe 2008) and aluminum alloys (Naumenko and Gariboldi 2014) leads to loss of the strength. To account for coarsening processes equations with respect to the size parameter—the mean particle diameter are required. Examples are presented by Kowalewski et al. (1994), Naumenko and Gariboldi (2014) for aluminum alloys and Dyson and McLean (2001), Blum (2008) for steels. Figure 1.50 provides a summary of several microstructural features discussed in this section, where size parameters, length scales and associated deformation or damage mechanisms are presented.

Microstructural features and microstructural size parameters may have different kinds of influences on the behavior of components at high temperature. For large structural components, for example power plant components, the local inelastic behavior is usually determined by the local stress state and the current state of microstructure defined in terms of mean quantities like dislocation density, mean diameter of precipitates, damage parameter etc. Such a description is possible since



Size parameter	Mechanism	Length scales
grain size	grain boundary sliding, diffusion, creep cavities	$1\ \mu\text{m} - 0.1\ \text{mm}$
cell size, subgrain size	interaction of, moving dislocations with subgrains, substructure evolution	$0.1\ \mu\text{m} - 1\ \mu\text{m}$
particle spacing	interaction of, moving dislocations with particles, coarsening of particles	$10\ \text{nm} - 0.1\ \mu\text{m}$

Fig. 1.50 Basic microstructure features of heat resistant materials, length scales, size parameters and mechanisms of changes in microstructure

a material point in the sense of continuum mechanics contains a huge number of microstructural elements, for example grains. An exception for large structural components is the behavior in the zones of stress concentrations, for example in the vicinity of notches. Here the macroscopic quantities like stress or strain may vary rapidly over a certain direction and the characteristic length of this change may be comparable with microstructural size quantities, for example the grain size. Figure 1.51 shows a sketch of a stress variation in the vicinity of the notch root. Far from the notch root, where stresses vary slowly a sample with a large number of microstructural features, for example grains can be used to identify the material response. In zones with higher stress gradients smaller samples are required to analyze the material behavior. For smaller samples microstructure features must be taken into account to capture the material behavior. Such a smaller volume element with microstructure, if subjected to a uniform elongation on the boundary would exhibit highly non-uniform stress distribution such that higher moments of the stress tensor might be required to capture the averaged stress state. Furthermore the local response in a material point at the macroscopic scale may be affected not only by the local stress state and the local state of the microstructure but also by the neighborhood.

In many cases variations of microstructure with respect to coordinates must be taken into account. Examples include gradient materials and welds. Figure 1.52 shows the microstructure of a multi-pass weld metal and the heat affected zone. Depending on the welding process the microstructure of the base metal will be changed in the heat affected zone. Major process parameters of welding that have an influence on the microstructure are the heating rate of the weld thermal cycle, the

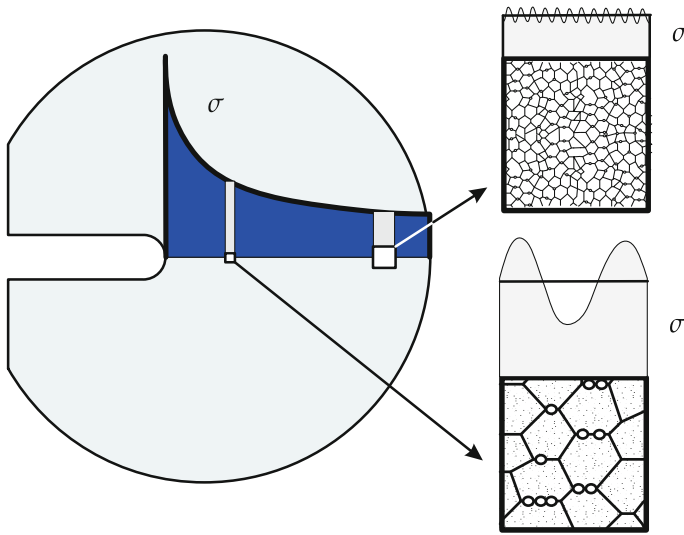


Fig. 1.51 Qualitative stress distribution in the vicinity of the notch root. To identify the behavior in zones with higher stress gradients smaller material samples are required

peak temperature, the dwell time and the cooling rate (Hyde et al. 2003b; Cerjak and Mayr 2008). The heat affected zone can be divided into a number of sub-zones with different microstructural features including the grain size, the distribution and size of precipitates, etc. There are no sharp boundaries between the different microstructural regions. The microstructure exhibits a continuous gradient from the fusion line between the deposited weld metal to the unaffected base material. Here one must consider that the stress-strain diagrams at room temperature are quite different for the weld metal, the heat-affected zone, and the base metal (parent material), in particular beyond the yield limit. At elevated temperature quite different inelastic strain versus time curves can be obtained in different zones even in the case of a constant moderate load. The results of creep tests of cross-weld specimens (Hyde et al. 1997, 1999), and specimens with a simulated microstructure (Lundin et al. 2001; Matsui et al. 2001; Wohlfahrt and Brinkmann 2001; Wu et al. 2004; Eggeler et al. 1994) show significant variation in creep properties in different material zones within the weld. Furthermore, they illustrate that the intercritical region of the heat-affected zone is the weakest part of the weld with respect to the creep properties. The specimen with the heat-affected zone microstructure usually exhibits the highest creep rate and the shortest time to failure if compared to other material zones within the weld for the same load and temperature.

For thick and moderately thick cross sections, multi-pass welding is usually preferred, where many stringer beads are deposited in a defined sequence. As a result of heating and cooling cycles during the welding process, the complex bead-type

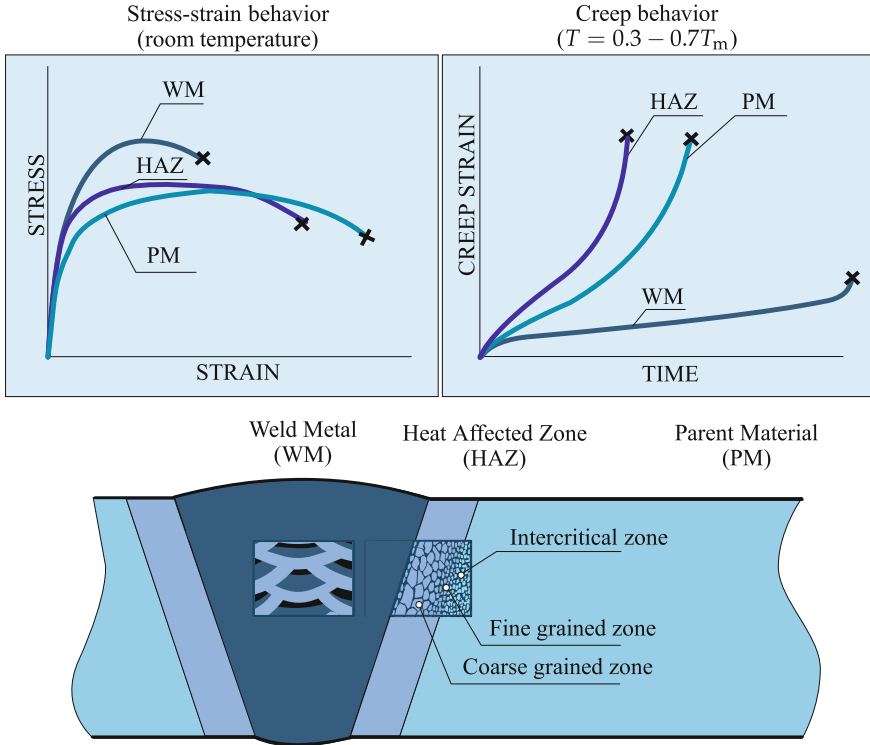


Fig. 1.52 Microstructure and inelastic behavior of welds after Naumenko and Altenbach (2005)

microstructure of the weld metal is formed, where every single bead consists of columnar, coarse-grained, and fine-grained regions, e.g., Hyde et al. (2003b).

In general, the coupling between different size dependencies of the properties of a material should be analyzed (Arzt 1998). To this end one has to deal with the interaction of the following two length scales. The first one is responsible for the phenomenon involved, for example variation of the stress state in the vicinity of a notch, and is usually called the characteristic length. The second one is a microstructural dimension, denoted as the size parameter.

Analysis of different length scale effects and their interactions is required in particular for small structures, such as components of microelectronics, thin films and coatings. Miniaturized components are frequently subjected to complex thermal and mechanical loading cycles. The dimension of such a part, for example, the diameter of a bondwire may be of several micrometers such that grain size and grain boundary effects should be taken into account in analysis of inelastic behavior. For thin films and thin layers the deformation or damage mechanism “feel” the presence of the surface or an interface (Arzt 1998; Kraft et al. 2010). As a result, the inelastic response of microcomponents and solder joints depends essentially on their

dimensions (Wiese et al. 2008; Wiese 2010). Experimental results on inelastic behavior of thin films and micropillars are reviewed in Kraft et al. (2010).

1.4 Temporal Scale Effects

Engineering structures are frequently subjected to complex loading conditions. Examples include thermo-mechanical loading profiles discussed in Sect. 1.1.1.4. Analysis of material behavior over many cycles of loading is crucial for life time estimations of components. Phenomena like cyclic hardening, cyclic softening, creep ratcheting, fatigue damage evolution, etc. are usually observable with respect to the global time scale after a certain number of loading cycles. On the other hand, the type of loading and the response within one loading cycle can be related to the local time scale. At elevated temperature not only the amplitudes of stresses/strains within a cycle, but also loading rates, hold times and many other factors have an influence on the component life. Simulations of components in inelastic range for many cycles of loading is time consuming, if ever possible. For an efficient analysis it is convenient to introduce two or more time scales (Altenbach et al. 2000a; Devulder et al. 2010; Fish et al. 2012). A “slow or macroscopic” time scale can be used to capture the global cyclic behavior like cyclic hardening, softening or creep ratcheting. For the structural analysis within one loading cycle “fast or microscopic” time scales are useful. As an example, Fig. 1.53 illustrates the accumulation of the inelastic strain as a result of cyclic force with hold times. Two regimes are clearly seen, the global one with the growth in the strain amplitude as a function of the “slow” time or cycle number and the rapid change of the inelastic strain within several cycles

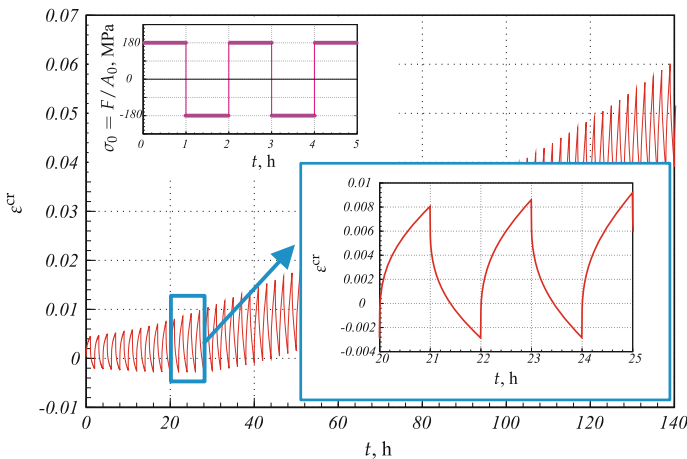


Fig. 1.53 Accumulation of inelastic strain for a 12% Cr steel at 600°C under cyclic force with hold times (simulation)

of loading. In Sect. 1.2.2.2 structural analysis results of a component subjected to thermo-mechanical cyclic loading are presented. Figure 1.48a illustrates the local changes of normalized strain and the normalized stress components over two cycles of thermo-mechanical loading. This “fast” time behavior determines to the structural response over many cycles. Figure 1.48b shows how the local hysteresis loop changes with respect to the cycle number. In particular, a shift towards the compressive stress and strain axes can be observed. Prediction of such “slow” stress and stress changes over the cycle number is crucial in the structural analysis of many components.

Inelastic behavior of structural materials at high temperature is controlled by several microstructural processes having different characteristic times. The inelastic deformation of crystalline materials can be explained by dislocation glide and dislocation climb (Frost and Ashby 1982; Nabarro and de Villiers 1995). The glide motion of dislocations dominates at lower homologous temperatures and higher stress levels, while the climb of dislocations over obstacles—a nonconservative motion controlled by the diffusion of lattice vacancies, becomes important in high-temperature regimes and moderate stress levels. As a thermally activated process, the diffusion of vacancies occurs over time scales that are much longer than the times required for glide steps. The difference in the time scales may be of many orders of magnitude depending on the stress and temperature levels.

1.5 Modeling Approaches and Objectives

Diverse approaches to the description of inelastic behavior are discussed in the literature. They can be classified with respect to pursued aims, involved assumptions and solution methods. In this section we review basic modeling approaches and discuss objectives of the book.

1.5.1 Modeling Approaches

The basic approaches to the description of inelastic behavior can be classified as follows. The *empirical modeling* is the study of correlations between the inelastic strain rate, stress, temperature and time. In addition, extrapolation methods are developed to predict time-dependent deformations and life time of a structure based on experimental data from short-term uni-axial creep tests. The aim of this approach is to derive simple formulae for an estimation of the structural behavior under creep conditions. An example is the Monkman-Grant relationship which states that the product of the minimum creep rate and the time to fracture is a constant (Monkman and Grant 1956).

$$\dot{\epsilon}_{\min} t_f = \text{const}, \quad (1.5.14)$$

where $\dot{\varepsilon}_{\min}$ is the minimum creep rate and t_f is the time to fracture. Once the constant is identified from a short-term creep test, Eq. (1.5.14) can be used to estimate the time to fracture for lower stress levels. To this end only the minimum creep rate versus stress dependence is required.

Another example is the linear damage summation rule for the life time assessment of components. Following Taira (1962)

$$L = L_f + L_c,$$

where the damage L in the creep-fatigue range is defined as a sum of pure fatigue damage L_f and creep damage L_c . A component failure is expected from this rule if the relative fatigue damage and the relative creep damage reach in the sum a critical value. Within the empirical approach the meaning of damage is related to the life time fraction. The fatigue damage is defined by the empirical rules of Palmgren (1924) and Miner (1945)

$$L_f = \sum_{i=1}^k \frac{N_i}{N_{A_i}}$$

where N_i and N_{A_i} are the number of cycles experienced and the number of cycles to failure at the constant strain amplitude, respectively. The sum over k loading cycles provides the relative fatigue life L_f . A similar rule to estimate creep damage was proposed by Robinson (1952)

$$L_c = \sum_{i=1}^k \frac{t_i}{t_{*i}}$$

where t_i is the time spent at constant stress and temperature levels and t_{*i} is the time to fracture for the same loading conditions.

Many different empirical relations of this type are reviewed in Penny and Marriott (1995), Viswanathan (1989). Empirical models are useful in early stages of design for a rapid estimation of the components operation life. It should be noted that the empirical approach provides one-dimensional relations. The dependencies of inelastic behavior on the type of stress state are not discussed. Furthermore, stress redistributions, creep-plasticity interactions, cyclic strain accumulations and many other effects cannot be considered.

Within the *materials science modeling*, the inelastic deformation process is characterized by a variety of microstructural rearrangements. According to assumed scenarios of transport processes in the microscale (diffusion of vacancies, climb and glide of dislocations, etc.) equations for the inelastic strain rate are derived. The form of the specific rate equation depends on the assumed deformation and damage mechanisms for specific stress and temperature regimes, e.g. (Frost and Ashby 1982). As an example consider the equation for the inelastic strain rate as proposed by Estrin (1996)

$$\dot{\varepsilon}^{\text{pl}} = \dot{\varepsilon}_0 \left(\frac{\sigma}{\hat{\sigma}} \right)^n, \quad (1.5.15)$$

where $\dot{\varepsilon}_0$ and n are constants, and the drag stress $\hat{\sigma}$ can be defined as a sum of dislocation and particle hardening contributions

$$\hat{\sigma} = M\alpha Gb\sqrt{\varrho} + M\chi Gb\frac{1}{l}, \quad (1.5.16)$$

where G is the shear modulus, M is the Taylor factor, b is the magnitude of the Burgers vector, ϱ is the dislocation density, l is the mean spacing between particles. α and χ are empirical constants. Equation (1.5.16) is based on the Taylor mechanism (dislocation-dislocation interactions) and the Orowan bowing mechanism (bypassing of dislocation over particles).

Mechanism based equations of this type are reviewed in François et al. (2012), Frost and Ashby (1982), Ilshner (1973), Kassner and Pérez-Prado (2004), Nabarro and de Villiers (1995), among others. In addition, kinetic equations for internal state variables are introduced. Examples for these variables include dislocation density (Estrin 1996) internal (back) stress, e.g. François et al. (2012), and various damage parameters associated with ageing and cavitation processes (Dyson and McLean 1998). The aim of the materials science models is to provide explicit correlations between quantities characterizing the type of microstructure and processing (grain size, types of alloying and hardening, etc.) and quantities characterizing the material behavior, e.g. the creep rate. Furthermore, the mechanisms based classification of different forms of creep equations including different stress and temperature functions is helpful in the structural analysis. However, the majority of models proposed within the materials science are one-dimensional and operate with scalar-valued quantities like magnitudes of stress and strain rates.

The objective of *continuum mechanics modeling* is to investigate inelastic behavior in idealized three-dimensional solids. The idealization is related to the hypothesis of a continuum, e.g. Haupt (2002). The approach is based on balance equations and assumptions regarding the kinematics of deformation and motion. Inelastic behavior is described by means of constitutive equations which relate multi-axial deformation and stress states. Topological details of microstructure are not considered. Processes associated with the microstructural changes like hardening, recovery, ageing and damage can be taken into account by means of hidden or internal state variables and corresponding evolution equations (Betten 2008; Chaboche 2008; Lemaitre and Desmorat 2005; Maugin 1992; Rabotnov 1969; Skrzypek and Ganczarski 1998). Various models and methods developed within the solid mechanics can be applied to the structural analysis in the inelastic range. Examples are theories of rods, plates shells and three-dimensional solids as well as direct variational methods, e.g. Altenbach et al. (1998), Betten (2008), Boyle and Spence (1983), Hyde et al. (2013), Malinin (1981), Podgorny et al. (1984), Skrzypek (1993). Numerical solution techniques, for example the finite element method, can be combined with various time step integration techniques to simulate time dependent structural behavior up to critical state of failure.

The classical continuum mechanics of solids takes into account only translational degrees of freedom for motion of material points. The local mechanical interactions

between the material points are characterized by forces. Moment interactions are not considered. Furthermore, it is assumed that the stress state at a point in the solid depends only on the deformations and state variables of a vanishingly small volume element surrounding the point. To account for the heterogeneous deformation various extensions to the classical continuum mechanics were proposed. Micropolar theories assume that a material point behaves like a rigid body, i.e. it has translation and rotation degrees of freedom. The mechanical interactions are due to forces and moments. Constitutive equations are formulated for force and moment stress tensors. An example, where the micropolar theory should be preferred over the classical one is the short-fiber reinforced material. Short fibers may rotate and align towards certain orientation states as a result of non-uniform deformation or flow during the processing. To account for the fiber orientation, rotational degrees of freedom are required (Altenbach et al. 2003, 2007; Eringen 2001). Micropolar theories of plasticity are presented in Forest et al. (1997), Altenbach and Eremeyev (2014), among others. Inelastic deformation process is highly heterogeneous at the microscale and several effects cannot be described by the classical continuum mechanics accurately. For example, the dependence of the yield strength on the mean grain size and on the mean size of precipitates, see Sect. 1.3, are not considered within the classical theories since they do not possess intrinsic length scales. To analyze such effects non-local continuum theories are developed. Examples include strain gradient (Fleck and Hutchinson 1993; Gao et al. 1999) and micromorphic theories (Forest 2009), where a gradient or the rotation (curl) of the inelastic strain are considered as additional degrees of freedom. Non-local and phase field theories of damage and fracture were recently advanced to capture initiation and propagation of cracks in solids (Miehe et al. 2010; Schmitt et al. 2013). One problem in the use of enhanced continuum theories is related to the forces thermodynamically conjugate to the introduced degrees of freedom. It is not easy to give a clear interpretation to the higher rank stress tensors associated with higher deformation gradients.

Continuum mechanics is widely used for the inelastic analysis of structures. Examples of high temperature applications are presented for circumferentially notched bars in Hayhurst (1994), pipe weldments in Hayhurst et al. (2002) and thin-walled tubes in Krieg (1999), where qualitative agreement between the theory and experiments carried out on model structures have been established. Constitutive equations with internal state variables have been found to be mostly suited for the inelastic analysis of structures (Hayhurst et al. 2002; Hyde et al. 2013; Naumenko and Altenbach 2007).

Classical or enhanced continuum mechanics approaches require experimental data to calibrate constitutive equations over a wide range of stress, strain rates and temperatures as well as for multi-axial stress states. Accurate experimental data, in particular data related to long term creep regime are rarely available.

The *micromechanical modeling* deals with discrete simulations of material behavior for a representative volume element with geometrically idealized microstructure. Simplifying assumptions are made for the behavior of constituents and their interactions, for the type of the representative volume element and for the exerted boundary conditions. Within the *continuum micromechanics* classical or enhanced

continuum models are used to analyze constituents and interfaces. An example is the continuum crystal viscoplasticity model. Here the discrete dislocation substructure in a crystal is ignored, considering instead that plastic deformation occurs in the form of smooth shearing deformations on certain planes and in certain directions—the slip systems (Rice 1971; Hutchinson 1976). Pioneering works to the micromechanics modeling of high-temperature inelasticity assumed idealized, usually two-dimensional microstructures and simplified constitutive models. Examples include numerical simulations of void growth in a power law creeping matrix material, e.g. Tvergaard (1990), van der Giessen et al. (1995), crack propagation through a two-dimensional polycrystal (Onck et al. 2000; van der Giessen and Tvergaard 1995). In the last two decades computational approaches were advanced to analyze realistic three-dimensional microstructures of polycrystals (Cailletaud et al. 2003; Roters et al. 2011). Figure 1.54 shows examples for microstructural polycrystal models generated by Voronoi tessellation. Based on such geometrical models several mechanisms of deformation and damage at the microscale can be analyzed. Examples include grain boundary sliding and grain boundary cavitation and—two important deformation and damage mechanisms under high temperature (Ozhoga-Maslovskaja et al. 2015; Ozhoga-Maslovskaja 2014).

The representative volume element (RVE) technique is widely used to analyze microstructural behavior in a bulk material. Indeed, a stress response of a RVE can be analyzed applying special types of deformation on the boundaries, for example periodic boundary conditions. By this approach gradient effects related to interfaces, free surfaces and notches cannot be captured. Recently polycrystal models with large numbers of grains are applied to analyze structures. As an example Fig. 1.55 shows geometrical polycrystal models for smooth and circumferentially notched cylindrical specimen generated by Voronoi tessellation. Simulations of inelastic behavior for such microstructural realizations and a subsequent statistical analysis contribute to understanding free-surface and notch stress effects in inelastic range (Prygorniev and Naumenko 2013).

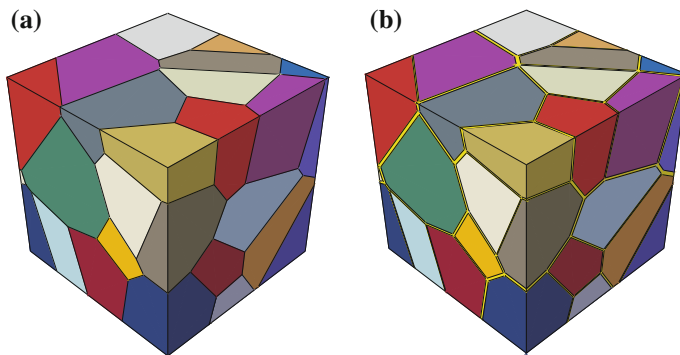


Fig. 1.54 Geometrical models of polycrystalline volume elements. **a** Zero grain boundary thickness, **b** finite grain boundary thickness (Ozhoga-Maslovskaja 2014)

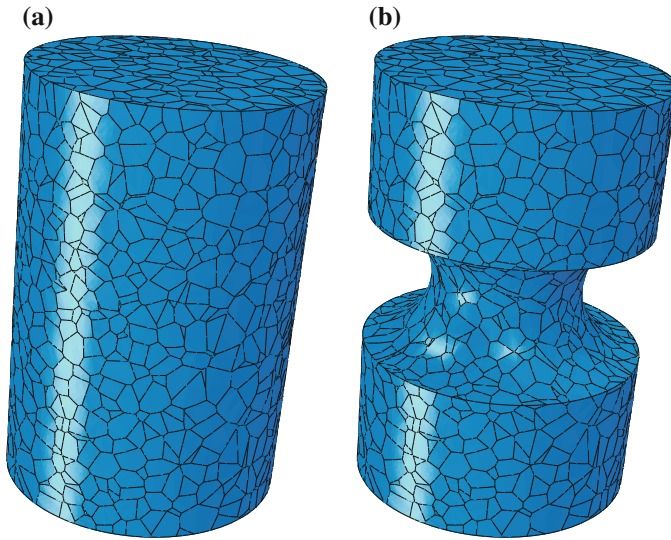


Fig. 1.55 Geometrical models of various polycrystalline cylindrical specimen. **a** Smooth specimen, **b** circumferentially notched specimen, after Prygoriev and Naumenko (2013)

Continuum micromechanics models are useful for the illustration of certain mechanisms of inelastic deformation. With respect to engineering applications the micromechanics approach suffers, however, from significant limitations. A typical high-temperature structural material, for example heat resistant steel, has a complex composition including dislocation structures, grain boundaries, dispersion particles, precipitates, etc. A reliable micromechanical description of inelastic behavior would therefore require a rather complex model of a multi-phase medium with many interacting constituents. Furthermore long term deformation at high temperature is usually accompanied by microstructural changes. For example subgrain boundaries may form, migrate and/or disappear. Voids form, grow and coalesce on grain boundaries leading to initiation of cracks and failure. Carbide precipitates coarsen during the high temperature exposure. Understanding of microstructural changes is crucial for design of high temperature materials. Direct simulations of topological changes in microstructure for real heat resistant alloys are time consuming, if ever possible.

Besides the continuum micromechanics several discrete methods were developed to analyze material behavior at lower length scales. The *discrete dislocation dynamics* (DDD) method is suitable for the analysis of plastic deformation on the microscale and mesoscale (i.e. the size range of a fraction of a micrometer to tens of micrometers). Dislocations are explicitly represented as line defects embedded in an elastic medium. The main idea is to derive and to solve equations of motion for dislocation loops. To this end driving forces (configurational forces) acting on dislocation line segments are defined. An example is the Peach-Köhler force, the energetic force work conjugate

to the dislocation motion in an elastic continuum (Maugin 1993, 2011). In the early versions of DDD, the collective behavior of dislocation ensembles was determined by interactions between infinitely long straight dislocations (Lepinoux and Kubin 1987). Simulations were two-dimensional and consisted of periodic cells containing multiple dislocations whose behavior was governed by a set of simplified rules. Recently, the DDD methodology is extended to the more physical, three-dimensional simulations (Kubin 2013).

DDD simulations give access to the dislocation patterning, interactions of dislocations with obstacles, subgrain boundaries, etc. but also to the mechanical response of a representative volume containing large number of dislocation lines. For thin films and small scale specimen DDD simulations explain the size dependency of the observed flow stress (Kraft et al. 2010). DDD is used for assessing the performance of enhanced continuum mechanics models in analysis of small scale structures and thin films (Aifantis et al. 2012) since it provides the knowledge of microscale stress and strain patterns, which are not easy to determine experimentally.

Several limitations exist when applying this method to the analysis of high-temperature phenomena. The inelastic strain at high temperature is mainly controlled by dislocation glide at a rate given by thermally-activated dislocation climb due to diffusion of vacancies (Frost and Ashby 1982). Numerical analysis of the phenomenon is challenging due to the complexity of incorporating both vacancies and dislocations in a single computational framework. Only recently two-dimensional DDD simulations are performed illustrating dislocation glide and climb such that power law creep phenomenon can be reproduced (Keralavarma et al. 2012).

1.5.2 Objectives, Modeling Requirements, and Steps for Structural Analysis

The objective of this book is to present current knowledge on modeling of high temperature material behavior for the structural analysis. Examples for high temperature applications include components of power plant, turbochargers, engines etc. Small scale components of microelectronics are further examples. The requirements for the modeling with respect to engineering applications are

- Ability to describe basic features of inelastic deformation, hardening, softening and damage processes for a wide range of stress, strain rate and temperature levels,
- Robustness and minimum number of functions and material properties to be identified from tests,
- Compatibility with structural mechanics methods, for example, FEM.

To met these requirements several theoretical and experimental approaches should be applied simultaneously. The continuum mechanics provides a rational framework for the analysis of real three-dimensional structures under complex thermo-mechanical loading paths. Appropriate stress and deformation measures are introduced to

capture complex local multi-axial loadings. General forms of constitutive and evolution equations are defined such that invariance requirements with respect to the choice of reference frame, laws of continuum thermodynamics and other principles are fulfilled. To specialize the constitutive equation results of basic tests of the material behavior, such as tensile test, creep test, relaxation test, etc. should be systematically analyzed. On the other hand basic features of materials microstructure in the reference state and after a course of inelastic deformation process should be established. For example, to formulate a robust model it is not enough to say, that a material exhibits anisotropic properties. Even in the case of linear elasticity 21 material constants must be identified from tests if the kind of anisotropy is not specified. Microstructural analysis and appropriate assumptions with regard to symmetries of microstructure would reduce the identification effort essentially. Different types of material symmetries and appropriate forms of constitutive laws are defined within the continuum mechanics, while microstructural analysis is usually the subject of the materials science.

Once a first guess to the constitutive model, for example, elasto-visco-plastic model with kinematic and isotropic hardening is selected, appropriate test programme to generate reliable databases, for example tensile tests for a range of temperatures and strain rates must be defined. The experimental data should be used to identify the constitutive functions, for example a function that captures the strain rate sensitivity. With the developed and identified constitutive model simulations of the material behavior under service-like loading conditions should be performed and compared with experimental data. For example, uni-axial tests under thermo-mechanical loading profile simulating start-up, running and shut-down stages of a component can be used for verification of the developed constitutive equation. Material testing under multi-axial stress states, for example tests on cruciform specimen as well as material testing under non-uniform stress states and stress concentrations, for example notched specimen, are useful to verify the modeling assumptions. The verification process may require to modify the model, for example to change the constitutive functions of stress and temperature. To this end additional information regarding deformation mechanisms is useful. Furthermore, loading profiles for laboratory testing must be extended to analyze the material behavior for wide ranges of stresses, strain rates and temperatures. Figure 1.56 provides a sketch of steps required to formulate a reliable constitutive model for structural analysis. The stress tensor is usually related to the strain tensor, the state variables like the inelastic strain tensor, backstress tensor, damage parameters, etc., and possibly their gradients. For the state variables evolution equations are required to capture microstructural changes in the course of inelastic deformation process.

In this book we focus on the continuum mechanics and continuum micromechanics approaches for the structural analysis applications. DDD and other discrete methods, for example molecular dynamics methods will be not considered. We discuss approaches to develop constitutive models, discuss identification techniques and present numerical methods in order to apply constitutive equations together with structural mechanics methods. In particular, we discuss how to develop user

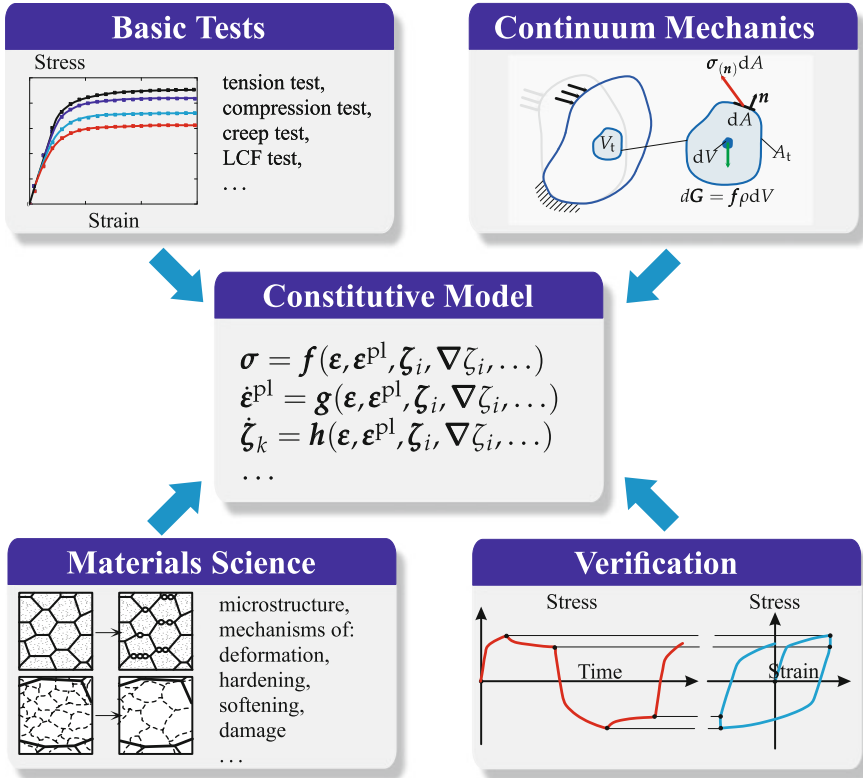


Fig. 1.56 Basic steps of constitutive modeling for structural analysis

material subroutines inside the commercial finite element codes for the structural analysis. Length scale and temporal scale approaches will be discussed to analyze heterogeneous deformation and to develop efficient time integration methods for cyclic loadings.

References

- Abe F (2008) Strengthening mechanisms in steel for creep and creep rupture. In: Abe F, Kern TU, Viswanathan R (eds) Creep-resistant steels. Woodhead Publishing, Cambridge, pp 279–304
- Abe F (2009) Analysis of creep rates of tempered martensitic 9% Cr steel based on microstructure evolution. Mater Sci Eng A 510:64–69
- Aifantis KE, Weygand D, Motz C, Nikitas N, Zaiser M (2012) Modeling microbending of thin films through discrete dislocation dynamics, continuum dislocation theory, and gradient plasticity. J Mater Res 27:612–618
- Aktaa J, Petersen C (2009) Challenges in the constitutive modeling of the thermo-mechanical deformation and damage behavior of EUROFER 97. Eng Fract Mech 76(10):1474–1484

- Altenbach H, Eremeyev V (2014) Strain rate tensors and constitutive equations of inelastic micropolar materials. *Int J Plast* 63:3–17
- Altenbach H, Naumenko K (1997) Creep bending of thin-walled shells and plates by consideration of finite deflections. *Comput Mech* 19:490–495
- Altenbach H, Naumenko K (2002) Shear correction factors in creep-damage analysis of beams, plates and shells. *JSME Int J Ser A, Solid Mech Mater Eng* 45:77–83
- Altenbach H, Morachkovsky O, Naumenko K, Sychov A (1997) Geometrically nonlinear bending of thin-walled shells and plates under creep-damage conditions. *Arch Appl Mech* 67:339–352
- Altenbach H, Altenbach J, Naumenko K (1998) *Ebene Flächentragwerke*. Springer, Berlin
- Altenbach H, Breslavsky D, Morachkovsky O, Naumenko K (2000a) Cyclic creep damage in thin-walled structures. *J Strain Anal Eng Des* 35(1):1–11
- Altenbach H, Kolarow G, Morachkovsky O, Naumenko K (2000b) On the accuracy of creep-damage predictions in thinwalled structures using the finite element method. *Comput Mech* 25:87–98
- Altenbach H, Kushnevsky V, Naumenko K (2001) On the use of solid- and shell-type finite elements in creep-damage predictions of thinwalled structures. *Arch Appl Mech* 71:164–181
- Altenbach H, Huang C, Naumenko K (2002) Creep damage predictions in thin-walled structures by use of isotropic and anisotropic damage models. *J Strain Anal Eng Des* 37(3):265–275
- Altenbach H, Naumenko K, Zhilin P (2003) A micro-polar theory for binary media with application to phase-transitional flow of fiber suspensions. *Continuum Mech Thermodyn* 15:539–570
- Altenbach H, Naumenko K, Pylypenko S, Renner B (2007) Influence of rotary inertia on the fiber dynamics in homogeneous creeping flows. *ZAMM-J Appl Math Mech/Zeitschrift für Angewandte Mathematik und Mechanik* 87(2):81–93
- Altenbach H, Gorash Y, Naumenko K (2008a) Steady-state creep of a pressurized thick cylinder in both the linear and the power law ranges. *Acta Mech* 195:263–274
- Altenbach H, Naumenko K, Gorash Y (2008b) Creep analysis for a wide stress range based on stress relaxation experiments. *Int J Mod Phys B* 22:5413–5418
- Altenbach H, Kozhar S, Naumenko K (2013) Modeling creep damage of an aluminum-silicon eutectic alloy. *Int J Damage Mech* 22(5):683–698
- Altenbach J, Altenbach H, Naumenko K (2004) Edge effects in moderately thick plates under creep damage conditions. *Tech Mechanik* 24(3–4):254–263
- Arzt E (1998) Size effects in materials due to microstructural and dimensional constraints: a comparative review. *Acta Mater* 46(16):5611–5626
- Berger C, Scholz A, Mueller F, Schwienherr M (2008) Creep fatigue behaviour and crack growth of steels. In: Abe F, Kern TU, Viswanathan R (eds) *Creep-resistant steels*. Woodhead Publishing, Cambridge, pp 446–471
- Bernhardt EO, Hanemann H (1938) Über den Kriechvorgang bei dynamischer Belastung und den Begriff der dynamischen Kriechfestigkeit. *Z Metallkd* 30(12):401–409
- Betten J (1976) Plastic anisotropy and Bauschinger-effect—general formulation and comparison with experimental yield curves. *Acta Mech* 25(1–2):79–94
- Betten J (2001) *Kontinuumsmechanik*. Springer, Berlin
- Betten J (2008) *Creep mechanics*, 3rd edn. Springer, Berlin
- Betten J, El-Magd E, Meydanli SC, Palmen P (1995) Untersuchung des anisotropen Kriechverhaltens vorgeschädigter Werkstoffe am austenitischen Stahl X8CrNiMoNb 1616. *Arch Appl Mech* 65:121–132
- Bielski J, Skrzypek J (1989) Failure modes of elastic-plastic curved tubes under external pressure with in-plane bending. *Int J Mech Sci* 31:435–458
- Blum W (2001) *Creep of crystalline materials: experimental basis, mechanisms and models*. *Mater Sci Eng: A* 319:8–15
- Blum W (2008) Mechanisms of creep deformation in steel. In: Abe F, Kern TU, Viswanathan R (eds) *Creep-resistant steels*. Woodhead Publishing, Cambridge, pp 365–402
- Boyle JT, Spence J (1983) *Stress analysis for creep*. Butterworth, London

- Bunch JO, McEvily AJ (1987) On the behavior of ferritic steels subjected to load controlled cycling at elevated temperatures. In: Rie KT (ed) *Cycle low fatigue and elasto-plastic behaviour of materials*, pp 252–257 Springer
- da C Andrade EN (1910) On the viscous flow of metals, and allied phenomena. *Proc R Soc Lond ALXXXIV*:1–12
- Cailletaud G, Forest S, Jeulin D, Feyel F, Galliet I, Mounoury V, Quilici S (2003) Some elements of microstructural mechanics. *Comput Mater Sci* 27(3):351–374
- Cerjak H, Mayr P (2008) Creep strength of welded joints of ferritic steels. In: Abe F, Kern TU, Viswanathan R (eds) *Creep-resistant steels*. Woodhead Publishing, Cambridge, pp 472–503
- Chaboche JL (2008) A review of some plasticity and viscoplasticity constitutive equations. *Int J Plast* 24:1642–1693
- Coble RL (1963) A model for boundary diffusion controlled creep in polycrystalline materials. *J Appl Phys* 34(6):1679–1682
- Coffin LF (1954) A study of the effects of cyclic thermal stresses on a ductile metal. *Am Soc Mech Eng* 76:931–950
- Colombo F, Mazza E, Holdsworth SR, Skelton RP (2008) Thermo-mechanical fatigue tests on uniaxial and component-like 1CrMoV rotor steel specimens. *Int J Fatigue* 30:241–248
- Cui L, Wang P (2014) Two lifetime estimation models for steam turbine components under thermomechanical creep-fatigue loading. *Int J Fatigue* 59:129–136
- Cui L, Scholz A, von Hartrott P, Schlesinger M (2009) Entwicklung von Modellen zur Lebensdauer vorhersage von Kraftwerksbauteilen unter thermisch-mechanischer Kriechermüdigungsbeanspruchung. Abschlussbericht, AVIF Vorhaben Nr. 895, FVV, Heft 888, Frankfurt am Main
- Cui L, Wang P, Hoche H, Scholz A, Berger C (2013) The influence of temperature transients on the lifetime of modern high-chromium rotor steel under service-type loading. *Mater Sci Eng: A* 560:767–780
- Devulder A, Aubry D, Puel G (2010) Two-time scale fatigue modelling: application to damage. *Comput Mech* 45(6):637–646
- Dyson BF, McLean M (1998) Microstructural evolution and its effects on the creep performance of high temperature alloys. In: Strang A, Cawley J, Greenwood GW (eds) *Microstructural Stability of creep resistant alloys for high temperature plant applications*. Cambridge University Press, Cambridge, pp 371–393
- Dyson BF, McLean M (2001) Micromechanism-quantification for creep constitutive equations. In: Murakami S, Ohno N (eds) *IUTAM Symposium on creep in structures*. Kluwer, Dordrecht, pp 3–16
- Eggeler G, Ramteke A, Coleman M, Chew B, Peter G, Burblies A, Hald J, Jefferey C, Rantala J, de Witte M, Mohrmann R (1994) Analysis of creep in a welded P91 pressure vessel. *Int J Press Vessels Pip* 60:237–257
- El-Magd E, Nicolini G (1999) Creep behaviour and microstructure of dispersion-strengthened pm-aluminium materials at elevated temperatures. In: Mughrabi H, Gottstein G, Mecking H, Riedel H, Tobolski J (eds) *Microstructure and mechanical properties of metallic high-temperature materials: research Report/DFG*. Wiley-VCH, Weinheim, pp 445–464
- El-Magd E, Betten J, Palmen P (1996) Auswirkung der Schädigungsanisotropie auf die Lebensdauer von Stählen bei Zeitstandsbeanspruchung. *Materialwiss Werkstofftech* 27:239–245
- Eringen AC (2001) *Microcontinuum field theories, vol II*. Fluent Media. Springer, New York
- Estrin Y (1996) Dislocation-density-related constitutive modelling. In: Krausz AS, Krausz K (eds) *Unified constitutive laws of plastic deformation*. Academic Press, San Diego, pp 69–104
- Faruque MO, Zaman M, Hossain MI (1996) Creep constitutive modelling of an aluminium alloy under multiaxial and cyclic loading. *Int J Plast* 12(6):761–780
- Fish J, Bailakanavar M, Powers L, Cook T (2012) Multiscale fatigue life prediction model for heterogeneous materials. *Int J Numer Meth Eng* 91(10):1087–1104
- Fleck NA, Hutchinson JW (1993) A phenomenological theory for strain gradient effects in plasticity. *J Mech Phys Solids* 41(12):1825–1857

- Forest S (2009) Micromorphic approach for gradient elasticity, viscoplasticity, and damage. *J Eng Mech* 135(3):117–131
- Forest S, Cailletaud G, Sievert R (1997) A Cosserat theory for elastoviscoplastic single crystals at finite deformation. *Arch Mech* 49:705–736
- Fournier B, Sauzay M, Caës C, Noblecourt M, Mottot M, Bougault A, Rabeau V, Pineau A (2008) Creep-fatigue-oxidation interactions in a 9Cr-1Mo martensitic steel. Part II: Effect of compressive holding period on fatigue lifetime. *Int J Fatigue* 30(4):663–676
- Fournier B, Dalle F, Sauzay M, Longour J, Salvi M, Caës C, Tournié I, Giroux PF, Kim SH (2011) Comparison of various 9–12 % Cr steels under fatigue and creep-fatigue loadings at high temperature. *Mater Sci Eng: A* 528(22):6934–6945
- François D, Pineau A, Zaoui A (2012) Mechanical behaviour of materials, mechanical behaviour of materials, vol I. Micro- and Macroscopic Constitutive Behaviour. Springer
- Frost HJ, Ashby MF (1982) Deformation-mechanism maps. Pergamon, Oxford
- Gao H, Huang Y, Nix WD, Hutchinson JW (1999) Mechanism-based strain gradient plasticity-I. Theory. *J Mech Phys Solids* 47(6):1239–1263
- Gariboldi E, Casaro F (2007) Intermediate temperature creep behaviour of a forged Al-Cu-Mg-Si-Mn alloy. *Mater Sci Eng: A* 462(1):384–388
- Gariboldi E, Naumenko K, Ozhoga-Maslovskaja O, Zappa E (2016) Analysis of anisotropic damage in forged Al-Cu-Mg-Si alloy based on creep tests, micrographs of fractured specimen and digital image correlations. *Mater Sci Eng: A* 652:175–185
- van der Giessen E, Tvergaard V (1995) Development of final creep failure in polycrystalline aggregates. *Acta metallurgica et materialia* 42:959–973
- van der Giessen E, van der Burg MWD, Needleman A, Tvergaard V (1995) Void growth due to creep and grain boundary diffusion at high triaxialities. *J Mech Phys Solids* 43:123–165
- Gooch DJ (2003) Remnant creep life prediction in ferritic materials. In: Saxena A (ed) *Comprehensive structural integrity*, vol 5., Creep and High-Temperature Failure Elsevier, Amsterdam, pp 309–359
- Gorash Y, Altenbach H, Lvov G (2012) Modelling of high-temperature inelastic behaviour of the austenitic steel AISI type 316 using a continuum damage mechanics approach. *J Strain Anal Eng Des* 47(4):229–243
- Hald J (1998) Service performance of a 12crmov steam pipe steel. In: Strang A, Cawley J, Greenwood GW (eds) *Microstructural stability of creep resistant alloys for high temperature plant applications*. Cambridge University Press, Cambridge, pp 173–184
- Hall EO (1951) The deformation and ageing of mild steel: III. Discussion of results. *Proc Phys Soc Sect B* 64(9):747
- Haupt P (2002) *Continuum mechanics and theory of materials*. Springer, Berlin
- Hayhurst DR (1994) The use of continuum damage mechanics in creep analysis for design. *J Strain Anal Eng Des* 25(3):233–241
- Hayhurst DR, Leckie FA (1990) High temperature creep continuum damage in metals. In: Boehler JP (ed) *Yielding, Damage and Failure of Anisotropic Solids*, Mechanical Engineering Publ, London, pp 445–464
- Hayhurst DR, Wong MT, Vakili-Tahami F (2002) The use of CDM analysis techniques in high temperature creep failure of welded structures. *JSME Int J SerA, Solid Mech Mater Eng* 45:90–97
- Herring C (1950) Diffusional viscosity of a polycrystalline solid. *J Appl Phys* 21(5):437–445
- Holdsworth S, Mazza E, Binda L, Ripamonti L (2007) Development of thermal fatigue damage in 1CrMoV rotor steel. *Nucl Eng Des* 237:2292–2301
- Hutchinson JW (1976) Bounds and self-consistent estimates for creep of polycrystalline materials. *Proc R Soc London Math Phys Sci* 348(1652):101–127
- Hyde T, Sun W, Hyde C (2013) *Applied creep mechanics*. McGraw-Hill Education
- Hyde TH, Xia L, Becker AA (1996) Prediction of creep failure in aeroengine materials under multi-axial stress states. *Int J Mech Sci* 38(4):385–403

- Hyde TH, Sun W, Becker AA, Williams JA (1997) Creep continuum damage constitutive equations for the base, weld and heat-affected zone materials of a service-aged 1/2Cr1/2Mo1/4V:2 1/4Cr1Mo multipass weld at 640°C. *J Strain Anal Eng Des* 32(4):273–285
- Hyde TH, Sun W, Williams JA (1999) Creep behaviour of parent, weld and HAZ materials of new, service aged and repaired 1/2Cr1/2Mo1/4V: 21/4Cr1Mo pipe welds at 640°C. *Mater High Temp* 16(3):117–129
- Hyde TH, Yaghi A, Becker AA, Earl PG (2002) Finite element creep continuum damage mechanics analysis of pressurised pipe bends with ovality. *JSME Int J Ser A, Solid Mech Mater Eng* 45(1):84–89
- Hyde TH, Sun W, Agyakwa PA, Shipeay PH, Williams JA (2003a) Anisotropic creep and fracture behaviour of a 9CrMoNbV weld metal at 650°C. In: Skrzypek JJ, Ganczarski AW (eds) *Anisotropic behaviour of damaged materials*. Springer, Berlin, pp 295–316
- Hyde TH, Sun W, Williams JA (2003b) Creep analysis of pressurized circumferential pipe weldments—a review. *J Strain Anal Eng Des* 38(1):1–29
- Ilschner B (1973) *Hochtemperatur-Plastizität*. Springer, Berlin et al
- Inoue T (1988) Inelastic constitutive models under plasticity-creep interaction condition—theories and evaluations. *JSME Int J Ser 1, Solid Mech Strength Mater* 31(4):653–663
- Kassner ME, Pérez-Prado MT (2004) *Fundamentals of creep in metals and alloys*. Elsevier, Amsterdam
- Kawai M (1989) Creep and plasticity of austenitic stainless steel under multiaxial non-proportional loadings at elevated temperatures. In: Hui D, Kozik TJ (eds) *Visco-plastic behavior of new materials*, ASME, PVP, vol. 184, pp 85–93. New York
- Keralavarma SM, Cagin T, Arsenlis A, Benzerga AA (2012) Power-law creep from discrete dislocation dynamics. *Phys Rev Lett* 109(26):265, 504
- Kimura K, Kushima H, Sawada K (2009) Long-term creep deformation properties of 9Cr-1Mo steel. *Mater Sci Eng A* 510–A511:58–63
- Kimura M, Yamaguchi K, Hayakawa M, Kobayashi K, Kanazawa K (2006) Microstructures of creep-fatigued 9–12% Cr ferritic heat-resisting steels. *Int J Fatigue* 28(3):300–308
- Kloc L, Sklenička V (1997) Transition from power-law to viscous creep behaviour of P-91 type heat-resistant steel. *Mater Sci Eng A* 234–A236:962–965
- Kloc L, Sklenička V (2004) Confirmation of low stress creep regime in 9% chromium steel by stress change creep experiments. *Mater Sci Eng A* 387–A389:633–638
- Kloc L, Sklenička V, Ventruba J (2001) Comparison of low creep properties of ferritic and austenitic creep resistant steels. *Mat Sci Eng A* 319–A321:774–778
- Kostenko Y, Almstedt H, Naumenko K, Linn S, Scholz A (2013) Robust methods for creep fatigue analysis of power plant components under cyclic transient thermal loading. In: *ASME turbo expo 2013: turbine technical conference and exposition*, American society of mechanical engineers, pp V05BT25A040–V05BT25A040
- Kowalewski ZL (1995) Experimental evaluation of the influence of the stress state type on the creep characteristics of copper at 523 K. *Arch Mech* 47(1):13–26
- Kowalewski ZL (2001) Assessment of the multiaxial creep data based on the isochronous creep surface concept. In: Murakami S, Ohno N (eds) *IUTAM Symposium on creep in structures*. Kluwer, Dordrecht, pp 401–418
- Kowalewski ZL, Hayhurst DR, Dyson BF (1994) Mechanisms-based creep constitutive equations for an aluminium alloy. *J Strain Anal Eng Des* 29(4):309–316
- Kraft O, Gruber PA, Mönig R, Weygand D (2010) Plasticity in confined dimensions. *Annu Rev Mater Res* 40:293–317
- Kraus H (1980) *Creep analysis*. John Wiley & Sons, New York
- Krausz AS, Krausz K (1996) *Unified constitutive laws of plastic deformation*. Academic Press, San Diego
- Krempel E (1999) Creep-plasticity interaction. In: Altenbach H, Skrzypek J (eds) *Creep and damage in materials and structures*, Springer, Wien, New York, pp 285–348, CISM Lecture Notes No. 399

- Krieg R (1999) Reactor pressure vessel under severe accident loading. Final Report of EU-Project Contract FI4S-CT95-0002. Technical report, Forschungszentrum Karlsruhe, Karlsruhe
- Kubin L (2013) Dislocations, mesoscale simulations and plastic flow. Oxford Series on Materials Modelling, OUP Oxford
- Laengler F, Mao T, Aleksanoglu H, Scholz A (2010) Phenomenological lifetime assessment for turbine housings of turbochargers. In: Proceedings of 9th international conference on multiaxial fatigue & fracture, 7th–9th June, 2010, Parma, Italy, (CD-ROM), Parma, pp 283–291
- Langdon TG (2006) Grain boundary sliding revisited: developments in sliding over four decades. *J Mater Sci* 41:597–609
- Längler F, Naumenko K, Altenbach H, Ievdokymov M (2014) A constitutive model for inelastic behavior of casting materials under thermo-mechanical loading. *J Strain Anal Eng Des* 49:421–428
- Lazan BJ (1949) Dynamic creep and rupture properties of temperature-resistant materials under tensile fatigue stress. *Proc ASTM* 49:757–787
- Le May I, da Silveria TL, Cheung-Mak SKP (1994) Uncertainties in the evaluations of high temperature damage in power stations and petrochemical plant. *Int J Press Vessels Pip* 59:335–343
- Lemaitre J, Desmorat R (2005) Engineering Damage mechanics: ductile, creep, fatigue and brittle failures. Springer
- Lepinoux J, Kubin L (1987) The dynamic organization of dislocation structures: a simulation. *Scr Metall* 21(6):833–838
- Libai A, Simmonds JG (1998) The nonlinear theory of elastic shells. Cambridge University Press, Cambridge
- Lucas GE, Pelloux RMN (1981) Texture and stress state dependent creep in Zircaloy-2. *Metall Trans A* 12A:1321–1331
- Lundin CD, Liu P, Prager M (2001) Creep behavior of weld heat affected zone regions for modified 9Cr-1Mo Steel. Proceedings of CREEP7. Japan Society of Mechanical Engineers, Tsukuba, pp 379–382
- Malinin NN (1981) Raschet na polzuchest' konstrukcionnykh elementov (Creep calculations of structural elements, in Russ.). Mashinostroenie, Moskva
- Manson SS (1953) Behavior of materials under conditions of thermal stress. NACA TN 2933
- Matsui M, Tabuchi M, Watanabe T, Kubo K, Kinugawa J, Abe F (2001) Degradation of creep strength in welded joint of 9%Cr steel. *Iron Steel Inst Jpn (ISIJ) Int* 41:S126–S130
- Maugin GA (1992) The thermomechanics of plasticity and fracture. Cambridge University Press, Cambridge
- Maugin GA (1993) Material inhomogeneities in elasticity. Chapman Hall, London
- Maugin GA (2011) Configurational forces: thermomechanics, physics, mathematics, and numerics. CRC Press, Boca Raton
- Miehe C, Hofacker M, Welschinger F (2010) A phase field model for rate-independent crack propagation: Robust algorithmic implementation based on operator splits. *Comput Methods Appl Mech Eng* 199(45–48):2765–2778
- Miller AK (ed) (1987) Unified constitutive equations for creep and plasticity. Elsevier, London, New York
- Miner M (1945) Cumulative damage in fatigue. *J Appl Mech* 12:159–164
- Monkman FC, Grant NJ (1956) An empirical relationship between rupture life and minimum creep rate in creep-rupture tests. *Proc ASTM* 56:593–620
- Mughrabi H (2009) Cyclic slip irreversibilities and the evolution of fatigue damage. *Metall Mater Trans B* 40(4):431–453
- Murakami S, Sanomura Y (1985) Creep and creep damage of copper under multiaxial states of stress. In: Sawczuk A, Bianchi B (eds) Plasticity today—modelling. Methods and Applications, New York, Elsevier, London, pp 535–551
- Nabarro FRN (1948) Report of a conference on the strength of solids. The Physical Society, London 75
- Nabarro FRN (2002) Creep at very low rates. *Metall Mater Trans A* 33(2):213–218

- Nabarro FRN, de Villiers HL (1995) *The physics of creep. Creep and creep-resistant alloys*. Taylor & Francis, London
- Nagode M, Längler F, Hack M (2011a) Damage operator based lifetime calculation under thermo-mechanical fatigue for application on Ni-resist D-5S turbine housing of turbocharger. *Eng Fail Anal* 18(6):1565–1575
- Nagode M, Längler F, Hack M (2011b) A time-dependent damage operator approach to thermo-mechanical fatigue of Ni-resist D-5S. *Int J Fatigue* 33(5):692–699
- Naumenko K (2000) On the use of the first order shear deformation models of beams, plates and shells in creep lifetime estimations. *Tech Mech* 20(3):215–226
- Naumenko K, Altenbach H (2005) A phenomenological model for anisotropic creep in a multi-pass weld metal. *Arch Appl Mech* 74:808–819
- Naumenko K, Altenbach H (2007) *Modelling of creep for structural analysis*. Springer, Berlin
- Naumenko K, Gariboldi E (2014) A phase mixture model for anisotropic creep of forged Al-Cu-Mg-Si alloy. *Mater Sci Eng: A* 618:368–376
- Naumenko K, Kostenko Y (2009) Structural analysis of a power plant component using a stress-range-dependent creep-damage constitutive model. *Mat. Sci. Eng. A510–A511*:169–174
- Naumenko K, Altenbach H, Gorash Y (2009) Creep analysis with a stress range dependent constitutive model. *Arch Appl Mech* 79:619–630
- Naumenko K, Altenbach H, Kutschke A (2011a) A combined model for hardening, softening and damage processes in advanced heat resistant steels at elevated temperature. *Int J Damage Mech* 20:578–597
- Naumenko K, Kutschke A, Kostenko Y, Rudolf T (2011b) Multi-axial thermo-mechanical analysis of power plant components from 9–12%Cr steels at high temperature. *Eng Fract Mech* 78:1657–1668
- Nikitentsov AF (1984) Eksperimental'noe obosnovanie gipotezy suschestvovaniya poverkhnosti polzuchesti v usloviyakh slozhnogo nagruzheniya, (experimental justification of the hypothesis on existence of the creep surface under complex loading conditions, in russ.). *Probl Prochn* 8:3–8
- Niu L, Kobayashi M, Takaku H (2002) Creep rupture properties of an austenitic steel with high ductility under multi-axial stresses. *Iron Steel Inst Jpn (ISIJ) Int* 42:1156–1181
- Nørbygaard T (2002) *Studies of grain boundaries in materials subjected to diffusional creep*. Ph.D. thesis, Risø National Laboratory, Roskilde
- Odqvist FKG (1974) *Mathematical theory of creep and creep rupture*. Oxford University Press, Oxford
- Odqvist FKG, Hult J (1962) *Kriechfestigkeit metallischer Werkstoffe*. Springer, Berlin
- Ohno N (1998) Constitutive modeling of cyclic plasticity with emphasis on ratchetting. *Int J Mech Sci* 40(2):251–261
- Ohno N, Takeuchi T (1994) Anisotropy in multiaxial creep of nickel-based single-crystal superalloy CMSX-2 (experiments and identification of active slip systems). *JSME Int J Ser A, Solid Mech Mater Eng* 37:129–137
- Ohno N, Kawabata M, Naganuma J (1990) Aging effects on monotonic, stress-paused, and alternating creep of type 304 stainless steel. *Int J Plast* 6:315–327
- Ohno N, Abdel-Karim M, Kobayashi M, Igari T (1998) Ratchetting characteristics of 316FR steel at high temperature, Part I: strain-controlled ratchetting experiments and simulations. *Int J Plast* 14(4):355–372
- Onck PR, Nguyen BN, Van der Giessen E (2000) Microstructural modelling of creep fracture in polycrystalline materials. In: Murakami S, Ohno N (eds) *Creep in structures*. Kluwer Academic Publishers, Dordrecht, pp 51–64
- Oytana C, Delobelle P, Mermet A (1982) Constitutive equations study in biaxial stress experiments. *J Eng Mater Technol* 104(3):1–11
- Ozhoga-Maslovskaja O (2014) *Micro scale modeling grain boundary damage under creep conditions*. Ph.D. thesis, Otto von Guericke University Magdeburg, Magdeburg

- Ozhoga-Maslovskaja O, Naumenko K, Altenbach H, Prygorniev O (2015) Micromechanical simulation of grain boundary cavitation in copper considering non-proportional loading. *Comput Mater Sci* 96(A):178–184
- Palmgren A (1924) Die Lebensdauer von Kugellagern. *Z Ver Dtsch Ing* 68(14):339–341
- Penkalla HJ, Schubert F, Nickel H (1988) Torsional creep of alloy 617 tubes at elevated temperature. In: Reichman S, Duhl DN, Maurer G, Antolovich S, Lund C (eds) *Superalloys 1988*, the metallurgical society, pp 643–652
- Penny RK, Mariott DL (1995) *Design for creep*. Chapman & Hall, London
- Perrin JJ, Hayhurst DR (1994) Creep constitutive equations for a 0.5Cr-0.5Mo-0.25V ferritic steel in the temperature range 600–675°C. *J Strain Anal Eng Des* 31(4):299–314
- Petch NJ (1953) The cleavage strength of polycrystals. *J Iron Steel Inst* 174:25–28
- Pintschovius L, Gering E, Munz D, Fett T, Soubeyroux JL (1989) Determination of non-symmetric secondary creep behaviour of ceramics by residual stress measurements using neutron diffraction. *J Mater Sci Lett* 8(7):811–813
- Podgorny AN, Bortovoj VV, Gontarovskiy PP, Kolomak VD, Lvov GI, Matyukhin YJ, Morachkovskiy OK (1984) Polzuchest' elementov mashinostroitel'nykh konstruykij (Creep of machinery structural members, in Russ.). *Naukova dumka*, Kiev
- Polák J (2003) 4.01–Cyclic deformation, crack initiation, and low-cycle fatigue. In: Karihaloo I, Milne R, Ritchie B (eds) *Comprehensive structural integrity*. Pergamon, Oxford, pp 1–39
- Polmear IJ (2004) Aluminium alloys—a century of age hardening. *Mater Forum* 28:1–14
- Prygorniev O, Naumenko K (2013) Surface layer effects in polycrystalline structures under cyclic viscoplasticity. In: *CanCNSM 2013*, 4th Canadian conference on nonlinear solid mechanics, montreal, Canada 2013.07.23–26, Published on CD-ROM, 6 pp
- Qin Y, Götz G, Blum W (2003) Subgrain structure during annealing and creep of the cast martensitic Cr-steel G-X12CrMoWVNbN 10-1-1. *Mater Sci Eng: A* 341(1):211–215
- Rabotnov YN (1969) Creep problems in structural members. North-Holland, Amsterdam
- Raj SV, Iskowitz IS, Freed AD (1996) Modeling the role of dislocation substructure during class M and exponential creep. In: Krausz AS, Krausz K (eds) *Unified constitutive laws of plastic deformation*. Academic Press, San Diego, pp 343–439
- Rice JR (1971) Inelastic constitutive relations for solids: an internal-variable theory and its application to metal plasticity. *J Mech Phys Solids* 19(6):433–455
- Rieth M, Falkenstein A, Graf P, Heger S, Jäntsch U, Klimiankou M, Materna-Morris E, Zimmermann H (2004) Creep of the austenitic steel AISI 316 L(N). Experiments and models. Technical report, Forschungszentrum Karlsruhe, FZKA 7065, Karlsruhe
- Robinson DN, Binienda WK, Ruggles MB (2003a) Creep of polymer matrix composites. I: Norton/Bailey Creep Law for transverse isotropy. *J Eng Mech* 129(3):310–317
- Robinson DN, Binienda WK, Ruggles MB (2003b) Creep of polymer matrix composites. II: Monkman-Grant failure relationship for transverse isotropy. *J Eng Mech* 129(3):318–323
- Robinson E (1952) Effect of temperature variation on the long-time rupture strength of steels. *Trans ASME* 74(5):777–781
- Roesler J, Harders H, Baeker M (2007) *Mechanical behaviour of engineering materials: Metals, Ceramics, Polymers, and Composites*. Springer
- Roters F, Eisenlohr P, Bieler T, Raabe D (2011) *Crystal plasticity finite element methods: in materials science and engineering*. Wiley
- Röttger D (1997) Untersuchungen zum Wechselverformungs- und Zeitstandverhalten der Stähle X20CrMoV121 und X10CrMoVNb91. Dissertation, Universität GH Essen, Fortschr.-Ber. VDI Reihe 5, Nr. 507, Düsseldorf
- Sakane M, Hosokawa T (2001) Biaxial and triaxial creep testing of type 304 stainless steel at 923 K. In: Murakami S, Ohno N (eds) *IUTAM symposium on creep in structures*. Kluwer, Dordrecht, pp 411–418
- Sakane M, Tokura H (2002) Experimental study of biaxial creep damage for type 304 stainless steel. *Int J Damage Mech* 11:247–262

- Samir A, Simon A, Scholz A, Berger C (2005) Deformation and life assessment of high temperature materials under creep fatigue loading. *Materialwiss Werkstofftech* 36:722–730
- Schmitt R, Müller R, Kuhn C, Urbassek H (2013) A phase field approach for multivariant martensitic transformations of stable and metastable phases. *Arch Appl Mech* 83:849–859
- Segle P, Tu ST, Storesund J, Samuelson LA (1996) Some issues in life assessment of longitudinal seam welds based on creep tests with cross-weld specimens. *Int J Press Vessels Pip* 66:199–222
- Shibli IA (2002) Performance of P91 thick section welds under steady and cyclic loading conditions: power plant and research experience. *OMMI* 1(3). <http://www.ommi.co.uk>
- Simon A (2007) Zur Berechnung betriebsnah belasteter Hochtemperaturstähle mit einem konstitutiven Werkstoffmodell. Dissertation, Technische Universität Darmstadt, Berichte aus der Werkstofftechnik, Band 4/2007, Shaker Verlag Aachen
- Skelton RP (2003) 5.02—Creep-Fatigue Interactions (Crack Initiation). In: Karihalo I, Milne R, Ritchie B (eds) *Comprehensive structural integrity*. Pergamon, Oxford, pp 25–112
- Sklenička V, Kuchařová K, Král P, Kvapilová M, Svobodová M, Čmakal J (2015) The effect of hot bending and thermal ageing on creep and microstructure evolution in thick-walled P92 steel pipe. *Mater Sci Eng: A* 644:297–309
- Skrzypek J, Ganczarski A (1998) Modelling of material damage and failure of structures. *Foundation of engineering mechanics*. Springer, Berlin
- Skrzypek JJ (1993) *Plasticity and creep*. CRC Press, Boca Raton
- Sosnin OV (1974) Energeticheskii variant teorii polzuchesti i dlitel'noi prochnosti. Polzuchest' i razrushenie neuprochnyayushikhysya materialov (Energetic variant of the creep and long-term strength theories. Creep and fracture of nonhardening materials, in Russ.). *Probl Prochn* 5:45–49
- Sosnin OV, Gorev BV, Nikitenko AF (1986) Energeticheskii variant teorii polzuchesti (Energetic variant of the creep theory, in Russ.). Institut Gidrodinamiki, Novosibirsk
- Stouffer DC, Dame LT (1996) *Inelastic deformation of metals*. John Wiley and Sons, New York
- Straub S (1995) Verformungsverhalten und Mikrostruktur warmfester martensitischer 12%-Chromstähle. Dissertation, Universität Erlangen-Nürnberg, VDI Reihe 5, Nr. 405, Düsseldorf
- Taira S (1962) Lifetime of structures subjected to varying load and temperature. In: Hoff NJ (ed) *Creep in structures*. Springer, Berlin, pp 96–119
- Taira S, Koterazawa R (1962) Dynamic creep and fatigue of an 18-8-Mo-Nb Steel. *Bulletin of JSME* 5(17):15–20
- Taira S, Ohtani R (1986) Teorija vysokotemperaturnoj prochnosti materialov (Theory of high-temperature strength of materials, in Russ.). Metallurgija, Moscow
- Trampczynski WA, Hayhurst DR, Leckie FA (1981) Creep rupture of copper and aluminium under non-proportional loading. *J Mech Phys Solids* 29:353–374
- Trivaudey F, Delobelle P (1993) Experimental study and modelization of creep damage under multi-axial loadings at high temperature. In: Wilshire B, Evans RW (eds) *Creep and fracture of engineering materials and structures*. Institute of Materials, London, pp 137–147
- Tvergaard V (1990) Material failure by void growth to coalescence. *Adv Appl Mech* 27:83–51
- Viswanathan R (1989) *Damage mechanisms and life assessment of high temperature components*. ASM International
- Wang P, Cui L, Scholz A, Linn S, Oechsner M (2014) Multiaxial thermomechanical creep-fatigue analysis of heat-resistant steels with varying chromium contents. *Int J Fatigue* 67:220–227
- Wiese S (2010) *Verformung und Schädigung von Werkstoffen der Aufbau- und Verbindungstechnik: das Verhalten im Mikrobereich*. Springer
- Wiese S, Roellig M, Mueller M, Wolter KJ (2008) The effect of downscaling the dimensions of solder interconnects on their creep properties. *Microelectron Reliab* 48(6):843–850
- Winstone MR (1998) Microstructure and alloy developments in nickel-based superalloys. In: Strang A, Cawley J, Greenwood GW (eds) *Microstructural stability of creep resistant alloys for high temperature plant applications*. Cambridge University Press, Cambridge, pp 27–47
- Wohlfahrt H, Brinkmann D (2001) Consideration of inhomogenities in application of deformation models, describing the inelastic behaviour of welded joints. In: Steck E, Ritter R, Peil U, Ziegen-

- bein A (eds) *Plasticity of metals: experiments, models, computation*. Final Report of the College Research Centre 319, Wiley-VCH, Weinheim, pp 361–382
- Wu R, Sandström R, Seitisleam F (2004) Influence of extra coarse grains on the creep properties of 9 percent CrMoV (P91) steel weldment. *J Eng Mater Technol* 26:87–94
- Yagi K, Merckling G, Kern TU, Irie H, Warlimont H (2004) Creep properties of heat resistant steels and superalloys. Numerical data and functional relationships in science and technology, Landolt-Börnstein—Group VIII Advanced Materials and Technologies. Springer, Berlin
- Yaguchi M, Takahashi Y (2005) Ratchetting of viscoplastic material with cyclic softening, part 1: experiments on modified 9Cr-1Mo steel. *Int J Plast* 21(1):43–65
- Zhang S, Harada M, Ozaki K, Sakane M (2007) Multiaxial creep-fatigue life using cruciform specimen. *Int J Fatigue* 29(5):852–859
- Zolocheskij AA (1988) Kriechen von Konstruktionselementen aus Materialien mit von der Belastung abhängigen Charakteristiken. *Tech Mech* 9:177–184

Chapter 2

Continuum Mechanics in One Dimension

This chapter gives a short introduction to the continuum mechanics applied to the uni-axial stress state. Here we consider a rod to illustrate main ideas of continuum mechanics in a simple, transparent manner, without jungles of tensors. However, to show parallels to the three-dimensional theory we apply the notation of continuum mechanics. For example, we use F to designate the “deformation gradient”, P to designate the Piola-Kirchhoff or engineering stress, etc. Three-dimensional equations will be discussed in Chap. 4.

The present chapter deals with basic equations of continuum mechanics applied to the theory of rods. A rod is a structural member with cross-section dimensions much less than the axial length. Rods can be subjected to different types of loadings including tension (compression), bending and torsion. A deformed configuration of a rod can be described by specifying the deformed rod axis, the actual cross-section area and triads of unit vectors to characterize the actual orientation of cross-sections. To define the deformed line only one coordinate is required. The problem to compute a deformed configuration for given loads is therefore one-dimensional.

Two approaches can be applied to formulate the theory of rods. The first one—called direct—considers a rod as a deformable line. The basic assumption is that every cross section behaves like a rigid body in the sense that translations and cross-section rotations are basic degrees of freedom for every point of the line. The mechanical interactions between two neighboring cross sections are (normal and/or shear) forces and (bending and/or twisting) moments. Basic balance equations of continuum mechanics are applied directly to the deformable line. Direct theories of rods are discussed in Altenbach et al. (2005, 2013), Antman (1995), Green et al. (1974b), Zhilin (2006) among others.

The second approach is based on equations of the three-dimensional continuum mechanics. With cross-section assumptions to the components of displacement vector and/or stress tensor, approximate one-dimensional equations for a rod can be derived, e.g. Green et al. (1974a).

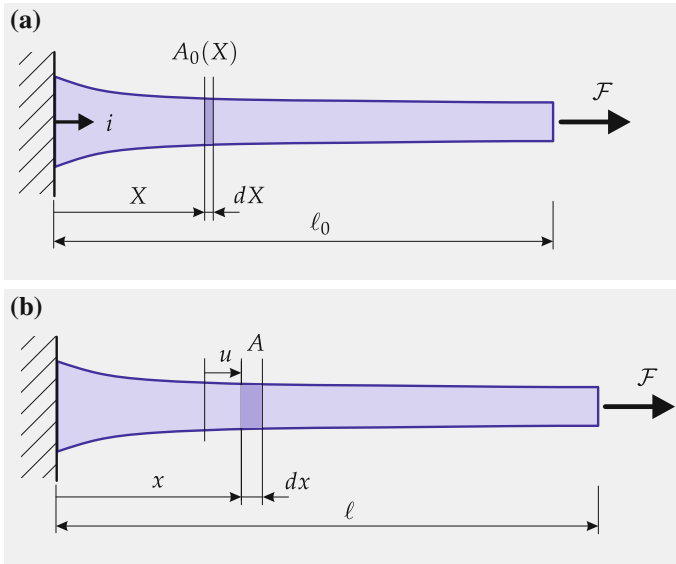


Fig. 2.1 A rod subjected to a tensile force. **a** Reference configuration, **b** actual configuration

In this section we assume that the rod is subjected to tensile (compressive) loading only. Figure 2.1 provides a sketch of a straight rod subjected to a tensile force. Let \mathbf{i} be the unit vector designating the direction of the rod axis, Fig. 2.1a. To describe the positions of cross sections of the rod in the reference configuration the vector $\mathbf{R} = X\mathbf{i}$ with the coordinate X is introduced. The corresponding position in the actual configuration is defined by the vector $\mathbf{r} = x\mathbf{i}$ with the coordinate x .

2.1 Motion, Derivatives, and Deformation

The motion of the rod is defined by the following mapping

$$x = \Phi(X, t) \tag{2.1.1}$$

The basic problem of continuum mechanics is to find the function Φ for all of $0 \leq X \leq \ell_0$, for the given time interval $t_0 \leq t \leq t_n$ as well as for defined external loads and temperature. It is obvious that $X = \Phi(X, t_0)$. The displacement u is defined as it follows (Fig. 2.1b)

$$u = x - X \tag{2.1.2}$$

To analyze the motion it is useful to introduce the rates of change of Φ with respect to the reference coordinate X and time t . The deformation gradient F is defined as follows¹

$$F = \frac{\partial \Phi}{\partial X} \quad (2.1.3)$$

The velocity field v is defined as follows

$$v = \frac{\partial \Phi}{\partial t} = \dot{u} \quad (2.1.4)$$

Within the one-dimensional theory the deformation gradient F is identical with the local stretch λ which is defined as

$$\lambda = \frac{dx}{dX}$$

dX and dx are line elements defined in the infinitesimal neighborhood of a cross section in the reference and actual configurations, respectively. The local strain ε can be defined as follows

$$\varepsilon = \frac{dx - dX}{dX} = \lambda - 1 = \frac{\partial u}{\partial X} \quad (2.1.5)$$

If the material properties and the cross section area do not depend on X then the rod is called homogeneous. The stretch and the strain can be computed as follows

$$\lambda = \frac{\ell}{\ell_0}, \quad \varepsilon = \frac{\ell - \ell_0}{\ell_0} \quad (2.1.6)$$

The formulas (2.1.6) are applied to evaluate strains from experimental data of uniaxial tests. If a rod is non-homogeneous than local strains should be evaluated. In this case a strain gauge should be placed in a position along the rod to provide the local strain value. The length of the strain gauge should be small such that the measured strain could be assumed constant. Otherwise the measured strain would depend on the length of the strain gauge. A similar assumption can be applied to motivate Eq. (2.1.5)—the value of the tested line element dX should be “small enough” such that the strain over dX is constant. This is the basic idea behind the classical continuum mechanics—the notions of infinitesimal volume, area and line elements are introduced such that the quantities like density, stress, strain etc. can be assumed uniform over the considered elements.

Assuming the mapping Φ to be invertible one may introduce the inverse of the deformation gradient as follows

$$F^{-1} = \frac{dX}{dx} \quad (2.1.7)$$

¹The deformation gradient is usually not introduced within the one-dimensional theory of rods. Here we introduce this and other quantities to explain basic ideas of continuum mechanics.

Let f be a field like density, displacement, stress, etc. f can be considered as a function of the coordinate X and time t . This is sometimes called Lagrangian description. Alternatively, one may refer f to the actual coordinate x and time. This kind of description is called spatial or Eulerian. The derivatives of a function f with respect to X and x can be specified as follows

$$\frac{\partial f}{\partial X} \equiv f'^0, \quad \frac{\partial f}{\partial x} \equiv f' \quad (2.1.8)$$

Between the derivatives the obvious relation exists

$$\frac{\partial f}{\partial X} = F \frac{\partial f}{\partial x} \quad \Rightarrow \quad f'^0 = F f' \quad (2.1.9)$$

As the motion Φ is assumed invertible

$$X = \Phi^{-1}(x, t), \quad (2.1.10)$$

the material and the spacial descriptions are equivalent in the sense that if f is known as a function of X and t , one may use the transformation (2.1.10) to find

$$f(X, t) = g(x, t)$$

For example the density ρ can be as a function of the reference coordinate and time or the actual coordinate and time

$$\rho = f(X, t) = g(x, t)$$

With Eqs. (2.1.3) and (2.1.4) the derivative of the velocity with respect to the reference coordinate can be computed as follows

$$v'^0 = \dot{F} \quad (2.1.11)$$

With (2.1.9) the derivative of the velocity with respect to the actual coordinate is

$$v' = \dot{F} F^{-1} \quad (2.1.12)$$

Assuming that $f(x)$ is continuous for $a \leq x \leq b$ the fundamental theorem of integral calculus provides

$$\int_a^b f'(x) dx = f(b) - f(a) \quad (2.1.13)$$

If $f(x)$ has n jumps at points $x_k, k = 1, 2, \dots, n$ within $a \leq x \leq b$ and $f'(x)$ is continuous between the jump points then

$$\int_a^b f'(x)dx = f(b) - f(a) + \sum_{k=1}^n \llbracket f(x_k) \rrbracket, \quad \llbracket f(x_k) \rrbracket \equiv f(x_k^+) - f(x_k^-) \quad (2.1.14)$$

Assume that the velocity field is given as a function of the spatial coordinate and the time, i.e. $v(x, t)$. The material time derivative of a field $f(x, t)$ is

$$\frac{d}{dt}f = \frac{\partial}{\partial t}f + vf' \quad (2.1.15)$$

2.2 Conservation of Mass

The mass of an infinitesimal part of the rod is

$$dm = \rho A dx = \rho_0 A_0 dX, \quad (2.2.16)$$

where ρ and ρ_0 is the density in the actual and the reference configurations, respectively. With Eq.(2.1.7) the conservation of mass (2.2.16) takes the form

$$F\rho A = \rho_0 A_0 \quad (2.2.17)$$

Introducing the change in the volume

$$J = \frac{dV}{dV_0} = \frac{A dx}{A_0 dX} = \frac{A}{A_0} F, \quad (2.2.18)$$

where dV and dV_0 are infinitesimal volume elements of the rod in the actual and reference configurations, respectively, the conservation of mass (2.2.16) yields

$$\frac{\rho_0}{\rho} = J \quad (2.2.19)$$

It is obvious that $J > 0$ and if $\rho = \rho_0$ one obtains $J = 1$.

2.3 Balance of Momentum

The momentum of an infinitesimal part of the rod is

$$dp = v dm = v\rho A dx$$

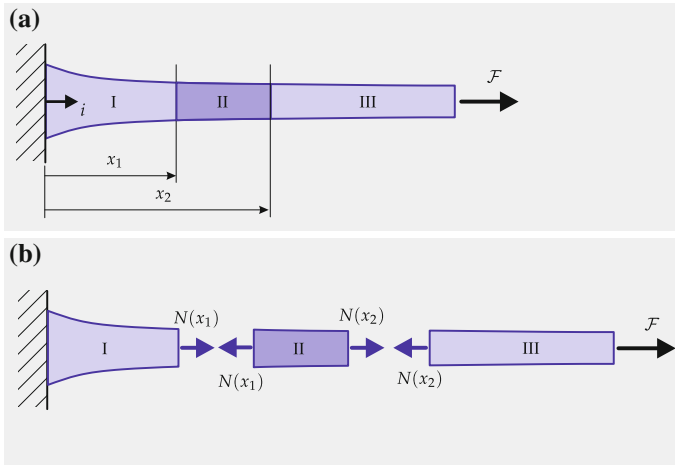


Fig. 2.2 Internal forces in a rod. **a** Rod in the actual configuration and two cutting planes, **b** free-body diagrams visualizing internal forces

Consider a part of the rod, for example, part II, Fig. 2.2b. The momentum for this part in the actual configuration is

$$p_{\text{II}} = \int_{x_1}^{x_2} v \rho A dx \quad (2.3.20)$$

The balance of momentum or the first law of dynamics states that the rate of change of momentum of a body is equal to the total force acting on the body. To introduce the forces acting on the part II of the rod let us cut it by two cross sections with the coordinates x_1 and x_2 . The parts I and III belong to the environment of the part II and the corresponding mechanical actions can be modeled by two forces: $\mathbf{N}_{\text{I-II}}$ —the action of the part I on the part II and $\mathbf{N}_{\text{III-II}}$ the action of the part III on the part II. Similarly, the actions on the parts I and III can be introduced. For example, $\mathbf{N}_{\text{II-I}}$ is the action of the part II on the part I. The following abbreviations can be introduced

$$\begin{aligned} \mathbf{N}_{\text{II-I}} &= \mathbf{N}_{(i)}(x_1) = N(x_1)\mathbf{i}, \\ \mathbf{N}_{\text{I-II}} &= \mathbf{N}_{(-i)}(x_1) = -N(x_1)\mathbf{i}, \\ \mathbf{N}_{\text{III-II}} &= \mathbf{N}_{(i)}(x_2) = N(x_2)\mathbf{i}, \\ \mathbf{N}_{\text{II-III}} &= \mathbf{N}_{(-i)}(x_2) = -N(x_2)\mathbf{i} \end{aligned} \quad (2.3.21)$$

With the free-body diagram presented in Fig. 2.2 the balance of momentum for the part II is²

$$\frac{d}{dt} \int_{x_1}^{x_2} v \rho A dx = N(x_2) - N(x_1) \quad (2.3.22)$$

²Body forces like the force of gravity are not included here for the sake of brevity.

With the fundamental theorem of integral calculus (2.1.13)³

$$N(x_2) - N(x_1) = \int_{x_1}^{x_2} N' dx \quad (2.3.23)$$

Applying the mass conservation equation (2.2.16) one may evaluate the rate of change of momentum as follows

$$\frac{d}{dt} \int_{x_1}^{x_2} v \rho A dx = \frac{d}{dt} \int_{X_1}^{X_2} v \rho_0 A_0 dX = \int_{x_1}^{x_2} \dot{v} \rho A dx \quad (2.3.24)$$

With Eqs. (2.3.23) and (2.3.24) the integral form of the balance of momentum is

$$\int_{x_1}^{x_2} (\dot{v} \rho A - N') dx = 0 \quad (2.3.25)$$

Equation (2.3.25) is valid for any part of the rod. Since x_1 and x_2 are arbitrary, the integral (2.3.25) is zero if

$$\rho A \dot{v} = N' \quad (2.3.26)$$

Multiplying both parts of Eq. (2.3.26) by F yields

$$F \rho A \dot{v} = F N' \quad (2.3.27)$$

With the conservation of mass (2.2.17) and the relation between the derivatives (2.1.9), Eq. (2.3.27) takes the following form

$$\rho_0 A_0 \dot{v} = N'^0 \quad (2.3.28)$$

2.4 Balance of Energy

The total energy E for any part of the rod is defined as the sum of the kinetic energy K and the internal energy U as follows

$$E = K + U, \quad K = \int_{x_1}^{x_2} \rho \mathcal{K} A dx, \quad U = \int_{x_1}^{x_2} \rho \mathcal{U} A dx, \quad \mathcal{K} = \frac{1}{2} v^2, \quad (2.4.29)$$

³Here and in the following derivations we assume that N and other field variables are smooth functions. In the case of finite jumps one should apply Eq. (2.1.14) and introduce the jump conditions.

where \mathcal{K} and \mathcal{U} are densities of the kinetic and the internal energy, respectively. The energy balance equation or the first law of thermodynamics states that the rate of change of the energy of a body is equal to the mechanical power plus the rate of change of non-mechanical energy, for example heat, supplied into the body. The energy balance equation is

$$\frac{d}{dt}E = L + Q, \quad (2.4.30)$$

where L is the mechanical power and Q is the rate of change of non-mechanical energy supply. The mechanical power of internal forces (2.3.21) is defined as follows

$$L = N(x_2)v(x_2) - N(x_1)v(x_1) = \int_{x_1}^{x_2} (Nv)' dx \quad (2.4.31)$$

The rate of change of energy supply through the cross sections of the parts I, II and III of the rod can be defined by analogy to Eqs. (2.3.21)

$$\begin{aligned} Q_{\text{II-I}} &= Q_{(i)}(x_1) = -Q(x_1), \\ Q_{\text{I-II}} &= Q_{(-i)}(x_1) = Q(x_1), \\ Q_{\text{III-II}} &= Q_{(i)}(x_2) = -Q(x_2), \\ Q_{\text{II-III}} &= Q_{(-i)}(x_2) = Q(x_2) \end{aligned} \quad (2.4.32)$$

The rate of change of the energy supply through the volume of the part II is

$$Q_{V_{\text{II}}} = \int_{x_1}^{x_2} \rho r A dx,$$

where r is the density of the energy supply. The total rate of energy supply into the part II is

$$Q(x_1) - Q(x_2) + \int_{x_1}^{x_2} \rho r A dx = \int_{x_1}^{x_2} (-Q' + \rho r A) dx \quad (2.4.33)$$

With Eqs. (2.4.29), (2.4.31) and (2.4.33) the energy balance equation (2.4.30) takes the form

$$\frac{d}{dt} \int_{x_1}^{x_2} \left(\rho \frac{1}{2} v^2 + \rho \mathcal{U} \right) A dx = \int_{x_1}^{x_2} (N'v + Nv' - Q' + \rho r A) dx \quad (2.4.34)$$

With the mass conservation equation (2.2.16) the rate of change of the total energy can be evaluated as follows

$$\begin{aligned}
\frac{d}{dt} \int_{x_1}^{x_2} (\rho \frac{1}{2} v^2 + \rho \mathcal{U}) A dx &= \frac{d}{dt} \int_{X_1}^{X_2} (\rho_0 \frac{1}{2} v^2 + \rho_0 \mathcal{U}) A_0 dX \\
&= \int_{X_1}^{X_2} (\dot{v} v + \dot{\mathcal{U}}) \rho_0 A_0 dX = \int_{x_1}^{x_2} (\dot{v} v + \dot{\mathcal{U}}) \rho A dx
\end{aligned} \tag{2.4.35}$$

The energy balance equation (2.4.34) takes the following form

$$\int_{x_1}^{x_2} [(\rho A \dot{v} - N')v + \rho A \dot{\mathcal{U}} - Nv' + Q' - \rho r A] dx = 0 \tag{2.4.36}$$

With the balance of momentum (2.3.26), Eq.(2.4.34) is simplified to

$$\int_{x_1}^{x_2} (\rho A \dot{\mathcal{U}} - Nv' + Q' - \rho r A) dx = 0 \tag{2.4.37}$$

As x_1 and $x_2 > x_1$ are arbitrary coordinates, the local (per unit length of the rod) form of the energy balance is

$$\rho A \dot{\mathcal{U}} = Nv' - Q' + \rho r \tag{2.4.38}$$

Multiplying both sides of (2.4.38) by F and using the conservation of mass (2.2.17) as well as the relation between the derivatives (2.1.9) provides the local form of the energy balance per unit length of the rod in the reference configuration

$$\rho_0 A_0 \dot{\mathcal{U}} = Nv'^0 - Q'^0 + \rho_0 A_0 r \tag{2.4.39}$$

2.5 Entropy Inequality

For historical overview of thermodynamics principles we refer to Ericksen (1998), Truesdell (1984), Müller (2007). The second law of thermodynamics states that the entropy production of a body is non-negative. This statement is given as the Clausius-Planck inequality

$$\frac{d}{dt} S - \frac{Q}{T} \geq 0, \tag{2.5.40}$$

where S is the entropy and T is the absolute temperature. The entropy of the part II of the rod (Fig. 2.2) is defined as follows

$$S = \int_{x_1}^{x_2} \rho \mathcal{S} A dx, \quad (2.5.41)$$

where \mathcal{S} is the entropy density. With Eqs. (2.4.32) and (2.1.13)

$$\left(\frac{Q}{T}\right)_{II} = -\frac{Q(x_2)}{T(x_2)} + \frac{Q(x_1)}{T(x_1)} + \int_{x_1}^{x_2} \frac{\rho Ar}{T} dx = -\int_{x_1}^{x_2} \left[\left(\frac{Q}{T}\right)' - \frac{\rho Ar}{T} \right] dx \quad (2.5.42)$$

Inserting (2.5.41) and (2.5.42) into (2.5.40) provides the integral form of the entropy inequality

$$\int_{x_1}^{x_2} \left[\rho \dot{\mathcal{S}} A + \left(\frac{Q}{T}\right)' - \frac{\rho Ar}{T} \right] dx \geq 0 \quad (2.5.43)$$

Since x_1 and $x_2 > x_1$ are arbitrary the local form of the entropy inequality can be given as follows

$$\rho \dot{\mathcal{S}} A \geq -\left(\frac{Q}{T}\right)' + \frac{\rho r A}{T} \quad (2.5.44)$$

This is a one-dimensional version of the Clausius-Duhem inequality. Multiplying the both sides of (2.5.44) by T it can be formulated as follows

$$\rho \dot{\mathcal{S}} T A \geq -Q' + Q \frac{T'}{T} + \rho r A \quad (2.5.45)$$

2.6 Dissipation Inequality, Free Energy, and Stress

From the energy balance Eq. (2.4.38) it follows

$$\rho Ar - Q' = \rho A \dot{U} - N v' \quad (2.6.46)$$

Inserting Eq. (2.6.46) into the entropy inequality (2.5.45) yields the dissipation inequality

$$N v' - \rho A \dot{U} + \rho \dot{\mathcal{S}} T A - Q \frac{T'}{T} \geq 0 \quad (2.6.47)$$

Dividing (2.6.47) by the cross section area provides the following local form of the dissipation inequality

$$\sigma v' - \rho \dot{U} + \rho \dot{\mathcal{S}} T - q \frac{T'}{T} \geq 0, \quad \sigma = \frac{N}{A}, \quad q = \frac{Q}{A}, \quad (2.6.48)$$

where σ is called stress or true stress and q is the heat supply through the infinitesimal cross section. Introducing the Helmholtz free energy density $\Phi = \mathcal{U} - ST$ the dissipation inequality (2.6.48) takes the following form

$$\sigma v' - \rho \dot{\Phi} - \rho S \dot{T} - q \frac{T'}{T} \geq 0 \quad (2.6.49)$$

With Eq.(2.1.12) it follows that

$$\sigma \dot{F} F^{-1} - \rho \dot{\Phi} - \rho S \dot{T} - q \frac{T'}{T} \geq 0 \quad (2.6.50)$$

Multiplying both sides of (2.6.47) by F and using the conservation of mass (2.2.17) as well as the relation between the derivatives (2.1.9), the local form of the dissipation inequality per unit length of the rod in the reference configuration can be obtained

$$N v'^0 - \rho_0 A_0 \dot{\mathcal{U}} + \rho_0 A_0 \dot{S} T - Q \frac{T'^0}{T} \geq 0 \quad (2.6.51)$$

Dividing by A_0 yields

$$P v'^0 - \rho_0 \dot{\mathcal{U}} + \rho_0 \dot{S} T - \tilde{q} \frac{T'^0}{T} \geq 0, \quad P = \frac{N}{A_0}, \quad \tilde{q} = \frac{Q}{A_0} \quad (2.6.52)$$

where P is the engineering stress and \tilde{q} is the heat flow through the infinitesimal cross section of the rod in the reference state. In terms of the free energy the inequality takes the following form

$$P v'^0 - \rho_0 \dot{\Phi} - \rho_0 S \dot{T} - \tilde{q} \frac{T'^0}{T} \geq 0 \quad (2.6.53)$$

With Eq.(2.1.11) the velocity derivative can be replaced by the rate of the deformation gradient leading to

$$P \dot{F} - \rho_0 \dot{\Phi} - \rho_0 S \dot{T} - \tilde{q} \frac{T'^0}{T} \geq 0 \quad (2.6.54)$$

Taking into account that the normal force is $N = P A_0 = \sigma A$ the following relation between the stress measures can be established

$$P A_0 = \sigma J A_0 F^{-1} \quad \Rightarrow \quad P = \sigma J F^{-1} \quad (2.6.55)$$

Similarly, with the heat flux $Q = q A = \tilde{q} A_0$

$$\tilde{q} = q J F^{-1} \quad (2.6.56)$$

References

- Altenbach H, Naumenko K, Zhilin PA (2005) A direct approach to the formulation of constitutive equations for rods and shells. In: Pietraszkiewicz W, Szymczak C (eds) *Shell Structures: Theory and Applications*, Taylor & Francis, Leiden, pp 87–90
- Altenbach H, Birsan M, Eremeyev VA (2013) Cosserat-type rods. In: Eremeyev VA, Altenbach H (eds) *Generalized Continua from the Theory to Engineering Applications*, Springer, pp 179–248
- Antman S (1995) *Nonlinear Problems of Elasticity*. Springer, Berlin
- Ericksen J (1998) *Introduction to the Thermodynamics of Solids*, Applied Mathematical Sciences, vol 131. Springer
- Green AE, Naghdi PM, Wrenner ML (1974a) On the theory of rods. I. Derivations from the three-dimensional equations. *Proc R Soc Lond A Math Phys Sci* 337(1611):451–483
- Green AE, Naghdi PM, Wrenner ML (1974b) On the theory of rods. II. Developments by direct approach. *Proc R Soc Lond A Math Phys Sci* 337(1611):485–507
- Müller I (2007) *A history of thermodynamics: the doctrine of energy and entropy*. Springer
- Truesdell C (1984) *Rational Thermodynamics*, 2nd edn. Springer, New York
- Zhilin PA (2006) Nonlinear theory of thin rods. In: Indeitsev D, Ivanova E, Krivtsov A (eds) *Advanced Problems in Mechanics*, vol 2. Nestor, St Petersburg, pp 227–249

Chapter 3

Elementary Uni-axial Constitutive Models

Basic information on the material behavior is usually obtained from a uni-axial test. The development of a constitutive model for a uni-axial stress state is the first step to the general structural analysis. This is a motivation to apply equations discussed in this chapter to develop constitutive models and to analyze restrictions to the response functions and material properties.

Materials are often subjected to complex thermo-mechanical loading conditions. To analyze material behavior under such conditions a combined model for thermo(visco)elasto-plasticity considering hardening, softening, damage and other processes is required. Such models are proposed and discussed in the literature. The idea of this chapter is to introduce elementary constitutive models, useful for the analysis of material behavior at high temperature.

3.1 Heat Transfer

Assume that the rod is mechanically isolated such that the local power of the internal force $\sigma \dot{F} F^{-1}$ in (2.6.50) is zero. This can be accomplished by keeping the deformation constant, for example, by setting $F = 1$. The internal force N and consequently the stress σ are not zeros and arise as reactions on the kinematical constraint. The inequality (2.6.50) simplifies to

$$-\rho \dot{\Phi} - \rho S \dot{T} - q \frac{T'}{T} \geq 0 \tag{3.1.1}$$

The independent variables in Eq. (3.1.1) are ρ , T and T' . Instead of the density ρ one may take the change in volume $J = \rho_0/\rho$ as the independent variable. The conjugate variables (sometimes called thermodynamic forces) are S and q . These can be assumed to be the functions of the independent variables, i.e.

$$S = S(J, T, T'), \quad q = q(J, T, T')$$

Consequently, the free energy Φ has the same arguments

$$\begin{aligned} \Phi &= \Phi(J, T, T') \\ \dot{\Phi} &= \frac{\partial \Phi}{\partial J} \dot{J} + \frac{\partial \Phi}{\partial T} \dot{T} + \frac{\partial \Phi}{\partial T'} \dot{T}' \end{aligned} \quad (3.1.2)$$

With Eq. (3.1.2) the inequality (3.1.1) takes the form

$$-\rho \frac{\partial \Phi}{\partial J} \dot{J} - \rho \left(\frac{\partial \Phi}{\partial T} + \mathcal{S} \right) \dot{T} - \rho \frac{\partial \Phi}{\partial T'} \dot{T}' - q \frac{T'}{T} \geq 0 \quad (3.1.3)$$

Inequality (3.1.3) can be formulated as follows

$$A \dot{J} + B \dot{T} + C \dot{T}' + D \geq 0, \quad (3.1.4)$$

where the coefficients

$$A = -\rho \frac{\partial \Phi}{\partial J}, \quad B = -\rho \left(\frac{\partial \Phi}{\partial T} + \mathcal{S} \right), \quad C = -\rho \frac{\partial \Phi}{\partial T'}, \quad D = -q \frac{T'}{T} \quad (3.1.5)$$

do not depend on the rates of independent variables. For arbitrary \dot{J} , \dot{T} and \dot{T}' the inequality is only satisfied if $A = 0$, $B = 0$, $C = 0$ and $D \geq 0$. From

$$\rho \frac{\partial \Phi}{\partial J} = 0, \quad \rho \frac{\partial \Phi}{\partial T'} = 0$$

it follows, that the free energy depends on the temperature only. Furthermore we obtain the constitutive equation for the entropy

$$\mathcal{S} = -\frac{\partial \Phi}{\partial T} \quad (3.1.6)$$

and the inequality

$$-q \frac{T'}{T} \geq 0 \quad (3.1.7)$$

The inequality (3.1.7) is satisfied with the Fourier law of heat conduction

$$q = -\kappa T', \quad (3.1.8)$$

where $\kappa(T) > 0$ is the thermal conductivity. The functions $\kappa(T)$ and $\mathcal{S}(T)$ must be identified experimentally. To discuss the identification procedure let us derive the

heat transfer equation. Neglecting the mechanical power the local energy balance (2.4.38) takes the form

$$\rho A \dot{\mathcal{U}} = -Q' + \rho A r \quad (3.1.9)$$

With $\mathcal{U} = \Phi + \mathcal{S}T$ and Eq. (3.1.6) the internal energy is the function of the temperature only. For the heat supply r assume the following constitutive equation

$$\rho r = h(T_e - T), \quad (3.1.10)$$

where $h(T) > 0$ and T_e is the temperature of the environment. Equation (3.1.10) is known as the Newton law of cooling. With Eqs. (3.1.8) and (3.1.10) the energy balance equation (3.1.9) takes the form

$$\rho c(T) \dot{T} = \frac{1}{A} (kAT')' + h(T_e - T), \quad c(T) = \frac{d\mathcal{U}}{dT}, \quad (3.1.11)$$

where $c(T)$ is the heat capacity. For a rod with the constant cross section area this simplifies to

$$\rho c(T) \dot{T} = (kT')' + h(T_e - T) \quad (3.1.12)$$

Furthermore, assuming that the expected temperature difference is small, one may linearize the temperature functions c , k and h about a reference temperature T_0 leading to the linear differential equation

$$\rho c_0 \dot{T} = k_0 T'' + h_0 (T_e - T), \quad (3.1.13)$$

where $c_0 = c(T_0)$, $k_0 = k(T_0)$ and $h_0 = h(T_0)$. Equation (3.1.13) is known as the heat equation or diffusion equation. The solution for the given initial condition and the boundary conditions with respect to the heat flux or the temperature provides the time-dependent temperature field in the rod. Several methods exist to identify the functions c , k and h , which are based on temperature measurements and solutions of the heat equation (3.1.13). For details the reader may consult textbooks on heat transfer and thermodynamics, for example, Granger (1994), Müller (2007), Nellis and Klein (2009).

Once the heat capacity $c(T)$ is identified the constitutive equation (3.1.6) allows us to compute the entropy as follows

$$\mathcal{S}(T) = \int_{T_0}^T \frac{c(\xi)}{\xi} d\xi$$

3.2 Thermo-elasticity

Within the framework of elasticity the basic assumption is that the stress is a function of the strain. This can be related to experimental observations from the tensile test, Sect. 1.1. After the loading and subsequent unloading within the elastic range the specimen takes the original length. The elastic behavior is reversible—no hysteresis loop is observable if the specimen is subjected to a closed cycle of strain under adiabatic or isothermal conditions.

Let us assume that the stress and consequently the free energy are functions of the following arguments

$$\sigma = \sigma(F, J, T, T') \Rightarrow \Phi = \Phi(F, J, T, T')$$

Then the inequality (2.6.50) takes the following form

$$\left(\sigma F^{-1} - \rho \frac{\partial \Phi}{\partial F} \right) \dot{F} - \rho \frac{\partial \Phi}{\partial J} \dot{J} - \rho \left(\frac{\partial \Phi}{\partial T} + \mathcal{S} \right) \dot{T} - \rho \frac{\partial \Phi}{\partial T'} \dot{T}' - q \frac{T'}{T} \geq 0 \quad (3.2.14)$$

The left hand side of the inequality (3.2.14) is a linear function of rates of independent variables. Therefore the inequality is satisfied if the following conditions are met (see Sect. 3.1 for a more detailed analysis)

$$\sigma = \rho F \frac{\partial \Phi}{\partial F}, \quad \frac{\partial \Phi}{\partial J} = 0, \quad \mathcal{S} = -\frac{\partial \Phi}{\partial T}, \quad \frac{\partial \Phi}{\partial T'} = 0, \quad -q \frac{T'}{T} \geq 0 \quad (3.2.15)$$

The first condition in Eq. (3.2.15) is the constitutive equation for the stress. With

$$F \frac{\partial \Phi(F)}{\partial F} = \frac{\partial \Phi(\varepsilon_H)}{\partial \varepsilon_H}, \quad \varepsilon_H = \ln F = \ln \lambda,$$

where ε_H is the Hencky strain (sometimes called true strain) and Eq. (2.2.19) it can be formulated as follows

$$\sigma = \rho \frac{\partial \Phi}{\partial \varepsilon_H} = \frac{\rho}{\rho_0} \frac{\partial \rho_0 \Phi}{\partial \varepsilon_H} = \frac{1}{J} \frac{\partial \rho_0 \Phi}{\partial \varepsilon_H} \quad (3.2.16)$$

From Eqs. (3.2.15) and (3.2.16) it follows that the free energy density must be formulated as a function of the Hencky strain and the temperature. For isothermal conditions, i.e. for $T(x, t) = T_0$ the work done by the stress $J\sigma$ on the infinitesimal change of the Hencky strain is the total differential of the strain energy density function

$$J\sigma d\varepsilon_H = d(\rho_0 \Phi) \quad (3.2.17)$$

The stress measure $J\sigma$ is called Kirchhoff stress. For adiabatic processes, i.e. for processes without heat transfer with the environment, one may use the local energy balance equation (2.4.38) to show that

$$J\sigma d\varepsilon_H = d(\rho_0\mathcal{U}) \quad (3.2.18)$$

Equations (3.2.17) and (3.2.18) are widely used in the theory of elasticity (Hahn 1985; Lurie 2010; Timoshenko and Goodier 1951) and structural mechanics (Altenbach et al. 1998; Gould 1988; Reddy 1997; Szilard 1974; Timoshenko and Woinowsky-Krieger 1959) for the formulation of variational principles.

The starting point for the analysis was the inequality (2.6.50). One may use the dissipation inequality (2.6.54) defined with respect to the reference configuration to find the relationship between the engineering stress P and the corresponding strain measure. Here we use the first equation in (3.2.15) and the relationship between the stress measures (2.6.55) to derive the following equation

$$P = \frac{\partial \rho_0 \Phi(F)}{\partial F} \quad (3.2.19)$$

To find a particular form of the strain energy density a constitutive equation for the stress is required. For many structural materials, for example steel, the elastic range is observed for small values of strain ε such that $\varepsilon^2 \ll \varepsilon < 1$. Furthermore, in this range the stress is proportional to the strain. In this case it follows $\varepsilon_H \approx \varepsilon$ and Eq. (3.2.15) can be linearized leading to

$$\sigma = \frac{\partial \rho_0 \Phi(\varepsilon)}{\partial \varepsilon} \quad (3.2.20)$$

Furthermore since $\lambda = 1 + \varepsilon$ one may use Eq. (3.2.19) to derive the linearized relation for the engineering stress P . Within the linear elasticity the difference between the stress measures is negligible. To find an expression for the free energy density we use the following linear constitutive equation

$$\sigma = E(\varepsilon - \varepsilon^{\text{th}}), \quad \varepsilon^{\text{th}} = \alpha_{\text{th}}\Theta, \quad \Theta = T - T_0, \quad (3.2.21)$$

where E is the Young's modulus and α_{th} is the thermal expansion coefficient. With Eq. (3.2.20)

$$\rho_0 \Phi = \frac{1}{2} E \varepsilon^2 - E \alpha_{\text{th}} \Theta \varepsilon + f(T) \quad (3.2.22)$$

To determine the function $f(T)$ compute

$$\frac{\partial \mathcal{U}}{\partial T} = T \frac{\partial S}{\partial T} = -T \frac{\partial^2 \oplus}{\partial T^2} \quad (3.2.23)$$

With Eq. (3.2.22) this results in

$$\frac{\partial \mathcal{U}}{\partial T} = \underline{-\frac{1}{\rho_0} T \frac{d^2 f}{dT^2}} - \frac{1}{2\rho_0} T \varepsilon^2 \frac{d^2 E}{dT^2} - \frac{1}{\rho_0} T \varepsilon \frac{d^2}{dT^2} (E \alpha_{\text{th}} \Theta)$$

The underlined term is the heat capacity without deformation, as defined by Eq. (3.1.11). Therefore the function f can be found from the following equation

$$-\frac{1}{\rho_0} T \frac{d^2 f}{dT^2} = c(T)$$

With Eqs. (3.1.10), (3.2.22) and (3.2.23) the energy balance equation (2.4.38) takes the following form

$$-\frac{\partial^2(\rho_0 \Phi)}{\partial T^2} \dot{T} - \frac{\partial^2(\rho_0 \Phi)}{\partial T \partial \varepsilon} \dot{\varepsilon} = \frac{1}{A} (kAT')' + h(T_e - T) \quad (3.2.24)$$

Assuming that the expected temperature difference is small one may linearize the functions $E(T)$, $\alpha_{\text{th}}(T)$, $c(T)$ and $h(T)$ about the reference temperature T_0 . The heat transfer equation (3.2.24) simplifies to

$$c_0 \dot{T} + E_0 \alpha_{\text{th}_0} \dot{\varepsilon} = \frac{1}{A} (k_0 AT')' + h_0 (T_e - T), \quad (3.2.25)$$

where $E_0 = E(T_0)$ and $\alpha_{\text{th}_0} = \alpha_{\text{th}}(T_0)$. The second term in the left-hand side of Eq. (3.2.25) is usually small and can be neglected (Landau et al. 1986). Therefore, within the linearized theory the deformation has minor influence on the heat transfer such that the heat equation can be solved independently providing the temperature $T(x, t)$. The balance of momentum (2.3.26) with the constitutive equation (3.2.21) yields

$$\rho A \ddot{u} = [EA(u' - \alpha_{\text{th}} \Theta)]'$$

3.3 Non-linear Viscosity, Viscoplasticity, and Rigid Plasticity

Assume that the stress σ is the function of the deformation rate $\dot{F}F^{-1} = \dot{\varepsilon}_{\text{H}}$ and the temperature. Furthermore, assume that the mechanical power $\sigma \dot{F}F^{-1}$ does not influence the free energy directly. The free energy and the entropy are then the functions of the temperature only. Then the inequality (2.6.50) takes the following form

$$-\rho \left(\frac{\partial \Phi}{\partial T} + \mathcal{S} \right) \dot{T} + \sigma \dot{\varepsilon}_{\text{H}} - q \frac{T'}{T} \geq 0 \quad (3.3.26)$$

The inequality (3.3.26) has the form $A(T)\dot{T} + B(T, \dot{\epsilon}_H) \geq 0$. For arbitrary (positive and negative) rates of temperature it can only be satisfied if $A = 0$ and $B \geq 0$. This leads to the constitutive equation for the entropy

$$\mathcal{S} = -\frac{\partial \Phi}{\partial T} \quad (3.3.27)$$

and the dissipation inequality

$$\sigma \dot{\epsilon}_H - q \frac{T'}{T} \geq 0 \quad (3.3.28)$$

Assuming that the heat flux q does not depend on the strain rate results in two inequalities

$$\sigma \dot{\epsilon}_H \geq 0, \quad -q \frac{T'}{T} \geq 0 \quad (3.3.29)$$

For the stress one may assume the constitutive equation in the form

$$\sigma(\dot{\epsilon}_H, T) = g_{\dot{\epsilon}_H}(|\dot{\epsilon}_H|) \text{sgn}(\dot{\epsilon}_H) g_T(T), \quad (3.3.30)$$

where $g_{\dot{\epsilon}_H}(|\dot{\epsilon}_H|) \geq 0$ is a function of strain rate with $g_{\dot{\epsilon}_H}(0) = 0$ and $g_T(T) > 0$ is a function of temperature. Both the functions can be identified from stress-strain diagrams in the saturation (steady state) regime, Fig. 1.2 by taking experimental data for the stress σ_{ss} as a function of the strain rate and the temperature. By inverting Eq. (3.3.31) the constitutive equation for the strain rate can be formulated as follows

$$\dot{\epsilon}_H = f_\sigma(|\sigma|) \text{sgn}(\sigma) f_T(T), \quad (3.3.31)$$

where $f_\sigma(|\sigma|) \geq 0$ is a function of stress with $f_\sigma(0) = 0$ and $f_T(T)$ is a function of temperature. These functions can be identified from experimental data of secondary (steady-state) creep, Fig. 1.5. To this end the minimum creep rates should be taken from experimental creep curves for different stress and temperature levels. Examples for stress and temperature functions include the power-law function of stress and the Arrhenius function of temperature

$$f_\sigma(\sigma) = \dot{\epsilon}_0 \left(\frac{\sigma}{\sigma_0} \right)^n, \quad f_T(T) = \exp\left(-\frac{Q}{RT}\right), \quad (3.3.32)$$

where ϵ_0 , σ_0 , n and Q are constants to be identified from experimental data and R is the universal gas constant. Examples for experimental data are shown in Fig. 1.8 for steels. With functions (3.3.32) the constitutive equation for the strain rate is

$$\dot{\epsilon}_H = \dot{\epsilon}_0 \exp\left(-\frac{Q}{RT}\right) \left(\frac{|\sigma|}{\sigma_0}\right)^n \text{sgn}(\sigma) \quad (3.3.33)$$

or in the inverse form

$$\sigma = \sigma_0 \exp\left(\frac{Q}{nRT}\right) \left(\frac{|\dot{\epsilon}_H|}{\dot{\epsilon}_0}\right)^{\frac{1}{n}} \text{sgn}(\dot{\epsilon}_H) \quad (3.3.34)$$

Let us note that constitutive equations (3.3.33) and/or (3.3.34) are applicable for narrow ranges of stress, strain rate and temperature. For example, for metals the activation energy decreases and the power exponent n increases with a decrease of temperature. To capture wide stress and temperature ranges advanced functions are required. Functions of stress (strain rate) and temperature will be discussed in Sect. 5.4.4.

For $n = 1$ the model of a linear viscous fluid follows from Eq. (3.3.34). For large values of n the strain rate sensitivity of stress according to Eq. (3.3.34) becomes negligible. For $n \rightarrow \infty$ the constitutive equation of rate-independent plasticity (St. Venant model) with the yield stress $\sigma_y = \sigma_0$ follows from Eq. (3.3.34)

$$\begin{cases} |\sigma| - \sigma_y \leq 0, & \text{if } \dot{\epsilon}_H = 0, \\ \sigma = \sigma_y \text{sgn} \dot{\epsilon}_H, & \text{if } \dot{\epsilon}_H \neq 0 \end{cases} \quad (3.3.35)$$

The inverse form of the rigid plasticity model is

$$\dot{\epsilon}_H = \dot{\lambda} \text{sgn} \sigma \quad \begin{cases} \dot{\lambda} = 0, & \text{if } |\sigma| - \sigma_y < 0, \\ \dot{\lambda} \geq 0, & \text{if } |\sigma| - \sigma_y = 0 \end{cases} \quad (3.3.36)$$

In rheology and theory of materials Eq. (3.3.30) is classified as a constitutive equation for non-linear viscous fluid, or non-linear viscous element, see for example Giesekus (1994), Krawietz (1986), Palmov (1998), Reiner (1969). On the other hand, for large values of n the model (3.3.34) is close to the model of rate-independent plasticity. Functions f_σ and f_T can be formulated such that experimental data including viscous flow and plasticity can be described. Therefore a model like (3.3.30) can be classified as viscoplasticity model. For example, viscoplasticity models proposed by Krempl (1996, 1999) do not contain the yield condition and are based on functions like (3.3.30). This definition of viscoplasticity may contradict again the classification in the rheology, where the viscoplastic model is a connection of viscous and rigid plastic elements.

The inelastic deformation of crystalline materials can be explained by dislocation glide and dislocation climb (Frost and Ashby 1982; Nabarro and de Villiers 1995). The glide motion of dislocations dominates at lower homologous temperatures and higher stress levels, while the climb of dislocations over obstacles is important in high-temperature regimes and moderate stress levels. From this point of view, the model like (3.3.30) can be classified as a model of high-temperature plasticity, as preferred in the materials science, see for example Ilshner (1973). In this book we classify the model like (3.3.30) as a model for high-temperature plasticity.

Multi-axial versions of the Eq. (3.3.30) are used in the analysis of hot deformation processes of metals, for example, friction welding (Schmicker et al. 2013, 2015). Constitutive equation (3.3.31) is used for the structural analysis in the steady-state creep range (Altenbach et al. 2008a; Boyle 2012; Naumenko et al. 2009).

3.4 Elasto-plasticity

Assume that the mechanical power $\mathcal{L} = \sigma \dot{F} F^{-1}$ can be additively decomposed in two parts $\mathcal{L} = \mathcal{L}_s + \mathcal{L}_d$ with

$$\mathcal{L}_s = \sigma_s \dot{F}_s F_s^{-1}, \quad \mathcal{L}_d = \sigma_d \dot{F}_d F_d^{-1},$$

where σ_s and σ_d are stress-like variables and F_s and F_d are deformation-like variables. Assume that σ_s depends only on the deformation-like variables and the temperature, while σ_d depends on the deformation rates and the temperature.¹ This decomposition is used to define a part of the mechanical power which is dissipated as heat, i.e. \mathcal{L}_d and can affect the free energy by means of temperature and the remaining part \mathcal{L}_s which directly affects the free energy and under certain conditions can be stored. For example, this is the case when $\dot{F}_d = 0$ and $T(x, t) = T_0$, i.e. for isothermal elasticity, as discussed in Sect. 3.2. In Ziegler (1983) \mathcal{L}_s is called quasi-conservative and \mathcal{L}_d —dissipated parts of mechanical power, respectively. Several approaches to define the corresponding stress and deformation parts are discussed in the literature. For example, one may consider various connections of rheological elements including a spring, a viscous element and a friction element (Krawietz 1986; Palmov 1998). A more general approach is to consider a mixture with several constituents having different properties and volume fractions (Besseling and van der Giessen 1994; Naumenko et al. 2011a). Alternatively, one may assume decompositions for the deformation gradient, rate of strain and/or stress (Besseling and van der Giessen 1994; Khan and Huang 1995; Maugin 1992).

In this section let us apply the so-called iso-stress approach with the following constitutive assumption

$$\sigma_s = \sigma_d = \sigma$$

The mechanical power can be given as follows

$$\mathcal{L} = \sigma \dot{F} F^{-1} = \sigma (\dot{F}_s F_s^{-1} + \dot{F}_d F_d^{-1}) \quad (3.4.37)$$

¹In general, σ_d may also depend on the deformation-like variables. Here we do not consider such a dependence, for the sake of brevity.

It is obvious, that in the uni-axial case the additive split of power with the iso-stress concept is equivalent to following splits of the deformation-like variables

$$\dot{F}F^{-1} = \dot{F}_s F_s^{-1} + \dot{F}_d F_d^{-1} \Rightarrow \frac{d}{dt} \ln F = \frac{d}{dt} \ln F_s + \frac{d}{dt} \ln F_d \Rightarrow F = F_s F_d \quad (3.4.38)$$

Vice versa, if we assume the multiplicative decomposition of the deformation gradient $F = F_s F_d$, then the additive split of the deformation rates and the additive split of the mechanical power (3.4.37) follow. In rheology this corresponds to the Maxwell model of viscoelasticity or Prandtl model of elastoplasticity, where a spring is connected with a dashpot or a friction element in series. For general multi-axial deformation states the multiplicative decomposition of the deformation gradient does not provide the additive decomposition of the deformation rates and the mechanical power, see for example, Besseling and van der Giessen (1994), Khan and Huang (1995), Xiao et al. (2006). Multi-axial constitutive assumptions will be discussed in Chap. 5. To illustrate basic ideas let us skip (3.4.38) and start with the iso-stress constitutive assumption which can be given in the following form

$$\sigma = \sigma_s(F, F_s, F_d, T) = \sigma_d(\dot{F}, \dot{F}_s, \dot{F}_d, T) \quad (3.4.39)$$

If constitutive equations for σ_s and σ_d are specified then Eq. (3.4.39) can be used to eliminate one of the kinematic variables, for example F_s . Indeed, assume that F , F_d and T are given as functions of time. Then Eq. (3.4.39) is the first-order ordinary differential equation with respect to F_s . It can be solved providing F_s as a function of remaining variables and time. Therefore the mechanical power can be decomposed as follows

$$\begin{aligned} \mathcal{L} &= \mathcal{L}_s + \mathcal{L}_d, \\ \mathcal{L}_s &= \sigma(F, F_d, T) \dot{F}F^{-1} - \sigma(F, F_d, T) \dot{F}_d F_d^{-1}, \\ \mathcal{L}_d &= \sigma(\dot{F}, \dot{F}_d, T) \dot{F}_d F_d^{-1} \end{aligned} \quad (3.4.40)$$

Therefore we can assume that the free energy is now a function of three variables F , F_d and T . The inequality (2.6.50) can be written as follows

$$\begin{aligned} \left(\sigma F^{-1} - \rho \frac{\partial \Phi}{\partial F} \right) \dot{F} - \left(\sigma F_d^{-1} + \rho \frac{\partial \Phi}{\partial F_d} \right) \dot{F}_d - \rho \left(\frac{\partial \Phi}{\partial T} + \mathcal{S} \right) \dot{T} \\ + \sigma \dot{F}_d F_d^{-1} - q \frac{T'}{T} \geq 0 \end{aligned} \quad (3.4.41)$$

The first line in Eq. (3.4.41) is a linear function of rates of the assumed independent variables. Therefore with procedures discussed in Sects. 3.1 and 3.2 the inequality (3.4.41) can be satisfied with

$$\sigma F^{-1} = \rho \frac{\partial \Phi}{\partial F}, \quad \sigma F_d^{-1} = -\rho \frac{\partial \Phi}{\partial F_d}, \quad \mathcal{S} = -\frac{\partial \Phi}{\partial T} \quad (3.4.42)$$

and

$$\sigma \dot{F}_d F_d^{-1} \geq 0, \quad -q \frac{T'}{T} \geq 0 \quad (3.4.43)$$

From the first and the second equation in (3.4.42) it follows

$$\sigma = \rho \frac{\partial \Phi}{\partial F} F = -\rho \frac{\partial \Phi}{\partial F_d} F_d \quad (3.4.44)$$

or

$$\frac{\partial \Phi}{\partial F} F + \frac{\partial \Phi}{\partial F_d} F_d = 0 \quad (3.4.45)$$

Equation (3.4.45) provides a restriction to the free energy and can be solved by the method of characteristics (Courant and Hilbert 1989). Indeed, the characteristic system of (3.4.45) is

$$\frac{dF}{ds} = F, \quad \frac{dF_d}{ds} = -F_d, \quad (3.4.46)$$

where s is a time-like variable. Two ordinary differential equations (3.4.46) possess one integral. To formulate it rewrite the second equation in Eqs. (3.4.46) as follows

$$\frac{dF_d^{-1}}{ds} = -\frac{1}{F_d^2} \frac{dF_d}{ds} = F_d^{-1}, \quad (3.4.47)$$

Now multiply the first equation in (3.4.46) with F_d^{-1} and the Eq. (3.4.47) with F and subtract leading to

$$\frac{d}{ds}(F F_d^{-1}) = 0 \quad \Rightarrow \quad F F_d^{-1} = C,$$

where C is an integration constant. Therefore $F F_d^{-1}$ is the integral curve of the free energy and

$$\Phi(F, F_d) = \Phi(F F_d^{-1})$$

With Eq. (3.4.44) the stress is given as follows

$$\sigma = \rho \frac{\partial \Phi}{\partial F} F = \rho \frac{\partial \Phi}{\partial F F_d^{-1}} F F_d^{-1} \quad (3.4.48)$$

By specifying $F^{\text{el}} = F F_d^{-1}$ we can formulate the thermoelasticity constitutive equations as it made in Sect. 3.2

$$\sigma = \rho \frac{\partial \Phi(F^{\text{el}})}{\partial F^{\text{el}}} F^{\text{el}} = \rho \frac{\partial \Phi(\varepsilon_{\text{H}}^{\text{el}})}{\partial \varepsilon_{\text{H}}^{\text{el}}}, \quad \mathcal{S} = -\frac{\partial \Phi}{\partial T}, \quad (3.4.49)$$

where $\varepsilon_{\text{H}}^{\text{el}} = \ln F^{\text{el}}$ is the elastic strain. Note the strain in the continuum mechanics is usually understood as a quantity that can be related to the deformation gradient, for example $\varepsilon_{\text{H}} = \ln F$. In this sense the “elastic strain” can only be identified as a strain if $F_{\text{d}} = 1$. Nevertheless, “elastic strain” is convenient to analyze and identify experimental data, for example initial strain in a strain versus time curve or elastic strain part in a stress-strain hysteresis loop, see examples presented in Sect. 1.1.1.

F_{d} can also be defined as a “plastic transformation” (Bertram 2012). The quantity $\varepsilon_{\text{H}}^{\text{pl}} = \ln(F^{\text{pl}})$ can be called the “plastic strain”, i.e. a strain upon an artificial unloading such that $F^{\text{el}} = 1$. Again “plastic strain”, “creep strain” or “inelastic strain” are useful to identify constitutive models, response functions and material properties from various tests, see Sect. 1.1.1. To define the plastic (inelastic) strain a kinetic equation is required. For example, one may use Eq. (3.3.31)

$$\dot{\varepsilon}_{\text{H}}^{\text{pl}} = f_{\sigma}(|\sigma|) \text{sgn}(\sigma) f_T(T) \quad (3.4.50)$$

Let us note, that a multiplicative decomposition of the deformation gradient or the additive decomposition of the deformation rates are not used in the presented derivations. However, to visualize the quantity like $F^{\text{el}} = F F_{\text{d}}^{-1}$ one may use the notion of an intermediate or relaxed configuration. For discussions related to controversial meanings of such configurations in the case of general three-dimensional deformation we refer to Bertram (2012), Naghdi (1990), Xiao et al. (2006), among others.

As an example let us consider an elastic-non-linear-viscous material behavior under isothermal loading conditions. To simplify the model assume that the elastic strain is small $(\varepsilon^{\text{el}})^2 \ll \varepsilon^{\text{el}} < 1$. Small elastic strains are usually observed for metals. Furthermore assume that the inelastic deformation does not produce a significant change in volume such that

$$J = J^{\text{el}} = (1 + \varepsilon^{\text{el}})(1 - \nu \varepsilon^{\text{el}})^2 \approx 1 + (1 - 2\nu)\varepsilon^{\text{el}}, \quad \sigma J \approx \sigma, \quad (3.4.51)$$

where ν is the Poisson ratio. The constitutive equation for the stress has the following form²

$$\sigma = \frac{\partial \rho_0 \Phi(\varepsilon_{\text{H}}^{\text{el}})}{\partial \varepsilon_{\text{H}}^{\text{el}}} = \frac{\partial \rho_0 \Phi(\varepsilon_{\text{H}} - \varepsilon_{\text{H}}^{\text{pl}})}{\partial (\varepsilon_{\text{H}} - \varepsilon_{\text{H}}^{\text{pl}})} = E(\varepsilon_{\text{H}} - \varepsilon_{\text{H}}^{\text{pl}}) \quad (3.4.52)$$

For the inelastic strain rate let us apply the power law type constitutive equation, as discussed in Sect. 3.2

$$\dot{\varepsilon}_{\text{H}}^{\text{pl}} = \dot{\varepsilon}_0 \left(\frac{|\sigma|}{\sigma_0} \right)^n \text{sgn}(\sigma) \quad (3.4.53)$$

²The linear thermal expansion is neglected for the sake of brevity.

Assume that the rod is fixed at the cross section $X = 0$, i.e. $x(0, t) = 0$, and loaded at $x = \ell$ by the force $\mathcal{F}(t)$. Furthermore assume that the load is quasi-static such that the balance of momentum (2.3.25) can be reduced to the balance of internal force providing $\sigma(x, t)A(t) = \mathcal{F}(t)$. First let us subject the rod to the time-dependent elongation (strain-controlled test) such that

$$\varepsilon_H(t) = \ln \frac{\ell(t)}{\ell_0} = \dot{\varepsilon}_{H_0} t, \quad (3.4.54)$$

where $\dot{\varepsilon}_{H_0}$ is a given constant strain rate. Let us compute the stresses $\sigma(x, t)$ and $P(x, t)$. To this end take the time derivative of Eq. (3.4.52) and apply the constitutive equation (3.4.53) to eliminate the inelastic strain rate. As a result the following differential equation for the stress σ can be derived

$$\dot{\sigma} + E \dot{\varepsilon}_0 \left(\frac{|\sigma|}{\sigma_0} \right)^n \text{sgn}(\sigma) = E \dot{\varepsilon}_H \quad (3.4.55)$$

For the loading defined by Eq. (3.4.54) the Eq. (3.4.55) can be put into the following normalized form

$$\frac{d\Sigma}{d\epsilon} + \frac{1}{\gamma} (\Sigma)^n = 1, \quad \Sigma = \frac{\sigma}{\sigma_0}, \quad \epsilon = \frac{E}{\sigma_0} \varepsilon_H, \quad \gamma = \frac{\dot{\varepsilon}_{H_0}}{\dot{\varepsilon}_0} \quad (3.4.56)$$

Equation (3.4.56) can be solved numerically with the initial condition $\Sigma(0) = 0$ providing the stress-strain curve. Figure 3.1a illustrates the results of the numerical integration for $n = 3$ and three different strain rates. The strain rate sensitivity of the inelastic range can be clearly observed. The flow stress in the steady state regime can be computed from Eq. (3.4.56) as follows

$$\frac{d\Sigma}{d\epsilon} = 0 \quad \Rightarrow \quad \Sigma_{ss} = \gamma^{\frac{1}{n}}$$

or

$$\sigma_{ss} = \sigma_0 \left(\frac{\dot{\varepsilon}_{H_0}}{\dot{\varepsilon}_0} \right)^{\frac{1}{n}} \quad (3.4.57)$$

Equation (3.4.57) can be used to identify the material properties $\dot{\varepsilon}_0$, σ_0 and n from stress-strain diagrams. Once the true stress σ is given the engineering stress P can be computed with Eqs. (2.6.55) and (3.4.51) as follows

$$P = \sigma F^{-1} = \sigma \exp\left(-\frac{\sigma_0}{E} \epsilon\right)$$

Furthermore the engineering strain defined by Eq. (2.1.5) can be related to the true strain as follows

$$\varepsilon = 1 - \exp(-\varepsilon_H)$$

Fig. 3.1 Strain rate sensitivity of stress-strain diagrams for $n = 3$ and $E/\sigma_0 = 10$. **a** Normalized true stress versus normalized true strain. **b** Normalized engineering stress versus normalized engineering strain

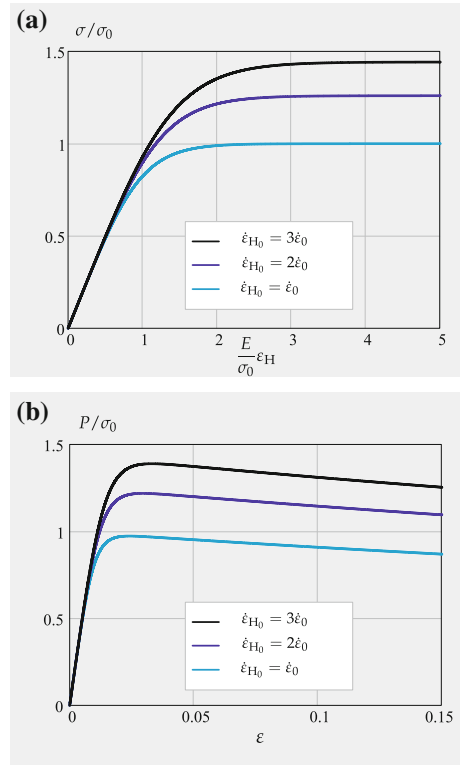


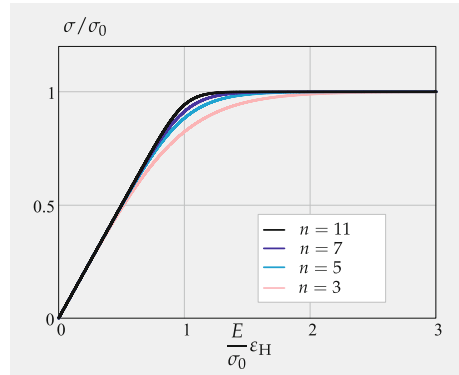
Figure 3.1b shows the engineering stress as a function of the engineering strain for $E/\sigma_0 = 10$ and different strain rates. The engineering stress-strain curve exhibits a descending branch as a result of the cross section shrinkage. Note, that we assumed uniform elongation and consequently uniform cross section change. For the analysis of strain localization and necking instability the cross section shrinkage and its gradient are required as additional degrees of freedom, e.g. Antman (1973), Coleman (1986).

Besides the strain rate sensitivity the exponent n controls the transition from the elastic to the inelastic regime. To discuss this Fig. 3.2 shows the true stress-strain curves for the strain rate $\dot{\varepsilon}_H = \dot{\varepsilon}_0$ and different values of n . With an increase of n the curves approach the elastic-ideal plastic rate-independent regime.

In the next example assume that the rod is subjected to the constant tensile force \mathcal{F} . The rate of strain follows from Eq. (3.4.55)

$$\dot{\varepsilon}_H \left(1 - \frac{P}{E} \exp(\varepsilon_H) \right) = \dot{\varepsilon}_0 \left(\frac{P}{\sigma_0} \right)^n \exp(n\varepsilon_H), \quad P = \frac{\mathcal{F}}{A_0} \quad (3.4.58)$$

Fig. 3.2 Normalized true stress versus normalized true strain for the constant strain rate $\dot{\varepsilon}_H = \dot{\varepsilon}_0$ and different values of the exponent n



Equation (3.4.55) can be solved in a closed analytical form providing the relation between the strain and the time. To simplify this relation assume that

$$\frac{P}{E} \exp(\varepsilon_{H_{\max}}) \ll 1$$

This can be well satisfied if the initial elastic strain after the loading is small, i.e. $P/E \ll 1$ and the maximum creep strain (strain before creep fracture) is $\varepsilon_{H_{\max}} < 1$. In this case Eq. (3.4.55) takes the form

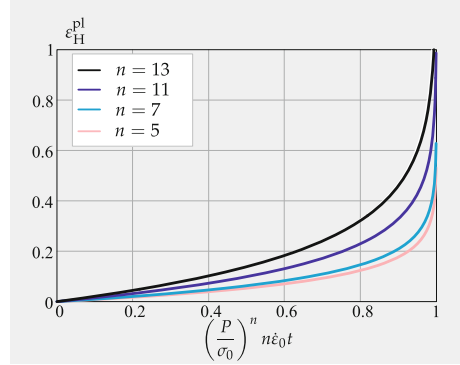
$$\dot{\varepsilon}_H = \dot{\varepsilon}_0 \left(\frac{P}{\sigma_0} \right)^n \exp(n\varepsilon_H) \quad (3.4.59)$$

The solution of Eq. (3.4.59) can be presented as follows

$$\varepsilon_H(t) = \varepsilon_H^{\text{el}} + \varepsilon_H^{\text{pl}}, \quad \varepsilon_H^{\text{pl}} = -\frac{1}{n} \ln \left(1 - \frac{t}{t_*} \right), \quad t_* = \frac{1}{\dot{\varepsilon}_0 n} \left(\frac{\sigma_0}{P} \right)^n, \quad (3.4.60)$$

where $\varepsilon_H^{\text{el}}$ is the initial elastic strain and t_* is the Hoff's time to ductile creep rupture (Hoff 1953). Figure 3.3 illustrates the creep curves according to Eqs. (3.4.60) for different values of the stress exponent. The introduced elasto-(visco)plastic model can capture the secondary creep stage and the tertiary creep stage due to the cross section shrinkage. Having a family of experimental creep curves for several stress levels one may identify the material properties $\dot{\varepsilon}_0$, σ_0 and n from creep curves. The value of σ_0 can be set arbitrarily, so that only two material constants in the power law creep are independent. Let us note that the power law creep is observed for narrow stress range. To capture creep behavior in a wide stress range advanced functions of stress are required (Altenbach et al. 2008b; Boyle 2012; Hosseini et al. 2013; Naumenko et al. 2009). Cross section shrinkage and the resulting tertiary creep were frequently observed in metals and alloys, for example Dünwald and

Fig. 3.3 Inelastic true strain versus normalized time for the constant force and different values of the exponent n



El-Magd (1996), El-Magd and Kranz (2000), Längler et al. (2014), Naumenko and Kostenko (2009). However, tertiary creep in metals and alloys may be controlled by additional material deterioration processes, see Sect. 1.2.1.2. Therefore Eq. (3.4.60) should be supplemented by additional kinetic equations to reflect softening, ageing and damage processes.

3.5 Hardening, Softening, and Ageing

Let us analyze several hardening mechanisms and present approaches to model macroscopic hardening phenomena. For the sake of brevity let us assume small strains such that the difference between true and engineering strain and stress measures is not essential and the geometrically-linear theory can be applied.

3.5.1 Strain Hardening

Inelastic flow of metals and alloys is accompanied by several hardening processes. An example is the dislocation generation as a result of inelastic strain accumulation. With the increase in dislocation density, the dislocation movement becomes more difficult such that the inelastic deformation rate decreases. At high temperature hardening effects may be reversed by annihilation processes that reduce the dislocation density. Therefore, the inelastic strain rate does not decrease towards zero, but attains a certain minimum or in some cases saturation value, see Sect. 1.1.1. A simple empirical approach is to introduce a strain hardening function h and to generalize a constitutive equation, for example a power law (3.4.53), as follows

$$\dot{\varepsilon}^{\text{pl}} = \dot{\varepsilon}_0 \left(\frac{|\sigma|}{\sigma_0} \right)^n \text{sgn}(\sigma) h(\varepsilon^{\text{pl}}) \quad (3.5.61)$$

A popular choice for h is a power function

$$h(\varepsilon^{\text{pl}}) = |\varepsilon^{\text{pl}}|^l,$$

where the power l , $-1 < l < 0$ has to be identified from experimental data. Limitations of the empirical approach will be discussed in Sect. 5.3.1. Alternatively, hardening can be considered as a process and described by an independent rate-type equation. In the materials science a mean dislocation density variable ϱ is introduced to capture a hardening state of the material. Following Estrin (1996) the power law (3.4.53) can be generalized as follows

$$\dot{\varepsilon}^{\text{pl}} = \dot{\varepsilon}_0 \left(\frac{|\sigma|}{\hat{\sigma}} \right)^n \text{sgn}\sigma, \quad (3.5.62)$$

where $\hat{\sigma}$ is called drag stress and defined as follows

$$\hat{\sigma} = M G b \sqrt{\varrho}, \quad (3.5.63)$$

where M is the Taylor factor and b is the magnitude of the Burgers vector. Equation (3.5.63) assumes a simple, linear relationship between the drag stress and the dislocation density. As the latter increases in the course of inelastic deformation, the strain rate decreases, according to Eq. (3.5.62). In the continuum mechanics variables like mean dislocation density do not appear in the balance equations, and are not introduced at the beginning together with displacement, strain, density and others. However, as the dislocation density variable affects the inelastic strain rate and the stress, one may apply a concept of internal state or hidden state variables as proposed by Coleman and Gurtin (1967).³ To explain this concept let us introduce a dimensionless hardening parameter

$$H = \sqrt{\frac{\varrho}{\varrho_0}}, \quad (3.5.64)$$

where ϱ_0 is a reference dislocation density. The constitutive equation (3.5.62) takes the form

$$\dot{\varepsilon}^{\text{pl}} = \dot{\varepsilon}_0 \left(\frac{|\sigma|}{\sigma_0 H} \right)^n \text{sgn}\sigma, \quad \sigma_0 = M G b \sqrt{\varrho_0} \quad (3.5.65)$$

³A historical essay on the development of theories with internal state variables is presented in Maugin (2015).

Under the assumption of small strains the inequality (2.6.50) takes the following form

$$\sigma \dot{\varepsilon} - \rho \dot{\Phi} - \rho S \dot{T} - q \frac{T'}{T} \geq 0 \quad (3.5.66)$$

Let us postulate the following split of the mechanical power

$$\begin{aligned} \mathcal{L} &= \sigma \dot{\varepsilon} = \mathcal{L}_s + \mathcal{L}_d, \\ \mathcal{L}_s &= \sigma_s(\varepsilon^{\text{el}}, T) \dot{\varepsilon}^{\text{el}}, \\ \mathcal{L}_d &= \sigma_d(\dot{\varepsilon}^{\text{pl}}, H, T) \dot{\varepsilon}^{\text{pl}} \end{aligned} \quad (3.5.67)$$

According to (3.5.67) the stored part is a function of the elastic strain and the temperature, while the dissipated part involves the new variable H to capture the influence of hardening on the inelastic process. As in the Sect. 3.5 let us use the iso-stress approach such that

$$\sigma = \sigma_s(\varepsilon^{\text{el}}, T) = \sigma_d(\dot{\varepsilon}^{\text{pl}}, H, T)$$

Furthermore, assume that the free energy now is a function of the elastic strain, the hardening and the temperature. The inequality (3.5.66) takes the form

$$\left(\sigma - \rho \frac{\partial \Phi}{\partial \varepsilon^{\text{el}}} \right) \dot{\varepsilon}^{\text{el}} - \rho \left(\frac{\partial \Phi}{\partial T} + S \right) \dot{T} + \sigma \dot{\varepsilon}^{\text{pl}} - \rho \frac{\partial \Phi}{\partial H} \dot{H} - q \frac{T'}{T} \geq 0 \quad (3.5.68)$$

To resolve the inequality assume that the internal state variable H is defined by the following evolution equation

$$\dot{H} = f_H(\varepsilon^{\text{el}}, T, H, \dot{\varepsilon}^{\text{pl}}) \quad (3.5.69)$$

Then, for $\dot{\varepsilon}^{\text{el}}$ and \dot{T} that can be positive or negative the inequality is satisfied for

$$\sigma = \rho \frac{\partial \Phi}{\partial \varepsilon^{\text{el}}}, \quad S = -\frac{\partial \Phi}{\partial T}, \quad -q \frac{T'}{T} \geq 0, \quad \sigma \dot{\varepsilon}^{\text{pl}} - \rho \frac{\partial \Phi}{\partial H} \dot{H} \geq 0 \quad (3.5.70)$$

The last inequality provides a restriction on the material properties and/or response functions that enter the model. As an example let us assume that the hardening part of the free energy is proportional to $(H_\infty - H)^2$, where H_∞ is the saturation value of the hardening variable, which may depend on the stress or minimum inelastic strain rate. Then

$$-\rho \frac{\partial \Phi}{\partial H} = A_h (H_\infty - H), \quad (3.5.71)$$

where A_h is a positive constant. For the hardening rate let us apply the following equation

$$\dot{H} = B (H_\infty - H) |\dot{\varepsilon}^{pl}|, \quad (3.5.72)$$

where B is a positive constant. Equation (3.5.72) assumes that the “driving force” for the hardening process is $(H_\infty - H)$, as given by Eq. (3.5.71), and that the kinetics of hardening is related to the inelastic strain rate magnitude. Equations like (3.5.71) are applied in Estrin (1996), Blum (2008), Naumenko and Gariboldi (2014), among others, for modeling hardening in several alloys. With the constitutive equations (3.5.62) and (3.5.71) as well as the evolution equation (3.5.71) we obtain

$$\sigma \dot{\varepsilon}^{pl} - \rho \frac{\partial \Phi}{\partial H} \dot{H} = [|\sigma| + A_h B (H_\infty - H)^2] |\dot{\varepsilon}^{pl}| \geq 0 \quad (3.5.73)$$

With the proposed constitutive Eq. (3.5.71) and evolution Eq. (3.5.72) the inequality (3.5.73) is satisfied.

As an example consider a small strain creep regime with $\sigma = \text{const} > 0$. For the constant stress Eq. (3.5.72) can be integrated providing the hardening variable as a function of the inelastic strain. As a result we obtain

$$H = H_\infty - (H_\infty - 1) \exp(-B \varepsilon^{pl}) \quad (3.5.74)$$

After inserting in the constitutive equation (3.5.65) we obtain

$$\dot{\varepsilon}^{pl} = \dot{\varepsilon}_0 \left(\frac{\sigma}{\sigma_0 H_\infty} \right)^n \left[1 - \left(1 - \frac{1}{H_\infty} \right) \exp(-B \varepsilon^{pl}) \right]^{-n} \quad (3.5.75)$$

Obviously, for the constant stress the model with the internal state variable provides the creep model with the exponential type strain hardening function. The material properties can be identified from a family of creep curves. As H_∞ is a function of stress, it is not possible to solve Eq. (3.5.72) in terms of elementary functions for other cases of loading, for example for the tensile regime. Standard numerical solution techniques for ordinary differential equations can be applied for the solution in a general case of loading.

Let us go back to the mean dislocation density model. With Eq. (3.5.64) the evolution equation (3.5.72) takes the following form

$$\dot{\varrho} = (k_1 \sqrt{\varrho} - k_2 \varrho) |\dot{\varepsilon}^{pl}|, \quad k_1 = 2B \sqrt{\varrho_\infty}, \quad k_2 = 2B \quad (3.5.76)$$

Similar equation is derived in Estrin (1996), where the term $k_1 \sqrt{\varrho}$ is associated with the storage of dislocations and $k_2 \varrho$ —with recovery of dislocations.

3.5.2 Kinematic Hardening

Another mechanism of hardening can be related to the micro-stress fields generated during the plastic flow, as a result of heterogeneous deformation on the micro-scale. Several microstructural zones, for example slip planes, grains with certain crystallographic orientations or certain regions within subgrains may exhibit higher levels of inelastic strain rate. The remaining part of microstructure behaves more or less elastically. This leads to changes of micro-stress states and to formation of residual stresses upon unloading. Residual micro-stress fields affect the overall deformation rate and provide an additional hardening.

To derive a robust phenomenological model by taking into account micro-stress fields consider again the following split of the mechanical power⁴

$$\mathcal{L} = \sigma \dot{\varepsilon} = \sigma \dot{\varepsilon}^{\text{el}} + \sigma \dot{\varepsilon}^{\text{pl}}$$

Now assume that a part of the mechanical power $\sigma \dot{\varepsilon}^{\text{pl}}$ is stored in the course of inelastic deformation. To this end let us consider the following decomposition

$$\sigma = \sigma_a + \beta, \quad \varepsilon^{\text{pl}} = \varepsilon^{\text{rec}} + \varepsilon^{\text{pm}}, \quad \sigma \dot{\varepsilon}^{\text{pl}} = \sigma_a \dot{\varepsilon}^{\text{pl}} + \beta \dot{\varepsilon}^{\text{rec}} + \beta \dot{\varepsilon}^{\text{pm}}, \quad (3.5.77)$$

where σ_a is the active stress and β is the backstress. ε^{rec} is the recoverable inelastic strain while ε^{pm} is the permanent inelastic strain. These strain components are illustrated in Fig. 1.11b. Now define the quasi-conservative and dissipated parts of the mechanical power as follows

$$\begin{aligned} \mathcal{L}_s &= \sigma(\varepsilon^{\text{el}}, T) \dot{\varepsilon}^{\text{el}} + \beta(\varepsilon^{\text{rec}}, T) \dot{\varepsilon}^{\text{rec}}, \\ \mathcal{L}_d &= \sigma_a(\dot{\varepsilon}^{\text{pl}}, T) \dot{\varepsilon}^{\text{pl}} + \beta(\dot{\varepsilon}^{\text{pm}}, T) \dot{\varepsilon}^{\text{pm}} \end{aligned} \quad (3.5.78)$$

Furthermore assume that the free energy depends on the elastic strain, the recoverable inelastic strain and the temperature. With these assumptions the inequality (3.5.66) takes the form

$$\begin{aligned} \left(\sigma - \rho \frac{\partial \Phi}{\partial \varepsilon^{\text{el}}} \right) \dot{\varepsilon}^{\text{el}} + \left(\beta - \rho \frac{\partial \Phi}{\partial \varepsilon^{\text{rec}}} \right) \dot{\varepsilon}^{\text{rec}} - \rho \left(\frac{\partial \Phi}{\partial T} + \mathcal{S} \right) \dot{T} \\ + \sigma_a \dot{\varepsilon}^{\text{pl}} + \beta \dot{\varepsilon}^{\text{pm}} - q \frac{T'}{T} \geq 0 \end{aligned} \quad (3.5.79)$$

The first line in (3.5.79) is a linear function of three independent rates $\dot{\varepsilon}^{\text{el}}$, $\dot{\varepsilon}^{\text{rec}}$ and T . Since these rates may be positive or negative, the inequality (3.5.79) can be resolved as follows

$$\begin{aligned} \sigma = \rho \frac{\partial \Phi}{\partial \varepsilon^{\text{el}}}, \quad \beta = \rho \frac{\partial \Phi}{\partial \varepsilon^{\text{rec}}}, \quad \mathcal{S} = - \frac{\partial \Phi}{\partial T}, \\ -q \frac{T'}{T} \geq 0, \quad \sigma_a \dot{\varepsilon}^{\text{pl}} + \beta \dot{\varepsilon}^{\text{pm}} \geq 0 \end{aligned} \quad (3.5.80)$$

⁴Here we assume again small strains for the sake of brevity.

For the stress and the backstress let us assume the following constitutive equations

$$\sigma = \rho \frac{\partial \Phi}{\partial \varepsilon^{\text{el}}} = E \varepsilon^{\text{el}}, \quad \beta = \rho \frac{\partial \Phi}{\partial \varepsilon^{\text{rec}}} = E_h \varepsilon^{\text{rec}}, \quad (3.5.81)$$

where E_h is the temperature-dependent hardening modulus. For the rate of the plastic strain let us apply Eq. (3.4.50) with respect to the active part of the stress

$$\dot{\varepsilon}^{\text{pl}} = f_\sigma(|\sigma_a|) \text{sgn}(\sigma_a) f_T(T) = f_\sigma(|\sigma - \beta|) \text{sgn}(\sigma - \beta) f_T(T), \quad (3.5.82)$$

For the rate of the permanent strain let us apply the following equation

$$\dot{\varepsilon}^{\text{pm}} = g_\sigma(|\beta|) \text{sgn}(\beta) g_T(T) \quad (3.5.83)$$

For f_σ and g_σ one may apply, for example, power law functions. For $f_T(T)$ and $g_T(T)$ Arrhenius type functions of temperature can be used. Response functions of stress and temperature will be discussed in Sect. 5.4.4. Alternatively, one may assume that the rate of the permanent strain is related to the rate of plastic strain and the backstress as follows

$$\dot{\varepsilon}^{\text{pm}} = \frac{\beta}{\beta_*} |\dot{\varepsilon}^{\text{pl}}|, \quad (3.5.84)$$

where β_* can be a function of stress and temperature. One may verify that with Eqs. (3.5.82) and (3.5.83) or (3.5.84) the last inequality in (3.5.80) is satisfied. Let us derive the rate equation for the backstress. To this end take the time derivative of the constitutive equation (3.5.81)₂

$$\dot{\beta} = \frac{dE_h}{dT} \dot{\varepsilon}^{\text{rec}} + E_h \dot{\varepsilon}^{\text{rec}} = \frac{1}{E_h} \frac{dE_h}{dT} \beta \dot{T} + E_h (\dot{\varepsilon}^{\text{pl}} - \dot{\varepsilon}^{\text{pm}}) \quad (3.5.85)$$

With the Eq. (3.5.83) we obtain

$$\dot{\beta} = \frac{1}{E_h} \frac{dE_h}{dT} \beta \dot{T} + E_h [\dot{\varepsilon}^{\text{pl}} - g_\sigma(|\beta|) \text{sgn}(\beta) g_T(T)] \quad (3.5.86)$$

Assuming isothermal loading conditions $\dot{T} = 0$, Eq. (3.5.86) simplifies to

$$\dot{\beta} = E_h [\dot{\varepsilon}^{\text{pl}} - g_\sigma(|\beta|) \text{sgn}(\beta) g_T(T)] \quad (3.5.87)$$

Equation (3.5.87) was postulated by Malinin and Khadjinsky (1972) without the analysis of the thermodynamic process and splitting the mechanical power. The constitutive equation (3.5.82) and the evolution equation (3.5.87) is an example of the hardening model with the backstress. As shown in Malinin and Khadjinsky (1972) such a model can describe various effects of inelastic deformation including creep recovery, cyclic hardening, etc. A more detailed analysis will be given in Sect. 5.3.2.

Applying the constitutive assumption (3.5.84) and with Eq. (3.5.85) we obtain

$$\dot{\beta} = \frac{1}{E_h} \frac{dE_h}{dT} \beta \dot{T} + E_h \left(\dot{\varepsilon}^{\text{pl}} - \frac{\beta}{\beta_*} |\dot{\varepsilon}^{\text{pl}}| \right) \quad (3.5.88)$$

For isothermal loading conditions this simplifies to

$$\dot{\beta} = E_h \left(\dot{\varepsilon}^{\text{pl}} - \frac{\beta}{\beta_*} |\dot{\varepsilon}^{\text{pl}}| \right) \quad (3.5.89)$$

Equation (3.5.89) was proposed by Frederick and Armstrong (2007).⁵ It is obvious, that different versions for a model with a backstress can be obtained by specifying the constitutive equation for the rate of permanent inelastic strain. A simplest version can be obtained assuming

$$\beta = E_h \varepsilon^{\text{pl}}$$

This linear hardening rule was proposed by Prager (1956). Instead the constitutive equation (3.4.50) one may use a rate-independent plasticity model of the type (3.3.36). The yield condition is then formulated with respect to the active stress i.e.

$$|\sigma - \beta| - \sigma_y = 0$$

For the given accumulated value of the backstress the actual yield condition is shifted or translated if compared to the original one with the zero backstress. Therefore this approach was called kinematic hardening. For different versions of the kinematic hardening rules we refer to Chaboche (1989, 2008), Lemaitre and Chaboche (1990), Lemaitre et al. (2009).

Let us analyze the constitutive equation for the plastic strain rate (3.5.82) and the evolution equation (3.5.89) for different loading cases. To this end let us specify the constitutive Eq. (3.5.82) assuming a power function of stress

$$\dot{\varepsilon}^{\text{pl}} = \dot{\varepsilon}_0 \left(\frac{|\sigma - \beta|}{\sigma_0} \right)^n \text{sgn}(\sigma - \beta), \quad (3.5.90)$$

where $\dot{\varepsilon}_0$, σ_0 and n are material properties. First consider a creep regime for the constant tensile stress. In this case the evolution equation (3.5.89) can be integrated in elementary functions. With the initial condition $\beta(0) = 0$ the result is

$$\beta = \beta_* \left[1 - \exp \left(- \frac{E_h}{\beta_*} \varepsilon^{\text{pl}} \right) \right] \quad (3.5.91)$$

⁵The model was first published in 1966 in a CEGB report, see Frederick and Armstrong (2007) for historical remarks.

With (3.5.90) the following expression for the inelastic strain rate can be obtained

$$\dot{\varepsilon}^{\text{pl}} = \dot{\varepsilon}_0 \left(\frac{\sigma}{\sigma_0} \right)^n \left[1 - \frac{\beta_*}{\sigma} + \frac{\beta_*}{\sigma} \exp \left(-\frac{E_h}{\beta_*} \varepsilon^{\text{pl}} \right) \right]^n \quad (3.5.92)$$

Equation (3.5.92) describes the primary stage of the creep curve. It is obvious that for the loading with constant stress the exponential type strain hardening function follows from the backstress model. The material parameters and the function β_* in Eq. (3.5.92) can be identified from a family of creep curves considering the primary creep stage.

To simulate strain and/or stress responses under timely varying loading Eqs. (3.5.82) and (3.5.89) can be solved numerically. Let us introduce new variables: the normalized time $\tau = \dot{\varepsilon}_0 t$, the normalized stress $\Sigma = \sigma/\sigma_0$ and the following dimensionless constants

$$\tilde{E}_h = \frac{\tilde{E}_h}{\sigma_0}, \quad \tilde{E} = \frac{\tilde{E}}{\sigma_0}$$

Equations (3.5.82) and (3.5.89) take the following form

$$\begin{aligned} \frac{d\varepsilon^{\text{pl}}}{d\tau} &= |\Sigma - \tilde{E}_h \varepsilon^{\text{rec}}|^n \text{sgn}(\Sigma - \tilde{E}_h \varepsilon^{\text{rec}}), \\ \frac{d\varepsilon^{\text{rec}}}{d\tau} &= \frac{d\varepsilon^{\text{pl}}}{d\tau} - \frac{\varepsilon^{\text{rec}}}{\varepsilon_*^{\text{rec}}} \left| \frac{d\varepsilon^{\text{pl}}}{d\tau} \right|, \end{aligned} \quad (3.5.93)$$

where

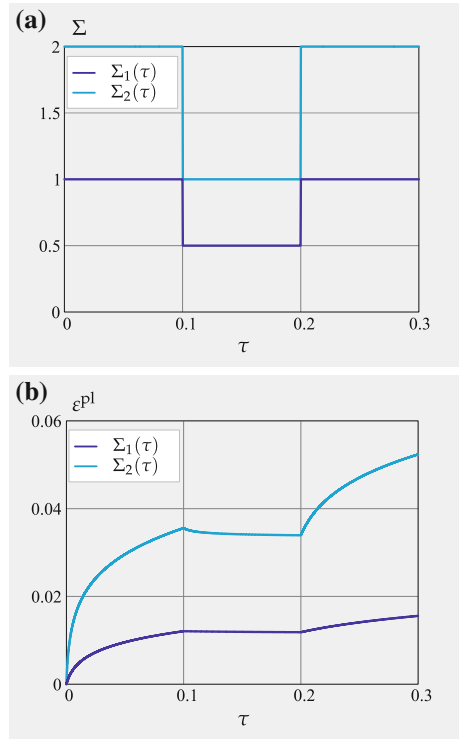
$$\varepsilon_*^{\text{rec}} = \frac{\beta_*}{\tilde{E}_h} \Sigma$$

For the simulations let us assume the following values

$$n = 3, \quad \tilde{E}_h = 100, \quad \tilde{E} = 1000, \quad B_* = 0.9 \quad (3.5.94)$$

Figure 3.4a shows two normalized stress versus normalized time profiles. Here three loading steps are assumed as follows. During the first step the stress is kept constant over a period of time. Then the stress value is reduced to the half of the value in the first cycle and kept constant for the same period of time. After that the stress is increased up to the original value and kept constant. Figure 3.4b illustrates the corresponding creep strain versus time responses. The first loading step provides a typical primary creep regime. After the unloading a creep recovery during the second loading step is observed. The loading to the same stress value leads again to the primary creep regime with a decrease of the inelastic strain rate over the time. However, the starting creep rate after the second loading is lower than the corresponding creep rate at the beginning of the loading sequence.

Fig. 3.4 Simulation of creep response under variable loading with Eqs. (3.5.93) and parameters (3.5.94).
a Loading profiles.
b Inelastic strain versus normalized time



Let us analyze stress responses under the strain control. Taking the time derivative of stress we obtain

$$\dot{\sigma} = E(\dot{\varepsilon} - \dot{\varepsilon}^{Pl})$$

With the introduced normalized variables this equation reads

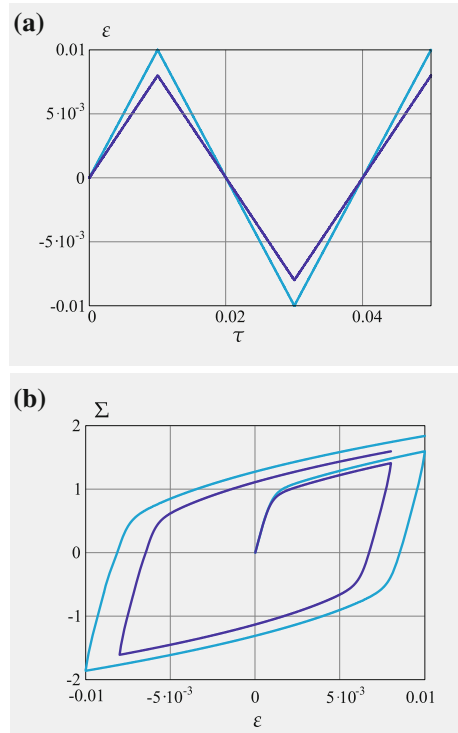
$$\frac{d\Sigma}{d\tau} = \tilde{E} \left(\frac{\dot{\varepsilon}}{\dot{\varepsilon}_0} - \frac{d\varepsilon^{Pl}}{d\tau} \right) \tag{3.5.95}$$

For a given strain profile $\varepsilon(\tau)$, Eq. (3.5.95) can be integrated numerically together with Eqs. (3.5.93). Figure 3.5a shows two strain versus time profiles corresponding to LCF loading regimes. The stress-strain hysteresis loops are presented in Fig. 3.5b. We observe that the Frederick-Armstrong type kinematic hardening model is able to reproduce several phenomena observed in LCF tests. They include the Bauschinger effect: in the first loading cycle the absolute value of the apparent yield point under compression is lower than the corresponding value under tension, the cyclic hardening: the stress amplitude increases in the course of cyclic loading, and the strain rate sensitivity: the stress-strain loop depends on the rate of loading. The Frederick-

Fig. 3.5 Simulation of stress response under cyclic strain with Eq. (3.5.95) and parameters (3.5.94).

a Loading profiles.

b Normalized stress versus strain



Armstrong model was calibrated and applied to describe inelastic behavior of many materials. Examples are presented in Altenbach et al. (2013), Chaboche (2008), Längler et al. (2014), among others. In describing material behavior over many loading cycles modifications may be required. For example the model can lead to an overestimation of cyclic strain accumulation in the creep ratchetting regime (Altenbach et al. 2013; Ohno et al. 1998; Ohno 1998). As discussed in Ohno et al. (1998) the deficiency is primarily related to the constitutive assumption (3.5.84). Various modifications of the Frederick-Armstrong model to capture the material behavior under cyclic loading are discussed by Ohno et al. (1998).

3.5.3 Phase Mixture Models for Hardening and Softening

Many materials contain relatively high dislocation density at the initial (virgin) state after the processing. Examples include 9–12% Cr ferritic steels, where a high density of dislocations is induced after martensitic transformation. High dislocation density, fine subgrain structure and different types of precipitates are examples of microstructural features that improve creep strength and high-temperature resistance

Abe (2009), Dyson and McLean (1998), Blum (2008), Straub (1995). For these materials the inelastic deformation is accompanied by softening processes such as recovery of dislocation substructures and coarsening of subgrains (Blum 2008). Stress-strain curves of softening materials show descending (softening) branch, Fig. 1.2 and creep curves exhibit accelerated regime immediately after the primary creep stage, Fig. 1.9.

To characterize hardening and softening processes a phase mixture model (or composite model) can be applied. The basic idea is to idealize the heterogeneous inelastic deformation in a volume element by considering a mixture with two or more constituents with different, but homogeneous inelastic properties. Assuming the total deformation of constituents to be the same, redistribution of stresses would take place, leading to the decrease of the overall inelastic strain rate. For example, in Straub (1995), Polcik et al. (1998), Polcik (1999), Barkar and Ågren (2005) two phases are introduced including the inelastic hard phase for subgrain boundaries with a relatively high dislocation density and the inelastic soft one for subgrain interiors. Two different sets of constitutive equations for inelastic strains are formulated. Furthermore, the volume fraction of the hard constituent is assumed to decrease over time to capture the coarsening process.

Let us explain the phase mixture approach by assuming two constituents with different inelastic behavior. For the sake of brevity, let us assume that constituents have the same elastic properties. Furthermore, as in the previous subsections we assume small strains, to keep the derivations brief and transparent. To designate the properties of the constituents the subscripts s (for inelastic-soft) and h (for inelastic hard) will be used. Let ε_s and ε_h be the strains of the constituents and σ_s and σ_h the corresponding effective stresses. For the stress of the composite the following mixture rule can be applied

$$\sigma = (1 - \eta_h)\sigma_s + \eta_h\sigma_h \quad (3.5.96)$$

where η_h is the volume fraction of the inelastic-hard constituent. With respect to the total strains let us postulate the following rule

$$\varepsilon = \varepsilon_h = \varepsilon_s \quad (3.5.97)$$

For the effective stress components the following constitutive equations can be assumed

$$\sigma_s = E(\varepsilon - \varepsilon_s^{pl}), \quad \sigma_h = E(\varepsilon - \varepsilon_h^{pl}) \quad (3.5.98)$$

With Eq. (3.5.96) the stress of the mixture is computed as follows

$$\sigma = E(\varepsilon - \varepsilon^{pl}), \quad \varepsilon^{pl} = (1 - \eta_h)\varepsilon_s^{pl} + \eta_h\varepsilon_h^{pl} \quad (3.5.99)$$

For the inelastic strain rates one may assume the following constitutive equations

$$\dot{\epsilon}_s^{\text{pl}} = f_s(|\sigma_s|)\text{sgn}\sigma_s, \quad \dot{\epsilon}_h^{\text{pl}} = f_h(|\sigma_h|)\text{sgn}\sigma_h, \quad (3.5.100)$$

where f_s and f_h are response functions of stress, for example power laws. Instead of Eq. (3.5.100) one may apply more advanced constitutive and evolution equations with dislocation type hardening or/and backstress as discussed in Sects. 3.5.1 and 3.5.2. Examples are presented in Straub (1995), Polcik et al. (1998), Polcik (1999), Barkar and Ågren (2005), Raj et al. (1996). Let us note that if the volume fractions are kept constant, then Eqs. (3.5.97)–(3.5.100) is nothing else as a connection of hard and soft elements in parallel, where both hard and soft elements is a series connection of an elastic spring and non-linear dashpots. Such connections in various combinations are discussed in rheology (Reiner 1969; Giesekus 1994; Palmov 1998). Rheological models, equipped with constant volume fractions were firstly applied in Besseling (1958), Besseling and van der Giessen (1994) to model inelastic material behavior and, in particular to motivate kinematic hardening rules. A more general approach is to introduce kinetic equations for the volume fractions. For example, assuming that the volume fraction of the hard constituent is decreasing over time, softening process associated with change of the microstructure can be described. In Straub (1995), Polcik et al. (1998), Polcik (1999), Barkar and Ågren (2005) the volume fraction η_h is related to the mean subgrain size. The increase in the subgrain size, or decrease of η_h is described with an exponential-type kinetic equation. It is calibrated against experimental data of substructure evolution based on in situ transmission electron microscope observations.

Equations (3.5.97)–(3.5.100) and a kinetic equation for the volume fraction can be used to simulate macroscopic material response for different types of loading. Such a simulation is feasible if material parameters in constitutive and evolution equations for constituents are well defined either from tests or from simulations at the microscale. An alternative approach is to reduce Eqs. (3.5.97)–(3.5.100) to obtain a macroscopic model with internal state variables. Then all response functions and material properties can be identified from macroscopic tests. As an example consider an approach presented in Naumenko et al. (2011a) to model hardening and softening in advanced steel. Instead of (3.5.100) the following constitutive equations are assumed

$$\dot{\epsilon}_s^{\text{pl}} = f_s(|\sigma_s|)\text{sgn}\sigma_s, \quad \dot{\epsilon}_h^{\text{pl}} = \frac{\sigma_h - \sigma}{\sigma_{h*} - \sigma} |\dot{\epsilon}^{\text{pl}}|, \quad (3.5.101)$$

where σ_{h*} is the saturation stress in the hard constituent. In Eqs. (3.5.101) the inelastic part of the soft constituent is determined by the non-linear viscosity function f_s . The inelastic strain rate of the hard constituent is proportional to the magnitude of the overall creep rate and the overstress $\sigma_{\text{ov}} = \sigma_h - \sigma$. As the elastic properties of constituents are assumed the same, after the loading in elastic range $\sigma_h = \sigma$, $\sigma_{\text{ov}} = 0$

and the inelastic strain rate of the hard constituent is zero. When $\sigma_h \rightarrow \sigma_{h*}$, where σ_{h*} is the saturation stress, the inelastic strain rate of the hard constituent in tensile regime approaches to the inelastic strain rate of the composite. Then $\dot{\varepsilon}_s^{\text{pl}} = \dot{\varepsilon}_h^{\text{pl}}$ and the stresses in both constituents approach the asymptotic values. For the sake of brevity let us assume isothermal loading. Taking the time derivative of Eq. (3.5.98) and applying Eq. (3.5.101) we obtain

$$\dot{\varepsilon}_s = \frac{\dot{\sigma}_s}{E} + f(|\sigma_s|)\text{sgn}\sigma_s, \quad \dot{\varepsilon}_h = \frac{\dot{\sigma}_h}{E} + \frac{\sigma_h - \sigma}{\sigma_{h*} - \sigma} |\dot{\varepsilon}^{\text{pl}}| \quad (3.5.102)$$

The strain rate of the mixture can be computed applying Eq. (3.5.99)₁ as follows

$$\dot{\varepsilon} = \frac{\dot{\sigma}}{E} + \dot{\varepsilon}^{\text{pl}} \quad (3.5.103)$$

For the identification it is convenient to introduce the following new variables

$$\beta = \frac{\eta_{h_0}}{1 - \eta_{h_0}} (\sigma_h - \sigma), \quad 0 \leq \beta \leq \beta_*, \quad \beta_* = \frac{\eta_{h_0}}{1 - \eta_{h_0}} (\sigma_{h*} - \sigma),$$

$$\Gamma = \frac{\eta_h}{1 - \eta_h} \frac{1 - \eta_{h_0}}{\eta_{h_0}}, \quad \Gamma_* \leq \Gamma \leq 1, \quad \Gamma_* = \frac{\eta_{h*}}{1 - \eta_{h*}} \frac{1 - \eta_{h_0}}{\eta_{h_0}},$$

where η_{h_0} is the reference value of η_h . Equations (3.5.97)–(3.5.100) and (3.5.101)–(3.5.103) can be transformed to

$$\dot{\varepsilon}^{\text{pl}} = f(|\sigma - \beta\Gamma|) \frac{\sigma - \beta\Gamma}{|\sigma - \beta\Gamma|} - \frac{1}{E} \frac{d}{dt}(\beta\Gamma), \quad (3.5.104)$$

$$\dot{\beta} = \frac{E}{c_h} \left(\dot{\varepsilon}^{\text{pl}} - |\dot{\varepsilon}^{\text{pl}}| \frac{\beta}{\beta_*} \right), \quad c_h = \frac{1 - \eta_{h_0}}{\eta_{h_0}}$$

In Eq. (3.5.104) β and Γ play now the role of internal state variables. If the fraction is kept constant then by setting $\Gamma = 1$ we obtain

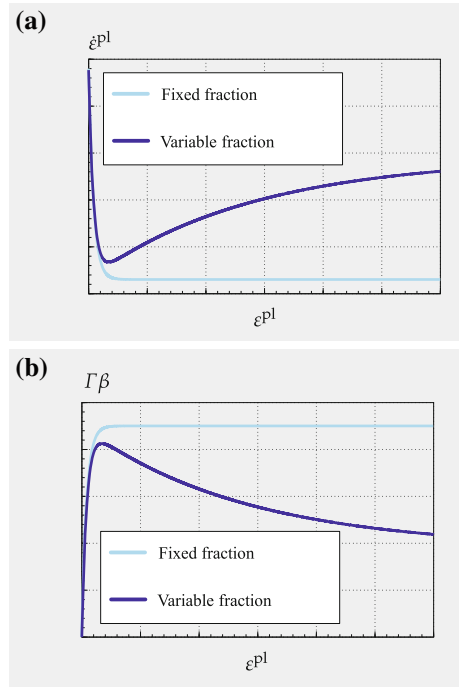
$$\dot{\varepsilon}^{\text{pl}} = f(|\sigma - \beta|) \frac{\sigma - \beta}{|\sigma - \beta|} - \frac{1}{E} \frac{d}{dt}(\beta), \quad (3.5.105)$$

$$\dot{\beta} = \frac{E}{c_h} \left(\dot{\varepsilon}^{\text{pl}} - |\dot{\varepsilon}^{\text{pl}}| \frac{\beta}{\beta_*} \right)$$

The underlined term influences the creep rate only at the beginning of the inelastic process. One may verify that if $c_h \gg 1$ then this term can be neglected. Then we obtain the kinematic hardening/recovery model proposed in Frederick and Armstrong (2007), see Sect. 3.5.2. Therefore, the variable β can be termed backstress or kinematic stress.

Fig. 3.6 Simulation of creep response under constant stress with Eqs. (3.5.104) and (3.5.106).

a Qualitative variation of inelastic strain rate versus inelastic strain. **b** Qualitative variation of backstress versus inelastic strain



For the variable Γ an additional evolution equation is required. Let us assume that Γ evolves by the exponential law with the increase of the mean inelastic strain towards the saturation value $\Gamma_*(\sigma)$, i.e.

$$\dot{\Gamma} = A_s(\Gamma_* - \Gamma)|\dot{\epsilon}^{pl}|, \quad (3.5.106)$$

where A_s is a constant. Then the set of Eqs. (3.5.104) and (3.5.106) describes the decrease of the inelastic strain rate as a result of stress redistribution between the constituents and the increase of the inelastic strain rate as a consequence of softening processes (decrease of the volume fraction of the hard constituent). As an example, consider a creep regime under the constant stress. Figure 3.6a illustrates the time variation of the inelastic strain rate as a function of the inelastic strain. Equations (3.5.104) and (3.5.106) describe the primary and the tertiary creep stages as a result of hardening and softening processes. If the volume fraction η_h is kept constant, and consequently $\Gamma = 1$, only the primary and the secondary creep stages can be described. In this case the backstress $\beta\Gamma$ attains a saturation value, Fig. 3.6b. If the volume fraction of the hard constituent is assumed to decrease, then Γ decreases and the backstress $\beta\Gamma$ decreases providing a possibility to describe the softening process. Equations (3.5.104) and (3.5.106) were identified in Naumenko et al. (2011a, b) based on creep data for several martensitic steels. Verification examples are presented illustrating a good performance of the model in describing hardening and softening for different loading paths.

3.5.4 Ageing

Strength characteristics of many materials is determined by precipitation and dispersion hardening. Heat-resistant steels contain several kinds of precipitate particles in the matrix and at grain boundaries including carbonitrides and intermetallic compounds (Abe 2008). Age-hardened aluminium alloys for high temperature applications, for example AA2014 alloy includes the θ' phase, in the form of rod-like precipitates aligned along the $\langle 001 \rangle$ crystallographic directions of the α -Al matrix (Naumenko and Gariboldi 2014). Dispersed fine precipitates are obstacles for mobile dislocations. Several mechanisms for interaction between mobile dislocations and particles are reviewed in Ilshner (1973), Kassner and Pérez-Prado (2004), Roesler et al. (2007) among others. An example is the Orowan bypassing mechanism, that predicts the yield stress to be inversely proportional to the mean spacing between particles or mean particle size, see Sect. 1.3. A decrease of the particle size would provide an increase of the yield stress. On the other hand, small particles can be sheared by dislocation. This shearing mechanism suggests the yield stress to decrease with a decrease in the particle size. The optimum strengthening can be achieved when an alloy contains precipitates that small enough to be bypassed and large enough to resist against shearing Roesler et al. (2007), Polmear (1996, 2004). The microstructural stability of many materials depends essentially on the precipitation sequences. For example, for age-hardenable Al alloys the high temperature exposure leads to the completion of precipitation and to coarsening of θ' particles (Gariboldi and Casaro 2007). Coarsening of carbide precipitates for steels is documented in (Abe 2008; Blum 2008; Straub 1995). The driving force of the coarsening process is the decrease in the mean surface energy. For example, for spherical particles the surface to the volume ratio is proportional to $1/D$, where D is the mean particle diameter. The increase of D would lead to a decrease of the surface energy. The process occurs by the growth of large particles at the expense of smaller ones which dissolve and is related to the diffusive mass transport. For example, the coarsening mechanism of θ' particles is governed by the diffusion of Cu in Al.

To describe the increase of the mean particle size the following equation is applied in Abe (2008), Blum (2008), Straub (1995), Gariboldi and Casaro (2007)

$$D^m = D_0^m + K(T)t, \quad K(T) = K_0 \exp\left(\frac{-Q_c}{RT}\right), \quad (3.5.107)$$

where K_0 is a material property and Q_c is the activation energy for the coarsening process. For spherical particles the exponent m takes the value 3, which is in accordance with the coarsening theories of Lifshitz and Slyozov (1961), Wagner (1961). For rod-like and plate-like particles m can take the value 2, as documented in Zhang et al. (2013), Gariboldi and Casaro (2007) for aluminum alloys. According to Eq. (3.5.107) the coarsening process is only related to the exposure time at high temperature. In several papers, for example, Nakajima et al. (2004) experimental data are presented, illustrating that inelastic deformation may affect the diffusion, and as a consequence the coarsening rate.

Though the evolution of the mean particle size can be examined by transmission electron microscopy, experimental analysis of how the mean particle size affects the inelastic strain rate is more challenging. Indeed, particles may affect the inelastic process directly and indirectly, as discussed by Ilschner (1973). The strain rate can be directly influenced by the mean particle spacing if the Orowan-type bypassing mechanism is assumed. As the particle volume fraction remains constant, the particle size is proportional to the particle spacing, see Sect. 1.3. Following Estrin (1996) the drag stress $\bar{\sigma}$ can be assumed as a superposition of the dislocation density and the particle hardening contributions as follows

$$\hat{\sigma} = M G b \left(\zeta \sqrt{\bar{\rho}} + \chi \frac{1}{D} \right), \quad (3.5.108)$$

where ζ and χ are weighting factors characterizing the contribution of the Taylor-type hardening due to dislocations and the Orowan-type hardening due to particles. With Eqs. (3.5.62) and (3.5.108) the increase in particle size leads to a decrease in the drag stress and increase in the creep rate. The particle hardening drag stress value is usually lower than the Orowan stress. This is explained by a variety of dislocation-particle interaction mechanisms operating in the creep range, e.g. dislocation climb over particles (Kassner and Pérez-Prado 2004).

Furthermore, the spacing or size of particles may affect the rates of hardening, recovery and softening. This constitutes an indirect influence on the inelastic strain rate, as pointed out by Ilschner (1973). For example, in the creep range, particles immobilize dislocations leading to formation of dislocation substructures. The storage/immobilization of dislocations can be related to the mean particle spacing.

Let us include the particle coarsening process into the constitutive equation for the inelastic strain rate and into the evolution equation for the dislocation density-type hardening variable given in Sect. 3.5.1. To this end let us modify the evolution equation for the mean dislocation density (3.5.76) as follows

$$\dot{\rho} = (k_1 \sqrt{\bar{\rho}} - k_2 \rho) |\dot{\epsilon}^{\text{pl}}|, \quad (3.5.109)$$

where

$$k_1 = 2B \sqrt{\bar{\rho}_*}, \quad k_2 = 2B, \quad \sqrt{\bar{\rho}_*} = \sqrt{\bar{\rho}_\infty} \frac{D_0}{D},$$

where D_0 is the mean particle size in the reference state. To describe the coarsening mechanism within the framework of continuum mechanics let us introduce the internal state variable $\Phi = D_0/D$ as proposed by Dyson and McLean (1998). From Eq. (3.5.107) the following kinetic equation can be derived

$$\dot{\Phi} = -\frac{A_s}{m} \Phi^{m+1}, \quad A_s(T) = A_0 \exp\left(\frac{-Q_c}{RT}\right), \quad A_0 = \frac{K_0}{D_0^m} \quad (3.5.110)$$

Furthermore let us introduce a hardening variable H as follows

$$H = \frac{\zeta D \sqrt{\rho} + \chi}{\zeta D_0 \sqrt{\rho_0} + \chi} \quad (3.5.111)$$

With the introduced state variables Φ and H and with Eq. (3.5.108) the constitutive equation (3.5.62) takes the following form

$$\dot{\varepsilon}^{\text{pl}} = \dot{\varepsilon}_0 \left(\frac{|\sigma|}{\sigma_0 H \Phi} \right)^n \text{sgn}(\sigma) \quad (3.5.112)$$

with

$$\sigma_0 = M G b \left(\zeta \sqrt{\varrho_0} + \frac{\chi}{D_0} \right)$$

The evolution equation (3.5.109) can be formulated as follows

$$\dot{H} = B (H_\infty - H) |\dot{\varepsilon}^{\text{pl}}| + (H - H_{D_*}) \frac{d}{dt} \ln \Phi, \quad (3.5.113)$$

with

$$H_\infty = \frac{\zeta D_0 \sqrt{\varrho_\infty} + \chi}{\zeta D_0 \sqrt{\rho_0} + \chi}, \quad H_{D_*} = \frac{\chi}{\zeta D_0 \sqrt{\varrho_0} + \chi}$$

The variable H can be considered as a modified hardening variable since it includes the influence of particles in addition to the mean dislocation density. Let us note that processes associated with change in dislocation density and coarsening of precipitates have usually quite different characteristic time. Therefore, two rate terms in the right-hand side of Eq. (3.5.113) may have different orders of magnitudes since the coarsening is much slower if compared to the hardening/recovery. In Dyson and McLean (2001), Kowalewski et al. (1994), Naumenko and Gariboldi (2014), Perrin and Hayhurst (1994) instead of Eq. (3.5.113) the following simplified equation for the hardening variable is used

$$\dot{H} = B (H_\infty - H) |\dot{\varepsilon}^{\text{pl}}| \quad (3.5.114)$$

Assuming the creep regime with the constant tensile stress, Eqs. (3.5.110) and (3.5.114) can be integrated providing the values of internal state variables in a closed analytical form. Then with Eq. (3.5.112) the inelastic strain rate follows

$$\dot{\varepsilon}^{\text{pl}} = \dot{\varepsilon}_0 \left(\frac{\sigma}{\sigma_0} \right)^n \frac{(1 + A_s t)^{\frac{n}{m}}}{[H_\infty - (H_\infty - 1) \exp(-B \varepsilon^{\text{pl}})]^n} \quad (3.5.115)$$

Equation (3.5.115) can be used to identify the material parameters A_s , B and σ_0 as well as the functions H_∞ and $\dot{\epsilon}_0$ from families of creep curves. An example of identification for forged AA2014 alloy is presented in Naumenko and Gariboldi (2014).

Advanced high-temperature materials, for example, high-chromium steel contain different types of precipitates having different coarsening rates. Furthermore, change in precipitation structures at grain or subgrain boundaries may promote strain softening and damage processes. For example, coarsening of precipitates at subgrain boundaries increase the rate at which subgrains coarsen. Kinetic equations for coarsening of different types of precipitates are discussed in the literature, a review presented by Straub (1995).

3.6 Damage

Softening and ageing phenomena discussed in Sects. 3.5.3 and 3.5.4 lead to a decrease of resistance against inelastic flow. As the inelastic strain rate increases and a specimen may fail as a result of necking, softening and ageing may be classified as material degradation processes. Inelastic deformation is often accompanied by damage processes—phenomena that can lead directly to macroscopic fracture. Examples include the formation, growth and coalescence of voids on grain boundaries, micro-cracks in particles of the second phase, decohesion at particle/matrix interfaces and surface relief. Defects in microstructure like voids and cracks may exist after the material processing, may nucleate in the early stages of loading, for example, during primary creep stage or even under spontaneous deformation in elastic range. The initially existing micro-defects have negligible influence on the macroscopic response such as inelastic strain rate. As their number and size increase, they weaken the material providing the decrease in the load-bearing capacity. The coalescence of cavities or propagation of micro-cracks lead to the final fracture. Damage mechanisms and damage processes are reviewed and classified in Ashby et al. (1979), François et al. (2012).

A micromechanics approach to damage modeling requires the analysis of many different mechanisms that may operate and interact in a specific material under specific loading conditions. As an example, consider different physical models related to grain boundary cavitation in the creep range, as discussed and reviewed in Kassner and Hayes (2003), Riedel (1987), François et al. (2012), Ozhoga-Maslovskaja et al. (2015).

A pragmatic approach is to introduce internal state variables to capture damage process in a phenomenological sense. For example, the tertiary creep stage is partly determined by the damage processes, Sect. 1.1.1.2. Therefore, one may develop and calibrate a damage evolution equation to describe the final stage of the creep curve. The idea of continuum damage mechanics is to formulate such damage laws to capture material behavior under various loading paths (Krajcinovic 1996; Lemaitre and Desmorat 2005; Murakami 2012).

3.6.1 Kachanov-Rabotnov Model

The phenomenological damage equations were firstly proposed by Kachanov (1958) and Rabotnov (1959) in order to characterize creep damage evolution. A new internal variable has been introduced to characterize “continuity” or “damage” of the material. The geometrical interpretation of the continuity variable starts from changes in the cross-section area of a uni-axial specimen. Specifying the initial cross-section area of a specimen by A_0 and the area of voids, cavities, micro-cracks, etc. by A_D , the Kachanov’s continuity is defined as follows (Kachanov 1986),

$$\psi = \frac{A_0 - A_D}{A_0}$$

The value $\psi = 1$ means the virgin, fully undamaged state, the condition $\psi = 0$ corresponds to the fracture (completely damaged cross-section).

Rabotnov (1959, 1963, 1969) introduced the dual damage variable ω . In Rabotnov (1963) he pointed out that the damage state variable ω “may be associated with the area fraction of cracks, but such an interpretation is connected with a rough scheme and is therefore not necessary”. Rabotnov assumed that the creep rate is additionally dependent on the current damage state. The constitutive equation should have the form

$$\dot{\varepsilon}^{\text{pl}} = f(\sigma, \omega) \quad (3.6.116)$$

Furthermore, the damage processes can be reflected in the evolution equation

$$\dot{\omega} = g(\sigma, \omega), \quad \omega|_{t=0} = 0, \quad \omega < \omega_*, \quad (3.6.117)$$

where ω_* is the critical value of the damage parameter for which the material fails. With the power functions of stress and damage the constitutive equation may be formulated as follows

$$\dot{\varepsilon}^{\text{pl}} = \frac{a|\sigma|^n}{(1-\omega)^m} \text{sgn}\sigma \quad (3.6.118)$$

Similarly, the damage rate can be expressed by

$$\dot{\omega} = \frac{b}{(1-\omega)^l} \left(\frac{\sigma + |\sigma|}{2} \right)^k \quad (3.6.119)$$

The material dependent parameters a , b , n , m , l and k should be identified from families of creep curves. It is easy to prove that for the damage free state ($\omega = 0$), the first equation results in the power law creep constitutive equation.

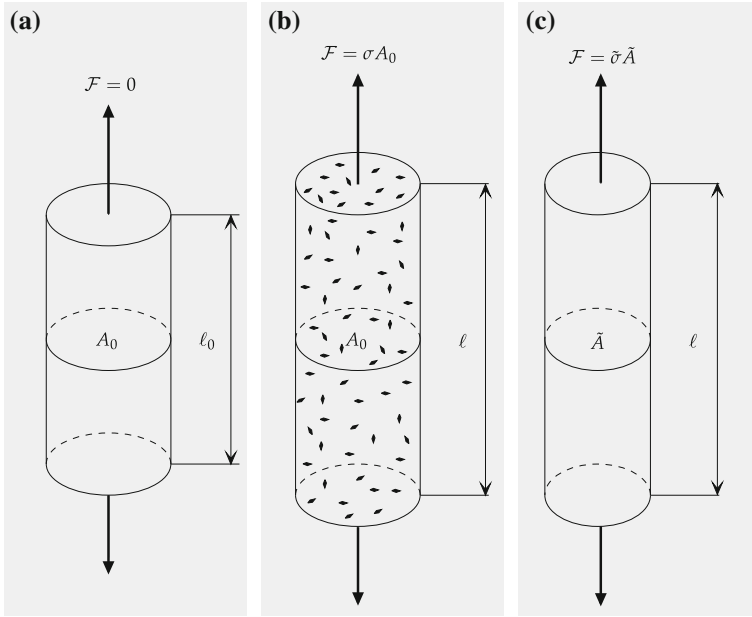


Fig. 3.7 Strain and damage of a bar. **a** Initial state. **b** Damaged state. **c** Fictitious undamaged state

Setting $m = n$ the first equation can be written as

$$\dot{\varepsilon}^{Pl} = a|\tilde{\sigma}|^n, \tag{3.6.120}$$

where $\tilde{\sigma} = \sigma/(1 - \omega)$ is the so-called net-stress or effective stress. With the effective stress Eq. (3.6.120) provides a way to generalize a secondary creep law for the description of tertiary creep process. Lemaitre and Chaboche (1990) proposed the effective stress concept to formulate constitutive equations for damaged materials based on available constitutive equation for “virgin” materials. An interpretation can be given for a tension bar, Fig. 3.7. Here A_0 denotes the initial cross-section area of the bar, Fig. 3.7a. From the given tensile force \mathcal{F} the stress can be computed as $\sigma = \mathcal{F}/A_0$. The axial strain for the loaded bar $\varepsilon = (l - l_0)/l_0$ can be expressed as a function of the stress and the actual damage $\varepsilon = f(\sigma, \omega)$, Fig. 3.7b. For the effective cross-section $\tilde{A} = A_0(1 - \omega)$ the effective stress is

$$\tilde{\sigma} = \frac{\mathcal{F}}{\tilde{A}} = \frac{\sigma}{1 - \omega} \tag{3.6.121}$$

Now a fictitious undamaged bar with a cross-section area \tilde{A} , Fig. 3.7c, having the same axial strain response as the actual damaged bar $\varepsilon = f(\tilde{\sigma}) = f(\sigma, \omega)$ is introduced. The strain equivalence principle (Lemaitre 1996) states that any strain constitutive equation for a damaged material may be derived in the same way as for

a virgin material except that the usual stress is replaced by the effective stress. Thus the constitutive equation for the creep rate (3.6.120) is the power law generalized for a damaged material. Note that the effective cross section area is not just understood as the initial area minus the area occupied by defects. This quantity and the effective stress are introduced to account for stress concentrations produced by cavities and/or microcracks in a phenomenological sense.

Equations (3.6.118) and (3.6.119) can be generalized to the non-isothermal conditions by replacing the parameters a and b by the functions of temperature. Assuming Arrhenius type temperature dependence the following relations can be applied

$$a(T) = a_0 \exp\left(-\frac{Q_a}{RT}\right), \quad b(T) = b_0 \exp\left(-\frac{Q_b}{RT}\right), \quad (3.6.122)$$

where Q_a and Q_b are the activation energies of creep and damage processes, respectively.

To identify the material parameters in Eqs. (3.6.118), (3.6.119) and (3.6.122) experimental data of uni-axial creep up to rupture for certain stress and temperature ranges are required. To illustrate the idea of identification let us ignore hardening, softening and ageing processes. Furthermore let us assume $m = n$ in Eq. (3.6.118) for the sake of brevity. Then the uni-axial creep model for $\sigma > 0$ takes the following form

$$\dot{\varepsilon}^{\text{pl}} = a \left(\frac{\sigma}{1 - \omega} \right)^n, \quad \dot{\omega} = \frac{b\sigma^k}{(1 - \omega)^l} \quad (3.6.123)$$

With $\omega = 0$ the first equation describes the secondary creep. The minimum (steady-state) creep rate is defined by the power law function of the applied stress

$$\dot{\varepsilon}_{\text{min}}^{\text{pl}} = a\sigma^n \quad (3.6.124)$$

In the steady-state creep range the creep curves are approximated by straight lines, Fig. 3.8a. From the family of creep curves the minimum creep rate versus stress curve can be obtained. A sketch for such a curve in a double logarithmic scale is presented in Fig. 3.8b. For a certain stress range $\log \dot{\varepsilon}_{\text{min}}^{\text{pl}}$ can be approximated by a linear function of $\log \sigma$. The parameters a and n can be determined from the steady-state creep. Let $\dot{\varepsilon}_{\text{min}1}^{\text{pl}}$ and $\dot{\varepsilon}_{\text{min}2}^{\text{pl}}$ be minimum creep rates for the constant stresses σ_1 and σ_2 , respectively. Then the material parameters can be estimated as follows

$$n = \frac{\log(\dot{\varepsilon}_{\text{min}1}^{\text{pl}}/\dot{\varepsilon}_{\text{min}2}^{\text{pl}})}{\log(\sigma_1/\sigma_2)}, \quad a = \frac{\dot{\varepsilon}_{\text{min}1}^{\text{pl}}}{\sigma_1^n} = \frac{\dot{\varepsilon}_{\text{min}2}^{\text{pl}}}{\sigma_2^n} \quad (3.6.125)$$

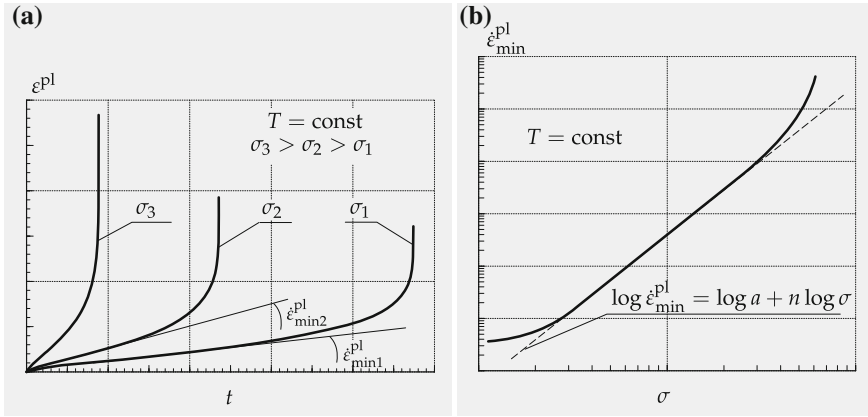


Fig. 3.8 Phenomenological description of uni-axial creep. **a** Creep strain versus time curves. **b** Minimum creep rate versus stress curve

For a constant stress σ the damage evolution equation in Eq. (3.6.123) can be integrated as follows

$$\int_0^{\omega_*} (1 - \omega)^l d\omega = \int_0^{t_*} b\sigma^k dt,$$

where t_* is the time to fracture of the specimen. Setting $\omega_* = 1$ and performing the integration one can obtain

$$t_* = \frac{1}{(l + 1)b\sigma^k} \tag{3.6.126}$$

This equation describes the time to creep fracture versus applied stress relation. For a number of metals and alloys experimental data for creep strength can be approximated by a straight line in a double logarithmic scale for a certain stress range. From Eq. (3.6.126) it follows

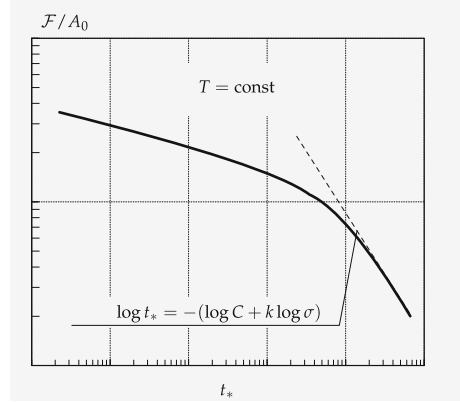
$$\log t_* = -(\log C + k \log \sigma), \quad C = b(l + 1) \tag{3.6.127}$$

A typical creep strength curve is sketched in Fig. 3.9. The linear approximation (3.6.127) is only valid for a specific stress range, Fig. 3.9. Based on Eq. (3.6.127) and the creep strength curve the following relations can be obtained

$$k = \frac{\log(t_{*2}/t_{*1})}{\log(\sigma_1/\sigma_2)}, \quad b(l + 1) = \frac{1}{t_{*1}\sigma_1^k} = \frac{1}{t_{*2}\sigma_2^k},$$

where t_{*1} and t_{*2} are values of time to fracture corresponding to the applied stresses σ_1 and σ_2 , respectively. Integration of the second Eq. (3.6.123) by use of Eq. (3.6.126)

Fig. 3.9 Creep strength curve



provides the damage parameter as a function of time

$$\omega(t) = 1 - \left(1 - \frac{t}{t_*}\right)^{\frac{1}{l+1}} \quad (3.6.128)$$

With Eq. (3.6.128) the creep rate equation (3.6.123) can be integrated leading to the creep strain versus time dependence

$$\varepsilon^{\text{pl}}(t) = \frac{a\sigma^{n-k}}{b(l+1-n)} \left[1 - \left(1 - \frac{t}{t_*}\right)^{\frac{l+1-n}{l+1}}\right] \quad (3.6.129)$$

From Eq. (3.6.129) it follows that the constant l must satisfy the condition $l > n - 1$ providing the positive strain for the positive stress values. By setting $t = t_*$ the creep strain before the fracture, i.e. $\varepsilon_*^{\text{pl}} = \varepsilon^{\text{pl}}(t_*)$, can be calculated as

$$\varepsilon_*^{\text{pl}} = \frac{a\sigma^{n-k}}{b(l+1-n)} \quad (3.6.130)$$

For $n > k$ the fracture strain increases with an increase in the stress value. Such a dependence is usually observed for many alloys in the case of moderate stresses. From Eqs. (3.6.124), (3.6.127) and (3.6.130) the following relations can be obtained

$$\varepsilon_*^{\text{pl}} = \frac{\dot{\varepsilon}_{\min}^{\text{pl}} t_*}{1 - \frac{n}{l+1}}, \quad \dot{\varepsilon}_{\min}^{\text{pl}} t_* = \frac{a}{b(l+1)} \sigma^{n-k} \quad (3.6.131)$$

In the special case $n = k$ the second equation in (3.6.131) reads

$$\dot{\varepsilon}_{\min}^{\text{pl}} t_* = \frac{a}{b(l+1)} = \text{const}$$

This is the Monkman-Grant relationship which states, that for a given material the product of the minimum creep rate and the time to fracture is a material constant. We observe, that the Monkman-Grant relationship follows from the Kachanov-Rabotnov model if the slopes of the minimum creep rate versus stress and the stress versus time to fracture dependencies coincide in the double logarithmic scale. In this case the strain before the creep fracture (creep ductility) should be stress independent, as it follows from the first equation in (3.6.131).

With Eq. (3.6.131) the creep strain versus time dependence (3.6.129) takes the form

$$\varepsilon^{\text{pl}}(t) = \frac{\dot{\varepsilon}_{\min}^{\text{pl}} t_*}{1 - \frac{n}{l+1}} \left[1 - \left(1 - \frac{t}{t_*} \right)^{1 - \frac{n}{l+1}} \right] \quad (3.6.132)$$

We observe that the constant l controls the shape of the tertiary creep stage. For $n/(l+1) \ll 1$ Eq. (3.6.132) can be approximated by

$$\varepsilon^{\text{pl}}(t) = \dot{\varepsilon}_{\min}^{\text{pl}} t, \quad 0 \leq t \leq t_*$$

In this case the tertiary creep stage is not observable. Instead of Eq. (3.6.123) one may apply the simplified constitutive model, where the influence of creep damage on the creep rate is ignored, i.e.

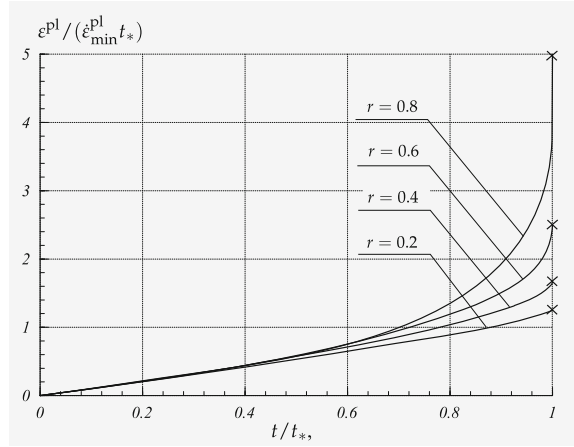
$$\dot{\varepsilon}^{\text{pl}} = a\sigma^n, \quad \dot{\omega} = \frac{b\sigma^k}{(1-\omega)^l} \quad (3.6.133)$$

In a slightly different form Eq. (3.6.133) were originally proposed by Kachanov (1958) under assumption that for brittle materials the damage processes have negligible influence on the creep rate.

Figure 3.10 provides the plots of Eq. (3.6.132) with respect to the normalized creep strain and normalized time for different values of $r \equiv n/(l+1)$. We observe that even for $r = 0.2$ the creep rate is almost constant. The increase of r leads to the increase of tertiary creep rate, the increase of the “duration” of the tertiary stage and increase of the fracture strain.

The phenomenological model (3.6.123) characterizes the effect of damage evolution and describes the tertiary creep in a uni-axial test. For a number of metals and alloys material parameters are available, see e.g. Altenbach et al. (1997), Altenbach and Naumenko (1997), Altenbach et al. (2000, 2001), Bodnar and Chrzanowski (1991), Boyle and Spence (1983), Hayhurst (1972), Hyde et al. (2003, 2000, 1997, 1999), Konkin and Morachkovskij (1987), Kowalewski (1996), Lemaitre (2001), Lemaitre and Chaboche (1990), Lemaitre et al. (2009), Murakami and Liu (1995). Instead of the power law functions of stress or damage it is possible to use another kind of functions, e.g. the hyperbolic sine functions in both the creep and damage evolution equations. In addition, by the introduction of suitable hardening, softening and ageing variables, the model can be extended to consider all creep stages. Examples are presented in Altenbach et al. (2013), Kowalewski et al. (1994), Naumenko

Fig. 3.10 Creep curves for different values of $r = n/(l + 1)$



and Kostenko (2009), Naumenko et al. (2011a, b), Naumenko and Altenbach (2005), Perrin and Hayhurst (1994).

In applying Eq. (3.6.123) to the analysis of structures one should bear in mind that the material parameters are usually estimated from experimental creep curves, available for a narrow range of stresses. The linear dependencies between $\log \dot{\varepsilon}_{\min}^{\text{cr}}$ and $\log \sigma$ or between $\log t_*$ and $\log \sigma$ do not hold for wide stress ranges. For example, it is known from materials science that for higher stresses the damage mode may change from inter-granular to trans-granular, e.g. Ashby et al. (1979). Furthermore, for higher values of the engineering stress the true stress increases due to the cross section shrinkage. This should be considered in calibrating the damage evolution equation based on experimental data on creep and/or creep strength. One may assume that the volume of the specimen does not change during the creep process providing the relation between the change in the cross section and the elongation, Sect. 3.4. With the relation between the true stress and the engineering stress the damage evolution equation (3.6.123) can be integrated providing a two-stage creep strength curve, Fig. 3.10. The related analysis is presented in Rabotnov (1963, 1969).

The damage evolution equation may be put in a different form, which is sometimes more convenient for the identification. To this end let us specify Eqs. (3.6.116) and (3.6.117) as follows

$$\dot{\varepsilon}^{\text{pl}} = f_{\sigma}(|\sigma|)f_{\omega}(\omega)\text{sgn}\sigma, \quad \dot{\omega} = g_{\sigma}(|\sigma|)g_{\omega}(\omega)\frac{1 + \text{sgn}\sigma}{2}, \quad (3.6.134)$$

where $f_{\sigma}(|\sigma|)$, $f_{\omega}(\omega)$, $g_{\sigma}(|\sigma|)$ and $g_{\omega}(\omega)$ are functions to be identified from experimental data. With the constitutive equation for the inelastic strain rate (3.6.134)₁ the damage evolution equation (3.6.134)₂ can be put in the following form

$$\dot{\omega} = h_{\omega}(\omega) \frac{1 + \operatorname{sgn} \sigma}{2} \frac{|\dot{\varepsilon}^{\text{pl}}|}{\varepsilon_*^{\text{pl}}(|\sigma|)}, \quad (3.6.135)$$

where

$$h_{\omega}(\omega) = \frac{g_{\omega}(\omega)}{f_{\omega}(\omega)} r(\omega_*), \quad r(\omega_*) = \int_0^{\omega_*} \frac{f_{\omega}(x)}{g_{\omega}(x)} dx, \quad \varepsilon_*(|\sigma|) = \frac{f_{\sigma}(|\sigma|)}{g_{\sigma}(|\sigma|)}$$

Integrating (3.6.135) for the constant positive true stress provides the relationship between the damage parameter and the inelastic strain

$$\Psi(\omega) = \frac{\varepsilon^{\text{pl}}}{\varepsilon_*^{\text{pl}}(|\sigma|)}, \quad (3.6.136)$$

where

$$\Psi(\omega) = \int_0^{\omega} \frac{dx}{h_{\omega}(x)}$$

Since $\Psi(\omega_*) = 1$, the function $\varepsilon_*^{\text{pl}}(|\sigma|)$ is the strain before the creep fracture under the constant true stress.

3.6.2 Continuum Damage Mechanics

Let us discuss how to introduce a damage parameter into the one-dimensional continuum mechanics framework. For the sake of brevity let us ignore hardening, softening and ageing. The dissipation inequality (2.6.50) with $\dot{F}F^{-1} = \dot{\varepsilon}_{\text{H}}$ has the following form (3.5.66)

$$\sigma \dot{\varepsilon}_{\text{H}} - \rho \dot{\Phi} - \rho S \dot{T} - q \frac{T'}{T} \geq 0 \quad (3.6.137)$$

Let us assume the following split of the mechanical power

$$\begin{aligned} \mathcal{L} &= \sigma \dot{\varepsilon}_{\text{H}} = \mathcal{L}_{\text{s}} + \mathcal{L}_{\text{d}}, \\ \mathcal{L}_{\text{s}} &= \sigma_{\text{s}}(\varepsilon_{\text{H}}^{\text{el}}, \omega, T) \dot{\varepsilon}_{\text{H}}^{\text{el}}, \\ \mathcal{L}_{\text{d}} &= \sigma_{\text{d}}(\dot{\varepsilon}_{\text{H}}^{\text{pl}}, \omega, T) \dot{\varepsilon}_{\text{H}}^{\text{pl}} \end{aligned} \quad (3.6.138)$$

As in the Sect. 3.5 let us assume the iso-stress approach such that

$$\sigma = \sigma_{\text{s}}(\varepsilon_{\text{H}}^{\text{el}}, \omega, T) = \sigma_{\text{d}}(\dot{\varepsilon}_{\text{H}}^{\text{pl}}, \omega, T)$$

Therefore, the free energy is now a function of the elastic strain, the damage parameter and the temperature. The inequality (3.5.66) takes the form

$$\left(\sigma - \rho \frac{\partial \Phi}{\partial \varepsilon_H^{\text{el}}} \right) \dot{\varepsilon}_H^{\text{el}} - \rho \left(\frac{\partial \Phi}{\partial T} + \mathcal{S} \right) \dot{T} + \sigma \dot{\varepsilon}^{\text{pl}} - \rho \frac{\partial \Phi}{\partial \omega} \dot{\omega} - q \frac{T'}{T} \geq 0 \quad (3.6.139)$$

To resolve the inequality assume that the internal state variable ω is defined by the following evolution equation

$$\dot{\omega} = g(\varepsilon_H^{\text{el}}, T, \omega, \dot{\varepsilon}_H^{\text{pl}}) \quad (3.6.140)$$

Furthermore, assume that the thermal conductivity is not affected by damage, for the sake of brevity.⁶ Then, for arbitrary $\dot{\varepsilon}^{\text{el}}$ and \dot{T} the inequality (3.6.139) is satisfied with

$$\sigma = \rho \frac{\partial \Phi}{\partial \varepsilon_H^{\text{el}}}, \quad \mathcal{S} = -\frac{\partial \Phi}{\partial T}, \quad -q \frac{T'}{T} \geq 0, \quad \sigma \dot{\varepsilon}_H^{\text{pl}} - \rho \frac{\partial \Phi}{\partial \omega} \dot{\omega} \geq 0 \quad (3.6.141)$$

For the stress let us assume the following constitutive equation

$$J\sigma = \frac{\partial \rho_0 \Phi}{\partial \varepsilon_H^{\text{el}}} = \begin{cases} E g_{\omega_T}(\omega) \varepsilon_H^{\text{el}}, & \varepsilon_H^{\text{el}} \geq 0, \\ E g_{\omega_C}(\omega) \varepsilon_H^{\text{el}}, & \varepsilon_H^{\text{el}} < 0, \end{cases} \quad (3.6.142)$$

where the functions $g_{\omega_T}(\omega)$ and $g_{\omega_C}(\omega)$ have the following properties

$$g_{\omega_i}(0) = 1, \quad g_{\omega_i}(\omega_*) = g_{*i}, \quad 0 < g_{*i} \ll 1, \quad \frac{dg_{\omega_i}}{d\omega} \leq 0, \quad i = T, C$$

These functions characterize the degradation of stiffness with progressive damage. As different damage mechanisms under tension and compression operate, different functions with subscripts T and C for tensile and compressive regimes are introduced. The material parameters g_{*T} and g_{*C} are introduced to evaluate the material stiffness under the critical damage state. Equation (3.6.142) can also be formulated as follows

$$J\sigma = E g_{\omega_T}(\omega) \frac{\varepsilon_H^{\text{el}} + |\varepsilon_H^{\text{el}}|}{2} + E g_{\omega_C}(\omega) \frac{\varepsilon_H^{\text{el}} - |\varepsilon_H^{\text{el}}|}{2} \quad (3.6.143)$$

With the constitutive equation (3.6.142), Eq. (3.6.141) can be integrated providing the following expression for the free energy

⁶The influence of damage on the heat transfer is analyzed in Skrzypek and Ganczarski (1998), Ganczarski and Skrzypek (2000).

$$\rho_0 \Phi = \left\{ \begin{array}{l} \frac{1}{2} E g_{\omega_T}(\omega) \varepsilon_H^{\text{el}^2}, \quad \varepsilon_H^{\text{el}} \geq 0 \\ \frac{1}{2} E g_{\omega_C}(\omega) \varepsilon_H^{\text{el}^2}, \quad \varepsilon_H^{\text{el}} < 0 \end{array} \right\} + \rho_0 \Phi_\omega(\omega) + \rho_0 \Phi_0, \quad (3.6.144)$$

where $\rho_0 \Phi_\omega(\omega)$ is the energy required to damage an infinitesimal volume element up to the value ω . It can be interpreted, as the energy required to form cavities of given radius and distribution, energy to form microcracks of given length and distribution, etc. With (3.6.144) the last inequality in (3.6.141) takes the following form

$$J \sigma \dot{\varepsilon}_H^{\text{pl}} + R(\varepsilon_H^{\text{el}}, \omega) \dot{\omega} \geq 0, \quad R(\varepsilon_H^{\text{el}}, \omega) = Y(\varepsilon_H^{\text{el}}, \omega) - h(\omega), \quad (3.6.145)$$

where

$$Y = -\frac{1}{2} E \varepsilon_H^{\text{el}^2} \left\{ \begin{array}{l} \frac{dg_{\omega_T}}{d\omega}, \quad \varepsilon_H^{\text{el}} \geq 0, \\ \frac{dg_{\omega_C}}{d\omega}, \quad \varepsilon_H^{\text{el}} < 0, \end{array} \right. \quad h(\omega) = \frac{d\rho_0 \Phi_\omega}{d\omega}, \quad (3.6.146)$$

The degradation functions g_{ω_T} , g_{ω_C} , the resistance function $h(\omega)$ as well as the damage evolution equation should be specified according to mechanisms of damage evolution for the given material, loading conditions and results of material testing. Many formulations related to brittle damage, ductile damage, creep damage, fatigue damage are discussed within the framework of continuum damage mechanics (Murakami 2012; Lemaitre and Desmorat 2005; Skrzypek and Ganczarski 1998). Let us consider some elementary examples.

With the strain equivalence principle, Sect. 3.6.1 the degradation functions can be given as follows, e.g. Lemaitre and Desmorat (2005)

$$g_{\omega_T} = 1 - \omega, \quad g_{\omega_C} = 1 - \kappa \omega, \quad 0 \leq \omega \leq \omega_*, \quad 0 \leq \kappa \leq 1 \quad (3.6.147)$$

where $\omega_* < 1$ is a critical value of the damage parameter, and the constant κ controls the tension-compression difference caused by damage. For $\kappa = 0$, damage does not affect the strain energy density under compression while for $\kappa = 1$ the behavior under tension and compression is the same. Let us assume $h(\omega) = h_0$, where h_0 is a constant. Furthermore, let us neglect the inelastic behavior and consider small elastic strains. Then the inequality (3.6.145) takes the following form

$$R(\varepsilon) \dot{\omega} \geq 0, \quad R(\varepsilon) = \left\{ \begin{array}{l} \frac{1}{2} E \varepsilon^2 - h_0, \quad \varepsilon \geq 0, \\ \frac{1}{2} \kappa E \varepsilon^2 - h_0, \quad \varepsilon < 0 \end{array} \right. \quad (3.6.148)$$

Assume that $\dot{\omega} \geq 0$, i.e. damage healing processes are excluded. Then the dissipation inequality (3.6.148) can be satisfied with the following damage evolution equation

$$\dot{\omega} = \Omega(< R(\varepsilon) >), \quad (3.6.149)$$

where $\Omega(x)$ is a monotonic function with $\Omega(x) \geq 0$ and $\Omega(0) = 0$. The Macaulay brackets $\langle x \rangle$ are defined as follows

$$\langle x \rangle = \frac{x + |x|}{2}$$

The function $R(\varepsilon)$ plays a role of a damage driving force similarly to the concept of crack driving force in the fracture mechanics (Rice 1978). An example for Ω is a power law-type function

$$\dot{\omega} = a_0 \left(\frac{\langle R(\varepsilon) \rangle}{R_0} \right)^p, \quad (3.6.150)$$

where a_0 , R_0 and p are material parameters. Instead of (3.6.150) one may apply a rate-independent formulation which includes the condition of the non-negative damage rate, i.e. $\dot{\omega} \geq 0$ and the admissibility condition for the driving force, i.e. $R(\varepsilon) \leq 0$. Furthermore it is assumed that $\dot{\omega} = 0$ if $R(\varepsilon) < 0$ and $\dot{\omega} > 0$ is only possible if $R(\varepsilon) = 0$. The rate-independent formulation can be given as follows

$$\dot{\omega} \geq 0, \quad R(\varepsilon) \leq 0, \quad \dot{\omega} R(\varepsilon) = 0 \quad (3.6.151)$$

With Eq. (3.6.143) one can compute the stress as follows

$$\sigma = E(1 - \omega) \frac{\varepsilon + |\varepsilon|}{2} + E(1 - \kappa\omega) \frac{\varepsilon - |\varepsilon|}{2} \quad (3.6.152)$$

Equations (3.6.148)–(3.6.152) can be used to model elasticity with damage based on the strain energy density criterion for damage evolution. Instead of the strain energy density one may apply the complementary energy density. The inverse of Eq. (3.6.152) provides

$$\varepsilon = \frac{\sigma + |\sigma|}{2E(1 - \omega)} + \frac{\sigma - |\sigma|}{2E(1 - \kappa\omega)} \quad (3.6.153)$$

Inserting into Eq. (3.6.148) yields the following stress based formulation

$$R_\sigma(\sigma, \omega) \dot{\omega} \geq 0, \quad R_\sigma(\sigma, \omega) = \begin{cases} \frac{\sigma^2}{2E(1 - \omega)^2} - h_0, & \sigma \geq 0, \\ \frac{\kappa\sigma^2}{2E(1 - \kappa\omega)^2} - h_0, & \sigma < 0 \end{cases} \quad (3.6.154)$$

The damage driving force $R_\sigma(\sigma, \omega)$ can also be given as follows

$$R_\sigma(\sigma, \omega) = \frac{\sigma^2}{2E(1 - \omega)^2} \left[\frac{1 + \text{sgn}\sigma}{2} + \kappa \frac{1 - \text{sgn}\sigma}{2} \left(\frac{1 - \omega}{1 - \kappa\omega} \right)^2 \right] - h_0 \quad (3.6.155)$$

With Eq. (3.6.155) the damage evolution equation can be formulated with respect to the stress. Depending on the type of material behavior and available experimental data different forms of damage evolution equations for brittle materials are proposed. The difference is in the type of the degradation functions, the type of damage resistance functions and the type of the damage driving force (Murakami 2012; Lemaitre and Desmorat 2005; Skrzypek and Ganczarski 1998).

To present examples of damage evolution equations for materials that exhibit inelastic material behavior let us apply the stress-based formulation. To this end we apply the inverse form of the constitutive equation (3.6.143)

$$\varepsilon_H^{\text{el}}(\sigma, \omega) = J \frac{\sigma + |\sigma|}{2E g_{\omega_T}(\omega)} + J \frac{\sigma - |\sigma|}{2E g_{\omega_C}(\omega)} \quad (3.6.156)$$

For the sake of brevity let us assume that under compression the effect of damage is negligible and set $g_{\omega_C}(\omega) = 1$. With Eq. (3.6.156) the dissipation inequality (3.6.145) can be formulated as follows

$$J\sigma \dot{\varepsilon}_H^{\text{pl}} + R_\sigma(\sigma, \omega)\dot{\omega} \geq 0, \quad R_\sigma(\sigma, \omega) = Y_\sigma(\sigma, \omega) - h(\omega), \quad (3.6.157)$$

where

$$Y_\sigma(\sigma, \omega) = -\frac{1}{2E} \left(\frac{J\sigma}{g_{\omega_T}} \right)^2 \frac{dg_{\omega_T}}{d\omega} \left(\frac{1 + \text{sgn}\sigma}{2} \right) \quad (3.6.158)$$

Many constitutive models of inelastic behavior coupled with damage that satisfy (3.6.157) were proposed, e.g. Murakami (2012), Lemaitre and Desmorat (2005), Skrzypek and Ganczarski (1998). One example is the following formulation

$$\dot{\varepsilon}^{\text{pl}} = f_\sigma(|\sigma|)f_\omega(\omega)\text{sgn}\sigma, \quad \dot{\omega} = \Omega(< R_\sigma >)|\dot{\varepsilon}^{\text{pl}}| \quad (3.6.159)$$

To specify the response functions f_σ , f_ω , Ω , g_{ω_T} and h experimental data are required. As an example consider the following functions

$$\begin{aligned} f_\sigma(x) &= a \left(\frac{x}{\sigma_0} \right)^n, & f_\omega(x) &= (1-x)^{-m}, \\ \Omega(x) &= b \left(\frac{x}{R_0} \right)^k, & g_{\omega_T}(x) &= (1-x), & h(x) &= h_0, \end{aligned}$$

where a , b , σ_0 , R_0 , h_0 , n and k are material parameters. Equations (3.6.159) take the following form

$$\begin{aligned} \dot{\varepsilon}^{\text{pl}} &= a \left(\frac{|\sigma|}{\sigma_0} \right)^n \frac{1}{(1-\omega)^m} \text{sgn}\sigma, \\ \dot{\omega} &= b \left(\frac{\langle R_\sigma \rangle}{R_0} \right)^k |\dot{\varepsilon}^{\text{pl}}|, & R_\sigma &= \frac{1}{2E} \left(\frac{J\sigma}{1-\omega} \right)^2 - h_0 \end{aligned} \quad (3.6.160)$$

References

- Abe F (2008) Strengthening mechanisms in steel for creep and creep rupture. In: Abe F, Kern TU, Viswanathan R (eds) *Creep-resistant steels*. Woodhead Publishing, Cambridge, pp 279–304
- Abe F (2009) Analysis of creep rates of tempered martensitic 9% Cr steel based on microstructure evolution. *Mater Sci Eng: A* 510:64–69
- Altenbach H, Naumenko K (1997) Creep bending of thin-walled shells and plates by consideration of finite deflections. *Comput Mech* 19:490–495
- Altenbach H, Morachkovsky O, Naumenko K, Sychov A (1997) Geometrically nonlinear bending of thin-walled shells and plates under creep-damage conditions. *Arch Appl Mech* 67:339–352
- Altenbach H, Altenbach J, Naumenko K (1998) *Ebene Flächentragwerke*. Springer, Berlin
- Altenbach H, Kolarow G, Morachkovsky O, Naumenko K (2000) On the accuracy of creep-damage predictions in thinwalled structures using the finite element method. *Comput Mech* 25:87–98
- Altenbach H, Kushnevsky V, Naumenko K (2001) On the use of solid- and shell-type finite elements in creep-damage predictions of thinwalled structures. *Arch Appl Mech* 71:164–181
- Altenbach H, Gorash Y, Naumenko K (2008a) Steady-state creep of a pressurized thick cylinder in both the linear and the power law ranges. *Acta Mech* 195:263–274
- Altenbach H, Naumenko K, Gorash Y (2008b) Creep analysis for a wide stress range based on stress relaxation experiments. *Int J Mod Phys B* 22:5413–5418
- Altenbach H, Kozhar S, Naumenko K (2013) Modeling creep damage of an aluminum-silicon eutectic alloy. *Int J Damage Mech* 22(5):683–698
- Antman SS (1973) Nonuniqueness of equilibrium states for bars in tension. *J Math Anal Appl* 44(2):333–349
- Ashby MF, Gandhi C, Taplin DMR (1979) Fracture-mechanism maps and their construction for f.c.c. metals and alloys. *Acta Metall* 27:699–729
- Barkar T, Ågren J (2005) Creep simulation of 9–12%Cr steels using the composite model with thermodynamically calculated input. *Mater Sci Eng A* 395:110–115
- Bertram A (2012) *Elasticity and plasticity of large deformations*, 3rd edn. Springer, Berlin
- Besseling JF (1958) A theory of elastic, plastic and creep deformation of an initially isotropic material showing anisotropic strain hardening, creep recovery and secondary creep. *Trans ASME J Appl Mech* 25(1):529–536
- Besseling JF, van der Giessen E (1994) *Mathematical modelling of inelastic deformation*. Chapman & Hall, London
- Blum W (2008) Mechanisms of creep deformation in steel. In: Abe F, Kern TU, Viswanathan R (eds) *Creep-resistant steels*. Woodhead Publishing, Cambridge, pp 365–402
- Bodnar A, Chrzanosowski M (1991) A non-unilateral damage in creeping plates. In: Zyczkowski M (ed) *Creep in structures*. Springer, Berlin, Heidelberg, pp 287–293
- Boyle JT (2012) The creep behavior of simple structures with a stress range-dependent constitutive model. *Arch Appl Mech* 82(4):495–514
- Boyle JT, Spence J (1983) *Stress analysis for creep*. Butterworth, London
- Chaboche JL (1989) Constitutive equations for cyclic plasticity and cyclic viscoplasticity. *Int J Plast* 5:247–302
- Chaboche JL (2008) A review of some plasticity and viscoplasticity constitutive equations. *Int J Plast* 24:1642–1693
- Coleman BD (1986) Necking and drawing in polymeric fibers under tension. The breadth and depth of continuum mechanics. Springer, Berlin Heidelberg, pp 19–41
- Coleman BD, Gurtin ME (1967) Thermodynamics with internal state variables. *J Chem Phys* 47(2):597–613
- Courant R, Hilbert D (1989) *Methods of mathematical physics, vol 2: partial differential equations*. Wiley Interscience Publication, New York
- Dünnwald J, El-Magd E (1996) Description of the creep behaviour of the precipitation-hardened material al-cu-mg alloy 2024 using finite element computations based on microstructure mechanical models. *Comput Mater Sci* 7(1):200–207

- Dyson BF, McLean M (1998) Microstructural evolution and its effects on the creep performance of high temperature alloys. In: Strang A, Cawley J, Greenwood GW (eds) *Microstructural stability of creep resistant alloys for high temperature plant applications*. Cambridge University Press, Cambridge, pp 371–393
- Dyson BF, McLean M (2001) Micromechanism-quantification for creep constitutive equations. In: Murakami S, Ohno N (eds) *IUTAM symposium on creep in structures*. Kluwer, Dordrecht, pp 3–16
- El-Magd E, Kranz A (2000) Ermittlung der inneren Rückspannung der Aluminiumlegierung AA2024 bei Kriechbelastung. *Materialwissenschaft und Werkstofftechnik* 31(1):96–101
- Estrin Y (1996) Dislocation-density-related constitutive modelling. In: Krausz AS, Krausz K (eds) *Unified constitutive laws of plastic deformation*. Academic Press, San Diego, pp 69–104
- François D, Pineau A, Zaoui A (2012) *Mechanical behaviour of materials, mechanical behaviour of materials, vol II: fracture mechanics and damage*. Springer
- Frederick CO, Armstrong PJ (2007) A mathematical representation of the multiaxial Bauschinger effect. *Mater High Temp* 24(1):1–26
- Frost HJ, Ashby MF (1982) *Deformation-mechanism maps*. Pergamon, Oxford
- Ganczarski A, Skrzypek J (2000) Damage effect on thermo-mechanical fields in a mid-thick plate. *J Theor Appl Mech* 38(2):271–284
- Gariboldi E, Casaro F (2007) Intermediate temperature creep behaviour of a forged Al-Cu-Mg-Si-Mn alloy. *Mater Sci Eng: A* 462(1):384–388
- Giesekus H (1994) *Phänomenologische Rheologie*. Springer, Berlin
- Gould PL (1988) *Analysis of shells and plates*. Springer, New York
- Granger R (1994) *Experiments in heat transfer and thermodynamics*. Cambridge University Press, Cambridge
- Hahn HG (1985) *Elastizitätstheorie*. Teubner, Stuttgart, B.G
- Hayhurst DR (1972) Creep rupture under multiaxial states of stress. *J Mech Phys Solids* 20:381–390
- Hoff NJ (1953) The necking and the rupture of rods subjected to constant tensile loads. *Trans ASME J Appl Mech* 20(1):105–108
- Hosseini E, Holdsworth SR, Mazza E (2013) Stress regime-dependent creep constitutive model considerations in finite element continuum damage mechanics. *Int J Damage Mech.* 22(8): 1186–1205
- Hyde TH, Sun W, Becker AA, Williams JA (1997) Creep continuum damage constitutive equations for the base, weld and heat-affected zone materials of a service-aged 1/2Cr1/2Mo1/4V:2 1/4Cr1Mo multipass weld at 640°C. *J Strain Anal Eng Des* 32(4):273–285
- Hyde TH, Sun W, Williams JA (1999) Creep behaviour of parent, weld and HAZ materials of new, service aged and repaired 1/2Cr1/2Mo1/4V: 21/4Cr1Mo pipe welds at 640°C. *Mater High Temp* 16(3):117–129
- Hyde TH, Sun W, Becker AA (2000) Failure prediction for multi-material creep test specimens using steady-state creep rupture stress. *Int J Mech Sci* 42:401–423
- Hyde TH, Sun W, Agyakwa PA, Shipeay PH, Williams JA (2003) Anisotropic creep and fracture behaviour of a 9CrMoNbV weld metal at 650°C. In: Skrzypek JJ, Ganczarski AW (eds) *Anisotropic behaviour of damaged materials*. Springer, Berlin, pp 295–316
- Ilschner B (1973) *Hochtemperatur-Plastizität*. Springer, Berlin
- Kachanov LM (1958) O vremeni razrusheniya v usloviyakh polzuchesti (on the time to rupture under creep conditions, in russ.). *Izv AN SSSR Otd Tekh Nauk* 8:26–31
- Kachanov LM (1986) *Introduction to continuum damage mechanics*. Martinus Nijhoff, Dordrecht
- Kassner ME, Hayes TA (2003) Creep cavitation in metals. *Int J Plast* 19:1715–1748
- Kassner ME, Pérez-Prado MT (2004) *Fundamentals of creep in metals and alloys*. Elsevier, Amsterdam
- Khan AS, Huang S (1995) *Continuum theory of plasticity*. Wiley, New York
- Konkin VN, Morachkovskij OK (1987) Polzuchest' i dlitel'naya prochnost' legkikh splavov, proyavlyayushchikh anizotropnye svoystva (Creep and long-term strength of light alloys with anisotropic properties, in Russ.). *Problemy prochnosti* 5:38–42

- Kowalewski ZL (1996) Creep rupture of copper under complex stress state at elevated temperature. Design and life assessment at high temperature. Mechanical Engineering Publ, London, pp 113–122
- Kowalewski ZL, Hayhurst DR, Dyson BF (1994) Mechanisms-based creep constitutive equations for an aluminium alloy. *J Strain Anal Eng Des* 29(4):309–316
- Krajcinovic D (1996) Damage mechanics. *Appl Math Mech* 41. North-Holland, Amsterdam
- Krawietz A (1986) *Materialtheorie: Mathematische Beschreibung des phänomenologischen thermomechanischen Verhalten*. Springer, Berlin
- Kreml E (1996) A small-strain viscoplasticity theory based on overstress. In: Krausz AS, Krausz K (eds) *Unified constitutive laws of plastic deformation*. Academic Press, San Diego, pp 281–318
- Kreml E (1999) Creep-plasticity interaction. In: Altenbach H, Skrzypek J (eds) *Creep and damage in materials and structures*. Springer, Wien, New York, pp 285–348, CISM Lecture Notes No. 399
- Landau LD, Lifshits EM, Kosevich AM, Pitaevskii LP (1986) *Theory of elasticity*. Butterworth-Heinemann, Course of theoretical physics
- Längler F, Naumenko K, Altenbach H, Ievdokymov M (2014) A constitutive model for inelastic behavior of casting materials under thermo-mechanical loading. *J Strain Anal Eng Des* 49: 421–428
- Lemaitre J (1996) *A course on damage mechanics*. Springer, Berlin
- Lemaitre J (ed) (2001) *Handbook of materials behavior models*. Academic Press, San Diego
- Lemaitre J, Chaboche JL (1990) *Mechanics of solid materials*. Cambridge University Press, Cambridge
- Lemaitre J, Desmorat R (2005) *Engineering damage mechanics: ductile, creep, fatigue and brittle failures*. Springer, Fatigue and Brittle Failures
- Lemaitre J, Chaboche J, Benallal A, Desmorat R (2009) *Mécanique des Matériaux Solides*, 3rd edn. Mechanics and thermodynamics, Dunod, Paris, The Addison-Wesley Series in the engineering sciences
- Lifshitz IM, Slyozov VV (1961) The kinetics of precipitation from supersaturated solid solutions. *J Phys Chem Solids* 19:35–50
- Lurie A (2010) *Theory of elasticity*. Springer, Foundations of Engineering Mechanics
- Malinin NN, Khadjinsky GM (1972) Theory of creep with anisotropic hardening. *Int J Mech Sci* 14:235–246
- Maugin GA (1992) *The thermomechanics of plasticity and fracture*. Cambridge University Press, Cambridge
- Maugin GA (2015) The saga of internal variables of state in continuum thermo-mechanics (1893–2013). *Mech Res Commun* 69:79–86
- Müller I (2007) *A history of thermodynamics: the doctrine of energy and entropy*. Springer
- Murakami S (2012) *Continuum damage mechanics: a continuum mechanics approach to the analysis of damage and fracture*. Springer, Solid Mechanics and Its Applications
- Murakami S, Liu Y (1995) Mesh-dependence in local approach to creep fracture. *Int J Damage Mech* 4:230–250
- Nabarro FRN, de Villiers HL (1995) *The physics of creep: creep and creep-resistant alloys*. Taylor & Francis, London
- Naghdi PM (1990) A critical review of the state of finite plasticity. *J Appl Math Phys (ZAMP)* 41:316–394
- Nakajima T, Takeda M, Endo T (2004) Accelerated coarsening of precipitates in crept Al-Cu alloys. *Mater Sci Eng: A* 387:670–673
- Naumenko K, Altenbach H (2005) A phenomenological model for anisotropic creep in a multi-pass weld metal. *Arch Appl Mech* 74:808–819
- Naumenko K, Gariboldi E (2014) A phase mixture model for anisotropic creep of forged Al-Cu-Mg-Si alloy. *Mater Sci Eng: A* 618:368–376
- Naumenko K, Kostenko Y (2009) Structural analysis of a power plant component using a stress-range-dependent creep-damage constitutive model. *Mater Sci Eng A510–A511:169–174*

- Naumenko K, Altenbach H, Gorash Y (2009) Creep analysis with a stress range dependent constitutive model. *Arch Appl Mech* 79:619–630
- Naumenko K, Altenbach H, Kutschke A (2011a) A combined model for hardening, softening and damage processes in advanced heat resistant steels at elevated temperature. *Int J Damage Mech* 20:578–597
- Naumenko K, Kutschke A, Kostenko Y, Rudolf T (2011b) Multi-axial thermo-mechanical analysis of power plant components from 9–12%Cr steels at high temperature. *Eng Fract Mech* 78:1657–1668
- Nellis G, Klein S (2009) Heat transfer. Cambridge University Press, Cambridge
- Ohno N (1998) Constitutive modeling of cyclic plasticity with emphasis on ratchetting. *Int J Mech Sci* 40(2):251–261
- Ohno N, Abdel-Karim M, Kobayashi M, Igari T (1998) Ratchetting characteristics of 316FR steel at high temperature, Part I: strain-controlled ratchetting experiments and simulations. *Int J Plast* 14(4):355–372
- Ozhoga-Maslovskaja O, Naumenko K, Altenbach H, Prygorniev O (2015) Micromechanical simulation of grain boundary cavitation in copper considering non-proportional loading. *Comput Mater Sci* 96, Part A:178–184
- Palmov V (1998) Vibrations in elasto-plastic bodies. Springer, Berlin
- Perrin JJ, Hayhurst DR (1994) Creep constitutive equations for a 0.5Cr-0.5Mo-0.25V ferritic steel in the temperature range 600–675°C. *J Strain Anal Eng Des* 31(4):299–314
- Polcik P (1999) Modellierung des Verformungsverhaltens der warmfesten 9–12% Chromstähle im Temperaturbereich von 550–560°C. Dissertation, Universität Erlangen-Nürnberg, Shaker Verlag Aachen
- Polcik P, Straub S, Henes D, Blum W (1998) Simulation of the creep behaviour of 9–12% CrMo-V steels on the basis of microstructural data. In: Strang A, Cawley J, Greenwood GW (eds) Microstructural stability of creep resistant alloys for high temperature plant applications. Cambridge University Press, Cambridge, pp 405–429
- Polmear IJ (1996) Recent developments in light alloys. *Mater Trans, Jpn Inst Met* 37(1):12–31
- Polmear IJ (2004) Aluminium alloys—a century of age hardening. *Mater Forum* 28:1–14
- Prager W (1956) A new method of analyzing stresses and strains in work-hardening plastic solids. *J Appl Mech* 23(4):493–496
- Rabotnov YN (1959) O mekhanizme dlitel'nogo razrusheniya (A mechanism of the long term fracture, in Russ.). *Voprosy prochnosti materialov i konstruktsii, AN SSSR* pp 5–7
- Rabotnov YN (1963) O razrushenii vsledstvie polzuchesti (On fracture as a consequence of creep, in Russ.). *Prikladnaya mekhanika i tekhnicheskaya fizika* 2:113–123
- Rabotnov YN (1969) Creep problems in structural members. North-Holland, Amsterdam
- Raj SV, Iskovitz IS, Freed AD (1996) Modeling the role of dislocation substructure during class M and exponential creep. In: Krausz AS, Krausz K (eds) Unified constitutive laws of plastic deformation. Academic Press, San Diego, pp 343–439
- Reddy JN (1997) Mechanics of laminated composite plates: theory and analysis. CRC Press, Boca Raton
- Reiner M (1969) Deformation and flow. an elementary introduction to rheology, 3rd edn. H.K. Lewis & Co., London
- Rice JR (1978) Thermodynamics of the quasi-static growth of griffith cracks. *J Mech Phys Solids* 26(2):61–78
- Riedel H (1987) Fracture at high temperatures. *Materials Research and Engineering*. Springer, Berlin
- Roesler J, Harders H, Baeker M (2007) Mechanical behaviour of engineering materials: metals, ceramics, polymers, and composites. Springer
- Schmicker D, Naumenko K, Strackeljan J (2013) A robust simulation of direct drive friction welding with a modified Carreau fluid constitutive model. *Comput Methods Appl Mech Eng* 265:186–194

- Schmicker D, Paczulla S, Nitzschke S, Groschopp S, Naumenko K, Jüttner S, Strackeljan J (2015) Experimental identification of flow properties of a S355 structural steel for hot deformation processes. *J Strain Anal Eng Des* 50(2):75–83
- Skrzypek J, Ganczarski A (1998) Modelling of material damage and failure of structures: foundation of engineering mechanics. Springer, Berlin
- Straub S (1995) Verformungsverhalten und Mikrostruktur warmfester martensitischer 12%-Chromstähle. Dissertation, Universität Erlangen-Nürnberg, VDI Reihe 5, Nr. 405, Düsseldorf
- Szilard R (1974) Theory and analysis of plates. Prentice-Hall, Englewood Cliffs, New Jersey
- Timoshenko SP, Goodier JN (1951) Theory of elasticity. McGraw-Hill, New York
- Timoshenko SP, Woinowsky-Krieger S (1959) Theory of plates and shells. McGraw-Hill, New York
- Wagner C (1961) Theorie der Alterung von Niederschlägen durch Umlösen (Ostwald-Reifung). *Zeitschrift für Elektrochemie, Berichte der Bunsengesellschaft für physikalische Chemie* 65 (7–8):581–591
- Xiao H, Bruhns OT, Meyers A (2006) Elastoplasticity beyond small deformations. *Acta Mech.* 182(1–2):31–111
- Zhang J, Deng Y, Zhang X (2013) Constitutive modeling for creep age forming of heat-treatable strengthening aluminum alloys containing plate or rod shaped precipitates. *Mater Sci Eng: A* 563:8–15
- Ziegler H (1983) An introduction to thermomechanics. North-Holland series in applied mathematics and mechanics, vol 21, North-Holland, Amsterdam

Chapter 4

Three-Dimensional Continuum Mechanics

The objective of continuum mechanics is to develop mathematical models to analyze the behavior of idealized three-dimensional bodies. The idealization is related to the hypothesis of a continuum, that is the matter is continuously distributed and fills the entire region of a body, e.g. Haupt (2002). The continuum mechanics is based on balance equations and assumptions regarding the kinematics of deformation and motion. Inelastic behavior is described by means of constitutive equations which relate multi-axial deformation and stress states. Topological details of microstructure are not considered. Processes associated with microstructural changes like hardening, recovery, ageing and damage can be taken into account by means of hidden or internal state variables and corresponding evolution equations. Various models developed within the continuum mechanics of solids can be applied to the structural analysis in the inelastic range.

The classical continuum mechanics of solids takes into account only translational degrees of freedom for motion of material points. The local mechanical interactions between material points are characterized by forces. Moment interactions are not considered. Furthermore, it is assumed that the stress state at a point in the solid depends only on the deformations and state variables of a vanishingly small volume element surrounding the point. To account for the heterogeneous deformation various extensions to the classical continuum mechanics were proposed. Micropolar theories assume that a material point behaves like a rigid body, i.e. it has translation and rotation degrees of freedom. The mechanical interactions are due to forces and moments. Constitutive equations are formulated for force and moment stress tensors. Micropolar theories of plasticity are presented in Forest et al. (1997), Altenbach and Eremeyev (2012), Eremeyev et al. (2012), Altenbach and Eremeyev (2014), among others. Inelastic deformation process is highly heterogeneous at the microscale and several effects cannot be described by the classical continuum mechanics accurately. For example, the dependence of the yield strength on the mean grain size and on the mean size of precipitates, see Sect. 1.3, are not considered within the classical theories since they do not possess intrinsic length scales. To analyze such effects, phase mixture, non-local and gradient-enhanced continuum theories are developed.

Examples for phase mixture models of inelastic deformation are presented in Naumenko and Gariboldi (2014), Naumenko et al. (2011). Strain gradient and micromorphic theories are discussed in Fleck and Hutchinson (1997), Gao et al. (1999), Forest (2009). Here a gradient or the rotation (curl) of the inelastic strain are considered as additional degrees of freedom. Non-local and phase field theories of damage and fracture were recently advanced to capture initiation and propagation of cracks in solids (Miehe et al. 2010; Schmitt et al. 2013).

This chapter provides basic equations of the classical three-dimensional continuum mechanics. To keep the presentation brief and transparent many details of mathematical derivations are omitted. Several rules of the direct tensor calculus, tensor analysis and special topics related to the theory of tensor functions and invariants are presented in Appendices A–B.5.

With regard to non-linear continuum mechanics there is a number of textbooks, for example Altenbach (2015), Bertram (2012), Eglit and Hodges (1996), Haupt (2002), Lai et al. (1993), Maugin (2013), Smith (1993), Truesdell and Noll (1992).

4.1 Motion, Derivatives and Deformation

4.1.1 Motion and Derivatives

Let \mathcal{R} be the position vector for a point P in a reference state of a solid, Fig. 4.1 and \mathbf{r} be the position vector of this point (designated by P') in the actual configuration. The displacement vector \mathbf{u} connects the points P and P' , Fig. 4.1. The position vector \mathcal{R} can be parameterized with the Cartesian coordinate system including the orthonormal basis \mathbf{i} , \mathbf{j} , \mathbf{k} and the coordinates X , Y , Z , i.e.

$$\mathcal{R}(X, Y, Z) = X\mathbf{i} + Y\mathbf{j} + Z\mathbf{k}$$

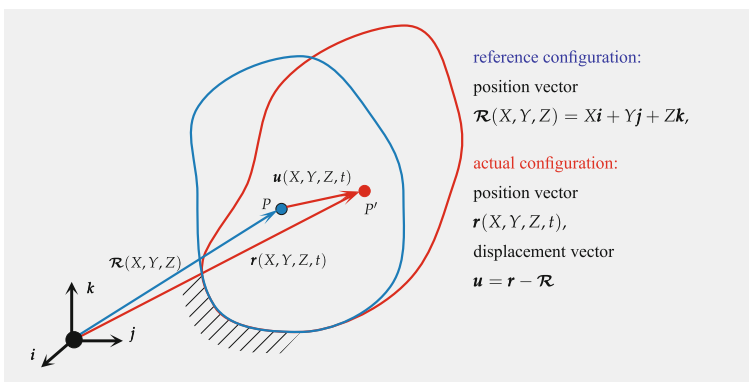


Fig. 4.1 Position vectors and displacement vector

In many cases it is more convenient to use curvilinear coordinates, for example cylindrical, spherical, skew etc. Specifying the curvilinear coordinates by $X^1 = q^1, X^2 = q^2, X^3 = q^3$, see Appendix B.1 the position vector is parameterized as follows

$$\mathcal{R}(X^1, X^2, X^3) = X(X^1, X^2, X^3)\mathbf{i} + Y(X^1, X^2, X^3)\mathbf{j} + Z(X^1, X^2, X^3)\mathbf{k}, \quad (4.1.1)$$

The directed line element in a differential neighborhood of P is

$$d\mathcal{R} = \mathcal{R}_i dX^i, \quad dX^i = d\mathcal{R} \cdot \mathcal{R}^i, \quad \mathcal{R}_i = \frac{\partial \mathcal{R}}{\partial X^i}, \quad i = 1, 2, 3, \quad (4.1.2)$$

where \mathcal{R}_i is the local basis and \mathcal{R}^i is the dual basis, Appendix B.1. The motion of the continuum is defined by the following mapping

$$\mathbf{r} = \Phi(\mathcal{R}, t) \quad (4.1.3)$$

The basic problem of continuum mechanics is to compute the function Φ for all vectors \mathcal{R} within the body in the reference configuration, for the given time interval $t_0 \leq t \leq t_n$ as well as for given external loads and temperature. It is obvious that $\mathcal{R} = \Phi(\mathcal{R}, t)$. The displacement vector \mathbf{u} is defined as follows (Fig. 4.1)

$$\mathbf{u} = \mathbf{r} - \mathcal{R} \quad (4.1.4)$$

The vector \mathbf{r} can be specified with the basis $\mathbf{i}, \mathbf{j}, \mathbf{k}$ as follows

$$\mathbf{r}(X^1, X^2, X^3, t) = x(X^1, X^2, X^3, t)\mathbf{i} + y(X^1, X^2, X^3, t)\mathbf{j} + z(X^1, X^2, X^3, t)\mathbf{k}$$

with the actual Cartesian coordinates x, y, z . The directed line element in a differential neighborhood of P' in the actual configuration is

$$d\mathbf{r} = \mathbf{r}_i dX^i, \quad dX^i = d\mathbf{r} \cdot \mathbf{r}^i, \quad \mathbf{r}_i = \frac{\partial \mathbf{r}}{\partial X^i}, \quad i = 1, 2, 3 \quad (4.1.5)$$

where \mathbf{r}_i is the local basis and \mathbf{r}^i is the dual basis in the actual configuration.

To analyze the motion it is useful to introduce the rates of change of functions with respect to the coordinates X^i and time t . Consider a tensor-valued function $\mathbf{f}(X^i, t)$. The total differential of \mathbf{f} for the fixed time variable is

$$d\mathbf{f} = dX^1 \frac{\partial \mathbf{f}}{\partial X^1} + dX^2 \frac{\partial \mathbf{f}}{\partial X^2} + dX^3 \frac{\partial \mathbf{f}}{\partial X^3} = dX^k \frac{\partial \mathbf{f}}{\partial X^k}$$

From Eq. (4.1.2)₂ we obtain

$$d\mathbf{f} = d\mathcal{R} \cdot \mathcal{R}^k \otimes \frac{\partial \mathbf{f}}{\partial X^k} = d\mathcal{R} \cdot \overset{\circ}{\nabla} \mathbf{f} \quad (4.1.6)$$

The operator $\overset{0}{\nabla}$ is the Hamilton (nabla) operator with dual basis vectors of the reference configuration

$$\overset{0}{\nabla} = \mathcal{R}^k \otimes \frac{\partial}{\partial X^k} \quad (4.1.7)$$

With $\mathbf{f} = \mathcal{R}$ Eq. (4.1.6) yields

$$d\mathcal{R} = d\mathcal{R} \cdot \overset{0}{\nabla} \mathcal{R}, \quad \overset{0}{\nabla} \mathcal{R} = \mathcal{R}^k \otimes \mathcal{R}_k = \mathbf{I} \quad (4.1.8)$$

Alternatively, one may use the spatial description by considering \mathbf{f} to be the function of \mathbf{r} and t . For the fixed time variable we may compute the total differential of \mathbf{f} as follows

$$d\mathbf{f} = dX^k \frac{\partial \mathbf{f}}{\partial X^k} = d\mathbf{r} \cdot \mathbf{r}^k \otimes \frac{\partial \mathbf{f}}{\partial X^k} = d\mathbf{r} \cdot \nabla \mathbf{f}, \quad (4.1.9)$$

where

$$\nabla = \mathbf{r}^k \otimes \frac{\partial}{\partial X^k} \quad (4.1.10)$$

is the Hamilton (nabla) operator with the dual basis of the actual configuration.

The velocity field \mathbf{v} is defined as follows

$$\mathbf{v} = \frac{\partial \Phi}{\partial t} = \dot{\mathbf{u}} = \dot{\mathbf{r}} \quad (4.1.11)$$

The description where \mathbf{f} is a function of \mathbf{R} and t is sometimes called Lagrangian or material. On the other hand if \mathbf{f} is a function of \mathbf{r} and t , the description is called Eulerian or spatial. As the mapping Φ is assumed invertible

$$\mathcal{R} = \Phi^{-1}(\mathbf{r}, t), \quad (4.1.12)$$

both the descriptions are equivalent in the sense that if \mathbf{f} is known as a function of \mathcal{R} and t , one may use the transformation (4.1.12) to get

$$\mathbf{f}(\mathcal{R}, t) = \mathbf{g}(\mathbf{r}, t)$$

Assuming that both \mathbf{v} and \mathbf{f} are functions of \mathbf{r} and t the material time derivative is defined as follows

$$\frac{d}{dt} \mathbf{f} = \frac{\partial}{\partial t} \mathbf{f} + \mathbf{v} \cdot \nabla \mathbf{f} \quad (4.1.13)$$

4.1.2 Deformation Gradient and Strain Tensors

Setting $\mathbf{f} = \mathbf{r}$ into Eq. (4.1.6) we obtain

$$d\mathbf{r} = d\mathcal{R} \cdot \overset{0}{\nabla} \mathbf{r}, \quad \overset{0}{\nabla} \mathbf{r} = \mathcal{R}^k \otimes \mathbf{r}_k \quad (4.1.14)$$

The second rank tensor

$$\mathbf{F} = (\overset{0}{\nabla} \mathbf{r})^T = \mathbf{r}_k \otimes \mathcal{R}^k \quad (4.1.15)$$

is called deformation gradient. With $\mathbf{u} = \mathbf{r} - \mathcal{R}$ and (4.1.8) the deformation gradient can be expressed through the displacement gradient as follows

$$\mathbf{F} = \mathbf{I} + \overset{0}{\nabla} \mathbf{u} \quad (4.1.16)$$

Once the deformation gradient is given, one may find the line element $d\mathbf{r}$ in the differential neighborhood of the point P' of the actual configuration for the given line element $d\mathcal{R}$ of the reference configuration. Consider three line elements $d\mathcal{R}_a$, $d\mathcal{R}_b$ and $d\mathcal{R}_c$ in the neighborhood of P such that

$$(d\mathcal{R}_a \times d\mathcal{R}_b) \cdot d\mathcal{R}_c = dV_0 > 0,$$

where dV_0 is the elementary volume of the parallelepiped spanned on $d\mathcal{R}_a$, $d\mathcal{R}_b$ and $d\mathcal{R}_c$. With Eqs. (4.1.15) and (A.4.7) we can compute the elementary volume of the actual configuration

$$\begin{aligned} dV &= (d\mathbf{r}_a \times d\mathbf{r}_b) \cdot d\mathbf{r}_c = [(\mathbf{F} \cdot d\mathcal{R}_a) \times (\mathbf{F} \cdot d\mathcal{R}_b)] \cdot \mathbf{F} \cdot d\mathcal{R}_c \\ &= \det \mathbf{F} (d\mathcal{R}_a \times d\mathcal{R}_b) \cdot d\mathcal{R}_c \\ &= \det \mathbf{F} dV_0 \end{aligned}$$

Hence

$$J = \det \mathbf{F} = \frac{dV}{dV_0} > 0 \quad (4.1.17)$$

The condition $\det \mathbf{F} > 0$ guarantees that the inverse \mathbf{F}^{-1} exists. It can be computed as follows

$$\mathbf{F}^{-1} = \mathcal{R}_k \otimes \mathbf{r}^k$$

Indeed

$$\mathbf{F}^{-1} \cdot \mathbf{F} = \mathcal{R}_k \otimes \mathbf{r}^k \cdot \mathbf{r}_i \otimes \mathcal{R}^i = \delta_i^k \mathcal{R}_k \otimes \mathcal{R}^i = \mathcal{R}_k \otimes \mathcal{R}^k = \mathbf{I}$$

Consider two line elements $d\mathcal{R}_a, d\mathcal{R}_b, d\mathcal{R}_a \times d\mathcal{R}_b \neq \mathbf{0}$ in the neighborhood of P . Let

$$NdA_0 = d\mathcal{R}_a \times d\mathcal{R}_b$$

be the infinitesimal oriented area element including the area of the parallelogram dA_0 having $d\mathcal{R}_a$ and $d\mathcal{R}_b$ as sides and the unit normal \mathbf{N} . With the identity (A.4.8)₁ one may compute the corresponding area element in the deformed configuration

$$J\mathbf{F}^{-T} \cdot (d\mathcal{R}_a \times d\mathcal{R}_b) = (\mathbf{F} \cdot d\mathcal{R}_a) \times (\mathbf{F} \cdot d\mathcal{R}_b)$$

or

$$J\mathbf{F}^{-T} \cdot (\mathbf{N}dA_0) = \mathbf{n}dA \quad (4.1.18)$$

With the deformation gradient the following relations between nabla operators (4.1.7) and (4.1.10) can be derived

$$\overset{0}{\nabla}(\dots) = \mathcal{R}^k \otimes \frac{\partial(\dots)}{\partial X^k} = \mathcal{R}^i \otimes \mathbf{r}_i \cdot \mathbf{r}^k \otimes \frac{\partial(\dots)}{\partial X^k} = \mathbf{F}^T \cdot \nabla(\dots) \quad (4.1.19)$$

As a result we obtain

$$\nabla(\dots) = \mathbf{F}^{-T} \cdot \overset{0}{\nabla}(\dots), \quad \overset{0}{\nabla}(\dots) = \mathbf{F}^T \cdot \nabla(\dots) \quad (4.1.20)$$

Once \mathbf{F} is given, one may compute the local strains. To this end consider a line element $d\mathcal{R}_a = \mathbf{M}dl_{a_0}$ in the neighborhood of the point P , where the unit vector \mathbf{M} is the direction of the element (direction of the strain measurement) and dl_{a_0} is the corresponding length. In the actual configuration $d\mathbf{r}_a = \mathbf{m}dl_a$. In the course of deformation both the orientation and the length of the element are changing. The local stretch and the local normal strain can be computed as follows

$$\lambda_{MM} = \frac{dl_a}{dl_{a_0}}, \quad \varepsilon_{MM} = \frac{dl_a - dl_{a_0}}{dl_{a_0}} \quad (4.1.21)$$

With the given deformation gradient and

$$d\mathbf{r}_a = \mathcal{R}_a \cdot \mathbf{F}^T = \mathbf{F} \cdot d\mathcal{R}_a$$

one may compute

$$dl_a^2 = d\mathbf{r}_a \cdot d\mathbf{r}_a = d\mathcal{R}_a \cdot \mathbf{F}^T \cdot \mathbf{F} \cdot d\mathcal{R}_a = (dl_{a_0})^2 \mathbf{M} \cdot \mathbf{F}^T \cdot \mathbf{F} \cdot \mathbf{M} \quad (4.1.22)$$

Hence

$$\lambda_{MM}^2 = (1 + \varepsilon_{MM})^2 = \mathbf{M} \cdot \mathbf{C} \cdot \mathbf{M}, \quad \mathbf{C} = \mathbf{F}^T \cdot \mathbf{F}, \quad (4.1.23)$$

where \mathbf{C} is the right Cauchy-Green tensor. For three orthogonal directions specified by the unit vectors \mathbf{e}_X , \mathbf{e}_Y and \mathbf{e}_Z Eq. (4.1.23) provides the corresponding stretches

$$\lambda_{XX}^2 = \mathbf{e}_X \cdot \mathbf{C} \cdot \mathbf{e}_X, \quad \lambda_{YY}^2 = \mathbf{e}_Y \cdot \mathbf{C} \cdot \mathbf{e}_Y, \quad \lambda_{ZZ}^2 = \mathbf{e}_Z \cdot \mathbf{C} \cdot \mathbf{e}_Z$$

These equations provide three components of the tensor \mathbf{C} with respect to the orthonormal basis. To define the remaining components consider two orthogonal line elements given by the vectors $d\mathcal{R}_a = \mathbf{M}dl_{a_0}$ and $d\mathcal{R}_b = \mathbf{N}dl_{b_0}$ in the neighborhood of the point P , where \mathbf{N} and \mathbf{M} , $\mathbf{N} \cdot \mathbf{M} = 0$ are unit vectors. dl_{a_0} and dl_{b_0} are reference lengths of the elements. The corresponding line elements in the actual configuration are $d\mathbf{r}_a = \mathbf{m}dl_a$ and $d\mathbf{r}_b = \mathbf{n}dl_b$. Let α_{MN} be the angle between the vectors $d\mathbf{r}_a$ and $d\mathbf{r}_b$. The local shear strain is defined as $\gamma_{MN} = \frac{\pi}{2} - \alpha_{MN}$. The scalar product of the vectors $d\mathbf{r}_a$ and $d\mathbf{r}_b$ yields

$$\begin{aligned} d\mathbf{r}_a \cdot d\mathbf{r}_b &= dl_a dl_b \cos \alpha_{MN} = dl_a dl_b \sin \gamma_{MN} \\ &= (1 + \varepsilon_{MM})(1 + \varepsilon_{NN}) \sin \gamma_{MN} dl_{a_0} dl_{b_0} \end{aligned} \quad (4.1.24)$$

For the given deformation gradient \mathbf{F}

$$d\mathbf{r}_a = d\mathcal{R}_a \cdot \mathbf{F}^T = dl_{a_0} \mathbf{M} \cdot \mathbf{F}^T, \quad d\mathbf{r}_b = \mathbf{F} \cdot d\mathcal{R}_b = dl_{b_0} \mathbf{F} \cdot \mathbf{N} \quad (4.1.25)$$

The scalar product yields

$$d\mathbf{r}_a \cdot d\mathbf{r}_b = \mathbf{M} \cdot \mathbf{F}^T \cdot \mathbf{F} \cdot \mathbf{N} dl_{a_0} dl_{b_0}$$

With Eq. (4.1.24) we obtain

$$\lambda_{MM} \lambda_{NN} \sin \gamma_{MN} = (1 + \varepsilon_{MM})(1 + \varepsilon_{NN}) \sin \gamma_{MN} = \mathbf{M} \cdot \mathbf{C} \cdot \mathbf{N} \quad (4.1.26)$$

Equation (4.1.26) provides the MN -component of the tensor \mathbf{C} . Since \mathbf{M} and \mathbf{N} are two arbitrary orthogonal unit vectors, one may compute six components of the tensor \mathbf{C} by taking the orthogonal unit vectors \mathbf{e}_X , \mathbf{e}_Y and \mathbf{e}_Z as directions of the shear strain measurement. Since the tensor \mathbf{C} is symmetric only three of them are independent, i.e.

$$\lambda_{XX} \lambda_{YY} \sin \gamma_{XY} = \mathbf{e}_X \cdot \mathbf{C} \cdot \mathbf{e}_Y,$$

$$\lambda_{XX} \lambda_{ZZ} \sin \gamma_{XZ} = \mathbf{e}_X \cdot \mathbf{C} \cdot \mathbf{e}_Z,$$

$$\lambda_{YY} \lambda_{ZZ} \sin \gamma_{YZ} = \mathbf{e}_Y \cdot \mathbf{C} \cdot \mathbf{e}_Z$$

The Cauchy-Green tensor is one example of many strain tensors that can be introduced in the non-linear continuum mechanics. To present several examples let us

apply the polar decomposition theorem (see Appendix A.4.18) to the deformation gradient

$$\mathbf{F} = \mathbf{R} \cdot \mathbf{U} = \mathbf{V} \cdot \mathbf{R}, \quad (4.1.27)$$

where \mathbf{R} is the rotation tensor. \mathbf{U} and \mathbf{V} are right and left stretch tensors respectively. These positive definite symmetric tensors have the following spectral representations

$$\mathbf{U} = \sum_{i=1}^3 \lambda_i \overset{u}{\mathbf{N}}_i \otimes \overset{u}{\mathbf{N}}_i, \quad \mathbf{V} = \sum_{i=1}^3 \lambda_i \overset{v}{\mathbf{n}}_i \otimes \overset{v}{\mathbf{n}}_i, \quad (4.1.28)$$

where $\lambda_i > 0$ are principal stretches. The orthonormal unit vectors $\overset{u}{\mathbf{N}}_i$ and $\overset{v}{\mathbf{n}}_i$ are principal directions of the tensors \mathbf{U} and \mathbf{V} , respectively. From (4.1.27) the following relations can be obtained

$$\overset{v}{\mathbf{n}}_i = \mathbf{R} \cdot \overset{u}{\mathbf{N}}_i, \quad \mathbf{R} = \sum_{i=1}^3 \overset{v}{\mathbf{n}}_i \otimes \overset{u}{\mathbf{N}}_i \quad (4.1.29)$$

Examples of strain tensors related to \mathbf{U} (sometimes called material strain tensors) are the Cauchy-Green strain tensor

$$\mathbf{G} = \frac{1}{2} (\mathbf{C} - \mathbf{I}) = \frac{1}{2} (\mathbf{U}^2 - \mathbf{I}) = \frac{1}{2} \sum_{i=1}^3 (\lambda_i^2 - 1) \overset{u}{\mathbf{N}}_i \otimes \overset{u}{\mathbf{N}}_i \quad (4.1.30)$$

the material Biot strain tensor

$$\mathbf{E}_B = \mathbf{U} - \mathbf{I} = \sum_{i=1}^3 (\lambda_i - 1) \overset{u}{\mathbf{N}}_i \otimes \overset{u}{\mathbf{N}}_i \quad (4.1.31)$$

and the material Hencky strain tensor

$$\mathbf{H} = \ln \mathbf{U} = \sum_{i=1}^3 \ln \lambda_i \overset{u}{\mathbf{N}}_i \otimes \overset{u}{\mathbf{N}}_i \quad (4.1.32)$$

Examples of strain tensors related to \mathbf{V} (spatial strain tensors) are the Almansi strain tensor

$$\mathbf{E}_A = \frac{1}{2} (\mathbf{I} - \mathbf{B}^{-1}) = \frac{1}{2} (\mathbf{I} - \mathbf{V}^{-2}) = \frac{1}{2} \sum_{i=1}^3 (1 - \lambda_i^{-2}) \overset{v}{\mathbf{n}}_i \otimes \overset{v}{\mathbf{n}}_i, \quad (4.1.33)$$

where $\mathbf{B} = \mathbf{V}^2 = \mathbf{F} \cdot \mathbf{F}^T$ is the left Cauchy-Green tensor. Further examples are the spatial Biot strain tensor

$$\mathbf{E}_b = \mathbf{I} - \mathbf{V}^{-1} = \sum_{i=1}^3 (1 - \lambda_i^{-1}) \mathbf{n}_i^v \otimes \mathbf{n}_i^v \quad (4.1.34)$$

and the spacial Hencky strain tensor

$$\mathbf{h} = \ln \mathbf{V} = \sum_{i=1}^3 \ln \lambda_i \mathbf{n}_i^v \otimes \mathbf{n}_i^v \quad (4.1.35)$$

For many structural analysis applications the local strains can be assumed small. With $\varepsilon_{MM} \ll 1$ and $\gamma_{MN} \ll 1$ the left hand side of Eqs. (4.1.23) and (4.1.26) can be linearized as follows

$$\begin{aligned} \lambda_{MM}^2 &= (\varepsilon_{MM} + 1)^2 \approx 2\varepsilon_{MM} + 1, \\ \lambda_{MM}\lambda_{NN} \sin \gamma_{MN} &= (\varepsilon_{MM} + 1)(\varepsilon_{NN} + 1) \sin \gamma_{MN} \approx \gamma_{MN} \end{aligned} \quad (4.1.36)$$

With Eqs. (4.1.23) and (4.1.36) the normal strain in the direction \mathbf{M} is

$$\begin{aligned} \varepsilon_{MM} &= \frac{1}{2} \mathbf{M} \cdot \mathbf{F}^T \cdot \mathbf{F} \cdot \mathbf{M} - \frac{1}{2} \\ &= \frac{1}{2} \mathbf{M} \cdot (\mathbf{C} - \mathbf{I}) \cdot \mathbf{M} \end{aligned}$$

The shear strain can be computed as follows

$$\gamma_{MN} = \mathbf{M} \cdot \mathbf{F}^T \cdot \mathbf{F} \cdot \mathbf{N}$$

With the Green-Lagrange strain tensor

$$\mathbf{G} = \frac{1}{2} (\mathbf{F}^T \cdot \mathbf{F} - \mathbf{I}),$$

the strains can be given as follows

$$\varepsilon_{MM} = \mathbf{M} \cdot \mathbf{G} \cdot \mathbf{M}, \quad \gamma_{MN} = 2\mathbf{M} \cdot \mathbf{G} \cdot \mathbf{N}$$

For the given tensor \mathbf{G} one may compute the strains with respect to any direction. For three orthogonal directions specified by the unit vectors \mathbf{e}_X , \mathbf{e}_Y and \mathbf{e}_Z the six components can be computed as follows

$$\begin{aligned} \varepsilon_{XX} &= \mathbf{e}_X \cdot \mathbf{G} \cdot \mathbf{e}_X, & \varepsilon_{YY} &= \mathbf{e}_Y \cdot \mathbf{G} \cdot \mathbf{e}_Y, & \varepsilon_{ZZ} &= \mathbf{e}_Z \cdot \mathbf{G} \cdot \mathbf{e}_Z, \\ \varepsilon_{XY} &= \mathbf{e}_X \cdot \mathbf{G} \cdot \mathbf{e}_Y, & \varepsilon_{XZ} &= \mathbf{e}_X \cdot \mathbf{G} \cdot \mathbf{e}_Z, & \varepsilon_{YZ} &= \mathbf{e}_Y \cdot \mathbf{G} \cdot \mathbf{e}_Z \end{aligned}$$

Although the normal and shear strains are assumed small, the difference between the unit vectors like \mathbf{M} and \mathbf{m} defined in the initial and actual configurations may be essential. To formulate geometrically-linear theory we have additionally to assume infinitesimal rotations.¹ The linearized rotation tensor \mathbf{R} can be given as follows

$$\mathbf{R} = \mathbf{I} + \boldsymbol{\varphi} \times \mathbf{I},$$

where $\boldsymbol{\varphi}$ is the vector of infinitesimal rotations. Then with Eqs. (4.1.27) and (4.1.16) the following linearized relations can be established

$$\begin{aligned} \mathbf{F} &= \mathbf{I} + \boldsymbol{\varepsilon} + \boldsymbol{\varphi} \times \mathbf{I}, \quad \overset{0}{\nabla} \mathbf{u} = \nabla \mathbf{u} = \boldsymbol{\varepsilon} + \boldsymbol{\varphi} \times \mathbf{I}, \\ \boldsymbol{\varepsilon} &= \frac{1}{2} [\nabla \mathbf{u} + (\nabla \mathbf{u})^T], \quad \boldsymbol{\varphi} = -\frac{1}{2} \nabla \times \mathbf{u} \end{aligned} \quad (4.1.37)$$

The tensor $\boldsymbol{\varepsilon}$ is called tensor of infinitesimal strains.

4.1.3 Velocity Gradient, Deformation Rate, and Spin Tensors

The time derivative of the deformation gradient, can be computed with (4.1.15) as follows

$$\dot{\mathbf{F}} = (\overset{0}{\nabla} \dot{\mathbf{r}})^T = \dot{\mathbf{r}}_k \otimes \mathcal{R}^k \quad (4.1.38)$$

With (4.1.11)

$$\frac{\partial \mathbf{v}}{\partial X^k} = \dot{\mathbf{r}}_k \quad (4.1.39)$$

Hence

$$\dot{\mathbf{F}} = (\overset{0}{\nabla} \mathbf{v})^T, \quad \overset{0}{\nabla} \mathbf{v} = \mathcal{R}^k \otimes \frac{\partial \mathbf{v}}{\partial X^k} \quad (4.1.40)$$

With the relation between nabla operators (4.1.20)₂ Eq. (4.1.40) takes the form

$$\dot{\mathbf{F}} = (\nabla \mathbf{v})^T \cdot \mathbf{F} \quad (4.1.41)$$

¹In many cases strains can be infinitesimal, but rotations finite. One example is a thin plate strip which can be bent into a ring such that the strains remain infinitesimal but cross section rotations are large.

The spatial velocity gradient $\mathbf{L} = (\nabla \mathbf{v})^T$ can be computed as follows

$$\mathbf{L} = (\nabla \mathbf{v})^T = \dot{\mathbf{F}} \cdot \mathbf{F}^{-1} = \frac{\partial \mathbf{v}}{\partial X^k} \otimes \mathbf{r}^k \quad (4.1.42)$$

The tensor \mathbf{L} can be additively decomposed into the symmetric and skew symmetric parts (see Appendix A.4.10)

$$\mathbf{L} = \mathbf{D} + \boldsymbol{\omega} \times \mathbf{I}, \quad (4.1.43)$$

where the symmetric part

$$\mathbf{D} = \frac{1}{2} [\nabla \mathbf{v} + (\nabla \mathbf{v})^T]$$

is called the deformation rate tensor² while

$$\boldsymbol{\omega} = -\frac{1}{2} \nabla \times \mathbf{v}$$

is called vorticity vector.

The time derivative of $J = \det \mathbf{F}$ can be computed as follows

$$\frac{dJ}{dt} = \frac{d\mathbf{F}}{dt} \cdot \left(\frac{\partial J}{\partial \mathbf{F}} \right)^T$$

With (B.4.13) we obtain

$$\frac{\partial J}{\partial \mathbf{F}} = \det \mathbf{F} \mathbf{F}^{-T}$$

Consequently

$$\dot{J} = J \dot{\mathbf{F}} \cdot \mathbf{F}^{-1} \quad (4.1.44)$$

Taking the trace of Eq. (4.1.42)

$$\text{tr } \mathbf{L} = \nabla \cdot \mathbf{v} = \dot{\mathbf{F}} \cdot \mathbf{F}^{-1}$$

With Eq. (4.1.44) we obtain

$$\frac{\dot{J}}{J} = \frac{d \ln J}{dt} = \nabla \cdot \mathbf{v} = \dot{\mathbf{F}} \cdot \mathbf{F}^{-1} \quad (4.1.45)$$

²The tensor \mathbf{D} is in general not a time derivative of a strain tensor.

Applying the polar decomposition (4.1.27) and the relations

$$\mathbf{F} = \mathbf{R} \cdot \mathbf{U} \quad \Rightarrow \quad \dot{\mathbf{F}} = \dot{\mathbf{R}} \cdot \mathbf{U} + \dot{\mathbf{U}} \cdot \mathbf{R} \quad \text{and} \quad \mathbf{F}^{-1} = \mathbf{U}^{-1} \cdot \mathbf{R}^T$$

the velocity gradient can be computed as follows

$$\mathbf{L} = \dot{\mathbf{F}} \cdot \mathbf{F}^{-1} = \dot{\mathbf{R}} \cdot \mathbf{R}^T + \mathbf{R} \cdot \dot{\mathbf{U}} \cdot \mathbf{U}^{-1} \cdot \mathbf{R}^T \quad (4.1.46)$$

For the rotation tensor \mathbf{R} let us introduce the angular velocity vector $\boldsymbol{\Omega}_R$ and the spin tensor $\boldsymbol{\Omega}_R \times \mathbf{I}$ as follows. According to the definition of the orthogonal tensor, see Appendix A.4.17, we obtain

$$\mathbf{R} \cdot \mathbf{R}^T = \mathbf{I} \quad \Rightarrow \quad \dot{\mathbf{R}} \cdot \mathbf{R}^T + \mathbf{R} \cdot \dot{\mathbf{R}}^T = \mathbf{0} \quad \Rightarrow \quad \dot{\mathbf{R}} \cdot \mathbf{R}^T = -(\dot{\mathbf{R}} \cdot \mathbf{R}^T)^T$$

The skew-symmetric tensor $\dot{\mathbf{R}} \cdot \mathbf{R}^T$ is called the left spin tensor or simply spin tensor. With the associated vector $\boldsymbol{\Omega}_R$ we obtain

$$\dot{\mathbf{R}} \cdot \mathbf{R}^T = \boldsymbol{\Omega}_R \times \mathbf{I}, \quad \boldsymbol{\Omega}_R = -\frac{1}{2}(\dot{\mathbf{R}} \cdot \mathbf{R}^T)_\times, \quad (4.1.47)$$

where $(\dots)_\times$ denotes the vector invariant or Gibbs cross of the second rank tensor, see Appendix A.4.15. The vector $\boldsymbol{\Omega}_R$ is called the left angular velocity vector of rotation or simply angular velocity of rotation. This vector is widely used in the mechanics of rigid bodies, e.g. Altenbach et al. (2007, 2009), Zhilin (1996). Equation (4.1.46) can be given as follows

$$\mathbf{D} + \boldsymbol{\omega} \times \mathbf{I} = \boldsymbol{\Omega}_R \times \mathbf{I} + \mathbf{R} \cdot \dot{\mathbf{U}} \cdot \mathbf{U}^{-1} \cdot \mathbf{R}^T \quad (4.1.48)$$

Taking the vector invariant of Eq. (4.1.48) the vorticity vector can be computed as follows

$$\boldsymbol{\omega} = \boldsymbol{\Omega}_R - \frac{1}{2}(\mathbf{R} \cdot \dot{\mathbf{U}} \cdot \mathbf{U}^{-1} \cdot \mathbf{R}^T)_\times \quad (4.1.49)$$

The symmetric part of Eq. (4.1.48) is

$$\mathbf{D} = \frac{1}{2}\mathbf{R} \cdot \mathbf{U}^{-1} \cdot \dot{\mathbf{U}} \cdot \mathbf{R}^T = \frac{1}{2}\mathbf{R} \cdot (\dot{\mathbf{U}} \cdot \mathbf{U}^{-1} + \mathbf{U}^{-1} \cdot \dot{\mathbf{U}}) \cdot \mathbf{R}^T \quad (4.1.50)$$

Equation (4.1.50) can be put in the following form

$$\mathbf{R}^T \cdot \mathbf{D} \cdot \mathbf{R} = \frac{1}{2}(\dot{\mathbf{U}} \cdot \mathbf{U}^{-1} + \mathbf{U}^{-1} \cdot \dot{\mathbf{U}})$$

or

$$\mathbf{F}^T \cdot \mathbf{D} \cdot \mathbf{F} = \frac{1}{2} \frac{d}{dt} (\mathbf{U}^2) = \frac{1}{2} \dot{\mathbf{C}} = \dot{\mathbf{G}} \quad (4.1.51)$$

Let us take the time derivatives of stretch tensors applying spectral representations (4.1.28)

$$\begin{aligned} \dot{\mathbf{U}} &= \sum_{i=1}^3 \left(\dot{\lambda}_i \overset{u}{\mathbf{N}}_i \otimes \overset{u}{\mathbf{N}}_i + \lambda_i \frac{d}{dt} \overset{u}{\mathbf{N}}_i \otimes \overset{u}{\mathbf{N}}_i + \lambda_i \overset{u}{\mathbf{N}}_i \otimes \frac{d}{dt} \overset{u}{\mathbf{N}}_i \right), \\ \dot{\mathbf{V}} &= \sum_{i=1}^3 \left(\dot{\lambda}_i \overset{v}{\mathbf{n}}_i \otimes \overset{v}{\mathbf{n}}_i + \lambda_i \frac{d}{dt} \overset{v}{\mathbf{n}}_i \otimes \overset{v}{\mathbf{n}}_i + \lambda_i \overset{v}{\mathbf{n}}_i \otimes \frac{d}{dt} \overset{v}{\mathbf{n}}_i \right) \end{aligned} \quad (4.1.52)$$

Consider a triple of fixed orthogonal unit vectors \mathbf{e}_i and the rotation tensor \mathbf{P}_U such that

$$\overset{u}{\mathbf{N}}_i = \mathbf{P}_U \cdot \mathbf{e}_i$$

Hence

$$\overset{v}{\mathbf{n}}_i = \mathbf{R} \cdot \mathbf{P}_U \cdot \mathbf{e}_i$$

or

$$\overset{v}{\mathbf{n}}_i = \mathbf{P}_V \cdot \mathbf{e}_i, \quad \mathbf{P}_V = \mathbf{R} \cdot \mathbf{P}_U \quad (4.1.53)$$

For the rotation tensors \mathbf{P}_U and \mathbf{P}_V the spin tensors and the angular velocity vectors can be introduced as follows

$$\begin{aligned} \dot{\mathbf{P}}_U \cdot \mathbf{P}_U^T &= \boldsymbol{\Omega}_U \times \mathbf{I}, \quad \dot{\mathbf{P}}_U = \boldsymbol{\Omega}_U \times \mathbf{P}_U, \\ \dot{\mathbf{P}}_V \cdot \mathbf{P}_V^T &= \boldsymbol{\Omega}_V \times \mathbf{I}, \quad \dot{\mathbf{P}}_V = \boldsymbol{\Omega}_V \times \mathbf{P}_V \end{aligned} \quad (4.1.54)$$

The time derivative of Eq. (4.1.53)₂ yields

$$\begin{aligned} \dot{\mathbf{P}}_V &= \dot{\mathbf{R}} \cdot \mathbf{P}_U + \mathbf{R} \cdot \dot{\mathbf{P}}_U \\ &= \boldsymbol{\Omega}_R \times \mathbf{R} \cdot \mathbf{P}_U + \mathbf{R} \cdot (\boldsymbol{\Omega}_U \times \mathbf{I}) \cdot \mathbf{R}^T \cdot \mathbf{R} \cdot \mathbf{P}_U \\ &= (\boldsymbol{\Omega}_R + \mathbf{R} \cdot \boldsymbol{\Omega}_U) \times \mathbf{P}_V \end{aligned}$$

Hence the following relationship between the angular velocity vectors can be established

$$\boldsymbol{\Omega}_V = \boldsymbol{\Omega}_R + \mathbf{R} \cdot \boldsymbol{\Omega}_U \quad (4.1.55)$$

With Eqs. (4.1.54) the rates of change of principal directions can be computed as follows

$$\frac{d}{dt} \overset{u}{\mathbf{N}}_i = \boldsymbol{\Omega}_U \times \overset{u}{\mathbf{N}}_i, \quad \frac{d}{dt} \overset{v}{\mathbf{n}}_i = \boldsymbol{\Omega}_V \times \overset{v}{\mathbf{n}}_i$$

Consequently the rates of change of stretch tensors (4.1.52) take the following form

$$\begin{aligned} \dot{\mathbf{U}} &= \sum_{i=1}^3 \dot{\lambda}_i \overset{u}{\mathbf{N}}_i \otimes \overset{u}{\mathbf{N}}_i + \boldsymbol{\Omega}_U \times \mathbf{U} - \mathbf{U} \times \boldsymbol{\Omega}_U, \\ \dot{\mathbf{V}} &= \sum_{i=1}^3 \dot{\lambda}_i \overset{v}{\mathbf{n}}_i \otimes \overset{v}{\mathbf{n}}_i + \boldsymbol{\Omega}_V \times \mathbf{V} - \mathbf{V} \times \boldsymbol{\Omega}_V \end{aligned} \quad (4.1.56)$$

With equation (4.1.56) and

$$\mathbf{U}^{-1} = \sum_{i=1}^3 \frac{1}{\lambda_i} \overset{u}{\mathbf{N}}_i \otimes \overset{u}{\mathbf{N}}_i,$$

one may compute

$$\mathbf{R} \cdot \dot{\mathbf{U}} \cdot \mathbf{U}^{-1} \cdot \mathbf{R}^T = \mathbf{R} \cdot \left[\sum_{i=1}^3 \dot{\lambda}_i \lambda_i^{-1} \overset{u}{\mathbf{N}}_i \otimes \overset{u}{\mathbf{N}}_i + \boldsymbol{\Omega}_U \times \mathbf{I} - (\mathbf{U} \times \boldsymbol{\Omega}_U) \cdot \mathbf{U} \right] \cdot \mathbf{R}^T$$

Applying Eqs. (4.1.53), (4.1.55) it can be simplified as follows

$$\begin{aligned} \mathbf{R} \cdot \dot{\mathbf{U}} \cdot \mathbf{U}^{-1} \cdot \mathbf{R}^T &= \sum_{i=1}^3 \dot{\lambda}_i \lambda_i^{-1} \overset{v}{\mathbf{n}}_i \otimes \overset{v}{\mathbf{n}}_i \\ &+ (\boldsymbol{\Omega}_V - \boldsymbol{\Omega}_R) \times \mathbf{I} - \mathbf{V} \cdot [(\boldsymbol{\Omega}_V - \boldsymbol{\Omega}_R) \times \mathbf{I}] \cdot \mathbf{V}^{-1} \end{aligned} \quad (4.1.57)$$

Taking the vector invariant of Eq. (4.1.57) and applying the identities (A.4.15) and (A.4.16) we obtain

$$(\mathbf{R} \cdot \dot{\mathbf{U}} \cdot \mathbf{U}^{-1} \cdot \mathbf{R}^T)_\times = -2(\boldsymbol{\Omega}_V - \boldsymbol{\Omega}_R) - \mathbf{A}_V \cdot (\boldsymbol{\Omega}_V - \boldsymbol{\Omega}_R), \quad (4.1.58)$$

where

$$\mathbf{A}_V = \sum_{i_1}^3 \lambda_{i_1} \overset{v}{\mathbf{n}}_{i_1} \times \mathbf{V}^{-1} \times \overset{v}{\mathbf{n}}_{i_1} = \sum_{i=1}^3 \sum_{j=1}^3 \frac{\lambda_i}{\lambda_j} \overset{v}{\mathbf{n}}_i \times \overset{v}{\mathbf{n}}_j \otimes \overset{v}{\mathbf{n}}_j \times \overset{v}{\mathbf{n}}_i$$

According to (A.4.16) and the Cayley-Hamilton theorem the tensor \mathbf{A}_V has the following representations

$$\mathbf{A}_V = J^{-1} \mathbf{V} \cdot [\mathbf{V}^2 - (\text{tr } \mathbf{V}^2) \mathbf{I}] = \mathbf{I} + \frac{J_{2V} - J_{1V}^2}{J} \mathbf{V} + \frac{J_{1V}}{J} \mathbf{V}^2,$$

where $J_{1\mathbf{v}}$, $J_{2\mathbf{v}}$ and $J = J_{3\mathbf{v}}$ are principal invariants of the tensor \mathbf{V} as defined by Eqs. (A.4.11). The spectral form of the tensor $\mathbf{A}_{\mathbf{V}}$ is

$$-\mathbf{A}_{\mathbf{V}} = \frac{\lambda_2^2 + \lambda_3^2}{\lambda_2\lambda_3} \mathbf{n}_1^{\mathbf{v}} \otimes \mathbf{n}_1^{\mathbf{v}} + \frac{\lambda_3^2 + \lambda_1^2}{\lambda_3\lambda_1} \mathbf{n}_2^{\mathbf{v}} \otimes \mathbf{n}_2^{\mathbf{v}} + \frac{\lambda_1^2 + \lambda_2^2}{\lambda_1\lambda_2} \mathbf{n}_3^{\mathbf{v}} \otimes \mathbf{n}_3^{\mathbf{v}} \quad (4.1.59)$$

With Eqs. (4.1.49) and (4.1.58) the following relationship between the angular velocities can be obtained

$$\boldsymbol{\omega} = \boldsymbol{\Omega}_{\mathbf{V}} + \frac{1}{2} \mathbf{A}_{\mathbf{V}} \cdot (\boldsymbol{\Omega}_{\mathbf{V}} - \boldsymbol{\Omega}_{\mathbf{R}}) \quad (4.1.60)$$

The relationship (4.1.60) can also be derived with the following decomposition

$$\mathbf{F} = \mathbf{V} \cdot \mathbf{R} \quad \Rightarrow \quad \mathbf{F}^{-1} = \mathbf{R}^T \cdot \mathbf{V}^{-1}$$

Therefore the velocity gradient is

$$\mathbf{L} = \dot{\mathbf{F}} \cdot \mathbf{F}^{-1} = \dot{\mathbf{V}} \cdot \mathbf{V}^{-1} + \mathbf{V} \cdot \dot{\mathbf{R}} \cdot \mathbf{R}^T \cdot \mathbf{V}^{-1} \quad (4.1.61)$$

With Eqs. (4.1.28), (4.1.47) and (4.1.56), Eq. (4.1.61) takes the form

$$\mathbf{L} = \sum_{i=1}^3 \dot{\lambda}_i \lambda_i^{-1} \mathbf{n}_i^{\mathbf{v}} \otimes \mathbf{n}_i^{\mathbf{v}} + \boldsymbol{\Omega}_{\mathbf{V}} \times \mathbf{I} + \mathbf{L}_{\boldsymbol{\Omega}}, \quad (4.1.62)$$

where

$$\mathbf{L}_{\boldsymbol{\Omega}} = \mathbf{V} \cdot (\tilde{\boldsymbol{\Omega}} \times \mathbf{I}) \cdot \mathbf{V}^{-1}, \quad \tilde{\boldsymbol{\Omega}} = \boldsymbol{\Omega}_{\mathbf{R}} - \boldsymbol{\Omega}_{\mathbf{V}}$$

Taking the vector invariant of Eq. (4.1.62) provides the relationship (4.1.60).

With the identity (A.4.8)₂ the tensor $\mathbf{L}_{\boldsymbol{\Omega}}$ can be represented as follows

$$\begin{aligned} \mathbf{L}_{\boldsymbol{\Omega}} &= \mathbf{a} \times \mathbf{V}^{-2} = \mathbf{V}^2 \times \mathbf{b}, \\ \mathbf{a} &= J\mathbf{V}^{-1} \cdot \tilde{\boldsymbol{\Omega}}, \quad \mathbf{b} = J^{-1}\mathbf{V} \cdot \tilde{\boldsymbol{\Omega}} \end{aligned} \quad (4.1.63)$$

The right dot product of Eq. (4.1.62) with \mathbf{V}^2 yields

$$\mathbf{L} \cdot \mathbf{V}^2 = \sum_{i=1}^3 \dot{\lambda}_i \lambda_i \mathbf{n}_i^{\mathbf{v}} \otimes \mathbf{n}_i^{\mathbf{v}} + \boldsymbol{\Omega}_{\mathbf{V}} \times \mathbf{V}^2 + \mathbf{a} \times \mathbf{I}, \quad (4.1.64)$$

With the decomposition of the velocity gradient (4.1.43), Eq. (4.1.64) takes the following form

$$\mathbf{D} \cdot \mathbf{V}^2 = \sum_{i=1}^3 \dot{\lambda}_i \lambda_i \mathbf{n}_i^{\mathbf{v}} \otimes \mathbf{n}_i^{\mathbf{v}} + (\boldsymbol{\Omega}_{\mathbf{V}} - \boldsymbol{\omega}) \times \mathbf{V}^2 + \mathbf{a} \times \mathbf{I} \quad (4.1.65)$$

Taking the vector invariant of Eq. (4.1.65) yields

$$\frac{1}{2J} \mathbf{V} \cdot (\mathbf{D} \cdot \mathbf{V}^2)_\times = \left(\mathbf{I} + \frac{1}{2} \mathbf{A}_V \right) \cdot \boldsymbol{\Omega}_V - \frac{1}{2} \mathbf{A}_V \cdot \boldsymbol{\omega} - \boldsymbol{\Omega}_R \quad (4.1.66)$$

From Eqs. (4.1.60) and (4.1.66) we obtain

$$\frac{1}{2J} \mathbf{V} \cdot (\mathbf{D} \cdot \mathbf{V}^2)_\times = \left(\mathbf{I} - \frac{1}{2} \mathbf{A}_V \right) \cdot (\boldsymbol{\omega} - \boldsymbol{\Omega}_R)$$

With Eq. (4.1.59) one may verify the tensor $\mathbf{I} - 1/2 \mathbf{A}_V$ is non-singular. Hence

$$\boldsymbol{\omega} - \boldsymbol{\Omega}_R = \mathbf{K}_V \cdot (\mathbf{D} \cdot \mathbf{V}^2)_\times, \quad \mathbf{K}_V = \frac{1}{2J} \left(\mathbf{I} - \frac{1}{2} \mathbf{A}_V \right)^{-1} \cdot \mathbf{V} \quad (4.1.67)$$

Applying Eq. (4.1.59) the following spectral representation of the tensor \mathbf{K}_V can be established

$$\mathbf{K}_V = \frac{1}{(\lambda_2 + \lambda_3)^2} \mathbf{n}_1^v \otimes \mathbf{n}_1^v + \frac{1}{(\lambda_3 + \lambda_1)^2} \mathbf{n}_2^v \otimes \mathbf{n}_2^v + \frac{1}{(\lambda_1 + \lambda_2)^2} \mathbf{n}_3^v \otimes \mathbf{n}_3^v \quad (4.1.68)$$

Let us relate the tensor \mathbf{D} to the time derivative of the Hencky strain tensor \mathbf{h} . To this end consider the symmetric part of Eq. (4.1.62)

$$\mathbf{D} = \sum_{i=1}^3 \dot{\lambda}_i \lambda_i^{-1} \mathbf{n}_i^v \otimes \mathbf{n}_i^v + \frac{1}{2} (\mathbf{V}^2 \times \mathbf{b} - \mathbf{b} \times \mathbf{V}^2) \quad (4.1.69)$$

The time derivative of the Hencky strain tensor (4.1.35) can be computed as follows

$$\dot{\mathbf{h}} = \sum_{i=1}^3 \dot{\lambda}_i \lambda_i^{-1} \mathbf{n}_i^v \otimes \mathbf{n}_i^v + \boldsymbol{\Omega}_V \times \mathbf{h} - \mathbf{h} \times \boldsymbol{\Omega}_V \quad (4.1.70)$$

Inserting into Eq. (4.1.69) yields

$$\mathbf{D} = \dot{\mathbf{h}} - \boldsymbol{\Omega}_V \times \mathbf{h} + \mathbf{h} \times \boldsymbol{\Omega}_V + \frac{1}{2} (\mathbf{V}^2 \times \mathbf{b} - \mathbf{b} \times \mathbf{V}^2) \quad (4.1.71)$$

The tensor

$$\mathbf{D}_\Omega = \frac{1}{2} (\mathbf{V}^2 \times \mathbf{b} - \mathbf{b} \times \mathbf{V}^2)$$

has the following representation

$$2\mathbf{D}_{\Omega} = \sum_{i=1}^3 \sum_{j=1}^3 (\lambda_i^2 - \lambda_j^2) \mathbf{b} \cdot (\mathbf{n}_i \times \mathbf{n}_j) (\mathbf{n}_i \otimes \mathbf{n}_j + \mathbf{n}_j \otimes \mathbf{n}_i) \quad (4.1.72)$$

Assuming that the tensor \mathbf{V} has distinct principal values λ_i let us consider the following identity

$$\begin{aligned} 2\mathbf{D}_{\Omega} &= \sum_{i=1}^3 \sum_{j=1}^3 (\ln \lambda_i - \ln \lambda_j) \frac{\lambda_i^2 - \lambda_j^2}{(\ln \lambda_i - \ln \lambda_j)} \mathbf{b} \cdot (\mathbf{n}_i \times \mathbf{n}_j) (\mathbf{n}_i \otimes \mathbf{n}_j + \mathbf{n}_j \otimes \mathbf{n}_i) \\ &= \sum_{i=1}^3 \sum_{j=1}^3 (\ln \lambda_i - \ln \lambda_j) \mathbf{c} \cdot (\mathbf{n}_i \times \mathbf{n}_j) (\mathbf{n}_i \otimes \mathbf{n}_j + \mathbf{n}_j \otimes \mathbf{n}_i) \\ &= \mathbf{h} \times \mathbf{c} - \mathbf{c} \times \mathbf{h}, \quad i \neq j \end{aligned} \quad (4.1.73)$$

where the components of vector \mathbf{c} are related to the components of vector \mathbf{b} as follows

$$\mathbf{c} \cdot (\mathbf{n}_i \times \mathbf{n}_j) = \frac{\lambda_i^2 - \lambda_j^2}{(\ln \lambda_i - \ln \lambda_j)} \mathbf{b} \cdot (\mathbf{n}_i \times \mathbf{n}_j), \quad i \neq j$$

Hence

$$\begin{aligned} \mathbf{c} \cdot \sum_{i=1}^3 \sum_{j=1}^3 \mathbf{n}_i \times \mathbf{n}_j \otimes \mathbf{n}_j \times \mathbf{n}_i \\ = \mathbf{b} \cdot \sum_{i=1}^3 \sum_{j=1}^3 \frac{\lambda_i^2 - \lambda_j^2}{(\ln \lambda_i - \ln \lambda_j)} \mathbf{n}_i \times \mathbf{n}_j \otimes \mathbf{n}_j \times \mathbf{n}_i, \quad i \neq j \end{aligned}$$

Applying the identity (A.4.14) we obtain

$$\sum_{i=1}^3 \sum_{j=1}^3 \mathbf{n}_i \times \mathbf{n}_j \otimes \mathbf{n}_j \times \mathbf{n}_i = \sum_{i=1}^3 \mathbf{n}_i \times \mathbf{I} \times \mathbf{n}_i = \sum_{i=1}^3 (\mathbf{n}_i \otimes \mathbf{n}_i - \mathbf{n}_i \cdot \mathbf{n}_i \mathbf{I}) = -2\mathbf{I}$$

Consequently

$$2\mathbf{c} = -\mathbf{b} \cdot \sum_{i=1}^3 \sum_{j=1}^3 \frac{\lambda_i^2 - \lambda_j^2}{(\ln \lambda_i - \ln \lambda_j)} \mathbf{n}_i \times \mathbf{n}_j \otimes \mathbf{n}_j \times \mathbf{n}_i, \quad i \neq j \quad (4.1.74)$$

With Eqs. (4.1.63), (4.1.71), (4.1.73) and (4.1.74) the tensor \mathbf{D} is related to the rate of the Hencky strain tensor \mathbf{h} as follows

$$\mathbf{D} = \dot{\mathbf{h}} - \boldsymbol{\Omega}_h \times \mathbf{h} + \mathbf{h} \times \boldsymbol{\Omega}_h, \quad \boldsymbol{\Omega}_h = \boldsymbol{\Omega}_V + \mathbf{A}_h \cdot (\boldsymbol{\Omega}_R - \boldsymbol{\Omega}_V) \quad (4.1.75)$$

where

$$\mathbf{A}_h = -\frac{1}{4J} \mathbf{V} \cdot \sum_{i=1}^3 \sum_{j=1}^3 \frac{\lambda_i^2 - \lambda_j^2}{(\ln \lambda_i - \ln \lambda_j)} \mathbf{n}_i^v \times \mathbf{n}_j^v \otimes \mathbf{n}_j^v \times \mathbf{n}_i^v, \quad i \neq j$$

The tensor \mathbf{A}_h has the following spectral representation

$$2\mathbf{A}_h = \frac{\lambda_2^2 - \lambda_3^2}{\lambda_2 \lambda_3 \ln \frac{\lambda_2}{\lambda_3}} \mathbf{n}_1^v \otimes \mathbf{n}_1^v + \frac{\lambda_3^2 - \lambda_1^2}{\lambda_3 \lambda_1 \ln \frac{\lambda_3}{\lambda_1}} \mathbf{n}_2^v \otimes \mathbf{n}_2^v + \frac{\lambda_1^2 - \lambda_2^2}{\lambda_1 \lambda_2 \ln \frac{\lambda_1}{\lambda_2}} \mathbf{n}_3^v \otimes \mathbf{n}_3^v$$

In Xiao et al. (1997) the tensor $\boldsymbol{\Omega}_h \times \mathbf{I}$ is called logarithmic spin. With Eqs. (4.1.55), (4.1.67) and (4.1.75) the vector $\boldsymbol{\Omega}_h$ can be computed as follows

$$\boldsymbol{\Omega}_h = \boldsymbol{\omega} + \mathbf{K}_h \cdot (\mathbf{D} \cdot \mathbf{V}^2)_\times, \quad (4.1.76)$$

where

$$2\mathbf{K}_h = \sum_{i=1}^3 \sum_{j=1}^3 \frac{1}{\lambda_i^2 - \lambda_j^2} \left(\frac{\lambda_i^2 + \lambda_j^2}{\lambda_i^2 - \lambda_j^2} - \frac{1}{\ln \frac{\lambda_i}{\lambda_j}} \right) \mathbf{n}_i^v \times \mathbf{n}_j^v \otimes \mathbf{n}_j^v \times \mathbf{n}_i^v, \quad i \neq j$$

Equation (4.1.76) is firstly derived by Xiao et al. (1997) in a different notation. The tensor \mathbf{K}_h has the following spectral representation

$$\begin{aligned} \mathbf{K}_h &= \frac{1}{\lambda_2^2 - \lambda_3^2} \left(\frac{1}{\ln \frac{\lambda_2}{\lambda_3}} - \frac{\lambda_2^2 + \lambda_3^2}{\lambda_2^2 - \lambda_3^2} \right) \mathbf{n}_1^v \otimes \mathbf{n}_1^v \\ &+ \frac{1}{\lambda_3^2 - \lambda_1^2} \left(\frac{1}{\ln \frac{\lambda_3}{\lambda_1}} - \frac{\lambda_3^2 + \lambda_1^2}{\lambda_3^2 - \lambda_1^2} \right) \mathbf{n}_2^v \otimes \mathbf{n}_2^v \\ &+ \frac{1}{\lambda_3^2 - \lambda_1^2} \left(\frac{1}{\ln \frac{\lambda_1}{\lambda_2}} - \frac{\lambda_1^2 + \lambda_2^2}{\lambda_1^2 - \lambda_2^2} \right) \mathbf{n}_3^v \otimes \mathbf{n}_3^v \end{aligned}$$

4.2 Conservation of Mass

The mass of an infinitesimal part of the body is

$$dm = \rho dV = \rho_0 dV_0, \quad (4.2.77)$$

where ρ and ρ_0 is the density in the actual and the reference configurations, respectively. With Eq. (4.1.17) the conservation of mass (4.2.77) takes the form

$$\frac{\rho_0}{\rho} = J \quad (4.2.78)$$

4.3 Balance of Momentum

The momentum of an infinitesimal part of the solid is defined as follows

$$d\mathbf{p} = \mathbf{v}dm = \mathbf{v}\rho dV$$

The momentum for a part of the solid with the volume V_p in the in the actual configuration is

$$\mathbf{p}_p = \int_{V_p} \mathbf{v}\rho dV \quad (4.3.79)$$

The balance of momentum or the first law of dynamics states that the rate of change of momentum of a body is equal to the total force acting on the body.

4.3.1 Stress Vector

Figure 4.2 illustrates a body under the given external loads. To visualize the internal forces let us cut the body in the actual configuration by a plane. The orientation of the plane is given by the unit normal vector \mathbf{n} . In the differential neighborhood of a point P consider an infinitesimal area element dA . To characterize the mechanical action of the part II on the part I of the body let us introduce the force vector $d\mathbf{T}_{II-I} = d\mathbf{T}_{(n)}$ as shown in Fig. 4.2. On the other hand the force vector $d\mathbf{T}_{I-II} = d\mathbf{T}_{(-n)}$ models the mechanical action of the part I on the part II. The intensity of these mechanical actions can be characterized by the stress vectors $\boldsymbol{\sigma}_{(n)}$ and $\boldsymbol{\sigma}_{(-n)}$. Both the magnitude

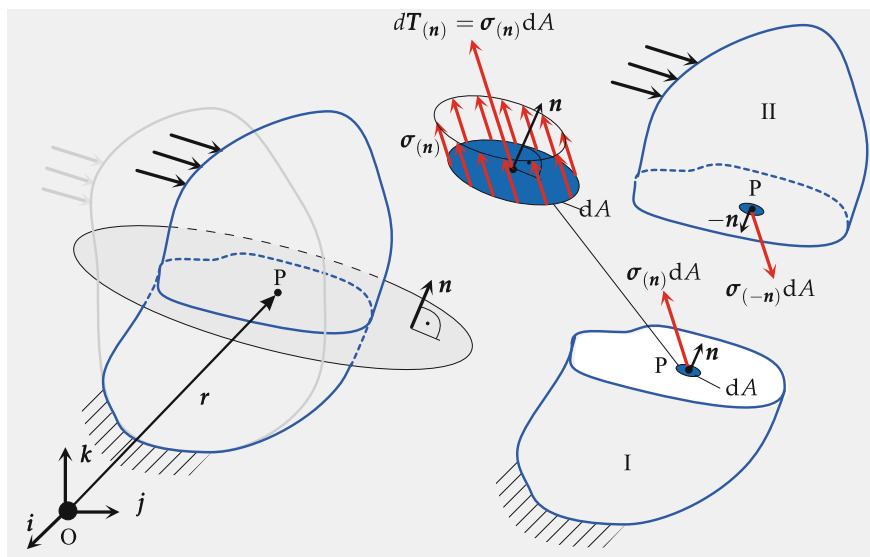


Fig. 4.2 Stress vector for the plane with the normal vector n

and the direction of the stress vector depend on the position within the body. Within the infinitesimal area element dA the stress vector is assumed constant such that

$$d\mathbf{T}_{(n)} = \boldsymbol{\sigma}_{(n)}dA, \quad d\mathbf{T}_{(-n)} = \boldsymbol{\sigma}_{(-n)}dA$$

One may prove that

$$d\mathbf{T}_{(n)} = -d\mathbf{T}_{(-n)} \Rightarrow \boldsymbol{\sigma}_{(n)} = -\boldsymbol{\sigma}_{(-n)} \quad (4.3.80)$$

4.3.2 Integral Form

Let us cut a part with the volume V_p and the surface area A_p from the body, as shown in Fig. 4.3. The mechanical actions on the part of the body can be classified as follows

- body forces, for example force of gravity, electric or magnetic forces acting on a part of the mass $dm = \rho dV$. This type of action is described with the force density vector \mathbf{f} such that the elementary body force is $d\mathcal{G} = \mathbf{f}dm = \mathbf{f}\rho dV$
- surface forces $d\mathbf{T}_{(n)} = \boldsymbol{\sigma}_{(n)}dA$ acting on the surface elements dA of A_p . These forces characterize the mechanical action of the environment (remainder of the body) on the given part V_p .

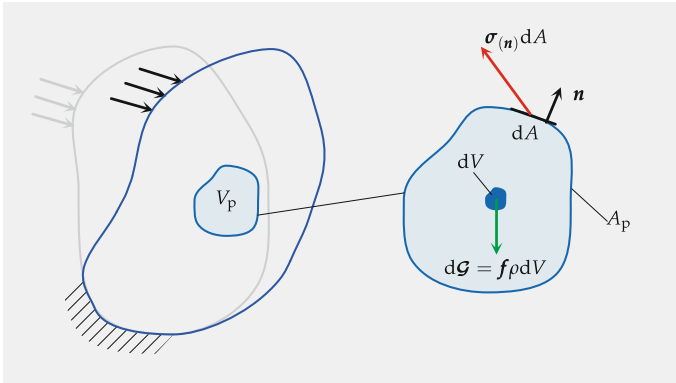


Fig. 4.3 Forces acting on a part of the body with the volume V_p

The resultant force vector is

$$\mathcal{F}_p = \int_{A_p} \boldsymbol{\sigma}_{(n)} dA + \int_{V_p} \mathbf{f} \rho dV$$

The balance of momentum for the part of the solid can be formulated as follows

$$\frac{d}{dt} \int_{V_p} \mathbf{v} \rho dV = \int_{A_p} \boldsymbol{\sigma}_{(n)} dA + \int_{V_p} \mathbf{f} \rho dV \tag{4.3.81}$$

4.3.3 Stress Tensor and Cauchy Formula

The balance of momentum (4.3.81) can be applied for any part of the body. Consider an infinitesimal tetrahedron ($A_p \rightarrow 0, V_p \rightarrow 0$) as a part of the body, Fig. 4.4. The orthonormal vectors $\mathbf{e}_1, \mathbf{e}_2$ and \mathbf{e}_3 are introduced to fix the orientation of the tetrahedron. The mechanical action of the environment on the tetrahedron cut from the body is characterized by forces and corresponding stress vectors. The cut planes, the corresponding areas as well as stress and force vectors are given in the Table 4.1. For the infinitesimal tetrahedron the volume integrals in Eq. (4.3.81) have lower order of magnitude compared to the surface integral such that

$$\int_{A_p} \boldsymbol{\sigma}_{(n)} dA = \mathbf{0} \tag{4.3.82}$$

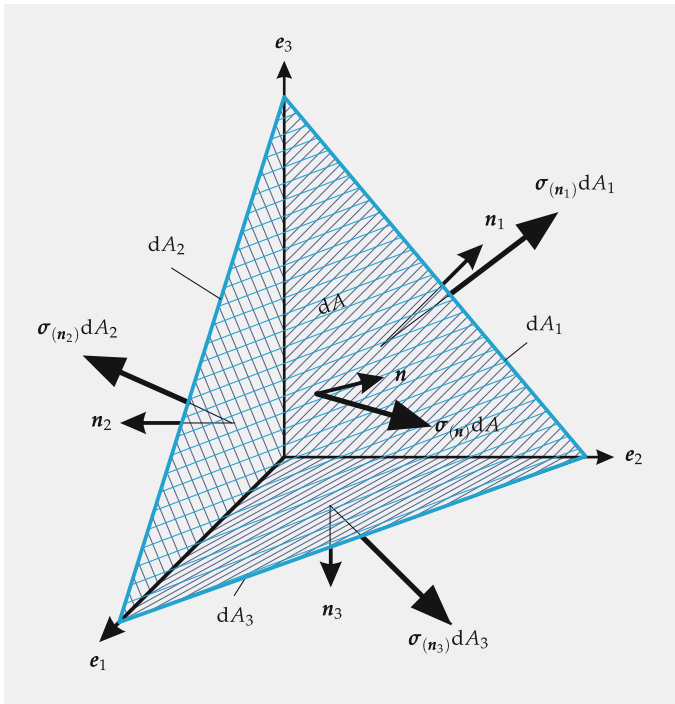


Fig. 4.4 Infinitesimal tetrahedron cut from the body

Table 4.1 Summary of formulae for the infinitesimal tetrahedron

Plane	Area	Stress vector	Force vector
$n_1 = -e_1$	dA_1	$\sigma_{(n_1)} = -\sigma_{(e_1)}$	$T_{(n_1)} = \sigma_{(n_1)}dA_1$
$n_2 = -e_2$	dA_2	$\sigma_{(n_2)} = -\sigma_{(e_2)}$	$T_{(n_2)} = \sigma_{(n_2)}dA_2$
$n_3 = -e_3$	dA_3	$\sigma_{(n_3)} = -\sigma_{(e_3)}$	$T_{(n_3)} = \sigma_{(n_3)}dA_3$
n	dA	$\sigma_{(n)}$	$T_{(n)} = \sigma_{(n)}dA$

Hence

$$\sigma_{(n_1)}dA_1 + \sigma_{(n_2)}dA_2 + \sigma_{(n_3)}dA_3 + \sigma_{(n)}dA = 0$$

Taking into account (4.3.80)

$$-\sigma_{(e_1)}dA_1 - \sigma_{(e_2)}dA_2 - \sigma_{(e_3)}dA_3 + \sigma_{(n)}dA = 0 \tag{4.3.83}$$

or

$$\sigma_{(n)}dA = \sigma_{(e_1)}dA_1 + \sigma_{(e_2)}dA_2 + \sigma_{(e_3)}dA_3 \tag{4.3.84}$$

In addition the following equation is valid for any part of the volume³

$$\int_{A_p} \mathbf{n} dA = \mathbf{0} \quad (4.3.85)$$

Applying (4.3.85) to the tetrahedron yields

$$\mathbf{n}_1 dA_1 + \mathbf{n}_2 dA_2 + \mathbf{n}_3 dA_3 + \mathbf{n} dA = \mathbf{0} \quad (4.3.86)$$

Therefore

$$\begin{aligned} \mathbf{n} dA &= \mathbf{e}_1 dA_1 + \mathbf{e}_2 dA_2 + \mathbf{e}_3 dA_3, \\ \mathbf{n} \cdot \mathbf{e}_1 dA &= dA_1, \quad \mathbf{n} \cdot \mathbf{e}_2 dA = dA_2, \quad \mathbf{n} \cdot \mathbf{e}_3 dA = dA_3 \end{aligned} \quad (4.3.87)$$

Inserting dA_i ($i = 1, 2, 3$) into Eq. (4.3.84) we obtain

$$\begin{aligned} \boldsymbol{\sigma}_{(\mathbf{n})} dA &= dA_1 \boldsymbol{\sigma}_{(\mathbf{e}_1)} + dA_2 \boldsymbol{\sigma}_{(\mathbf{e}_2)} + dA_3 \boldsymbol{\sigma}_{(\mathbf{e}_3)} \\ &= \mathbf{n} \cdot \mathbf{e}_1 dA \boldsymbol{\sigma}_{(\mathbf{e}_1)} + \mathbf{n} \cdot \mathbf{e}_2 dA \boldsymbol{\sigma}_{(\mathbf{e}_2)} + \mathbf{n} \cdot \mathbf{e}_3 dA \boldsymbol{\sigma}_{(\mathbf{e}_3)} \end{aligned}$$

This can be simplified as follows

$$\begin{aligned} \boldsymbol{\sigma}_{(\mathbf{n})} &= \mathbf{n} \cdot \mathbf{e}_1 \boldsymbol{\sigma}_{(\mathbf{e}_1)} + \mathbf{n} \cdot \mathbf{e}_2 \boldsymbol{\sigma}_{(\mathbf{e}_2)} + \mathbf{n} \cdot \mathbf{e}_3 \boldsymbol{\sigma}_{(\mathbf{e}_3)} \\ &= \mathbf{n} \cdot [\mathbf{e}_1 \otimes \boldsymbol{\sigma}_{(\mathbf{e}_1)} + \mathbf{e}_2 \otimes \boldsymbol{\sigma}_{(\mathbf{e}_2)} + \mathbf{e}_3 \otimes \boldsymbol{\sigma}_{(\mathbf{e}_3)}] \end{aligned} \quad (4.3.88)$$

With the tensor

$$\boldsymbol{\sigma} = \mathbf{e}_1 \otimes \boldsymbol{\sigma}_{(\mathbf{e}_1)} + \mathbf{e}_2 \otimes \boldsymbol{\sigma}_{(\mathbf{e}_2)} + \mathbf{e}_3 \otimes \boldsymbol{\sigma}_{(\mathbf{e}_3)} \quad (4.3.89)$$

Eq. (4.3.88) takes the following form

$$\boldsymbol{\sigma}_{(\mathbf{n})} = \mathbf{n} \cdot \boldsymbol{\sigma} \quad (4.3.90)$$

Equation (4.3.90) is the Cauchy formula⁴ that allows one to compute the stress vector for any plane with the unit normal \mathbf{n} if the Cauchy stress tensor $\boldsymbol{\sigma}$ is given.

³This can be verified applying the integral theorem (B.3.4)₁ with $\varphi = 1$.

⁴In some books of continuum mechanics and applied mathematics the stress tensor is defined as $\boldsymbol{\sigma} = \boldsymbol{\sigma}_{(\mathbf{e}_1)} \otimes \mathbf{e}_1 + \boldsymbol{\sigma}_{(\mathbf{e}_2)} \otimes \mathbf{e}_2 + \boldsymbol{\sigma}_{(\mathbf{e}_3)} \otimes \mathbf{e}_3$ such that the Cauchy formula is $\boldsymbol{\sigma}_{(\mathbf{n})} = \boldsymbol{\sigma} \cdot \mathbf{n}$. Formally this definition differs from (4.3.89) by transpose. It might be more convenient, as it is closer to the matrix algebra. For engineers dealing with internal forces it is more natural to use (4.3.89). Indeed, to analyze a stress state we need to cut the body first and to specify the normal to the cut plane. Only after that we can introduce the internal force. The sequence of these operations is clearly seen in (4.3.89).

4.3.4 Local Forms

With the Cauchy formula (4.3.90) and the integral theorem (B.3.5)₂ the surface integral in (4.3.81) is transformed as follows

$$\int_{A_p} \boldsymbol{\sigma}(\mathbf{n}) dA = \int_{A_p} \mathbf{n} \cdot \boldsymbol{\sigma} dA = \int_{V_p} \nabla \cdot \boldsymbol{\sigma} dV \quad (4.3.91)$$

Now the balance of momentum takes the form

$$\int_{V_p} (\rho \dot{\mathbf{v}} - \nabla \cdot \boldsymbol{\sigma} - \rho \mathbf{f}) dV = \mathbf{0} \quad (4.3.92)$$

Since Eq. (4.3.92) is valid for any part of the solid, the following local form of the balance of momentum can be established

$$\rho \dot{\mathbf{v}} = \nabla \cdot \boldsymbol{\sigma} + \rho \mathbf{f} \quad (4.3.93)$$

With the identity (4.1.18) the surface integral (4.3.91) can be transformed as follows

$$\int_{A_p} \boldsymbol{\sigma}(\mathbf{n}) dA = \int_{A_p} \mathbf{n} \cdot \boldsymbol{\sigma} dA = \int_{A_{p_0}} \mathbf{N} \cdot \mathbf{P} dA_0 = \int_{V_{p_0}} \overset{0}{\nabla} \cdot \mathbf{P} dV_0, \quad (4.3.94)$$

where

$$\mathbf{P} = \mathbf{J} \mathbf{F}^{-1} \cdot \boldsymbol{\sigma} \quad (4.3.95)$$

is the Piola-Kirchhoff stress tensor. With Eqs. (4.3.94) and (4.2.78) the balance of momentum can be formulated as follows

$$\int_{V_{p_0}} (\rho_0 \dot{\mathbf{v}} - \overset{0}{\nabla} \cdot \mathbf{P} - \rho_0 \mathbf{f}) dV_0 = \mathbf{0} \quad (4.3.96)$$

The corresponding local form is

$$\rho_0 \dot{\mathbf{v}} = \overset{0}{\nabla} \cdot \mathbf{P} + \rho_0 \mathbf{f} \quad (4.3.97)$$

4.4 Balance of Angular Momentum

With respect to the point O the angular momentum and the resultant moment vectors for a part of the body are defined as follows⁵

$$\mathbf{q}_{pO} = \int_{V_p} \mathbf{r} \times \mathbf{v} \rho dV, \quad \mathcal{M}_{pO} = \int_{A_p} \mathbf{r} \times \boldsymbol{\sigma}_{(\mathbf{n})} dA + \int_{V_p} \mathbf{r} \times \mathbf{f} \rho dV \quad (4.4.98)$$

The balance of angular momentum or the second law of dynamics states that the rate of change of angular momentum of a body is equal to the resultant moment acting on the body. The surface integral in Eq. (4.4.98) can be transformed applying (B.3.5)₂ as follows

$$\int_{A_p} \mathbf{r} \times (\mathbf{n} \cdot \boldsymbol{\sigma}) dA = - \int_{A_p} \mathbf{n} \cdot \boldsymbol{\sigma} \times \mathbf{r} dA = - \int_{V_p} \nabla \cdot (\boldsymbol{\sigma} \times \mathbf{r}) dV \quad (4.4.99)$$

Applying the identity (B.2.3) we obtain

$$\nabla \cdot (\boldsymbol{\sigma} \times \mathbf{r}) = (\nabla \cdot \boldsymbol{\sigma}) \times \mathbf{r} - \boldsymbol{\sigma}_{\times}$$

The balance of angular momentum can be formulated as follows

$$\dot{\mathbf{q}}_{pO} = \int_{V_p} \mathbf{r} \times \dot{\mathbf{v}} \rho dV = \int_{V_p} [\mathbf{r} \times (\nabla \cdot \boldsymbol{\sigma} + \boldsymbol{\rho} f) + \boldsymbol{\sigma}_{\times}] dV$$

or

$$\int_{V_p} \mathbf{r} \times (\dot{\mathbf{v}} \rho - \nabla \cdot \boldsymbol{\sigma} + \boldsymbol{\rho} f) dV = \int_{V_p} \boldsymbol{\sigma}_{\times} dV$$

Taking into account the balance of momentum (4.3.93) this results in

$$\boldsymbol{\sigma}_{\times} = \mathbf{0} \quad \Rightarrow \quad \boldsymbol{\sigma} = \boldsymbol{\sigma}^T \quad (4.4.100)$$

⁵With regard to structural analysis applications discussed in this book it is enough to identify the angular momentum as the moment of momentum and the resultant moment as the moment of forces. In contrast, within the micropolar theories material points are equipped by tensor of inertia. The resultant moment includes surface and body moments which are not related to moment of forces, e.g. Altenbach et al. (2003), Eringen (1999), Nowacki (1986).

4.5 Balance of Energy

The total energy E_p of the part of the body, is defined as a sum of the kinetic energy K_p and the internal energy U_p as follows

$$E_p = K_p + U_p,$$

$$K_p = \int_{V_p} \rho \mathcal{K} dV, \quad U_p = \int_{V_p} \rho \mathcal{U} dV, \quad \mathcal{K} = \frac{1}{2} \mathbf{v} \cdot \mathbf{v}, \quad (4.5.101)$$

where \mathcal{K} and \mathcal{U} are densities of the kinetic and the internal energy, respectively. The energy balance equation or the first law of thermodynamics states that the rate of change of the energy of a body is equal to the mechanical power plus the rate of change of non-mechanical energy, for example heat, supplied into the body. The energy balance equation is

$$\frac{d}{dt} E_p = L_p + Q_p, \quad (4.5.102)$$

where L_p is the mechanical power and Q_p is the rate of change of non-mechanical energy supply. The mechanical power of forces introduced in Sect. 4.3.2 is defined as follows

$$L_p = \int_{A_p} \boldsymbol{\sigma}^{(n)} \cdot \mathbf{v} dA + \int_{V_p} \mathbf{f} \cdot \mathbf{v} \rho dV \quad (4.5.103)$$

With Eqs. (4.3.90) and (B.3.5)₂ the surface integral in (4.5.103) is transformed to

$$\int_{A_p} \boldsymbol{\sigma}^{(n)} \cdot \mathbf{v} dA = \int_{A_p} \mathbf{n} \cdot \boldsymbol{\sigma} \cdot \mathbf{v} dA = \int_{V_p} \nabla \cdot (\boldsymbol{\sigma} \cdot \mathbf{v}) dV \quad (4.5.104)$$

With the identity (B.2.2) we obtain

$$\nabla \cdot (\boldsymbol{\sigma} \cdot \mathbf{v}) = (\nabla \cdot \boldsymbol{\sigma}) \cdot \mathbf{v} + \boldsymbol{\sigma} \cdot \cdot (\nabla \otimes \mathbf{v})^T$$

The mechanical power can be now given as follows

$$L_p = \int_{V_p} [(\nabla \cdot \boldsymbol{\sigma} + \rho \mathbf{f}) \cdot \mathbf{v} + \boldsymbol{\sigma} \cdot \cdot (\nabla \otimes \mathbf{v})^T] dV \quad (4.5.105)$$

The energy balance equation (4.5.102) takes the form

$$\int_{V_p} \rho(\dot{\mathbf{v}} \cdot \mathbf{v} + \dot{\mathcal{U}})dV = \int_{V_p} [(\nabla \cdot \boldsymbol{\sigma} + \rho \mathbf{f}) \cdot \mathbf{v} + \boldsymbol{\sigma} \cdot (\nabla \otimes \mathbf{v})^T]dV + Q_p \quad (4.5.106)$$

With the balance of momentum (4.3.93), Eq. (4.5.106) simplifies to

$$\int_{V_p} \rho \dot{\mathcal{U}}dV = \int_{V_p} \boldsymbol{\sigma} \cdot (\nabla \otimes \mathbf{v})^T dV + Q_p \quad (4.5.107)$$

The rate of change of the energy supply includes the contributions through the outer surface and within the volume of the part p

$$Q_p = \int_{A_p} q_{(n)}dA + \int_{V_p} r\rho dV \quad (4.5.108)$$

Equation (4.5.107) takes the following form

$$\int_{V_p} [\rho \dot{\mathcal{U}} - \boldsymbol{\sigma} \cdot (\nabla \otimes \mathbf{v})^T - \rho r]dV = \int_{A_p} q_{(n)}dA \quad (4.5.109)$$

Equation (4.5.109) is valid for any part of the body. Considering an infinitesimal tetrahedron the energy balance reduces to

$$\int_{A_p} q_{(n)}dA = 0$$

Applying the procedures discussed in Sect. 4.3.3 one may derive the following equation

$$q_{(n)} = -\mathbf{n} \cdot \mathbf{q}, \quad (4.5.110)$$

where \mathbf{q} is the heat flow vector. With (B.3.5)₁ and (4.5.110) the surface integral can be transformed into the volume one as follows

$$\int_{A_p} q_{(n)}dA = - \int_{V_p} \nabla \cdot \mathbf{q}dV \quad (4.5.111)$$

Equation (4.5.108) takes the form

$$\int_{V_p} [\rho \dot{\mathcal{U}} - \boldsymbol{\sigma} \cdot (\nabla \otimes \mathbf{v})^T + \nabla \cdot \mathbf{q} - \rho r]dV = 0 \quad (4.5.112)$$

Equation (4.5.112) is valid for any part of the deformed body. Hence

$$\rho \dot{\mathcal{L}} = \boldsymbol{\sigma} \cdot (\nabla \otimes \mathbf{v})^T - \nabla \cdot \mathbf{q} + \rho r \quad (4.5.113)$$

With the identity (4.1.18) the surface integral (4.5.111) can be transformed as follows

$$\int_{A_p} q_{(n)} dA = - \int_{A_p} \mathbf{n} \cdot \mathbf{q} dA = - \int_{A_{p_0}} \mathbf{N} \cdot \hat{\mathbf{q}} dA_0 - \int_{V_{p_0}} \overset{0}{\nabla} \cdot \hat{\mathbf{q}} dV_0, \quad (4.5.114)$$

where by analogy to the Piola-Kirchhoff stress tensor the following heat flow vector can be introduced

$$\hat{\mathbf{q}} = J \mathbf{F}^{-1} \cdot \mathbf{q} \quad (4.5.115)$$

Now it is not difficult to derive the local form of the energy balance per unit volume of the body in the reference configuration

$$\rho_0 \dot{\mathcal{L}} = \mathbf{P} \cdot (\overset{0}{\nabla} \otimes \mathbf{v})^T - \overset{0}{\nabla} \cdot \hat{\mathbf{q}} + \rho_0 r \quad (4.5.116)$$

4.6 Entropy and Dissipation Inequalities

The second law of thermodynamics states that the entropy production of a body is non-negative. This statement is given as the Clausius-Planck inequality

$$\frac{d}{dt} S_p - \left(\frac{Q}{T} \right)_p \geq 0, \quad (4.6.117)$$

where S is the entropy and T is the absolute temperature. The entropy of the part of the body is defined as follows

$$S_p = \int_{V_p} \rho S dV, \quad (4.6.118)$$

where \mathcal{S} is the entropy density. For the part of the body we define

$$\left(\frac{Q}{T}\right)_p = \int_{A_p} \frac{q(\mathbf{n})}{T} dA + \int_{V_p} \frac{r}{T} \rho dV \quad (4.6.119)$$

Applying Eqs. (4.5.110) and (B.3.5)₁ we obtain

$$\left(\frac{Q}{T}\right)_p = \int_{V_p} \left[-\nabla \cdot \left(\frac{\mathbf{q}}{T}\right) + \frac{r}{T} \rho \right] dV \quad (4.6.120)$$

With Eqs. (4.6.118) and (4.6.120) the entropy inequality (4.6.117) can be formulated as follows

$$\int_{V_p} \left[\rho \dot{\mathcal{S}} + \nabla \cdot \left(\frac{\mathbf{q}}{T}\right) - \frac{r}{T} \rho \right] dV \geq 0 \quad (4.6.121)$$

Since (4.6.121) is valid for any part of the body the local form of the entropy inequality is

$$\rho \dot{\mathcal{S}} \geq -\nabla \cdot \left(\frac{\mathbf{q}}{T}\right) + \frac{\rho r}{T} \quad (4.6.122)$$

With the identity (B.2.1)

$$\nabla \cdot \left(\frac{\mathbf{q}}{T}\right) = \frac{\nabla \cdot \mathbf{q}}{T} - \frac{\mathbf{q} \cdot \nabla T}{T^2}$$

Multiplying both sides of (4.6.122) by T yields the Clausius-Duhem inequality

$$\rho \dot{\mathcal{S}} T \geq -\nabla \cdot \mathbf{q} + \frac{\mathbf{q} \cdot \nabla T}{T} + r \rho \quad (4.6.123)$$

The energy balance equation (4.5.113) can be formulated as follows

$$\rho r - \nabla \cdot \mathbf{q} = \rho \dot{\mathcal{U}} - \boldsymbol{\sigma} \cdot (\nabla \otimes \mathbf{v})^T \quad (4.6.124)$$

Inserting into the entropy inequality (4.6.123) yields the dissipation inequality

$$\boldsymbol{\sigma} \cdot (\nabla \otimes \mathbf{v})^T - \rho \dot{\mathcal{U}} + \rho \dot{\mathcal{S}} T - \frac{\mathbf{q} \cdot \nabla T}{T} \geq 0 \quad (4.6.125)$$

Introducing the Helmholtz free energy density $\Phi = \mathcal{U} - ST$ the dissipation inequality (4.6.125) can be put into the following form

$$\boldsymbol{\sigma} \cdot (\nabla \otimes \mathbf{v})^T - \rho \dot{\Phi} - \rho S \dot{T} - \frac{\mathbf{q} \cdot \nabla T}{T} \geq 0 \quad (4.6.126)$$

With Eqs. (4.2.78), (4.3.95) and (4.5.115) as well as the relationships between the gradients (4.1.20) the dissipation inequality (4.6.126) can be given with respect to the reference configuration as follows

$$\mathbf{P} \cdot (\overset{0}{\nabla} \otimes \mathbf{v})^T - \rho_0 \dot{\Phi} - \rho_0 S \dot{T} - \frac{\hat{\mathbf{q}} \cdot \overset{0}{\nabla} T}{T} \geq 0 \quad (4.6.127)$$

References

- Altenbach H (2015) *Kontinuumsmechanik: Einführung in die materialunabhängigen und materialabhängigen Gleichungen*. Springer
- Altenbach H, Eremeyev V (2012) *Generalized Continua - from the Theory to Engineering Applications*. Springer, CISM International Centre for Mechanical Sciences
- Altenbach H, Eremeyev V (2014) Strain rate tensors and constitutive equations of inelastic micropolar materials. *Int J Plast* 63:3–17
- Altenbach H, Naumenko K, Zhilin PA (2003) A micro-polar theory for binary media with application to phase-transitional flow of fiber suspensions. *Continuum Mech Thermodyn* 15:539–570
- Altenbach H, Naumenko K, Pylypenko S, Renner B (2007) Influence of rotary inertia on the fiber dynamics in homogeneous creeping flows. *ZAMM-J Appl Math Mech/Zeitschrift für Angewandte Mathematik und Mechanik* 87(2):81–93
- Altenbach H, Brigadnov I, Naumenko K (2009) Rotation of a slender particle in a shear flow: influence of the rotary inertia and stability analysis. *ZAMM-J Appl Math Mech/Zeitschrift für Angewandte Mathematik und Mechanik* 89(10):823–832
- Bertram A (2012) *Elasticity and plasticity of large deformations*, 3rd edn. Springer, Berlin
- Eglt M, Hodges D (1996) *Continuum mechanics via problems and exercises: theory and problems*. World Scientific
- Eremeyev VA, Lebedev LP, Altenbach H (2012) *Foundations of micropolar mechanics*. Springer Science & Business Media
- Eringen AC (1999) *Microcontinuum field theories, vol. I*. In: *Foundations and solids*. Springer, New York
- Fleck NA, Hutchinson JW (1997) Strain gradient plasticity. In: Hutchinson JW, Wu TY (eds) *Advances in applied mechanics, vol 33*. Academic Press, New York, pp 295–361
- Forest S (2009) Micromorphic approach for gradient elasticity, viscoplasticity, and damage. *J Eng Mech* 135(3):117–131
- Forest S, Cailletaud G, Sievert R (1997) A Cosserat theory for elastoviscoplastic single crystals at finite deformation. *Arch Mech* 49:705–736
- Gao H, Huang Y, Nix WD, Hutchinson JW (1999) Mechanism-based strain gradient plasticity - I. Theory. *J Mech Phys Solids* 47(6):1239–1263
- Haupt P (2002) *Continuum mechanics and theory of materials*. Springer, Berlin
- Lai WM, Rubin D, Krempf E (1993) *Introduction to continuum mechanics*. Pergamon Press, Oxford

- Maugin G (2013) Continuum mechanics through the twentieth century: a concise historical perspective. In: Solid mechanics and its applications. Springer
- Miehe C, Hofacker M, Welschinger F (2010) A phase field model for rate-independent crack propagation: robust algorithmic implementation based on operator splits. *Comput Meth Appl Mech Eng* 199(45–48):2765–2778
- Naumenko K, Gariboldi E (2014) A phase mixture model for anisotropic creep of forged Al-Cu-Mg-Si alloy. *Mater Sci Eng: A* 618:368–376
- Naumenko K, Altenbach H, Kutschke A (2011) A combined model for hardening, softening and damage processes in advanced heat resistant steels at elevated temperature. *Int J Damage Mech* 20:578–597
- Nowacki W (1986) Theory of asymmetric elasticity. Pergamon Press, Oxford
- Schmitt R, Müller R, Kuhn C, Urbassek H (2013) A phase field approach for multivariant martensitic transformations of stable and metastable phases. *Arch Appl Mech* 83:849–859
- Smith DR (1993) An introduction to continuum mechanics. Kluwer, Dordrecht
- Truesdell C, Noll W (1992) The non-linear field theories of mechanics, 2nd edn. Springer, Berlin
- Xiao H, Bruhns OT, Meyers A (1997) Logarithmic strain, logarithmic spin and logarithmic rate. *Acta Mechanica* 124(1–4):89–105
- Zhilin PA (1996) A new approach to the analysis of free rotations of rigid bodies. *ZAMM-J Appl Math Mech/Zeitschrift für Angewandte Mathematik und Mechanik* 76(4):187–204

Chapter 5

Constitutive Models

In this chapter we discuss constitutive equations to describe material behavior of high-temperature materials under multi-axial stress state. To analyze material behavior under complex thermo-mechanical loading a combined model for thermo(visco)elasto-plasticity considering hardening, softening, damage and other processes is required. The idea of this chapter is to introduce basic ingredients, useful for the formulation of such unified material models. They include the heat transfer modeling, modeling of elasto-plastic deformations, hardening and softening rules as well as ageing and damage evolution equations. The corresponding uni-axial models were discussed in Chap. 3. To generalize these models to the multi-axial stress state several additional assumptions must be introduced. Appropriate stress and deformation measures must be introduced to capture complex local multi-axial loadings. General forms of constitutive and evolution equations must be defined such that invariance requirements with respect to the choice of reference frame, laws of continuum thermodynamics and other principles are fulfilled. To specialize the constitutive equation results of basic tests of the material behavior, such as tensile test, creep test, relaxation test, etc. should be systematically analyzed. On the other hand basic features of materials microstructure in the reference state and after a course of inelastic deformation process should be established. Microstructural analysis and appropriate assumptions with regard to symmetries of microstructure would reduce the identification effort essentially. Different types of material symmetries and appropriate forms of constitutive laws will be discussed.

All equations are presented in the direct tensor notation. This notation guarantees the invariance with respect to the choice of the coordinate system and has the advantage of transparent and compact representation of constitutive assumptions. The basic rules of the direct tensor calculus as well as some new results for basic sets of invariants with respect to different symmetry classes are presented in Appendices A–B.5.

5.1 Heat Transfer

Assume that the local power of the internal forces $\boldsymbol{\sigma} \cdot (\nabla \otimes \mathbf{v})^T$ in (4.6.126) is zero. The inequality (4.6.126) simplifies to

$$-\rho \dot{\Phi} - \rho S \dot{T} - \frac{\mathbf{q} \cdot \nabla T}{T} \geq 0 \quad (5.1.1)$$

The independent variables in Eq. (5.1.1) are T and ∇T . The conjugate variables (sometimes called thermodynamic forces) are S and \mathbf{q} . These can be assumed to be the functions of the independent variables, i.e.

$$S = S(T, \nabla T), \quad \mathbf{q} = \mathbf{q}(T, \nabla T), \quad \Phi = \Phi(T, \nabla T)$$

Consequently

$$\dot{\Phi} = \frac{\partial \Phi}{\partial T} \dot{T} + \frac{\partial \Phi}{\partial \nabla T} \cdot (\nabla T) \quad (5.1.2)$$

With Eq. (5.1.2) the inequality (5.1.1) takes the form

$$-\rho \left(\frac{\partial \Phi}{\partial T} + S \right) \dot{T} - \rho \frac{\partial \Phi}{\partial \nabla T} \cdot (\nabla T) - \frac{\mathbf{q} \cdot \nabla T}{T} \geq 0 \quad (5.1.3)$$

Inequality (3.1.3) can be formulated as follows

$$A \dot{T} + \mathbf{b} \cdot (\nabla T) + C \geq 0, \quad (5.1.4)$$

where

$$A = -\rho \left(\frac{\partial \Phi}{\partial T} + S \right), \quad \mathbf{b} = -\rho \frac{\partial \Phi}{\partial \nabla T}, \quad C = -\frac{\mathbf{q} \cdot \nabla T}{T} \quad (5.1.5)$$

do not depend on the velocities. For arbitrary \dot{T} and (∇T) the inequality is only satisfied if $A = 0$, $\mathbf{b} = \mathbf{0}$ and $C \geq 0$. From $\mathbf{b} = \mathbf{0}$ it follows

$$\rho \frac{\partial \Phi}{\partial \nabla T} = 0$$

and the free energy depends on the temperature only. From $A = 0$ the constitutive equation for the entropy can be obtained

$$S = -\frac{\partial \Phi}{\partial T} \quad (5.1.6)$$

With $C \geq 0$

$$-\frac{\mathbf{q} \cdot \nabla T}{T} \geq 0 \quad (5.1.7)$$

The inequality (5.1.7) can be satisfied with the Fourier law of heat conduction

$$\mathbf{q} = -\boldsymbol{\kappa} \cdot \nabla T, \quad (5.1.8)$$

where the positive semi-definite symmetric tensor $\boldsymbol{\kappa}(T)$ is called tensor of thermal conductivity. The functions $\boldsymbol{\kappa}(T)$ and $\mathcal{S}(T)$ must be identified experimentally.

Neglecting the mechanical power the local energy balance (4.5.113) takes the form

$$\rho \dot{\mathcal{U}} = -\nabla \cdot \mathbf{q} + \rho r = 0 \quad (5.1.9)$$

With $\mathcal{U} = \Phi + \mathcal{S}T$ and Eq. (5.1.6) the internal energy is the function of the temperature only. For the heat supply r assume the following constitutive equation

$$\rho r = h(T_e - T), \quad (5.1.10)$$

where $h(T) > 0$ and T_e is the temperature of the environment. Equation (5.1.10) is the Newton law of cooling. With Eqs. (5.1.8) and (5.1.10) the energy balance equation (5.1.9) takes the form

$$\rho c(T) \dot{T} = \nabla \cdot (\boldsymbol{\kappa} \cdot \nabla T) + h(T_e - T), \quad c(T) = \frac{d\mathcal{U}}{dT}, \quad (5.1.11)$$

where $c(T)$ is the heat capacity. For homogeneous bodies this simplifies to

$$\rho c(T) \dot{T} = \boldsymbol{\kappa} \cdot \nabla \nabla T + h(T_e - T) \quad (5.1.12)$$

Assuming that the expected temperature difference is small, one may linearize the temperature functions c , $\boldsymbol{\kappa}$ and h about a reference temperature T_0 leading to the linear differential equation

$$\rho c_0 \dot{T} = \boldsymbol{\kappa}_0 \cdot \nabla \nabla T + h_0(T_e - T), \quad (5.1.13)$$

where $c_0 = c(T_0)$, $\boldsymbol{\kappa}_0 = \boldsymbol{\kappa}(T_0)$ and $h_0 = h(T_0)$. Equation (5.1.13) is known as the heat equation or diffusion equation. The solution for the given initial condition and the boundary conditions with respect to the heat flux or the temperature provides the time-dependent temperature field in the body. Several methods exist to identify the functions c , k and h , which are based on temperature measurements and solutions of the heat equation (5.1.13). For details the reader may consult textbooks on heat transfer and thermodynamics, for example, Granger (1994), Müller (2007), Nellis and

Klein (2009). Once the the heat capacity $c(T)$ is identified the constitutive equation (5.1.6) can be used to compute the entropy as follows

$$\mathcal{S}(T) = \int_{T_0}^T \frac{c(\xi)}{\xi} d\xi$$

Assuming $c(T) = c_0$

$$\mathcal{S}(T) = c_0 \ln \frac{T}{T_0}$$

Integration of the constitutive equation (5.1.6) provides the following expression for the free energy

$$\Phi = c_0 \left[(T - T_0) - T \ln \frac{T}{T_0} \right] + \Phi_0$$

5.2 Material and Physical Symmetries

The tensor of thermal conductivity introduced in Sect. 5.1 includes six components that should be identified experimentally. In this section we discuss the concepts of material symmetry, physical symmetry, symmetry transformation and symmetry group. We take the thermal conductivity tensor as an example to illustrate how to apply these principles to the analysis of the material behavior.

The material symmetry group is related to the symmetries of the materials microstructure, e.g. the crystal symmetries, the symmetries due to the arrangement of fibers in a fiber-reinforced materials, etc. The symmetry transformations are described by means of orthogonal tensors. Two important of them are

- the mirror reflection

$$\mathbf{Q}(\mathbf{n}) = \mathbf{I} - 2\mathbf{n} \otimes \mathbf{n}, \quad (5.2.14)$$

where \mathbf{n} is the unit normal to the mirror plane,

- the rotation about a fixed axis

$$\mathbf{Q}(\varphi\mathbf{m}) = \mathbf{m} \otimes \mathbf{m} + \cos \varphi (\mathbf{I} - \mathbf{m} \otimes \mathbf{m}) + \sin \varphi \mathbf{m} \times \mathbf{I}, \quad (5.2.15)$$

where \mathbf{m} is the axis of rotation and φ is the angle of rotation.

Any arbitrary rotation of a rigid body can be described as a composition of three rotations (5.2.15) about three fixed axes (Zhilin 1996). Any symmetry transformation can be represented by means of rotations and reflections, i.e. the tensors of the type (5.2.14) and (5.2.15). The notion of the symmetry group as a set of symmetry

transformations was introduced in Noll (1972). According to Truesdell and Noll (1992) a “simple material” is called aelotropic or anisotropic, if its symmetry group is a proper subgroup of the orthogonal group.

The concept of the “physical symmetry group” is related to the symmetries of the material behavior, e.g. thermal conductivity, linear elasticity, thermal expansion, plasticity, creep, etc. It can only be established based on experimental observations. Physical symmetries must be taken into account in the formulation of constitutive equations and constitutive functions. Assume that the tensor of thermal conductivity $\boldsymbol{\kappa}$ is identified from experiments. Then the element \boldsymbol{Q} of the physical symmetry group can be found from the following equation

$$\boldsymbol{\kappa}' = \boldsymbol{Q} \cdot \boldsymbol{\kappa} \cdot \boldsymbol{Q}^T = \boldsymbol{\kappa} \quad (5.2.16)$$

Vice versa, if the physical symmetry group is known then one can find the general structure of the thermal conductivity tensor with Eq. (5.2.16). Clearly, neither the thermal conductivity tensor nor the physical symmetry group of the thermal conductivity can be exactly found from tests. However, one can relate physical symmetries to the known symmetries of materials microstructure. According to the Neumann principle widely used in different branches of physics and continuum mechanics, e.g. Altenbach and Zhilin (1988), Nye (1992), Zhilin (1982)

The symmetry group of the reason belongs to the symmetry group of the consequence.

Considering the material symmetries as one of the “reasons” and the physical symmetries as a “consequence” one can apply the following statement (Zheng and Boehler 1994)

For a material element and for any of its physical properties every material symmetry transformation of the material element is a physical symmetry transformation of the physical property.

In many cases the material symmetry elements are evident from the arrangement of the materials microstructure as a consequence of manufacturing conditions, for example. The above principle states that the physical behavior, e.g. the thermal conductivity, contains all elements of the material symmetry group. The physical symmetry group usually possesses more elements than the material symmetry group, e.g. Nye (1992).

Assume that the mirror reflection $\boldsymbol{Q}_1 = \boldsymbol{Q}(\boldsymbol{n}_1) = \boldsymbol{I} - 2\boldsymbol{n}_1 \otimes \boldsymbol{n}_1$ is the element of the material symmetry group. Since \boldsymbol{Q}_1 is symmetric, Eq. (5.2.16) yields

$$\boldsymbol{\kappa} \cdot \boldsymbol{Q}_1 = \boldsymbol{Q}_1 \cdot \boldsymbol{\kappa} \quad \text{or} \quad (\boldsymbol{\kappa} \cdot \boldsymbol{Q}_1)_{\times} = \mathbf{0}$$

Taking the vector invariant we obtain

$$\boldsymbol{n}_1 \times (\boldsymbol{\kappa} \cdot \boldsymbol{n}_1) = \mathbf{0} \quad \Rightarrow \quad \boldsymbol{\kappa} \cdot \boldsymbol{n}_1 = \lambda \boldsymbol{n}_1$$

Hence \mathbf{n}_1 is the principal direction of the tensor $\boldsymbol{\kappa}$. The spectral form of the tensor $\boldsymbol{\kappa}$ is

$$\boldsymbol{\kappa} = \kappa_1 \mathbf{n}_1 \otimes \mathbf{n}_1 + \kappa_2 \mathbf{n}_2 \otimes \mathbf{n}_2 + \kappa_3 \mathbf{n}_3 \otimes \mathbf{n}_3, \quad (5.2.17)$$

where κ_i are principal values and the orthonormal unit vectors \mathbf{n}_i are principal directions. Equation (5.2.17) specifies the tensor $\boldsymbol{\kappa}$ for materials having a mirror reflection as a symmetry group, i.e. for monoclinic materials. It is obvious that also the mirror reflections $\mathbf{Q}_2 = \mathbf{Q}(\mathbf{n}_2) = \mathbf{I} - 2\mathbf{n}_2 \otimes \mathbf{n}_2$ and $\mathbf{Q}_3 = \mathbf{Q}(\mathbf{n}_3) = \mathbf{I} - 2\mathbf{n}_3 \otimes \mathbf{n}_3$ belong to the symmetry group of the tensor (5.2.17). Hence the representation (5.2.17) is valid for orthotropic materials with \mathbf{n}_i being the axes of orthotropy.

Let (5.2.15), i.e. the rotation about the axis \mathbf{m} with any angle φ be the symmetry transformation. Equation (5.2.16) takes the form

$$\mathbf{Q}(\varphi \mathbf{m}) \cdot \boldsymbol{\kappa} \cdot \mathbf{Q}^T(\varphi \mathbf{m}) = \boldsymbol{\kappa} \quad (5.2.18)$$

The right hand side of (5.2.18) does not depend on φ . Therefore the derivative of the left hand side with respect to φ is the zero tensor¹

$$\mathbf{m} \times \boldsymbol{\kappa} - \boldsymbol{\kappa} \times \mathbf{m} = \mathbf{0} \quad (5.2.19)$$

The right scalar product with \mathbf{m} yields

$$\mathbf{m} \times (\boldsymbol{\kappa} \cdot \mathbf{m}) = \mathbf{0} \quad \Rightarrow \quad \boldsymbol{\kappa} \cdot \mathbf{m} = \lambda \mathbf{m}$$

Hence \mathbf{m} is the eigenvector of $\boldsymbol{\kappa}$. Let \mathbf{n} be a unit vector orthogonal to the vector \mathbf{m} and let $\mathbf{p} = \mathbf{n} \times \mathbf{m}$. The right scalar product of Eq. (5.2.19) mit \mathbf{n} yields

$$\mathbf{m} \times \boldsymbol{\kappa} \cdot \mathbf{n} - \boldsymbol{\kappa} \cdot (\mathbf{m} \times \mathbf{n}) = \mathbf{0}$$

Since \mathbf{n} and \mathbf{p} are eigenvectors of $\boldsymbol{\kappa}$ too we have

$$\mathbf{m} \times (\kappa_n \mathbf{n}) - \kappa_p \mathbf{p} = \mathbf{0}, \quad \Rightarrow \quad (\kappa_n - \kappa_p) \mathbf{p} = \mathbf{0},$$

where

$$\kappa_n = \mathbf{n} \cdot \boldsymbol{\kappa} \cdot \mathbf{n}, \quad \kappa_p = \mathbf{p} \cdot \boldsymbol{\kappa} \cdot \mathbf{p}$$

are principal values of the tensor $\boldsymbol{\kappa}$. Specifying $\kappa_L = \lambda$ and $\kappa_T = \kappa_n = \kappa_p$ the tensor $\boldsymbol{\kappa}$ has the following representation

$$\boldsymbol{\kappa} = \kappa_L \mathbf{m} \otimes \mathbf{m} + \kappa_T (\mathbf{I} - \mathbf{m} \otimes \mathbf{m}), \quad (5.2.20)$$

¹The derivative of the rotation tensor with the fixed axis of rotation is $d\mathbf{Q}(\varphi \mathbf{m}) = \mathbf{m} \times \mathbf{Q}(\varphi \mathbf{m})d\varphi$, see also Appendix B.7.

Materials with the symmetry group defined by arbitrary rotation about the axis \mathbf{m} (5.2.15) are called transversely-isotropic. Examples include fiber composites, directionally solidified alloys etc., Appendix B.7. The constants κ_L and κ_T are thermal conductivities in the longitudinal, for example fiber direction, and the transverse direction, respectively.

For isotropic materials Eq. (5.2.16) must be valid for any symmetry transformations. Therefore

$$\boldsymbol{\kappa} = \kappa_0 \mathbf{I},$$

where κ_0 is the thermal conductivity.

The notion of material and physical symmetries is widely applied in the material theory. Tensors of material properties of different rank, e.g. the fourth rank elasticity tensor can be specified in a similar way if the symmetry group is given.

5.3 Thermo-elasticity

5.3.1 Preliminary Remarks

With (4.1.42) the dissipation inequality (4.6.126) can be formulated as follows

$$\boldsymbol{\sigma} \cdot (\dot{\mathbf{F}} \cdot \mathbf{F}^{-1}) - \rho \dot{\Phi} - \rho S \dot{T} - \frac{\mathbf{q} \cdot \nabla T}{T} \geq 0 \quad (5.3.21)$$

Within the framework of elasticity the basic assumption is that the stress tensor is a function of the deformation. This can be related to experimental observations from the tensile test, Sect. 1.1. After the loading and subsequent unloading within the elastic range the specimen takes the original length. The elastic behavior is reversible—no hysteresis loop is observable if the specimen is subjected to a closed cycle of strain under adiabatic or isothermal conditions. Furthermore, the current state of stress is not influenced by the loading history and deformation rate.

Let us assume that the stress tensor and consequently the free energy are functions of the following arguments

$$\boldsymbol{\sigma} = \boldsymbol{\sigma}(\mathbf{F}, T) \quad \Rightarrow \quad \Phi = \Phi(\mathbf{F}, T)$$

Then the dissipation inequality (5.3.21) takes the following form²

$$\dot{\mathbf{F}} \cdot \left[\mathbf{F}^{-1} \cdot \boldsymbol{\sigma} - \rho \left(\frac{\partial \Phi}{\partial \mathbf{F}} \right)^T \right] - \rho \left(\frac{\partial \Phi}{\partial T} + S \right) \dot{T} - \frac{\mathbf{q} \cdot \nabla T}{T} \geq 0 \quad (5.3.22)$$

²The rules for derivatives of scalar-valued functions with respect to tensors are given in Appendix B.4.

With

$$\mathbf{A} = \mathbf{F}^{-1} \cdot \boldsymbol{\sigma} - \rho \left(\frac{\partial \Phi}{\partial \mathbf{F}} \right)^{\text{T}}, \quad B = -\frac{\partial \Phi}{\partial T} - S, \quad C = -\frac{\mathbf{q} \cdot \nabla T}{T}$$

the inequality (5.3.22) takes the form

$$\dot{\mathbf{F}} \cdot \mathbf{A} + \dot{T} B + C \geq 0, \quad (5.3.23)$$

Since \mathbf{A} , B and C do not depend on the velocities and $\dot{\mathbf{F}}$ and \dot{T} can be arbitrary the inequality is satisfied if $\mathbf{A} = \mathbf{0}$, $B = 0$ and $C \geq 0$. Hence

$$\boldsymbol{\sigma} = \rho \mathbf{F} \cdot \left(\frac{\partial \Phi}{\partial \mathbf{F}} \right)^{\text{T}}, \quad S = -\frac{\partial \Phi}{\partial T}, \quad -\frac{\mathbf{q} \cdot \nabla T}{T} \geq 0 \quad (5.3.24)$$

As the Cauchy stress tensor is symmetric (see Sect.4.4)

$$\boldsymbol{\sigma} = \boldsymbol{\sigma}^{\text{T}} \Rightarrow \mathbf{A} \cdot \boldsymbol{\sigma} = 0$$

for the skew-symmetric tensor $\mathbf{A} = \mathbf{a} \times \mathbf{I}$ with any vector $\mathbf{a} \neq \mathbf{0}$. Therefore the constitutive equation for the stress tensor (5.3.24)₁ can be written as follows

$$\mathbf{A} \cdot \left[\mathbf{F} \cdot \left(\frac{\partial \Phi}{\partial \mathbf{F}} \right)^{\text{T}} \right] = 0 \Rightarrow \mathbf{A} \cdot \mathbf{F} \cdot \left(\frac{\partial \Phi}{\partial \mathbf{F}} \right)^{\text{T}} = 0 \quad (5.3.25)$$

The first order partial differential equation (5.3.25) can be solved by the method of characteristics (Courant and Hilbert 1989). To this end consider a family of deformation gradients depending on the parameter τ , i.e. $\mathbf{F}(\tau)$. As the free energy depends on the parameter τ such that $\Phi(\mathbf{F}(\tau)) = \hat{\Phi}(\tau)$ we compute the derivative

$$\frac{d\hat{\Phi}}{d\tau} = \frac{d\mathbf{F}}{d\tau} \cdot \left(\frac{\partial \Phi}{\partial \mathbf{F}} \right)^{\text{T}} \quad (5.3.26)$$

Let us set

$$\frac{d\mathbf{F}}{d\tau} \cdot \left(\frac{\partial \Phi}{\partial \mathbf{F}} \right)^{\text{T}} = \mathbf{A} \cdot \mathbf{F} \cdot \left(\frac{\partial \Phi}{\partial \mathbf{F}} \right)^{\text{T}} \Rightarrow \frac{d\mathbf{F}}{d\tau} = \mathbf{A} \cdot \mathbf{F} \quad (5.3.27)$$

With Eq. (5.3.25) we have

$$\frac{d\hat{\Phi}}{d\tau} = 0 \Rightarrow \hat{\Phi}(\tau) = \hat{\Phi}(\tau_0) = \Phi(\mathbf{F}_0) = \text{const} \quad (5.3.28)$$

Hence, any solution of the partial differential equation (5.3.25) takes a constant (independent on τ) value on the integral (characteristic) curves $\mathbf{F}(\tau)$ defined by the set of ordinary differential equations

$$\frac{d\mathbf{F}}{d\tau} = \mathbf{A} \cdot \mathbf{F} \quad \Rightarrow \quad \frac{d\mathbf{F}}{d\tau} = \mathbf{a} \times \mathbf{F} \quad (5.3.29)$$

If \mathbf{F}_0 is the rotation tensor then (5.3.29) is the Darboux problem, known from the dynamics of rigid bodies, e.g. Altenbach et al. (2007, 2009), Zhilin (1996). The solution is the rotation tensor corresponding to the angular velocity vector \mathbf{a} . For arbitrary \mathbf{F}_0 the general solution to (5.3.29) can be given as

$$\mathbf{F}(\tau) = \mathbf{R}(\tau) \cdot \mathbf{U}_0, \quad \mathbf{U}_0 = (\mathbf{F}_0^T \cdot \mathbf{F}_0)^{1/2} \quad (5.3.30)$$

The rotation tensor $\mathbf{R}(\tau)$ has to be computed by solving the following Darboux problem

$$\frac{d\mathbf{R}}{d\tau} = \mathbf{a} \times \mathbf{R}, \quad \mathbf{R} = \mathbf{R}_0$$

Since the free energy remains constant on characteristic curves the solution of (5.3.25) is a function of first integrals of (5.3.29), as shown in Courant and Hilbert (1989). The ninth order system (5.3.29) has eight independent first integrals. Eliminating the parameter τ from the solution (5.3.30) we obtain six integrals which do not depend on the vector \mathbf{a}

$$\mathbf{F}^T \cdot \mathbf{F} = \mathbf{F}_0^T \cdot \mathbf{F}_0,$$

Two integrals

$$\mathbf{n}_a \cdot \mathbf{R} = \mathbf{n}_a \cdot \mathbf{R}_0, \quad \mathbf{n}_a = \frac{\mathbf{a}}{|\mathbf{a}|}$$

include the arbitrary vector \mathbf{a} and can be omitted. Hence, the free energy is an arbitrary function of the right Cauchy-Green strain tensor $\mathbf{C} = \mathbf{F}^T \cdot \mathbf{F}$

$$\Phi(\mathbf{F}) = \tilde{\Phi}(\mathbf{C}) \quad \Rightarrow \quad \frac{\partial \Phi}{\partial \mathbf{F}} = 2 \frac{\partial \tilde{\Phi}}{\partial \mathbf{C}} \cdot \mathbf{F}^T \quad (5.3.31)$$

The constitutive equation (5.3.24) takes the form³

$$\boldsymbol{\sigma} = 2\rho \mathbf{F} \cdot \frac{\partial \Phi}{\partial \mathbf{C}} \cdot \mathbf{F}^T = \frac{2}{J} \mathbf{F} \cdot \frac{\partial \rho_0 \Phi}{\partial \mathbf{C}} \cdot \mathbf{F}^T \quad (5.3.32)$$

³For the sake of brevity tilde is omitted.

With the Piola-Kirchhoff stress tensor (4.3.95)

$$\mathbf{P} = 2 \frac{\partial \rho_0 \Phi}{\partial \mathbf{C}} \cdot \mathbf{F}^T \quad (5.3.33)$$

Introducing the second Piola-Kirchhoff stress tensor

$$\mathbf{P}_{2PK} = \mathbf{P} \cdot \mathbf{F}^T$$

the constitutive equation (5.3.33) takes the form

$$\mathbf{P}_{2PK} = 2 \frac{\partial \rho_0 \Phi}{\partial \mathbf{C}} \quad (5.3.34)$$

For known physical symmetries of elastic material behavior the free energy can be specified as a function of certain invariants of \mathbf{C} relative to the given symmetry group.

5.3.2 Isotropic Materials

For isotropic materials the free energy must satisfy the following restriction

$$\Phi(\mathbf{C}') = \Phi(\mathbf{C}), \quad \mathbf{C}' = \mathbf{Q} \cdot \mathbf{C} \cdot \mathbf{Q}^T, \quad (5.3.35)$$

where \mathbf{Q} is any orthogonal tensor. The physical meaning of Eq. (5.3.35) can be explained as follows. Consider an experiment, in which a specimen cut from the material is isothermally deformed by \mathbf{F} . In the next experiment subject the specimen to a symmetry transformation \mathbf{Q} and then deform it by the same way such that the resulting deformation gradient is $\mathbf{F}' = \mathbf{F} \cdot \mathbf{Q}$. Equation (5.3.35) states that the amount of free energy stored will be the same in both the experiments. Following Zhilin (2003) consider a family of rotation tensors⁴ specified by $\mathbf{Q}(\tau)$, where τ is a time-like variable. Equation (5.3.35) takes the form

$$\Phi(\mathbf{C}'(\tau)) = \Phi(\mathbf{C}), \quad \mathbf{C}'(\tau) = \mathbf{Q}(\tau) \cdot \mathbf{C} \cdot \mathbf{Q}^T(\tau), \quad (5.3.36)$$

Taking the derivative of both Eqs. in (5.3.36) with respect to τ results in

$$\frac{d\Phi}{d\tau} = \frac{d\mathbf{C}'}{d\tau} \cdot \frac{\partial \Phi}{\partial \mathbf{C}'} = 0, \quad \frac{d\mathbf{C}}{d\tau} = \boldsymbol{\omega} \times \mathbf{Q} - \mathbf{Q} \times \boldsymbol{\omega}, \quad (5.3.37)$$

⁴The orthogonal symmetry group includes also reflections. Since any reflection is the composition of a rotation and the inversion $-\mathbf{I}$, it is possible to consider the proper orthogonal group first and then apply the inversion.

where $\boldsymbol{\omega}$ is the angular velocity vector corresponding to the rotation tensor \boldsymbol{Q} such that

$$\frac{d\boldsymbol{Q}}{d\tau} = \boldsymbol{\omega} \times \boldsymbol{Q}$$

Assuming $\boldsymbol{Q}(0) = \boldsymbol{I}$ and $\boldsymbol{\omega}(0) = \boldsymbol{\omega}_0$ and setting $\tau = 0$ in Eq. (5.3.37) the following partial differential equation can be obtained

$$(\boldsymbol{\omega}_0 \times \boldsymbol{Q} - \boldsymbol{Q} \times \boldsymbol{\omega}_0) \cdot \frac{\partial \Phi}{\partial \boldsymbol{C}} = 0 \quad (5.3.38)$$

The general solution can be found applying the method of characteristics. Let us skip the derivations since a similar procedure is discussed in the previous subsection to solve Eq. (5.3.25). The result is

$$\Phi(\boldsymbol{C}) = \Phi(J_{1\boldsymbol{C}}, J_{2\boldsymbol{C}}, J_{3\boldsymbol{C}}),$$

where $J_{1\boldsymbol{C}}$, $J_{2\boldsymbol{C}}$ and $J_{3\boldsymbol{C}}$ are principal invariants of the tensor \boldsymbol{C} as defined by Eq. (A.4.11). Note that these invariants can be computed in terms of principal stretches λ_i and

$$J_{i\boldsymbol{C}} = J_{i\boldsymbol{B}} = J_{i\nu^2} = J_{i\nu^2}, \quad i = 1, 2, 3$$

With Eq. (5.3.34) we obtain

$$\boldsymbol{P}_{2PK} = 2 \frac{\partial \rho_0 \Phi}{\partial \boldsymbol{C}} = 2 \frac{\partial \rho_0 \Phi}{\partial J_{1\boldsymbol{C}}} \frac{J_{1\boldsymbol{C}}}{\partial \boldsymbol{C}} + 2 \frac{\partial \rho_0 \Phi}{\partial J_{2\boldsymbol{C}}} \frac{J_{2\boldsymbol{C}}}{\partial \boldsymbol{C}} + 2 \frac{\partial \rho_0 \Phi}{\partial J_{3\boldsymbol{C}}} \frac{J_{3\boldsymbol{C}}}{\partial \boldsymbol{C}} \quad (5.3.39)$$

Applying the derivatives of the principal invariants (B.4.12), Eq. (5.3.39) takes the form

$$\boldsymbol{P}_{2PK} = 2 \frac{\partial \rho_0 \Phi}{\partial J_{1\boldsymbol{C}}} \boldsymbol{I} + 2 \frac{\partial \rho_0 \Phi}{\partial J_{2\boldsymbol{C}}} (J_{1\boldsymbol{C}} \boldsymbol{I} - \boldsymbol{C}) + 2 \frac{\partial \rho_0 \Phi}{\partial J_{3\boldsymbol{C}}} J_{3\boldsymbol{C}} \boldsymbol{C}^{-1} \quad (5.3.40)$$

With Eq. (5.3.32) the constitutive equation for the Cauchy stress tensor can be derived as follows

$$\boldsymbol{\sigma} = \frac{2}{J} \left(\frac{\partial \rho_0 \Phi}{\partial J_{1\boldsymbol{B}}} \boldsymbol{B} + \frac{\partial \rho_0 \Phi}{\partial J_{2\boldsymbol{B}}} (J_{1\boldsymbol{B}} \boldsymbol{B} - \boldsymbol{B}^2) + \frac{\partial \rho_0 \Phi}{\partial J_{3\boldsymbol{B}}} J_{3\boldsymbol{B}} \boldsymbol{I} \right) \quad (5.3.41)$$

We refer to textbooks on non-linear elasticity (Bertram 2012; Lurie 1990; Ogden 1997), among others, for many different representations of constitutive equations with respect to various stress and strain measures.

5.3.3 Anisotropic Materials

Assume that the free energy function satisfies the following restrictions

$$\Phi(\mathbf{Q}(\varphi\mathbf{M}) \cdot \mathbf{C} \cdot \mathbf{Q}^T(\varphi\mathbf{M})) = \Phi(\mathbf{C}), \quad \Phi(\mathbf{Q}_N \cdot \mathbf{C} \cdot \mathbf{Q}_N^T) = \Phi(\mathbf{C}), \quad (5.3.42)$$

where

$$\mathbf{Q}(\varphi\mathbf{M}) = \mathbf{M} \otimes \mathbf{M} + \cos \varphi (\mathbf{I} - \mathbf{M} \otimes \mathbf{M}) + \sin \varphi \mathbf{M} \times \mathbf{I},$$

is the tensor characterizing the rotation about a fixed axis \mathbf{M} with the angle ϕ and

$$\mathbf{Q}_N = \mathbf{Q}(\pi\mathbf{N}) = 2\mathbf{N} \otimes \mathbf{N} - \mathbf{I}, \quad \mathbf{N} \cdot \mathbf{M} = 0$$

is the rotation about the axis \mathbf{N} with the angle π . The symmetry group given by the tensors $\mathbf{Q}(\varphi\mathbf{M})$ and \mathbf{Q}_N is an example of the transverse isotropy or cylindrical symmetry group.⁵ The unit vector \mathbf{M} defines the preferential direction (anisotropy direction) of the microstructure in the reference configuration. This direction can be assigned to be the direction of aligned fibers in a fiber-reinforced composite, e.g. Ogden (2015), Altenbach et al. (2003a). The physical meaning of Eq. (5.3.42)₁ is: any rotation of the solid about \mathbf{M} and subsequent deformation under a constant temperature lead to the same value of the stored energy. Furthermore a rotation with the angle π about any axis \mathbf{N} which is orthogonal to \mathbf{M} is the symmetry transformation as well. Let us note, that the symmetry transformation can be defined for the whole solid in the reference state, as it usually the case for composites reinforced by long fibers (Chawla 1987; Ogden 2015; Altenbach et al. 2004). In this case the symmetry transformation can be understood as a change of the reference placement of the solid, e.g. Bertram (2012). However, materials may possess symmetries only locally. An example is the short-fiber reinforced composite, produced by injection molding (Kröner et al. 2009; Altenbach et al. 2003a). In this case a testpiece from the material should be deformed after a symmetry transformation to detect a kind of anisotropy.

The right-hand side of Eq. (5.3.42)₁ does not depend on the arbitrary angle φ . Setting the derivative of the left-hand side with respect to φ to zero results in the following partial differential equation (Altenbach et al. 2006), see Appendix B.7.1

$$(\mathbf{M} \times \mathbf{C} - \mathbf{C} \times \mathbf{M}) \cdot \left(\frac{\partial \Phi}{\partial \mathbf{C}} \right)^T = 0 \quad (5.3.43)$$

The general solution to (5.3.43) is a function of five independent invariants relative to the symmetry group of rotations about a fixed axis. Six invariants (B.7.28) and

⁵Five different cases of the transverse isotropy can be defined, see, for example, Spencer (1987), Zheng and Boehler (1994).

a relationship between them (B.7.29) are presented in Appendix B.7.1. With the additional symmetry transformation (5.3.42)₂ the list of invariants is reduced to the three principal invariants J_{1c} , J_{2c} and J_{3c} of the tensor \mathbf{C} as defined by Eqs. (A.4.11) and two following invariants

$$J_{4c} = \mathbf{M} \cdot \mathbf{C} \cdot \mathbf{M} = \mathbf{C} \cdot \mathbf{M} \otimes \mathbf{M}, \quad J_{5c} = \mathbf{M} \cdot \mathbf{C}^2 \cdot \mathbf{M} = \mathbf{C}^2 \cdot \mathbf{M} \otimes \mathbf{M}, \quad (5.3.44)$$

With Eq. (5.3.34) we obtain

$$\begin{aligned} \mathbf{P}_{2PK} = & 2W_1 \mathbf{I} + 2W_2 (J_{1c} \mathbf{I} - \mathbf{C}) + 2W_3 J_{3c} \mathbf{C}^{-1} \\ & + 2W_4 \mathbf{M} \otimes \mathbf{M} + 2W_5 (\mathbf{C} \cdot \mathbf{M} \otimes \mathbf{M} + \mathbf{M} \otimes \mathbf{M} \cdot \mathbf{C}) \end{aligned} \quad (5.3.45)$$

where

$$W_i = \frac{\partial \rho_0 \Phi}{\partial J_{ic}}, \quad i = 1, 2, \dots, 5$$

Let us introduce the unit vector \mathbf{m} as follows

$$\mathbf{m} = \frac{\mathbf{F} \cdot \mathbf{M}}{\sqrt{\mathbf{M} \cdot \mathbf{F}^T \cdot \mathbf{F} \cdot \mathbf{M}}} \quad (5.3.46)$$

With Eq. (5.3.32) the following constitutive equation for the Cauchy stress tensor can be derived

$$\begin{aligned} \boldsymbol{\sigma} = & \frac{2}{J} (W_1 \mathbf{B} + W_2 (J_{1B} \mathbf{B} - \mathbf{B}^2) + W_3 J_{3B} \mathbf{I} \\ & + W_4 J_{4c} \mathbf{m} \otimes \mathbf{m} + W_5 J_{5c} (\mathbf{B} \cdot \mathbf{m} \otimes \mathbf{m} + \mathbf{m} \otimes \mathbf{m} \cdot \mathbf{B})) \end{aligned} \quad (5.3.47)$$

Instead the invariants J_{3c} and J_{4c} one may introduce the following invariants with respect to the spatial tensor \mathbf{B} and the vector \mathbf{m}

$$J_{4c} = \frac{1}{\mathbf{m} \cdot \mathbf{B}^{-1} \cdot \mathbf{m}} \quad J_{5c} = \frac{\mathbf{m} \cdot \mathbf{B} \cdot \mathbf{m}}{\mathbf{m} \cdot \mathbf{B}^{-1} \cdot \mathbf{m}} \quad (5.3.48)$$

With Eq. (5.3.46) the time derivative of the vector \mathbf{m} can be computer as follows

$$\dot{\mathbf{m}} = \boldsymbol{\omega} \times \mathbf{m} + \mathbf{m} \cdot \mathbf{D} \cdot (\mathbf{I} - \mathbf{m} \otimes \mathbf{m}) \quad (5.3.49)$$

From Eqs. (5.3.44) and (5.3.45) we may conclude that the constitutive equation for a transversely-isotropic material can be formulated as follows

$$\Phi(\mathbf{C}) = \hat{\Phi}(\mathbf{C}, \mathbf{M} \otimes \mathbf{M}), \quad \mathbf{P}_{2PK} = \mathbf{g}(\mathbf{C}, \mathbf{M} \otimes \mathbf{M}), \quad (5.3.50)$$

where $\hat{\phi}$ and \mathbf{g} are the isotropic scalar-valued and tensor-valued tensor functions of \mathbf{C} and $\mathbf{M} \otimes \mathbf{M}$, respectively. Similarly, we may define the elasticity law for transversely-isotropic materials in the actual configuration. To this end consider the following transformation

$$\hat{\phi}(\mathbf{C}, \mathbf{M} \otimes \mathbf{M}) = \hat{\phi}\left(\mathbf{R}^T \cdot \mathbf{B} \cdot \mathbf{R}, \frac{\mathbf{R}^T \cdot \mathbf{V}^{-1} \cdot \mathbf{m} \otimes \mathbf{m} \cdot \mathbf{V}^{-1} \cdot \mathbf{R}}{\mathbf{m} \cdot \mathbf{B}^{-1} \cdot \mathbf{m}}\right)$$

Assume two actual configurations of the solid, one defined by the tensors \mathbf{V} , \mathbf{R} and $\mathbf{m} \otimes \mathbf{m}$ and one defined by the the symmetry transformation \mathbf{Q} and the subsequent deformation. With $\mathbf{F}^* = \mathbf{F} \cdot \mathbf{Q}^T$ the corresponding tensors take the form

$$\mathbf{V}^* = \mathbf{V}, \quad \mathbf{B}^* = \mathbf{B}, \quad \mathbf{R}^* = \mathbf{R} \cdot \mathbf{Q}^T, \quad \mathbf{m}^* \otimes \mathbf{m}^* = \mathbf{m} \otimes \mathbf{m}$$

Therefore

$$\begin{aligned} & \hat{\phi}\left(\mathbf{R}^T \cdot \mathbf{B} \cdot \mathbf{R}, \frac{\mathbf{R}^T \cdot \mathbf{V}^{-1} \cdot \mathbf{m} \otimes \mathbf{m} \cdot \mathbf{V}^{-1} \cdot \mathbf{R}}{\mathbf{m} \cdot \mathbf{B}^{-1} \cdot \mathbf{m}}\right) \\ &= \hat{\phi}\left(\mathbf{Q} \cdot \mathbf{R}^T \cdot \mathbf{B} \cdot \mathbf{R} \cdot \mathbf{Q}^T, \frac{\mathbf{Q} \cdot \mathbf{R}^T \cdot \mathbf{V}^{-1} \cdot \mathbf{m} \otimes \mathbf{m} \cdot \mathbf{V}^{-1} \cdot \mathbf{R} \cdot \mathbf{Q}^T}{\mathbf{m} \cdot \mathbf{B}^{-1} \cdot \mathbf{m}}\right) \end{aligned} \quad (5.3.51)$$

Since \mathbf{Q} is arbitrary, we select $\mathbf{Q} = \mathbf{R}$. Equation (5.3.51) takes the form

$$\begin{aligned} & \hat{\phi}\left(\mathbf{R}^T \cdot \mathbf{B} \cdot \mathbf{R}, \frac{\mathbf{R}^T \cdot \mathbf{V}^{-1} \cdot \mathbf{m} \otimes \mathbf{m} \cdot \mathbf{V}^{-1} \cdot \mathbf{R}}{\mathbf{m} \cdot \mathbf{B}^{-1} \cdot \mathbf{m}}\right) \\ &= \hat{\phi}\left(\mathbf{B}, \frac{\mathbf{V}^{-1} \cdot \mathbf{m} \otimes \mathbf{m} \cdot \mathbf{V}^{-1}}{\mathbf{m} \cdot \mathbf{B}^{-1} \cdot \mathbf{m}}\right) = \tilde{\phi}(\mathbf{B}, \mathbf{m} \otimes \mathbf{m}) \end{aligned} \quad (5.3.52)$$

The free energy must be invariant under any superimposed rigid body rotation in the actual configuration. Considering again two states: one defined by \mathbf{F} and $\mathbf{m} \otimes \mathbf{m}$ and one defined by

$$\mathbf{F}^* = \mathbf{Q} \cdot \mathbf{F}, \quad \mathbf{m}^* \otimes \mathbf{m}^* = \mathbf{Q} \cdot \mathbf{m} \otimes \mathbf{m} \cdot \mathbf{Q}^T,$$

where \mathbf{Q} describes the superimposed rotation we obtain

$$\tilde{\phi}(\mathbf{Q} \cdot \mathbf{B} \cdot \mathbf{Q}^T, \mathbf{Q} \cdot \mathbf{m} \otimes \mathbf{m} \cdot \mathbf{Q}^T) = \tilde{\phi}(\mathbf{B}, \mathbf{m} \otimes \mathbf{m}) \quad (5.3.53)$$

Therefore, the free energy can be specified as an isotropic function of \mathbf{B} and $\mathbf{m} \otimes \mathbf{m}$. Furthermore, Eq. (5.3.47) can be given as follows

$$\boldsymbol{\sigma} = \tilde{\mathbf{g}}(\mathbf{B}, \mathbf{m} \otimes \mathbf{m}),$$

where the vector $\tilde{\mathbf{g}}$ is the isotropic tensor function of two arguments. The free energy or the elasticity law specified in the actual configuration must be supplemented by the evolution equation for the vector \mathbf{m} (5.3.49). An observation can be made that from Eq. (5.3.53) it follows that the free energy can be locally defined as a transversely-isotropic function with respect to the actual vector \mathbf{m} such that

$$\mathcal{Q}(\varphi\mathbf{m}) = \mathbf{m} \otimes \mathbf{m} + \cos \varphi(\mathbf{I} - \mathbf{m} \otimes \mathbf{m}) + \sin \varphi \mathbf{m} \times \mathbf{I}, \quad \mathcal{Q}_n = 2\mathbf{n} \otimes \mathbf{n} - \mathbf{I}$$

are elements of the symmetry group, where the unit vectors \mathbf{m} and \mathbf{n} , $\mathbf{n} \cdot \mathbf{m} = 0$ are defined in the actual configuration.

Another observation is that a free energy function subjected to a group of symmetry transformations, for example (5.3.42) can be extended to the isotropic function of \mathbf{C} and $\mathbf{M} \otimes \mathbf{M}$. This approach is called isotropic extension of anisotropic tensor functions, and is widely used in the development of constitutive theories. The dyad $\mathbf{M} \otimes \mathbf{M}$ is an example of the so-called structure tensor—a tensor whose symmetry group coincides with the material symmetry group. Structure tensors of different rank are listed in Lokhin and Sedov (1963) for different symmetry classes. An example for the approach of isotropic extension is presented in Appendix B.8 to find invariants with respect to the group of orthotropic symmetry.

5.3.4 Linear Elasticity

For many structural materials, for example steel, the elastic material behavior is observed within the range of small strains. Furthermore, in this range the stress is proportional to the strain, as observed in the uni-axial tensile test. With the linearized kinematical relations (4.1.37) one may show that the difference between the stress measures can be ignored such that the constitutive Eq. (5.3.32) can be put in the following form

$$\boldsymbol{\sigma} = \frac{\partial \rho_0 \Phi(\boldsymbol{\varepsilon})}{\partial \boldsymbol{\varepsilon}} \quad (5.3.54)$$

There are two ways to specify the constitutive equation (5.3.54). One may specify a free energy as a quadratic form of the strain tensor and the temperature and then to define the stress tensor by Eq. (5.3.54). Another approach is to start with the constitutive equation for the stress tensor and then compute the free energy density by integrating Eq. (5.3.54). If the linear relationship between the stress and the strain is observed in stress-strain diagrams then we may generalize the uni-axial constitutive equation (3.2.21) as follows

$$\boldsymbol{\sigma} = {}^{(4)}\mathbf{C} \cdot (\boldsymbol{\varepsilon} - \boldsymbol{\varepsilon}^{\text{th}}), \quad \boldsymbol{\varepsilon}^{\text{th}} = \boldsymbol{\alpha}_{\text{th}} \Theta, \quad \Theta = T - T_0, \quad (5.3.55)$$

The fourth rank elasticity tensor ${}^{(4)}\mathbf{C}$ must satisfy the following restrictions

$$\mathbf{a} \cdot \cdot {}^{(4)}\mathbf{C} \cdot \cdot \mathbf{a} \geq 0, \quad \mathbf{a} \cdot \cdot {}^{(4)}\mathbf{C} = {}^{(4)}\mathbf{C} \cdot \cdot \mathbf{a}, \quad \mathbf{c} \cdot \cdot {}^{(4)}\mathbf{C} = \mathbf{0},$$

$$\forall \mathbf{a}, \mathbf{c} \text{ with } \mathbf{a} = \mathbf{a}^T, \quad \mathbf{c} = -\mathbf{c}^T, \quad (5.3.56)$$

where \mathbf{a} and \mathbf{c} are second rank tensors. The symmetric second rank tensor $\boldsymbol{\alpha}_{\text{th}}$ is called tensor of thermal expansion. Both the elasticity and the thermal expansion tensors can be specified if the material symmetry group is known. For example, if the orthogonal tensor \mathbf{Q} stands for a symmetry element, the structure of the tensor ${}^{(4)}\mathbf{C}$ can be established from the following equation

$${}^{(4)}\mathbf{C}' = C^{ijkl} \mathbf{Q} \cdot \mathbf{e}_i \otimes \mathbf{Q} \cdot \mathbf{e}_j \otimes \mathbf{Q} \cdot \mathbf{e}_k \otimes \mathbf{Q} \cdot \mathbf{e}_l = {}^{(4)}\mathbf{C}, \quad (5.3.57)$$

where $\mathbf{e}_i, i = 1, 2, 3$ are basis vectors. The structure of the thermal expansion tensor can be established from the following equation

$$\mathbf{Q} \cdot \boldsymbol{\alpha}^{\text{th}} \cdot \mathbf{Q}^T = \boldsymbol{\alpha}^{\text{th}} \quad (5.3.58)$$

Symmetry groups of the second rank tensors and restrictions of the type (5.3.58) are discussed in Sect. 5.2. The fourth rank tensors satisfying the restrictions (5.3.57) for different material symmetry classes are well-known. The components of these tensors are given in the matrix notation in many textbooks on linear elasticity as well as in books and monographs on composite materials, e.g. Altenbach et al. (1996, 1998), Altenbach (2012), Gibson (1994), Powell (1994), Ting (1996). Furthermore, different coordinate free representations of fourth rank tensors are discussed in the literature. For a review we refer to Böhlke (2000). One may prove that only eight basic symmetry classes can be distinguished within the framework of linear elasticity (Ting 1996). These symmetry classes and the corresponding number of independent coordinates of the tensor ${}^{(4)}\mathbf{C}$ are listed in Table 5.1. The number of independent coordinates coincides with the number of material parameters to be identified from

Table 5.1 Basic symmetry classes and number of independent coordinates of the tensor ${}^{(4)}\mathbf{C}$

Symmetry class	Number of independent coordinates of ${}^{(4)}\mathbf{C}$
Triclinic symmetry	21
Monoclinic symmetry	13
Orthotropic or rhombic symmetry	9
Trigonal symmetry	6
Tetragonal symmetry	6
Transverse isotropy or hexagonal symmetry	5
Cubic symmetry	3
Isotropic symmetry	2

tests. With Eqs. (5.3.54) and (5.3.55) the free energy density can be specified as follows

$$\rho_0 \Phi = \frac{1}{2} \boldsymbol{\varepsilon} \cdot \cdot {}^{(4)}\mathbf{C} \cdot \cdot \boldsymbol{\varepsilon} - \boldsymbol{\varepsilon} \cdot \cdot {}^{(4)}\mathbf{C} \cdot \cdot \boldsymbol{\alpha}_{\text{th}} \Theta + g(T) \quad (5.3.59)$$

To determine the function $g(T)$ let us compute

$$\frac{\partial \mathcal{U}}{\partial T} = T \frac{\partial \mathcal{S}}{\partial T} = -T \frac{\partial^2 \Phi}{\partial T^2} \quad (5.3.60)$$

With the free energy density (5.3.59) this results in

$$\frac{\partial \mathcal{U}}{\partial T} = \underline{-\frac{1}{\rho_0} T \frac{d^2 f}{dT^2}} - \frac{1}{2\rho_0} T \boldsymbol{\varepsilon} \cdot \cdot \frac{d^2}{dT^2} [{}^{(4)}\mathbf{C}] \cdot \cdot \boldsymbol{\varepsilon} - \frac{1}{\rho_0} T \boldsymbol{\varepsilon} \cdot \cdot \frac{d^2}{dT^2} [{}^{(4)}\mathbf{C} \cdot \cdot \boldsymbol{\alpha}_{\text{th}} \Theta]$$

The underlined term is the heat capacity without deformation, see Eq. (5.1.11). Therefore the function f can be obtained from the following differential equation

$$-\frac{1}{\rho_0} T \frac{d^2 f}{dT^2} = c(T)$$

With Eqs. (5.1.10), (5.3.59) and (5.3.60) the energy balance equation (4.5.113) takes the following form

$$-\frac{\partial^2(\rho_0 \Phi)}{\partial T^2} \dot{T} - \frac{\partial^2(\rho_0 \Phi)}{\partial T \partial \boldsymbol{\varepsilon}} \cdot \cdot \dot{\boldsymbol{\varepsilon}} = \nabla \cdot (\boldsymbol{\kappa} \cdot \nabla T) + h(T_e - T) \quad (5.3.61)$$

Assuming that the expected temperature difference is small one may linearize the functions ${}^{(4)}\mathbf{C}(T)$, $\boldsymbol{\alpha}_{\text{th}}(T)$, $c(T)$ and $h(T)$ about the reference temperature T_0 . The heat transfer equation (5.3.61) simplifies to

$$c_0 \dot{T} + \boldsymbol{\alpha}_{\text{th}_0} \cdot \cdot {}^{(4)}\mathbf{C}_0 \cdot \cdot \dot{\boldsymbol{\varepsilon}} = \nabla \cdot (\boldsymbol{\kappa}_0 \cdot \nabla T) + h_0(T_e - T), \quad (5.3.62)$$

where ${}^{(4)}\mathbf{C}_0 = {}^{(4)}\mathbf{C}(T_0)$, $\boldsymbol{\alpha}_{\text{th}_0} = \boldsymbol{\alpha}_{\text{th}}(T_0)$. The second term in the left-hand side of Eq. (5.3.62) is usually small and can be neglected (Landau et al. 1986). Therefore, within the linearized theory the deformation has minor influence on the heat transfer such that the simplified heat equation

$$c_0 \dot{T} = \nabla \cdot (\boldsymbol{\kappa}_0 \cdot \nabla T) + h_0(T_e - T)$$

can be solved independently providing the temperature field $T(\mathbf{r}, t)$. The balance of momentum (4.3.93) with the constitutive equation (5.3.55) yields

$$\rho \ddot{\mathbf{u}} = \nabla \cdot \left[{}^{(4)}\mathbf{C} \cdot \cdot \left(\frac{1}{2} \nabla \mathbf{u} + \frac{1}{2} (\nabla \mathbf{u})^T - \boldsymbol{\alpha}_{\text{th}} \Theta \right) \right] + \rho \mathbf{f} \quad (5.3.63)$$

For isotropic materials the elasticity tensor and the tensor of thermal expansion have the following representations

$${}^{(4)}\mathbf{C} = \lambda \mathbf{I} \otimes \mathbf{I} + \mu (\mathbf{e}_k \otimes \mathbf{I} \otimes \mathbf{e}^k + \mathbf{e}_i \otimes \mathbf{e}_k \otimes \mathbf{e}^i \otimes \mathbf{e}^k), \quad \boldsymbol{\alpha}_T = \alpha_T \mathbf{I} \quad (5.3.64)$$

where λ and μ are Lamé's constants and α_T is the coefficient of thermal expansion. The Lamé's constants can be computed as follows

$$\mu = G = \frac{E}{2(1+\nu)}, \quad \lambda = \frac{\nu E}{(1+\nu)(1-2\nu)}, \quad (5.3.65)$$

where E is the Young's modulus, G is the shear modulus and ν is the Poisson's ratio. For isotropic homogeneous materials Eq. (5.3.63) takes the following form

$$\rho \ddot{\mathbf{u}} = \frac{\mu}{1-2\nu} \nabla \nabla \cdot \mathbf{u} + \mu \Delta \mathbf{u} - 2\mu \frac{1+\nu}{1-2\nu} \alpha_{\text{th}} \nabla \Theta + \rho \mathbf{f} \quad (5.3.66)$$

A wide class of problems is related to the analysis of slow (quasi-static) deformation in structures. To find the displacement field the following second order partial differential equation has to be solved

$$\frac{\mu}{1-2\nu} \nabla \nabla \cdot \mathbf{u} + \mu \Delta \mathbf{u} - 2\mu \frac{1+\nu}{1-2\nu} \alpha_{\text{th}} \nabla \Theta + \rho \mathbf{f} = \mathbf{0} \quad (5.3.67)$$

We refer to the classical texts on linear elasticity (Hahn 1985; Landau et al. 1986; Lurie 2010; Muskhelishvili 2013; Neuber 2013; Timoshenko and Goodier 1951), where solutions to Eq. (5.3.67) for various problems of structural mechanics are derived.

5.4 Non-linear Viscosity, Viscoplasticity, and Rigid Plasticity

5.4.1 Preliminary Remarks

Consider the dissipation inequality (4.6.126)

$$\boldsymbol{\sigma} \cdot \mathbf{L} - \rho \dot{\phi} - \rho S \dot{T} - \frac{\mathbf{q} \cdot \nabla T}{T} \geq 0 \quad (5.4.68)$$

Assume that the Cauchy stress tensor $\boldsymbol{\sigma}$ is the function of the velocity gradient \mathbf{L} and the temperature. Furthermore, assume that the mechanical power $\boldsymbol{\sigma} \cdot \mathbf{L}$ does not influence the free energy directly. The free energy and the entropy are then the

functions of the temperature only. Then the inequality (5.4.68) can be specified as follows

$$-\rho \left(\frac{\partial \Phi}{\partial T} + \mathcal{S} \right) \dot{T} + \boldsymbol{\sigma} \cdot \mathbf{L} - \frac{\mathbf{q} \cdot \nabla T}{T} \geq 0 \quad (5.4.69)$$

The inequality (5.4.69) has the form $A(T)\dot{T} + B(T, \mathbf{L}) \geq 0$. For arbitrary (positive and negative) rates of temperature it can only be satisfied if $A = 0$ and $B \geq 0$. This leads to the constitutive equation for the entropy

$$\mathcal{S} = -\frac{\partial \Phi}{\partial T} \quad (5.4.70)$$

and the dissipation inequality

$$\boldsymbol{\sigma} \cdot \mathbf{L} - \frac{\mathbf{q} \cdot \nabla T}{T} \geq 0 \quad (5.4.71)$$

Assuming that the heat flux vector \mathbf{q} does not depend on the strain rate results in two inequalities

$$\boldsymbol{\sigma} \cdot \mathbf{L} \geq 0, \quad -\frac{\mathbf{q} \cdot \nabla T}{T} \geq 0 \quad (5.4.72)$$

Since the Cauchy stress tensor is symmetric the former inequality can be reduced to

$$\boldsymbol{\sigma} \cdot \mathbf{D} \geq 0 \quad (5.4.73)$$

For the stress tensor let us assume the following constitutive equation

$$\boldsymbol{\sigma}(\mathbf{L}, T) = g_T(T)\mathbf{g}(\mathbf{L}), \quad (5.4.74)$$

Functions of temperature $f_T(T)$ will be discussed in Sect. 5.4.4. To specify the function $\mathbf{g}(\mathbf{L})$ consider two motions: one characterized by the deformation gradient \mathbf{F} and one defined by $\mathbf{F}^* = \mathbf{Q} \cdot \mathbf{F}$, where $\mathbf{Q}(t)$ is an arbitrary rotation tensor. The corresponding velocity gradients are specified by \mathbf{L} and

$$\mathbf{L}^* = \boldsymbol{\Omega}_{\mathbf{Q}} \times \mathbf{I} + (\mathbf{Q} \cdot \boldsymbol{\omega}) \times \mathbf{I} + \mathbf{Q} \cdot \mathbf{D} \cdot \mathbf{Q}^T,$$

where $\boldsymbol{\Omega}_{\mathbf{Q}}$ is the angular velocity vector for \mathbf{Q} . Assuming that under the superimposed rigid rotation the Cauchy stress tensor is $\boldsymbol{\sigma}^* = \mathbf{Q} \cdot \boldsymbol{\sigma} \cdot \mathbf{Q}^T$ the following restriction on the function $\mathbf{g}_L(\mathbf{L})$ can be formulated⁶

$$\mathbf{Q} \cdot \mathbf{g}(\mathbf{L}) \cdot \mathbf{Q}^T = \mathbf{g}(\mathbf{L}^*)$$

⁶This assumption is deduced from the principle of invariance under superimposed rigid body motions, e.g. Bertram (2012).

As a result we obtain

$$\mathbf{Q} \cdot \mathbf{g}(\boldsymbol{\omega} \times \mathbf{I} + \mathbf{D}) \cdot \mathbf{Q}^T = \mathbf{g}[(\boldsymbol{\Omega}_{\mathbf{Q}} + \mathbf{Q} \cdot \boldsymbol{\omega}) \times \mathbf{I} + \mathbf{Q} \cdot \mathbf{D} \cdot \mathbf{Q}^T] \quad (5.4.75)$$

Since $\boldsymbol{\Omega}_{\mathbf{Q}}$ is an arbitrary angular velocity vector, we may specify

$$\boldsymbol{\Omega}_{\mathbf{Q}} = -\mathbf{Q} \cdot \boldsymbol{\omega}$$

Now Eq. (5.4.75) takes the form

$$\mathbf{Q} \cdot \mathbf{g}(\boldsymbol{\omega} \times \mathbf{I} + \mathbf{D}) \cdot \mathbf{Q}^T = \mathbf{g}(\mathbf{Q} \cdot \mathbf{D} \cdot \mathbf{Q}^T) \quad (5.4.76)$$

For $\mathbf{Q} = \mathbf{I}$ this results in

$$\mathbf{g}(\boldsymbol{\omega} \times \mathbf{I} + \mathbf{D}) = \mathbf{g}(\mathbf{D}) = \mathbf{g}_{\mathbf{D}}(\mathbf{D})$$

Omitting the skew-symmetric tensor $\boldsymbol{\omega} \times \mathbf{I}$, Eq. (5.4.76) takes the form

$$\mathbf{Q} \cdot \mathbf{g}(\mathbf{D}) \cdot \mathbf{Q}^T = \mathbf{g}(\mathbf{Q} \cdot \mathbf{D} \cdot \mathbf{Q}^T)$$

Therefore \mathbf{g} is the isotropic function of \mathbf{D} and has the following general representation⁷

$$\mathbf{g} = \alpha_0 \mathbf{I} + \alpha_1 \mathbf{D} + \alpha_2 \mathbf{D}^2,$$

where α_i are functions of invariants of \mathbf{D} . The Cauchy stress tensor is co-axial with the tensor \mathbf{D} and Eq. (5.4.74) takes the form

$$\boldsymbol{\sigma}(\mathbf{D}, T) = g_T(T) (\alpha_0 \mathbf{I} + \alpha_1 \mathbf{D} + \alpha_2 \mathbf{D}^2), \quad (5.4.77)$$

From (5.4.73) it follows that the functions α_i must satisfy the following inequality

$$\alpha_0 \text{tr } \mathbf{D} + \alpha_1 \text{tr } \mathbf{D}^2 + \alpha_2 \text{tr } \mathbf{D}^3 \geq 0 \quad (5.4.78)$$

Specific forms of the constitutive equation (5.4.77) are discussed in the rheology, e.g. Giesekus (1994), Reiner (1969), Palmov (1998). An example is a model of an incompressible non-linear viscous fluid. To introduce this model let us decompose the tensor $\boldsymbol{\sigma}$ into the spherical and deviatoric parts

$$\boldsymbol{\sigma} = \sigma_m \mathbf{I} + \mathbf{s}, \quad \text{tr } \mathbf{s} = 0 \quad \Rightarrow \quad \sigma_m = \frac{1}{3} \text{tr } \boldsymbol{\sigma}, \quad (5.4.79)$$

⁷From this consideration it does not follow that only isotropic materials can be described. Indeed, we assumed that the stress tensor depends only on the velocity gradient, which is not true for anisotropic materials. Extensions will be discussed in Sect. 5.4.3.

where \mathbf{s} is the stress deviator and σ_m is the mean (hydrostatic) stress. For the tensor \mathbf{D} we can write

$$\mathbf{D} = d_0 \mathbf{I} + \mathbf{d}, \quad \text{tr } \mathbf{d} = 0 \quad \Rightarrow \quad d_0 = \frac{1}{3} \nabla \cdot \mathbf{v}, \quad (5.4.80)$$

The constitutive model for an incompressible fluid can be formulated as follows

$$\mathbf{s}(\mathbf{d}, T) = g_T(T) \left[\tilde{\alpha}_1 \mathbf{d} + \tilde{\alpha}_2 \left(\mathbf{d}^2 - \frac{1}{3} \text{tr } \mathbf{d}^2 \mathbf{I} \right) \right], \quad (5.4.81)$$

where $\tilde{\alpha}_1$ and $\tilde{\alpha}_2$ depend on two invariants of the tensor \mathbf{d} . The hydrostatic stress is not defined by the constitutive equation. It can be computed from the balance of momentum. Further specification of the constitutive equation can be made based on experimental observations. For example assume the shear flow

$$\mathbf{v}(x, y, z) = z \dot{\gamma} \mathbf{e}_x, \quad \Rightarrow \quad \mathbf{L} = \dot{\gamma} \mathbf{e}_x \otimes \mathbf{e}_z, \quad \mathbf{d} = \mathbf{D} = \dot{\gamma} (\mathbf{e}_x \otimes \mathbf{e}_z + \mathbf{e}_z \otimes \mathbf{e}_x),$$

where the unit vector \mathbf{e}_x designates the flow (velocity) direction and the unit vector \mathbf{e}_z , is the normal to the plane xy and $\dot{\gamma}$ is the shear rate. With Eq. (5.4.81) the stress deviator is

$$\mathbf{s} = g_T(T) \tilde{\alpha}_1 \dot{\gamma} (\mathbf{e}_x \otimes \mathbf{e}_z + \mathbf{e}_z \otimes \mathbf{e}_x) + g_T(T) \tilde{\alpha}_2 \dot{\gamma}^2 \left(\frac{1}{3} \mathbf{I} - \mathbf{e}_y \otimes \mathbf{e}_y \right)$$

The first term is the shear stress state in the xz plane with the magnitude $g_T(T) \tilde{\alpha}_1 \dot{\gamma}$. The second term is the “out of plane” stress state with the magnitude $g_T(T) \tilde{\alpha}_2 \dot{\gamma}^2$. This may be important to describe complex material responses, for example the Weissenberg effect observed for several non-Newtonian fluids, e.g. Ziegler (1983), Giesekus (1994). In many cases, for example for hot deformation processes of metals such effects are usually negligible. With $\tilde{\alpha}_2 = 0$ Eq. (5.4.81) is simplified to

$$\mathbf{s}(\mathbf{d}, T) = g_T(T) \tilde{\alpha}_1 \mathbf{d}, \quad (5.4.82)$$

where $\tilde{\alpha}_1$ may depend on two invariants of \mathbf{d} .

For the identification the following inverse form of Eq. (5.4.77) may be convenient⁸

$$\mathbf{D}(\boldsymbol{\sigma}, T) = f_T(T) \mathbf{f}(\boldsymbol{\sigma}), \quad \mathbf{f}(\boldsymbol{\sigma}) = \beta_0 \mathbf{I} + \beta_1 \boldsymbol{\sigma} + \beta_2 \boldsymbol{\sigma}^2, \quad (5.4.83)$$

where β_i are functions of three invariants of the stress tensor. For many materials, the inelastic deformation does not produce an essential change in volume. Setting

⁸For example, to identify creep of metals, the creep rate is considered as a function of the stress based on results of uni-axial creep tests.

the trace of Eq. (5.4.83) to zero, we obtain

$$\mathbf{d}(\boldsymbol{\sigma}, T) = f_T(T) \left[\tilde{\beta}_1 \mathbf{s} + \tilde{\beta}_2 \left(\mathbf{s}^2 - \frac{1}{3} \text{tr} \mathbf{s}^2 \mathbf{I} \right) \right], \quad (5.4.84)$$

where $\tilde{\beta}_i$ depend on two invariants of the stress deviator. To specify these functions, experimental data from tests under different stress states are required. As an example, consider the shear stress state which can be obtained if a thin-walled tube is subjected to the torsion, see Sect. 1.1.2

$$\boldsymbol{\sigma} = \mathbf{s} = \tau (\mathbf{e}_x \otimes \mathbf{e}_z + \mathbf{e}_z \otimes \mathbf{e}_x),$$

where τ is the magnitude of the shear stress. Equation (5.4.84) yields

$$\mathbf{d} = f_T(T) \tilde{\beta}_1 \tau (\mathbf{e}_x \otimes \mathbf{e}_z + \mathbf{e}_z \otimes \mathbf{e}_x) + f_T(T) \tilde{\beta}_2 \tau^2 \left(\frac{1}{3} \mathbf{I} - \mathbf{e}_y \otimes \mathbf{e}_y \right) \quad (5.4.85)$$

For the fixed temperature a family of creep curves for different values of the shear stress can be recorded. From the steady creep state one may obtain the components of the creep rate tensor and identify the functions $\tilde{\beta}_i$. Equation (5.4.85) predicts that the shear stress leads to shear creep rate, and additionally to the axial creep rates (Poynting-Swift effect). Within the engineering mechanics of small inelastic deformation such effects are usually neglected and one may set $\tilde{\beta}_2 = 0$. This leads to the following equation

$$\mathbf{d}(\boldsymbol{\sigma}, T) = f_T(T) \tilde{\beta}_1 \mathbf{s} \quad (5.4.86)$$

In this case the dissipation inequality (5.4.73) reads

$$f_T(T) \tilde{\beta}_1 \mathbf{s} \cdot \mathbf{s} \geq 0$$

Since $f_T(T) > 0$, we obtain the restriction for the function $\tilde{\beta}_1 \geq 0$. From Eq. (5.4.86) can also be written as follows

$$\mathbf{d}^2 = f_T^2 \tilde{\beta}_1^2 \mathbf{s}^2, \quad \Rightarrow \quad \text{tr} \mathbf{d}^2 = f_T^2 \tilde{\beta}_1^2 \text{tr} \mathbf{s}^2 \quad (5.4.87)$$

Introducing the von Mises equivalent stress and deformation rate

$$\sigma_{\text{vM}} = \sqrt{\frac{3}{2} \text{tr} \mathbf{s}^2} = \sqrt{\frac{3}{2} \mathbf{s} \cdot \mathbf{s}}, \quad d_{\text{vM}} = \sqrt{\frac{2}{3} \text{tr} \mathbf{d}^2} = \sqrt{\frac{2}{3} \mathbf{d} \cdot \mathbf{d}} \quad (5.4.88)$$

Equation (5.4.87)₂ takes the following form

$$\frac{3}{2} d_{\text{vM}}^2 = f_T^2 \tilde{\beta}_1^2 \frac{2}{3} \sigma_{\text{vM}}^2, \quad \Rightarrow \quad f_T \tilde{\beta}_1 = \frac{3}{2} \frac{d_{\text{vM}}}{\sigma_{\text{vM}}} \quad (5.4.89)$$

Now Eq. (5.4.86) can be put into the following equivalent form

$$\mathbf{d} = \frac{3}{2} \frac{d_{\text{VM}}}{\sigma_{\text{VM}}} \mathbf{s} \quad (5.4.90)$$

A class of constitutive equations is usually based on the concept of the plastic or creep potentials and the flow rule. The associated flow rule has the origin in the engineering theory of plasticity. The basic assumptions of this theory are:

- The existence of a yield condition (creep condition, see Betten (1993), for example) expressed by the equation $F(\boldsymbol{\sigma}) = 0$, where F is a scalar valued function. The function F depends not only on the stress tensor but also on the internal state variables and the temperature (Malinin 1981; Rabotnov 1969), i.e. the yield condition has a form

$$F(\boldsymbol{\sigma}, H_i, \omega_j, T) = 0, \quad i = 1, \dots, n, \quad j = 1, \dots, m, \quad (5.4.91)$$

where H_i are hardening variables and ω_j are damage variables.

- The existence of a flow potential as a function of the stress tensor $\Phi(\boldsymbol{\sigma})$.

The flow rule (sometimes called the normality rule) is the following assumption for the inelastic deformation rate tensor

$$\mathbf{D} = \dot{\lambda} \frac{\partial \Phi}{\partial \boldsymbol{\sigma}}, \quad \begin{cases} \dot{\lambda} = 0, & \text{if } F(\boldsymbol{\sigma}) < 0, \\ \dot{\lambda} \geq 0, & \text{if } F(\boldsymbol{\sigma}) = 0 \end{cases} \quad (5.4.92)$$

Details of the rate-independent plasticity theory including different arguments leading to (5.4.92) can be found in textbooks, e.g. Hill (1950), Kachanov (1969), Kaliszky (1984), Khan and Huang (1995), Malinin (1975), Malinin (1992), Skrzypek (1993).

Within the mechanics of inelastic deformation at elevated temperature, the flow theory is usually applied without the concept of the yield stress or yield condition. This is motivated by the fact that high-temperature plasticity is a thermally activated process and the material starts to creep even under low and moderate stress values below the apparent yield point.⁹ Furthermore, within the temperature range $0.5T_m < T < 0.7T_m$ the dominant creep mechanism for metals and alloys is the diffusion of vacancies, e.g. Frost and Ashby (1982). Under this condition the existence of a yield or a creep limit cannot be verified. In Betten (1993, 2008), Malinin (1975, 1981), Penny and Mariott (1995) the flow rule is applied as follows

$$\mathbf{D} = \dot{\lambda} \frac{\partial \Phi}{\partial \boldsymbol{\sigma}}, \quad \dot{\lambda} > 0 \quad (5.4.93)$$

Equation (5.4.93) states the “normality” of the strain rate tensor to the surfaces $\Phi(\boldsymbol{\sigma}) = \text{const}$. The scalar factor $\dot{\lambda}$ is determined according to the hypothesis of the

⁹At high temperature the yield point cannot be defined, the $R_{p0.2}$ stress value is used instead in most cases, see Sect. 1.1.1.1.

equivalence of the dissipation power (Altenbach 1999; Betten 2008). With the dissipation power $P = \mathbf{D} \cdot \boldsymbol{\sigma}$ it is assumed that $P = \dot{\epsilon}_{\text{eq}} \sigma_{\text{eq}}$, where $\dot{\epsilon}_{\text{eq}}$ is the equivalent strain rate and σ_{eq} is the equivalent stress. The equivalent measures of stress and strain rate are convenient to compare experimental data under different stress states (see Sect. 1.1.2). From the above hypothesis it follows

$$\dot{\lambda} = \frac{P}{\frac{\partial \Phi}{\partial \boldsymbol{\sigma}} \cdot \boldsymbol{\sigma}} = \frac{\dot{\epsilon}_{\text{eq}} \sigma_{\text{eq}}}{\frac{\partial \Phi}{\partial \boldsymbol{\sigma}} \cdot \boldsymbol{\sigma}} \quad (5.4.94)$$

The equivalent strain rate is defined as a function of the equivalent stress according to the experimental data for uni-axial creep as well as creep mechanisms operating for the given stress range. An example is the power law stress function

$$\dot{\epsilon}_{\text{eq}}(\sigma_{\text{eq}}) = a \sigma_{\text{eq}}^n \quad (5.4.95)$$

Another form of the flow rule without the yield condition has been proposed by Odqvist (Odqvist 1974; Odqvist and Hult 1962). The steady-state creep theory of Odqvist, see Odqvist (1974), is based on the variational equation $\delta W = \delta \boldsymbol{\sigma} \cdot \mathbf{D}$ leading to the flow rule

$$\mathbf{D} = \frac{\partial W}{\partial \boldsymbol{\sigma}}, \quad (5.4.96)$$

where the scalar valued function $W(\boldsymbol{\sigma})$ plays the role of the creep potential.¹⁰ In order to specify the creep potential, the equivalent stress $\sigma_{\text{eq}}(\boldsymbol{\sigma})$ is introduced. Taking into account that $W(\boldsymbol{\sigma}) = W(\sigma_{\text{eq}}(\boldsymbol{\sigma}))$ the flow rule (5.4.96) can be formulated as follows

$$\mathbf{D} = \frac{\partial W}{\partial \sigma_{\text{eq}}} \frac{\partial \sigma_{\text{eq}}}{\partial \boldsymbol{\sigma}} = \dot{\epsilon}_{\text{eq}} \frac{\partial \sigma_{\text{eq}}}{\partial \boldsymbol{\sigma}}, \quad \dot{\epsilon}_{\text{eq}} = \frac{\partial W}{\partial \sigma_{\text{eq}}} \quad (5.4.97)$$

The creep potential $W(\sigma_{\text{eq}})$ is defined according to experimental data of creep under uni-axial stress state for the specific stress range. An example is the Norton-Bailey-Odqvist creep potential

$$W = \frac{\sigma_0}{n+1} \left(\frac{\sigma_{\text{vM}}}{\sigma_0} \right)^{n+1}, \quad (5.4.98)$$

widely used for the description of steady-state creep of metals and alloys. In (5.4.98) σ_0 and n are material parameters and σ_{vM} is the von Mises equivalent stress. Below we discuss various restrictions on the potentials, e.g. the symmetries of the creep behavior and the inelastic incompressibility.

¹⁰The dependence on the temperature is dropped for the sake of brevity.

In order to compare the flow rules (5.4.93) and (5.4.96) let us compute the dissipation power. From (5.4.97) it follows

$$P = \dot{\boldsymbol{\varepsilon}} \cdot \boldsymbol{\sigma} = \frac{\partial W}{\partial \sigma_{\text{eq}}} \frac{\partial \sigma_{\text{eq}}}{\partial \boldsymbol{\sigma}} \cdot \boldsymbol{\sigma} = \dot{\varepsilon}_{\text{eq}} \frac{\partial \sigma_{\text{eq}}}{\partial \boldsymbol{\sigma}} \cdot \boldsymbol{\sigma}$$

We observe that the equivalence of the dissipation power follows from (5.4.97) if the equivalent stress satisfies the following partial differential equation

$$\frac{\partial \sigma_{\text{eq}}}{\partial \boldsymbol{\sigma}} \cdot \boldsymbol{\sigma} = \sigma_{\text{eq}} \quad (5.4.99)$$

Furthermore, in this case the flow rules (5.4.93) and (5.4.96) lead to the same creep constitutive equation. Many equivalent stress formulations proposed in the literature satisfy (5.4.99).

The above potential formulations originate from the works of Richard von Mises, where the existence of variational principles is assumed in analogy to those known from the theory of elasticity (the principle of the minimum of the complementary elastic energy, for example). Richard von Mises wrote (von Mises 1928): “Die Formänderung regelt sich derart, daß die pro Zeiteinheit von ihr verzehrte Arbeit unverändert bleibt gegenüber kleinen Variationen der Spannungen innerhalb der Fließgrenze. Da die Elastizitätstheorie einen ähnlichen Zusammenhang zwischen den Deformationsgrößen und dem elastischen Potential lehrt, so nenne ich die Spannungsfunktion F auch das “plastische Potential” oder “Fließpotential”.”¹¹ It can be shown that the variational principles of linear elasticity are special cases of the energy balance equation (for isothermal or adiabatic processes), see e.g. Lurie (2010), for example. Many attempts have been made to prove or to motivate the potential formulations within the framework of irreversible thermodynamics. For quasi-static irreversible processes various extremum principles (e.g. the principle of least irreversible force) are stipulated in Ziegler (1963, 1983). Based on these principles and additional arguments like material stability, the potential formulations and the flow rules (5.4.93) and (5.4.96) can be verified. In Lemaitre and Chaboche (1990) a complementary dissipation potential as a function of the stress tensor as well as the number of additional forces conjugate to internal state variables is postulated, whose properties, e.g. the convexity, are sufficient conditions to satisfy the dissipation inequality. In Maugin (1992) theories of plasticity and visco-plasticity are based on the notion of the dissipation pseudo-potentials. However, as far as we know, the flow rules (5.4.93) and (5.4.96) still represent the assumptions confirmed by various experimental observations of steady-state creep in metals rather than consequences

¹¹The change in shape is governed in such a way that the the work per unit time remains unchanged compared to small variations of the stresses within the yield limit. Since the elasticity theory provides a similar relationship between the deformations and the elastic potential, so I call the stress function F also the “plastic potential” or “flow potential”.

of the fundamental laws. The advantage of variational statements is that they are convenient for the formulation of initial-boundary value problems and for the numerical analysis of creep in engineering structures. The direct variational methods (for example, the Ritz method, the Galerkin method, the finite element method) can be applied for the numerical solution.

Let us note that, constitutive equations of inelastic flow can be developed without the notion of flow or creep potentials. Examples are Eqs. (5.4.80) and (5.4.83). The existence of the potential requires that α_i or β_i must satisfy integrability conditions (Betten 2008; Lurie 1990; Rivlin and Erickson 1955).

In rheology and theory of materials equations like (5.4.77), (5.4.83) or (5.4.96) are classified as a constitutive equation for non-linear viscous fluids, or non-linear viscous elements, see, for example, Giesekus (1994), Krawietz (1986), Palmov (1998), Reiner (1969). On the other hand, for large values of n the creep potential (5.4.98) is close to the potential of rate-independent plasticity. Functions \mathbf{f} and f_T can be formulated such that experimental data including non-linear viscous flow and plasticity can be described. Therefore equations like (5.4.80), (5.4.83) or (5.4.96) can be classified as viscoplasticity model. An example is the viscoplasticity model proposed by Krempl (1996, 1999) where the yield condition is not included. This definition of a viscoplasticity model like (5.4.77), (5.4.83) or (5.4.96) may contradict the classification in the rheology, where the viscoplastic model is defined as a connection of viscous and rigid plastic elements.

The inelastic deformation of crystalline materials is related to dislocation glide and dislocation climb (Frost and Ashby 1982; Nabarro and de Villiers 1995). The glide motion of dislocations dominates at lower homologous temperatures and higher stress levels, while the climb of dislocations over obstacles is important in high-temperature regimes and moderate stress levels. From this point of view, equations like (5.4.77), (5.4.83) or (5.4.96) can be classified as models of high-temperature plasticity, as preferred in the materials science, see, for example, Ilschner (1973).

Constitutive Equations like (5.4.80), (5.4.83) or (5.4.96) are used in the analysis of hot deformation processes of metals, for example, friction welding (Schmicker et al. 2013, 2015). Constitutive equations (5.4.90) and (5.4.96) are applied for the structural analysis in the steady-state creep range (Altenbach et al. 2008; Boyle 2012; Naumenko et al. 2009; Naumenko and Altenbach 2007).

5.4.2 *Isotropic Materials*

In many cases creep behavior can be assumed to be isotropic. In what follows the classical potential and the potential formulated in terms of three invariants of the stress tensor are introduced.

5.4.2.1 Classical Creep Potential

The starting point is the Odqvist flow rule (5.4.96). Under the assumption of the isotropic creep, the potential depends only on the stress tensor and must satisfy the following restriction

$$W(\mathbf{Q} \cdot \boldsymbol{\sigma} \cdot \mathbf{Q}^T) = W(\boldsymbol{\sigma}) \quad (5.4.100)$$

for any symmetry transformation \mathbf{Q} , $\mathbf{Q} \cdot \mathbf{Q}^T = \mathbf{I}$, $\det \mathbf{Q} = \pm 1$. From (5.4.100) it follows that the potential depends only on the three invariants of the stress tensor (see Appendix B.6). Applying the principal invariants

$$\begin{aligned} J_1(\boldsymbol{\sigma}) &= \text{tr } \boldsymbol{\sigma}, & J_2(\boldsymbol{\sigma}) &= \frac{1}{2}[(\text{tr } \boldsymbol{\sigma})^2 - \text{tr } \boldsymbol{\sigma}^2], \\ J_3(\boldsymbol{\sigma}) &= \det \boldsymbol{\sigma} = \frac{1}{6}(\text{tr } \boldsymbol{\sigma})^3 - \frac{1}{2}\text{tr } \boldsymbol{\sigma} \text{tr } \boldsymbol{\sigma}^2 + \frac{1}{3}\text{tr } \boldsymbol{\sigma}^3 \end{aligned} \quad (5.4.101)$$

one can write

$$W(\boldsymbol{\sigma}) = W(J_1, J_2, J_3)$$

The stress tensor can be decomposed into the spherical and deviatoric parts as follows

$$\boldsymbol{\sigma} = \sigma_m \mathbf{I} + \mathbf{s}, \quad \text{tr } \mathbf{s} = 0 \quad \Rightarrow \quad \sigma_m = \frac{1}{3} \text{tr } \boldsymbol{\sigma},$$

where \mathbf{s} is the stress deviator and σ_m is the mean stress. With the principal invariants of the stress deviator

$$J_{2D} = -\frac{1}{2} \text{tr } \mathbf{s}^2 = -\frac{1}{2} \mathbf{s} \cdot \mathbf{s}, \quad J_{3D} = \frac{1}{3} \text{tr } \mathbf{s}^3 = \frac{1}{3} (\mathbf{s} \cdot \mathbf{s}) \cdot \mathbf{s}$$

the potential takes the form

$$W = W(J_1, J_{2D}, J_{3D}),$$

Applying the rule for the derivative of a scalar valued function with respect to a second rank tensor (see Appendix B.4) and Eq. (5.4.96) one can obtain

$$\mathbf{D} = \frac{\partial W}{\partial J_1} \mathbf{I} - \frac{\partial W}{\partial J_{2D}} \mathbf{s} + \frac{\partial W}{\partial J_{3D}} \left(\mathbf{s}^2 - \frac{1}{3} \text{tr } \mathbf{s}^2 \mathbf{I} \right) \quad (5.4.102)$$

In the classical creep theory it is assumed that the inelastic deformation does not produce a significant change in volume. The spherical part of the deformation rate tensor is neglected, i.e. $\text{tr } \mathbf{D} = 0$. Setting the trace of (5.4.102) to zero results in

$$\text{tr } \mathbf{D} = 3 \frac{\partial W}{\partial J_1} = 0 \quad \Rightarrow \quad W = W(J_{2D}, J_{3D})$$

From this follows that the creep behavior is not sensitive to the hydrostatic stress state $\boldsymbol{\sigma} = -p\mathbf{I}$, where $p > 0$ is the hydrostatic pressure. The creep equation (5.4.102) can be formulated as

$$\mathbf{D} = \mathbf{d} = -\frac{\partial W}{\partial J_{2D}} \mathbf{s} + \frac{\partial W}{\partial J_{3D}} \left(\mathbf{s}^2 - \frac{1}{3} \text{tr } \mathbf{s}^2 \mathbf{I} \right) \quad (5.4.103)$$

The last term in the right-hand side of (5.4.103) is non-linear with respect to the stress deviator \mathbf{s} . Equations of this type are called tensorial non-linear equations, e.g. Backhaus (1983), Betten (2008), Malinin (1981), Rabotnov (1969). With the tensorial non-linearity several non-classical or second order effects of the material behavior can be considered (Backhaus 1983; Billington 1985). As an example consider the shear stress state $\mathbf{s} = \tau(\mathbf{m} \otimes \mathbf{n} + \mathbf{n} \otimes \mathbf{m})$, where τ is the magnitude of the shear stress and \mathbf{m} and \mathbf{n} are orthogonal unit vectors. From (5.4.103) it follows

$$\mathbf{d} = -\frac{\partial W}{\partial J_{2D}} \tau(\mathbf{m} \otimes \mathbf{n} + \mathbf{n} \otimes \mathbf{m}) + \frac{\partial W}{\partial J_{3D}} \tau^2 \left(\frac{1}{3} \mathbf{I} - \mathbf{p} \otimes \mathbf{p} \right),$$

where the unit vector \mathbf{p} is orthogonal to the plane spanned on \mathbf{m} and \mathbf{n} . We observe that the pure shear load leads to shear creep rate, and additionally to the axial creep rates (Poynting-Swift effect). Within the engineering creep mechanics such effects are usually neglected.

The assumption that the potential is a function of the second invariant of the stress deviator only, i.e.

$$W = W(J_{2D})$$

leads to the classical von Mises type potential (von Mises 1928). In applications it is convenient to introduce the equivalent stress which allows to compare the creep behavior under different stress states including the uni-axial tension. The von Mises equivalent stress is defined as follows

$$\sigma_{\text{vM}} = \sqrt{\frac{3}{2} \mathbf{s} \cdot \mathbf{s}} = \sqrt{-3J_{2D}}, \quad (5.4.104)$$

where the factor $3/2$ is used for convenience (in the case of the uni-axial tension with the stress σ the above expression provides $\sigma_{\text{vM}} = \sigma$). With $W = W(\sigma_{\text{vM}}(\boldsymbol{\sigma}))$ the flow rule (5.4.96) results in

$$\mathbf{d} = \frac{\partial W(\sigma_{\text{vM}})}{\partial \sigma_{\text{vM}}} \frac{\partial \sigma_{\text{vM}}}{\partial \boldsymbol{\sigma}} = \frac{\partial W(\sigma_{\text{vM}})}{\partial \sigma_{\text{vM}}} \frac{3}{2} \frac{\mathbf{s}}{\sigma_{\text{vM}}} \quad (5.4.105)$$

The second invariant of \mathbf{d} can be calculated as follows

$$\mathbf{d} \cdot \mathbf{d} = \frac{3}{2} \left[\frac{\partial W(\sigma_{\text{vM}})}{\partial \sigma_{\text{vM}}} \right]^2$$

Introducing the notation $\dot{\varepsilon}_{\text{vM}}^2 = \frac{2}{3} \mathbf{d} \cdot \mathbf{d}$ and taking into account that

$$P = \frac{\partial W(\sigma_{\text{vM}})}{\partial \sigma_{\text{vM}}} \sigma_{\text{vM}} \geq 0$$

we obtain

$$\mathbf{d} = \frac{3}{2} \frac{\dot{\varepsilon}_{\text{vM}}}{\sigma_{\text{vM}}} \mathbf{s}, \quad \dot{\varepsilon}_{\text{vM}} = \frac{\partial W(\sigma_{\text{vM}})}{\partial \sigma_{\text{vM}}} \quad (5.4.106)$$

The constitutive equation of steady-state creep (5.4.106) was proposed by Odqvist and Hult (1962). Experimental verifications of this equation can be found, for example, in Sosnin (1971) for steel 45, in Nikitenko (1984) for titanium alloy Ti-6Al-4V and in Oytana et al. (1982) for alloys Al-Si, Fe-Co-V and XC 48. In these works tubular specimens were loaded by tension force and torque leading to the plane stress state $\boldsymbol{\sigma} = \sigma \mathbf{n} \otimes \mathbf{n} + \tau (\mathbf{n} \otimes \mathbf{m} + \mathbf{m} \otimes \mathbf{n})$, where σ and τ are the magnitudes of the normal and shear stresses (see Sect. 1.1.2). Surfaces $\sigma_{\text{vM}}^2 = \sigma^2 + 3\tau^2 = \text{const}$ corresponding to the same steady state values of $\dot{\varepsilon}_{\text{vM}}$ were recorded. Assuming the Norton-Bailey type potential (5.4.98), from (5.4.106) it follows

$$\mathbf{d} = \frac{3}{2} a \sigma_{\text{vM}}^{n-1} \mathbf{s} \quad (5.4.107)$$

This model is widely used for the analysis steady-state creep in structures, e.g. Boyle and Spence (1983), Burlakov et al. (1977), Odqvist and Hult (1962), Penny and Mariott (1995), Rabotnov (1969).

5.4.2.2 Potentials with Three Invariants of the Stress Tensor

In some cases, deviations from the von Mises type equivalent stress were found in experiments. For example, different secondary creep rates under tensile and compressive loading were observed in Lucas and Pelloux (1981) for Zircaloy-2, in El-Magd and Nicolini (1999) for aluminium alloy ALC101 and in Stouffer and Dame (1996) for the nickel-based alloy René 95. One way to consider such effects is to construct the creep potential as a function of three invariants of the stress tensor. Below we discuss a generalized creep potential, proposed in Altenbach et al. (1995). This potential leads to tensorial non-linear constitutive equations and allows to predict the stress state dependent creep behavior and second order effects. The 6 unknown parameters in this law can be identified by some basic tests. Creep potentials formulated

in terms of three invariants of the stress tensor are termed non-classical (Altenbach et al. 1995).

By analogy to the classical creep equations, the dependence on the stress tensor is defined by means of the equivalent stress σ_{eq} . Various equivalent stress expressions have been proposed in the literature for the formulation of yield or failure criteria, e.g. Altenbach and Zolochovsky (1996). In the case of creep, different equivalent stress expressions are summarized in Kawai (2002). In Altenbach et al. (1995) the following equivalent stress is proposed

$$\sigma_{\text{eq}} = \alpha\sigma_1 + \beta\sigma_2 + \gamma\sigma_3 \quad (5.4.108)$$

with the linear, the quadratic and the cubic invariants

$$\sigma_1 = \mu_1 I_1, \quad \sigma_2^2 = \mu_2 I_1^2 + \mu_3 I_2, \quad \sigma_3^3 = \mu_4 I_1^3 + \mu_5 I_1 I_2 + \mu_6 I_3, \quad (5.4.109)$$

where $I_i = \text{tr } \boldsymbol{\sigma}^i$ ($i = 1, 2, 3$) are basic invariants of the stress tensor (see Appendix B.6), μ_j ($j = 1, \dots, 6$) are parameters, which depend on the material properties. α, β, γ are numerical coefficients for weighting the influence of the different parts in the equivalent stress expression (5.4.108). Such a weighting is usual in phenomenological modeling of material behavior. For example, in Hayhurst (1972) similar coefficients are introduced for characterizing different failure modes.

The von Mises equivalent stress (5.4.104) can be obtained from (5.4.108) by setting $\alpha = \gamma = 0, \beta = 1$ and $\mu_3 = 1.5, \mu_2 = -0.5$. In what follows we set $\beta = 1$ and the equivalent stress takes the form

$$\sigma_{\text{eq}} = \alpha\sigma_1 + \sigma_2 + \gamma\sigma_3 \quad (5.4.110)$$

It can be verified that the equivalent stress (5.4.110) satisfies (5.4.99).

The flow rule (5.4.96) allows to formulate the constitutive equation for the creep rate tensor

$$\mathbf{D} = \frac{\partial W(\sigma_{\text{eq}})}{\partial \sigma_{\text{eq}}} \frac{\partial \sigma_{\text{eq}}}{\partial \boldsymbol{\sigma}} = \frac{\partial W(\sigma_{\text{eq}})}{\partial \sigma_{\text{eq}}} \left(\alpha \frac{\partial \sigma_1}{\partial \boldsymbol{\sigma}} + \frac{\partial \sigma_2}{\partial \boldsymbol{\sigma}} + \gamma \frac{\partial \sigma_3}{\partial \boldsymbol{\sigma}} \right) \quad (5.4.111)$$

Taking into account the relations between the invariants σ_i and the basic invariants I_i and using the rules for the derivatives of the invariants (see Appendix B.4), we obtain

$$\begin{aligned} \frac{\partial \sigma_1}{\partial \boldsymbol{\sigma}} &= \mu_1 \mathbf{I}, & \frac{\partial \sigma_2}{\partial \boldsymbol{\sigma}} &= \frac{\mu_2 I_1 \mathbf{I} + \mu_3 \boldsymbol{\sigma}}{\sigma_2}, \\ \frac{\partial \sigma_3}{\partial \boldsymbol{\sigma}} &= \frac{\mu_4 I_1^2 \mathbf{I} + \frac{\mu_5}{3} I_2 \mathbf{I} + \frac{2}{3} \mu_5 I_1 \boldsymbol{\sigma} + \mu_6 \boldsymbol{\sigma} \cdot \boldsymbol{\sigma}}{\sigma_3^2} \end{aligned} \quad (5.4.112)$$

As a result, the creep constitutive equation can be formulated as follows

$$\mathbf{D} = \frac{\partial W(\sigma_{\text{eq}})}{\partial \sigma_{\text{eq}}} \left[\alpha \mu_1 \mathbf{I} + \frac{\mu_2 I_1 \mathbf{I} + \mu_3 \boldsymbol{\sigma}}{\sigma_2} + \gamma \frac{\left(\mu_4 I_1^2 + \frac{\mu_5}{3} I_2 \right) \mathbf{I} + \frac{2}{3} \mu_5 I_1 \boldsymbol{\sigma} + \mu_6 \boldsymbol{\sigma} \cdot \boldsymbol{\sigma}}{\sigma_3^2} \right] \quad (5.4.113)$$

Introducing the notation

$$\dot{\varepsilon}_{\text{eq}} \equiv \frac{\partial W(\sigma_{\text{eq}})}{\partial \sigma_{\text{eq}}}$$

the constitutive equation takes the form

$$\mathbf{D} = \dot{\varepsilon}_{\text{eq}} \left[\alpha \mu_1 \mathbf{I} + \frac{\mu_2 I_1 \mathbf{I} + \mu_3 \boldsymbol{\sigma}}{\sigma_2} + \gamma \frac{\left(\mu_4 I_1^2 + \frac{\mu_5}{3} I_2 \right) \mathbf{I} + \frac{2}{3} \mu_5 I_1 \boldsymbol{\sigma} + \mu_6 \boldsymbol{\sigma} \cdot \boldsymbol{\sigma}}{\sigma_3^2} \right] \quad (5.4.114)$$

Equation (5.4.114) is non-linear with respect to the stress tensor. Therefore, second order effects, e.g. Backhaus (1983), Betten (1998), Truesdell (1964) are included in the material behavior description. In addition, the volumetric creep rate can be calculated from (5.4.114) as follows

$$\dot{\varepsilon}_V = \dot{\varepsilon}_{\text{eq}} \left[3\alpha \mu_1 + \frac{(3\mu_2 + \mu_3) I_1}{\sigma_2} + \gamma \frac{(9\mu_4 + 2\mu_5) I_1^2 + 3(\mu_5 + \mu_6) I_2}{3\sigma_3^2} \right] \quad (5.4.115)$$

The volumetric creep rate is different from 0, i.e. the compressibility or dilatation can be considered.

The derived creep equation has the form (5.4.83) of the general relation between two coaxial tensors. The comparison of (5.4.83) and (5.4.114) provides

$$\begin{aligned} f_T \beta_0 &= \dot{\varepsilon}_{\text{eq}} \left(\alpha \mu_1 + \frac{\mu_2 I_1}{\sigma_2} + \gamma \frac{3\mu_4 I_1^2 + \mu_5 I_2}{3\sigma_3^2} \right), \\ f_T \beta_1 &= \dot{\varepsilon}_{\text{eq}} \left(\frac{\mu_3}{\sigma_2} + \gamma \frac{2\mu_5 I_1}{3\sigma_3^2} \right), \\ f_T \beta_2 &= \dot{\varepsilon}_{\text{eq}} \gamma \frac{\mu_6}{\sigma_3^2} \end{aligned} \quad (5.4.116)$$

In Altenbach et al. (1995) the power law function of the equivalent stress (5.4.95) is applied to model creep behavior of several materials. Four independent creep tests are required to identify the material constants. The stress states realized in tests should

include uni-axial tension, uni-axial compression, torsion and hydrostatic pressure. Let us note that experimental data which allows to identify the full set of material constants in (5.4.114) are usually not available. In applications one may consider the following special cases of (5.4.114) with reduced number of material constants.

The classical creep equation based on the von Mises equivalent stress can be derived assuming the following values of material constants

$$\alpha = \gamma = 0, \quad \mu_2 = -1/2, \quad \mu_3 = 3/2, \quad (5.4.117)$$

$$\sigma_{\text{eq}} = \sigma_2 = \sqrt{-\frac{1}{2}I_1^2 + \frac{3}{2}I_2} = \sqrt{\frac{3}{2}\mathbf{s} \cdot \mathbf{s}} = \sigma_{\text{vM}} \quad (5.4.118)$$

The creep rate tensor takes the form

$$\mathbf{D} = \dot{\varepsilon}_{\text{eq}} \left(\sqrt{\frac{3}{2}\mathbf{s} \cdot \mathbf{s}} \right) \frac{3\boldsymbol{\sigma} - I_1\mathbf{I}}{2\sqrt{\frac{3}{2}\mathbf{s} \cdot \mathbf{s}}} = \frac{3}{2} \frac{\dot{\varepsilon}_{\text{eq}}(\sigma_{\text{vM}})}{\sigma_{\text{vM}}} \mathbf{s} \quad (5.4.119)$$

Assuming identical behavior in tension and compression and neglecting second order effects from $\alpha = \gamma = 0$, the following equivalent stress can be obtained

$$\sigma_{\text{eq}} = \sigma_2 = \sqrt{\mu_2 I_1^2 + \mu_3 I_2} \quad (5.4.120)$$

The corresponding creep constitutive equation takes the form

$$\mathbf{D} = \dot{\varepsilon}_{\text{eq}}(\sigma_2) \frac{\mu_2 I_1 \mathbf{I} + \mu_3 \boldsymbol{\sigma}}{\sigma_2} \quad (5.4.121)$$

The parameters μ_2 and μ_3 can be determined from uni-axial tension and torsion tests. Based on the experimental data presented in Kowalewski (1987, 1991) for technical pure copper M1E (Cu 99.9%) at $T = 573$ K the parameters μ_2 and μ_3 are identified in Altenbach et al. (1991).

Neglecting the influence of the third invariant ($\gamma = 0$), the creep rate tensor can be expressed as follows

$$\mathbf{D} = \dot{\varepsilon}_{\text{eq}}(\sigma_{\text{eq}}) \left(\alpha \mu_1 \mathbf{I} + \frac{\mu_2 I_1 \mathbf{I} + \mu_3 \boldsymbol{\sigma}}{\sigma_2} \right) \quad (5.4.122)$$

Equation (5.4.122) describes different behavior in tension and compression, and includes the volumetric creep rate. Three independent tests, e.g. tension, compression and torsion are required to identify the material constants μ_1 , μ_2 and μ_3 .

With the quadratic invariant and the reduced cubic invariant several special cases with three material constants can be considered. Setting ($\alpha \mu_1 = \mu_4 = \mu_5 = 0$) the

tensorial non-linear equation can be obtained

$$\mathbf{D} = \dot{\varepsilon}_{\text{eq}}(\sigma_{\text{eq}}) \left(\frac{\mu_2 I_1 \mathbf{I} + \mu_3 \boldsymbol{\sigma}}{\sigma_2} + \gamma \frac{\mu_6 \boldsymbol{\sigma} \cdot \boldsymbol{\sigma}}{\sigma_3^2} \right) \quad (5.4.123)$$

With $\alpha \mu_1 = \mu_4 = \mu_6 = 0$ the deformation rate tensor takes the form

$$\mathbf{D} = \dot{\varepsilon}_{\text{eq}}(\sigma_{\text{eq}}) \left(\frac{\mu_2 I_1 \mathbf{I} + \mu_3 \boldsymbol{\sigma}}{\sigma_2} + \gamma \frac{\mu_5 (I_2 \mathbf{I} + 2I_1 \boldsymbol{\sigma})}{\sigma_3^2} \right) \quad (5.4.124)$$

The material parameters in (5.4.122), (5.4.123) and (5.4.124) were identified in Altenbach (1999), Altenbach and Zolochovsky (1994) according to data from multi-axial creep tests for plastics (PVC) at room temperature (Lewin and Lehmann 1977) and aluminium alloy AK4-1T at 473 K (Cvelodub 1991; Gorev et al. 1979; Soločevskij et al. 1985). Furthermore, simulations have been performed in Altenbach (1999), Altenbach and Zolochovsky (1994) to compare Eqs. (5.4.122), (5.4.123) and (5.4.124) as they characterize creep behavior under different loading conditions. The conclusion was made that cubic invariants applied in (5.4.123) and (5.4.124) do not deliver any significant improvement in the material behavior description.

5.4.3 Initially Anisotropic Materials

Anisotropic creep behavior and anisotropic creep modeling are subjects which are rarely discussed in the classical monographs and textbooks on creep mechanics (only in some books one may find the flow potentials introduced by von Mises (1928) and Hill (1950). The reason for this is that the experimental data from creep tests usually show large scatter within the range of 20% or even more. Therefore, it was often difficult to recognize whether the difference in creep curves measured for different specimens (cut from the same material in different directions) is the result of the anisotropy. Therefore, it was no use for anisotropic models with higher order complexity, since the identification of material constants was difficult or even impossible. In the last three decades the importance in modeling anisotropic creep behavior of materials and structures is discussed in many publications. In Bertram and Olschewski (1996), Mahnken (2002), Qi (1998), Qi and Bertram (1997), Qi and Bertram (1998), Qi and Bertram (1999) experimental results of creep of superalloys SRR99 and CMSX-4 are reported, which demonstrate significant anisotropy of creep behavior for different orientations of specimens with respect to the crystallographic axes. In Hyde et al. (2003a) experimental creep curves of a 9CrMoNbV weld metal are presented. They show significant difference for specimens sampled in longitudinal (welding) direction and transverse directions. In Gariboldi and Casaro (2007), Naumenko and Gariboldi (2014) creep curves for a forged aluminum alloy are presented. The results illustrate the essential difference of creep rates for specimens sampled longitudinal (forging) and transverse directions. Further examples are

materials reinforced by fibers, showing different creep behavior in direction of fibers and in the transverse direction, e.g. Robinson et al. (2003a, b), Kröner et al. (2009).

Constitutive models for anisotropic materials include the orientation of microstructure, specified by vectors and tensors of different rank, besides the actual stress and/or deformation rate states. Examples for the material directions are the orientation of fibers in a fiber reinforced material, the direction of forging in a forged alloy, the orientation of crystallographic axes in a single crystal alloy, etc. By analogy to the elasticity, Sect. 5.3.3, the flow potential can be introduced as a function of the stress tensor and a set of structure tensors. Within the framework of elasticity, the actual state of the microstructure can be determined through the deformation gradient, cp. Eq. (5.3.46) providing the actual orientation of a structure tensor. For example, flexible fibers deform with the matrix material without any sliding/debonding such that after the unloading the initial orientation of the material microstructure is recovered. In contrast, the material microstructure during the inelastic flow cannot be related to the deformation gradient and/or velocity gradient only. For example, short fibers may change the orientation in a viscous medium as a result of their rotary inertia (Altenbach et al. 2007, 2009; Lundell 2011; Lundell and Carlsson 2010). Therefore, additional evolution equations are required to define the current state of microstructure. Several kinds of anisotropy can be distinguished. The initial anisotropy is usually the result of the material processing, the information to the material symmetries including the orientation of material vectors is defined in the reference state. The deformation and/or damage induced anisotropy is the result of changes in the symmetry group during the deformation, for example during the creep exposure. In a simple case only the orientation of material orientation is changing and the material possesses the same symmetry group relative to the actual material vectors. In a more complex case the symmetries are lost during the deformation, as a result of damage, for example.

In this section we consider only the case of the initial anisotropy. Furthermore, we assume that the state of the material orientation is stable, such that the associated structure tensors can be assumed constant. Examples for constitutive equations for induced anisotropy will be discussed in Sects. 5.3.2 and 5.5.2.

5.4.3.1 Quadratic Potentials

Here we discuss constitutive equations for steady-state creep based on the flow rule (5.4.96) and assumption that the creep potential has a quadratic form with respect to the invariants of the stress tensor. These invariants must be established according to the assumed symmetry elements of the creep behavior. The assumption of the quadratic form of the flow potential originates from the von Mises work on plasticity of crystals (von Mises 1928). Therefore, the equations presented below may be termed as von Mises type equations.

Transverse Isotropy

In this case the potential $W(\boldsymbol{\sigma})$ must satisfy the following restriction

$$W(\mathbf{Q} \cdot \boldsymbol{\sigma} \cdot \mathbf{Q}^T) = W(\boldsymbol{\sigma}), \quad \mathbf{Q}(\varphi \mathbf{m}) = \mathbf{m} \otimes \mathbf{m} + \cos \varphi (\mathbf{I} - \mathbf{m} \otimes \mathbf{m}) + \sin \varphi \mathbf{m} \times \mathbf{I} \quad (5.4.125)$$

In (5.4.125) $\mathbf{Q}(\varphi \mathbf{m})$ is the assumed element of the symmetry group, whereby \mathbf{m} is a constant unit vector and φ is the arbitrary angle of rotation about \mathbf{m} . From the restriction (5.4.125) follows that the potential W must satisfy the following partial differential equation (see Appendix B.7)

$$(\mathbf{m} \times \boldsymbol{\sigma} - \boldsymbol{\sigma} \times \mathbf{m}) \cdot \left(\frac{\partial W}{\partial \boldsymbol{\sigma}} \right)^T = 0 \quad (5.4.126)$$

The set of integrals of this equation represent the set of functionally independent scalar valued arguments of the potential W with respect to the symmetry transformation (5.4.125). The characteristic system of (5.4.126) is the system of ordinary differential equations

$$\frac{d\boldsymbol{\sigma}}{ds} = (\mathbf{m} \times \boldsymbol{\sigma} - \boldsymbol{\sigma} \times \mathbf{m}) \quad (5.4.127)$$

Any system of n linear ordinary differential equations has not more than $n - 1$ functionally independent integrals (Courant and Hilbert 1989). Since $\boldsymbol{\sigma}$ is symmetric, (5.4.127) is a system of six ordinary differential equations and has not more than five functionally independent integrals. The lists of these integrals are presented by (B.7.28) and (B.7.39). Within the classical von Mises type theory second order effects are neglected. Therefore, we have to neglect the arguments which are cubic with respect to the stress tensor. In this case the difference between various kinds of transverse isotropy considered in Appendix B.7 vanishes. It is possible to use different lists of of scalar arguments. The linear and quadratic arguments from (B.7.28) are

$$\text{tr } \boldsymbol{\sigma}, \quad \text{tr } \boldsymbol{\sigma}^2, \quad \mathbf{m} \cdot \boldsymbol{\sigma} \cdot \mathbf{m}, \quad \mathbf{m} \cdot \boldsymbol{\sigma}^2 \cdot \mathbf{m} \quad (5.4.128)$$

Instead of (5.4.128) one can use other arguments, for example

$$\begin{aligned} \text{tr } \boldsymbol{\sigma}, \quad \text{tr } \boldsymbol{\sigma}^2 &= \text{tr } \boldsymbol{\sigma}^2 - \frac{1}{3}(\text{tr } \boldsymbol{\sigma})^2, \\ \mathbf{m} \cdot \boldsymbol{\sigma} \cdot \mathbf{m} &= \mathbf{m} \cdot \boldsymbol{\sigma} \cdot \mathbf{m} - \frac{1}{3}\text{tr } \boldsymbol{\sigma}, \\ \mathbf{m} \cdot \boldsymbol{\sigma}^2 \cdot \mathbf{m} &= \mathbf{m} \cdot \boldsymbol{\sigma}^2 \cdot \mathbf{m} - \frac{2}{3}\mathbf{m} \cdot \boldsymbol{\sigma} \cdot \mathbf{m} \text{tr } \boldsymbol{\sigma} - \frac{1}{9}(\text{tr } \boldsymbol{\sigma})^2, \end{aligned} \quad (5.4.129)$$

as proposed in Robinson et al. (2003a). In what follows we prefer another set of invariants which can be related to (5.4.128) but has a more clear mechanical interpretation.

Let us decompose the stress tensor as follows

$$\boldsymbol{\sigma} = \sigma_{mm} \mathbf{m} \otimes \mathbf{m} + \boldsymbol{\sigma}_p + \boldsymbol{\tau}_m \otimes \mathbf{m} + \mathbf{m} \otimes \boldsymbol{\tau}_m \tag{5.4.130}$$

with the projections

$$\begin{aligned} \sigma_{mm} &= \mathbf{m} \cdot \boldsymbol{\sigma} \cdot \mathbf{m}, \\ \boldsymbol{\sigma}_p &= (\mathbf{I} - \mathbf{m} \otimes \mathbf{m}) \cdot \boldsymbol{\sigma} \cdot (\mathbf{I} - \mathbf{m} \otimes \mathbf{m}), \\ \boldsymbol{\tau}_m &= \mathbf{m} \cdot \boldsymbol{\sigma} \cdot (\mathbf{I} - \mathbf{m} \otimes \mathbf{m}) \end{aligned} \tag{5.4.131}$$

The meaning of the decomposition (5.4.130) is obvious. σ_{mm} is the normal stress acting in the plane with the unit normal \mathbf{m} , $\boldsymbol{\sigma}_p$ stands for the “plane” part of the stress tensor representing the stress state in the isotropy plane. $\boldsymbol{\tau}_m$ is the shear stress vector in the plane with the unit normal \mathbf{m} . For the orthonormal basis \mathbf{k}, \mathbf{l} and \mathbf{m} the projections are (see Fig. 5.1)

$$\begin{aligned} \boldsymbol{\tau}_m &= \tau_{mk} \mathbf{k} + \tau_{ml} \mathbf{l}, \\ \boldsymbol{\sigma}_p &= \sigma_{kk} \mathbf{k} \otimes \mathbf{k} + \sigma_{ll} \mathbf{l} \otimes \mathbf{l} + \tau_{kl} (\mathbf{k} \otimes \mathbf{l} + \mathbf{l} \otimes \mathbf{k}) \end{aligned}$$

The plane part of the stress tensor can be further decomposed as follows

$$\boldsymbol{\sigma}_p = \mathbf{s}_p + \frac{1}{2} \text{tr} \boldsymbol{\sigma}_p (\mathbf{I} - \mathbf{m} \otimes \mathbf{m}), \quad \text{tr} \mathbf{s}_p = 0 \tag{5.4.132}$$

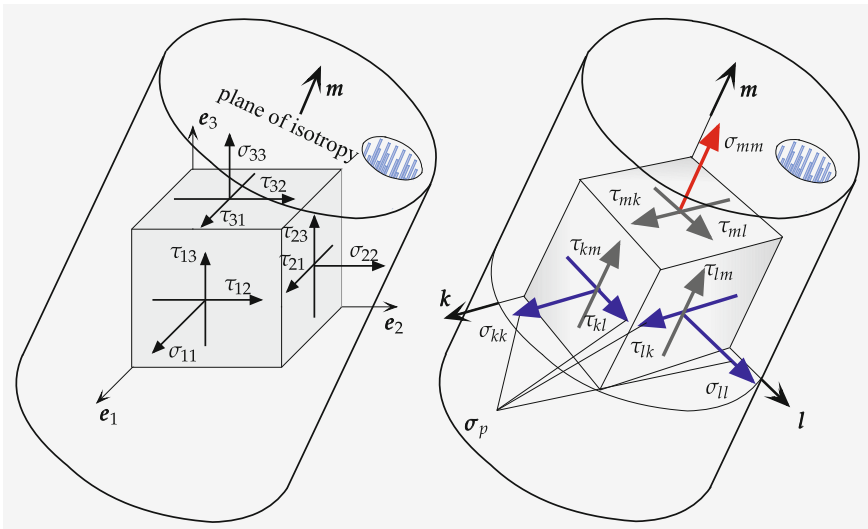


Fig. 5.1 Stress state in a transversely isotropic medium with the preferential (fiber) direction \mathbf{m} and corresponding projections σ_{mm} , $\boldsymbol{\sigma}_p$ and $\boldsymbol{\tau}_m$

Now we can introduce the following set of transversely isotropic invariants

$$\begin{aligned}
 I_{1m} &= \sigma_{mm} = \mathbf{m} \cdot \boldsymbol{\sigma} \cdot \mathbf{m}, \\
 I_{2m} &= \text{tr } \boldsymbol{\sigma}_p = \text{tr } \boldsymbol{\sigma} - \mathbf{m} \cdot \boldsymbol{\sigma} \cdot \mathbf{m}, \\
 I_{3m} &= \frac{1}{2} \text{tr } \mathbf{s}_p^2 = \frac{1}{2} \text{tr } \boldsymbol{\sigma}_p^2 - \frac{1}{4} (\text{tr } \boldsymbol{\sigma}_p)^2 \\
 &= \frac{1}{2} (\text{tr } \boldsymbol{\sigma}^2 + (\mathbf{m} \cdot \boldsymbol{\sigma} \cdot \mathbf{m})^2) - \mathbf{m} \cdot \boldsymbol{\sigma}^2 \cdot \mathbf{m} - \frac{1}{4} (\text{tr } \boldsymbol{\sigma} - \mathbf{m} \cdot \boldsymbol{\sigma} \cdot \mathbf{m})^2, \\
 I_{4m} &= \boldsymbol{\tau}_m \cdot \boldsymbol{\tau}_m = \mathbf{m} \cdot \boldsymbol{\sigma}^2 \cdot \mathbf{m} - (\mathbf{m} \cdot \boldsymbol{\sigma} \cdot \mathbf{m})^2 = (\mathbf{m} \times \boldsymbol{\sigma} \cdot \mathbf{m}) \cdot (\mathbf{m} \times \boldsymbol{\sigma} \cdot \mathbf{m})
 \end{aligned} \tag{5.4.133}$$

In the above list I_{2m} and I_{3m} are two invariants of $\boldsymbol{\sigma}_p$ and $I_{4m} = \boldsymbol{\tau}_m^2 = \boldsymbol{\tau}_m \cdot \boldsymbol{\tau}_m$ is the square of the length of the shear stress vector acting in the plane with the unit normal \mathbf{m} . It is shown in Appendix B.7 that the above invariants are integrals of Eq. (5.4.127).

Taking into account the relations

$$\begin{aligned}
 \frac{\partial I_{1m}}{\partial \boldsymbol{\sigma}} &= \mathbf{m} \otimes \mathbf{m}, & \frac{\partial I_{2m}}{\partial \boldsymbol{\sigma}} &= \mathbf{I} - \mathbf{m} \otimes \mathbf{m}, \\
 \frac{\partial I_{3m}}{\partial \boldsymbol{\sigma}} &= \mathbf{s}_p, & \frac{\partial I_{4m}}{\partial \boldsymbol{\sigma}} &= \boldsymbol{\tau}_m \otimes \mathbf{m} + \mathbf{m} \otimes \boldsymbol{\tau}_m
 \end{aligned}$$

and the flow rule (5.4.96) we obtain the following creep equation

$$\begin{aligned}
 \mathbf{D} &= \frac{\partial W}{\partial I_{1m}} \mathbf{m} \otimes \mathbf{m} + \frac{\partial W}{\partial I_{2m}} (\mathbf{I} - \mathbf{m} \otimes \mathbf{m}) + \frac{\partial W}{\partial I_{3m}} \mathbf{s}_p \\
 &+ \frac{\partial W}{\partial I_{4m}} (\boldsymbol{\tau}_m \otimes \mathbf{m} + \mathbf{m} \otimes \boldsymbol{\tau}_m)
 \end{aligned} \tag{5.4.134}$$

The next assumption of the classical theory is the zero volumetric creep rate. Taking the trace of Eq. (5.4.134) we obtain

$$\text{tr } \mathbf{D} = \frac{\partial W}{\partial I_{1m}} + 2 \frac{\partial W}{\partial I_{2m}} = 0 \quad \Rightarrow \quad W = W(I_{1m} - \frac{1}{2} I_{2m}, I_{3m}, I_{4m}) \tag{5.4.135}$$

Introducing the notation

$$J_m \equiv I_{1m} - \frac{1}{2} I_{2m} = \mathbf{m} \cdot \boldsymbol{\sigma} \cdot \mathbf{m} - \frac{1}{2} \text{tr } \boldsymbol{\sigma}_p$$

the creep equation (5.4.134) takes the form

$$\mathbf{D} = \mathbf{d} = \frac{1}{2} \frac{\partial W}{\partial J_m} (3\mathbf{m} \otimes \mathbf{m} - \mathbf{I}) + \frac{\partial W}{\partial I_{3m}} \mathbf{s}_p + \frac{\partial W}{\partial I_{4m}} (\boldsymbol{\tau}_m \otimes \mathbf{m} + \mathbf{m} \otimes \boldsymbol{\tau}_m) \tag{5.4.136}$$

By analogy to the isotropic case we formulate the equivalent stress as follows

$$\begin{aligned}\sigma_{\text{eq}}^2 &= \alpha_1 J_m^2 + 3\alpha_2 I_{3m} + 3\alpha_3 I_{4m} \\ &= \alpha_1 \left(\mathbf{m} \cdot \boldsymbol{\sigma} \cdot \mathbf{m} - \frac{1}{2} \text{tr} \boldsymbol{\sigma}_p \right)^2 + \frac{3}{2} \alpha_2 \text{tr} \mathbf{s}_p^2 + 3\alpha_3 \tau_m^2\end{aligned}\quad (5.4.137)$$

The positive definiteness of the quadratic form (5.4.137) is provided by the conditions $\alpha_i > 0$, $i = 1, 2, 3$. The deviatoric part \mathbf{s} of the stress tensor and its second invariant can be computed by

$$\begin{aligned}\mathbf{s} &= J_m \left(\mathbf{m} \otimes \mathbf{m} - \frac{1}{3} \mathbf{I} \right) + \mathbf{s}_p + \boldsymbol{\tau}_m \otimes \mathbf{m} + \mathbf{m} \otimes \boldsymbol{\tau}_m, \\ \text{tr} \mathbf{s}^2 &= \frac{2}{3} J_m^2 + \text{tr} \mathbf{s}_p^2 + 2\tau_m^2\end{aligned}$$

Consequently, the von Mises equivalent stress (5.4.104) follows from Eq. (5.4.137) by setting $\alpha_1 = \alpha_2 = \alpha_3 = 1$.

The advantage of the introduced invariants over (5.4.128) or (5.4.129) is that they can be specified independently from each other. For example, set the second invariant in Eq. (5.4.128) to zero, i.e. $\text{tr} \boldsymbol{\sigma}^2 = \boldsymbol{\sigma} \cdot \boldsymbol{\sigma} = 0$. From this follows that $\boldsymbol{\sigma} = \mathbf{0}$ and consequently all other invariants listed in Eq. (5.4.128) are simultaneously equal to zero. In addition, the introduced invariants can be related to typical stress states which should be realized in creep tests for the identification of constitutive functions and material constants. With the equivalent stress (5.4.137) the creep equation (5.4.136) can be rewritten as follows

$$\mathbf{d} = \frac{3}{2\sigma_{\text{eq}}} \frac{\partial W}{\partial \sigma_{\text{eq}}} \left[\alpha_1 J_m \left(\mathbf{m} \otimes \mathbf{m} - \frac{1}{3} \mathbf{I} \right) + \alpha_2 \mathbf{s}_p + \alpha_3 (\boldsymbol{\tau}_m \otimes \mathbf{m} + \mathbf{m} \otimes \boldsymbol{\tau}_m) \right] \quad (5.4.138)$$

With the notation $\dot{\varepsilon}_{\text{eq}} \equiv \frac{\partial W}{\partial \sigma_{\text{eq}}}$ Eq. (5.4.138) takes the form

$$\mathbf{d} = \frac{3}{2} \frac{\dot{\varepsilon}_{\text{eq}}}{\sigma_{\text{eq}}} \left[\alpha_1 J_m \left(\mathbf{m} \otimes \mathbf{m} - \frac{1}{3} \mathbf{I} \right) + \alpha_2 \mathbf{s}_p + \alpha_3 (\boldsymbol{\tau}_m \otimes \mathbf{m} + \mathbf{m} \otimes \boldsymbol{\tau}_m) \right] \quad (5.4.139)$$

Let us introduce the following parts of the creep rate tensor

$$\begin{aligned}d_{mm} &\equiv \mathbf{m} \cdot \mathbf{d} \cdot \mathbf{m}, \\ \mathbf{D}_p &\equiv (\mathbf{I} - \mathbf{m} \otimes \mathbf{m}) \cdot \mathbf{d} (\mathbf{I} - \mathbf{m} \otimes \mathbf{m}), \\ \mathbf{d}_p &\equiv \mathbf{D}_p - \frac{1}{2} d_{mm} (\mathbf{I} - \mathbf{m} \otimes \mathbf{m}), \\ \boldsymbol{\gamma}_m &\equiv \mathbf{m} \cdot \mathbf{d} \cdot (\mathbf{I} - \mathbf{m} \otimes \mathbf{m})\end{aligned}\quad (5.4.140)$$

From Eq. (5.4.138) we obtain

$$d_{mm} = \alpha_1 \frac{\dot{\epsilon}_{\text{eq}}}{\sigma_{\text{eq}}} J_m, \quad \mathbf{d}_p = \frac{3}{2} \alpha_2 \frac{\dot{\epsilon}_{\text{eq}}}{\sigma_{\text{eq}}} \mathbf{s}_p, \quad \boldsymbol{\gamma}_m = \frac{3}{2} \alpha_3 \frac{\dot{\epsilon}_{\text{eq}}}{\sigma_{\text{eq}}} \boldsymbol{\tau}_m \quad (5.4.141)$$

Similarly to the isotropic case the equivalent creep rate can be calculated as follows

$$\dot{\epsilon}_{\text{eq}} = \sqrt{\frac{1}{\alpha_1} d_{mm}^2 + \frac{2}{3} \frac{1}{\alpha_2} \mathbf{d}_p \cdot \mathbf{d}_p + \frac{4}{3} \frac{1}{\alpha_3} \boldsymbol{\gamma}_m \cdot \boldsymbol{\gamma}_m} \quad (5.4.142)$$

The equivalent creep rate (5.4.142) is useful for the verification of the creep potential hypothesis and the assumed quadratic form of the equivalent stress with respect to the transversely isotropic invariants of the stress tensor. The introduced creep equation contains three material constants α_i and the equivalent creep rate $\dot{\epsilon}_{\text{eq}}$.

The assumptions of transverse isotropy and the quadratic form of the equivalent stress are widely used in models of elasticity, plasticity, creep and failure of fiber reinforced composites, e.g. Altenbach et al. (1996), Boehler (1987d), Robinson et al. (2003a, b), Rogers (1990), Spencer (1984), directionally solidified superalloys (Bernhardi and Mücke 2000; Mücke and Bernhardi 2003), forged alloys, e.g. Naumenko and Gariboldi (2014) and multi-pass weld metals (Naumenko and Altenbach 2005; Lvov et al. 2014).

Orthotropic Symmetry

In this case the potential $W(\boldsymbol{\sigma})$ must satisfy the following restriction

$$W(\mathbf{Q}_i \cdot \boldsymbol{\sigma} \cdot \mathbf{Q}_i^T) = W(\boldsymbol{\sigma}), \quad \mathbf{Q}_i = \mathbf{I} - 2\mathbf{n}_i \otimes \mathbf{n}_i, \quad i = 1, 2, 3 \quad (5.4.143)$$

In (5.4.143) \mathbf{Q}_i denote the assumed symmetry elements—three reflections with respect to the planes with unit normals $\pm \mathbf{n}_i$, Fig. 5.2. The unit vectors $\pm \mathbf{n}_1$, $\pm \mathbf{n}_2$, $\pm \mathbf{n}_3$ are assumed to be orthogonal, i.e. $\mathbf{n}_i \cdot \mathbf{n}_j = 0$, $i \neq j$. In Appendix B.8 the sets of scalar arguments which satisfy the above restrictions are presented. As in the previous paragraph we assume the quadratic form of the potential with respect to the stress tensor. One can use different sets of scalar arguments of the stress tensor satisfying (5.4.143), see, for example, Boehler (1987c),

$$\begin{aligned} & \mathbf{n}_1 \cdot \boldsymbol{\sigma} \cdot \mathbf{n}_1, \quad \mathbf{n}_2 \cdot \boldsymbol{\sigma} \cdot \mathbf{n}_2, \quad \mathbf{n}_3 \cdot \boldsymbol{\sigma} \cdot \mathbf{n}_3, \\ & \mathbf{n}_1 \cdot \boldsymbol{\sigma}^2 \cdot \mathbf{n}_1, \quad \mathbf{n}_2 \cdot \boldsymbol{\sigma}^2 \cdot \mathbf{n}_2, \quad \mathbf{n}_3 \cdot \boldsymbol{\sigma}^2 \cdot \mathbf{n}_3 \end{aligned}$$

Figure 5.2 shows the components of the stress tensor in a Cartesian frame \mathbf{e}_i , three planes of symmetry characterized by the unit vectors $\pm \mathbf{n}_i$ and components of the stress tensor with respect to the planes of symmetry. The stress tensor can be represented as follows

$$\begin{aligned} \boldsymbol{\sigma} = & \sigma_{\mathbf{n}_1 \mathbf{n}_1} \mathbf{n}_1 \otimes \mathbf{n}_1 + \sigma_{\mathbf{n}_2 \mathbf{n}_2} \mathbf{n}_2 \otimes \mathbf{n}_2 + \sigma_{\mathbf{n}_3 \mathbf{n}_3} \mathbf{n}_3 \otimes \mathbf{n}_3 \\ & + \tau_{\mathbf{n}_1 \mathbf{n}_2} (\mathbf{n}_1 \otimes \mathbf{n}_2 + \mathbf{n}_2 \otimes \mathbf{n}_1) + \tau_{\mathbf{n}_1 \mathbf{n}_3} (\mathbf{n}_1 \otimes \mathbf{n}_3 + \mathbf{n}_3 \otimes \mathbf{n}_1) \\ & + \tau_{\mathbf{n}_2 \mathbf{n}_3} (\mathbf{n}_2 \otimes \mathbf{n}_3 + \mathbf{n}_3 \otimes \mathbf{n}_2) \end{aligned}$$

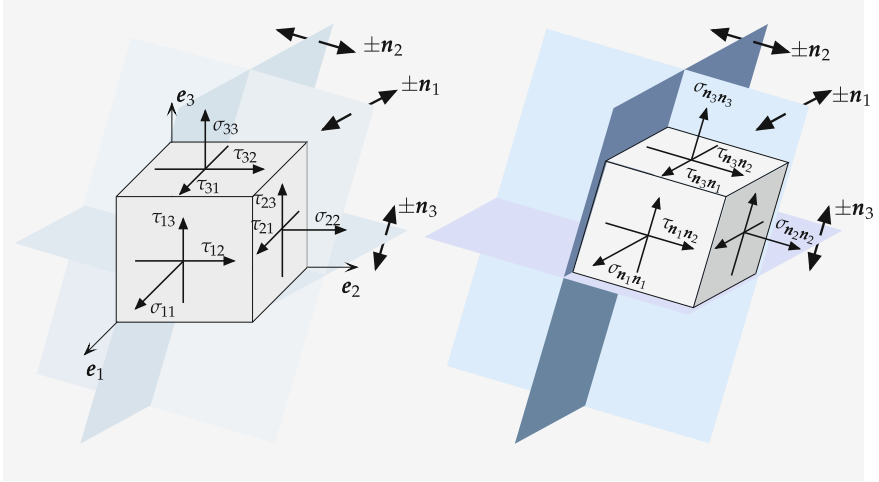


Fig. 5.2 Stress state in an orthotropic medium with the symmetry planes \mathbf{n}_i . Components of the stress tensor σ_{ij} in a basis \mathbf{e}_i and corresponding projections $\sigma_{\mathbf{n}_i \mathbf{n}_i}$, $\tau_{\mathbf{n}_i \mathbf{n}_j}$

with

$$\begin{aligned} \sigma_{\mathbf{n}_1 \mathbf{n}_1} &= \mathbf{n}_1 \cdot \boldsymbol{\sigma} \cdot \mathbf{n}_1, \quad \sigma_{\mathbf{n}_2 \mathbf{n}_2} = \mathbf{n}_2 \cdot \boldsymbol{\sigma} \cdot \mathbf{n}_2, \quad \sigma_{\mathbf{n}_3 \mathbf{n}_3} = \mathbf{n}_3 \cdot \boldsymbol{\sigma} \cdot \mathbf{n}_3, \\ \tau_{\mathbf{n}_1 \mathbf{n}_2} &= \mathbf{n}_1 \cdot \boldsymbol{\sigma} \cdot \mathbf{n}_2, \quad \tau_{\mathbf{n}_1 \mathbf{n}_3} = \mathbf{n}_1 \cdot \boldsymbol{\sigma} \cdot \mathbf{n}_3, \quad \tau_{\mathbf{n}_2 \mathbf{n}_3} = \mathbf{n}_2 \cdot \boldsymbol{\sigma} \cdot \mathbf{n}_3 \end{aligned}$$

According to Appendix B.8 we use the following orthotropic invariants of the stress tensor

$$\begin{aligned} I_{\mathbf{n}_1 \mathbf{n}_1} &= \sigma_{\mathbf{n}_1 \mathbf{n}_1}, \quad I_{\mathbf{n}_2 \mathbf{n}_2} = \sigma_{\mathbf{n}_2 \mathbf{n}_2}, \quad I_{\mathbf{n}_3 \mathbf{n}_3} = \sigma_{\mathbf{n}_3 \mathbf{n}_3}, \\ I_{\mathbf{n}_1 \mathbf{n}_2} &= \tau_{\mathbf{n}_1 \mathbf{n}_2}^2, \quad I_{\mathbf{n}_1 \mathbf{n}_3} = \tau_{\mathbf{n}_1 \mathbf{n}_3}^2, \quad I_{\mathbf{n}_2 \mathbf{n}_3} = \tau_{\mathbf{n}_2 \mathbf{n}_3}^2 \end{aligned} \quad (5.4.144)$$

Assuming that the creep potential is a function of six arguments introduced, the flow rule (5.4.96) leads to the following creep equation

$$\begin{aligned} \mathbf{D} &= \frac{\partial W}{\partial I_{\mathbf{n}_1 \mathbf{n}_1}} \mathbf{n}_1 \otimes \mathbf{n}_1 + \frac{\partial W}{\partial I_{\mathbf{n}_2 \mathbf{n}_2}} \mathbf{n}_2 \otimes \mathbf{n}_2 + \frac{\partial W}{\partial I_{\mathbf{n}_3 \mathbf{n}_3}} \mathbf{n}_3 \otimes \mathbf{n}_3 \\ &+ \frac{\partial W}{\partial I_{\mathbf{n}_1 \mathbf{n}_2}} \mathbf{n}_1 \cdot \boldsymbol{\sigma} \cdot \mathbf{n}_2 (\mathbf{n}_1 \otimes \mathbf{n}_2 + \mathbf{n}_2 \otimes \mathbf{n}_1) \\ &+ \frac{\partial W}{\partial I_{\mathbf{n}_1 \mathbf{n}_3}} \mathbf{n}_1 \cdot \boldsymbol{\sigma} \cdot \mathbf{n}_3 (\mathbf{n}_1 \otimes \mathbf{n}_3 + \mathbf{n}_3 \otimes \mathbf{n}_1) \\ &+ \frac{\partial W}{\partial I_{\mathbf{n}_2 \mathbf{n}_3}} \mathbf{n}_2 \cdot \boldsymbol{\sigma} \cdot \mathbf{n}_3 (\mathbf{n}_2 \otimes \mathbf{n}_3 + \mathbf{n}_3 \otimes \mathbf{n}_2) \end{aligned} \quad (5.4.145)$$

The assumption of zero volumetric creep rate leads to

$$\text{tr } \mathbf{D} = \frac{\partial W}{\partial I_{\mathbf{n}_1 \mathbf{n}_1}} + \frac{\partial W}{\partial I_{\mathbf{n}_2 \mathbf{n}_2}} + \frac{\partial W}{\partial I_{\mathbf{n}_3 \mathbf{n}_3}} = 0 \quad (5.4.146)$$

From the partial differential equation (5.4.146) follows that the potential W is a function of five scalar arguments of the stress tensor. The characteristic system of (5.4.146) is

$$\frac{dI_{n_1n_1}}{ds} = 1, \quad \frac{dI_{n_2n_2}}{ds} = 1, \quad \frac{dI_{n_3n_3}}{ds} = 1 \quad (5.4.147)$$

The above system of three ordinary differential equations has two independent integrals. One can verify that the following invariants

$$J_1 = \frac{1}{2}(I_{n_2n_2} - I_{n_3n_3}), \quad J_2 = \frac{1}{2}(I_{n_3n_3} - I_{n_1n_1}), \quad J_3 = \frac{1}{2}(I_{n_1n_1} - I_{n_2n_2}) \quad (5.4.148)$$

are integrals of (5.4.147). Only two of them are independent due to the relation $J_1 + J_2 + J_3 = 0$. If the principal directions of the stress tensor coincide with the directions \mathbf{n}_i then $\tau_{n_i n_j} = 0, i \neq j$ and the above invariants represent the principal shear stresses. An alternative set of integrals of (5.4.147) is

$$\tilde{J}_1 = I_{n_1n_1} - \frac{1}{3}\text{tr } \boldsymbol{\sigma}, \quad \tilde{J}_2 = I_{n_2n_2} - \frac{1}{3}\text{tr } \boldsymbol{\sigma}, \quad \tilde{J}_3 = I_{n_3n_3} - \frac{1}{3}\text{tr } \boldsymbol{\sigma} \quad (5.4.149)$$

If the principal directions of the stress tensor coincide with \mathbf{n}_i then the above invariants are the principal values of the stress deviator. For the formulation of the creep potential in terms of invariants the relation $\tilde{J}_1 + \tilde{J}_2 + \tilde{J}_3 = 0$ must be taken into account.

In what follows we apply the invariants (5.4.148). The equivalent stress can be formulated as follows

$$\sigma_{\text{eq}}^2 = 2\beta_1 J_1^2 + 2\beta_2 J_2^2 + 2\beta_3 J_3^2 + 3\beta_{12} I_{n_1n_2} + 3\beta_{13} I_{n_1n_3} + 3\beta_{23} I_{n_2n_3} \quad (5.4.150)$$

The von Mises equivalent stress (5.4.104) follows from Eq. (5.4.150) by setting $\beta_1 = \beta_2 = \beta_3 = \beta_{12} = \beta_{13} = \beta_{23} = 1$. Applying the flow rule (5.4.96) we obtain the following creep equation

$$\begin{aligned} \mathbf{d} = \frac{\dot{\epsilon}_{\text{eq}}}{\sigma_{\text{eq}}} & \left[\beta_1 J_1 (\mathbf{n}_2 \otimes \mathbf{n}_2 - \mathbf{n}_3 \otimes \mathbf{n}_3) \right. \\ & + \beta_2 J_2 (\mathbf{n}_3 \otimes \mathbf{n}_3 - \mathbf{n}_1 \otimes \mathbf{n}_1) \\ & + \beta_3 J_3 (\mathbf{n}_1 \otimes \mathbf{n}_1 - \mathbf{n}_2 \otimes \mathbf{n}_2) \\ & + \frac{3}{2} \beta_{12} \tau_{n_1 n_2} (\mathbf{n}_1 \otimes \mathbf{n}_2 + \mathbf{n}_2 \otimes \mathbf{n}_1) \\ & + \frac{3}{2} \beta_{13} \tau_{n_1 n_3} (\mathbf{n}_1 \otimes \mathbf{n}_3 + \mathbf{n}_3 \otimes \mathbf{n}_1) \\ & \left. + \frac{3}{2} \beta_{23} \tau_{n_2 n_3} (\mathbf{n}_2 \otimes \mathbf{n}_3 + \mathbf{n}_3 \otimes \mathbf{n}_2) \right] \end{aligned} \quad (5.4.151)$$

The equivalent stress and the creep equation includes six independent material parameters. Therefore six independent homogeneous stress states should be realized in order to identify the whole set of constants. In addition, the dependence of the creep rate on the equivalent stress must be fitted from the results of uni-axial creep tests for different constant stress values. For example, if the power law stress function provides a satisfactory description of steady-state creep then the constant n must be additionally identified.

An example of orthotropic creep is discussed in Konkin and Morachkovskij (1987) for the aluminium alloy D16AT. Plane specimens were removed from rolled sheet along three directions: the rolling direction, the transverse direction as well as under the angle of 45° to the rolling direction. Uni-axial creep tests were performed at 273°C and 300°C within the stress range 63-90 MPa. The results have shown that at 273°C creep curves depend on the loading direction while at 300°C the creep behavior is isotropic.

General Case of Quadratic Potential

The previous models are based on the assumption of the quadratic form of the creep potential with respect to the stress tensor. The most general quadratic form can be formulated as follows

$$\sigma_{\text{eq}}^2 = \frac{3}{2} \boldsymbol{\sigma} \cdot \cdot {}^{(4)}\mathbf{B} \cdot \cdot \boldsymbol{\sigma}, \quad (5.4.152)$$

where σ_{eq} plays the role of the equivalent stress. The fourth rank tensor ${}^{(4)}\mathbf{B}$ must satisfy the following restrictions

$$\begin{aligned} \mathbf{a} \cdot \cdot {}^{(4)}\mathbf{B} \cdot \cdot \mathbf{a} \geq 0, \quad \mathbf{a} \cdot \cdot {}^{(4)}\mathbf{B} = {}^{(4)}\mathbf{B} \cdot \cdot \mathbf{a}, \quad \mathbf{c} \cdot \cdot {}^{(4)}\mathbf{B} = \mathbf{0}, \\ \forall \mathbf{a}, \mathbf{c} \text{ with } \mathbf{a} = \mathbf{a}^T, \quad \mathbf{c} = -\mathbf{c}^T, \end{aligned} \quad (5.4.153)$$

where \mathbf{a} and \mathbf{c} are second rank tensors. Additional restrictions follow from the assumed symmetries of the steady-state creep behavior. For example, if the orthogonal tensor \mathbf{Q} stands for a symmetry element, the structure of the tensor ${}^{(4)}\mathbf{B}$ can be established from the following equation

$${}^{(4)}\mathbf{B}' = B^{ijkl} \mathbf{Q} \cdot \mathbf{e}_i \otimes \mathbf{Q} \cdot \mathbf{e}_j \otimes \mathbf{Q} \cdot \mathbf{e}_k \otimes \mathbf{Q} \cdot \mathbf{e}_l = {}^{(4)}\mathbf{B}, \quad (5.4.154)$$

where $\mathbf{e}_i, i = 1, 2, 3$ are basis vectors.

The flow rule (5.4.96) provides the following generalized anisotropic creep equation

$$\mathbf{D} = \frac{3}{2} \frac{\dot{\varepsilon}_{\text{eq}}}{\sigma_{\text{eq}}} {}^{(4)}\mathbf{B} \cdot \cdot \boldsymbol{\sigma}, \quad \dot{\varepsilon}_{\text{eq}} \equiv \frac{\partial W}{\partial \sigma_{\text{eq}}} \quad (5.4.155)$$

The fourth rank tensors satisfying the restrictions (5.4.153) are well-known from the theory of linear elasticity. They are used to represent elastic material properties in the generalized Hooke's law, see Sect. 5.3.4.

Let us recall that (5.4.155) is the consequence of the flow potential hypothesis and the quadratic form of the equivalent stress with respect to the stress tensor. Similarly to the case of linear elasticity (Ting 1996) one can prove that only eight basic symmetry classes are relevant according to these assumptions. The basic symmetry classes and the corresponding number of independent coordinates are listed in Table 5.1. The number of independent coordinates indicates the number of material properties which should be identified from creep tests. This number can be reduced if the volume constancy is additionally assumed. For example, in the cases of transverse isotropy and orthotropic symmetry the number of independent coordinates of \mathbf{B} reduces to 3 and 5, respectively (see previous paragraphs).

Cubic Symmetry

As in the previous cases the creep potential can be assumed as an isotropic function of the stress tensor and a system of direction tensors associated with the orientation of the materials microstructure. For example, consider the point group O_h (the symmetry group of the FCC lattice). The creep potential should be formulated as an isotropic function of the following two arguments

$$W = W(\boldsymbol{\sigma}, \mathbb{O}), \quad \mathbb{O} = \sum_{i=1}^3 \mathbf{n}_i \otimes \mathbf{n}_i \otimes \mathbf{n}_i \otimes \mathbf{n}_i, \quad (5.4.156)$$

where the fourth-rank tensor \mathbb{O} is the structure tensor for O_h , as shown in Lokhin and Sedov (1963) and \mathbf{n}_i is the orthonormal basis of the crystal lattice. With the theory of isotropic scalar-valued tensor functions it is possible to derive a system of independent arguments of W corresponding to the given symmetry group. Here let us consider the quadratic form of the creep potential. For materials with the cubic symmetry the tensor $^{(4)}\mathbf{B}$ can be specified as follows (Bertram and Olschewski 1996, 2001; Mahnken 2002)

$$^{(4)}\mathbf{B} = \alpha_1 \mathbb{P}_1 + \alpha_2 \mathbb{P}_2 + \alpha_3 \mathbb{P}_3, \quad (5.4.157)$$

where α_i are material parameters and

$$\begin{aligned} \mathbb{P}_1 &= \frac{1}{3} \mathbf{I} \otimes \mathbf{I}, \quad \mathbb{P}_2 = \sum_{i=1}^3 \mathbf{n}_i \otimes \mathbf{n}_i \otimes \mathbf{n}_i \otimes \mathbf{n}_i - \mathbb{P}_1, \quad \mathbb{P}_3 = \mathbb{I} - \mathbb{P}_1 - \mathbb{P}_2, \\ \mathbb{I} &= \frac{1}{2} [\mathbf{n}_i \otimes \mathbf{I} \otimes \mathbf{n}^i + \mathbf{n}_i \otimes \mathbf{n}^j \otimes \mathbf{n}_i \otimes \mathbf{n}^j] \end{aligned}$$

Inserting Eq. (5.4.157) into Eq. (5.4.155) we obtain

$$\mathbf{D} = \frac{3}{2} \frac{\dot{\epsilon}_{\text{eq}}}{\sigma_{\text{eq}}} \left(\sum_{i=1}^3 \alpha_i \mathbb{P}_i \right) \cdot \boldsymbol{\sigma} \quad (5.4.158)$$

With $\text{tr } \mathbf{D} = 0$ it follows that $\alpha_1 = 0$ and Eq. (5.4.158) simplifies to

$$\mathbf{D} = \mathbf{d} = \frac{3}{2} \frac{\dot{\epsilon}_{\text{eq}}}{\sigma_{\text{eq}}} \left(\sum_{i=2}^3 \alpha_i \mathbb{P}_i \right) \cdot \boldsymbol{\sigma}, \quad \sigma_{\text{eq}}^2 = \frac{3}{2} \boldsymbol{\sigma} \cdot \left(\sum_{i=2}^3 \alpha_i \mathbb{P}_i \right) \cdot \boldsymbol{\sigma} \quad (5.4.159)$$

Assuming the power law creep and with $\xi = \alpha_3/\alpha_2$, Eqs. (5.4.159) can also be specified as follows

$$\mathbf{d} = \frac{3}{2} a \alpha_2 \sigma_{\text{eq}}^n (\mathbb{P}_2 + \xi \mathbb{P}_3) \cdot \boldsymbol{\sigma}, \quad \sigma_{\text{eq}}^2 = \frac{3}{2} \alpha_2 \boldsymbol{\sigma} \cdot (\mathbb{P}_2 + \xi \mathbb{P}_3) \cdot \boldsymbol{\sigma}, \quad (5.4.160)$$

where a and n are material parameters. The parameter α_2 can be selected arbitrarily. For example one may set $\alpha_2 = 1$. For $\xi = 1$ Eq. (5.4.155) provides the creep constitutive equation (5.4.106) for isotropic materials. Equation (5.4.160) can also be written as follows

$$\begin{aligned} \mathbf{d} = & \frac{3}{2} a \sigma_{\text{eq}}^{n-1} \left[\sigma_{\mathbf{n}_1 \mathbf{n}_1} \left(\mathbf{n}_1 \otimes \mathbf{n}_1 - \frac{1}{3} \mathbf{I} \right) + \sigma_{\mathbf{n}_2 \mathbf{n}_2} \left(\mathbf{n}_2 \otimes \mathbf{n}_2 - \frac{1}{3} \mathbf{I} \right) \right. \\ & + \sigma_{\mathbf{n}_3 \mathbf{n}_3} \left(\mathbf{n}_3 \otimes \mathbf{n}_3 - \frac{1}{3} \mathbf{I} \right) + \xi \sigma_{\mathbf{n}_1 \mathbf{n}_2} \left(\mathbf{n}_1 \otimes \mathbf{n}_2 + \mathbf{n}_2 \otimes \mathbf{n}_1 \right) \\ & \left. + \xi \sigma_{\mathbf{n}_1 \mathbf{n}_3} \left(\mathbf{n}_1 \otimes \mathbf{n}_3 + \mathbf{n}_3 \otimes \mathbf{n}_1 \right) + \xi \sigma_{\mathbf{n}_2 \mathbf{n}_3} \left(\mathbf{n}_2 \otimes \mathbf{n}_3 + \mathbf{n}_3 \otimes \mathbf{n}_2 \right) \right], \end{aligned} \quad (5.4.161)$$

where

$$\begin{aligned} 2\sigma_{\text{eq}}^2 = & (\sigma_{\mathbf{n}_1 \mathbf{n}_1} - \sigma_{\mathbf{n}_2 \mathbf{n}_2})^2 + (\sigma_{\mathbf{n}_1 \mathbf{n}_1} - \sigma_{\mathbf{n}_3 \mathbf{n}_3})^2 + (\sigma_{\mathbf{n}_2 \mathbf{n}_2} - \sigma_{\mathbf{n}_3 \mathbf{n}_3})^2 \\ & + 6\xi (\sigma_{\mathbf{n}_1 \mathbf{n}_2}^2 + \sigma_{\mathbf{n}_2 \mathbf{n}_2}^2 + \sigma_{\mathbf{n}_1 \mathbf{n}_3}^2) \end{aligned} \quad (5.4.162)$$

and

$$\sigma_{\mathbf{n}_i \mathbf{n}_j} = \mathbf{n}_i \cdot \boldsymbol{\sigma} \cdot \mathbf{n}_j$$

Equation (5.4.161) is applied in Ozhoga-Maslovskaja (2014), Ozhoga-Maslovskaja et al. (2015) to model creep of single crystal alloys as well as for creep inside individual grains in polycrystalline aggregates.

5.4.3.2 Non-quadratic Potentials

Non-quadratic potential can be used to capture the dependence of inelastic deformation rate on the kind of loading as well as second order effects as discussed in Sect. 5.4.2.2 for isotropic materials. Examples of such behavior are different creep rates under tensile and compressive stress or the effect of reversal of the shear stress.

The last case is observed in creep tests on tubular specimens under applied torque. The change of the direction of the applied torque leads to different values of the shear strain rate. The effect of shear stress reversal is usually explained to be the result of the anisotropy induced by the deformation process (e.g. anisotropic hardening) or anisotropy induced by damage evolution. Phenomenological models of induced anisotropy will be introduced in Sects. 5.3.2 and 5.5. Here we consider the case of initial anisotropy without analysis of deformation, damage or manufacturing process histories. Nevertheless, a phenomenological model of anisotropic creep should be able to reflect the above mentioned effects once they are observed experimentally. In order to describe non-classical effects the quadratic form of the creep potential should be replaced by a more general form including all invariants of the stress tensor for the assumed symmetry group. In this case the number of material parameters increases essentially. Furthermore, the identification and verification of the model requires creep tests under combined multi-axial stress states. In what follows we limit ourselves to some remarks regarding the general structure of constitutive equations and kinds of tests for the identification.

Transverse Isotropy

The creep potential must satisfy the restriction (5.4.125) leading to the partial differential equation (5.4.126). The integrals represent the set of functionally independent arguments of the creep potential. They are listed in Appendix B.7 for two transverse isotropy groups. The first group is formed by all the rotations about a given axis \mathbf{m} , i.e.

$$\mathcal{Q}(\psi \mathbf{m}) = \mathbf{m} \otimes \mathbf{m} + \cos \psi (\mathbf{I} - \mathbf{m} \otimes \mathbf{m}) + \sin \psi \mathbf{m} \times \mathbf{I}$$

The second group additionally includes rotations on the angle π about any axis orthogonal to \mathbf{m} , i.e.

$$\mathcal{Q}_1 = \mathcal{Q}(\pi \mathbf{p}) = 2\mathbf{p} \otimes \mathbf{p} - \mathbf{I}, \quad \det \mathcal{Q} = 1, \quad \mathbf{p} \cdot \mathbf{m} = 0$$

Let us note that there is an essential difference in these two groups since the creep potential depends on different non-quadratic arguments of the stress tensor. Here we limit our considerations to the second case which is widely discussed in the literature on anisotropic elasticity, plasticity and creep (Betten 2008; Boehler 1987c; Cazacu and Barlat 2003; Rogers 1990; Schröder and Neff 2003), where the following invariants are applied¹²

$$\text{tr } \boldsymbol{\sigma}, \quad \text{tr } \boldsymbol{\sigma}^2, \quad \text{tr } \boldsymbol{\sigma}^3, \quad \mathbf{m} \cdot \boldsymbol{\sigma} \cdot \mathbf{m}, \quad \mathbf{m} \cdot \boldsymbol{\sigma}^2 \cdot \mathbf{m} \quad (5.4.163)$$

To be consistent with derivations presented in Sect. 5.4.3.1 let us use the decomposition of the stress tensor (5.4.130) and the following set of invariants

¹²For the description of elastic material behavior instead of $\boldsymbol{\sigma}$ a strain tensor, e.g. the Cauchy-Green strain tensor is introduced. The five transversely isotropic invariants are the arguments of the strain energy density function, see Sect. 5.3.3.

$$\begin{aligned}
I_{1m} &= \sigma_{mm} = \mathbf{m} \cdot \boldsymbol{\sigma} \cdot \mathbf{m}, \\
I_{2m} &= \text{tr } \boldsymbol{\sigma}_p = \text{tr } \boldsymbol{\sigma} - \mathbf{m} \cdot \boldsymbol{\sigma} \cdot \mathbf{m}, \\
I_{3m} &= \frac{1}{2} \text{tr } \boldsymbol{s}_p^2 = \frac{1}{2} \text{tr } \boldsymbol{\sigma}_p^2 - \frac{1}{4} (\text{tr } \boldsymbol{\sigma}_p)^2 \\
&= \frac{1}{2} [\text{tr } \boldsymbol{\sigma}^2 + (\mathbf{m} \cdot \boldsymbol{\sigma} \cdot \mathbf{m})^2] - \mathbf{m} \cdot \boldsymbol{\sigma}^2 \cdot \mathbf{m} - \frac{1}{4} (\text{tr } \boldsymbol{\sigma} - \mathbf{m} \cdot \boldsymbol{\sigma} \cdot \mathbf{m})^2, \\
I_{4m} &= \boldsymbol{\tau}_m \cdot \boldsymbol{\tau}_m = \mathbf{m} \cdot \boldsymbol{\sigma}^2 \cdot \mathbf{m} - (\mathbf{m} \cdot \boldsymbol{\sigma} \cdot \mathbf{m})^2 = (\mathbf{m} \times \boldsymbol{\sigma} \cdot \mathbf{m}) \cdot (\mathbf{m} \times \boldsymbol{\sigma} \cdot \mathbf{m}) \\
I_{5m} &= \boldsymbol{\tau}_m \cdot \boldsymbol{s}_p \cdot \boldsymbol{\tau}_m = \mathbf{m} \cdot \boldsymbol{\sigma}^3 \cdot \mathbf{m} - 2(\mathbf{m} \cdot \boldsymbol{\sigma} \cdot \mathbf{m})(\mathbf{m} \cdot \boldsymbol{\sigma}^2 \cdot \mathbf{m}) \\
&\quad + (\mathbf{m} \cdot \boldsymbol{\sigma} \cdot \mathbf{m})^3 - \frac{1}{2} (\text{tr } \boldsymbol{\sigma} - \mathbf{m} \cdot \boldsymbol{\sigma} \cdot \mathbf{m}) [\mathbf{m} \cdot \boldsymbol{\sigma}^2 \cdot \mathbf{m} - (\mathbf{m} \cdot \boldsymbol{\sigma} \cdot \mathbf{m})^2]
\end{aligned} \tag{5.4.164}$$

The meaning of the first four invariants is explained in Sect. 5.4.3.1. The last cubic invariant is introduced instead $\text{tr } \boldsymbol{\sigma}^3$. One can prove the following relation

$$\text{tr } \boldsymbol{\sigma}^3 = I_{1m}^3 + 3I_{1m}I_{4m} + 3I_{2m}I_{3m} + \frac{3}{2}I_{2m}I_{4m} + \frac{1}{2}I_{2m}^3 + 3I_{5m}$$

Assuming that the creep potential W is a function of five scalar arguments (5.4.164) and applying the flow rule (5.4.96) we obtain the following creep equation

$$\begin{aligned}
\mathbf{D} &= h_1 \mathbf{m} \otimes \mathbf{m} + (h_2 - \frac{1}{2} h_5 I_{4m}) (\mathbf{I} - \mathbf{m} \otimes \mathbf{m}) + h_3 \boldsymbol{\sigma}_p + h_4 (\boldsymbol{\tau}_m \otimes \mathbf{m} + \mathbf{m} \otimes \boldsymbol{\tau}_m) \\
&\quad + h_5 (\boldsymbol{\tau}_m \otimes \boldsymbol{\tau}_m + \mathbf{m} \otimes \boldsymbol{\sigma}_p \cdot \boldsymbol{\tau}_m + \boldsymbol{\tau}_m \cdot \boldsymbol{\sigma}_p \otimes \mathbf{m}),
\end{aligned} \tag{5.4.165}$$

where

$$h_i = \frac{\partial W}{\partial I_{im}}, \quad i = 1, 2, \dots, 5$$

The last term in the right-hand side of Eq. (5.4.165) describes second order effects. To illustrate this consider a stress state with a non-zero ‘‘transverse shear stress’’ vector

$$\boldsymbol{\tau}_m = \mathbf{m} \cdot \boldsymbol{\sigma} \cdot (\mathbf{I} - \mathbf{m} \otimes \mathbf{m})$$

The last term in Eq. (5.4.165) includes a dyad $\boldsymbol{\tau}_m \otimes \boldsymbol{\tau}_m$. Therefore the deformation rate in the direction of $\boldsymbol{\tau}_m$ can be considered. The vector $\boldsymbol{\zeta}_m = \boldsymbol{s}_p \cdot \boldsymbol{\tau}_m$ belongs to the isotropy plane, i.e. $\boldsymbol{\zeta}_m \cdot \mathbf{m} = 0$. In the case that $\boldsymbol{\zeta}_m \neq \mathbf{0}$ Eq. (5.4.165) describes an additional ‘‘transverse shear strain rate’’ effect.

In order to formulate the creep constitutive equation one should specify an expression for the equivalent stress as a function of the introduced invariants. As an example we present the equivalent stress by use of polynomials of the type (5.4.108) and (5.4.109)

$$\sigma_{\text{eq}} = \alpha \sigma_1 + \sigma_2 + \gamma \sigma_3, \tag{5.4.166}$$

with

$$\begin{aligned}
 \sigma_1 &= \mu_{11} I_{1m} + \mu_{12} I_{2m}, \\
 \sigma_2^2 &= \mu_{21} I_{1m}^2 + \mu_{22} I_{1m} I_{2m} + \mu_{23} I_{2m}^2 + \mu_{24} I_{3m} + \mu_{25} I_{4m}, \\
 \sigma_3^3 &= \mu_{31} I_{1m}^3 + \mu_{32} I_{1m}^2 I_{2m} + \mu_{33} I_{1m} I_{2m}^2 + \mu_{34} I_{2m}^3 + \mu_{35} I_{1m} I_{3m} \\
 &\quad + \mu_{36} I_{2m} I_{3m} + \mu_{37} I_{1m} I_{4m} + \mu_{38} I_{2m} I_{4m} + \mu_{39} I_{5m}
 \end{aligned} \tag{5.4.167}$$

The equivalent stress (5.4.166) includes 16 material constants μ_{ij} and two weighting factors α and γ . The identification of all material constants requires different independent creep tests under multi-axial stress states. For example, in order to find the constant μ_{39} creep tests under stress states with nonzero cubic invariant I_{5m} should be carried out. An example is the tension in the isotropy plane combined with the transverse shear stress leading to the stress state of the type $\boldsymbol{\sigma} = \sigma_0 \mathbf{n}_1 \otimes \mathbf{n}_1 + \tau_0 (\mathbf{n}_1 \otimes \mathbf{m} + \mathbf{m} \otimes \mathbf{n}_1)$, where $\sigma_0 > 0$ and $\tau_0 > 0$ are the magnitudes of the applied stresses, \mathbf{n}_1 is the direction of tension and $\mathbf{n}_1 \cdot \mathbf{m} = 0$. In this case

$$\mathbf{s}_p = \frac{1}{2} \sigma_0 (\mathbf{n}_1 \otimes \mathbf{n}_1 - \mathbf{n}_2 \otimes \mathbf{n}_2), \quad \mathbf{n}_1 \cdot \mathbf{n}_2 = 0, \quad \boldsymbol{\tau}_m = \tau_0 \mathbf{n}_1, \quad I_{5m} = \frac{1}{2} \sigma_0 \tau_0^2$$

By analogy to non-quadratic potentials for isotropic materials discussed in Sect. 5.4.2.2 different special cases can be introduced. Setting $\gamma = 0$ in (5.4.167), second order effects will be neglected. The resulting constitutive model takes into account different behavior under tension and compression. To find the constants μ_{11} and μ_{12} creep tests under tension (compression) along the direction \mathbf{m} as well as tension (compression) along any direction in the isotropy plane should be carried out. Setting $\alpha = 0$ the model with the quadratic form of the creep potential with 5 constants can be obtained. The assumption of the zero volumetric creep rate would lead to the model discussed in Sect. 5.4.3.1.

Second order effects of anisotropic creep were discussed by Betten (1984, 2008). He found disagreements between creep equations based on the theory of isotropic functions and the creep equation of the type (5.4.165) according to the potential hypothesis and the flow rule. The conclusion was made that the potential theory leads to restrictive forms of constitutive equations if compared to the representations of tensor functions.

Let us recall the results following from the algebra of isotropic tensor functions (Boehler 1987a). In the case of transverse isotropy group characterized by the symmetry elements (B.7.31) the basic problem is to find the general representation of the isotropic tensor function of the stress tensor $\boldsymbol{\sigma}$ and the dyad $\mathbf{m} \otimes \mathbf{m}$ (structure tensor). The constitutive equation describing the creep behavior must be found as follows

$$\mathbf{D} = \mathbf{f}(\boldsymbol{\sigma}, \mathbf{m} \otimes \mathbf{m}),$$

where \mathbf{f} is an isotropic tensor function of two tensor arguments. The general representation of this function is Boehler (1987c)

$$\begin{aligned} \mathbf{f}(\boldsymbol{\sigma}, \mathbf{m} \otimes \mathbf{m}) = & f_1 \mathbf{m} \otimes \mathbf{m} + f_2 (\mathbf{I} - \mathbf{m} \otimes \mathbf{m}) + f_3 \boldsymbol{\sigma} + f_4 \boldsymbol{\sigma}^2 \\ & + f_5 (\mathbf{m} \otimes \mathbf{m} \cdot \boldsymbol{\sigma} + \boldsymbol{\sigma} \cdot \mathbf{m} \otimes \mathbf{m}) + f_6 (\mathbf{m} \otimes \mathbf{m} \cdot \boldsymbol{\sigma}^2 + \boldsymbol{\sigma}^2 \cdot \mathbf{m} \otimes \mathbf{m}), \end{aligned} \quad (5.4.168)$$

where the scalars f_i , $i = 1, \dots, 6$, depend on the five invariants of the stress tensor (5.4.163). Betten found that the last term in Eq. (5.4.168) is missing in the constitutive equation which is based on the potential theory. In order to discuss the meaning of the last term in (5.4.168) let us introduce the identities which follow from the decomposition of the stress tensor by Eqs. (5.4.130) and (5.4.132)

$$\begin{aligned} \boldsymbol{\sigma}^2 = & I_{2m} \mathbf{s}_p + (I_{3m} + \frac{1}{4} I_{2m}^2) (\mathbf{I} - \mathbf{m} \otimes \mathbf{m}) + \bar{\mathbf{m}} \otimes \mathbf{s}_p \cdot \boldsymbol{\tau}_m + \boldsymbol{\tau}_m \cdot \mathbf{s}_p \otimes \bar{\mathbf{m}} \\ & + (I_{1m} + \frac{1}{2} I_{2m}) (\boldsymbol{\tau}_m \otimes \bar{\mathbf{m}} + \bar{\mathbf{m}} \otimes \boldsymbol{\tau}_m) + (I_{1m}^2 + I_{4m}) \bar{\mathbf{m}} \otimes \bar{\mathbf{m}} + \boldsymbol{\tau}_m \otimes \boldsymbol{\tau}_m, \end{aligned} \quad (5.4.169)$$

$$\begin{aligned} \bar{\mathbf{m}} \otimes \bar{\mathbf{m}} \cdot \boldsymbol{\sigma} + \boldsymbol{\sigma} \cdot \bar{\mathbf{m}} \otimes \bar{\mathbf{m}} &= \boldsymbol{\tau}_m \otimes \bar{\mathbf{m}} + \bar{\mathbf{m}} \otimes \boldsymbol{\tau}_m + 2I_{1m} \bar{\mathbf{m}} \otimes \bar{\mathbf{m}}, \\ \bar{\mathbf{m}} \otimes \bar{\mathbf{m}} \cdot \boldsymbol{\sigma}^2 + \boldsymbol{\sigma}^2 \cdot \bar{\mathbf{m}} \otimes \bar{\mathbf{m}} &= \bar{\mathbf{m}} \otimes \mathbf{s}_p \cdot \boldsymbol{\tau}_m + \boldsymbol{\tau}_m \cdot \mathbf{s}_p \otimes \bar{\mathbf{m}} \\ &+ (I_{1m} + \frac{1}{2} I_{2m}) (\boldsymbol{\tau}_m \otimes \bar{\mathbf{m}} + \bar{\mathbf{m}} \otimes \boldsymbol{\tau}_m) \\ &+ 2(I_{4m} + I_{1m}^2) \bar{\mathbf{m}} \otimes \bar{\mathbf{m}} \end{aligned}$$

After inserting (5.4.169), (5.4.130) and (5.4.132) into (5.4.168) we obtain the following creep equation

$$\begin{aligned} \mathbf{D} = & g_1 \bar{\mathbf{m}} \otimes \bar{\mathbf{m}} + g_2 (\mathbf{I} - \bar{\mathbf{m}} \otimes \bar{\mathbf{m}}) + g_3 \mathbf{s}_p + g_4 (\bar{\mathbf{m}} \otimes \boldsymbol{\tau}_m + \boldsymbol{\tau}_m \otimes \bar{\mathbf{m}}) \\ & + g_5 (\bar{\mathbf{m}} \otimes \mathbf{s}_p \cdot \boldsymbol{\tau}_m + \boldsymbol{\tau}_m \cdot \mathbf{s}_p \otimes \bar{\mathbf{m}}) + g_6 \boldsymbol{\tau}_m \otimes \boldsymbol{\tau}_m \end{aligned} \quad (5.4.170)$$

with

$$\begin{aligned} g_1 &= f_1 + f_4 (I_{1m}^2 + I_{4m}) + 2f_5 I_{1m} + 2f_6 (I_{4m} + I_{1m}^2), \\ g_2 &= f_2 + \frac{1}{2} f_3 I_{2m} + f_4 (I_{3m} + \frac{1}{4} I_{2m}^2), \\ g_3 &= f_3 + I_{2m} f_4, \\ g_4 &= (f_4 + f_6) (I_{1m} + \frac{1}{2} I_{2m}) + f_5, \\ g_5 &= f_4 + f_6, \\ g_6 &= f_4 \end{aligned}$$

We observe that Eq. (5.4.170) based on the theory of isotropic tensor functions does not deliver any new second order effect in comparison to Eq. (5.4.165). The only difference is that the two last terms in Eq. (5.4.170) characterizing the second order

effects appear with two different influence functions. The comparison of Eq. (5.4.170) with Eq. (5.4.165) provides the following conditions for the existence of the flow potential

$$\begin{aligned} \frac{\partial W}{\partial I_{1m}} &= g_1, & \frac{\partial W}{\partial I_{2m}} &= g_2 + \frac{1}{2}g_5 I_{4m}, \\ \frac{\partial W}{\partial I_{3m}} &= g_3, & \frac{\partial W}{\partial I_{4m}} &= g_4, & \frac{\partial W}{\partial I_{5m}} &= g_5, & g_6 &= g_5 \end{aligned}$$

Furthermore, the functions g_i must satisfy the integrability conditions which can be obtained by equating the mixed derivatives of the potential with respect to invariants, i.e.

$$\frac{\partial^2 W}{\partial I_{im} \partial I_{km}} = \frac{\partial^2 W}{\partial I_{km} \partial I_{im}}, \quad i \neq k, \quad i, k = 1, 2, \dots, 5$$

Let us note that the models (5.4.165) and (5.4.170) are restricted to the special case of transverse isotropy. In the general case one should analyze the creep potential with the invariants listed in Eq. (B.7.39).

Other Cases

Alternatively a phenomenological constitutive equation of anisotropic creep can be formulated with the help of material tensors, e.g. Altenbach (1999). Introducing three material tensors \mathbf{A} , ${}^{(4)}\mathbf{B}$ and ${}^{(6)}\mathbf{C}$ the equivalent stress (5.4.166) can be generalized as follows

$$\sigma_{\text{eq}} = \alpha \sigma_1 + \sigma_2 + \gamma \sigma_3 \quad (5.4.171)$$

with

$$\sigma_1 = \mathbf{A} \cdot \cdot \boldsymbol{\sigma}, \quad \sigma_2^2 = \boldsymbol{\sigma} \cdot \cdot {}^{(4)}\mathbf{B} \cdot \cdot \boldsymbol{\sigma}, \quad \sigma_3^3 = \boldsymbol{\sigma} \cdot \cdot ({}^{(6)}\mathbf{C} \cdot \cdot \boldsymbol{\sigma}) \quad (5.4.172)$$

The structure of the material tensors must be established from the following restrictions

$$\begin{aligned} \mathbf{A}' &= \mathbf{Q} \cdot \mathbf{A} \cdot \mathbf{Q}^T = A^{ij} \mathbf{Q} \cdot \mathbf{e}_i \otimes \mathbf{Q} \cdot \mathbf{e}_j = \mathbf{A}, \\ {}^{(4)}\mathbf{B}' &= B^{ijkl} \mathbf{Q} \cdot \mathbf{e}_i \otimes \mathbf{Q} \cdot \mathbf{e}_j \otimes \mathbf{Q} \cdot \mathbf{e}_k \otimes \mathbf{Q} \cdot \mathbf{e}_l = {}^{(4)}\mathbf{B}, \\ {}^{(6)}\mathbf{C}' &= C^{ijklmn} \mathbf{Q} \cdot \mathbf{e}_i \otimes \mathbf{Q} \cdot \mathbf{e}_j \otimes \mathbf{Q} \cdot \mathbf{e}_k \otimes \mathbf{Q} \cdot \mathbf{e}_l \otimes \mathbf{Q} \cdot \mathbf{e}_m \otimes \mathbf{Q} \cdot \mathbf{e}_n = {}^{(6)}\mathbf{C}, \end{aligned} \quad (5.4.173)$$

where \mathbf{Q} is an element of the physical symmetry group. The creep potential hypothesis and the flow rule (5.4.96) lead to the following creep equation

$$\mathbf{D} = \frac{\partial W}{\partial \sigma_{\text{eq}}} \left(\alpha \frac{\partial \sigma_1}{\partial \boldsymbol{\sigma}} + \frac{\partial \sigma_2}{\partial \boldsymbol{\sigma}} + \gamma \frac{\partial \sigma_3}{\partial \boldsymbol{\sigma}} \right) \quad (5.4.174)$$

Taking into account the relations

$$\frac{\partial \sigma_1}{\partial \boldsymbol{\sigma}} = \mathbf{A}, \quad \frac{\partial \sigma_2}{\partial \boldsymbol{\sigma}} = \frac{{}^{(4)}\mathbf{B} \cdot \cdot \boldsymbol{\sigma}}{\sigma_2}, \quad \frac{\partial \sigma_3}{\partial \boldsymbol{\sigma}} = \frac{\boldsymbol{\sigma} \cdot \cdot {}^{(6)}\mathbf{C} \cdot \cdot \boldsymbol{\sigma}}{\sigma_3^2} \quad (5.4.175)$$

a generalized anisotropic creep equation can be formulated as follows

$$\mathbf{D} = \dot{\varepsilon}_{\text{eq}} \left(\alpha \mathbf{A} + \frac{{}^{(4)}\mathbf{B} \cdot \cdot \boldsymbol{\sigma}}{\sigma_2} + \gamma \frac{\boldsymbol{\sigma} \cdot \cdot {}^{(6)}\mathbf{C} \cdot \cdot \boldsymbol{\sigma}}{\sigma_3^2} \right), \quad \dot{\varepsilon}_{\text{eq}} \equiv \frac{\partial W}{\partial \sigma_{\text{eq}}} \quad (5.4.176)$$

In Betten (1982), Rabotnov (1969) the following anisotropic creep equation is proposed

$$\mathbf{D} = \mathbf{H} + {}^{(4)}\mathbf{M} \cdot \cdot \boldsymbol{\sigma} + {}^{(6)}\mathbf{L} \cdot \cdot \boldsymbol{\sigma} \cdot \cdot \boldsymbol{\sigma} \quad (5.4.177)$$

Comparing the Eqs. (5.4.176) and (5.4.177) the material tensors \mathbf{H} , ${}^{(4)}\mathbf{M}$ and ${}^{(6)}\mathbf{L}$ can be related to the tensors \mathbf{A} , ${}^{(4)}\mathbf{B}$ and ${}^{(6)}\mathbf{C}$.

The tensors \mathbf{A} , ${}^{(4)}\mathbf{B}$ and ${}^{(6)}\mathbf{C}$ contain 819 coordinates (\mathbf{A} -9, ${}^{(4)}\mathbf{B}$ -81, ${}^{(6)}\mathbf{C}$ -729). From the symmetry of the stress tensor and the deformation rate tensor as well as from the potential hypothesis it follows that “only” 83 coordinates are independent (\mathbf{A} -6, ${}^{(4)}\mathbf{B}$ -21, ${}^{(6)}\mathbf{C}$ -56). Further reduction is based on the symmetry considerations. The structure of material tensors and the number of independent coordinates can be obtained by solving Eq. (5.4.173).

Another possibility of simplification is the establishing of special cases of Eq. (5.4.176). For instance, equations with a reduced number of parameters can be derived as follows

- $\alpha = 1, \gamma = 0$:

$$\sigma_{\text{eq}} = \sigma_1 + \sigma_2, \quad \mathbf{D} = \dot{\varepsilon}_{\text{eq}} \left(\mathbf{A} + \frac{{}^{(4)}\mathbf{B} \cdot \cdot \boldsymbol{\sigma}}{\sigma_2} \right), \quad (5.4.178)$$

- $\alpha = 0, \gamma = 1$:

$$\sigma_{\text{eq}} = \sigma_2 + \sigma_3, \quad \mathbf{D} = \dot{\varepsilon}_{\text{eq}} \left(\frac{{}^{(4)}\mathbf{B} \cdot \cdot \boldsymbol{\sigma}}{\sigma_2} + \frac{\boldsymbol{\sigma} \cdot \cdot {}^{(6)}\mathbf{C} \cdot \cdot \boldsymbol{\sigma}}{\sigma_3^2} \right), \quad (5.4.179)$$

- $\alpha = 0, \gamma = 0$:

$$\sigma_{\text{eq}} = \sigma_2, \quad \mathbf{D} = \dot{\varepsilon}_{\text{eq}} \left(\frac{{}^{(4)}\mathbf{B} \cdot \cdot \boldsymbol{\sigma}}{\sigma_2} \right) \quad (5.4.180)$$

The last case has been discussed in Sect. 5.4.3.1. Examples of application of constitutive equation (5.4.176) as well as different cases of symmetries are discussed in Altenbach (1999), Altenbach et al. (1995).

5.4.4 Functions of Stress and Temperature

In constitutive equations discussed in Sects. 5.4.2 and 5.4.3 the flow potential or the equivalent strain rate must be specified as functions of the equivalent stress and the temperature, i.e.

$$\dot{\epsilon}_{\text{eq}} = \frac{\partial W}{\partial \sigma_{\text{eq}}} = f(\sigma_{\text{eq}}, T)$$

In Krempl (1999) the function f is called constitutive or response function. For the formulation of constitutive functions one may apply theoretical foundations from materials science with regard to mechanisms of inelastic deformation and related forms of stress and temperature functions. Furthermore, experimental data including families of creep curves obtained from uni-axial creep tests for certain ranges of stress and temperature as well as stress-strain curves for a range of strain rates and temperatures are required. It is convenient to present these curves in a form of equivalent strain rate versus stress and equivalent strain rate versus temperature. Examples are discussed in Sect. 1.1.

Several empirical functions of stress and temperature have been proposed to fit experimental data. For reviews we refer to Chaboche (2008), Ilschner (1973), Odqvist and Hult (1962), Penny and Marriott (1995), Rabotnov (1979), Skrzypek (1993). For many materials within certain ranges of stress and temperature the equivalent inelastic deformation rate can be approximated by a product of two separate functions of stress and temperature as follows

$$\dot{\epsilon}_{\text{eq}} = f_{\sigma}(\sigma_{\text{eq}}) f_T(T)$$

Examples of stress functions include:

- power law

$$f_{\sigma}(\sigma_{\text{eq}}) = \dot{\epsilon}_0 \left(\frac{\sigma_{\text{eq}}}{\sigma_0} \right)^n \quad (5.4.181)$$

The power law (5.4.181) contains three material parameters ($\dot{\epsilon}_0$, σ_0 , n) but only two of them are independent. Instead of $\dot{\epsilon}_0$ and σ_0 one constant

$$a = \frac{\dot{\epsilon}_0}{\sigma_0^n}$$

can be introduced.

- power law including the creep limit

$$f_{\sigma}(\sigma_{\text{eq}}) = \dot{\epsilon}'_0 \left(\frac{\sigma_{\text{eq}}}{\sigma'_0} - 1 \right)^{n'}, \quad \sigma_{\text{eq}} > \sigma'_0$$

If $\sigma_{\text{eq}} \leq \sigma'_0$ the deformation rate is equal zero. In this case σ'_0 is the assumed creep limit.

- exponential law

$$f_{\sigma}(\sigma_{\text{eq}}) = \dot{\varepsilon}_0 \exp \frac{\sigma_{\text{eq}}}{\sigma_0}$$

$\dot{\varepsilon}_0$, σ_0 are material parameters. The disadvantage of this expression is that it predicts a nonzero creep rate for a zero equivalent stress

$$f_{\sigma}(0) = \dot{\varepsilon}_0 \neq 0$$

- hyperbolic sine law

$$f_{\sigma}(\sigma_{\text{eq}}) = \dot{\varepsilon}_0 \sinh \frac{\sigma_{\text{eq}}}{\sigma_0} \quad (5.4.182)$$

For low stress values $\sigma_{\text{eq}} \ll \sigma_0$ this function provides the linear dependence on the stress

$$f_{\sigma}(\sigma_{\text{eq}}) \approx \dot{\varepsilon}_0 \frac{\sigma_{\text{eq}}}{\sigma_0}$$

while for high stress values $\sigma_{\text{eq}} \gg \sigma_0$ the exponential law can be obtained

$$f_{\sigma}(\sigma_{\text{eq}}) \approx \frac{\dot{\varepsilon}_0}{2} \exp \frac{\sigma_{\text{eq}}}{\sigma_0}$$

- double power law

$$f_{\sigma}(\sigma_{\text{eq}}) = \dot{\varepsilon}_0 \left[\frac{\sigma_{\text{eq}}}{\sigma_0} + \left(\frac{\sigma_{\text{eq}}}{\sigma_0} \right)^n \right] \quad (5.4.183)$$

For low stress values $\sigma_{\text{eq}} \ll \sigma_0$ this function provides the linear dependence on the stress while for $\sigma_{\text{eq}} \gg \sigma_0$ the power law stress dependence (5.4.181) can be obtained

- power law breakdown equation

$$f_{\sigma}(\sigma_{\text{eq}}) = \dot{\varepsilon}_0 \left[\sinh \left(\frac{\sigma_{\text{eq}}}{\sigma_0} \right) \right]^n \quad (5.4.184)$$

For $\sigma_{\text{eq}} \ll \sigma_0$ the power law stress function (5.4.181) follows from Eq. (5.4.184) while for $\sigma_{\text{eq}} \gg \sigma_0$ the exponential law

$$f_{\sigma}(\sigma_{\text{eq}}) = \frac{\dot{\varepsilon}_0}{2} \exp \left(n \frac{\sigma_{\text{eq}}}{\sigma_0} \right)$$

can be obtained. Equation (5.4.184) describes both the power law and the power law breakdown regimes

The dependence on the temperature is usually expressed by the Arrhenius law

$$f_T(T) = \exp[-Q/RT],$$

where Q and R denote the activation energy and the universal gas constant, respectively.

For the use of stress and temperature functions one should take into account that different deformation mechanisms may operate for different specific ranges of stress and temperature. An overview is provided by the deformation mechanisms map, as proposed by Frost and Ashby (1982), Fig. 5.3. Contours of constant strain rates are presented as functions of the normalized equivalent stress σ_{eq}/G and the homologous temperature T/T_m , where G is the shear modulus and T_m is the melting temperature. For a given combination of the stress and the temperature, the map provides the dominant mechanism and of the high-temperature plasticity and an approximate value of the strain rate.

Let us briefly discuss different regions on the map, the mechanisms of inelastic deformation and constitutive functions derived in materials science. For comprehensive reviews one may consult François et al. (2012), Kassner and Pérez-Prado (2004), Nabarro and de Villiers (1995). The origins of the inelastic deformation at the temperature range $0.5 < T/T_m < 0.7$ are transport processes associated with

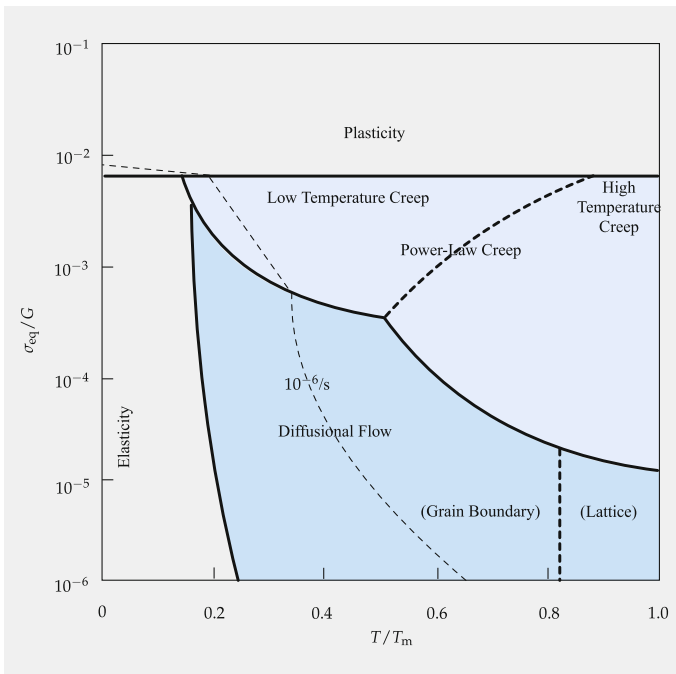


Fig. 5.3 Schematic deformation-mechanism map

motion and interaction of dislocations and diffusion of vacancies. Two typical classes of physical models are the dislocation creep and the diffusion creep. Various creep rate equations within the dislocation creep range are based on the Bailey-Orowan recovery hypothesis. An internal barrier stress σ_{int} being opposed to the dislocation movement is assumed. When the plastic strain occurs the internal stress increases as a result of work hardening due to accumulation of deformation and due to increase of the dislocation density. As the material is subjected to the load and temperature over certain time, the internal stress σ_{int} decreases as a result of diffusion processes. In the uni-axial case the rate of change of the internal stress is assumed as follows

$$\dot{\sigma}_{\text{int}} = h\dot{\epsilon}^{\text{pl}} - r\sigma_{\text{int}},$$

where h and r are material properties related to hardening and recovery, respectively. In the steady state $\dot{\sigma}_{\text{int}} = 0$ so that

$$\dot{\epsilon} = \frac{r\sigma_{\text{int}}}{h}$$

Specifying the values for r , h and σ_{int} various models for the steady-state creep rate have been derived. An example is the following expression (for details of derivation we refer to (François et al. 1998))

$$\dot{\epsilon} \propto \frac{D}{RT} \frac{\sigma^4}{G^3} \exp\left(-\frac{Q}{RT}\right),$$

where D is the diffusion coefficient.

Further models of dislocation creep are derived under the assumption of the climb-plus-glide deformation mechanism. At high temperatures and moderate stresses, dislocations can climb as well as glide. The glide of dislocations produced by the applied stress is opposed by obstacles. Due to diffusion of vacancies, the dislocations can climb around strengthening particles. The inelastic strain is then controlled by the glide, while its rate is determined by the climb. The climb-plus-glide mechanism can be related to the recovery-hardening hypothesis. The hardening results from the resistance to glide due to interaction of moving dislocations with other dislocations, precipitates, etc. The recovery mechanism is the diffusion controlled climb which releases the glide barriers. The climb-plus-glide based creep rate models can be found in François et al. (1998), Frost and Ashby (1982), Nabarro and de Villiers (1995). The common result is the power-law creep

$$\dot{\epsilon}_{\text{eq}} \propto \left(\frac{\sigma_{\text{eq}}}{G}\right)^n \exp\left(-\frac{Q}{RT}\right) \quad (5.4.185)$$

Equation (5.4.185) can be used to fit experimental data for a range of stresses up to $10^{-3}G$. The exponent n varies from 3 to about 10 for metallic materials. At higher stresses above $10^{-3}G$ the power law (5.4.185) breaks down. The measured strain rate

is greater than the Eq. (5.4.185) predicts. Within the range of the power-law break down a transition from the climb-plus-glide to the glide mechanism is assumed (Frost and Ashby 1982). The following empirical equation can be applied, e.g. Frost and Ashby (1982), Nabarro and de Villiers (1995),

$$\dot{\epsilon}_{\text{eq}} \propto \left[\sinh \left(\alpha \frac{\sigma_{\text{eq}}}{G} \right) \right]^n \exp \left(-\frac{Q}{RT} \right), \quad (5.4.186)$$

where α is a material constant. If $\alpha \sigma_{\text{eq}}/G < 1$ then (5.4.186) reduces to (5.4.185).

At higher temperatures ($T/T_m > 0.7$) diffusion mechanisms control the creep rate. The deformation occurs at much lower stresses and results from diffusion of vacancies. The mechanism of grain boundary diffusion (Coble creep) assumes diffusive transport of vacancies through and around the surfaces of grains. The deviatoric part of the stress tensor changes the chemical potential of atoms at the grain boundaries. Because of different orientations of grain boundaries a potential gradient occurs. This gradient is the driving force for the grain boundary diffusion. The diffusion through the matrix (bulk diffusion) is the dominant creep mechanism (Nabarro-Herring creep) for temperatures close to the melting point. For details concerning the Coble and the Nabarro-Herring creep models we refer to François et al. (1998), Nabarro and de Villiers (1995). These models predict the diffusion controlled creep rate to be a linear function of the stress.

In addition to the dislocation and the diffusion creep, the grain boundary sliding is the important mechanism for poly-crystalline materials. This mechanism occurs because the grain boundaries are weaker than the ordered crystalline structure of the grains (Nabarro and de Villiers 1995; Riedel 1987). Furthermore, the formation of voids and micro-cracks on grain boundaries contributes to the sliding (Ozhoga-Maslovskaja et al. 2015). The whole deformation rate depends on the grain size and the grain aspect ratio (ratio of the grain dimensions parallel and perpendicular to the tensile stress direction). Samples with a larger grain size usually exhibit a lower strain rate.

5.5 Elasto-plasticity

Assume that the mechanical power $\mathcal{L} = \boldsymbol{\sigma} \cdot \mathbf{L}$ can be additively decomposed in two parts $\mathcal{L} = \mathcal{L}_s + \mathcal{L}_d$ with

$$\mathcal{L}_s = \boldsymbol{\sigma}_s \cdot \mathbf{L}_s, \quad \mathcal{L}_d = \boldsymbol{\sigma}_d \cdot \mathbf{L}_d,$$

where $\boldsymbol{\sigma}_s$ and $\boldsymbol{\sigma}_d$ are quasi-conservative and dissipative stress tensors, respectively, and \mathbf{L}_s and \mathbf{L}_d are deformation rate-like variables. By analogy to the uni-axial case, see Sect. 3.4 assume that $\boldsymbol{\sigma}_s$ may depend only on the deformation-like variables and the temperature, while $\boldsymbol{\sigma}_d$ may depend on the deformation rates and the temperature. This additive decomposition can be applied to define a part of the mechanical power

which is dissipated as heat, i.e. \mathcal{L}_d and can affect the free energy by means of temperature and the remaining part \mathcal{L}_s which directly affects the free energy and under certain conditions can be stored. For example, this is the case for isothermal elasticity, as discussed in Sect. 3.2. In Ziegler (1983) \mathcal{L}_s is called quasi-conservative and \mathcal{L}_d —dissipated parts of mechanical power, respectively. Several approaches to define the corresponding stress and deformation parts are discussed in the literature. For example, one may consider various connections of rheological elements including a spring, a viscous element and a friction element (Krawietz 1986; Palmov 1998). Another approach, which is more appropriate for the three-dimensional continuum mechanics is to consider a mixture with several (elastic and inelastic) constituents having different properties and volume fractions (Atkin and Craine 1976; Altenbach et al. 2003b). Alternatively, one may assume a multiplicative decomposition for the deformation gradient, and appropriate decompositions for the rate of deformations and/or stress tensors (Besseling and van der Giessen 1994; Khan and Huang 1995; Maugin 1992; Nemat-Nasser 2004).

5.5.1 Multiplicative Decomposition of Deformation Gradient

The following decomposition of the deformation gradient is assumed

$$\mathbf{F} = \mathbf{F}^{\text{el}} \cdot \mathbf{F}^{\text{pl}} \quad (5.5.187)$$

The elastic \mathbf{F}^{el} and the plastic \mathbf{F}^{pl} parts are not deformation gradients in the sense that they are not gradients of position vectors in a certain configuration of a body. Indeed, the decomposition (5.5.187) can also be given as follows

$$\mathbf{r}_i \otimes \mathcal{R}^i = \mathbf{r}_i \otimes \mathbf{g}^i \cdot \mathbf{g}_k \otimes \mathcal{R}^k, \quad (5.5.188)$$

where the vectors \mathcal{R}_i in the reference configuration are defined by Eq. (4.1.2), the vectors \mathbf{r}_i in the actual configuration are given by Eq. (4.1.5) and the tripple of vectors \mathbf{g}_i must satisfy the condition $(\mathbf{g}_1 \times \mathbf{g}_2) \cdot \mathbf{g}_3 \neq 0$. The vectors \mathbf{g}_i are not derivatives of the position vector in a configuration of a body with respect to the coordinates. To motivate the sequence of parts in the decomposition (5.5.187): the plastic part at the first place and then the elastic part in the second one, the notion of an unloaded or intermediate configuration is introduced.¹³ As the body is locally subjected to the deformation gradient \mathbf{F} , one may assume the “elastic” unloading from the actual configuration by \mathbf{F}^{el} . The remaining part $\mathbf{F}^{\text{pl}} = (\mathbf{F}^{\text{el}})^{-1} \cdot \mathbf{F}$ is assumed to be “stress-free”. The local configuration after this unloading procedure is interpreted as an intermediate (stress-free). In order to formulate constitutive equation the multiplicative

¹³The intermediate configuration can only be used as illustrative since it has a number of conceptual shortcomings. Historical essays and critical remarks to the multiplicative decomposition are presented in Naghdi (1990), Bertram (2012), Xiao et al. (2006).

decomposition (5.5.187) should be supplemented by the rules as how the tripple of vectors \mathbf{g}_i transform by the change of the reference configuration and how these vectors are affected by a superimposed rotation. Let \mathbf{Q} be an orthogonal tensor. Consider the deformation gradient \mathbf{F} and the transformed deformation gradient $\mathbf{F}_* = \mathbf{F} \cdot \mathbf{Q}^T$ after the change of the reference configuration. For the parts in the multiplicative decomposition we may assume, for example,

$$\mathbf{F}_*^{\text{el}} = \mathbf{F}^{\text{el}} \cdot \mathbf{Q}^T, \quad \mathbf{F}_*^{\text{pl}} = \mathbf{Q} \cdot \mathbf{F}^{\text{pl}} \cdot \mathbf{Q}^T \quad (5.5.189)$$

Another choice could be

$$\mathbf{F}_*^{\text{el}} = \mathbf{F}^{\text{el}} \cdot \bar{\mathbf{Q}}^T, \quad \mathbf{F}_*^{\text{pl}} = \bar{\mathbf{Q}} \cdot \mathbf{F}^{\text{pl}} \cdot \mathbf{Q}^T, \quad (5.5.190)$$

where $\bar{\mathbf{Q}}$ is an orthogonal tensor. Now assume that the body is subjected to a superimposed rotation $\mathbf{Q}(t)$. The transformed deformation gradient is $\mathbf{F}_{**} = \mathbf{Q} \cdot \mathbf{F}$. For the elastic and plastic parts one may assume

$$\mathbf{F}_{**}^{\text{el}} = \mathbf{Q} \cdot \mathbf{F}^{\text{el}}, \quad \mathbf{F}_{**}^{\text{pl}} = \mathbf{F}^{\text{pl}} \quad (5.5.191)$$

Another choice could be

$$\mathbf{F}_{**}^{\text{el}} = \mathbf{Q} \cdot \mathbf{F}^{\text{el}} \cdot \bar{\mathbf{Q}}^T, \quad \mathbf{F}_{**}^{\text{pl}} = \bar{\mathbf{Q}} \cdot \mathbf{F}^{\text{pl}}, \quad (5.5.192)$$

where $\bar{\mathbf{Q}}(t)$ is a rotation tensor.

With the multiplicative decomposition the velocity gradient is computed as follows

$$\mathbf{L} = \dot{\mathbf{F}} \cdot \mathbf{F}^{-1} = \dot{\mathbf{F}}^{\text{el}} \cdot \mathbf{F}^{\text{el}-1} + \mathbf{F}^{\text{el}} \cdot \dot{\mathbf{F}}^{\text{pl}} \cdot \mathbf{F}^{\text{pl}-1} \cdot \mathbf{F}^{\text{el}-1} \quad (5.5.193)$$

The mechanical power can be computed as follows

$$\begin{aligned} \mathcal{L} &= \mathcal{L}_s + \mathcal{L}_d, \\ \mathcal{L}_s &= \boldsymbol{\sigma} \cdot \left(\dot{\mathbf{F}}^{\text{el}} \cdot \mathbf{F}^{\text{el}-1} \right), \quad \mathcal{L}_d = \left(\mathbf{F}^{\text{el}-1} \cdot \boldsymbol{\sigma} \cdot \mathbf{F}^{\text{el}} \right) \cdot \left(\dot{\mathbf{F}}^{\text{pl}} \cdot \mathbf{F}^{\text{pl}-1} \right) \end{aligned}$$

Obviously the quasi-conservative stress tensor is $\boldsymbol{\sigma}_s = \boldsymbol{\sigma}$ while the dissipative stress tensor can be defined as follows

$$\boldsymbol{\sigma}_d = \mathbf{F}^{\text{el}-1} \cdot \boldsymbol{\sigma} \cdot \mathbf{F}^{\text{el}} \quad (5.5.194)$$

Let us assume that $\boldsymbol{\sigma}_s$ depends on \mathbf{F}^{el} and the temperature T , while $\boldsymbol{\sigma}_d$ depends on $\dot{\mathbf{F}}^{\text{pl}}$ and temperature. With $\Phi = \Phi(\mathbf{F}^{\text{el}}, T)$ the dissipation inequality (5.3.21) takes the following form

$$\begin{aligned} \dot{\mathbf{F}}^{\text{el}} \cdot \left[\mathbf{F}^{\text{el}^{-1}} \cdot \boldsymbol{\sigma} - \rho \left(\frac{\partial \Phi}{\partial \mathbf{F}^{\text{el}}} \right)^T \right] - \rho \left(\frac{\partial \Phi}{\partial T} + \mathcal{S} \right) \dot{T} \\ + \boldsymbol{\sigma}_d \cdot \left(\dot{\mathbf{F}}^{\text{pl}} \cdot \mathbf{F}^{\text{pl}^{-1}} \right) - \frac{\mathbf{q} \cdot \nabla T}{T} \geq 0 \end{aligned} \quad (5.5.195)$$

The inequality is satisfied with¹⁴

$$\boldsymbol{\sigma} = \rho \mathbf{F}^{\text{el}} \cdot \left(\frac{\partial \Phi}{\partial \mathbf{F}^{\text{el}}} \right)^T, \quad \mathcal{S} = -\frac{\partial \Phi}{\partial T} \quad (5.5.196)$$

and

$$\boldsymbol{\sigma}_d \cdot \left(\dot{\mathbf{F}}^{\text{pl}} \cdot \mathbf{F}^{\text{pl}^{-1}} \right) \geq 0, \quad -\frac{\mathbf{q} \cdot \nabla T}{T} \geq 0 \quad (5.5.197)$$

From the symmetry of the Cauchy stress tensor it follows, see Eqs. (5.3.25)–(5.3.32)

$$\Phi(\mathbf{F}^{\text{el}}, T) = \Phi(\mathbf{C}^{\text{el}}, T),$$

and

$$\boldsymbol{\sigma} = 2\rho \mathbf{F}^{\text{el}} \cdot \frac{\partial \Phi}{\partial \mathbf{C}^{\text{el}}} \cdot \mathbf{F}^{\text{el}^T} = \frac{2}{J} \mathbf{F}^{\text{el}} \cdot \frac{\partial \rho_0 \Phi}{\partial \mathbf{C}^{\text{el}}} \cdot \mathbf{F}^{\text{el}^T}, \quad \mathbf{C}^{\text{el}} = \mathbf{F}^{\text{el}^T} \cdot \mathbf{F}^{\text{el}} \quad (5.5.198)$$

With Eq. (5.5.194) the dissipative stress tensor takes the form

$$\boldsymbol{\sigma}_d = \frac{2}{J} \frac{\partial \rho_0 \Phi}{\partial \mathbf{C}^{\text{el}}} \cdot \mathbf{C}^{\text{el}} \quad (5.5.199)$$

Let us assume that the physical symmetry group of elasticity is the full orthogonal group, i.e. the material exhibits isotropic behavior. One may show by the use of either (5.5.189)₁ or (5.5.190)₂ that the free energy depends on the three invariants of the tensor \mathbf{C}^{el} , see Sect. 5.3.2. Constitutive equations like (5.3.40) can be derived. Alternatively the following constitutive equation can be applied

$$\boldsymbol{\sigma} = \frac{2}{J} \frac{\partial \rho_0 \Phi}{\partial \mathbf{B}^{\text{el}}} \cdot \mathbf{B}^{\text{el}}, \quad \mathbf{B}^{\text{el}} = \mathbf{F}^{\text{el}} \cdot \mathbf{F}^{\text{el}^T} \quad (5.5.200)$$

For isotropic elasticity the free energy can also be assumed to be a function of the Hencky strain tensor such that

$$\Phi(\mathbf{F}^{\text{el}}, T) = \Phi(\mathbf{h}^{\text{el}}, T)$$

¹⁴See the analysis presented in Sect. 5.3.1.

and

$$\boldsymbol{\sigma} = \frac{1}{J} \frac{\partial \rho_0 \Phi}{\partial \mathbf{h}^{\text{el}}}, \quad \mathbf{h}^{\text{el}} = \ln \mathbf{V}^{\text{el}} = \frac{1}{2} \ln \mathbf{B}^{\text{el}} \quad (5.5.201)$$

An example of the constitutive equation for an isotropic elastic material (Hencky material) is

$$J \boldsymbol{\sigma} = \lambda (\text{tr } \mathbf{h}^{\text{el}}) \mathbf{I} + 2\mu \mathbf{h}^{\text{el}}, \quad (5.5.202)$$

where the Lamé constants λ and μ are defined by (5.3.65). With the polar decomposition

$$\mathbf{F}^{\text{el}} = \mathbf{V}^{\text{el}} \cdot \mathbf{R}^{\text{el}}$$

the dissipative stress (5.5.194) can be computed as follows

$$\boldsymbol{\sigma}_d = \mathbf{R}^{\text{elT}} \cdot \mathbf{V}^{\text{el}^{-1}} \cdot \boldsymbol{\sigma} \cdot \mathbf{V}^{\text{el}} \cdot \mathbf{R}^{\text{el}} \quad (5.5.203)$$

Since the Cauchy tensor is coaxial with the tensor \mathbf{V}^{el} , Eq. (5.5.203) takes the following form

$$\boldsymbol{\sigma}_d = \mathbf{R}^{\text{elT}} \cdot \boldsymbol{\sigma} \cdot \mathbf{R}^{\text{el}} \quad (5.5.204)$$

To proceed with the inelastic deformation one should specify the rotation tensor \mathbf{R}^{el} . An assumption is made in Lee (1969) that the elastic unloading takes place without rotation such that $\mathbf{R}^{\text{el}} = \mathbf{I}$. Then $\boldsymbol{\sigma}_d = \boldsymbol{\sigma}_s = \boldsymbol{\sigma}$ leading to the iso-stress approach, as postulated in the uni-axial case, see Sect. 3.4. For the dissipative stress tensor let us postulate the following constitutive equation

$$\boldsymbol{\sigma}_d(\boldsymbol{\Lambda}^{\text{pl}}, T) = \boldsymbol{\sigma}(\boldsymbol{\Lambda}^{\text{pl}}, T) = g_T(T) \mathbf{g}(\boldsymbol{\Lambda}^{\text{pl}}), \quad \boldsymbol{\Lambda}^{\text{pl}} = \dot{\mathbf{F}}^{\text{pl}} \cdot \mathbf{F}^{\text{pl}^{-1}} \quad (5.5.205)$$

With $\mathbf{R}^{\text{el}} = \mathbf{I}$ the tensor \mathbf{F}^{el} is symmetric and the transformation (5.5.192) takes the form

$$\mathbf{F}_{**}^{\text{el}} = \mathbf{Q} \cdot \mathbf{F}^{\text{el}} \cdot \mathbf{Q}^T, \quad \mathbf{F}_{**}^{\text{pl}} = \mathbf{Q} \cdot \mathbf{F}^{\text{pl}}, \quad (5.5.206)$$

With the decomposition

$$\boldsymbol{\Lambda}^{\text{pl}} = \mathbf{D}^{\text{pl}} + \boldsymbol{\omega}^{\text{pl}} \times \mathbf{I}$$

the following transformation rule can be obtained

$$\boldsymbol{\Lambda}_{**}^{\text{pl}} = \boldsymbol{\Omega}_{\mathbf{Q}} \times \mathbf{I} + (\mathbf{Q} \cdot \boldsymbol{\omega}^{\text{pl}}) \times \mathbf{I} + \mathbf{Q} \cdot \mathbf{D}^{\text{pl}} \cdot \mathbf{Q}^T,$$

where $\boldsymbol{\Omega}_Q$ is the angular velocity vector for the rotation tensor Q . Under superimposed rigid rotation the Cauchy stress tensor is $\boldsymbol{\sigma}_{**} = Q \cdot \boldsymbol{\sigma} \cdot Q^T$, and the following restriction on the function $g(\Lambda^{pl})$ can be formulated

$$Q \cdot g(\Lambda^{pl}) \cdot Q^T = g(\Lambda_{**}^{pl})$$

As a result we obtain

$$Q \cdot g(D^{pl} + \boldsymbol{\omega}^{pl} \times I) \cdot Q^T = g[(\boldsymbol{\Omega}_Q + Q \cdot \boldsymbol{\omega}^{pl}) \times I + Q \cdot D^{pl} \cdot Q^T] \quad (5.5.207)$$

Since $\boldsymbol{\Omega}_Q$ is an arbitrary angular velocity vector, we may specify

$$\boldsymbol{\Omega}_Q = -Q \cdot \boldsymbol{\omega}^{pl}$$

Equation (5.5.207) takes the form

$$Q \cdot g(D^{pl} + \boldsymbol{\omega}^{pl} \times I) \cdot Q^T = g(Q \cdot D^{pl} \cdot Q^T) \quad (5.5.208)$$

For $Q = I$ this results in

$$g(D^{pl} + \boldsymbol{\omega}^{pl} \times I) = g(D^{pl})$$

Omitting the skew-symmetric tensor $\boldsymbol{\omega}^{pl} \times I$, Eq. (5.5.208) takes the form

$$Q \cdot g(D^{pl}) \cdot Q^T = g(Q \cdot D^{pl} \cdot Q^T)$$

Therefore g is the isotropic function of D^{pl} and has the following general representation¹⁵

$$g = \alpha_0 I + \alpha_1 D^{pl} + \alpha_2 D^{pl^2},$$

where α_i are functions of invariants of D^{pl} . The Cauchy stress tensor is co-axial with the tensor D^{pl} . From (5.5.197) it follows that the functions α_i must satisfy the following inequality

$$\alpha_0 \text{tr } D^{pl} + \alpha_1 \text{tr } D^{pl^2} + \alpha_2 \text{tr } D^{pl^3} \geq 0 \quad (5.5.209)$$

Specific forms of the function g or its inverse were discussed in Sect. 5.4. As an example consider the following tensorial-linear constitutive equation

$$D^{pl} = f_T(T)\beta(\mathbf{s})\mathbf{s}, \quad \text{tr } D^{pl} = 0, \quad \det F^{pl} = 1, \quad (5.5.210)$$

¹⁵From this consideration it does not follow that only isotropic plasticity can be described. Indeed, we assumed that the stress tensor depends only on Λ^{pl} , which is not true for anisotropic materials.

where $f_T(T)$ is a function of temperature and β is a function of invariants of the stress deviator.

With Eq. (5.5.193) and $\mathbf{R}^{\text{el}} = \mathbf{I}$ the velocity gradient can be decomposed as follows

$$\mathbf{D} + \boldsymbol{\omega} \times \mathbf{I} = \mathbf{D}^{\text{el}} + \boldsymbol{\omega}^{\text{el}} \times \mathbf{I} + \mathbf{V}^{\text{el}} \cdot \mathbf{D}^{\text{pl}} \cdot \mathbf{V}^{\text{el}^{-1}} + \mathbf{V}^{\text{el}} \cdot (\boldsymbol{\omega}^{\text{pl}} \times \mathbf{I}) \cdot \mathbf{V}^{\text{el}^{-1}} \quad (5.5.211)$$

With the constitutive assumptions (5.5.210) and (5.5.200) it is obvious that the tensors \mathbf{V}^{el} and \mathbf{D}^{pl} are coaxial. Therefore

$$\mathbf{V}^{\text{el}} \cdot \mathbf{D}^{\text{pl}} \cdot \mathbf{V}^{\text{el}^{-1}} = \mathbf{D}^{\text{pl}} \quad (5.5.212)$$

With (A.4.8)₂ the last term in Eq. (5.5.211) can be transformed as follows

$$\mathbf{V}^{\text{el}} \cdot (\boldsymbol{\omega}^{\text{pl}} \times \mathbf{I}) \cdot \mathbf{V}^{\text{el}^{-1}} = \frac{1}{J} \mathbf{V}^{\text{el}^2} \times \tilde{\boldsymbol{\omega}}^{\text{pl}}, \quad \tilde{\boldsymbol{\omega}}^{\text{pl}} = \mathbf{V}^{\text{el}} \cdot \boldsymbol{\omega}^{\text{pl}}$$

Taking the vector invariant of Eq. (5.5.211) and applying the identity (A.4.16) we obtain the following relationship between the angular velocities

$$\boldsymbol{\omega} = \boldsymbol{\omega}^{\text{el}} - \frac{1}{2} \mathbf{A}_{\mathbf{V}^{\text{el}}} \cdot \boldsymbol{\omega}^{\text{pl}}, \quad (5.5.213)$$

where

$$\mathbf{A}_{\mathbf{V}^{\text{el}}} = \sum_{i=1}^3 \lambda_i^{\text{el}} \mathbf{n}_i^{\text{el}} \times \mathbf{V}^{\text{el}^{-1}} \times \mathbf{n}_i^{\text{el}} = \sum_{i=1}^3 \sum_{j=1}^3 \frac{\lambda_i^{\text{el}}}{\lambda_j^{\text{el}}} \mathbf{n}_i^{\text{el}} \times \mathbf{n}_j^{\text{el}} \otimes \mathbf{n}_j^{\text{el}} \times \mathbf{n}_i^{\text{el}},$$

where λ_i^{el} are principal values and \mathbf{n}_i^{el} are principal axes of the tensor \mathbf{V}^{el} , respectively. According to (A.4.16) and the Cayley-Hamilton theorem the tensor $\mathbf{A}_{\mathbf{V}^{\text{el}}}$ has the following representations

$$\mathbf{A}_{\mathbf{V}^{\text{el}}} = J^{-1} \mathbf{V}^{\text{el}} \cdot [\mathbf{V}^{\text{el}^2} - (\text{tr } \mathbf{V}^{\text{el}^2}) \mathbf{I}] = \mathbf{I} + \frac{J_{2_{\mathbf{V}^{\text{el}}}} - J_{1_{\mathbf{V}^{\text{el}}}^2}}{J} \mathbf{V}^{\text{el}} + \frac{J_{1_{\mathbf{V}^{\text{el}}}}}{J} \mathbf{V}^{\text{el}^2},$$

where $J_{1_{\mathbf{V}^{\text{el}}}}$, $J_{2_{\mathbf{V}^{\text{el}}}}$ and $J = J_{3_{\mathbf{V}^{\text{el}}}}$ are principal invariants of the tensor \mathbf{V}^{el} as defined by Eqs. (A.4.11).

With Eq. (5.5.211) the symmetric part of Eq. (5.5.212) is

$$\mathbf{D} = \mathbf{D}^{\text{el}} + \mathbf{D}^{\text{pl}} + \frac{1}{2} \left[\mathbf{V}^{\text{el}} \cdot (\boldsymbol{\omega}^{\text{pl}} \times \mathbf{I}) \cdot \mathbf{V}^{\text{el}^{-1}} - \mathbf{V}^{\text{el}^{-1}} \cdot (\boldsymbol{\omega}^{\text{pl}} \times \mathbf{I}) \cdot \mathbf{V}^{\text{el}} \right] \quad (5.5.214)$$

With Eq. (A.4.8)₂ Eq. (5.5.214) can be transformed as follows

$$\mathbf{D} = \mathbf{D}^{\text{el}} + \mathbf{D}^{\text{pl}} + \mathbf{V}^{\text{el}2} \times \tilde{\boldsymbol{\omega}}^{\text{pl}} - \tilde{\boldsymbol{\omega}}^{\text{pl}} \times \mathbf{V}^{\text{el}2}, \quad (5.5.215)$$

where

$$\tilde{\boldsymbol{\omega}}^{\text{pl}} = \frac{1}{2J} \mathbf{V}^{\text{el}} \cdot \boldsymbol{\omega}^{\text{pl}}$$

To complete the theory one should define the vectors $\boldsymbol{\omega}^{\text{pl}}$ and $\boldsymbol{\Omega}_{\mathbf{R}}^{\text{pl}}$. For example, one may set, cp. Belytschko et al. (2014), Besseling and van der Giessen (1994)

$$\boldsymbol{\omega}^{\text{pl}} = \mathbf{0} \quad (5.5.216)$$

Then Eq. (5.5.215) simplifies to

$$\mathbf{D} = \mathbf{D}^{\text{el}} + \mathbf{D}^{\text{pl}}, \quad (5.5.217)$$

i.e. the deformation rate tensor can be decomposed into the elastic and plastic parts. Furthermore, from Eq. (5.5.213) it follows that

$$\boldsymbol{\omega} = \boldsymbol{\omega}^{\text{el}} \quad (5.5.218)$$

With Eq. (4.1.75) we can replace the elastic part of the deformation rate through the time derivative of the Hencky strain tensor as follows

$$\mathbf{D}^{\text{el}} = \dot{\mathbf{h}}^{\text{el}} - \boldsymbol{\Omega}_{\mathbf{h}^{\text{el}}} \times \mathbf{h}^{\text{el}} + \mathbf{h}^{\text{el}} \times \boldsymbol{\Omega}_{\mathbf{h}^{\text{el}}}, \quad \boldsymbol{\Omega}_{\mathbf{h}^{\text{el}}} = (\mathbf{I} - \mathbf{A}_{\mathbf{h}^{\text{el}}}) \cdot \boldsymbol{\Omega}_{\mathbf{V}^{\text{el}}}, \quad (5.5.219)$$

where¹⁶

$$\mathbf{A}_{\mathbf{h}^{\text{el}}} = -\frac{1}{4J} \mathbf{V}^{\text{el}} \cdot \sum_{i=1}^3 \sum_{j=1}^3 \frac{\lambda_i^{\text{el}2} - \lambda_j^{\text{el}2}}{(\ln \lambda_i^{\text{el}} - \ln \lambda_j^{\text{el}})} \mathbf{n}_i^{\text{el}} \times \mathbf{n}_j^{\text{el}} \otimes \mathbf{n}_j^{\text{el}} \times \mathbf{n}_i^{\text{el}}, \quad i \neq j$$

The tensor $\mathbf{A}_{\mathbf{h}^{\text{el}}}$ has the following spectral representation

$$\begin{aligned} 2\mathbf{A}_{\mathbf{h}^{\text{el}}} &= \frac{\lambda_2^{\text{el}2} - \lambda_3^{\text{el}2}}{\lambda_2^{\text{el}} \lambda_3^{\text{el}} \ln \frac{\lambda_2^{\text{el}}}{\lambda_3^{\text{el}}}} \mathbf{n}_1^{\text{el}} \otimes \mathbf{n}_1^{\text{el}} \\ &+ \frac{\lambda_3^{\text{el}2} - \lambda_1^{\text{el}2}}{\lambda_3^{\text{el}} \lambda_1^{\text{el}} \ln \frac{\lambda_3^{\text{el}}}{\lambda_1^{\text{el}}}} \mathbf{n}_2^{\text{el}} \otimes \mathbf{n}_2^{\text{el}} + \frac{\lambda_1^{\text{el}2} - \lambda_2^{\text{el}2}}{\lambda_1^{\text{el}} \lambda_2^{\text{el}} \ln \frac{\lambda_1^{\text{el}}}{\lambda_2^{\text{el}}}} \mathbf{n}_3^{\text{el}} \otimes \mathbf{n}_3^{\text{el}} \end{aligned}$$

¹⁶Here we assumed that the tensor \mathbf{V}_{el} has distinct principal values.

With Eqs. (4.1.60) and (5.5.218) we obtain

$$\boldsymbol{\omega} = \left(\mathbf{I} + \frac{1}{2} \mathbf{A}_{\mathbf{V}^{\text{el}}} \right) \cdot \boldsymbol{\Omega}_{\mathbf{V}^{\text{el}}} \quad (5.5.220)$$

or in the inverse form

$$\boldsymbol{\Omega}_{\mathbf{V}^{\text{el}}} = \left(\mathbf{I} - \tilde{\mathbf{A}}_{\mathbf{V}^{\text{el}}} \right) \cdot \boldsymbol{\omega}, \quad (5.5.221)$$

where

$$\begin{aligned} \tilde{\mathbf{A}}_{\mathbf{V}^{\text{el}}} = & \frac{\lambda_2^{\text{el}2} + \lambda_3^{\text{el}2}}{(\lambda_2^{\text{el}} - \lambda_3^{\text{el}})^2} \mathbf{n}_1^{\text{el}} \otimes \mathbf{n}_1^{\text{el}} \\ & + \frac{\lambda_3^{\text{el}2} + \lambda_1^{\text{el}2}}{(\lambda_3^{\text{el}} - \lambda_1^{\text{el}})^2} \mathbf{n}_2^{\text{el}} \otimes \mathbf{n}_2^{\text{el}} + \frac{\lambda_1^{\text{el}2} + \lambda_2^{\text{el}2}}{(\lambda_1^{\text{el}} - \lambda_2^{\text{el}})^2} \mathbf{n}_3^{\text{el}} \otimes \mathbf{n}_3^{\text{el}} \end{aligned}$$

With Eqs. (5.5.219)₂ and (5.5.221) the vector $\boldsymbol{\Omega}_{\mathbf{h}^{\text{el}}}$ can be computed as follows

$$\boldsymbol{\Omega}_{\mathbf{h}^{\text{el}}} = (\mathbf{I} - \mathbf{A}_{\mathbf{h}^{\text{el}}}) \cdot \left(\mathbf{I} - \tilde{\mathbf{A}}_{\mathbf{V}^{\text{el}}} \right) \cdot \boldsymbol{\omega} \quad (5.5.222)$$

The inverse form of the constitutive equation (5.5.202) is

$$\mathbf{h}^{\text{el}} = \frac{\boldsymbol{\tau}}{2\mu} - \frac{\lambda}{2\mu} \frac{(\text{tr } \boldsymbol{\tau}) \mathbf{I}}{3\lambda + 2\mu}, \quad (5.5.223)$$

where $\boldsymbol{\tau} = \mathbf{J}\boldsymbol{\sigma}$ is the Kirchhoff stress tensor. Taking the time derivative of (5.5.223) and applying Eqs. (5.5.217) and (5.5.219) we obtain the relationship between the rate of deformation tensor and the Kirchhoff stress tensor

$$\mathbf{D} = \frac{d}{dt} \left(\frac{\boldsymbol{\tau}}{2\mu} - \frac{\lambda}{2\mu} \frac{(\text{tr } \boldsymbol{\tau}) \mathbf{I}}{3\lambda + 2\mu} \right) + \frac{1}{2\mu} (\boldsymbol{\tau} \times \boldsymbol{\Omega}_{\mathbf{h}^{\text{el}}} - \boldsymbol{\Omega}_{\mathbf{h}^{\text{el}}} \times \boldsymbol{\tau}) + \mathbf{D}^{\text{pl}} \quad (5.5.224)$$

Equations (5.5.224), (5.5.222) and (5.5.223) together with constitutive equation for \mathbf{D}^{pl} , for example, Eq. (5.5.210) can be applied to compute stress response for the given velocity gradient \mathbf{L} . Let us note, that the “plastic part” of the deformation gradient \mathbf{F}^{pl} is not defined as long as $\boldsymbol{\Omega}_{\mathbf{R}}^{\text{pl}}$.

Another possibility is to assume

$$\boldsymbol{\omega}^{\text{pl}} = \boldsymbol{\Omega}_{\mathbf{R}}^{\text{pl}} \quad (5.5.225)$$

instead of (5.5.216). From Eq. (4.1.67) it follows that $(\mathbf{D}^{\text{pl}} \cdot \mathbf{V}^{\text{pl}2})_{\times} = \mathbf{0}$, i.e. the tensor \mathbf{V}^{pl} is co-axial with the tensor \mathbf{D}^{pl} . Furthermore, if we accept the constitutive Eqs. (5.5.210) and (5.5.202) then the tensor \mathbf{D}^{pl} is co-axial with the tensor \mathbf{V}^{el} . Therefore, the tensors \mathbf{V}^{el} and \mathbf{V}^{pl} are co-axial too, and the tensor $\mathbf{V}^{\text{el}} \cdot \mathbf{V}^{\text{pl}}$ is symmetric.

With $\mathbf{R}^{\text{pl}} = \mathbf{I}$ the multiplicative decomposition (5.5.187) takes the form

$$\mathbf{F} = \mathbf{V}^{\text{el}} \cdot \mathbf{V}^{\text{pl}} \cdot \mathbf{R}^{\text{pl}}$$

Since $\mathbf{V} = \mathbf{V}^{\text{el}} \cdot \mathbf{V}^{\text{pl}}$ is symmetric, from the polar decomposition theorem we may identify $\mathbf{R} = \mathbf{R}^{\text{pl}}$. For the Hencky strain tensor the additive decomposition can be applied

$$\mathbf{h} = \mathbf{h}^{\text{el}} + \mathbf{h}^{\text{pl}}$$

Furthermore, the principal axes of the tensors \mathbf{V}^{el} , \mathbf{V}^{pl} and \mathbf{V} rotate with the same angular velocities

$$\boldsymbol{\Omega}_{\mathbf{V}} = \boldsymbol{\Omega}_{\mathbf{V}^{\text{el}}} = \boldsymbol{\Omega}_{\mathbf{V}^{\text{pl}}}$$

Since $\boldsymbol{\omega}^{\text{pl}} = \boldsymbol{\Omega}_{\mathbf{R}^{\text{pl}}} = \boldsymbol{\Omega}_{\mathbf{R}}$, it follows from the relationship (4.1.55) that $\boldsymbol{\Omega}_{\mathbf{V}^{\text{pl}}} = \boldsymbol{\Omega}_{\mathbf{R}}$ and consequently $\boldsymbol{\Omega} = \boldsymbol{\Omega}_{\mathbf{R}}$. This is only possible if the tensor \mathbf{D} is co-axial with the tensor \mathbf{V} , as it follows from Eqs. (4.1.55) and (4.1.67). This condition restricts the class of allowable deformations.

We refer to Lubarda (2001), Nemat-Nasser (2004) for various versions of the multiplicative decomposition as well as to several formulations for rotation tensors and associated spins.

5.5.2 Small Strains

Many high-temperature components are designed such that local deformations cannot exceed some small allowable values. For the structural analysis the geometrically-linear theory (small strain theory) can be applied. Within the linearized theory of elasto-plasticity the additive split of strain tensors can be assumed as follows

$$\boldsymbol{\varepsilon} = \boldsymbol{\varepsilon}^{\text{el}} + \boldsymbol{\varepsilon}^{\text{pl}} \quad (5.5.226)$$

The time derivative of Eq. (5.5.226) provides the additive split of strain rates

$$\mathbf{D} = \mathbf{D}^{\text{el}} + \mathbf{D}^{\text{pl}}, \quad \mathbf{D} = \dot{\boldsymbol{\varepsilon}}, \quad \mathbf{D}^{\text{el}} = \dot{\boldsymbol{\varepsilon}}^{\text{el}}, \quad \mathbf{D}^{\text{pl}} = \dot{\boldsymbol{\varepsilon}}^{\text{pl}} \quad (5.5.227)$$

In the general case of thermo-elasto-plasticity one should add thermal strains, see Sect. 5.3.4

$$\boldsymbol{\varepsilon} = \boldsymbol{\varepsilon}^{\text{el}} + \boldsymbol{\varepsilon}^{\text{pl}} + \boldsymbol{\varepsilon}^{\text{th}}, \quad \boldsymbol{\varepsilon}^{\text{th}} = \boldsymbol{\alpha}_{\text{th}} \Theta \quad (5.5.228)$$

As an example, consider the isotropic linear-elasticity coupled with isotropic von Mises-Odqvist type inelastic flow. The stress tensor is then defined as follows

$$\boldsymbol{\sigma} = \lambda(\text{tr } \boldsymbol{\varepsilon})\mathbf{I} + 2\mu(\boldsymbol{\varepsilon} - \boldsymbol{\varepsilon}^{\text{pl}}) - (3\lambda + 2\mu)\alpha_{\text{th}}\Theta\mathbf{I}, \quad (5.5.229)$$

where the Lamé constants λ and μ are defined by (5.3.65). With the decomposition of the stress tensor (5.4.79) we obtain

$$\sigma_{\text{m}} = K(\varepsilon_V - 3\alpha_{\text{th}}\Theta), \quad \mathbf{s} = 2\mu(\boldsymbol{\varepsilon} - \boldsymbol{\varepsilon}^{\text{pl}}), \quad (5.5.230)$$

where

$$K = \frac{3\lambda + 2\mu}{3} = \frac{E}{3(1 - 2\nu)}$$

is the bulk modulus, $\varepsilon_V = \text{tr } \boldsymbol{\varepsilon}$ is the volumetric strain and

$$\boldsymbol{\varepsilon} = \boldsymbol{\varepsilon} - \frac{1}{3}\varepsilon_V\mathbf{I} \quad (5.5.231)$$

is the strain deviator. The inelastic strain rate tensor can be defined by Eq. (5.4.106) as follows

$$\dot{\boldsymbol{\varepsilon}}^{\text{pl}} = \frac{3}{2}\dot{\varepsilon}_{\text{vM}}\frac{\mathbf{s}}{\sigma_{\text{vM}}}, \quad \dot{\varepsilon}_{\text{vM}} = \frac{\partial W(\sigma_{\text{vM}})}{\partial \sigma_{\text{vM}}} \quad (5.5.232)$$

With Eqs. (5.5.230) and (5.5.231) the strain tensor can be computed

$$\boldsymbol{\varepsilon} = \frac{\sigma_{\text{m}}}{3K}\mathbf{I} + \frac{\mathbf{s}}{2\mu} + \alpha_{\text{th}}\Theta\mathbf{I} + \boldsymbol{\varepsilon}^{\text{pl}} \quad (5.5.233)$$

The time derivative of Eq. (5.5.233) yields

$$\dot{\boldsymbol{\varepsilon}} = \frac{d}{dt} \left(\frac{\sigma_{\text{m}}}{3K}\mathbf{I} + \frac{\mathbf{s}}{2\mu} + \alpha_{\text{th}}\Theta\mathbf{I} \right) + \dot{\boldsymbol{\varepsilon}}^{\text{pl}} \quad (5.5.234)$$

With Eq. (5.5.232) we obtain

$$\dot{\boldsymbol{\varepsilon}} = \frac{d}{dt} \left(\frac{\sigma_{\text{m}}}{3K}\mathbf{I} + \frac{\mathbf{s}}{2\mu} + \alpha_{\text{th}}\Theta\mathbf{I} \right) + \frac{3}{2}\dot{\varepsilon}_{\text{vM}}\frac{\mathbf{s}}{\sigma_{\text{vM}}} \quad (5.5.235)$$

For isothermal condition Eq. (5.5.235) simplifies to

$$\dot{\boldsymbol{\varepsilon}} = \frac{\dot{\sigma}_{\text{m}}}{3K}\mathbf{I} + \frac{\dot{\mathbf{s}}}{2\mu} + \frac{3}{2}\dot{\varepsilon}_{\text{vM}}\frac{\mathbf{s}}{\sigma_{\text{vM}}} \quad (5.5.236)$$

5.6 Hardening and Softening Rules

In the case of rapid changes of external loading one must take into account transient effects of inelastic material behavior. Let us discuss some experimental results related to high-temperature plasticity under variable multi-axial loading conditions and small strains. The majority of multi-axial tests have been performed on thin-walled tubes under combined action of tension (compression) force and torque. In this case the uniform stress state $\boldsymbol{\sigma} = \sigma \mathbf{n} \otimes \mathbf{n} + \tau (\mathbf{n} \otimes \mathbf{m} + \mathbf{m} \otimes \mathbf{n})$ is assumed, where σ and τ are calculated from the force and torque as well as the geometry of the cross section (see Sect. 1.1.2). Figure 5.4 presents a sketch of experimental data for type 304 steel ($2\frac{1}{4}\text{Cr-1Mo}$) at 600°C (Inoue 1988). A tube was loaded the first 5 h by the constant tension force and the constant torque. After that the direction of the force was reversed while the torque kept constant. The normal strain versus time creep curve under compressive force after the reversal differs substantially from the reference creep curve under tensile force, Fig. 5.4a. The absolute value of the strain rate before and after the reversal differs significantly. Furthermore, the shear strain versus time creep curve is influenced by the reversal of the axial force, Fig. 5.4b.

Figure 5.5 shows a sketch of experimental results obtained in Penkalla et al. (1988) for INCONEL Alloy 617 (NiCr22Co12Mo) tubes at 900°C under cyclic torsion. Every 100h the applied torque was reversed leading to the change of the sign of the shear stress. The inelastic shear strain accumulated after each cycle of positive (negative) torque decreases rapidly after few cycles of reversals. Similar behavior is reported in Ohno et al. (1990) for the type 304 steel, where, in addition, the effect of thermal exposure before and during the loading is discussed. Creep behavior of steels is usually accompanied by the thermally induced evolution of structure of carbide precipitates (coarsening or new precipitation). The effect of ageing has a significant influence on the transient creep of steels as discussed in Ohno et al. (1990). For example, the decrease of inelastic shear strain under alternating torsion

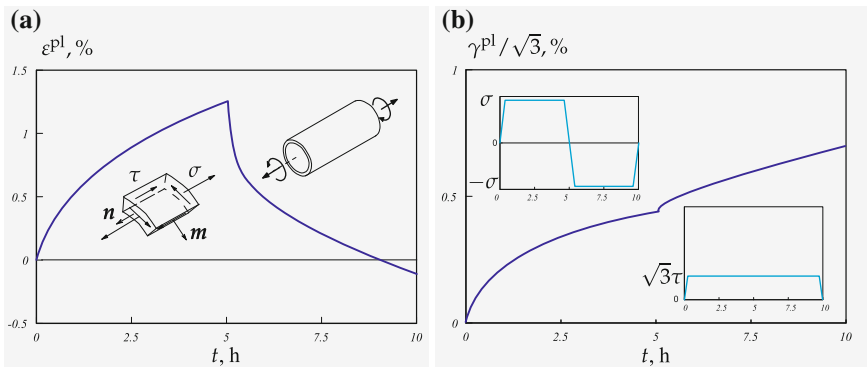


Fig. 5.4 Transient creep at combined tension and torsion. Effect of the normal stress reversal. **a** Normal strain versus time, **b** shear strain versus time, after Inoue (1988)

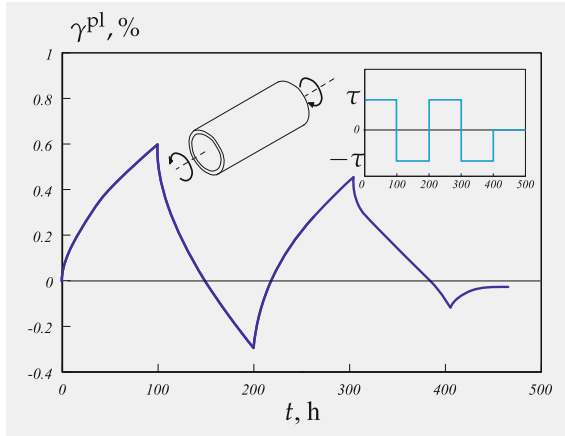


Fig. 5.5 Creep under shear stress reversals, after Penkalla et al. (1988)

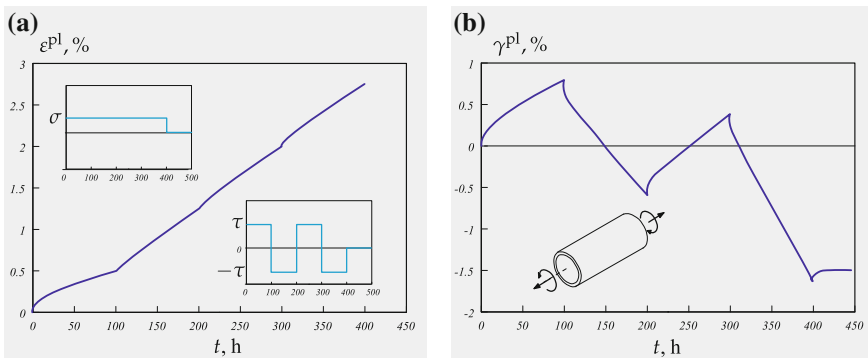


Fig. 5.6 Creep at combined tension and torsion—effect of the shear stress reversals. **a** Normal strain versus time, **b** shear strain versus time, after Penkalla et al. (1988)

was not observed if tubular specimens were subjected to the thermal exposure within the time interval of 500 h before the loading.

Additional effects have been observed in the case of reversals of the applied torque combined with the constant tension force, Fig. 5.6. Here the axial strain response is significantly influenced by the cyclic torsion. Furthermore, the rate of the shear strain depends on the sign of the applied torque. Such a response indicates the anisotropic nature of the hardening processes.

Multi-axial inelastic behavior is significantly influenced by the deformation history. As an example, Fig. 1.25 presents a sketch of results reported in Kawai (1989) for type 304 stainless steel. Tubular specimens were first loaded up to the stress σ_1 leading to the plastic strain of 3%. After that the specimens were unloaded to σ_0 . Subsequent creep tests have been performed under combined constant normal strain σ and shear strain τ . Tests under different stress states leading to the same value of

the von Mises stress $\sigma_{vM} = \sqrt{\sigma^2 + 3\tau^2} = \sigma_0$ were performed. The results show that the tensile creep curve of the material after plastic pre-straining differs significantly from the creep curve of the “virgin material” (curve a). Furthermore, the von Mises inelastic strain versus time curves after plastic pre-straining depend significantly on the type of the applied stress state (compare, for example, tension, curve a, torsion, curve b, and compression, curve e).

In this section we discuss phenomenological models to describe primary creep and inelastic transients under multi-axial stress states. We start with empirical models of time and strain hardening. Then we introduce the concept of kinematic hardening to characterize transient creep effects under constant and varying loading. Our purpose is to discuss general ideas rather than enter into details of empirical functions of stress and temperature as well as different forms of evolution equations for hardening variables (the so-called hardening rules). Regarding the hardening rules one may consult the comprehensive reviews (Chaboche 1989; Ohno 1990; Chaboche 2008) and monographs (Krausz and Krausz 1996; Lemaitre and Chaboche 1990; Miller 1987; Stouffer and Dame 1996). For classification and assessment of different unified models of high-temperature plasticity we refer to Inoue (1988), Inoue et al. (1989).

5.6.1 Time and Strain Hardening

The time hardening model assumes a relationship between the equivalent creep rate, the equivalent stress and the time at fixed temperature, i.e.

$$f_t(\dot{\epsilon}_{eq}^{pl}, \sigma_{eq}, t) = 0$$

The strain hardening model postulates a relationship between the equivalent creep rate, the equivalent creep strain and the equivalent stress at fixed temperature. In this case

$$f_s(\dot{\epsilon}_{eq}^{pl}, \epsilon_{eq}^{pl}, \sigma_{eq}) = 0$$

Figure 5.7 illustrates the uni-axial creep response after reloading (stress jump from σ_1 to σ_2 at $t = t_r$). Based on the time hardening model the strain rate at $t \geq t_r$ is determined by the stress σ_2 and the time t_r only. Thus the creep curve for $t \geq t_r$ can be obtained by translation of the curve BC to the point D . Following the strain hardening model the strain rate depends on the stress and the accumulated strain. The creep curve after the stress jump can be determined by translating the curve AC (the creep curve for the stress σ_2 starting from the creep strain ϵ_A^{pl} accumulated over time t_r) along the time axis.

It can be shown that for specific functions of stress, time and strain as well as under the assumption of the constant stress and temperature the strain and the time hardening models provide the same description. For example, if we set

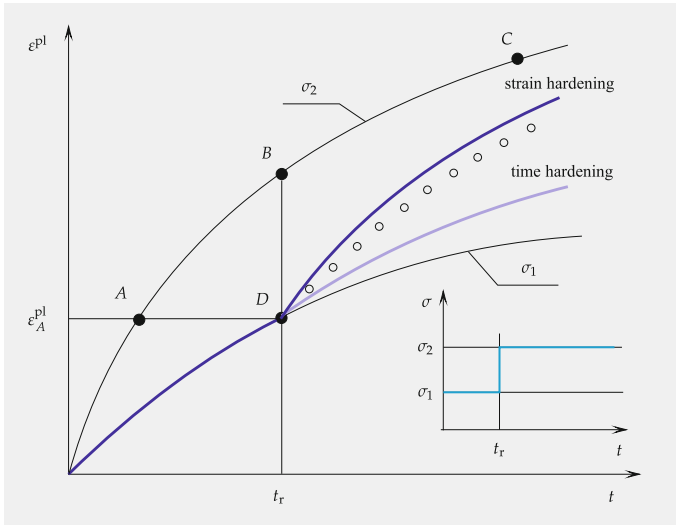


Fig. 5.7 Creep response at variable loading (the open circles denote typical experimental values)

$$\dot{\epsilon}_{eq}^{pl} = a\sigma_{eq}^n t^m \tag{5.6.237}$$

according to the time hardening with a , n and m as the material parameters, the integration with respect to the time variable assuming $\sigma_{eq} = \text{const}$ and $\epsilon_{eq}^{pl} = 0$ at $t = 0$ leads to

$$\epsilon_{eq}^{pl} = a\sigma_{eq}^n \frac{1}{m + 1} t^{m+1} \tag{5.6.238}$$

On the other hand applying the strain hardening model, the creep equation can be formulated as

$$\dot{\epsilon}_{eq}^{pl} = b\sigma_{eq}^k (\epsilon_{eq}^{pl})^l \tag{5.6.239}$$

Taking into account (5.6.238) the time variable can be eliminated from (5.6.237). As a result the following relations between the material parameters can be obtained

$$b = [a(m + 1)^m]^{\frac{1}{m+1}}, \quad k = \frac{n}{m + 1}, \quad l = \frac{m}{m + 1}$$

Vice versa, the strain hardening equation (5.6.238) can be integrated for the special choice of k and l and for $\sigma_{eq} = \text{const}$. Again, if $\epsilon_{eq}^{pl} = 0$ at $t = 0$, we obtain Eq. (5.6.238).

Applying the time hardening model the von Mises-Odqvist creep theory (see Sect. 5.4.2.1) can be generalized as follows

$$\dot{\boldsymbol{\varepsilon}}^{\text{pl}} = \frac{3}{2} a \sigma_{\text{VM}}^{n-1} t^m \mathbf{s} \quad (5.6.240)$$

By analogy one can formulate the creep constitutive equation with the strain hardening

$$\dot{\boldsymbol{\varepsilon}}^{\text{pl}} = \frac{3}{2} b \sigma_{\text{VM}}^{k-1} (\varepsilon_{\text{VM}}^{\text{pl}})^l \mathbf{s} \quad (5.6.241)$$

The time and the strain hardening models provide simple empirical description of the uni-axial creep curve within the range of primary creep and are popular in characterizing the material behavior, e.g. Hayhurst et al. (2002), Hyde et al. (2003b), Kowalewski et al. (1994). Despite the simplicity, both the models suffer from several limitations, even if applied stress and temperature are constant. The disadvantage of the time hardening model is that the time variable appears explicitly in Eq. (5.6.237) for the creep rate. An additional drawback is that the constants m and l take usually the values $-1 < m < 0$, $-1 < l < 0$ as the result of curve fitting. If $\varepsilon_{\text{eq}}^{\text{pl}} = 0$ at $t = 0$ then Eq. (5.6.239) provides an infinite starting creep rate. One can avoid this problem in a time-step based numerical procedure assuming a small non-zero creep equivalent strain at the starting time step. Finally, both models can be applied only for the case of the constant or slowly varying stresses. Transient creep effects under rapid changes of loading and in particular under stress reversals cannot be described.

Many details of time and strain hardening models can be found in Kraus (1980), Penny and Marriott (1995). In Kraus (1980) a modified strain hardening model is proposed based on the concept of creep strain origins.

5.6.2 Kinematic Hardening

The common approach in describing transient inelastic effects under complex loading paths is the introduction of internal state variables and appropriate evolution equations (the so-called hardening rules). The scalar-valued internal state variables are applied to characterize isotropic hardening and ageing processes. Examples are discussed in Sect. 3.5. Several “non-classical” effects observed in tests under non-proportional loading have motivated the use of tensor-valued variables (usually second rank tensors).

The idea of kinematic hardening (translation of the yield surface in the stress space) originates from the theory of plasticity and has been proposed by Prager (1956). In the creep mechanics the kinematic hardening was introduced by Malinin and Khadjinsky (1969, 1972) and Frederick and Armstrong (2007).¹⁷

¹⁷The model was first published in 1966 in a CEBG report, see Frederick and Armstrong (2007) for historical remarks.

The starting point is the additive decomposition of the stress tensor into two parts: $\boldsymbol{\sigma} = \bar{\boldsymbol{\sigma}} + \boldsymbol{\alpha}$, where $\bar{\boldsymbol{\sigma}}$ is called the active or the effective part of the stress tensor and $\boldsymbol{\alpha}$ denotes the additional or translation part of the stress tensor (backstress tensor). The introduced tensors can be further decomposed into spherical and deviatoric parts

$$\begin{aligned}\bar{\boldsymbol{\sigma}} &= \frac{1}{3} \text{tr } \bar{\boldsymbol{\sigma}} \mathbf{I} + \bar{\mathbf{s}}, & \text{tr } \bar{\mathbf{s}} &= 0, \\ \boldsymbol{\alpha} &= \frac{1}{3} \text{tr } \boldsymbol{\alpha} \mathbf{I} + \boldsymbol{\beta}, & \text{tr } \boldsymbol{\beta} &= 0, \\ \boldsymbol{\sigma} &= \frac{1}{3} (\text{tr } \bar{\boldsymbol{\sigma}} + \text{tr } \boldsymbol{\alpha}) \mathbf{I} + \mathbf{s}, & \mathbf{s} &= \bar{\mathbf{s}} + \boldsymbol{\beta}\end{aligned}\quad (5.6.242)$$

It is assumed that the inelastic strain rate is determined by the active part of the stress tensor. The flow potential is then a function of the active part of the stress tensor, i.e. $W = W(\bar{\boldsymbol{\sigma}}) = W(\boldsymbol{\sigma} - \boldsymbol{\alpha})$, e.g. Oytana et al. (1982). As in the case of the isotropic creep (Sect. 5.4.2.1) only the second invariant of the deviator $\bar{\mathbf{s}}$ is considered. Introducing the von Mises equivalent stress

$$\bar{\sigma}_{\text{vM}} = \sqrt{\frac{3}{2} \bar{\mathbf{s}} \cdot \bar{\mathbf{s}}} = \sqrt{\frac{3}{2} (\mathbf{s} - \boldsymbol{\beta}) \cdot (\mathbf{s} - \boldsymbol{\beta})} \quad (5.6.243)$$

the flow rule (5.4.96) leads to the following constitutive equation

$$\dot{\boldsymbol{\epsilon}}^{\text{pl}} = \frac{3}{2} \frac{\dot{\bar{\sigma}}_{\text{vM}}^{\text{pl}}}{\bar{\sigma}_{\text{vM}}} \bar{\mathbf{s}}, \quad \dot{\bar{\sigma}}_{\text{vM}}^{\text{pl}} = \sqrt{\frac{2}{3} \dot{\boldsymbol{\epsilon}}^{\text{pl}} \cdot \dot{\boldsymbol{\epsilon}}^{\text{pl}}} \quad (5.6.244)$$

The equivalent creep rate can be expressed by the use of stress and temperature functions discussed in Sect. 5.4.4. For example, the power law stress function and the Arrhenius temperature dependence can be applied as follows

$$\dot{\bar{\sigma}}_{\text{vM}}^{\text{pl}} = a \bar{\sigma}_{\text{vM}}^n, \quad a = a_0 \exp\left(-\frac{Q}{RT}\right) \quad (5.6.245)$$

Equations (5.6.244) contain the deviatoric part of the back stress $\boldsymbol{\beta}$. This internal state variable is defined by the evolution equation and the initial condition. In Malinin (1975, 1981) the following evolution equation is postulated

$$\dot{\boldsymbol{\beta}} = \frac{2}{3} b \dot{\boldsymbol{\epsilon}}^{\text{pl}} - \frac{g(\alpha_{\text{vM}})}{\alpha_{\text{vM}}} \boldsymbol{\beta} \quad (5.6.246)$$

with

$$\alpha_{\text{vM}} = \sqrt{\frac{3}{2} \boldsymbol{\beta} \cdot \boldsymbol{\beta}}$$

In Malinin (1975, 1981) the function g is postulated as follows

$$g(\alpha_{\text{VM}}) = c\alpha_{\text{VM}}^n, \quad c = c_0 \exp\left(-\frac{Q_r}{RT}\right)$$

Equation (5.6.246) is the multi-axial utilization of the Bailey-Orowan recovery hypothesis, see Sect. 5.4.4, b and c_0 are material parameters and Q_r is the activation energy of recovery.

The Armstrong-Frederick type evolution equation for the backstress deviator can be formulated as follows (Frederick and Armstrong 2007; Längler et al. 2014)

$$\dot{\boldsymbol{\beta}} = \frac{1}{E_h(T)} \frac{dE_h}{dT} \dot{T} \boldsymbol{\beta} + \frac{2}{3} E_h \left[\dot{\boldsymbol{\epsilon}}^{\text{pl}} - \frac{3}{2} \dot{\epsilon}_{\text{VM}} \frac{\boldsymbol{\beta}}{\beta_*(\sigma_{\text{VM}}, T)} \right], \quad (5.6.247)$$

where $E_h(T)$ is a function of the temperature, and $\beta_*(\sigma_{\text{VM}}, T)$ is a function of the von Mises equivalent stress

$$\sigma_{\text{VM}} = \sqrt{\frac{3}{2} \mathbf{s} \cdot \mathbf{s}}$$

and the temperature.

Let us show how the kinematic hardening model behaves for the uni-axial homogeneous stress state $\boldsymbol{\sigma}(t) = \sigma(t) \mathbf{n} \otimes \mathbf{n}$, where $\sigma(t)$ is the magnitude of the applied stress and \mathbf{n} is the unit vector. With $\boldsymbol{\alpha}(0) = \mathbf{0}$ one can assume that $\boldsymbol{\alpha}(t)$ is coaxial with the stress tensor. Therefore one can write (Malinin 1975, 1981)

$$\boldsymbol{\alpha} = \alpha \mathbf{n} \otimes \mathbf{n}, \quad \boldsymbol{\beta} = \alpha \left(\mathbf{n} \otimes \mathbf{n} - \frac{1}{3} \mathbf{I} \right), \quad \bar{\sigma}_{\text{VM}} = |\sigma - \alpha|, \quad \alpha_{\text{VM}} = |\alpha|$$

From Eqs. (5.6.245) and (5.6.246) it follows

$$\begin{aligned} \dot{\epsilon}^{\text{pl}} &= a \text{sign}(\sigma - \alpha) |\sigma - \alpha|^n, & \dot{\boldsymbol{\epsilon}}^{\text{pl}} &= \mathbf{n} \cdot \dot{\epsilon}^{\text{pl}} \cdot \mathbf{n}, \\ \dot{\alpha} &= b \dot{\epsilon}^{\text{pl}} - c \text{sign} \alpha |\alpha|^n \end{aligned} \quad (5.6.248)$$

Let us assume that $\sigma(t) = \sigma_0 > 0$, $\alpha(0) = 0$, $\sigma_0 - \alpha > 0$. In addition, let us introduce the variable $H = \alpha/\sigma_0$. From (5.6.248) we obtain

$$\dot{\epsilon}^{\text{pl}} = a \sigma_0^n (1 - H)^n, \quad \dot{H} = \sigma_0^{n-1} [ba(1 - H)^n - cH^n] \quad (5.6.249)$$

The constitutive and evolution Eqs. (5.6.249) describe the primary and the secondary stages of a uni-axial creep curve, Fig. 5.8. In the considered case of the uni-axial tension the parameter $0 \leq H < H_* < 1$ is equal to zero at the beginning of the creep process and increases over time. In the steady state $H = H_*$, where H_* is the saturation value. From the second equation in (5.6.249) we obtain

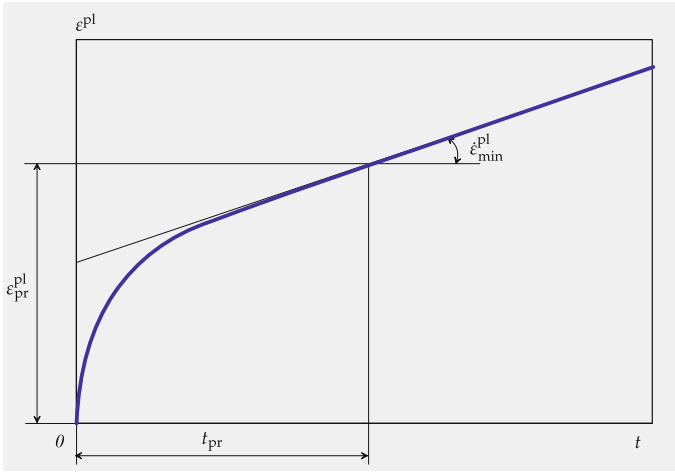


Fig. 5.8 Primary and secondary creep stages of a uni-axial creep curve

$$H_* = \frac{1}{1 + \mu^{\frac{1}{n}}}, \quad \mu = \frac{c}{ab} \tag{5.6.250}$$

The minimum creep rate in the steady creep state is calculated by

$$\dot{\varepsilon}_{\min}^{\text{pl}} = a\sigma_0^n(1 - H_*)^n = \tilde{a}\sigma_0^n, \quad \tilde{a} \equiv a(1 - H_*)^n \tag{5.6.251}$$

The constants \tilde{a} and n can be obtained from the experimental data of steady-state creep. For the given value of H_* the second equation in (5.6.249) can be integrated providing the duration time of primary creep t_{pr} (see Fig. 5.8)

$$t_{\text{pr}} = \frac{\varphi(H_*)}{ba\sigma_0^n}, \quad \varphi(H_*) = \int_0^{H_*} \frac{dH}{(1 - H)^n - \mu H^n}$$

From the first equation in Eqs. (5.6.249) the creep strain $\varepsilon_{\text{pr}}^{\text{pl}}$ follows at $t = t_{\text{pr}}$ (see Fig. 5.8) as

$$\varepsilon_{\text{pr}}^{\text{pl}} = \frac{\sigma_0}{b} \int_0^{H_*} \frac{(1 - H)^n dH}{(1 - H)^n - \mu H^n}$$

The above equations can be used for the identification of material parameters.

To discuss the model predictions for the case of the uni-axial cyclic loading let us introduce the following dimensionless variables

$$\tilde{\sigma} = \frac{\sigma(t)}{\sigma_0}, \quad \tau = \frac{t}{t_{pr}}, \quad \epsilon = \frac{\epsilon^{pl}}{a(1 - H_*)\sigma_0^n t_{pr}},$$

where σ_0 denotes the constant stress value in the first loading cycle. Equations (5.6.248) take the form

$$\begin{aligned} \frac{d\epsilon}{d\tau} &= a \text{sign}(\tilde{\sigma} - H) \frac{|\tilde{\sigma} - H|^n}{1 - H_*}, \\ \frac{dH}{d\tau} &= \varphi(H_*) \left[\text{sign}(\tilde{\sigma} - H) |\tilde{\sigma} - H|^n - \text{sign}(H) \left(\frac{1 - H_*}{H_*} \right)^n |H|^n \right] \end{aligned} \quad (5.6.252)$$

Figures 5.9 and 5.10 illustrate the results of the numerical integration of Eqs. (5.6.252) with $n = 3$, $H_* = 0.7$ and the initial conditions $\epsilon(0) = 0$ and $H(0) = 0$. In the first

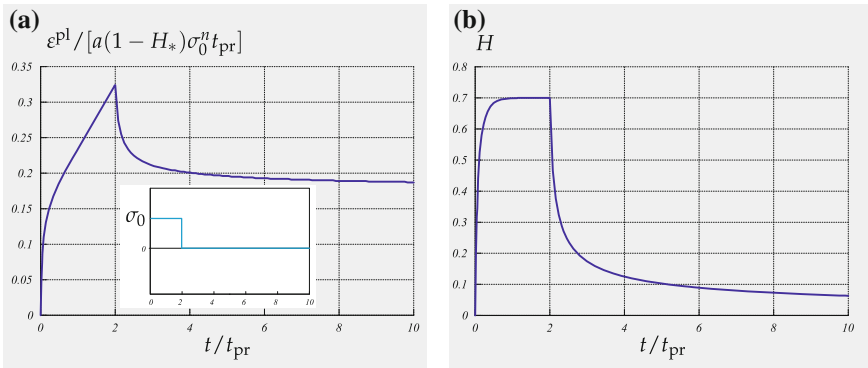


Fig. 5.9 Uni-axial creep after unloading—simulations based on Eqs. (5.6.252) for the case $n = 3$ and $H_* = 0.7$. **a** Creep strain versus time, **b** hardening variable versus time

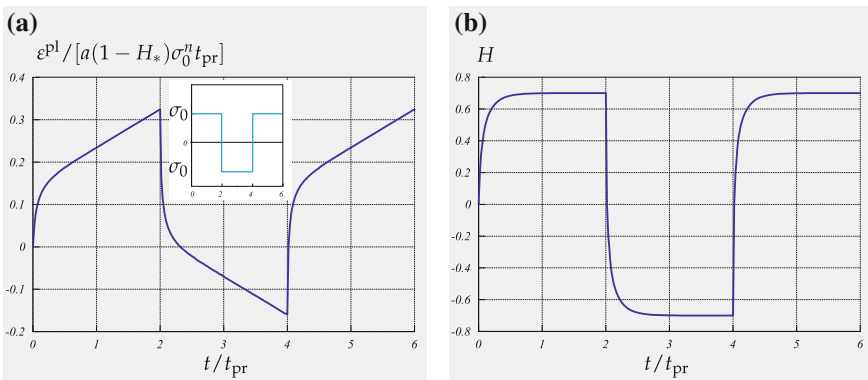


Fig. 5.10 Uni-axial creep under cyclic loading—simulations based on Eqs. (5.6.252) for the case $n = 3$ and $H_* = 0.7$. **a** Creep strain versus time, **b** hardening variable versus time

case presented in Fig. 5.9 we assume $\sigma = \sigma_0$ within the time interval $[0; 2t_{pr}]$, so that the hardening variable increases up to the saturation value and remains constant. The creep curve exhibits both the primary and the secondary stages, Fig. 5.9a. At $t = 2t_{pr}$ we assume a spontaneous unloading, i.e. $\sigma = 0$. We observe that the model (5.6.252) is able to describe the creep recovery (see Fig. 1.11b). Figure 5.10 presents the numerical results for the case of cyclic loading. Three loading cycles with the constant stresses $\pm\sigma_0$ and the holding time $\Delta t = 2t_{pr}$, Fig. 5.10a, are considered. We observe that the model (5.6.252) predicts identical creep responses for the first and the third loading cycle.

Let us analyze the model predictions under multi-axial stress state. To this end we consider the loading case with the constant stress deviator \mathbf{s} within a given interval of time $[t_0, t]$. Equations (5.6.244) and (5.6.246) can be rewritten as follows

$$\dot{\boldsymbol{\varepsilon}}^{pl} = \frac{3}{2} \frac{f(\bar{\sigma}_{vM})}{\bar{\sigma}_{vM}} (\mathbf{s} - \boldsymbol{\beta}), \quad \dot{\boldsymbol{\beta}} = b \frac{f(\bar{\sigma}_{vM})}{\bar{\sigma}_{vM}} (\mathbf{s} - \boldsymbol{\beta}) - \frac{g(\alpha_{vM})}{\alpha_{vM}} \boldsymbol{\beta} \quad (5.6.253)$$

In the steady creep state $\boldsymbol{\beta} = \boldsymbol{\beta}_*$, where $\boldsymbol{\beta}_*$ is the saturation value of the back stress deviator. From Eq. (5.6.253)₂ it follows

$$b \frac{f(\bar{\sigma}_{vM_*})}{\bar{\sigma}_{vM_*}} (\mathbf{s} - \boldsymbol{\beta}_*) = \frac{g(\alpha_{vM_*})}{\alpha_{vM_*}} \boldsymbol{\beta}_*, \quad (5.6.254)$$

where

$$\bar{\sigma}_{vM_*} = \sqrt{\frac{3}{2} (\mathbf{s} - \boldsymbol{\beta}_*) \cdot (\mathbf{s} - \boldsymbol{\beta}_*)}, \quad \alpha_{vM_*} = \sqrt{\frac{3}{2} \boldsymbol{\beta}_* \cdot \boldsymbol{\beta}_*}$$

The double inner product of (5.6.254) with itself results in

$$[bf(\bar{\sigma}_{vM_*})]^2 = [g(\alpha_{vM_*})]^2$$

Since $f(\bar{\sigma}_{vM_*}) > 0$ and $g(\alpha_{vM_*}) > 0$ we obtain

$$bf(\bar{\sigma}_{vM_*}) = g(\alpha_{vM_*}) \quad (5.6.255)$$

From (5.6.254) it follows

$$\boldsymbol{\beta}_* = \frac{\alpha_{vM_*}}{\bar{\sigma}_{vM_*} + \alpha_{vM_*}} \mathbf{s} \Rightarrow \bar{\sigma}_{vM_*} = \sigma_{vM} + \alpha_{vM_*} \quad (5.6.256)$$

Now the steady state value of the back stress deviator can be calculated

$$\boldsymbol{\beta}_* = \alpha_{vM_*} \frac{\mathbf{s}}{\sigma_{vM}} \quad (5.6.257)$$

Let us assume power functions for f and g . Then from Eq. (5.6.255) we obtain

$$ba(\sigma_{\text{VM}} - \alpha_{\text{VM}_*})^n = c\alpha_{\text{VM}_*}^n$$

As in the uni-axial case we introduce the hardening variable $H = \alpha_{\text{VM}}/\sigma_{\text{VM}}$. The saturation value H_* is then determined by (5.6.250). From Eq. (5.6.253)₁ we obtain

$$\dot{\boldsymbol{\varepsilon}}_{\text{st}}^{\text{pl}} = \frac{3}{2}\tilde{a}\sigma_{\text{VM}}^{n-1}\boldsymbol{s}, \quad \tilde{a} \equiv a(1 - H_*)^n \quad (5.6.258)$$

We observe that the kinematic hardening model (5.6.253) results in the Norton-Bailey-Odqvist constitutive equation of steady-state creep discussed in Sect. 5.4.2.1. This model predicts isotropic steady-state creep independently from the initial condition for the back stress deviator $\boldsymbol{\beta}$. Furthermore, different stress states leading to the same value of the von Mises equivalent stress will provide the same steady state value of the equivalent creep rate.

As an example let us consider a thin-walled tube subjected to the axial force and the torque (see Sect. 1.1.2). Let us assume that in the first loading cycle the force and the torque are kept constant over a certain period of time such that the creep rates attain the steady state values. The stress deviator has the following form

$$\boldsymbol{s}_1 = \sigma(\boldsymbol{k} \otimes \boldsymbol{k} - \frac{1}{3}\boldsymbol{I}) + \tau(\boldsymbol{e}_\varphi \otimes \boldsymbol{k} + \boldsymbol{k} \otimes \boldsymbol{e}_\varphi), \quad (5.6.259)$$

where σ is the normal stress, τ is the shear stress and the unit vectors \boldsymbol{k} and \boldsymbol{e}_φ designate the axial and the circumferential direction, respectively (cp. Fig. 1.22). In addition, we assume that in the second loading cycle the tube is loaded by the same tensile force but the reversed constant shear stress. In this case the stress deviator is

$$\boldsymbol{s}_2 = \sigma(\boldsymbol{k} \otimes \boldsymbol{k} - \frac{1}{3}\boldsymbol{I}) - \tau(\boldsymbol{e}_\varphi \otimes \boldsymbol{k} + \boldsymbol{k} \otimes \boldsymbol{e}_\varphi), \quad (5.6.260)$$

From Eqs. (5.6.259) and (5.6.260) we find that

$$\boldsymbol{s}_2 = \boldsymbol{Q} \cdot \boldsymbol{s}_1 \cdot \boldsymbol{Q}^T, \quad \boldsymbol{Q} = \boldsymbol{Q}^T = 2\boldsymbol{k} \otimes \boldsymbol{k} - \boldsymbol{I} \quad (5.6.261)$$

The kinematic hardening model (5.6.253) predicts the following relation between the steady state creep rates in the first and the second loading cycle

$$\dot{\boldsymbol{\varepsilon}}_{\text{st}_2}^{\text{pl}} = \boldsymbol{Q} \cdot \dot{\boldsymbol{\varepsilon}}_{\text{st}_1}^{\text{pl}} \cdot \boldsymbol{Q}^T$$

Consequently, the normal strain rates and the magnitudes of the shear strain rates will be the same at the end of the loading cycles.

The model (5.6.253) is applied in Malinin (1981), Oytana et al. (1982) for the description of creep for different materials under simple or non-proportional loading conditions. It is demonstrated that the predictions agree well with experimental data.

However, in many cases deviations from the Norton-Bailey-Odqvist type steady-state creep can be observed in experiments. For example, in the case shown in Fig. 5.6 the steady state shear creep rate changes significantly after the shear stress reversals, although the von Mises equivalent stress remains constant. The results presented in Fig. 1.25 indicate that the initial hardening state due to plastic pre-strain is the reason for the stress state dependence of the subsequent creep behavior. This effect is not described by the model (5.6.253).

The model with the back stress of the type (5.6.253) are sometimes called anisotropic hardening model, e.g. Malinin (1981). The type of anisotropy is then determined by the symmetry group of the back stress tensor or deviator. The symmetry group of any symmetric second rank tensor includes always eight elements, e.g. Lurie (1990). For the tensor $\boldsymbol{\beta}$ the symmetry elements are

$$\boldsymbol{Q}_{\boldsymbol{\beta}} = \pm \boldsymbol{n}_1 \otimes \boldsymbol{n}_1 \pm \boldsymbol{n}_2 \otimes \boldsymbol{n}_2 \pm \boldsymbol{n}_3 \otimes \boldsymbol{n}_3, \quad (5.6.262)$$

where \boldsymbol{n}_i are the principal axes of the tensor $\boldsymbol{\beta}$. The flow potential formulated in terms of the stress deviator and the back stress deviator satisfies the following condition

$$W(\boldsymbol{s}, \boldsymbol{\beta}) = W(\boldsymbol{Q}_{\boldsymbol{\beta}} \cdot \boldsymbol{s} \cdot \boldsymbol{Q}_{\boldsymbol{\beta}}^T, \boldsymbol{Q}_{\boldsymbol{\beta}} \cdot \boldsymbol{\beta} \cdot \boldsymbol{Q}_{\boldsymbol{\beta}}^T) = W(\boldsymbol{Q}_{\boldsymbol{\beta}} \cdot \boldsymbol{s} \cdot \boldsymbol{Q}_{\boldsymbol{\beta}}^T, \boldsymbol{\beta})$$

Consequently the flow potential is an orthotropic function of the stress deviator with the symmetry group defined by (5.6.262). As shown in Boehler (1987b) any kinematic hardening model of the type (5.6.253) leads to a restrictive form of orthotropic inelastic behavior. In order to demonstrate this let us put the back stress deviator in the following form

$$\begin{aligned} \boldsymbol{\beta} &= \beta_1 \boldsymbol{n}_1 \otimes \boldsymbol{n}_1 + \beta_2 \boldsymbol{n}_2 \otimes \boldsymbol{n}_2 - (\beta_1 + \beta_2) \boldsymbol{n}_3 \otimes \boldsymbol{n}_3 \\ &= \beta_1 (\boldsymbol{n}_1 \otimes \boldsymbol{n}_1 - \boldsymbol{n}_3 \otimes \boldsymbol{n}_3) + \beta_2 (\boldsymbol{n}_2 \otimes \boldsymbol{n}_2 - \boldsymbol{n}_3 \otimes \boldsymbol{n}_3), \end{aligned}$$

where β_1 and β_2 are the principal values and $\boldsymbol{n}_1, \boldsymbol{n}_2$ and \boldsymbol{n}_3 are the principal directions of $\boldsymbol{\beta}$. For the given back stress deviator $\boldsymbol{\beta}$ the equivalent stress (5.6.243) takes the form

$$\begin{aligned} \bar{\sigma}_{\text{VM}}^2 &= 3\tilde{J}_1^2 \left(1 - \frac{\beta_1}{\tilde{J}_1}\right)^2 + 3\tilde{J}_2^2 \left(1 - \frac{\beta_2}{\tilde{J}_2}\right)^2 + \frac{3}{2}\tilde{J}_1\tilde{J}_2 \left(1 - \frac{\beta_1}{\tilde{J}_1}\right) \left(1 - \frac{\beta_2}{\tilde{J}_2}\right) \\ &+ 3I_{\boldsymbol{n}_1\boldsymbol{n}_2}^2 + 3I_{\boldsymbol{n}_1\boldsymbol{n}_3}^2 + 3I_{\boldsymbol{n}_2\boldsymbol{n}_3}^2, \end{aligned} \quad (5.6.263)$$

where the invariants \tilde{J}_i are defined by Eqs. (5.4.149) and the invariants $I_{\boldsymbol{n}_i\boldsymbol{n}_j}$ are defined by Eqs. (5.4.144). Steady state creep with initial orthotropic symmetry is discussed in Sect. 5.4.3. In this case the von Mises type equivalent stress includes 6 invariants and 6 independent material parameters. The equivalent stress (5.6.263) contains all 6 orthotropic invariants. However, the last three terms (three shear stresses with respect to the three planes of the orthotropic symmetry) are not affected by the

hardening. Furthermore, in the steady state range these terms vanish since the back stress deviator β_* is coaxial with the stress deviator according to (5.6.257).

Several possibilities to refine the kinematic hardening model are discussed in the literature. Examples include:

- Introduction of additional state variables like isotropic hardening variable, e.g. Chaboche (1989, 2008), ageing variable, e.g. Ohno et al. (1990), Naumenko and Gariboldi (2014), or damage variables, e.g. Dyson and McLean (1998), Naumenko et al. (2011a, b),
- Formulation of the creep potential as a general isotropic function of two tensors σ and α . Such an approach is proposed in Boehler (1987b) for the case of plasticity and includes different special cases of kinematic hardening,
- Consideration of the initial anisotropy of the material behavior, e.g. Inoue (1988), Naumenko and Gariboldi (2014).

Creep models with kinematic hardening of the type (5.6.244) and different specific forms of the hardening evolution equation are discussed in Kawai (1996), Kawai (1997), Malinin (1981), Ohno et al. (1990), Oytana et al. (1982), Robinson (1984) among others. For the description of creep and creep-plasticity interaction at complex loading conditions a variety of unified models is available including the hardening variables as second rank tensors. For details we refer to Krausz and Krausz (1996), Krempl (1999), Lemaitre and Chaboche (1990), Miller (1987). Several unified models are reviewed and evaluated in Inoue (1988); Inoue et al. (1989). The historical background of the development of non-linear kinematic hardening rules is presented in Chaboche (1989, 2008).

5.6.3 Phase Mixture Models for Hardening and Softening

Advanced heat resistant steels contain relatively high dislocation density at the initial state after the processing. Fine subgrain structure and different types of precipitates are examples of microstructural features that improve creep strength and high-temperature resistance Abe (2009), Dyson and McLean (1998), Blum (2008), Straub (1995). For such materials the inelastic deformation is accompanied by softening processes including recovery of dislocation substructures and coarsening of subgrains (Blum 2008). Stress-strain curves of softening materials show descending (softening) branch, Fig. 1.2 and creep curves exhibit accelerated regime immediately after the primary creep stage, Fig. 1.9.

In Sect. 3.5.3 a phase mixture model (or composite model) is applied to characterize hardening and softening processes. The basic idea is to idealize the heterogeneous inelastic deformation in a volume element by considering a mixture with two or more constituents with different, but homogeneous inelastic properties. Assuming the total deformation of constituents to be the same, redistribution of stresses would take place,

leading to the decrease of the overall inelastic strain rate. In Straub (1995), Polcik et al. (1998), Polcik (1999), Barkar and Ågren (2005) two phases are introduced including the inelastic hard phase to characterize subgrain boundaries with a relatively high dislocation density and the inelastic soft one to model subgrain interiors. Two different sets of constitutive equations for inelastic strains are formulated. Furthermore, the volume fraction of the hard constituent is assumed to decrease over time to capture the coarsening process. Below let us generalize the phase mixture model to the multi-axial stress state. For the sake of simplicity let us assume small strains such that the geometrically-linear theory can be applied.

Let us consider a composite material with two constituents. We assume that constituents have the same thermo-elastic properties. To designate the properties of the constituents the subscripts s (for inelastic-soft) and h (for inelastic-hard) will be used. Let $\boldsymbol{\varepsilon}$ be the strain tensor and $\boldsymbol{\sigma}$ the Cauchy stress tensor. We specify by $\boldsymbol{\varepsilon}_s$ and $\boldsymbol{\varepsilon}_h$ the infinitesimal strain tensors of the constituents and by $\boldsymbol{\sigma}_s$ and $\boldsymbol{\sigma}_h$ the corresponding effective stress tensors. To generalize the constitutive equations discussed in Sect. 3.5.3 we assume isotropic thermo-elasticity and creep for both the constituents. Furthermore, we assume that the constituents have the same temperature. With Eq. (5.5.234) the constitutive equations for the constituents are

$$\begin{aligned}\dot{\boldsymbol{\varepsilon}}_h &= \frac{d}{dt} \left(\frac{\sigma_{m_h}}{3K} \mathbf{I} + \frac{\mathbf{s}_h}{2\mu} + \alpha_{th} \Theta \mathbf{I} \right) + \dot{\boldsymbol{\varepsilon}}_h^{pl}, \\ \dot{\boldsymbol{\varepsilon}}_s &= \frac{d}{dt} \left(\frac{\sigma_{m_s}}{3K} \mathbf{I} + \frac{\mathbf{s}_s}{2\mu} + \alpha_{th} \Theta \mathbf{I} \right) + \dot{\boldsymbol{\varepsilon}}_s^{pl},\end{aligned}\tag{5.6.264}$$

where

$$\begin{aligned}\sigma_{m_h} &= \frac{1}{3} \text{tr} \boldsymbol{\sigma}_h, & \mathbf{s}_h &= \boldsymbol{\sigma}_h - \sigma_{m_h} \mathbf{I}, \\ \sigma_{m_s} &= \frac{1}{3} \text{tr} \boldsymbol{\sigma}_s, & \mathbf{s}_s &= \boldsymbol{\sigma}_s - \sigma_{m_s} \mathbf{I}\end{aligned}$$

The corresponding equation for the composite is

$$\dot{\boldsymbol{\varepsilon}} = \frac{d}{dt} \left(\frac{\sigma_m}{3K} \mathbf{I} + \frac{\mathbf{s}}{2\mu} + \alpha_{th} \Theta \mathbf{I} \right) + \dot{\boldsymbol{\varepsilon}}^{pl}\tag{5.6.265}$$

For the inelastic strain rates of the constituents let us assume the following constitutive equations

$$\begin{aligned}\dot{\boldsymbol{\varepsilon}}_s^{pl} &= \frac{3}{2} \frac{\dot{\varepsilon}_{vM_s}}{\sigma_{vM_s}} \mathbf{s}_s, & \dot{\varepsilon}_{vM_s} &= f(\sigma_{vM_s}) g(T), \\ \dot{\boldsymbol{\varepsilon}}_h^{pl} &= \frac{3}{2} \frac{\dot{\varepsilon}_{vM}}{\sigma_{vM_s}} (\mathbf{s}_h - \mathbf{s}),\end{aligned}\tag{5.6.266}$$

where

$$\begin{aligned}\sigma_{vM_s} &= \sqrt{\frac{3}{2} \mathbf{s}_s \cdots \mathbf{s}_s}, & \sigma_{vM_*} &= \sqrt{\frac{3}{2} (\mathbf{s}_{h_*} - \mathbf{s}) \cdots (\mathbf{s}_{h_*} - \mathbf{s})}, \\ \dot{\varepsilon}_{vM} &= \sqrt{\frac{2}{3} \dot{\boldsymbol{\varepsilon}}^{pl} \cdots \dot{\boldsymbol{\varepsilon}}^{pl}}, & \dot{\varepsilon}_{vM_s} &= \sqrt{\frac{2}{3} \dot{\boldsymbol{\varepsilon}}_s^{pl} \cdots \dot{\boldsymbol{\varepsilon}}_s^{pl}},\end{aligned}\quad (5.6.267)$$

and \mathbf{s}_{h_*} is the saturation stress deviator which is assumed to be collinear with \mathbf{s} . The stress and the strain tensors of the composite are defined by the following mixture rules

$$\boldsymbol{\sigma} = (1 - \eta_h) \boldsymbol{\sigma}_s + \eta_h \boldsymbol{\sigma}_h, \quad \boldsymbol{\varepsilon} = (1 - \eta_h) \boldsymbol{\varepsilon}_s + \eta_h \boldsymbol{\varepsilon}_h, \quad (5.6.268)$$

where η_h is the volume fraction of the hard constituent. To complete the model a rule for the interaction between the constituents is required. Here let us apply the iso-strain approach such that

$$\boldsymbol{\varepsilon}_h = \boldsymbol{\varepsilon}_s = \boldsymbol{\varepsilon} \quad (5.6.269)$$

The traces of Eqs. (5.6.268)₁ and (5.6.269) yield

$$\sigma_m = (1 - \eta_h) \sigma_{m_s} + \eta_h \sigma_{m_h}, \quad \varepsilon_V = \varepsilon_{V_h} = \varepsilon_{V_s},$$

where $\varepsilon_V = \text{tr } \boldsymbol{\varepsilon}$, $\varepsilon_{V_h} = \text{tr } \boldsymbol{\varepsilon}_h$ and $\varepsilon_{V_s} = \text{tr } \boldsymbol{\varepsilon}_s$ are volumetric strains. From constitutive Eqs. (5.6.264) it follows

$$\varepsilon_{V_h} - 3\alpha_{th}\Theta = \frac{\sigma_{m_h}}{K}, \quad \varepsilon_{V_s} - 3\alpha_{th}\Theta = \frac{\sigma_{m_s}}{K}, \quad \varepsilon_V - 3\alpha_{th}\Theta = \frac{\sigma_m}{K}$$

Hence

$$\sigma_m = \sigma_{m_h} = \sigma_{m_s} = K(\varepsilon_V - 3\alpha_{th}\Theta) \quad (5.6.270)$$

Since the bulk moduli of the constituents are assumed to be the same and the spherical parts of the creep rate tensors are zeros, the mean stresses have identical values. Then for the deviatoric parts of the stress and the strain tensors we have

$$\mathbf{s} = (1 - \eta_h) \mathbf{s}_s + \eta_h \mathbf{s}_h, \quad \boldsymbol{\varepsilon} = \boldsymbol{\varepsilon}_h = \boldsymbol{\varepsilon}_s \quad (5.6.271)$$

For the identification of functions and material properties in the phase mixture model it is convenient to introduce the following new variables

$$\boldsymbol{\beta} = \frac{\eta_{h_0}}{1 - \eta_{h_0}} (\mathbf{s}_h - \mathbf{s}), \quad \Gamma = \frac{\eta_h}{1 - \eta_h} \frac{1 - \eta_{h_0}}{\eta_{h_0}}, \quad (5.6.272)$$

where η_{h_0} is the reference value of the volume fraction. From Eqs. (5.6.264)₁, (5.6.265), (5.6.266)₂, (5.6.269) and (5.6.270) we obtain

$$\dot{\boldsymbol{\beta}} = \frac{1}{\mu} \frac{d\mu}{dT} \dot{T} \boldsymbol{\beta} + \frac{2\mu}{c_h} \left[\dot{\boldsymbol{\epsilon}}^{\text{pl}} - \frac{3}{2} \dot{\epsilon}_{\text{vM}} \frac{\boldsymbol{\beta}}{\beta_*} \right], \quad (5.6.273)$$

where

$$c_h = \frac{1 - \eta_{h_0}}{\eta_{h_0}}, \quad \beta_* = \sqrt{\frac{3}{2} \boldsymbol{\beta}_* \cdots \boldsymbol{\beta}_*}, \quad \beta_* = \frac{1}{c_h} (s_{h_*} - s)$$

With Eqs. (5.6.264)₂, (5.6.265), (5.6.266)₁, (5.6.269) and (5.6.270) the inelastic strain rate tensor can be computed as follows

$$\dot{\boldsymbol{\epsilon}}^{\text{pl}} = \frac{3}{2} f(\bar{\sigma}_{\text{vM}}) g(T) \frac{\bar{\boldsymbol{s}}}{\bar{\sigma}_{\text{vM}}} - \frac{d}{dt} \left(\frac{\boldsymbol{\beta} \Gamma}{2\mu} \right), \quad (5.6.274)$$

where

$$\bar{\boldsymbol{s}} = \boldsymbol{s} - \boldsymbol{\beta} \Gamma, \quad \bar{\sigma}_{\text{vM}} = \sqrt{\frac{3}{2} \bar{\boldsymbol{s}} \cdots \bar{\boldsymbol{s}}} \quad (5.6.275)$$

In Eq. (5.6.274) the introduced variables $\boldsymbol{\beta}$ and Γ play the role of internal state variables. If the volume fraction of the hard constituent does not evolve over time, i.e. $\eta_h = \eta_{h_0}$ then according to Eq. (5.6.272) $\Gamma = 1$. Equations (5.6.273) and (5.6.274) simplify to

$$\begin{aligned} \dot{\boldsymbol{\epsilon}}^{\text{pl}} &= \frac{3}{2} f(\bar{\sigma}_{\text{vM}}) g(T) \frac{\bar{\boldsymbol{s}}}{\bar{\sigma}_{\text{vM}}} - \frac{d}{dt} \left(\frac{\boldsymbol{\beta}}{2\mu} \right), \quad \bar{\boldsymbol{s}} = \boldsymbol{s} - \boldsymbol{\beta} \Gamma \\ \dot{\boldsymbol{\beta}} &= \frac{1}{\mu} \frac{d\mu}{dT} \dot{T} \boldsymbol{\beta} + \frac{2\mu}{c_h} \left[\dot{\boldsymbol{\epsilon}}^{\text{pl}} - \frac{3}{2} \dot{\epsilon}_{\text{vM}} \frac{\boldsymbol{\beta}}{\beta_*} \right] \end{aligned} \quad (5.6.276)$$

For $c_h \gg 1$ the underlined term has a minor influence and can be neglected. With $E_h = 3\mu/c_h$ and without the underlined term Eqs. (5.6.276) coincide with Frederick-Armstrong type constitutive and evolution equations, cp. Eqs. (5.6.244) and (5.6.247).

To consider softening processes an additional evolution equation is required for the variable Γ . Let us assume that Γ evolves by the exponential law with the increase of the mean inelastic strain towards the saturation value $\Gamma_*(\sigma)$, i.e.

$$\dot{\Gamma} = A_s [\Gamma_*(\sigma_{\text{vM}}) - \Gamma] \dot{\epsilon}_{\text{vM}}^{\text{pl}} \quad (5.6.277)$$

Then, as discussed in Sect. 3.5.3 the introduced model describes the decrease of the inelastic strain rate as a result of stress redistribution between the constituents and the increase of the inelastic strain rate as a consequence of softening processes (decrease of the volume fraction of the hard constituent).

5.7 Damage Processes and Damage Mechanics

Inelastic deformation is often accompanied by damage processes. Examples include the formation, growth and coalescence of voids on grain boundaries, microcracks in particles of the second phase, decohesion at particle/matrix interfaces and surface relief and surface cracks under cyclic loading. In contrast to softening and ageing, leading to the increase of inelastic strain rate, damage processes cause formation of cracks and final fracture of solids. The characterization of damage processes under multi-axial stress state is important for life-time estimation of a component designed for high-temperature application.

Continuum damage mechanics is a powerful approach to characterize various damage phenomena in materials and structures (Krajcinovic 1996; Lemaitre and Desmorat 2005; Murakami 2012). Several examples of damage evolution equations for uni-axial stress state are presented in Sect. 3.6. In this Section we discuss generalizations to the multi-axial stress state. The damage rate and the inelastic strain rate are determined by the stress level, the accumulated damage and the temperature. These dependencies can be established based on experimental data from uni-axial tests, for example creep tests. If the material is subjected to multi-axial loading, the kind of stress state has a significant influence on the damage growth. Tension and compression lead to different creep rates. Different stress states corresponding to the same von Mises equivalent stress lead, in general, to different equivalent tertiary creep rates while the equivalent strain rate in the secondary stage is approximately the same. These facts are established from the data of creep tests under combined tension and torsion, e.g. Kowalewski (1996, 2001), as well as from biaxial and triaxial creep tests (Sakane and Hosokawa 2001; Sakane and Tokura 2002). Stress state effects must be considered in the damage evolution equation. In Sect. 5.7.1 we discuss various possibilities to characterize the tertiary creep behavior by means of scalar-valued damage parameters. Under non-proportional loading conditions, the additional factor is the influence of the damage induced anisotropy. Examples are creep tests under combined tension and alternating torsion, e.g. Murakami and Sanomura (1985), and creep tests under biaxial loading with alternating direction of the first principal stress (Sakane and Tokura 2002). In both cases the assumption of isotropic creep behavior and the scalar measure of damage lead to disagreement with experimental observations. In Sect. 5.7.2 we review some experimental results illustrating the damage induced anisotropy and discuss creep-damage models with tensor-valued damage variables. In this Section we focus on the description of creep damage—a main factor that usually limits the lifetime of a high-temperature component.

5.7.1 *Scalar-Valued Damage Variables*

Many microstructural observations show the directional effect of creep damage. For example, during a cyclic torsion test on copper, voids nucleate and grow

predominantly on those grain boundaries, which are perpendicular to the first principal direction of the stress tensor, e.g. Hayhurst (1999). Creep damage has therefore an anisotropic nature and should be characterized by a tensor. However, if the initially isotropic material is subjected to constant or monotonic loading the influence of the damage anisotropy on the observed creep behavior, i.e. the strain versus time curves, is not significant. If the state of damage is characterized by a tensor (see Sect. 5.7.2) then such a tensor can be assumed to be coaxial with the stress tensor under monotonic loading conditions. In such a case only the scalar damage measures will enter the creep constitutive equation. Below we introduce different models of tertiary creep including the phenomenological, the so-called micromechanically consistent and mechanism based models. The effect of damage is described by means of scalar valued damage parameters and corresponding evolution equations. The stress state influences are expressed in the equivalent stress responsible for the damage evolution.

5.7.1.1 Kachanov-Rabotnov Model

To generalize Eqs. (3.6.118) and (3.6.119) to the multi-axial stress states Rabotnov (1963) assumed that

- the creep process is determined by the effective stress tensor $\tilde{\sigma} = \mathbf{f}(\boldsymbol{\sigma}, \omega)$,
- the creep potential for the damaged material has the same form as for the secondary creep

For example, the Norton-Bailey-Odqvist creep potential (5.4.98) can be generalized as follows

$$W(\tilde{\sigma}) = \frac{\sigma_0}{n+1} \left(\frac{\tilde{\sigma}_{\text{VM}}}{\sigma_0} \right)^{n+1}, \quad \tilde{\sigma}_{\text{VM}} = \sqrt{\frac{3}{2} \tilde{\mathbf{s}} \cdot \tilde{\mathbf{s}}}, \quad \tilde{\mathbf{s}} = \tilde{\boldsymbol{\sigma}} - \frac{1}{3} \text{tr} \tilde{\boldsymbol{\sigma}} \mathbf{I} \quad (5.7.278)$$

Rabotnov (1963, 1967) proposed the following effective stress tensor

$$\tilde{\boldsymbol{\sigma}} = \frac{\sigma_I}{1-\omega} \mathbf{n}_I \otimes \mathbf{n}_I + \sigma_{II} \mathbf{n}_{II} \otimes \mathbf{n}_{II} + \sigma_{III} \mathbf{n}_{III} \otimes \mathbf{n}_{III} \quad (5.7.279)$$

for the case of distinct principal values of the stress tensor $\sigma_I > \sigma_{II} > \sigma_{III}$ and $\sigma_I > 0$. Equation (5.7.279) implies that the effect of damage is only significant in the planes perpendicular to the first principal direction associated with the maximum tensile stress. Hence the constitutive equation for the creep rate would have the form

$$\dot{\boldsymbol{\epsilon}}^{\text{pl}} = \dot{\lambda}(\tilde{\sigma}_{\text{VM}}) \left[\mathbf{s} + \frac{\omega}{1-\omega} \sigma_I (\mathbf{n}_I \otimes \mathbf{n}_I - \frac{1}{3} \mathbf{I}) \right], \quad (5.7.280)$$

Equation (5.7.280) suggests that the proportionality between the creep rate tensor and the stress deviator is violated in the tertiary creep range. Leckie and Hayhurst

(1977) analyzed experimental data of combined tension and torsion for copper and aluminium alloys. They concluded that the strain trajectories (see Fig. 1.24) are not sensibly affected by the damage processes. Therefore, the creep rate can be assumed in the form

$$\dot{\boldsymbol{\epsilon}}^{\text{pl}} = \dot{\lambda}(\tilde{\sigma}_{\text{VM}})\mathbf{s}$$

Leckie and Hayhurst (1977) proposed to generalize the von Mises-type secondary creep equation (see Sect. 5.4.2.1) as follows

$$\dot{\boldsymbol{\epsilon}}^{\text{pl}} = \frac{3}{2}a \left(\frac{\sigma_{\text{VM}}}{1-\omega} \right)^n \frac{\mathbf{s}}{\sigma_{\text{VM}}} \quad (5.7.281)$$

Equation (5.7.281) can be also derived applying the strain equivalence principle (Lemaitre and Chaboche 1990) and the effective stress tensor in the form $\tilde{\boldsymbol{\sigma}} = \boldsymbol{\sigma}/(1-\omega)$.

The next step is the formulation of the damage evolution equation. By analogy with the uni-axial case, the damage rate should have a form

$$\dot{\omega} = \dot{\omega}(\boldsymbol{\sigma}, \omega)$$

The dependence on the stress tensor can be expressed by means of the “damage equivalent stress” $\sigma_{\text{eq}}^{\omega}(\boldsymbol{\sigma})$ which allows the comparison of creep strength behavior under different stress states. With the damage equivalent stress, the uni-axial equation (3.6.119) can be generalized as follows

$$\dot{\omega} = \frac{b(\sigma_{\text{eq}}^{\omega})^k}{(1-\omega)^l} \quad (5.7.282)$$

The material parameters a , b , n , k and l can be identified from uni-axial creep curves. In order to find a suitable expression for the damage equivalent stress, the data from multi-axial creep tests up to rupture are required. For isotropic materials, $\sigma_{\text{eq}}^{\omega}$ can be formulated in terms of three invariants of the stress tensor, for example the basic invariants

$$\sigma_{\text{eq}}^{\omega} = \sigma_{\text{eq}}^{\omega}[I_1(\boldsymbol{\sigma}), I_2(\boldsymbol{\sigma}), I_3(\boldsymbol{\sigma})]$$

Similarly to the uni-axial case, see Eq. (3.6.126), the damage evolution equation (5.7.282) can be integrated assuming that the stress tensor is constant during the test. As a result, the relationship between the time to creep fracture and the equivalent stress can be obtained

$$t_* = \frac{1}{(l+1)b} (\sigma_{\text{eq}}^{\omega})^{-k} \quad (5.7.283)$$

Sdobyrev (1959) carried out long term tests on tubular specimens made from alloys EI-237B (Ni-based alloy) and EI-405 (Fe-based alloy) under tension, torsion and combined tension-torsion. The results of tests are collected for different temperatures and presented as equivalent stress versus fracture time plots. The following dependence was established

$$\frac{1}{2}(\sigma_I + \sigma_{vM}) = f(\log t_*) \quad (5.7.284)$$

Sdobyrev found that the linear function f provides a satisfactory description of the experimental data. The equivalent stress responsible to the long term strength at high temperatures is then $\sigma_{eq}^* = \frac{1}{2}(\sigma_I + \sigma_{vM})$. Based on different mechanisms which control creep failure, the influence of three stress state parameters (the mean stress $\sigma_m = I_1/3$, the first positive principal stress or the maximum tensile stress $\sigma_{max\ t} = (\sigma_I + |\sigma_I|)/2$ and the von Mises stress) is discussed by Trunin (1965). The Sdobyrev criterion was extended as follows

$$\sigma_{eq}^* = \frac{1}{2}(\sigma_{vM} + \sigma_{max\ t}) a^{1-2\eta}, \quad \eta = \frac{3\sigma_m}{\sigma_{vM} + \sigma_{max\ t}}, \quad (5.7.285)$$

where a is a material constant. For special loading cases this equivalent stress yields

- uni-axial tension

$$\sigma_{eq}^* = \sigma, \quad \eta = \frac{1}{2}$$

- uni-axial compression

$$\sigma_{eq}^* = \frac{\sigma a^3}{2}, \quad \eta = -1$$

- pure torsion

$$\sigma_{eq}^* = \frac{\sqrt{3} + 1}{2} \tau a, \quad \eta = 0$$

The constant a can be calculated from the ultimate stress values leading to the same fracture time for a given temperature. For example, if the ultimate tension and shear stresses are σ_u and τ_u , respectively, then

$$a = \frac{2}{\sqrt{3} + 1} \frac{\sigma_u}{\tau_u}$$

Hayhurst (1972) proposed the following relationship

$$t_* = A(\alpha\sigma_{max\ t} + \beta I_1 + \gamma\sigma_{vM})^{-\chi}, \quad (5.7.286)$$

where A and χ are material constants, $I_1 = 3\sigma_m$ and $\alpha + \beta + \gamma = 1$. Comparing this equation with Eq. (5.7.283) one can obtain

$$A = \frac{1}{(l+1)b}, \quad \chi = k, \quad \sigma_{\text{eq}}^\omega = \alpha\sigma_{\text{max } t} + \beta I_1 + \gamma\sigma_{\text{vM}} \quad (5.7.287)$$

Hayhurst introduced the normalized stress tensor $\bar{\sigma} = \sigma/\sigma_0$ and the normalized time to fracture $\bar{t}_* = t_*/t_{*0}$, where t_{*0} is the time to fracture in a uni-axial test conducted at the stress σ_0 . From Eqs. (3.6.126) and (5.7.283) it follows

$$\bar{t}_* = \left(\frac{\sigma_{\text{eq}}^\omega}{\sigma_0} \right)^{-k} = (\bar{\sigma}_{\text{eq}}^\omega)^{-k}$$

By setting the normalized rupture time equal to unity, the equation $\bar{\sigma}_{\text{eq}}^\omega = 1$ follows, which defines the stress states leading to the equal rupture time. In Hayhurst (1972) the data of biaxial tests (biaxial tension test, combined tension and torsion of tubular specimens) are collected for different materials. It was found convenient to present the results in terms of the isochronous rupture surface, which is the plot of the equation $\bar{\sigma}_{\text{eq}}^\omega = 1$ for the specified values of α and β in the normalized stress space. For plane stress states the isochronous rupture loci can be presented in the normalized principal stress axes. Examples for different materials are discussed by Hayhurst (1972). The coefficients α and β are specific for each material and, in addition, they may depend on the temperature. Figure 5.11 shows the isochronous rupture loci for three special cases: $\bar{\sigma}_{\text{eq}}^\omega = \bar{\sigma}_{\text{max } t}$, $\bar{\sigma}_{\text{eq}}^\omega = \bar{\sigma}_{\text{vM}}$ and $\bar{\sigma}_{\text{eq}}^\omega = 3\bar{\sigma}_m$. The first two represent the limit cases of the material behavior (Leckie and Hayhurst 1977).

A generalized expression for the damage equivalent stress can be formulated by the use of three invariants of the stress tensor. With the first invariant I_1 , the von Mises equivalent stress σ_{vM} and

$$\sin 3\xi = -\frac{27}{2} \frac{(\mathbf{s} \cdot \mathbf{s}) \cdot \mathbf{s}}{\sigma_{\text{vM}}^3}, \quad -\frac{\pi}{6} \leq \xi \leq \frac{\pi}{6},$$

as a cubic invariant, the following equivalent stress has been proposed in Altenbach and Zolochovsky (1996)

$$\sigma_{\text{eq}}^\omega = \lambda_1\sigma_{\text{vM}} \sin \xi + \lambda_2\sigma_{\text{vM}} \cos \xi + \lambda_3\sigma_{\text{vM}} + \lambda_4 I_1 + \lambda_5 I_1 \sin \xi + \lambda_6 I_1 \cos \xi \quad (5.7.288)$$

The identification of coefficients λ_i , $i = 1, \dots, 6$ requires six independent tests. Equation (5.7.288) contains a number of known failure criteria as special cases, see Altenbach and Zolochovsky (1996). Setting $\lambda_1 = \lambda_2 = \lambda_4 = \lambda_5 = \lambda_6 = 0$ the equation provides the von Mises equivalent stress. Taking into account

$$\sigma_I = \frac{1}{3} \left[2\sigma_{\text{vM}} \sin \left(\xi + \frac{2\pi}{3} \right) + I_1 \right] = -\frac{1}{3}\sigma_{\text{vM}} \sin \xi + \frac{\sqrt{3}}{3}\sigma_{\text{vM}} \cos \xi + \frac{1}{3}I_1$$

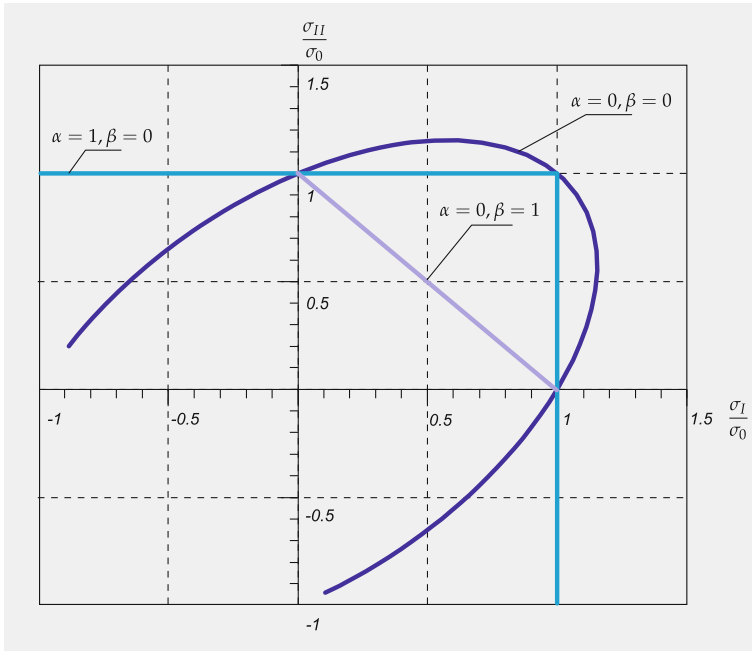


Fig. 5.11 Plane stress isochronous rupture loci, for details see Hayhurst (1972)

and with

$$\lambda_1 = -\frac{1}{6}, \quad \lambda_2 = \frac{\sqrt{3}}{6}, \quad \lambda_3 = \frac{1}{2}, \quad \lambda_4 = \frac{1}{6}, \quad \lambda_5 = \lambda_6 = 0$$

one can obtain $\sigma_{eq}^\omega = \frac{1}{2}(\sigma_I + \sigma_{vM})$. With

$$\lambda_1 = -\frac{1}{3}\alpha, \quad \lambda_2 = \frac{\sqrt{3}}{3}\alpha, \quad \lambda_3 = \beta, \quad \lambda_4 = 1 - \frac{2}{3}\alpha - \beta, \quad \lambda_5 = \lambda_6 = 0$$

Equation (5.7.288) yields $\sigma_{eq}^\omega = \alpha\sigma_I + \beta\sigma_{vM} + (1 - \alpha - \beta)I_1$. Other examples are discussed in Altenbach (2001).

In order to identify the material constants, e.g., a in Eqs. (5.7.285) or α and β in Eq. (5.7.286), the values of the ultimate stresses leading to the same failure time for different stress states are necessary. Therefore series of independent creep tests up to rupture are required. For each kind of test the creep strength curve (stress vs. time to fracture curve), see Fig. 3.9, must be obtained. For example, a series of torsion tests (at least two) under different stress values should be performed. Usually, experimental data from creep tests under complex stress states are limited and the scatter of the experimental results is unavoidable. Therefore, the constitutive and the evolution equation (5.7.281) and (5.7.282) with the two-parametric damage

equivalent stress (5.7.287) are widely used in modeling tertiary creep. Examples of material parameters as well as structural mechanics applications can be found in Altenbach et al. (1997, 2000, 2001b), Altenbach and Naumenko (1997), Bodnar and Chrzanowski (1991), Boyle and Spence (1983), Hayhurst (1972), Hyde et al. (1997, 1999, 2000), Konkin and Morachkovskij (1987), Kowalewski (1996) among others.

5.7.1.2 Micromechanically-Consistent Models

The creep constitutive equation (5.7.281) includes the effect of damage by means of the equivalent stress concept. An alternative approach to formulate the creep constitutive equation can be based on micromechanics. Rodin and Parks (1986) considered an infinite block from incompressible isotropic material containing a given distribution of cracks and subjected to a far field homogeneous stress. As a measure of damage $\rho = a^3 N/V$ is proposed, where N is the number of cracks (voids) in a volume V and a is the averaged radius of a crack. Assuming power law creep the creep potential for such a material has the following form

$$W(\boldsymbol{\sigma}, \rho, n) = \frac{\dot{\varepsilon}_0 \sigma_0}{n+1} f(\zeta(\boldsymbol{\sigma}), \rho, n) \left(\frac{\sigma_{vM}}{\sigma_0} \right)^{n+1}, \quad (5.7.289)$$

where $\dot{\varepsilon}_0$ is the reference creep rate, σ_0 is the reference stress and n is a material constant. $\zeta(\boldsymbol{\sigma})$ is a function representing the influence of the kind of stress state. In Rodin and Parks (1986) the following particular expression is proposed

$$\zeta(\boldsymbol{\sigma}) = \frac{\sigma_I}{\sigma_{vM}},$$

where σ_I is the maximum principal stress. The creep potential (5.7.289) and the flow rule (5.4.96) give

$$\begin{aligned} \dot{\boldsymbol{\varepsilon}}^{pl} &= \frac{\partial W}{\partial \boldsymbol{\sigma}} = \frac{\partial W}{\partial \sigma_{vM}} \frac{\partial \sigma_{vM}}{\partial \boldsymbol{\sigma}} + \frac{\partial W}{\partial \zeta} \frac{\partial \zeta}{\partial \boldsymbol{\sigma}} \\ &= \dot{\varepsilon}_0 \left(\frac{\sigma_{vM}}{\sigma_0} \right)^n \left[\frac{3}{2} \left(f - \frac{\zeta f_{,\zeta}}{n+1} \right) \frac{\boldsymbol{s}}{\sigma_{vM}} + \frac{f_{,\zeta}}{n+1} \boldsymbol{n}_I \otimes \boldsymbol{n}_I \right], \end{aligned} \quad (5.7.290)$$

where \boldsymbol{n}_I is the first principal direction of the stress tensor. The function f must satisfy the following convexity condition (Rodin and Parks 1986)

$$f f_{,\zeta \zeta} - \frac{n}{n+1} f_{,\zeta}^2 > 0,$$

The form of the function f is established for the assumed particular distribution of cracks and by use of a self-consistent approach. In Rodin and Parks (1988) the

following expression is proposed

$$f(\zeta, \rho, n) = \left[1 + \alpha(\rho, n)\zeta^2\right]^{\frac{n+1}{2}},$$

$$\alpha(\rho, n) = \frac{2\rho}{n+1} + \frac{(2n+3)\rho^2}{n(n+1)^2} + \frac{(n+3)\rho^3}{9n(n+1)^3} + \frac{(n+3)\rho^4}{108n(n+1)^4}$$

Models of the type (5.7.290) are popular in materials science related literature, e.g. Gaudig et al. (1999), Mohrmann and Sester (1999). They are based on micromechanical considerations and therefore seem to be more preferable for creep-damage analysis. However, only idealized damage states, e.g. dilute non-interacting cracks or voids with a given density and specific distribution can be considered. Furthermore, there is no micromechanically-consistent way to establish the form of the evolution equation for the assumed damage variable. Different empirical equations are proposed in the literature. For example, Mohrmann and Sester (1999) assume that the cavity nucleation is strain controlled and recommend the following equation

$$\frac{\rho}{\rho_f} = \left(\frac{\varepsilon_{vM}}{\varepsilon_f}\right)^\gamma,$$

where ρ_f , ε_f and γ are material constants which should be identified from “macroscopic” creep responses.

Bassani and Hawk (1990) proposed to use a phenomenological damage parameter ω (see Sect. 5.7.1.1) instead of ρ . The function f is then postulated as follows

$$f(\zeta, \omega, n) = \frac{1}{(1-\omega)^k} (1 - \alpha_0\omega + \alpha_0\omega\zeta^2)^{\frac{n+1}{2}} \quad (5.7.291)$$

Here

$$\zeta = (1 - \alpha_1) \frac{\sigma_I}{\sigma_{vM}} + \alpha_1 \frac{\sigma_H}{\sigma_{vM}}$$

and k , n , α_0 and α_1 are material constants. From Eqs. (5.7.290) and (5.7.291) follows

$$\dot{\boldsymbol{\varepsilon}}^{pl} = \dot{\varepsilon}_0 \left(\frac{\sigma_{vM}}{\sigma_0}\right)^n \frac{1}{(1-\omega)^k} (1 - \alpha_0\omega + \alpha_0\omega\zeta^2)^{\frac{n-1}{2}} \times \left\{ \frac{3}{2}(1 - \alpha_0\omega) \frac{\boldsymbol{s}}{\sigma_{vM}} + \alpha_0\omega\zeta [(1 - \alpha_1)\mathbf{n}_I \otimes \mathbf{n}_I + \alpha_1\mathbf{I}] \right\} \quad (5.7.292)$$

With $\alpha_0 = 0$, $\alpha_1 = 1$ and $k = n$ Eq. (5.7.292) reduces to the Kachanov-Rabotnov type constitutive equation (5.7.281). By setting $\alpha_0 = 1$, $k = (n+1)/2$ and $\omega \ll 1$ Eq. (5.7.292) approximates the Rodin and Parks micro-mechanically consistent model (Rodin and Parks 1986). For the case $k = n$, $\alpha_0 = 1$ and $\alpha_1 = 1$ the constitutive equation for the creep rate can be presented as follows

$$\dot{\boldsymbol{\varepsilon}}^{\text{pl}} = \dot{\varepsilon}_0 \left[\frac{\sigma_{\text{vM}}}{\sigma_0(1-\omega)} \right]^n (1-\omega + \omega\zeta^2)^{\frac{n-1}{2}} \left[\frac{3}{2}(1-\omega) \frac{\boldsymbol{s}}{\sigma_{\text{vM}}} + \omega\zeta \mathbf{I} \right], \quad \zeta = \frac{\sigma_H}{\sigma_{\text{vM}}} \quad (5.7.293)$$

Equation (5.7.293) is applied in Bassani and Hawk (1990) to the finite element simulation of creep crack growth.

From Eq. (5.7.292) one can calculate the volumetric creep rate

$$\dot{\varepsilon}_V = \text{tr } \dot{\boldsymbol{\varepsilon}}^{\text{pl}} = \dot{\varepsilon}_0 \left(\frac{\sigma_{\text{vM}}}{\sigma_0} \right)^n \frac{1}{(1-\omega)^k} (1 - \alpha_0\omega + \alpha_0\omega\zeta^2)^{\frac{n-1}{2}} [\alpha_0\omega\zeta(1 + 2\alpha_1)]$$

We observe that for $\alpha_0 \neq 0$ the damage growth induces dilatation. Creep constitutive equations (5.7.290) or (5.7.292) include the first principal direction of the stress tensor. It should be noted that the dyad $\mathbf{n}_I \otimes \mathbf{n}_I$ can be only found if $\sigma_I \neq 0$, $\sigma_I \neq \sigma_{II}$ and $\sigma_I \neq \sigma_{III}$. In this case, e.g. Lurie (1990)

$$\mathbf{n}_I \otimes \mathbf{n}_I = \frac{1}{(\sigma_I - \sigma_{II})(\sigma_I - \sigma_{III})} \left[\boldsymbol{\sigma}^2 - (\text{tr } \boldsymbol{\sigma} - \sigma_I)\boldsymbol{\sigma} + \frac{\det \boldsymbol{\sigma}}{\sigma_I} \mathbf{I} \right] \quad (5.7.294)$$

Inserting Eq. (5.7.294) into Eq. (5.7.290) or Eq. (5.7.292) we observe that not only the volumetric strain but also second order effects (see Sect. 5.4.2.2 for discussion) are “induced” by damage.

5.7.1.3 Mechanism-Based Models

The constitutive and evolution equations (5.7.281) and (5.7.282) are formulated in terms of power law functions of stress. It is known from materials science that the power law stress dependence guarantees the correct description of the creep rate only for a specific stress range. In addition, the power law stress and damage functions used in Eqs. (5.7.281) and (5.7.282) may lead to numerical problems in finite element simulations of creep in structures with stress concentrations or in attempts to predict the creep crack growth (Liu and Murakami 1998; Saanouni et al. 1989).

The uni-axial creep tests are usually performed under increased stress and temperature levels in order to accelerate the creep process. For the long term analysis of structures the material model should be able to predict creep rates for wide stress ranges including moderate and small stresses. Within the materials science many different damage mechanisms which may operate depending on the stress level and the temperature are discussed, e.g., Dyson (1992). Each of the damage mechanisms can be considered by a state variable with an appropriate kinetic equation.

Within the so-called mechanism-based approach the internal state variables are introduced according to those creep and damage mechanisms which dominate for a specific material and specific loading conditions. Furthermore, different functions of stress and temperature proposed in materials science can be utilized. The form and the validity frame of such a function depend on many factors including the

stress and temperature levels, type of alloying, grain size, etc. The materials science formulations do not provide the values of material constants (only the bounds are given). They must be identified from the data of standard tests, e.g. uni-axial creep test. Examples of mechanism-based models can be found in Hayhurst (1994, 1999), Kowalewski et al. (1994), Othman et al. (1994), Perrin and Hayhurst (1994), Naumenko et al. (2011a, b), Naumenko and Gariboldi (2014). Here let us discuss the model proposed by Perrin and Hayhurst (1994) for a 0.5Cr-0.5Mo-0.25V ferritic steel in the temperature range 600–675 °C.

The starting point is the assumption that the rate of the local grain boundary deformation is approximately a constant fraction of the overall deformation rate. From this follows that the constitutive equations for the overall creep rate can be formulated in terms of empirical relationships between the local grain boundary deformation rate and the stress, the temperature, the cavitation rate, etc.

For ferritic steels the nucleation of cavities has been observed at carbide particles on grain boundaries due to the local accumulation of dislocations. The nucleation kinetics can be therefore related to the local deformation. Furthermore, the cavity nucleation depends on the stress state characterized by σ_I/σ_{VM} . Cane (1981) observed that the area fraction of intergranular cavities in the plane normal to the applied stress increases uniformly with the accumulated creep strain. He proposed that the nucleation and growth can be combined into an overall measure of cavitation. The cavitated area fraction A_f can be related to the von Mises equivalent creep strain, the von Mises equivalent stress and the maximum principal stress by the equation

$$A_f = D\varepsilon_{VM} \left(\frac{\sigma_I}{\sigma_{VM}} \right)^\mu, \quad (5.7.295)$$

where D and μ are constants depending on the material microstructure. Perrin and Hayhurst define the damage state variable ω as the cavitated area fraction. The failure condition in a uni-axial creep test is the complete cavitation of all grain boundaries normal to the applied stress. The cavitated area fraction at failure is approximately 1/3. Therefore, the critical state at which the material fails, can be characterized by $\omega_* = 1/3$.

The ageing mechanism for the ferritic steel under consideration is the temperature dependent coarsening of carbide precipitates. First, the carbide precipitates restrict the deformation of the grain interior and second, they provide sites for nucleation of cavities. Following Dyson (1992), the particle coarsening can be characterized by the state variable $\phi = 1 - l_i/l$ related to the initial (l_i) and current (l) spacing of precipitates. The kinetic equation is derived from the coarsening theory (Dyson 1992; Dyson and McLean 1998), see Sect. 3.5.4

$$\dot{\phi} = \left(\frac{K_c}{3} \right) (1 - \phi)^4 \quad (5.7.296)$$

with K_c as the material dependent constant for a given temperature. The rate of the coarsening variable is independent from the applied stress and can be integrated with respect to time.

The primary creep is characterized by the work hardening due to the formation of the dislocation substructure. For this purpose a scalar hardening state variable H is introduced. This variable varies from zero to a saturation value H_* , at which no further hardening takes place. The proposed evolution equation is

$$\dot{H} = \frac{h_c \dot{\varepsilon}_{vM}^{pl}}{\sigma_{vM}} \left(1 - \frac{H}{H_*} \right) \quad (5.7.297)$$

with h_c as the material constant.

The creep rate is controlled by the climb plus glide deformation mechanism. For the stress dependence of the creep rate, the hyperbolic sine stress function is used. The materials science arguments for the use of hyperbolic sine function instead of power law function are discussed, for example, by Dyson and McLean (2001). With the assumed mechanisms of hardening, cavitation and ageing as well as the corresponding state variables the following equation for the von Mises creep rate is proposed

$$\dot{\varepsilon}_{vM}^{pl} = A \sinh \frac{B \sigma_{vM} (1 - H)}{(1 - \phi)(1 - \omega)} \quad (5.7.298)$$

Equations (5.7.295)–(5.7.298) are formulated under assumption of constant temperature. The influence of the temperature on the processes of creep deformation, creep cavitation and coarsening can be expressed by Arrhenius functions with appropriate activation energies. Further details of the physical motivation are discussed in Perrin and Hayhurst (1994). The following set of constitutive and evolution equations has been proposed

$$\begin{aligned} \dot{\varepsilon}^{pl} &= \frac{3}{2} \frac{s}{\sigma_{vM}} A \sinh \frac{B \sigma_{vM} (1 - H)}{(1 - \phi)(1 - \omega)}, \\ \dot{H} &= \frac{h_c \dot{\varepsilon}_{vM}^{pl}}{\sigma_{vM}} \left(1 - \frac{H}{H_*} \right), \\ \dot{\phi} &= \left(\frac{K_c}{3} \right) (1 - \phi)^4, \\ \dot{\omega} &= DN \dot{\varepsilon}_{vM}^{pl} \left(\frac{\sigma_I}{\sigma_{vM}} \right)^v, \\ A &= A_0 B \exp \left(-\frac{Q_A}{RT} \right), \quad B = B_0 \exp \left(-\frac{Q_B}{RT} \right), \\ K_c &= \frac{K_{c0}}{B^3} \exp \left(-\frac{Q_{K_c}}{RT} \right), \quad D = D_0 \exp \left(-\frac{Q_D}{RT} \right), \end{aligned} \quad (5.7.299)$$

where $N = 1$ for $\sigma_I > 0$ and $N = 0$ for $\sigma_I \leq 0$. $A_0, B_0, D_0, K_{c_0}, h_c, H_*, Q_A, Q_B, Q_D$ and Q_{K_c} are material constants which must be identified from uni-axial creep tests. The material property ν , the so-called stress state index, can be determined from multi-axial creep rupture data. These constants are identified in Perrin and Hayhurst (1994) based on the experimental data of uni-axial creep over the stress range of 28–110 MPa and over the temperature range of 615–690°C. In Perrin and Hayhurst (1999) Eqs. (5.7.299) are applied to model creep in different zones of a weldment at 640°C including the weld metal, the heat-affected zone and the parent material.

It should be noted that Eqs. (5.7.299) are specific for the considered material and can only be applied with respect to the dominant mechanisms of the creep deformation and damage evolution. Further examples of mechanism based material models are presented in Othman et al. (1993) for a nickel-based super-alloy and in Kowalewski et al. (1994) for an aluminium alloy.

5.7.1.4 Models Based on Dissipation

Sosnin (1974), Sosnin et al. (1986) proposed to characterize the material damage by the specific dissipation work. The following damage variable has been introduced

$$q = \int_0^t \sigma \dot{\epsilon}^{pl} d\tau \quad (5.7.300)$$

For the variable q the evolution equation was postulated

$$\dot{q} = f_\sigma(\sigma) f_T(T) f_q(q)$$

For the multi-axial stress state this variable is defined as follows

$$q = \int_0^t \boldsymbol{\sigma} \cdot \dot{\boldsymbol{\epsilon}}^{pl} d\tau$$

In Sosnin et al. (1986) experimental data for various titanium and aluminium alloys are presented in a form of q versus time curves. It was established that a critical value q_* exists at which the material fails under creep conditions. The value q_* does not depend on the kind of the applied stress state.

For isotropic materials the creep rate equation can be formulated as follows (see Sect. 5.4.2)

$$\dot{\boldsymbol{\epsilon}}^{pl} = \frac{3}{2} \frac{P}{\sigma_{vM}} \mathbf{s}, \quad P = \boldsymbol{\sigma} \cdot \dot{\boldsymbol{\epsilon}}^{pl} = \sigma_{vM} \dot{\epsilon}_{vM}^{pl} \quad (5.7.301)$$

Sosnin assumed the dissipation power P to be a function of the von Mises equivalent stress, the temperature and the internal state variable q as follows

$$\dot{q} \equiv P = f_{\sigma}(\sigma_{\text{vM}}) f_T(T) f_q(q)$$

The following empirical equation provides a satisfactory agreement with experimental results

$$\dot{q} = \frac{b\sigma_{\text{vM}}^n}{q^k(q_*^{k+1} - q^{k+1})^m}, \quad (5.7.302)$$

where b , n , k , m and q_* are material constants. In Sosnin et al. (1986) experimental data obtained from uni-axial tests and tests on tubular specimens under combined tension and torsion are presented. In particular the results of combined tension and torsion tests show that the q versus t curves do not depend on the kind of the stress state. The material constants are identified for titanium alloys OT-4, BT-5 and BT-9, for the aluminium alloy D16T and for the steel 45. In Altenbach and Zolochovsky (1994) the Sosnin's dissipation damage measure is applied to the description of creep-damage of the titanium alloy OT-4 and the aluminium alloy D16T considering stress state effects. In Zyczkowski (2000) the dissipation power P was calculated starting from the Kachanov-Rabotnov constitutive equation (5.7.281). It was found that for a class of materials it is possible to express the damage evolution equation (5.7.282) in terms of the dissipation power. A conclusion was made that the number of material constants to be determined from creep tests can be significantly reduced if applying a dissipation based damage model.

5.7.2 Damage-Induced Anisotropy

For many metals and alloys the dominant damage mechanism is the nucleation and growth of cavities and formation of micro-cracks. Cavities nucleate on grain boundaries having different orientations. At the final stages of deformation before creep rupture the coalescence of cavities and the formation of oriented micro-cracks is observed. The preferential direction of micro-cracks depends on the material microstructure and on the kind of the applied stress. For example, micrographs of copper specimens tested under torsion show that the micro-cracks dominantly occur on the grain boundaries whose normals coincide with the direction of the maximum positive principal stress (Hayhurst 1999; Hayhurst and Leckie 1990; Morishita and Hirao 1997). The strongly oriented micro-cracks may induce anisotropic creep responses, in particular, at the last stage of the creep process. Creep behavior of the austenitic steel X8 CrNiMoNb 1616 and the ferritic steel 13 CrMo 4 4 is experimentally studied in Betten et al. (1995), El-Magd et al. (1996) with respect to different loading orientations. Figure 5.12 schematically presents the results of testing. Uni-axial creep tests were carried out on flat specimens at different stress and temperature

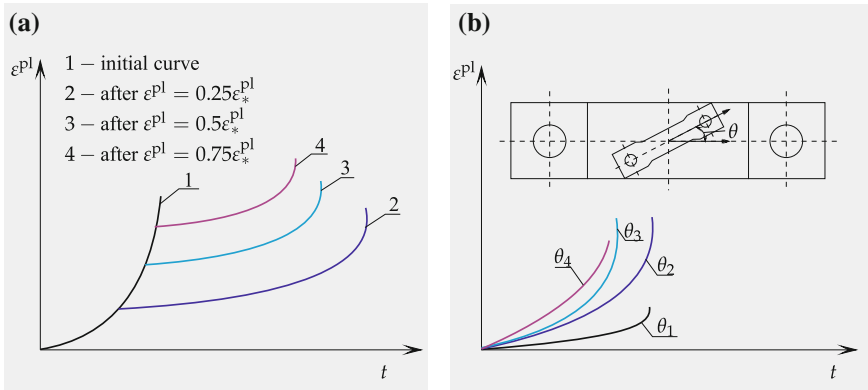


Fig. 5.12 Uni-axial creep tests with different orientations of the loading direction. **a** Creep curve for a flat specimen and creep curves for small specimens after different prestraining, **b** creep curves for different loading directions after pre-straining of $0.75\epsilon_*^{pl}$ (Betten et al. 1995; El-Magd et al. 1996)

levels. In order to establish the influence of the creep history (pre-loading and pre-damage), series of flat specimens were tested up to different values of the creep strain. The values of the creep pre-straining were $\epsilon^{pl} = 0.25\epsilon_*^{pl}; 0.5\epsilon_*^{pl}; 0.75\epsilon_*^{pl}$, where ϵ_*^{pl} is the creep strain at fracture. After unloading, small specimens were manufactured from the pre-strained flat specimens with different orientation to the loading axis, Fig. 5.12b. The uni-axial tests performed on the small specimens show that the creep responses depend on the angle of the orientation θ . In El-Magd et al. (1996) it is demonstrated that for small specimens pre-strained up to $0.25\epsilon_*^{pl}$ the creep response is not sensitive to the angle θ . The significant dependence of the creep curves and the fracture times on the angle θ has been observed for specimens pre-strained up to $0.75\epsilon_*^{pl}$.

In Murakami and Sanomura (1985) creep tests were carried out on thin-walled copper tubes under combined tension and torsion. The loading history and the creep responses are schematically presented in Fig. 1.27. During the first cycle the specimens were preloaded by constant normal and shear stresses within the time interval $[0, t_1]$. In the second cycle from t_1 up to creep rupture the specimens were loaded under the same constant normal stress but the reversed constant shear stress. The stress state after the reversal is characterized by the change of the principal directions. The angle between the first principal direction in the reference loading cycle and after the reversal can be controlled by the values of the normal and the shear stresses. Creep curves for different angles are presented in Murakami and Sanomura (1985). It is demonstrated that the creep-damage model with a scalar damage parameter is not able to predict the creep behavior after the shear stress reversal. In particular, the fracture time is underestimated in all loading cases. Similar results are discussed in Murakami et al. (1986) based on tests on Nimonic 80A.

The introduced examples of experimental observations indicate that the creep rate and the lifetime of a specimen additionally depend on the orientation of micro-defects with respect to the principal axes of the stress tensor. One way to consider such a dependence is the use of a tensor-valued damage parameter. A second rank damage tensor was firstly introduced by Vakulenko and Kachanov (1971) for the description of elastic-brittle damage. The first attempt to use a tensor-valued damage parameter in creep mechanics is due to Murakami and Ohno (Murakami 1983; Murakami and Ohno 1981). They considered a characteristic volume V in the material having N wedge cracks and specified the area of the grain boundary occupied by the k th crack by dA_g^k . They assumed that the state of damage can be characterized by the following second rank symmetric tensor

$$\boldsymbol{\Omega} = \frac{3}{A_g(V)} \sum_{k=1}^N \int_V [\mathbf{m}^k \otimes \mathbf{m}^k + w^k (\mathbf{I} - \mathbf{m}^k \otimes \mathbf{m}^k)] dA_g^k, \quad (5.7.303)$$

where \mathbf{m}^k is the unit normal vector to the k th crack and $A_g(V)$ is the total area of all grain boundaries in V . w^k characterizes the effect of the k th crack on the area reduction in the planes whose normals are perpendicular to \mathbf{m}^k . Specifying the three principal values of $\boldsymbol{\Omega}$ by Ω_j , $j = 1, 2, 3$, and the corresponding principal directions by the unit vectors \mathbf{n}_j the damage tensor can be formulated in the spectral form

$$\boldsymbol{\Omega} = \sum_{j=1}^3 \Omega_j \mathbf{n}_j \otimes \mathbf{n}_j \quad (5.7.304)$$

The principal values of the damage tensor Ω_j are related to the cavity area fractions in three orthogonal planes with the unit normals $\pm \mathbf{n}_j$. The cases $\Omega_j = 0$ and $\Omega_j = 1$ correspond to the undamaged state and the creep-rupture in the j th plane, respectively. By analogy with the uni-axial bar (see Fig. 3.7) Murakami and Ohno introduced a fictitious undamaged configuration in a solid by means of effective infinitesimal area elements. From three orthogonal planes having the unit normals $-\mathbf{n}_j$ an infinitesimal tetrahedron is constructed with area elements $-\tilde{\mathbf{n}}_i d\tilde{A}_i$ and $\tilde{\mathbf{n}} d\tilde{A}$ so that

$$\tilde{\mathbf{n}} d\tilde{A} = \sum_{j=1}^3 \mathbf{n}_j d\tilde{A}_j = \sum_{j=1}^3 (1 - \Omega_j) \mathbf{n}_j dA_j \quad (5.7.305)$$

With $\Omega_j \mathbf{n}_j = \mathbf{n}_j \cdot \boldsymbol{\Omega} = \boldsymbol{\Omega} \cdot \mathbf{n}_j$

$$\tilde{\mathbf{n}} d\tilde{A} = (\mathbf{I} - \boldsymbol{\Omega}) \cdot \mathbf{n} dA \quad (5.7.306)$$

The stress vector acting in the plane with the unit normal \mathbf{n} can be specified by $\boldsymbol{\sigma}_{(\mathbf{n})}$. The resultant force vector acting in the plane dA is

$$dA\boldsymbol{\sigma}_{(\mathbf{n})} = dA\mathbf{n} \cdot \boldsymbol{\sigma} = d\tilde{A}\tilde{\mathbf{n}} \cdot (\mathbf{I} - \boldsymbol{\Omega})^{-1} \cdot \boldsymbol{\sigma} = d\tilde{A}\tilde{\mathbf{n}} \cdot \tilde{\boldsymbol{\sigma}}, \quad \tilde{\boldsymbol{\sigma}} \equiv (\mathbf{I} - \boldsymbol{\Omega})^{-1} \cdot \boldsymbol{\sigma}, \quad (5.7.307)$$

where $\tilde{\boldsymbol{\sigma}}$ is the effective stress tensor. Introducing the so-called damage effect tensor $\boldsymbol{\Phi} \equiv (\mathbf{I} - \boldsymbol{\Omega})^{-1}$ one can write

$$\tilde{\boldsymbol{\sigma}} = \boldsymbol{\Phi} \cdot \boldsymbol{\sigma} \quad (5.7.308)$$

According to the strain equivalence principle (Lemaitre and Chaboche 1990), the constitutive equation for the virgin material, for example the constitutive equation for the secondary creep, can be generalized to the damaged material replacing the Cauchy stress tensor $\boldsymbol{\sigma}$ by the net-stress tensor $\tilde{\boldsymbol{\sigma}}$. The net stress tensor (5.7.308) is non-symmetric. Introducing the symmetric part

$$\tilde{\boldsymbol{\sigma}}^s = \frac{1}{2}(\boldsymbol{\sigma} \cdot \boldsymbol{\Phi} + \boldsymbol{\Phi} \cdot \boldsymbol{\sigma}) \quad (5.7.309)$$

the secondary creep equation is generalized as follows (Murakami et al. 1986)

$$\dot{\boldsymbol{\epsilon}}^{\text{pl}} = \frac{3}{2}a\tilde{\sigma}_{\text{VM}}^{n-1}\tilde{\boldsymbol{s}}^s, \quad \tilde{\boldsymbol{s}}^s = \tilde{\boldsymbol{\sigma}}^s - \frac{1}{3}\text{tr}\tilde{\boldsymbol{\sigma}}^s \mathbf{I}, \quad \tilde{\sigma}_{\text{VM}} = \sqrt{\frac{3}{2}\tilde{\boldsymbol{s}}^s \cdot \tilde{\boldsymbol{s}}^s} \quad (5.7.310)$$

The rate of the damage tensor is postulated as a function of the stress tensor and the current damage state. The following evolution equation is proposed in Murakami and Sanomura (1985) for the description of creep damage of copper

$$\dot{\boldsymbol{\Omega}} = b[\alpha\tilde{\sigma}_l^s + (1 - \alpha)\tilde{\sigma}_{\text{VM}}^s]^k (\mathbf{n}_l^{\tilde{\boldsymbol{\sigma}}} \cdot \boldsymbol{\Phi} \cdot \mathbf{n}_l^{\tilde{\boldsymbol{\sigma}}})^l \mathbf{n}_l^{\tilde{\boldsymbol{\sigma}}} \otimes \mathbf{n}_l^{\tilde{\boldsymbol{\sigma}}}, \quad (5.7.311)$$

where b , α , k and l are material constants and the unit vector $\mathbf{n}_l^{\tilde{\boldsymbol{\sigma}}}$ denotes the direction corresponding to the first positive principal stress $\tilde{\sigma}_l$. The constitutive and evolution equations (5.7.310) and (5.7.311) have been applied in Murakami et al. (1986) for the description of creep-damage behavior of Nimonic 80A. The second rank damage tensor (5.7.304) and the net stress (5.7.309) have been used in Murakami and Sanomura (1985) with McVetty-type creep equations for the prediction of creep-damage of copper. The results suggest that the model with the damage tensor provides better agreement with experimental data if compared to the model with a scalar-valued damage parameter. In Murakami and Ohno (1981) the following damage evolution equation is utilized

$$\dot{\boldsymbol{\Omega}} = b[\alpha\tilde{\sigma}_l^s + \beta\tilde{\sigma}_m + (1 - \alpha - \beta)\tilde{\sigma}_{\text{VM}}^s]^k (\text{tr} \boldsymbol{\Phi}^2)^{1/2} \left[\eta \mathbf{I} + (1 - \eta)\mathbf{n}_l^{\tilde{\boldsymbol{\sigma}}} \otimes \mathbf{n}_l^{\tilde{\boldsymbol{\sigma}}} \right], \quad (5.7.312)$$

where β and η are material constants. This equation takes into account the influence of the mean stress σ on the damage rate. Furthermore, the isotropic part of the damage tensor associated with the growth of voids is included.

To discuss the damage tensor (5.7.304) let us consider a uni-axial homogeneous stress state $\boldsymbol{\sigma} = \sigma_0 \mathbf{m} \otimes \mathbf{m}$ with $\sigma_0 > 0$ and $\mathbf{m} = \text{const}$. Let us specify $\boldsymbol{\Omega} = \mathbf{0}$ as the initial condition. The evolution equation (5.7.311) takes the form

$$\dot{\boldsymbol{\Omega}}(t) = \dot{\omega}(t) \mathbf{m} \otimes \mathbf{m}, \quad \dot{\omega} = \frac{b\sigma_0^k}{(1-\omega)^{k+l}}, \quad \omega(0) = 0 \quad (5.7.313)$$

The equation for the scalar ω can be integrated as shown in Sect. 3.6.1. As a result one can find the relation between the time to fracture and the stress σ_0 . Based on this relation and experimental data one can estimate the values of material constants b , k and l (Sect. 3.6.1). According to the introduced damage measure (5.7.304) the damage state $\boldsymbol{\Omega} = \omega \mathbf{m} \otimes \mathbf{m}$ corresponds to the case of uniformly distributed penny-shaped cracks (circular planes) with the unit normals \mathbf{m} .

Now let us assume that the damage state $\boldsymbol{\Omega} = \omega_0 \mathbf{m} \otimes \mathbf{m}$, $0 < \omega_0 < 1$ is induced as a result of the constant stress $\boldsymbol{\sigma} = \sigma_0 \mathbf{m} \otimes \mathbf{m}$ exerted over a period of time $[0, t_1]$ and in the next loading cycle the stress $\boldsymbol{\sigma} = \sigma_0 \mathbf{p} \otimes \mathbf{p}$, $\mathbf{p} \cdot \mathbf{m} = 0$ is applied. In this case the solution of (5.7.311) can be written down as follows

$$\boldsymbol{\Omega}(t) = \omega_0 \mathbf{m} \otimes \mathbf{m} + \omega_1(t) \mathbf{p} \otimes \mathbf{p}, \quad \dot{\omega}_1 = \frac{b\sigma_0^k}{(1-\omega_1)^{k+l}}, \quad \omega_1(0) = 0 \quad (5.7.314)$$

Equation (5.7.314) predicts that in the second cycle the material behaves like a virgin material. Then the total time to fracture can be calculated as follows

$$t_* = t_1 + \frac{1}{(k+l+1)b\sigma_0^k}$$

We observe that t_* does not depend on the damage value ω_0 induced during the first loading cycle. The rate of nucleation and growth of new voids (cracks) on the planes orthogonal to \mathbf{p} will not be affected by cracks formed in the first loading cycle. Furthermore, if a compressive stress, i.e., $\boldsymbol{\sigma} = -\sigma_0 \mathbf{p} \otimes \mathbf{p}$ is applied in the second cycle the model predicts no damage accumulation.

Let us note that the evolution equations (5.7.311) and (5.7.312) can only be applied if $\tilde{\sigma}_I \neq 0$, $\tilde{\sigma}_I \neq \tilde{\sigma}_{II}$ and $\tilde{\sigma}_I \neq \tilde{\sigma}_{III}$. In this case the dyad $\mathbf{n}_I^{\tilde{\sigma}} \otimes \mathbf{n}_I^{\tilde{\sigma}}$ can be found from the identity (5.7.294). For the stress states $\boldsymbol{\sigma} = a_0 \mathbf{I}$ or $\boldsymbol{\sigma} = a \mathbf{p} \otimes \mathbf{p} + b(\mathbf{I} - \mathbf{p} \otimes \mathbf{p})$, $a < b$, there is an infinite number of first principal directions. Such stress states are typical for engineering structural components. For example, the stress state of the type $\boldsymbol{\sigma} = a \mathbf{p} \otimes \mathbf{p} + b(\mathbf{I} - \mathbf{p} \otimes \mathbf{p})$ arises in the midpoint of a transversely loaded square plate with all four edges to be fixed (e.g. supported or clamped edges), (Altenbach et al. 2002). In the loaded (top) surface of such a plate $b < a < 0$ while in the bottom surface $b > a$, $a < 0$, $b > 0$. Stress states of the same type arise in different rotationally symmetric problems of structural mechanics. For analysis of such

problems a modified form of the evolution equation (5.7.312) is required (Ganczarski and Skrzypek 2001).

Various forms of creep-damage constitutive equations with second rank damage tensors have been utilized. In Altenbach et al. (2001a) the effective stress tensor

$$\tilde{\sigma} = \Phi^{1/2} \cdot \sigma \cdot \Phi^{1/2} \quad (5.7.315)$$

originally proposed in Cordebois and Sidoroff (1983), is applied to formulate the creep-damage constitutive equation. Mechanisms of damage activation and deactivation are taken into account. The model predictions are compared with experimental data of creep in copper. In Qi (1998), Qi and Bertram (1997, 1998, 1999) a second rank damage tensor is applied for the modeling of creep of nickel-based single crystal super-alloys SRR 99 and CMSX-6 at 760°C. The proposed constitutive equations take into account both the initial anisotropy and the damage induced anisotropy.

The symmetry group of a symmetric second rank tensor includes at least eight elements. With the second rank damage tensor and the effective stress tensors (5.7.309) or (5.7.315) only restrictive forms of orthotropic tertiary creep can be considered (a similar situation is discussed in Sect. 5.6.2). Therefore in many publications it is suggested to introduce higher order damage tensors. For different definitions of damage tensors one may consult Altenbach et al. (1990), Altenbach and Blumener (1989), Betten (1993), Krajcinovic (1996), Lemaitre (1996), Skrzypek and Ganczarski (1998), Lemaitre and Desmorat (2005), Murakami (2012). A critical review is given in Schiesse (1994). Usually, the available experimental data on creep responses is not enough to verify whether the orthotropic symmetry is an appropriate symmetry assumption for the modeling of anisotropic creep-damage processes. From the micro-structural point of view one may imagine rather complex three-dimensional patterns of voids and cracks which nucleate and propagate as the result of multi-axial non-proportional loadings. An attempt to predict these patterns would result in a complex mathematical model with a large (or even infinite) number of internal variables including tensors of different rank. A model to characterize different patterns of cracks may be based on the orientation distribution function, orientation averaging and the so-called orientation tensors. This approach is widely used in different branches of physics and materials science for the statistical modeling of oriented micro-structures. Examples include fiber suspensions (Leal and Hinch 1973), mixtures (Faria 2001), polymers and polymer composites (Altenbach et al. 2003a; Tamuzh and Kuksenko 1978; Kröner et al. 2009). The application of orientational averaging to characterize damage states under creep conditions is discussed in Morishita and Hirao (1997), Onat and Leckie (1988), Stamm and von Estroff (1993).

Let us note, that the material behavior at high temperature and non-proportional loading is accompanied by a complex interaction of different deformation and damage mechanisms such as hardening, recovery, softening, creep-damage, fatigue-damage, etc. Several unified models utilize constitutive equations of creep with kinematic and/or isotropic hardening and include damage effects by means of the effective stress concept and the strain equivalence principle. In Kawai (1996) the Malinin-Khadjinsky kinematic hardening rule, see Sect. 5.6.2 and isotropic

Kachanov-Rabotnov type damage variable are discussed. The damage rate is additionally governed by the magnitude of the hardening variable, so that the coupling effect of damage and strain hardening/softening can be taken into account. It is shown that the kinematic hardening coupled with isotropic damage predicts well the effect of longer life-time after the stress reversal. In Dunne and Hayhurst (1992) the Chaboche-Rousselier visco-plasticity model is modified to predict the coupled creep-plasticity-damage behavior. The scalar damage variable is introduced as a sum of the accumulated time-dependent and cycle-dependent components. Various approaches to formulate a unified material model within the framework of continuum damage mechanics and thermodynamics of dissipative processes are discussed in Chaboche (1988a, b), Chaboche (1999), Lemaitre and Chaboche (1990), Kostenko et al. (2013), Altenbach et al. (2013), Naumenko et al. (2011b).

The verification of a unified model with non-linear anisotropic hardening and damage coupling requires a large number of independent tests under non-proportional loading. As a rule, accurate experimental data are rarely available. Furthermore, non-uniform stress and strain fields may be generated in a standard uni-axial specimen under non-proportional cyclic loading conditions Lin et al. (1999). They may be the reason for the large scatter of experimental data and misleading interpretations.

References

- Abe F (2009) Analysis of creep rates of tempered martensitic 9% Cr steel based on microstructure evolution. *Mater Sci Eng: A* 510:64–69
- Altenbach H (1999) Classical and nonclassical creep models. In: Altenbach H, Skrzypek J (eds) *Creep and damage in materials and structures*. Springer, Wien, New York, pp. 45–95, CISM Lecture Notes No. 399
- Altenbach H (2001) A generalized limit criterion with application to strength, yielding, and damage of isotropic materials. In: Lemaitre J (ed) *Handbook of materials behaviour models*. Academic Press, San Diego, pp 175–186
- Altenbach H (2012) *Kontinuumsmechanik - Einführung in die materialunabhängigen und materialabhängigen Gleichungen*, 2nd edn. Springer, Berlin
- Altenbach H, Blumenauer H (1989) *Grundlagen und Anwendungen der Schädigungsmechanik*. Neue Hütte 34(6):214–219
- Altenbach H, Naumenko K (1997) Creep bending of thin-walled shells and plates by consideration of finite deflections. *Comput Mech* 19:490–495
- Altenbach H, Zhilin PA (1988) Osnovnye uravneniya neklassicheskoi teorii uprugikh obolochek (Basic equations of a non-classical theory of elastic shells, in Russ.). *Adv Mech* 11:107–148
- Altenbach H, Zolochovsky A (1996) A generalized failure criterion for three-dimensional behaviour of isotropic materials. *Eng Fract Mech* 54(1):75–90
- Altenbach H, Zolochovsky AA (1994) Eine energetische Variante der Theorie des Kriechens und der Langzeitfestigkeit für isotrope Werkstoffe mit komplizierten Eigenschaften. *ZAMM-J Appl Math Mech/Zeitschrift für Angewandte Mathematik und Mechanik* 74(3):189–199
- Altenbach H, Altenbach J, Schießle P (1990) Konzepte der schädigungsmechanik und ihre anwendung bei der werkstoffmechanischen bauteilanalyse. *Technische Mechanik* 11(2):81–93
- Altenbach H, Schießle P, Zolochovsky A (1991) Zum Kriechen isotroper Werkstoffe mit komplizierten Eigenschaften. *Rheol Acta* 30:388–399

- Altenbach H, Altenbach J, Zolochovsky A (1995) *Erweiterte Deformationsmodelle und Versagenkriterien der Werkstoffmechanik*. Deutscher Verlag für Grundstoffindustrie, Stuttgart
- Altenbach H, Altenbach J, Rikards R (1996) *Einführung in die Mechanik der Laminat- und Sandwichtragwerke*. Deutscher Verlag für Grundstoffindustrie, Stuttgart
- Altenbach H, Morachkovsky O, Naumenko K, Sychov A (1997) Geometrically nonlinear bending of thin-walled shells and plates under creep-damage conditions. *Arch Appl Mech* 67:339–352
- Altenbach H, Altenbach J, Naumenko K (1998) *Ebene Flächentragwerke*. Springer, Berlin
- Altenbach H, Kolarow G, Morachkovsky O, Naumenko K (2000) On the accuracy of creep-damage predictions in thinwalled structures using the finite element method. *Comput Mech* 25:87–98
- Altenbach H, Huang C, Naumenko K (2001a) Modelling of creep damage under the reversed stress states considering damage activation and deactivation. *Technische Mechanik* 21(4):273–282
- Altenbach H, Kushnevsky V, Naumenko K (2001b) On the use of solid- and shell-type finite elements in creep-damage predictions of thinwalled structures. *Arch Appl Mech* 71:164–181
- Altenbach H, Huang C, Naumenko K (2002) Creep damage predictions in thin-walled structures by use of isotropic and anisotropic damage models. *J Strain Anal Eng Des* 37(3):265–275
- Altenbach H, Naumenko K, L'vov GI, Pylypenko S (2003a) Numerical estimation of the elastic properties of thin-walled structures manufactured from short-fiber reinforced thermoplastics. *Mech Compos Mater* 39:221–234
- Altenbach H, Naumenko K, Zhilin P (2003b) A micro-polar theory for binary media with application to phase-transitional flow of fiber suspensions. *Continuum Mech Thermodyn* 15:539–570
- Altenbach H, Altenbach J, Kissing W (2004) *Mechanics of composite structural elements*. Springer, Berlin
- Altenbach H, Naumenko K, Zhilin P (2006) A note on transversely isotropic invariants. *ZAMM-J Appl Math Mech/Zeitschrift für Angewandte Mathematik und Mechanik* 86:162–168
- Altenbach H, Naumenko K, Pylypenko S, Renner B (2007) Influence of rotary inertia on the fiber dynamics in homogeneous creeping flows. *ZAMM-J Appl Math Mech/Zeitschrift für Angewandte Mathematik und Mechanik* 87(2):81–93
- Altenbach H, Gorash Y, Naumenko K (2008) Steady-state creep of a pressurized thick cylinder in both the linear and the power law ranges. *Acta Mech* 195:263–274
- Altenbach H, Brigadnov I, Naumenko K (2009) Rotation of a slender particle in a shear flow: influence of the rotary inertia and stability analysis. *ZAMM-J Appl Math Mech/Zeitschrift für Angewandte Mathematik und Mechanik* 89(10):823–832
- Altenbach H, Kozhar S, Naumenko K (2013) Modeling creep damage of an aluminum-silicon eutectic alloy. *Int J Damage Mech* 22(5):683–698
- Atkin RJ, Craine RE (1976) Continuum theories of mixtures: basic theory and historical development. *Q J Mech Appl Math* 29:209–244
- Backhaus G (1983) *Deformationsgesetze*. Akademie-Verlag, Berlin
- Barkar T, Ågren J (2005) Creep simulation of 9–12%Cr steels using the composite model with thermodynamically calculated input. *Mater Sci Eng A* 395:110–115
- Bassani JL, Hawk DE (1990) Influence of damage on crack-tip fields under small-scale-creep conditions. *Int J Fract* 42:157–172
- Belytschko T, Liu WK, Moran B, Elkhodary K (2014) *Nonlinear finite elements for continua and structures*. Wiley
- Bernhardi O, Mücke R (2000) A lifetime prediction procedure for anisotropic materials. *Commun Numer Meth Eng* 16:519–527
- Bertram A (2012) *Elasticity and plasticity of large deformations*, 3rd edn. Springer, Berlin
- Bertram A, Olschewski J (1996) Anisotropic modelling of the single crystal superalloy SRR99. *Comput Mater Sci* 5:12–16
- Bertram A, Olschewski J (2001) A phenomenological anisotropic creep model for cubic single crystals. In: Lemaitre J (ed) *Handbook of materials behaviour models*. Academic Press, San Diego, pp 303–307
- Besseling JF, van der Giessen E (1994) *Mathematical modelling of inelastic deformation*. Chapman & Hall, London

- Betten J (1982) Zur Aufstellung einer Integritätsbasis für Tensoren zweiter und vierter Stufe. *ZAMM-J Appl Math Mech/Zeitschrift für Angewandte Mathematik und Mechanik* 62(5):T274–T275
- Betten J (1984) Materialgleichungen zur Beschreibung des sekundären und tertiären Kriechverhaltens anisotroper Stoffe. *ZAMM-J Appl Math Mech/Zeitschrift für Angewandte Mathematik und Mechanik* 64:211–220
- Betten J (1993) *Kontinuumsmechanik*. Springer, Berlin
- Betten J (1998) Anwendungen von Tensorfunktionen in der Kontinuumsmechanik anisotroper Materialien. *ZAMM-J Appl Math Mech/Zeitschrift für Angewandte Mathematik und Mechanik* 78(8):507–521
- Betten J (2008) *Creep mechanics*, 3rd edn. Springer, Berlin
- Betten J, El-Magd E, Meydanli SC, Palmen P (1995) Untersuchung des anisotropen Kriechverhaltens vorgeschädigter Werkstoffe am austenitischen Stahl X8CrNiMoNb 1616. *Arch Appl Mech* 65:121–132
- Billington EW (1985) The Poynting-Swift effect in relation to initial and post-yield deformation. *Int J Solids Struct* 21(4):355–372
- Blum W (2008) Mechanisms of creep deformation in steel. In: Abe F, Kern TU, Viswanathan R (eds) *Creep-resistant steels*. Woodhead Publishing, Cambridge, pp 365–402
- Bodnar A, Chrzanowski M (1991) A non-unilateral damage in creeping plates. In: Zyczkowski M (ed) *Creep in structures*. Springer, Heidelberg, pp 287–293
- Boehler JP (ed) (1987a) Application of tensor functions in solid mechanics. *CISM Lecture Notes No. 292*. Springer, Wien
- Boehler JP (1987b) On a rational formulation of isotropic and anisotropic hardening. In: Boehler JP (ed) *Applications of tensor functions in solid mechanics*. Springer, Wien, pp 99–122, *CISM Lecture Notes No. 292*
- Boehler JP (1987c) Representations for isotropic and anisotropic non-polynomial tensor functions. In: Boehler JP (ed) *Applications of tensor functions in solid mechanics*. Springer, Wien, pp 31–53, *CISM Lecture Notes No. 292*
- Boehler JP (1987d) Yielding and failure of transversely isotropic solids. In: Boehler JP (ed) *Applications of tensor functions in solid mechanics*. Springer, Wien, pp 67–97, *CISM Lecture Notes No. 292*
- Böhlke T (2000) *Crystallographic texture evolution and elastic anisotropy. Simulation, modelling and applications*, PhD-Thesis. Shaker Verlag, Aachen
- Boyle JT (2012) The creep behavior of simple structures with a stress range-dependent constitutive model. *Arch Appl Mech* 82(4):495–514
- Boyle JT, Spence J (1983) *Stress analysis for creep*. Butterworth, London
- Burlakov AV, Lvov GI, Morachkovsky OK (1977) Polzuchest' tonkikh obolochek (Creep of thin shells, in Russ.). Kharkov State Univ. Publ., Kharkov
- Cane BJ (1981) Creep fracture of dispersion strengthened low alloy ferritic steels. *Acta Metall* 29:1581–1591
- Cazacu O, Barlat F (2003) Application of the theory of representation to describe yielding of anisotropic aluminium alloys. *Int J Eng Sci* 41:1367–1385
- Chaboche JL (1988a) Continuum damage mechanics: part I—general concepts. *J Appl Mech* 55:59–64
- Chaboche JL (1988b) Continuum damage mechanics: part II—damage growth, crack initiation, and crack growth. *J Appl Mech* 55:65–71
- Chaboche JL (1989) Constitutive equations for cyclic plasticity and cyclic viscoplasticity. *Int J Plast* 5:247–302
- Chaboche JL (1999) Thermodynamically founded cdm models for creep and other conditions. In: Altenbach H, Skrzypek J (eds) *Creep and damage in materials and structures*, Springer, Wien, New York, pp 209–283, *CISM Lecture Notes No. 399*
- Chaboche JL (2008) A review of some plasticity and viscoplasticity constitutive equations. *Int J Plast* 24:1642–1693

- Chawla KK (1987) Composite materials. Springer, New York
- Cordebois J, Sidoroff F (1983) Damage induced elastic anisotropy. In: Boehler JP (ed) Mechanical behaviours of anisotropic solids. Martinus Nijhoff Publishers, Boston, pp 761–774
- Courant R, Hilbert D (1989) Methods of mathematical physics, vol. 2. Partial differential equations. Wiley Interscience Publication, New York
- Cvelodub IY (1991) Postulat ustoichivosti i ego prilozheniya v teorii polzuchesti metallicheskih materialov (On the stability postulate and its application in the creep theory of metallic materials, in Russ.). Institute Gidrodinamiki, Novosibirsk
- Dunne FPE, Hayhurst DR (1992) Continuum damage based constitutive equations for copper under high temperature creep and cyclic plasticity. Proc R Soc London A: Math Phys Eng Sci A437:545–566
- Dyson BF (1992) Material data requirements, creep damage mechanisms, and predictive models. In: Larson LH (ed) High temperature structural design. Mechanical Engineering Publ, London, pp 335–354
- Dyson BF, McLean M (1998) Microstructural evolution and its effects on the creep performance of high temperature alloys. In: Strang A, Cawley J, Greenwood GW (eds) Microstructural stability of creep resistant alloys for high temperature plant applications. Cambridge University Press, Cambridge, pp 371–393
- Dyson BF, McLean M (2001) Micromechanism-quantification for creep constitutive equations. In: Murakami S, Ohno N (eds) IUTAM symposium on creep in structures. Kluwer, Dordrecht, pp 3–16
- El-Magd E, Nicolini G (1999) Creep behaviour and microstructure of dispersion-strengthened pm-aluminium materials at elevated temperatures. In: Mughrabi H, Gottstein G, Mecking H, Riedel H, Tobolski J (eds) Microstructure and mechanical properties of metallic high-temperature materials: research report/DFG. Wiley-VCH, Weinheim, pp 445–464
- El-Magd E, Betten J, Palmen P (1996) Auswirkung der Schädigungsanisotropie auf die Lebensdauer von Stählen bei Zeitstandbeanspruchung. Materialwiss Werkstofftech 27:239–245
- Faria SH (2001) Mixtures with continuous diversity: general theory and application to polymer solutions. Continuum Mech Thermodyn 13:91–120
- François D, Pineau A, Zaoui A (1998) Mechanical behavior of materials, vol II. Kluwer Academic Publishers, Dordrecht
- François D, Pineau A, Zaoui A (2012) Mechanical behaviour of materials, vol ii. In: Fracture mechanics and damage, vol 191. Springer Science & Business Media
- Frederick CO, Armstrong PJ (2007) A mathematical representation of the multiaxial Bauschinger effect. Mater High Temp 24(1):1–26
- Frost HJ, Ashby MF (1982) Deformation-mechanism maps. Pergamon, Oxford
- Ganczarski A, Skrzypiek J (2001) Application of the modified Murakami's anisotropic creep-damage model to 3d rotationally-symmetric problem. Technische Mechanik 21(4):251–260
- Gariboldi E, Casaro F (2007) Intermediate temperature creep behaviour of a forged Al-Cu-Mg-Si-Mn alloy. Mater Sci Eng: A 462(1):384–388
- Gaudig W, Kussmaul K, Maile K, Tramer M, Granacher J, Kloos KH (1999) A microstructural model to predict the multiaxial creep and damage in 12 Cr steel grade at 550°C. In: Mughrabi H, Gottstein G, Mecking H, Riedel H, Tobolski J (eds) Microstructure and mechanical properties of metallic high-temperature materials: research report/DFG. Wiley-VCH, Weinheim, pp 192–205
- Gibson RF (1994) Principles of composite materials. McGraw-Hill, New York
- Giesekus H (1994) Phänomenologische Rheologie. Springer, Berlin
- Gorev BV, Rubanov VV, Sosnin OV (1979) O polzuchesti materialov s raznymi svoistvami pri rastyazhenii i szhatii (on the creep of materials with different properties in tension and compression, in russ.). Problemy prochnosti 7:62–67
- Granger R (1994) Experiments in heat transfer and thermodynamics. Cambridge University Press
- Hahn HG (1985) Elastizitätstheorie. Teubner, Stuttgart, B.G
- Hayhurst DR (1972) Creep rupture under multiaxial states of stress. J Mech Phys Solids 20:381–390

- Hayhurst DR (1994) The use of continuum damage mechanics in creep analysis for design. *J Strain Anal Eng Des* 25(3):233–241
- Hayhurst DR (1999) Materials data bases and mechanisms-based constitutive equations for use in design. In: Altenbach H, Skrzypek J (eds) *Creep and damage in materials and structures*. Springer, Wien, New York, pp 285–348, CISM Lecture Notes No. 399
- Hayhurst DR, Leckie FA (1990) High temperature creep continuum damage in metals. In: Boehler JP (ed) *Yielding damage and failure of anisotropic solids*. Mechanical Engineering Publ, London, pp 445–464
- Hayhurst DR, Wong MT, Vakili-Tahami F (2002) The use of CDM analysis techniques in high temperature creep failure of welded structures. *JSME Int J Series A, Solid Mech Mater Eng* 45:90–97
- Hill R (1950) *Math Theor Plast Mater Res Eng*. Oxford University Press, London
- Hyde TH, Sun W, Becker AA, Williams JA (1997) Creep continuum damage constitutive equations for the base, weld and heat-affected zone materials of a service-aged 1/2Cr1/2Mo1/4V:2 1/4Cr1Mo multipass weld at 640°C. *J Strain Anal Eng Des* 32(4):273–285
- Hyde TH, Sun W, Williams JA (1999) Creep behaviour of parent, weld and HAZ materials of new, service aged and repaired 1/2Cr1/2Mo1/4V: 21/4Cr1Mo pipe welds at 640°C. *Mater High Temp* 16(3):117–129
- Hyde TH, Sun W, Becker AA (2000) Failure prediction for multi-material creep test specimens using steady-state creep rupture stress. *Int J Mech Sci* 42:401–423
- Hyde TH, Sun W, Agyakwa PA, Shipeay PH, Williams JA (2003a) Anisotropic creep and fracture behaviour of a 9CrMoNbV weld metal at 650°C. In: Skrzypek JJ, Ganczarski AW (eds) *Anisotropic behaviour of damaged materials*. Springer, Berlin, pp 295–316
- Hyde TH, Sun W, Williams JA (2003b) Creep analysis of pressurized circumferential pipe weldments—a review. *J Strain Anal Eng Des* 38(1):1–29
- Ilschner B (1973) *Hochtemperatur-Plastizität*. Springer, Berlin
- Inoue T (1988) Inelastic constitutive models under plasticity-creep interaction condition—theories and evaluations. *JSME Int J Series 1, Solid Mech Strength Mater* 31(4):653–663
- Inoue T, Ohno N, Suzuki A, Igari T (1989) Evaluation of inelastic constitutive models under plasticity-creep interaction for 21/4Cr-1Mo steel at 600°C. *Nucl Eng Des* 114:259–309
- Kachanov LM (1969) *Osnovy teorii plastichnosti* (Basics of the theory of plasticity, in Russ.). Nauka, Moskva
- Kaliszky S (1984) *Plastizitätslehre Theorie und Technische Anwendung*. VDI-Verlag, Düsseldorf
- Kassner ME, Pérez-Prado MT (2004) *Fundamentals of creep in metals and alloys*. Elsevier, Amsterdam
- Kawai M (1989) Creep and plasticity of austenitic stainless steel under multiaxial non-proportional loadings at elevated temperatures. In: Hui D, Kozik TJ (eds) *Visco-plastic behavior of new materials*. ASME, PVP-vol 184. New York, pp 85–93
- Kawai M (1996) Coupled creep-damage modelling for isotropic hardening and kinematic hardening materials. Design and life assessment at high temperature. Mechanical Engineering Publ, London, pp 91–100
- Kawai M (1997) Coupled inelasticity and damage model for metal matrix composites. *Int J Damage Mech* 6:453–478
- Kawai M (2002) Constitutive modelling of creep and damage behaviors of the non-Mises type for a class of polycrystalline metals. *Int J Damage Mech* 11:223–245
- Khan AS, Huang S (1995) *Continuum theory of plasticity*. Wiley, New York
- Konkin VN, Morachkovskij OK (1987) Polzuchest' i dlitel'naya prochnost' legkikh splavov, proyavlyayushchikh anizotropnye svoystva (Creep and long-term strength of light alloys with anisotropic properties, in Russ.). *Problemy prochnosti* 5:38–42
- Kostenko Y, Almstedt H, Naumenko K, Linn S, Scholz A (2013) Robust methods for creep fatigue analysis of power plant components under cyclic transient thermal loading. In: ASME Turbo Expo 2013: Turbine Technical Conference and Exposition, American Society of Mechanical Engineers, pp V05BT25A040–V05BT25A040

- Kowalewski Z (1987) The surface of constant rate of energy dissipation under creep and its experimental determination. *Arch Mech* 39:445–459
- Kowalewski Z (1991) Creep behaviour of copper under plane stress state. *Int J Plast* 7:387–400
- Kowalewski ZL (1996) Creep rupture of copper under complex stress state at elevated temperature. Design and life assessment at high temperature. *Mechanical Engineering Publ, London*, pp 113–122
- Kowalewski ZL (2001) Assessment of the multiaxial creep data based on the isochronous creep surface concept. In: Murakami S, Ohno N (eds) *IUTAM symposium on creep in structures*. Kluwer, Dordrecht, pp 401–418
- Kowalewski ZL, Hayhurst DR, Dyson BF (1994) Mechanisms-based creep constitutive equations for an aluminium alloy. *J Strain Anal Eng Des* 29(4):309–316
- Krajcinovic D (1996) Damage mechanics. In: *Applied mathematics and mechanics*, vol 41. North-Holland, Amsterdam
- Kraus H (1980) *Creep analysis*. Wiley, New York
- Krausz AS, Krausz K (1996) *Unified constitutive laws of plastic deformation*. Academic Press, San Diego
- Krawietz A (1986) *Materialtheorie. Mathematische Beschreibung des phänomenologischen thermomechanischen Verhalten*. Springer, Berlin
- Kreml E (1996) A small-strain viscoplasticity theory based on overstress. In: Krausz AS, Krausz K (eds) *Unified constitutive laws of plastic deformation*. Academic Press, San Diego, pp 281–318
- Kreml E (1999) Creep-plasticity interaction. In: Altenbach H, Skrzypek J (eds) *Creep and damage in materials and structures*. Springer, Wien, New York, pp 285–348, *CISM Lecture Notes No. 399*
- Kröner C, Altenbach H, Naumenko K (2009) Coupling of a structural analysis and flow simulation for short-fiber-reinforced polymers: property prediction and transfer of results. *Mech Compos Mater* 45(3):249–256
- Landau LD, Lifshits EM, Kosevich AM, Pitaevskii LP (1986) *Theory of elasticity*. In: *Course of theoretical physics*. Butterworth-Heinemann
- Längler F, Naumenko K, Altenbach H, Ievdokymov M (2014) A constitutive model for inelastic behavior of casting materials under thermo-mechanical loading. *J Strain Anal Eng Des* 49:421–428
- Leal LG, Hinch EJ (1973) Theoretical studies of a suspension of rigid particles affected by brownian couples. *Rheol Acta* 12:127–132
- Leckie FA, Hayhurst DR (1977) Constitutive equations for creep rupture. *Acta Metall* 25:1059–1070
- Lee EH (1969) Elastic-plastic deformation at finite strains. *J Appl Mech* 36(1):1–6
- Lemaitre J (1996) *A course on damage mechanics*. Springer, Berlin
- Lemaitre J, Chaboche JL (1990) *Mechanics of solid materials*. Cambridge University Press, Cambridge
- Lemaitre J, Desmorat R (2005) *Engineering damage mechanics: ductile, creep, fatigue and brittle failures*. Springer
- Lewin G, Lehmann B (1977) Ergebnisse über das Spannungs-Verformungsverhalten von PVC, dargestellt an einem zylindrischen Bauelement. *Wissenschaftliche Zeitschrift der Technischen Hochschule Magdeburg* 21:415–422
- Lin J, Dunne FPE, Hayhurst DR (1999) Aspects of testpiece design responsible for errors in cyclic plasticity experiments. *Int J Damage Mech* 8:109–137
- Liu Y, Murakami S (1998) Damage localization of conventional creep damage models and proposition of a new model for creep damage analysis. *JSME Int J Series A, Solid Mech Mater Eng* 41:57–65
- Lokhin VV, Sedov LI (1963) Nonlinear tensor functions of several tensor arguments. *J Appl Math Mech* 27(3):597–629
- Lubarda V (2001) *Elastoplasticity theory*. CRC Press
- Lucas GE, Pelloux RMN (1981) Texture and stress state dependent creep in Zircaloy-2. *Metall Trans A* 12A:1321–1331

- Lundell F (2011) The effect of particle inertia on triaxial ellipsoids in creeping shear: from drift toward chaos to a single periodic solution. *Phys Fluids* 23(1):011, 704
- Lundell F, Carlsson A (2010) Heavy ellipsoids in creeping shear flow: transitions of the particle rotation rate and orbit shape. *Phys Rev E* 81(1):016, 323
- Lurie AI (1990) *Nonlinear theory of elasticity*. Dordrecht
- Lurie AI (2010) *Theory of elasticity*. In: *Foundation of engineering mechanics*. Springer
- Lvov I, Naumenko K, Altenbach H (2014) Homogenisation approach in analysis of creep behaviour in multipass weld. *Mater Sci Technol* 30(1):50–53
- Mahnken R (2002) Anisotropic creep modeling based on elastic projection operators with applications to CMSX-4 superalloy. *Comput Meth Appl Mech Eng* 191(15):1611–1637
- Malinin NN (1975) *Prikladnaya teoriya plastichnosti i polzuchesti* (Applied theory of plasticity and creep, in Russ.). Mashinostroenie, Moskva
- Malinin NN (1981) *Raschet na polzuchest' konstrukcionnykh elementov* (Creep calculations of structural elements, in Russ.). Mashinostroenie, Moskva
- Malinin NN, Khadjinsky GM (1969) *K postroeniyu teorii polzuchesti s anizotropnym uprochneniem* (On the formulation of a creep theory with anisotropic hardening, in Russ.). *Izv AN SSSR Mechanika tverdogo tela* 3:148–152
- Malinin NN, Khadjinsky GM (1972) Theory of creep with anisotropic hardening. *Int J Mech Sci* 14:235–246
- Maugin GA (1992) *The thermomechanics of plasticity and fracture*. Cambridge University Press, Cambridge
- Miller AK (ed) (1987) *Unified constitutive equations for creep and plasticity*. Elsevier, London, New York
- von Mises R (1928) *Mechanik der plastischen Formänderung von Kristallen*. *ZAMM-J Appl Math Mechanics/Zeitschrift für Angewandte Mathematik und Mechanik* 8(3):161–185
- Mohrmann R, Sester M (1999) A multi-axial model for the evolution of the microstructure and for the mechanical behaviour of a 12% chromium steel under creep conditions. In: Mughrabi H, Gottstein G, Mecking H, Riedel H, Tobolski J (eds) *Microstruct Mech Prop Metall High-Temp Mater: Res Report/DFG*. Wiley-VCH, Weinheim, pp 206–221
- Morishita T, Hirao M (1997) Creep damage modelling based on ultrasonic velocities in copper. *Int J Solids Struct* 34:1169–1182
- Mücke R, Bernhardt O (2003) A constitutive model for anisotropic materials based on Neuber's rule. *Comput Meth Appl Mech Eng* 192:4237–4255
- Müller I (2007) *A history of thermodynamics: the doctrine of energy and entropy*. Springer
- Murakami S (1983) Notion of continuum damage mechanics and its application to anisotropic creep damage theory. *J Eng Mater Technol* 105:99–105
- Murakami S (2012) *Continuum damage mechanics: a continuum mechanics approach to the analysis of damage and fracture*. In: *Solid mechanics and its applications*. Springer
- Murakami S, Ohno N (1981) A continuum theory of creep and creep damage. In: Ponter ARS, Hayhurst DR (eds) *Creep in structures*. Springer, Berlin, pp 422–444
- Murakami S, Sanomura Y (1985) Creep and creep damage of copper under multiaxial states of stress. In: Sawczuk A, Bianchi B (eds) *Plasticity today—modelling, methods and applications*. Elsevier, London, New York, pp 535–551
- Murakami S, Sanomura Y, Hattori M (1986) Modelling of the coupled effect of plastic damage and creep damage in nimonic 80a. *Int J Solids Struct* 22(4):373–386
- Muskhelishvili N (2013) *Some basic problems of the mathematical theory of elasticity*. Springer, Netherlands
- Nabarro FRN, de Villiers HL (1995) *The physics of creep*. In: *Creep and creep-resistant alloys*. Taylor & Francis, London
- Naghdi PM (1990) A critical review of the state of finite plasticity. *J Appl Math Phys (ZAMP)* 41:316–394
- Naumenko K, Altenbach H (2005) A phenomenological model for anisotropic creep in a multi-pass weld metal. *Arch Appl Mech* 74:808–819

- Naumenko K, Altenbach H (2007) Modelling of creep for structural analysis. Springer, Berlin
- Naumenko K, Gariboldi E (2014) A phase mixture model for anisotropic creep of forged Al-Cu-Mg-Si alloy. *Mater Sci Eng: A* 618:368–376
- Naumenko K, Altenbach H, Gorash Y (2009) Creep analysis with a stress range dependent constitutive model. *Arch Appl Mech* 79:619–630
- Naumenko K, Altenbach H, Kutschke A (2011a) A combined model for hardening, softening and damage processes in advanced heat resistant steels at elevated temperature. *Int J Damage Mech* 20:578–597
- Naumenko K, Kutschke A, Kostenko Y, Rudolf T (2011b) Multi-axial thermo-mechanical analysis of power plant components from 9–12%Cr steels at high temperature. *Eng Fract Mech* 78:1657–1668
- Nellis G, Klein S (2009) Heat transfer. Cambridge University Press
- Nemat-Nasser S (2004) Plasticity: A treatise on finite deformation of heterogeneous inelastic materials. Cambridge University Press, Cambridge Monographs on Mechanics
- Neuber H (2013) Kerbspannungslehre: Theorie der Spannungskonzentration. Genaue Berechnung der Festigkeit. Klassiker der Technik, Springer
- Nikitenko AF (1984) Eksperimental'noe obosnovanie gipotezy suschestvovaniya poverkhnosti polzuchesti v usloviyakh slozhnogo nagruzheniya, (experimental justification of the hypothesis on existence of the creep surface under complex loading conditions, in russ.). *Problemy prochnosti* 8:3–8
- Noll W (1972) A new mathematical theory of simple materials. *Arch Ration Mech Anal* 48:1–50
- Nye JF (1992) Physical properties of crystals. Oxford Science Publications, Oxford
- Odqvist FKG (1974) Mathematical theory of creep and creep rupture. Oxford University Press, Oxford
- Odqvist FKG, Hult J (1962) Kriechfestigkeit metallischer Werkstoffe. Springer, Berlin u.a
- Ogden R (1997) Non-linear elastic deformations. Dover Publications, Dover Civil and Mechanical Engineering
- Ogden RW (2015) Nonlinear elasticity with application to soft fibre-reinforced materials. In: Dorfmann L, Ogden RW (eds) Nonlinear mechanics of soft fibrous materials, cism international centre for mechanical sciences, vol 559, Springer, pp 1–48
- Ohno N (1990) Recent topics in constitutive modelling of cyclic plasticity and viscoplasticity. *Appl Mech Rev* 43:283–295
- Ohno N, Kawabata M, Naganuma J (1990) Aging effects on monotonic, stress-paused, and alternating creep of type 304 stainless steel. *Int J Plast* 6:315–327
- Onat ET, Leckie FA (1988) Representation of mechanical behavior in the presence of changing internal structure. *J Appl Mech* 55:1–10
- Othman AM, Hayhurst DR, Dyson BF (1993) Skeletal point stresses in circumferentially notched tension bars undergoing tertiary creep modelled with physically-based constitutive equations. *Proc R Soc London A: Math Phys Eng Sci* A441:343–358
- Othman AM, Dyson BF, Hayhurst DR, Lin J (1994) Continuum damage mechanics modelling of circumferentially notched tension bars undergoing tertiary creep with physically-based constitutive equations. *Acta Metall Mater* 42(3):597–611
- Oytana C, Delobelle P, Mermet A (1982) Constitutive equations study in biaxial stress experiments. *J Eng Mater Technol* 104(3):1–11
- Ozhoga-Maslovskaja O (2014) Micro scale modeling grain boundary damage under creep conditions. PhD thesis, Otto von Guericke University Magdeburg, Magdeburg
- Ozhoga-Maslovskaja O, Naumenko K, Altenbach H, Prygorniev O (2015) Micromechanical simulation of grain boundary cavitation in copper considering non-proportional loading. *Comput Mater Sci* 96, Part A:178–184
- Palmov V (1998) Vibrations in elasto-plastic bodies. Springer, Berlin
- Penkalla HJ, Schubert F, Nickel H (1988) Torsional creep of alloy 617 tubes at elevated temperature. In: Reichman S, Duhl DN, Maurer G, Antolovich S, Lund C (eds) Super alloys 1988. The Metallurgical Society, pp 643–652

- Penny RK, Mariott DL (1995) Design for creep. Chapman & Hall, London
- Perrin IJ, Hayhurst DR (1994) Creep constitutive equations for a 0.5Cr-0.5Mo-0.25V ferritic steel in the temperature range 600–675°C. *J Strain Anal Eng Des* 31(4):299–314
- Perrin IJ, Hayhurst DR (1999) Continuum damage mechanics analyses of type IV creep failure in ferritic steel crossweld specimens. *Int J Press Vessels Pip* 76:599–617
- Polcik P (1999) Modellierung des Verformungsverhaltens der warmfesten 9–12% Chromstähle im Temperaturbereich von 550–560°C. Dissertation, Universität Erlangen-Nürnberg, Shaker Verlag Aachen
- Polcik P, Straub S, Henes D, Blum W (1998) Simulation of the creep behaviour of 9–12% CrMo-V steels on the basis of microstructural data. In: Strang A, Cawley J, Greenwood GW (eds) Microstructural stability of creep resistant alloys for high temperature plant applications. Cambridge University Press, Cambridge, pp 405–429
- Powell PC (1994) Engineering with fiber-reinforced laminates. Chapman & Hall, London
- Prager W (1956) A new method of analyzing stresses and strains in work-hardening plastic solids. *J Appl Mech* 23(4):493–496
- Qi W (1998) Modellierung der Kriechschädigung einkristalliner Superlegierungen im Hochtemperaturbereich, Fortschrittberichte VDI, Reihe 18, Nr. 230. VDI Verlag, Düsseldorf
- Qi W, Bertram A (1997) Anisotropic creep damage modelling of single crystal superalloys. *Technische Mechanik* 17(4):313–322
- Qi W, Bertram A (1998) Damage modeling of the single crystal superalloy srr99 under monotonous creep. *Comput Mater Sci* 13:132–141
- Qi W, Bertram A (1999) Anisotropic continuum damage modeling for single crystals at high temperatures. *Int J Plast* 15:1197–1215
- Rabotnov YN (1963) O razrushenii vsledstvie polzuchesti (On fracture as a consequence of creep, in Russ.). *Prikladnaya mekhanika i tekhnicheskaya fizika* 2:113–123
- Rabotnov YN (1967) Vliyanie konsentratsii napryazhenij na dlitel'nyu prochnost' (Influence of stress concentration on the long-term strength, in Russ.). *Prikladnaya mekhanika i tekhnicheskaya fizika* 3:36–41
- Rabotnov YN (1969) Creep problems in structural members. North-Holland, Amsterdam
- Rabotnov YN (1979) Mekhanika deformiruemogo tverdogo tela (Mechanics of the deformable solid, in Russ.). Nauka, Moskva
- Reiner M (1969) Deformation and flow. An elementary introduction to rheology, 3rd edn. H.K. Lewis & Co., London
- Riedel H (1987) Fracture at high temperatures. In: Materials research and engineering. Springer, Berlin
- Rivlin R, Erickson J (1955) Stress-deformation-relations for isotropic material. *J Ration Mech Anal* 4:323–425
- Robinson DN (1984) Constitutive relationships for anisotropic high-temperature alloys. *Nucl Eng Des* 83:389–396
- Robinson DN, Binienda WK, Ruggles MB (2003a) Creep of polymer matrix composites. I: Norton/Bailey creep law for transverse isotropy. *J Eng Mech* 129(3):310–317
- Robinson DN, Binienda WK, Ruggles MB (2003b) Creep of polymer matrix composites. II: Monkman-Grant failure relationship for transverse isotropy. *J Eng Mech* 129(3):318–323
- Rodin GJ, Parks DM (1986) Constitutive models of a power-law matrix containing aligned penny-shaped cracks. *Mech Mater* 5:221–228
- Rodin GJ, Parks DM (1988) A self-consistent analysis of a creeping matrix with aligned cracks. *J Mech Phys Solids* 36:237–249
- Rogers TG (1990) Yield criteria, flow rules and hardening in anisotropic plasticity. In: Boehler JP (ed) Yielding, damage and failure of anisotropic solids. Mechanical Engineering Publ, London, pp 53–79
- Saanouni K, Chaboche JL, Lense PM (1989) On the creep crack-growth prediction by a non-local damage formulation. *Eur J Mech A Solids* 8(6):437–459

- Sakane M, Hosokawa T (2001) Biaxial and triaxial creep testing of type 304 stainless steel at 923 K. In: Murakami S, Ohno N (eds) IUTAM symposium on creep in structures. Kluwer, Dordrecht, pp 411–418
- Sakane M, Tokura H (2002) Experimental study of biaxial creep damage for type 304 stainless steel. *Int J Damage Mech* 11:247–262
- Schiesse P (1994) Ein Beitrag zur Berechnung des Deformationsverhaltens anisotrop gescheädigter Kontinua unter Berücksichtigung der thermoplastischer Kopplung. Dissertation, Ruhr-Universität Bochum, Mitteilungen aus dem Institut für Mechanik 89
- Schmicker D, Naumenko K, Strackeljan J (2013) A robust simulation of direct drive friction welding with a modified Carreau fluid constitutive model. *Comput Methods Appl Mech Eng* 265:186–194
- Schmicker D, Paczulla S, Nitzschke S, Groschopp S, Naumenko K, Jüttner S, Strackeljan J (2015) Experimental identification of flow properties of a S355 structural steel for hot deformation processes. *J Strain Anal Eng Des* 50(2):75–83
- Schröder J, Neff P (2003) Invariant formulation of hyperelastic transverse isotropy based on polyconvex free energy functions. *Int J Solids Struct* 40:401–445
- Sdobryev VP (1959) Kriterij dlitel'noj prochnosti dlya nekotorykh zharoprochnykh splavov pri slozhnom napryazhenom sostoyanii, (Criterion of long term strength of some high-temperature alloys under multiaxial stress state, in Russ.). *Izv AN SSSR OTN Mekh i Mashinostroenie* 6:93–99
- Skrzypek J, Ganczarski A (1998) Modelling of material damage and failure of structures. In: Foundation of engineering mechanics. Springer, Berlin
- Skrzypek JJ (1993) Plasticity and creep. CRC Press, Boca Raton
- Soločevskij A, Konkin V, Moračkovskij O, Koczyk S (1985) Eine Theorie zur nichtlinearen Verformung anisotroper Körper und ihre Anwendung auf die Berechnung des Kriechverhaltens dünner Schalen. *Technische Mechanik* 6(4):27–36
- Sosnin OV (1971) K voprosu o suschestvovanii potentsiala polzuchseti, (On the question on existence of creep potential, in Russ.). *Izv AN SSSR Mekhanika tverdogo tela* 5:85–89
- Sosnin OV (1974) Energeticheskii variant teorii polzuchesti i dlitel'noi prochnosti. Polzuchest' i razrushenie neuprochnyayushikhhsya materialov (Energetic variant of the creep and long-term strength theories. Creep and fracture of nonhardening materials, in Russ.). *Problemy prochnosti* 5:45–49
- Sosnin OV, Gorev BV, Nikitenko AF (1986) Energeticheskii variant teorii polzuchesti (Energetic variant of the creep theory, in Russ.). Institut Gidrodinamiki, Novosibirsk
- Spencer AJM (1984) Linear elastic constitutive equations for fibre-reinforced material. In: Spencer AJM (ed) Continuum theory of the mechanics of fibre-reinforced composites. Springer-Verlag, Wien, pp 1–32, CISM Lecture Notes No. 282
- Spencer AJM (1987) Isotropic polynomial invariants and tensor functions. In: Boehler J (ed) Applications of tensor functions in solid mechanics. Springer, Wien, pp 141–169, CISM Lecture Notes No. 292
- Stamm H, von Estroff U (1993) Determination of damage parameters for microcrack formation under creep conditions. In: Ainsworth RA, Skelton RP (eds) Behaviour of defects at high temperatures. Mechanical Engineering Publ, London, pp 123–151
- Stouffer DC, Dame LT (1996) Inelastic deformation of metals. Wiley, New York
- Straub S (1995) Verformungsverhalten und Mikrostruktur warmfester martensitischer 12%-Chromstähle. Dissertation, Universität Erlangen-Nürnberg, VDI Reihe 5, Nr. 405, Düsseldorf
- Tamuzh VP, Kuksenko VS (1978) Mikromechanika razrusheniya polimernykh materialov (Micro-mechanics of fracture of polymeric materials, in Russ.). Zinatne, Riga
- Timoshenko SP, Goodier JN (1951) Theory of elasticity. McGraw-Hill, New York
- Ting TCT (1996) Anisotropic elasticity. In: Theory and applications. Oxford University Press, Oxford
- Truesdell C (1964) Second-order effects in the mechanics of materials. In: Reiner M, Abir D (eds) Second-order effects in elasticity, plasticity and fluid dynamics. Pergamon Press, Oxford, pp 228–251

- Truesdell C, Noll W (1992) *The non-linear field theories of mechanics*, 2nd edn. Springer, Berlin
- Trunin II (1965) Kriterii prochnosti v usloviyakh polzuchesti pri slozhnom napryazhennom sostoyanii (Failure criteria under creep conditions in multiaxial stress state, in Russ.). *Prikl Mekhanika* 1(7):77–83
- Vakulenko AA, Kachanov ML (1971) Kontinual'naya teoriya s treshchinami (Continuum theory of a medium with cracks, in Russ.). *Izv AN SSSR Mekhanika tverdogo tela* 4:159–166
- Xiao H, Bruhns OT, Meyers A (2006) Elastoplasticity beyond small deformations. *Acta Mech* 182(1–2):31–111
- Zheng QS, Boehler JP (1994) The description, classification and reality of material and physical symmetries. *Acta Mech* 102:73–89
- Zhilin PA (1982) Osnovnye uravneniya neklassicheskoi teorii obolochek (basic equations of a non-classical theory of shells, in russ.). *Dinamika i prochnost' mashin*, Trudy LPI 386:29–46
- Zhilin PA (1996) A new approach to the analysis of free rotations of rigid bodies. *ZAMM-J Appl Math Mech/Zeitschrift für Angewandte Mathematik und Mechanik* 76(4):187–204
- Zhilin PA (2003) Modifizirovannaya teoriya simmetrii tenzorov i tenzornykh invariantov (A modified theory of symmetry for tensors and tensor invariants, in Russ.). *Izvestiya vuzov Estestvennyye Nauki* pp 176–195
- Ziegler H (1963) Some extremum principles in irreversible thermodynamics with application to continuum mechanics. In: Sneddon IN, Hill R (eds) *Progress in solid mechanics*. North-Holland, Amsterdam, pp 93–192
- Ziegler H (1983) An introduction to thermomechanics. In: *North-Holland Series in Applied Mathematics and Mechanics*, vol 21. North-Holland, Amsterdam
- Zyczkowski M (2000) Creep damage evolution equations expressed in terms of dissipated power. *Int J Mech Sci* 42:755–769

Chapter 6

Examples of Constitutive Equations for Various Materials

In Chaps. 3 and 5 various constitutive equations to characterize behavior of materials at high temperature are presented. These equations include a number of material dependent parameters like Young's modulus, creep exponent, hardening modulus etc., to be identified from experimental data. Furthermore functions of stress, strain rate and temperature (sometimes called response functions) are unknown in advance and should be formulated according to available experimental data for given ranges of loading and specific material.

This chapter presents several examples of constitutive equations, response functions of stress and temperature as well as material parameters for selected engineering materials. In order to find a set of material parameters, uni-axial tests under constant temperature leading to homogeneous stress and deformation states are required. The majority of available experimental data is presented as tensile curves (stress-strain curves) and creep curves (creep strain vs. time curves) obtained from standard uni-axial tests. Based on such curves the response functions and material parameters are identified.

Section 6.1 provides an overview of approaches to calibrate constitutive models against experimental data of high-temperature material behavior. In Sect. 6.2 constitutive equations of isotropic high-temperature plasticity of several alloys are presented. The objective of Sect. 6.3 is to discuss anisotropic inelastic behavior. Two examples of initially anisotropic materials including a forged aluminium alloy and a multi-pass weld metal from an advanced steel are presented.

6.1 Basic Approaches of Identification

The problem to identify the material parameters (also known as the inverse problem) can be solved with the following steps

- Formulate the functional with respect to the unknown material parameters by the use of the (weighted) least squares method,
- Minimize the functional by specifying appropriate guess for the material parameters.

For simplified constitutive equations, e.g. power law creep or deformation plasticity, the above steps are enough to fit the deformation response with a desired accuracy. Various examples for applications of least square methods to compute material parameters in constitutive equations of creep are presented in Boyle and Spence (1983). Mathematical and numerical aspects of identification procedures are discussed in Mahnken and Stein (1996, 1997), among others.

In contrast, the identification of material properties in unified constitutive models to capture several phenomena of inelastic deformation like hardening/recovery, softening and damage under different loading paths can be ill-posed for the following reasons

- The unified model should be calibrated for wide strain rate, stress and temperature ranges to capture both creep and LCF regimes. For example, for cast iron materials the inelastic strain rate ranges from 10^{-7} to 10 1/h (Längler et al. 2014). Therefore, not only the material parameters but also functions of strain rate, stress and temperature are unknown in advance and should be found during the identification process,
- The resolution of experimental data is usually not fine enough to perform a stable minimization. For example, inelastic strain rates at the beginning of the creep process after the loading are usually not well defined,
- Experimental data may show a large scatter generated by testing a series of specimens removed from the same material. The origins of scatter in creep tests are discussed, for example, in Dyson (1996),
- Inelastic behavior may significantly depend on the kind of processing of specimens, e.g. the heat treatment. As a result, different data sets for the material with the same chemical composition may be found in the literature. For example, one may compare experimental data for 9Cr1Mo (P91) ferritic steel obtained in different laboratories (Abe 2001; Choudhary et al. 2001; Eggeler et al. 1994; Kloc et al. 2001; Orlová et al. 1998; Wu et al. 2004).

An alternative approach is to develop a step-by-step identification procedure. For example, one may develop the identification procedure based on the following steps

- Experimental creep curves (creep strain versus time curves) are smoothed and transformed to the creep rate versus creep strain curves,
- Initial and minimum inelastic strain rates as functions of stress and temperature are processed from experimental data for creep and tensile regimes,
- Response functions of stress and temperature are identified from experimental data on initial and steady strain rates,
- Evolution equations for softening, ageing and damage are calibrated against experimental creep rate versus creep strain curves within the tertiary creep range

Step-by-step identification procedures are presented in Samir et al. (2005), Kostenko et al. (2006, 2009a), Längler et al. (2014), Naumenko and Gariboldi (2014), among others. An example will be presented in Sect. 6.2.3.

6.2 Isotropic Materials

In this section examples of constitutive equations for isotropic high-temperature behavior of several alloys are presented. Sections 6.2.1 and 6.2.2 provide simplified creep-damage constitutive equations. Here the hardening processes are ignored and the tertiary creep is described by a single damage variable. In Sects. 6.2.3 and 6.2.4 mechanisms-based models are discussed in detail. Examples of evolution equations for hardening/recovery, softening and ageing are presented. In all examples response functions of stress and temperature as well as values of material parameters are presented.

6.2.1 Type 316 Steel

The first example is type 316 stainless steel at 650 °C. In Liu et al. (1994) the following creep equations are applied

$$\begin{aligned} \dot{\boldsymbol{\varepsilon}}^{\text{pl}} &= \frac{3}{2} f_1(\sigma_{\text{VM}}) g_1(\omega) \frac{\boldsymbol{s}}{\sigma_{\text{VM}}}, \quad \dot{\omega} = f_2 \left[\sigma_{\text{eq}}^\omega(\boldsymbol{\sigma}) \right] g_2(\omega), \\ \boldsymbol{\varepsilon}^{\text{pl}}|_{t=0} &= \mathbf{0}, \quad \omega|_{t=0} = 0, \quad 0 \leq \omega \leq \omega_*, \\ \boldsymbol{s} &= \boldsymbol{\sigma} - \frac{1}{3} \text{tr} \boldsymbol{\sigma} \mathbf{I}, \quad \sigma_{\text{VM}} = \sqrt{\frac{3}{2} \boldsymbol{s} \cdot \boldsymbol{s}} \end{aligned} \quad (6.2.1)$$

Here $\boldsymbol{\varepsilon}^{\text{pl}}$ is the creep strain tensor, $\boldsymbol{\sigma}$ is the stress tensor, ω is the scalar-valued damage parameter and $\sigma_{\text{eq}}^\omega$ is the damage equivalent stress (see Sect. 5.7.1.1). The response functions f_1 , f_2 , g_1 , and g_2 are

$$\begin{aligned} f_1(\sigma) &= a \sigma^n, \quad g_1(\omega) = (1 - \omega)^{-n}, \\ f_2(\sigma) &= b \sigma^k, \quad g_2(\omega) = (1 - \omega)^{-k} \end{aligned} \quad (6.2.2)$$

The material parameters are presented in Liu et al. (1994) as follows

$$\begin{aligned} a &= 2.13 \cdot 10^{-13} \text{ MPa}^{-n} / \text{h}, \quad b = 9.1 \cdot 10^{-10} \text{ MPa}^{-k} / \text{h}, \\ n &= 3.5, \quad k = 2.8 \end{aligned} \quad (6.2.3)$$

Note, that the constants a and b in Eqs. (6.2.2) are identified for the constant temperature. In the general case they must be replaced by functions of temperature. It

is assumed that the damage evolution is controlled by the maximum tensile stress. Therefore the damage equivalent stress takes the form

$$\sigma_{\text{eq}}^{\omega}(\boldsymbol{\sigma}) = \frac{\sigma_I + |\sigma_I|}{2},$$

where σ_I is the first principal stress. The elastic material behavior is characterized by the following values of the Young's modulus E and the Poisson's ratio ν

$$E = 1.44 \cdot 10^5 \text{ MPa}, \quad \nu = 0.314 \quad (6.2.4)$$

Equations (6.2.1) can be applied for the analysis of creep under constant or proportional slowly varying loading. Response functions and material parameters in Eqs. (6.2.1) can be found in the literature for numerous metals and alloys. Examples are presented in the monographs by Boyle and Spence (1983), Lemaitre and Chaboche (1990), Malinin (1981), Penny and Marriott (1995), Podgorny et al. (1984), Rabotnov (1969), Skrzypek and Ganczarski (1998), Hyde et al. (2013). Experimental data from long-term creep tests are usually limited and the scatter is unavoidable. Therefore, robust equations (6.2.1) are widely used in modeling creep behavior and in structural analysis. Examples of material parameters as well as structural mechanics applications can be found in Altenbach et al. (1997b), Altenbach and Naumenko (1997), Altenbach et al. (2000, 2001), Bodnar and Chrzanowski (1991), Hayhurst (2001), Hyde et al. (1997, 1999, 2000), Konkin and Morachkovskij (1987), Kowalewski (1996), among others.

6.2.2 Steel 13CrMo4-5

In Segle et al. (1996) the creep behavior of steel 13CrMo4-5 at 550°C is described by (6.2.1) with the following response functions

$$\begin{aligned} f_1(\sigma) &= a\sigma^n, & g_1(\omega) &= 1 - \zeta + \zeta(1 - \omega)^{-n}, \\ f_2(\sigma) &= b\sigma^k, & g_2(\omega) &= (1 - \omega)^{-l} \end{aligned} \quad (6.2.5)$$

The material parameters are

$$\begin{aligned} a &= 1.94 \cdot 10^{-15} \text{ MPa}^{-n}/\text{h}, & b &= 3.302 \cdot 10^{-13} \text{ MPa}^{-k}/\text{h}, \\ n &= 4.354, & k &= 3.955, & l &= 1.423, & \zeta &= 0.393 \end{aligned} \quad (6.2.6)$$

The damage equivalent stress is assumed in the form

$$\sigma_{\text{eq}}^{\omega}(\boldsymbol{\sigma}) = \alpha \frac{\sigma_I + |\sigma_I|}{2} + (1 - \alpha)\sigma_{\text{VM}}$$

with $\alpha = 0.43$. The Young's modulus and Poisson's ratio are $E = 1.6 \cdot 10^5$ MPa and $\nu = 0.3$, respectively. Equations (6.2.1) with response functions (6.2.5) are applied in Naumenko and Altenbach (2007) for the long-term strength analysis of a steam transfer line, see also Sect. 1.2.1.2.

6.2.3 Steel X20CrMoV12-1

In this section we present a set of constitutive and evolution equations to describe the inelastic behavior of advanced 9–12% Cr heat resistant steels. These materials are designed for the use at steam temperatures up to 650 °C (Mayer and Masuyama 2008). If compared to the low alloy steels, they have a rather complex composition and show complicated inelastic behavior (see Chap. 1). The main features are

- The uni-axial creep curves do not exhibit a secondary (steady-state) stage. The dependence of the minimum creep rate on the stress essentially deviates from the power law (Kloc and Sklenička 2004; Kimura et al. 2009; Kostenko et al. 2009a).
- The transition from the primary to the tertiary creep stage is controlled by softening processes, e.g. the coarsening of the subgrain microstructure (Straub 1995; Polcik et al. 1998).
- The final part of the tertiary creep is influenced by damage processes, e.g. the formation and growth of voids and micro-cracks (Straub 1995; Rauch et al. 2004; Simon 2007).
- The damage and softening processes are more or less dominant for different stress ranges. As a result the slope of the creep term strength curve (stress versus time to rupture in a double logarithmic scale) continuously decreases with a decrease of the stress level (Naumenko and Kostenko 2009).
- The stress-strain curves show descending (softening) branches, Fig. 1.2.

The conventional approach in the creep continuum damage mechanics is to introduce damage parameter(s) and to calibrate the damage evolution equation(s) against the tertiary stage of the creep curve. As proposed by Rabotnov (1963) a single damage parameter can be used to describe tertiary creep and long term strength in the range of “brittle” creep rupture, see Sect. 3.6.1. On the other hand, the Hoff's kinematical model of ductile creep predicts tertiary creep as a result of the shrinkage of the specimens cross section (Hoff 1953), see Sect. 3.3. The combination of Rabotnov's and Hoff's models provides the two-slope long term strength curve including both the ductile and the brittle creep regimes (Rabotnov 1963; Odqvist 1974). Further developments of this approach were related to quantification of different damage mechanisms, e.g. creep constrained or continuum cavity nucleation and growth (Lin et al. 2005) as well as processes that accompany and influence the damage evolution, e.g. the coarsening of carbide precipitates (Dyson and McLean 2001). The resulting models include several independent internal state variables that account for different deterioration processes and characterize tertiary creep in a more precise manner (Hayhurst 1999).

Below we extend the conventional approach by quantifying hardening/recovery, softening, and damage processes. For the sake of simplicity we introduce a single damage parameter to characterize creep cavitation. The influence of ageing processes like coarsening of carbide precipitates will be ignored. We focus on the modeling of softening associated with the evolution of subgrain structure usually observed in advanced heat resistant steels. In particular, we show that a combined model including hardening, softening, and damage variables describes well the inelastic response under constant and variable loading. Furthermore, such a model allows us to reproduce the long term strength behavior in a wide stress range.

To describe hardening and softening phenomena we apply a phase mixture model discussed in Sects. 3.5.3 and 5.6.3. The response functions of stress and temperature as well as material parameters are calibrated against experimental data for X20CrMoV12-1 steel presented in Straub (1995). Creep tests under tension and compression were performed for a range of stresses and temperatures. For the compressive true stress the tertiary creep is primarily determined by the softening processes. Based on the corresponding creep curves the phase mixture model will be calibrated. For the tensile stress, additional rapid increase of the creep rate is controlled by damage evolution. This fact is confirmed by microstructural observations presented in Straub (1995), where voids and micro-cracks were detected only for tension specimen. To describe the final part of the creep curve the scalar-valued damage variable and the damage evolution equation will be utilized.

To verify the developed model, creep curves under stress changes will be simulated and the results will be compared with experimental data. To validate the coupled softening and damage evolution equations time to fracture will be simulated for different uni-axial stress levels. To discuss the applicability range of the model we simulate the inelastic behavior under strain controlled tension.

6.2.3.1 Hardening and Softening

The constitutive model for the inelastic deformation considering hardening/recovery and softening processes is presented in Sect. 5.6.3. The model includes the constitutive equation for the inelastic strain rate tensor (5.6.274), the evolution equation for the backstress deviator (5.6.273) and the evolution equation for the softening variable (5.6.277). For isothermal conditions the constitutive model can be formulated as follows

$$\begin{aligned}\dot{\boldsymbol{\epsilon}}^{\text{pl}} &= \frac{3}{2} f(\bar{\sigma}_{\text{vM}}) g(T) \frac{\bar{\boldsymbol{s}}}{\bar{\sigma}_{\text{vM}}} - \frac{d}{dt} \left(\frac{\boldsymbol{\beta} \Gamma}{2\mu} \right), \\ \dot{\boldsymbol{\beta}} &= \frac{2\mu}{c_h} \left(\dot{\boldsymbol{\epsilon}}^{\text{pl}} - \frac{3}{2} \dot{\boldsymbol{\epsilon}}_{\text{vM}}^{\text{pl}} \frac{\boldsymbol{\beta}}{\beta_*} \right), \\ \dot{\Gamma} &= A_s [\Gamma_*(\sigma_{\text{vM}}) - \Gamma] \dot{\boldsymbol{\epsilon}}_{\text{vM}}^{\text{pl}},\end{aligned}\tag{6.2.7}$$

where the active stress deviator $\bar{\boldsymbol{s}}$ and the corresponding von Mises equivalent stress $\bar{\sigma}_{\text{vM}}$ are defined as follows

$$\underline{\bar{s}} = \underline{s} - \underline{\beta} \Gamma, \quad \bar{\sigma}_{\text{VM}} = \sqrt{\frac{3}{2} \underline{\bar{s}} \cdot \underline{\bar{s}}} \quad (6.2.8)$$

The underlined term in Eq. (6.2.7)₁ has minor influence on the inelastic strain rates and can be neglected, as proposed in Naumenko et al. (2011a,b), Kostenko et al. (2013). For the uni-axial stress state the stress deviator \underline{s} and the backstress deviator $\underline{\beta}$ take the following forms

$$\underline{s} = \sigma (\underline{e} \otimes \underline{e} - \frac{1}{3} \underline{I}), \quad \underline{\beta} = \beta (\underline{e} \otimes \underline{e} - \frac{1}{3} \underline{I}), \quad (6.2.9)$$

where σ is the uni-axial stress, β is the uni-axial backstress and the unit vector \underline{e} stands for the loading direction. The constitutive model (6.2.7) takes the following form

$$\begin{aligned} \dot{\varepsilon}^{\text{pl}} &= f(|\sigma - \beta \Gamma|) g(T) \frac{\sigma - \beta \Gamma}{|\sigma - \beta \Gamma|}, \\ \dot{\beta} &= \frac{3\mu}{c_h} \left(\dot{\varepsilon}^{\text{pl}} - |\dot{\varepsilon}^{\text{pl}}| \frac{\beta}{\beta_*} \right), \\ \dot{\Gamma} &= A_s [\Gamma_* (|\sigma|) - \Gamma] |\dot{\varepsilon}^{\text{pl}}| \end{aligned} \quad (6.2.10)$$

Assuming a constant stress value $\sigma = \text{const}$ and with a new variable $H = \beta/\sigma_0$ Eqs. (6.2.10) can be simplified as follows

$$\begin{aligned} \dot{\varepsilon}^{\text{pl}} &= f[|\sigma|(1 - H\Gamma)] g(T) \text{sgn}\sigma, \\ \dot{H} &= \frac{3\mu}{c_h \sigma} \left(1 - \frac{H}{H_*} \right) \dot{\varepsilon}^{\text{pl}}, \quad H_* = \frac{\beta_*}{|\sigma|} \\ \dot{\Gamma} &= A_s [\Gamma_* (|\sigma|) - \Gamma] \dot{\varepsilon}^{\text{pl}} \text{sgn}\sigma \end{aligned} \quad (6.2.11)$$

With the initial condition $H(0) = 0$ the hardening evolution equation in (6.2.11)₂ can be integrated leading to

$$H(\sigma, \varepsilon^{\text{pl}}) = H_* \left[1 - \exp \left(-\frac{3\mu}{c_h H_*} \frac{\varepsilon^{\text{pl}}}{\sigma} \right) \right] \quad (6.2.12)$$

Neglecting the softening, i.e. setting in (6.2.11)₃ $A_s = 0$ and with the initial condition $\Gamma(0) = 1$ the creep constitutive equation (6.2.11)₁ takes now the form

$$\dot{\varepsilon}^{\text{pl}} = f \left\{ |\sigma| \left[1 - H_* + H_* \exp \left(-\frac{3\mu}{c_h H_*} \frac{\varepsilon^{\text{pl}}}{\sigma} \right) \right] \right\} g(T) \text{sgn}\sigma \quad (6.2.13)$$

Equation (6.2.13) describes the primary stage of a creep curve, i.e. the decrease of the creep rate towards a steady-state value $\dot{\varepsilon}_{\text{ss}}^{\text{pl}} = f[|\sigma|(1 - H_*)] g(T) \text{sgn}\sigma$ with an increase of the creep strain. Constitutive and evolution Eqs. (6.2.11)₁ and (6.2.11)₂ with $\Gamma = 1$ were used in Dyson and McLean (2001), Kowalewski et al. (1994), Perrin and Hayhurst (1994) to describe primary creep of various materials, see Sects. 5.7.1.3

and 6.2.4. We observe, that Eqs. (6.2.11)₁ and (6.2.11)₂ are only applicable for the constant stress value.

For the constant stress value σ and with the initial condition $\Gamma(0) = 1$ the softening evolution equation (6.2.11)₃ can be integrated providing the softening variable as the following function of stress and inelastic strain

$$\Gamma(\sigma, \varepsilon^{pl}) = \Gamma_*(|\sigma|) + [1 - \Gamma_*(|\sigma|)] \exp(-A_s \varepsilon^{pl} \text{sgn}\sigma) \tag{6.2.14}$$

With Eqs. (6.2.12) and (6.2.14) the inelastic strain rate (6.2.10)₁ is the function of the inelastic strain and the applied stress.

Figure 6.1 shows the experimental data for X20CrMoV12-1 steel at 873 K presented in Straub (1995). Creep tests were performed under constant compressive true stress. From the absolute strain values the creep rate was evaluated and plotted against the logarithmic creep strain. The resulting creep rate versus creep strain curves clearly show the hardening and softening regimes, Fig. 6.1. The experimental data is used to identify the material parameters and response functions in Eqs. (6.2.10)₁, (6.2.12) and (6.2.14). To calibrate a constitutive model a family of creep curves in wide stress and temperature ranges is usually required. Creep curves presented in Fig. 6.1 are given for one temperature level and for a narrow stress range. Therefore additional experimental data on minimum creep rates is applied for the identification. Figure 6.1 shows the minimum creep rate as a function of stress for three temperature levels. The experimental data is collected by Straub (1995) from several publications and based on own creep tests. To fit the data various response functions of stress and temperature, which are more or less physically motivated, can be applied. Overviews are presented in Sect. 5.4.4. One example is the hyperbolic sine law

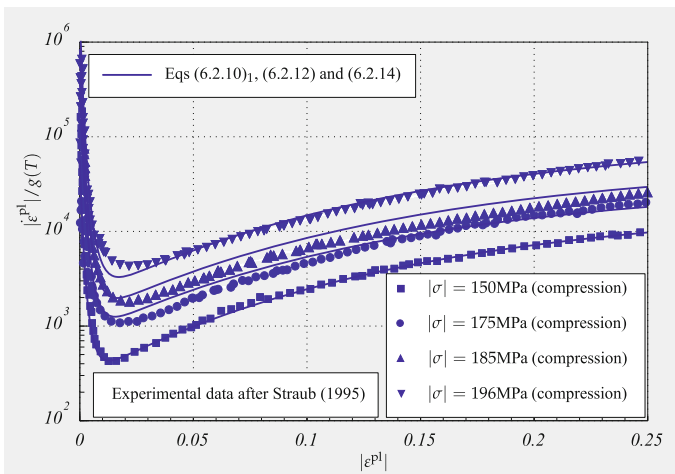


Fig. 6.1 Normalized creep rate versus creep strain curves for X20CrMoV12-1 steel at 873 K and different stress levels

$$\dot{\epsilon}_{\min} = g(T) \sinh(B\sigma), \tag{6.2.15}$$

where B is a constant and $g(T)$ is the Arrhenius function of the absolute temperature T . Equation (6.2.15) is applied in Dyson and McLean (2001), Kowalewski et al. (1994), Perrin and Hayhurst (1994). Another way is to assume that the minimum creep rate is the sum of the linear and the power law stress functions. As pointed out in Frost and Ashby (1982) power law and diffusion creep mechanisms involve different defects and may be assumed independent such that the corresponding creep rates add. The constitutive equation can be formulated as follows

$$\dot{\epsilon}_{\min} = \dot{\epsilon}_0(T) \frac{\sigma}{\sigma_0(T)} + \dot{\epsilon}_0(T) \left(\frac{\sigma}{\sigma_0(T)} \right)^n, \tag{6.2.16}$$

where n is a constant and $\dot{\epsilon}_0(T)$, $\sigma_0(T)$ are Arrhenius functions of the temperature. The response function (6.2.16) is applied in Kloc and Sklenička (2004), Rieth et al. (2004), Naumenko and Kostenko (2009), Naumenko et al. (2009) to describe the minimum creep rate for various advanced steels. The results of fitting by the use of Eqs. (6.2.15) and (6.2.16) are presented in Fig. 6.2. In what follows let us apply the hyperbolic sine law. The identified response functions in Eqs. (6.2.10) can be summarized as follows

$$\begin{aligned} f(x) &= \sinh(Bx), & g(T) &= a_0 \exp\left(-\frac{\alpha}{T}\right), \\ \Gamma_*(x) &= \frac{a_\Gamma}{1 + b_\Gamma e^{-\frac{x}{c_\Gamma}}}, & \beta_*(x) &= H_* x \end{aligned} \tag{6.2.17}$$

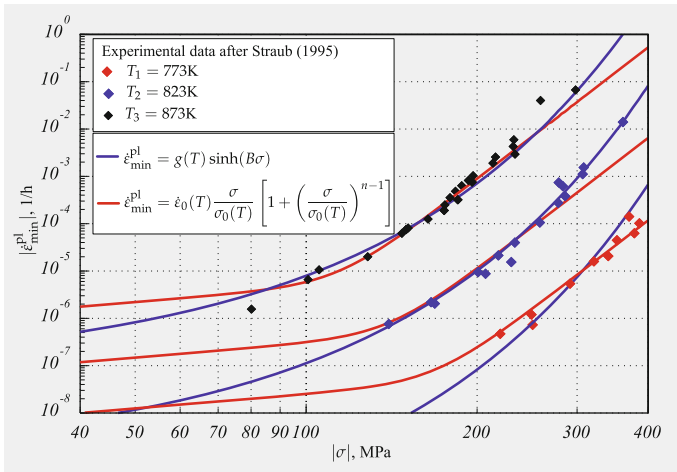


Fig. 6.2 Minimum creep rate versus stress curves for X20CrMoV12-1 steel at three temperature levels

with $B = 7.74 \cdot 10^{-2}$ 1/MPa, $a_0 = 4.64 \cdot 10^{23}$ 1/h, $\alpha = 6.12 \cdot 10^4$ 1/K, $a_\Gamma = 0.42$, $b_\Gamma = 9.12 \cdot 10^6$, $c_\Gamma = 9.46$ MPa, $H_* = 0.46$. The additional material parameters in Eqs. (6.2.10) are identified as $c_h = 8.84$ and $A_s = 7.21$. The Young's modulus E and the shear modulus μ are functions of temperature. The corresponding temperature dependencies are given in Straub (1995) as follows

$$E(T) = -a_E + b_E T, \quad \mu(T) = -a_\mu + b_\mu T \quad (6.2.18)$$

with

$$\begin{aligned} a_E &= 95.597 \text{ MPa/K}, & b_E &= 252334.26 \text{ MPa}, \\ a_\mu &= 38.773 \text{ MPa/K}, & b_\mu &= 97398.16 \text{ MPa} \end{aligned}$$

6.2.3.2 Damage Processes and Creep Strength

Damage processes are usually associated with nucleation, growth and coalescence of voids on grain or subgrain boundaries as well as nucleation of voids and microcracks around carbide precipitates. For low-alloy steels the damage evolution equations are usually calibrated against the tertiary stage of the creep curve. For advanced steels the essential part of the tertiary creep is related to softening processes (e.g. coarsening of subgrain structure) as documented in Polcik et al. (1999), Kimura (2006), Kostenko and Naumenko (2008), see also Fig. 1.9. For 9%Cr steels the voids on former austenite grain boundaries and/or carbides can be observed after prolonged test durations and essentially higher values of the creep strain if compared to the low alloy steels, e.g. Rauch et al. (2004), Maile and Scheck (2008). Let us describe the uni-axial creep curves for X20CrMoV12-1 steel presented in Straub (1995). To this end we introduce the Kachanov-Rabotnov damage parameter (Rabotnov 1963) and apply the strain equivalence principle as proposed in Lemaitre and Chaboche (1990), see Sects. 3.6.1 and 5.7.1.1. The constitutive equation (6.2.10)₁ can be modified as follows

$$\dot{\varepsilon}^{\text{pl}} = f \left(\frac{|\sigma - \beta \Gamma|}{1 - \omega} \right) \frac{\sigma - \beta \Gamma}{|\sigma - \beta \Gamma|} \quad (6.2.19)$$

For the damage parameter ω the evolution (3.6.135) equation is applied

$$\dot{\omega} = h_\omega(\omega) \frac{1 + \text{sgn}\sigma}{2} \frac{|\dot{\varepsilon}^{\text{pl}}|}{\varepsilon_*^{\text{pl}}(|\sigma|)}, \quad (6.2.20)$$

where $h_\omega(\omega)$ and $\varepsilon_*^{\text{pl}}(|\sigma|)$ are response functions. Figure 6.3 shows creep curves for X20CrMoV12-1 steel obtained from tension tests under constant true stress levels. For the comparison the creep curves under compression for the same stress levels are presented. The results of metallographic analysis presented in Straub (1995) show that the increase in the creep rate under tension is primarily connected with the nucleation and growth of voids. Therefore the continuum damage mechanics can be applied to describe the whole creep process including the final part before the

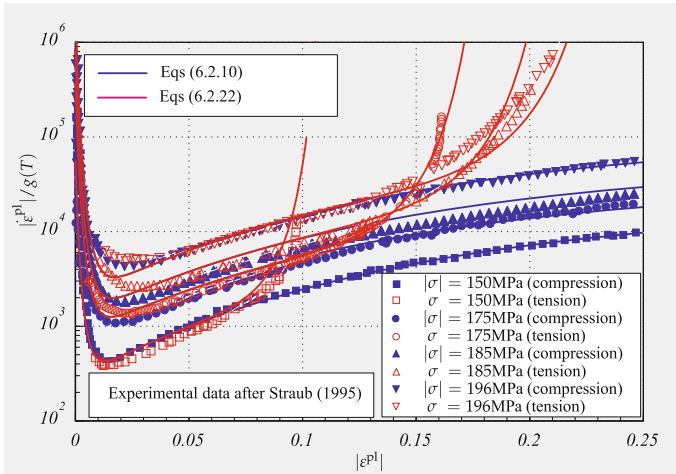


Fig. 6.3 Normalized creep rate versus creep strain curves for X20CrMoV12-1 steel at 873 K and different stress levels

fracture. Let us summarize all constitutive and evolution equations for the uni-axial stress state as follows

$$\begin{aligned}
 \dot{\varepsilon}^{pl} &= f(|\sigma - \beta\Gamma|)g(T) \frac{\sigma - \beta\Gamma}{|\sigma - \beta\Gamma|}, \\
 \dot{\beta} &= \frac{3\mu}{c_h} \left(\dot{\varepsilon}^{pl} - |\dot{\varepsilon}^{pl}| \frac{\beta}{\beta_*} \right), \\
 \dot{r} &= A_s [\Gamma_*(|\sigma|) - \Gamma] |\dot{\varepsilon}^{pl}|, \\
 \dot{\omega} &= h_\omega(\omega) \frac{1 + \text{sgn}\sigma}{2} \frac{|\dot{\varepsilon}^{pl}|}{\varepsilon_*^{pl}(|\sigma|)},
 \end{aligned} \tag{6.2.21}$$

The response functions in the damage evolution equation are identified as follows

$$h_\omega(\omega) = l\omega^{\frac{l-1}{l}}, \quad \varepsilon_*^{pl}(|\sigma|) = \varepsilon_{br} + \frac{a_\varepsilon}{1 + b_\varepsilon \exp\left(-\frac{|\sigma|}{c_\varepsilon}\right)} \tag{6.2.22}$$

with $l = 8$, $\varepsilon_{br} = 0.09$, $a_\varepsilon = 0.2$, $b_\varepsilon = 8.39 \cdot 10^5$, $c_\varepsilon = 12.67$ MPa.

Numerical integration of Eqs. (6.2.21) over time provides the relation between the applied stress and the time to rupture. Figure 6.4 shows the results of integration according to three different model assumptions. The model of ductile creep rupture proposed by Hoff (1953) ignores softening and damage processes. The tertiary creep stage is the result of the specimens cross section shrinkage only, see Sect. 3.4. This approach provides a rough estimation of the time to creep rupture, Fig. 6.4. If softening processes are taken into account then the long term strength curve shifts

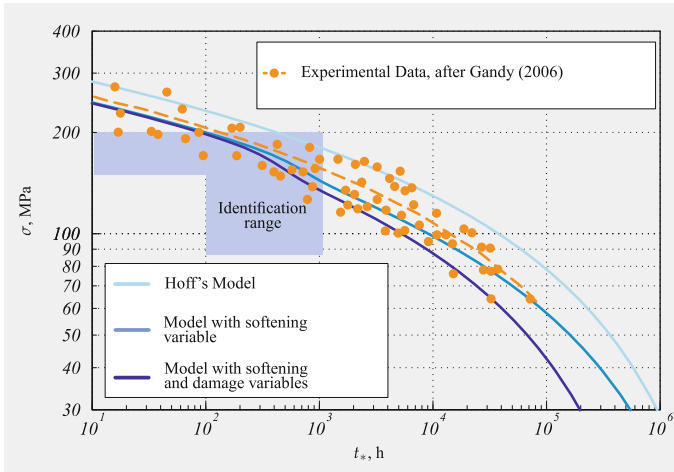


Fig. 6.4 Engineering stress versus time to rupture for X20CrMoV12-1 steel at 873 K

down along the stress axis. Furthermore, a sigmoidal inflection of the creep strength curve can be observed, Fig. 6.4. Such sigmoidal inflection is documented in many experimental studies related to advanced 9–12 % Cr steels (Abe 2004; Kimura et al. 1997; Sklenička et al. 2003).

If we consider both the softening and the damage processes an additional decrease of the slope of the long term strength curve can be described. Let us note that hardening, softening and damage evolution equations are calibrated against the creep curves in a narrow stress range (identification range). To check the quality of lifetime prediction in the wide stress range let us compare the results with experimental data plotted by dots in Fig. 6.4 after Gandy (2006). Despite a relatively large scatter of the data, we may conclude that the Hoff's model overestimates the rupture life in the range of moderate and low stress levels. The softening model leads to the result closer to experimental data while the additional consideration of damage provides a conservative estimation of the lifetime.

Voids and microcracks usually nucleate and grow on those planes which are perpendicular to the direction of the maximum tensile stress, e.g. Naumenko and Altenbach (2007), Betten (2008). The microstructural observations and the analysis of void size distributions in crept specimen from steels X20CrMoV12-1 and X22CrMoV12-1 are presented in Straub (1995). The biggest voids were found within the angles 60° – 90° to the stress axis. The topology of the directional damage state can be characterized by damage tensors of different rank, see Sect. 5.7.2. To establish the influence of the directional damage on the creep rate, creep tests under non-proportional loading conditions are required. Examples include creep tests on thin-walled tubes under combined tension and torsion (Murakami and Sanomura 1985) and biaxial creep tests on cruciform specimens (Sakane and Tokura 2002). The results of such tests can be applied to calibrate the tensor-valued damage evolu-

tion equations. Multi-axial test data for 9–12% Cr steels are currently not published. Here we neglect the directional nature of damage. The damage evolution equation (6.2.20) can be generalized as follows

$$\dot{\omega} = h_{\omega}(\omega) \frac{1}{2} \frac{(\sigma_I + |\sigma_I|)}{\sigma_{vM}} \frac{\dot{\epsilon}_{vM}^{pl}}{\epsilon_*^{pl}(\sigma_{vM})}, \tag{6.2.23}$$

where σ_I is the first principal stress. Applying the strain equivalence principle (Lemaitre and Chaboche 1990; Lemaitre 1996) the constitutive equation (6.2.7)₁ can be generalized as follows

$$\dot{\epsilon}^{pl} = \frac{3}{2} f \left(\frac{\bar{\sigma}_{vM}}{1 - \omega} \right) g(T) \frac{\bar{s}}{\bar{\sigma}_{vM}} \tag{6.2.24}$$

6.2.3.3 Creep Under Stress Changes

To verify the constitutive model let us simulate creep behavior under variable loading conditions. Figure 6.5 shows the experimental creep curve under compressive stress changes obtained in Straub (1995). During the test the specimen was initially subjected to the constant compressive true stress with the value of 196 MPa. After a certain hold time the stress was rapidly reduced to the value of 150 MPa. Several loading/unloading cycles with hold time were performed up to the reaching of the creep strain value of 25%. As Fig. 6.5 shows the stress changes were performed within the tertiary creep stage.

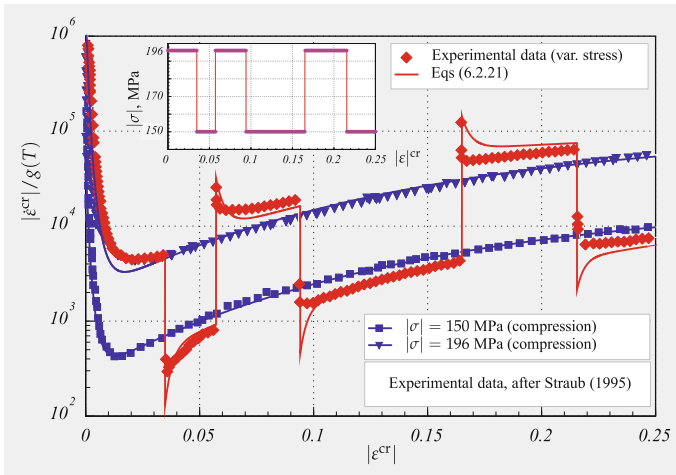


Fig. 6.5 Normalized creep rate versus creep strain for X20CrMoV 12-1 steel at $T = 600\text{ }^{\circ}\text{C}$ and variable compressive stress

The inelastic strain rate versus inelastic strain curve predicted by Eqs. (6.2.21) is presented in Fig. 6.5 by the solid line. For the comparison, two creep curves under the constant upper and lower stress values are shown. We observe that the model underestimates the creep rates after the rapid loading reduction. This slight disagreement may be related to the deficiency of the assumed constitutive equation for the inelastic-hard constituent in the phase mixture model, see Sect. 5.6.3. Despite this inaccuracy, the creep behavior under stress changes is well represented by the composite model with the varying volume fraction. One feature of the softening process is well reproduced by the model. After the stress decrease the creep rate remains lower, while after the stress increase remains higher than the corresponding creep rates under the constant stress levels.

6.2.3.4 Tensile Behavior Under Constant Strain Rate

The next verification test is to simulate tensile behavior under a constant strain rate. To compute the stress response we integrate the equation

$$\dot{\varepsilon} = \frac{\dot{\sigma}}{E} + \dot{\varepsilon}^{\text{pl}} = \text{const} \quad (6.2.25)$$

together with the constitutive model (6.2.21). Figure 6.6 shows the experimental stress-strain diagram obtained with $\dot{\varepsilon} = 2.63 \cdot 10^{-4} \text{ s}^{-1}$ and 803 K (Röttger 1997). The results of the model prediction are presented by the solid line. In addition, a zoom of the transition from the linear-elastic to the inelastic behavior is given in the left smaller diagram. The right smaller diagram shows the backstress variable β as a function of the strain. The elastic behavior up to 300 MPa is almost exactly described. The beginning of the inelastic behavior is observed at the strain value $\varepsilon \approx 0.0015$. Up to this value the backstress remains almost zero. It is obvious that there is no kink in the progress of the global stress-strain curve, although the change of the slope is too abrupt if compared to the experimental data. The too strict transition from the linear-elastic to the inelastic behavior and a low slope of the curve at the beginning of the inelastic range may again be related to the deficiency of the assumed constitutive equation for the inelastic-hard constituent in the phase mixture model, see Sect. 5.6.3. Nevertheless, the maximum stress value and the softening behavior are well reproduced by the model. For strains higher than 16 % the model overestimates the stress values. This may be caused by the start of necking of the specimen, which is not taken into account in the uni-axial model.

6.2.3.5 Summary of Constitutive and Evolution Equations

The proposed constitutive model includes three state variables: the backstress deviator β , the softening variable Γ and the damage variable ω . The inelastic strain tensor and the internal state variables are defined by the following equations

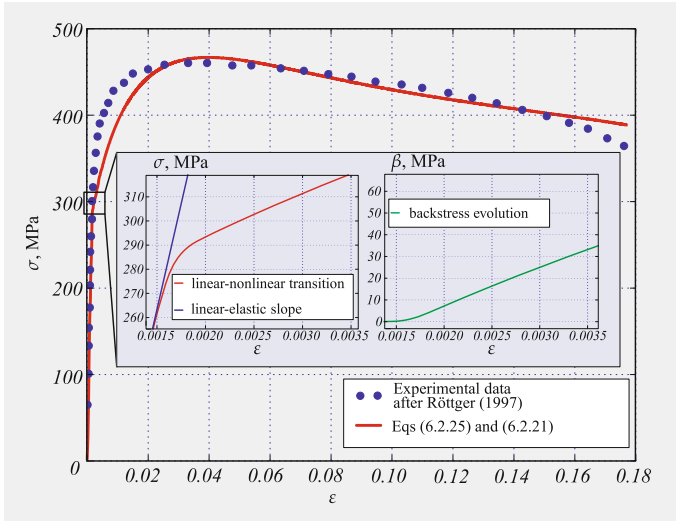


Fig. 6.6 Stress-strain diagram for X20CrMoV12-1 steel with $\dot{\epsilon} = 2.63 \cdot 10^{-4} \text{ s}^{-1}$ at 803 K

$$\begin{aligned}
 \dot{\epsilon}^{\text{pl}} &= \frac{3}{2} f \left(\frac{\bar{\sigma}_{\text{vM}}}{1 - \omega} \right) g(T) \frac{\bar{s}}{\bar{\sigma}_{\text{vM}}}, \\
 \dot{\beta} &= \frac{2\mu}{c_h} \left[\dot{\epsilon}^{\text{pl}} - \frac{3}{2} \dot{\epsilon}_{\text{vM}}^{\text{pl}} \frac{\beta}{\beta_*(\sigma_{\text{vM}})} \right], \\
 \dot{\Gamma} &= A_s [\Gamma_*(\sigma_{\text{vM}}) - \Gamma] \dot{\epsilon}_{\text{vM}}^{\text{pl}}, \\
 \dot{\omega} &= h_\omega(\omega) \frac{1}{2} \frac{(\sigma_I + |\sigma_I|)}{\sigma_{\text{vM}}} \frac{\dot{\epsilon}_{\text{vM}}^{\text{pl}}}{\epsilon_*^{\text{pl}}(\sigma_{\text{vM}})}
 \end{aligned} \tag{6.2.26}$$

with the active stress deviator \bar{s} and the corresponding von Mises equivalent stress $\bar{\sigma}_{\text{vM}}$

$$\bar{s} = s - \beta \Gamma, \quad \bar{\sigma}_{\text{vM}} = \sqrt{\frac{3}{2} \bar{s} \cdot \bar{s}} \tag{6.2.27}$$

The response functions f , g , β_* , Γ_* , h_ω and ϵ_*^{pl} and the material parameters c_h , A_s must be identified from families of creep and tensile curves for a range of stresses, temperatures and strain rates. For 12%Cr steel X20CrMoV12-1 these functions are calibrated from experimental data on creep as follows

$$\begin{aligned}
 f(x) &= \sinh(Bx), \quad g(T) = a_0 \exp\left(-\frac{\alpha}{T}\right), \\
 \Gamma_*(x) &= \frac{a_\Gamma}{1 + b_\Gamma \exp\left(-\frac{x}{c_\Gamma}\right)}, \quad \beta_*(x) = H_* x, \\
 h_\omega(\omega) &= l\omega^{\frac{l-1}{l}}, \quad \varepsilon_*^{\text{pl}}(|\sigma|) = \varepsilon_{br} + \frac{a_\varepsilon}{1 + b_\varepsilon \exp\left(-\frac{|\sigma|}{c_\varepsilon}\right)}
 \end{aligned} \tag{6.2.28}$$

with the material parameters

$$\begin{aligned}
 B &= 7.74 \cdot 10^{-2} \text{ 1/MPa}, \quad a_0 = 4.64 \cdot 10^{23} \text{ 1/h}, \quad \alpha = 6.12 \cdot 10^4 \text{ 1/K}, \\
 c_h &= 8.84, \quad H_* = 0.46, \\
 A_s &= 7.21, \quad a_\Gamma = 0.42, \quad b_\Gamma = 9.12 \cdot 10^6, \quad c_\Gamma = 9.46 \text{ MPa}
 \end{aligned} \tag{6.2.29}$$

The Young's modulus E and the shear modulus μ are identified in Straub (1995) as follows

$$E(T) = -a_E + b_E T, \quad \mu(T) = -a_\mu + b_\mu T \tag{6.2.30}$$

with

$$\begin{aligned}
 a_E &= 95.597 \text{ MPa/K}, \quad b_E = 252334.26 \text{ MPa}, \\
 a_\mu &= 38.773 \text{ MPa/K}, \quad b_\mu = 97398.16 \text{ MPa}
 \end{aligned}$$

In a slightly modified form Eqs. (6.2.26) are applied in Kostenko and Naumenko (2008), Kostenko et al. (2009a, b), Naumenko et al. (2011b), Kostenko et al. (2013) to describe inelastic behavior of 10%Cr steels.

The advantage of the phase mixture model is the possibility to describe the inelastic behavior with a minimum number of response functions and material parameters. The developed model is compatible with the standard structural mechanics and can be implemented inside any finite element code. Since the model incorporates both the softening and damage variables and reproduces the descending branch of the stress-strain curve, regularization techniques (de Borst 2004) might be necessary to avoid spurious mesh dependence.

To improve the model, in particular for the better description of inelastic transients under rapid loading changes, the constitutive equation for the inelastic hard constituent should be refined. Another possibility is to consider a phase mixture with three or more constituents. This would lead to several backstress variables and increase the number of material parameters.

6.2.4 Aluminium Alloy BS 1472

The experimental data for aluminium alloy BS 1472 at $150 \pm 0.5^\circ\text{C}$ (Al, Cu, Fe, Ni, Mg and Si alloy) are published in Kowalewski et al. (1994). The authors proposed to describe the uni-axial creep curves (loading conditions 227.53, 241.3 and 262 MPa) by use of two constitutive models. The first model is based on Eqs. (6.2.1) and the time hardening function

$$\dot{\boldsymbol{\varepsilon}}^{\text{pl}} = \frac{3}{2} \frac{a\sigma_{\text{vM}}^{n-1}}{(1-\omega)^n} \boldsymbol{s} t^m, \quad \dot{\omega} = \frac{b(\sigma_{\text{eq}}^\omega)^k}{(1-\omega)^l} t^m \quad (6.2.31)$$

with $\sigma_{\text{eq}}^\omega = \sigma_{\text{vM}}$. The material parameters in Eqs. (6.2.31) are identified as follows (Kowalewski et al. 1994)

$$\begin{aligned} a &= 3.511 \cdot 10^{-31} \text{ MPa}^{-n}/\text{h}^{m+1}, & b &= 1.960 \cdot 10^{-23} \text{ MPa}^{-k}/\text{h}^{m+1}, \\ n &= 11.034, & k &= 8.220, & l &= 12.107, & m &= -0.3099 \end{aligned} \quad (6.2.32)$$

The Young's modulus and Poisson's ratio are $E = 0.71 \cdot 10^5$ MPa and $\nu = 0.3$. Equations (6.2.31) include the time hardening function. One shortcoming of the time hardening model is that the creep behavior depends on the choice of the time scale (see Sect. 5.6.1).

Alternatively the experimental data presented in Kowalewski et al. (1994) can be described by the following equations

$$\dot{\boldsymbol{\varepsilon}}^{\text{pl}} = \frac{3}{2} \frac{a\sigma_{\text{vM}}^{n-1}}{(1-\omega)^m} \boldsymbol{s}, \quad \dot{\omega} = \frac{b(\sigma_{\text{eq}}^\omega)^k}{(1-\omega)^l} \quad (6.2.33)$$

with the following set of material parameters

$$\begin{aligned} a &= 1.35 \cdot 10^{-39} \text{ MPa}^{-n}/\text{h}, & b &= 3.029 \cdot 10^{-35} \text{ MPa}^{-k}/\text{h}, \\ n &= 14.37, & k &= 12.895, & l &= 12.5, & m &= 10 \end{aligned} \quad (6.2.34)$$

In the above equations the primary creep effect is neglected. Figure 6.7 presents the experimental results and the predictions by Eqs. (6.2.31) and (6.2.33).

The second approach applied in Kowalewski et al. (1994) is based on the mechanism-based model (see Sect. 5.7.1.3). The constitutive model can be summarized as follows

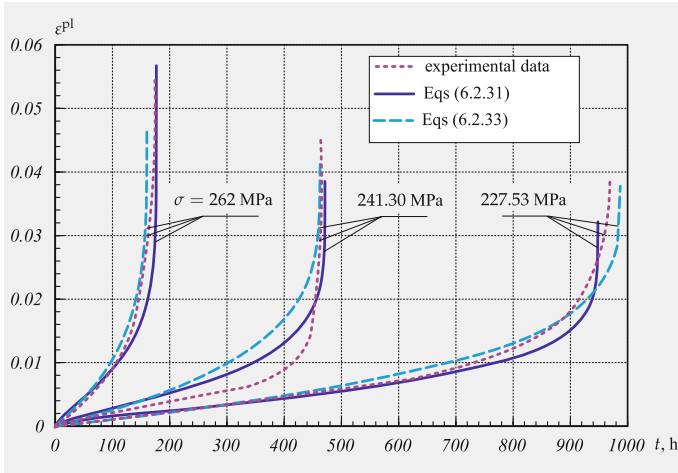


Fig. 6.7 Experimental data and model predictions for the aluminium alloy BS 1472 at $150 \pm 0.5^\circ\text{C}$, after Kowalewski et al. (1994)

$$\begin{aligned}
 \dot{\varepsilon}^{\text{pl}} &= \frac{3}{2} \frac{A}{(1-\omega)^n} \frac{s}{\sigma_{\text{VM}}} \sinh \left[\frac{B\sigma_{\text{VM}}(1-H)}{1-\Phi} \right], \\
 \dot{H} &= \frac{h_c}{\sigma_{\text{VM}}} \frac{A}{(1-\omega)^n} \sinh \left[\frac{B\sigma_{\text{VM}}(1-H)}{1-\Phi} \right] \left(1 - \frac{H}{H_*} \right), \\
 \dot{\Phi} &= \frac{K_c}{3} (1-\Phi)^4, \\
 \dot{\omega} &= \frac{DA}{(1-\omega)^n} \left(\frac{\sigma_I}{\sigma_{\text{VM}}} \right)^v N \sinh \left[\frac{B\sigma_{\text{VM}}(1-H)}{1-\Phi} \right], \\
 n &= \frac{B\sigma_{\text{VM}}(1-H)}{1-\Phi} \coth \left[\frac{B\sigma_{\text{VM}}(1-H)}{1-\Phi} \right], \\
 N &= 1 \text{ for } \sigma_I > 0, \quad N = 0 \text{ for } \sigma_I \leq 0, \\
 0 &\leq \omega < 0.3, \quad 0 \leq \Phi < 1, \quad 0 \leq H \leq H_*
 \end{aligned} \tag{6.2.35}$$

The set of equations (6.2.35) includes the creep constitutive equation and evolution equations with respect to three internal state variables. The hardening variable H is introduced to describe primary creep. The variable Φ characterizes the ageing process. The variable ω is responsible for the grain boundary creep constrained cavitation.

The material parameters in Eqs. (6.2.35) may be divided into three groups: the constants h_c and H_* must be obtained from the primary creep stage; A and B characterize the secondary creep (minimum creep rate versus stress); and K_c and D must be found from the tertiary creep stage. The parameter v is the so-called stress state index, which characterizes the stress state dependence of the damage evolution. The material constants are identified in Kowalewski et al. (1994) as follows

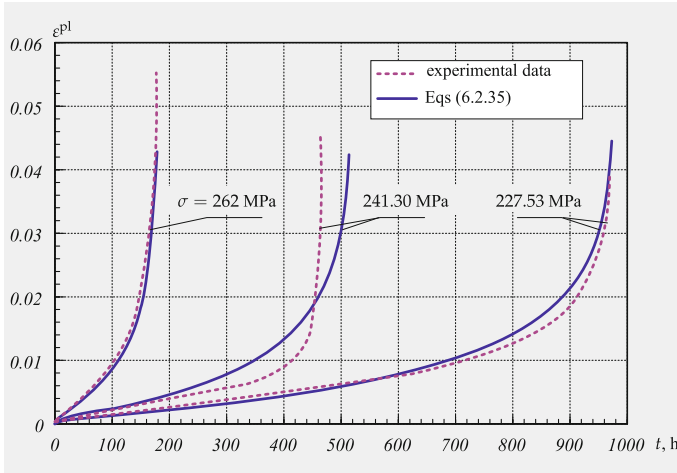


Fig. 6.8 Experimental data and simulations for the aluminium alloy BS 1472 at $150 \pm 0.5^\circ\text{C}$, after Kowalewski et al. (1994)

$$\begin{aligned}
 A &= 2.960 \cdot 10^{-11} \text{ h}^{-1}, & B &= 7.167 \cdot 10^{-2} \text{ MPa}^{-1}, \\
 h_c &= 1.370 \cdot 10^5 \text{ MPa}, & H_* &= 0.2032, \\
 K_c &= 19.310 \cdot 10^{-5} \text{ h}^{-1}, & D &= 6.630
 \end{aligned}
 \tag{6.2.36}$$

Figure 6.8 presents the experimental creep curves and predictions based on Eqs. (6.2.35). To identify the stress state index ν experimental data from multi-axial creep tests up to creep rupture are required. The isochronous rupture loci obtained according to Eqs. (6.2.35) for different values of ν in the range $0 \leq \nu \leq 12$ are presented in Kowalewski et al. (1994).

This example illustrates that the same experimental data can be described by different relations (6.2.31), (6.2.33) and (6.2.35). The model (6.2.35) seems to be more preferable since it is based on material science foundations. One feature of Eqs. (6.2.35) is the use of a hyperbolic function for the dependence of the minimum creep rate on the stress instead of the power function in Eqs. (6.2.33). Let us compare how the models (6.2.33) and (6.2.35) describe the secondary creep rate for a wide stress range. For this purpose we assume $\omega \ll 1$ in Eqs. (6.2.33) leading to the Norton-Bailey creep equation $\dot{\epsilon}_{\min}^{\text{cr}} = a\sigma^n$. In Eq. (6.2.35) we set $H = H_*$, $\omega \ll 1$ and $\Phi \ll 1$ resulting in $\dot{\epsilon}_{\min}^{\text{cr}} = A \sinh[B\sigma(1 - H_*)]$. Figure 6.9 shows the minimum creep rate as a function of stress calculated by the use of material parameters (6.2.34) and (6.2.36). We observe that within the stress range 227–262 MPa the minimum creep rate versus stress curves almost coincide. The coincidence of curves is not surprising since the material parameters in both models were identified from creep tests carried out within the stress range 227–262 MPa. This stress range is marked in Fig. 6.9 as the identification range. Furthermore, a wider stress range exist, for which the power law and the hyperbolic sine functions provide nearly the same

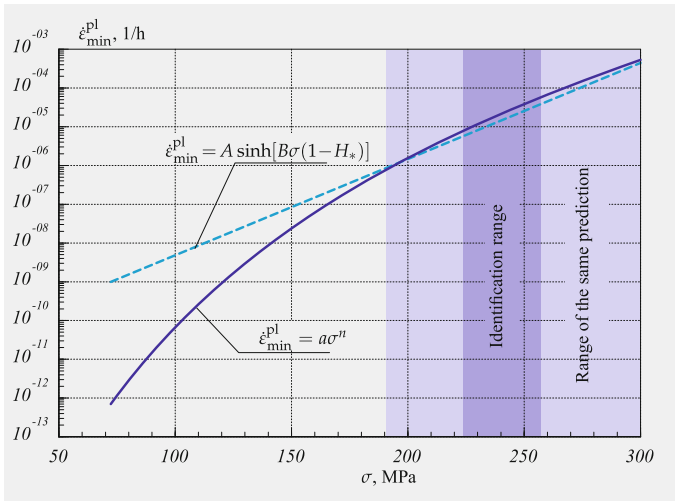


Fig. 6.9 Minimum creep rate versus stress by use of the power law and sinh functions

inelastic strain rates, Fig. 6.9. If a structure is loaded in such a way that the von Mises equivalent stress lies within this range, then both the models would lead to similar results of structural analysis, e.g. time dependent deformation, stress redistribution etc.

However, in most applications one has to analyze statically indeterminate structures. In this case, if the external loads are constant, the stresses may rapidly relax down at the beginning of the creep process. Therefore, the range of moderate and small stress values is important in the structural analysis. For this range the two applied models lead to quite different predictions, Fig. 6.9. In Altenbach et al. (1997a, c) we utilized the models (6.2.33) and (6.2.35) for the structural analysis of pressurized cylindrical shells and transversely loaded rectangular plates. The maximum values of the von Mises equivalent stress in the reference elastic state of structures were within the identification range. The results of creep analysis based on the models (6.2.33) and (6.2.35) qualitatively agree only at the beginning of the creep process as long as the maximum values of the von Mises equivalent stress lay within the range of the same prediction. With the relaxation and redistribution of stresses, the discrepancy between the results increases leading to quite different long term predictions. The differences in estimated life times were of up to a factor 5.

6.3 Initially Anisotropic Materials

Many materials exhibit anisotropic inelastic behavior as a result of processing. This Section presents examples of constitutive equations for initially-anisotropic materi-

als. The first one is related to the forged aluminium alloy AA2014. Microstructural observations and experimental data suggest that the anisotropy of inelastic behavior is primarily caused by elongated grains and grain boundaries as a result of material processing. The second example deals with a multi-pass weld metal. Here the arrangement of weld beads and microstructural zones is the reason for anisotropic creep.

6.3.1 Forged Al-Cu-Mg-Si Alloy

Age-hardenable alloys based on the aluminum-copper system (known as AA2xxx alloys) exhibit superior creep strength and are widely used in structural components operating at elevated temperatures (Polmear 1996, 2004). Complex shape parts produced from these alloys usually exhibit microstructural anisotropy as a result of processing (Gariboldi and Conte 2013). Furthermore, the creep properties of age-hardenable alloys strongly depend on the heat treatment and ageing conditions (Gariboldi and Casaro 2007). Origins of anisotropic creep include elongated grains, crystallographic texture, non-uniform distribution of particles, oriented grain boundary cavities, etc. One approach to formulate a constitutive equation for anisotropic creep is based on the theory of symmetries and representation of tensor-valued functions, see Sect. 5.4.3. For the assumed symmetry class, e.g. a transverse isotropy, a creep potential is formulated as a function of appropriate invariants of the stress tensor. The resulting creep constitutive equation includes a number of material parameters to be identified from experimental creep curves for different stress states and different loading directions. This approach provides a general form of a constitutive equation. However, the identification of all required parameters is usually not feasible since the required experimental creep curves are rarely available.

6.3.1.1 Basic Features of Microstructure

Al-Cu-Mg-Si alloy forging had displayed anisotropic effects in longitudinal (L), transverse (T) and radial (R) sampling directions (Gariboldi et al. 2016). Two sets of $20 \times 20 \times 100 \text{ mm}^3$ bars were sampled from the as supplied forging with their longer side in L, T and R directions, respectively. Tensile tests were performed at temperatures within the range 20–170 °C. Creep tests were conducted under constant load at 130, 150 and 170 °C (homologous temperature range 0.44–0.49) under stresses that led to a range of times to rupture t_* from several hours to more than 10,000 h. Crept specimens were diametrically cut in order to investigate microstructure features along the gauge length.

The investigated forging was characterized by grains elongated in the main plastic flow path experienced during the processing. Their mean size of grains was about 300, 80 and 50 μm along the L, T and R directions, respectively. Figure 6.10 shows light optical microscope micrographs of the microstructure of the forged part in

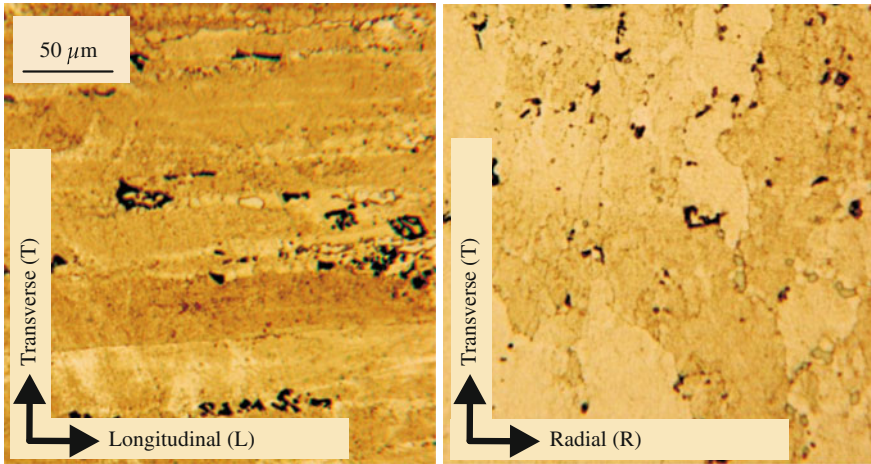


Fig. 6.10 Light optical microscope micrographs of the forged part from AA2014 in different metallographic sections, after Gariboldi et al. (2016)

2014 alloy in different metallographic sections. Two kinds of coarse intermetallic particles were present in the microstructure: globular Al_2Cu (θ) particles (bright particles in Fig. 6.10) and blocky shaped clustered particles containing Fe, Mn, Si and Cu (darker particles in Fig. 6.10). These latter secondary phase clustered particles are elongated in the L direction. In most of the volume of the forging, macrographic analyzes revealed the large intermetallic particles longitudinally oriented, suggesting the same direction of the plastic flow during the processing.

In addition, transmission electron microscopy images published in Angella et al. (2008) illustrate the presence of θ' phase, in the form of plate-like precipitates in $\{100\}$ crystallographic planes of the α -Al matrix. These precipitates play an important role in strengthening of the alloy. The forging was supplied in the T6 condition, that is the solution treatment at 778 K and aging at 433 K for 16h. During the subsequent creep overageing processes take place leading to the increase of particles size and distance between particles with time.

6.3.1.2 Minimum Creep Rates

Creep curves of the material sampled in L and T direction are presented and analyzed in Naumenko and Gariboldi (2014). Figure 6.11 shows minimum creep rate vs stress curves. To normalize the data the reference stress $\sigma_0 = 320$ MPa, the reference strain rate $\dot{\epsilon}_0 = 1.026$ 1/h and the Arrhenius function of the temperature

$$g(T) = \exp\left(-\frac{Q}{RT}\right) \quad (6.3.37)$$

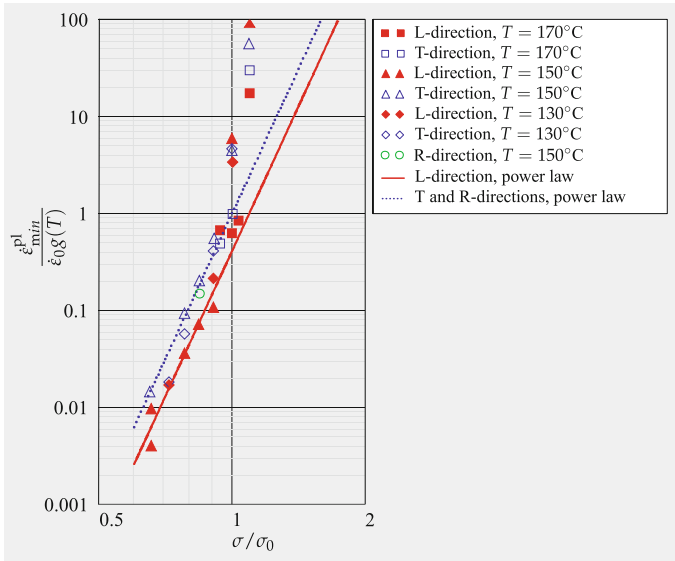


Fig. 6.11 Normalized minimum creep rate versus normalized stress for longitudinal, transverse and radial creep tests of AA2014 at 150 °C, after Gariboldi et al. (2016)

with apparent activation energy Q , the universal gas constant R and absolute temperature T is applied. The value $Q = 175.42$ kJ/mol is used as given in Gariboldi and Casaro (2007), Naumenko and Gariboldi (2014). The reference stress σ_0 is introduced to split the ranges of power law creep and power law breakdown, as shown in Fig. 6.11. According to experimental data presented in Fig. 6.11 the anisotropy is primarily observable in the power law range. The following relation

$$\dot{\epsilon}_{T_{min}}^{pl} = \alpha \dot{\epsilon}_{L_{min}}^{pl}, \quad \alpha = 2.43$$

indicates that the creep rate in the T direction is 2.43 times higher than the creep rate in the L direction for the same stress level. In the power law breakdown range the difference between L and T data is not significant, if compared to the usual scatter of experimental data in the creep range, and can be neglected. The minimum creep rates for T-specimen can be described by the following equation

$$\dot{\epsilon}_{T_{min}}^{pl} = \dot{\epsilon}_0 g(T) \left(\frac{\sigma}{\sigma_0} \right)^n$$

with $n = 9.94$. Two additional creep tests at 150 °C for specimens sampled in R direction were performed in Gariboldi et al. (2016). The results indicate that the difference in creep rates for T and R directions is not significant, Fig. 6.11. This supports the assumption of transversely-isotropic creep made in Naumenko and Gariboldi (2014).

6.3.1.3 Constitutive Model

In what follows let us assume that the minimum creep rates in R and T directions are approximately the same and the plane spanned on R and T directions to be the isotropy plane. Constitutive equations of transversely-isotropic steady-state creep were applied in Betten (2008) to modeling deep drawing sheets and in Naumenko and Altenbach (2005) to characterize multi-pass weld metals, for example. Let \mathbf{e}_L be the unit vector that designates the direction L, \mathbf{I} the second rank unit tensor and $\mathbf{P} = \mathbf{I} - \mathbf{e}_L \otimes \mathbf{e}_L$ the projector onto the RT plane. For anisotropic materials different parts of the stress state cause different creep responses. Therefore let us decompose the stress state characterized by the stress tensor $\boldsymbol{\sigma}$ into the three parts including the tension (compression) along L σ_{LL} , the plane stress state in the RT-plane $\boldsymbol{\sigma}_p$ and the out of plane shear characterized by the shear stress vector $\boldsymbol{\tau}_L$. Figure 6.12 illustrates the corresponding components of the stress tensor. The decomposition has the following form

$$\boldsymbol{\sigma} = \sigma_{LL} \mathbf{e}_L \otimes \mathbf{e}_L + \boldsymbol{\sigma}_p + \boldsymbol{\tau}_L \otimes \mathbf{e}_L + \mathbf{e}_L \otimes \boldsymbol{\tau}_L \quad (6.3.38)$$

By subtracting the hydrostatic stress state the stress deviator \mathbf{s} can be given as follows

$$\mathbf{s} = \mathbf{s}_L + \mathbf{s}_p + \boldsymbol{\tau}_L \otimes \mathbf{e}_L + \mathbf{e}_L \otimes \boldsymbol{\tau}_L, \quad (6.3.39)$$

where

$$\mathbf{s}_L = \left(\sigma_{LL} - \frac{1}{2} \text{tr} \boldsymbol{\sigma}_p \right) \left(\mathbf{e}_L \otimes \mathbf{e}_L - \frac{1}{3} \mathbf{I} \right), \quad \mathbf{s}_p = \boldsymbol{\sigma}_p - \frac{1}{2} \text{tr} \boldsymbol{\sigma}_p (\mathbf{I} - \mathbf{e}_L \otimes \mathbf{e}_L) \quad (6.3.40)$$

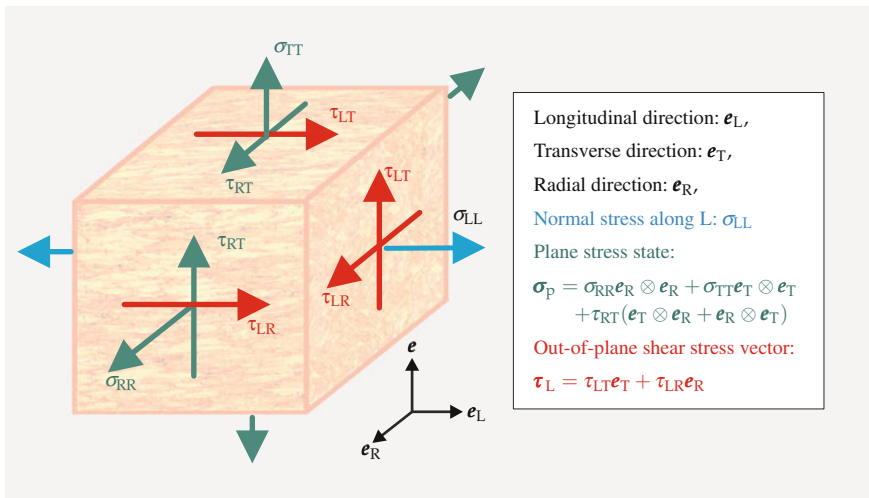


Fig. 6.12 Stress state in a forged material with elongated grains and preference (forging) direction $\mathbf{m} = \mathbf{e}_L$, after Naumenko and Gariboldi (2014)

With the decomposition (6.3.39), the creep potential hypothesis and the assumption that the volumetric creep rate is negligible, the constitutive equation can be formulated as follows, see Sect. 5.4.3.1

$$\dot{\boldsymbol{\varepsilon}}^{\text{pl}} = \frac{3}{2} \dot{\varepsilon}_0 g(T) \left(\frac{\sigma_{\text{eq}}}{\sigma_0} \right)^n \frac{1}{\sigma_{\text{eq}}} \left[\alpha_1 \mathbf{s}_L + \alpha_2 \mathbf{s}_p + \alpha_3 (\boldsymbol{\tau}_L \otimes \mathbf{e}_L + \mathbf{e}_L \otimes \boldsymbol{\tau}_L) \right], \quad (6.3.41)$$

where $\boldsymbol{\varepsilon}^{\text{pl}}$ is the tensor of inelastic strains, $\dot{\varepsilon}_0$, σ_0 , n and α_i , $i = 1, 2, 3$ are material parameters. The equivalent stress σ_{eq} is defined as follows

$$\sigma_{\text{eq}}^2 = \frac{3}{2} \left(\alpha_1 \text{tr} \mathbf{s}_L^2 + \alpha_2 \text{tr} \mathbf{s}_p^2 + 2\alpha_3 \boldsymbol{\tau}_L \cdot \boldsymbol{\tau}_L \right) \quad (6.3.42)$$

To identify the material parameters families of creep curves for different stress levels for three independent kinds of loading are required. These include the loading in L and T directions, respectively as well as any kind of loading that leads to non-zero out-of-plane shear stress. For $\alpha_1 = \alpha_2 = \alpha_3 = 1$ the von Mises equivalent stress follows from Eq. (6.3.42). Equation (6.3.41) reduces to the Norton-Bailey-Odqvist equation of isotropic creep in the power law range (5.4.107).

For the tensile stress σ_{LL} the longitudinal creep rate $\dot{\varepsilon}_{\text{TT}}^{\text{pl}}$ can be computed from Eq. (6.3.41) as follows

$$\dot{\varepsilon}_{\text{LL}}^{\text{pl}} = \dot{\varepsilon}_0 g(T) \left(\frac{\sigma_{LL}}{\sigma_0} \right)^n \alpha_1^{\frac{n+1}{2}} \quad (6.3.43)$$

The creep rate in the transverse direction for the applied stress σ_{TT} is

$$\dot{\varepsilon}_{\text{TT}}^{\text{pl}} = \dot{\varepsilon}_0 g(T) \left(\frac{\sigma_{\text{TT}}}{\sigma_0} \right)^n \left(\frac{\alpha_1 + 3\alpha_2}{4} \right)^{\frac{n+1}{2}} \quad (6.3.44)$$

The function $g(T)$ and the parameter $\dot{\varepsilon}_0$ can be identified from minimum creep rate versus stress data generated from transverse creep curves, Fig. 6.11. In this case the parameter α_2 can be set to one. To identify the parameter α_1 the ratio of creep rates α for the same stress level can be computed from Eqs. (6.3.43) and (6.3.44) as follows

$$\alpha = \frac{\dot{\varepsilon}_{\text{TT}}^{\text{pl}}}{\dot{\varepsilon}_{\text{LL}}^{\text{pl}}} = \left(\frac{\alpha_1 + 3}{4\alpha_1} \right)^{\frac{n+1}{2}} \quad (6.3.45)$$

For the given values of α and n the solution of Eq. (6.3.45) is $\alpha_1 = 0.81$.

6.3.2 *Multi-pass Weld Metal*

For many structures designed for high-temperature applications, e.g., piping systems and pressure vessels, an important problem is the assessment of creep strength of welded joints. The lifetime of the welded structure is primarily determined by the behavior in the local zones of welds, where time-dependent creep and damage processes dominate. Different types of creep failure that have occurred in recent years are discussed in Shibli (2002), for example. The design of welded structures and their residual life estimations require engineering mechanics models that would be able to characterize creep strains, stress redistributions, and damage evolution in the zones of welds.

A weld is usually considered as a metallurgical notch. The reason for this is the complex microstructure in the weld metal itself and in the neighboring heat-affected zone. Many research activities have been directed to the study of welded joints. First, theoretical and experimental studies have addressed the welding process with the aim of predicting the formation of the microstructure of the welds and analyzing residual stresses (Aurich et al. 1999). Second, the behavior of welded joints under the mechanical and thermal loadings was investigated (Hyde et al. 2003b). Here one must consider that the stress-strain response at room temperature is quite different for the weld metal, the heat-affected zone, and the base metal (parent material), particularly if they are loaded beyond the yield limit. At elevated temperatures quite different inelastic strain versus time curves can be obtained in different zones even in the case of a constant moderate load. Figure 1.52 illustrates zones with different microstructures and the variation in material behavior within the weld.

The results of creep tests of cross-weld specimens (Hyde et al. 1997, 1999), and specimens with a simulated microstructure (Lundin et al. 2001; Matsui et al. 2001; Wohlfahrt and Brinkmann 2001; Wu et al. 2004) show significant variation in creep properties in different material zones within the weld. Furthermore, they illustrate that the intercritical region of the heat-affected zone is the weakest part of the weld with respect to the creep properties. The material with the heat-affected zone microstructure usually exhibits the highest creep rate and the shortest time to failure if compared to other material zones within the weld for the same load and temperature.

For thick and moderately thick cross sections, multi-pass welding is usually preferred, where many stringer beads are deposited in a defined sequence. As a result of heating and cooling cycles during the welding process, the complex bead-type microstructure of the weld metal is formed, where every single bead consists of columnar, coarse-grained, and fine-grained regions (Hyde et al. 2003b). The results of uni-axial creep tests for the weld metal 9CrMoNbV are reported in Hyde et al. (2003a). They show that the creep strain versus time curves significantly differ for specimens removed from the weld metal in the longitudinal (welding) direction and the transverse direction. Furthermore, different types of damage were observed for the longitudinal and the transverse specimens.

One possibility for studying the creep behavior in structures is the use of continuum damage mechanics (Altenbach and Naumenko 2002; Altenbach et al. 2001; Hayhurst 1994). The application of this approach to welded joints is discussed in Hall and Hayhurst (1991), Hayhurst et al. (2002), Hyde et al. (2003b), for example. Here the weld is considered as a heterogeneous structure composed of at least three constituents—the weld metal, the heat-affected zone, and the parent material with different creep properties. Constitutive and evolution equations that are able to reflect experimental data of primary, secondary, and tertiary creep in different zones of the welded joint are presented in Eggeler et al. (1994), Hall and Hayhurst (1991), Hayhurst et al. (2002), Hyde et al. (2003b), Wohlfahrt and Brinkmann (2001), among others. The results of finite element simulations illustrate stress redistributions, creep strains, and damage evolution in different zones of the weld (Eggeler et al. 1994; Hall and Hayhurst 1991; Hayhurst et al. 2002; Hyde et al. 2003b). Furthermore, they are useful to analyze the influence of numerous factors like weld dimensions, types of external loading, and material properties on the creep behavior of welded structures (Hyde et al. 2003b).

6.3.2.1 Basic Features of Microstructure

A weld bead produced by a single pass welding has a columnar solidification microstructure. During the multi-pass welding many weld beads are deposited in the groove by a defined sequence. As a subsequent weld bead is laid, the part of the metal produced in previous cycles is subjected to the local reheating and cooling. As a result, the weld beads consist of columnar, coarse-grained and fine-grained microstructural zones (Hyde et al. 2003a, b). A sketch for the typical microstructure of a multi-pass weld metal is presented in Fig. 6.13. This microstructure depends on many factors of the welding process like bead size, travel speed, buildup sequence, interpass temperature, and type of postweld heat treatment (Hyde et al. 2003a). The resulting inelastic material behavior will be apparently determined by the distribution and size of columnar, coarse-grained, and fine-grained zones as well as residual stresses in the weld metal. It is well established that creep behavior is very sensitive to the type of microstructure and, in particular, to grain size. Experimental data illustrating the significant influence of grain size on creep behavior are presented for copper in Kowalewski (1992) and for various types of steel in Lundin et al. (2001), Wohlfahrt and Brinkmann (2001), Wu et al. (2004). The grain size dependence is explained in materials science by two creep mechanisms: grain boundary sliding and grain boundary diffusion. These mechanisms operate under moderate loading and within a temperature range of $0.5 < T/T_m < 0.7$, where T_m is the melting temperature (see Sect. 1.3). The principal damage mechanism is the nucleation and growth of voids on grain boundaries. Many experimental observations show that the finer the grain structure, the higher the secondary creep rate and the higher the damage rate for the same loading and temperature conditions.

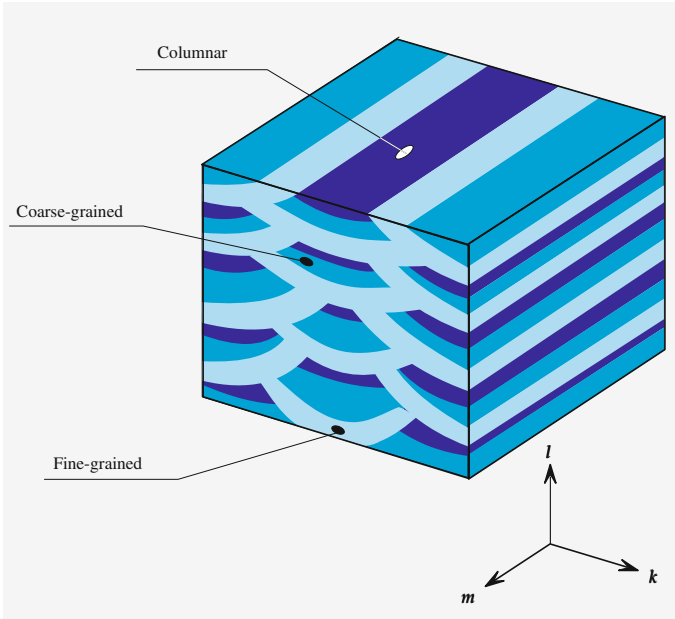


Fig. 6.13 Microstructure of the weld metal, after Naumenko and Altenbach (2005)

6.3.2.2 Elementary Micromechanics Model

To discuss the origins of the anisotropic creep in a weld metal let us consider a uni-axial model of a binary structure composed of constituents with different creep properties. In what follows let us term the first constituent “fine-grained” or “creep-weak” and the second one “coarse-grained” or “creep-strong.” Let us describe the creep behavior of the constituents by use of the Kachanov-Rabotnov model (see Sect. 3.6.1)

$$\dot{\epsilon}^{pl} = \frac{a\sigma^n}{(1-\omega)^n}, \quad \dot{\omega} = \frac{b\sigma^k}{(1-\omega)^l} \tag{6.3.46}$$

In what follows we use the subscripts f and c for the fine-grained and coarse-grained constituents, respectively. For the sake of simplicity we assume that the constituents have the same value of Young’s modulus E and the same values of parameters n, k and l in (6.3.46). Let us introduce the dimensionless quantities

$$s = \frac{\sigma}{\sigma_0}, \quad \epsilon = \frac{\epsilon}{\epsilon_0}, \quad \epsilon^{pl} = \frac{\epsilon^{pl}}{\epsilon_0}, \quad \tau = \frac{t}{t_{*f}}, \tag{6.3.47}$$

where t_{*f} is the time to fracture of the fine-grained constituent, σ_0 is the reference stress and ϵ_0 is the elastic strain at σ_0 , i.e. $\epsilon_0 = \sigma_0/E$. Equations (6.3.46) can be formulated for two constituents as follows

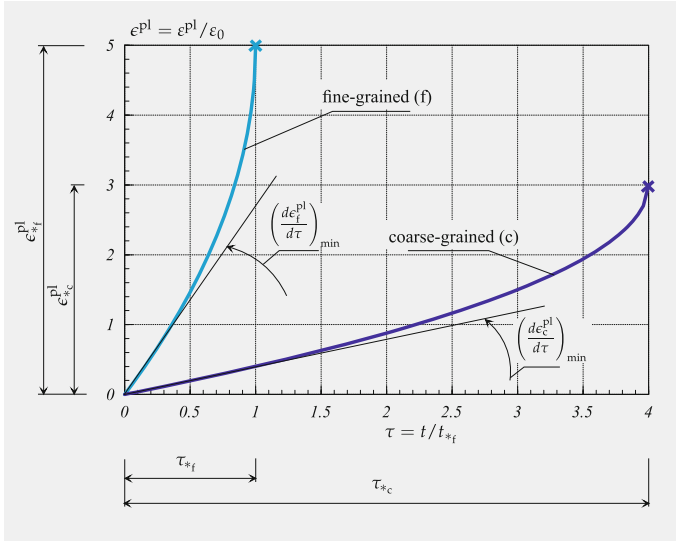


Fig. 6.14 Creep curves for constituents

$$\begin{cases} \frac{d\epsilon_f^{pl}}{d\tau} = \tilde{a} \frac{s^n}{(1 - \omega_f)^n} \\ \frac{d\omega_f}{d\tau} = \tilde{b} \frac{s^k}{(1 - \omega_f)^l} \end{cases}, \quad \begin{cases} \frac{d\epsilon_c^{pl}}{d\tau} = \alpha \tilde{a} \frac{s^n}{(1 - \omega_c)^n} \\ \frac{d\omega_c}{d\tau} = \beta \tilde{b} \frac{s^k}{(1 - \omega_c)^l} \end{cases}, \quad (6.3.48)$$

where

$$\tilde{a} = \epsilon_{*f} \left(1 - \frac{n}{l+1} \right), \quad \tilde{b} = \frac{1}{l+1}, \quad \alpha = \frac{\dot{\epsilon}_{\min_c}^{pl}}{\dot{\epsilon}_{\min_f}^{pl}}, \quad \beta = \frac{t_{*f}}{t_{*c}}$$

Figure 6.14 illustrates creep curves obtained after integration of Eqs. (6.3.48) for the cases $n = 3, k = n + 1, l = n + 2, \epsilon_{*f} = 5, \alpha = 0.15, \beta = 0.25, s = 1$.

Let us consider a connection of constituents in parallel, as it usually assumed for composite materials (Altenbach et al. 2004; Chawla 1987). The strains and the strain rates can be assumed to be the same (iso-strain concept)

$$\epsilon = \epsilon_f = \epsilon_c, \quad \dot{\epsilon} = \dot{\epsilon}_f = \dot{\epsilon}_c \quad (6.3.49)$$

We assume that a constant load $\mathcal{F} = \sigma_0 A$, Fig. 6.15, is applied to the composite, where A is the cross section area. Specifying by N_f and N_c the internal forces in the constituents such that $N_f + N_c = \mathcal{F}$ we can write

$$\sigma_f A_f + \sigma_c A_c = \sigma_0 A, \quad \eta_f \sigma_f + (1 - \eta_f) \sigma_c = \sigma_0, \quad \eta_f s_f + (1 - \eta_f) s_c = 1 \quad (6.3.50)$$

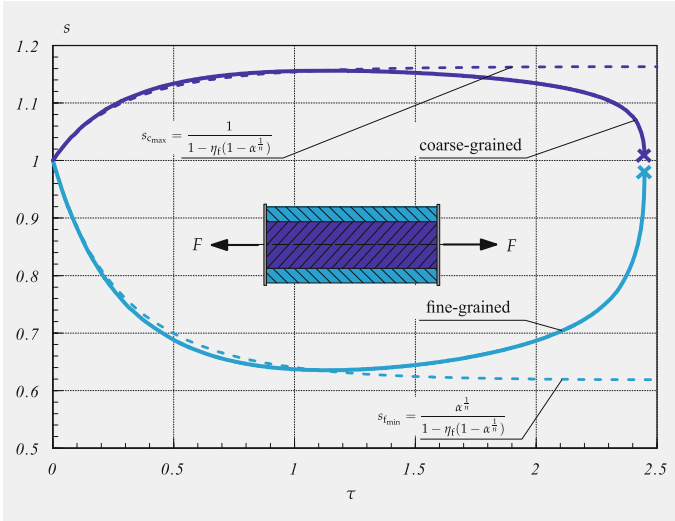


Fig. 6.15 Normalized stresses versus normalized time for connection of constituents in parallel

where $\eta_f = A_f/A$ is the volume fraction of the fine-grained constituent. For the stresses we apply the following constitutive equations

$$\sigma_f = E(\varepsilon - \varepsilon_f^{pl}), \quad \sigma_c = E(\varepsilon - \varepsilon_c^{pl}) \tag{6.3.51}$$

Based on Eqs. (6.3.48)–(6.3.51) one can formulate a system of ordinary differential equations describing the stress redistribution between constituents. With respect to the stress in the fine-grained constituent the following equation can be obtained

$$\frac{ds_f}{d\tau} = \bar{a}(1 - \eta_f) \left[\frac{\alpha}{(1 - \eta_f)^n} \frac{(1 - \eta_f s_f)^n}{(1 - \omega_c)^n} - \frac{s_f^n}{(1 - \omega_f)^n} \right] \tag{6.3.52}$$

Equation (6.3.52) is numerically solved together with the evolution equations for the damage parameters (6.3.48) and initial conditions $s_f = 1, \omega_f = \omega_c = 0$ providing time variation of the stress s_f . The stress s_c can be then computed from Eqs. (6.3.50). The results are shown in Fig. 6.15 for the case $\eta_f = 0.3$. In addition, Fig. 6.16 presents creep strains and the damage parameters in the constituents as well as the creep strain of the mixture $\varepsilon^{pl} = \varepsilon - 1$. At the beginning of the creep process the creep rate is higher in the fine-grained constituent, Fig. 6.16a. Therefore, the stress in the fine-grained constituent relaxes down while the stress in the coarse-grained constituent increases, Fig. 6.15. If we neglect the influence of damage on the creep process, i.e. set $\omega_f = \omega_c = 0$ in (6.3.52), we obtain the steady-state creep solution. The corresponding results are plotted in Fig. 6.15 by dotted lines. We observe that the maximum value of s_c and the minimum value of s_f in the case of creep-damage almost coincide with the corresponding steady-state values. The steady-state solution for s_f follows from Eqs. (6.3.52) by setting $\omega_f = \omega_c = 0$ and $\frac{ds_f}{d\tau} = 0$. The corresponding

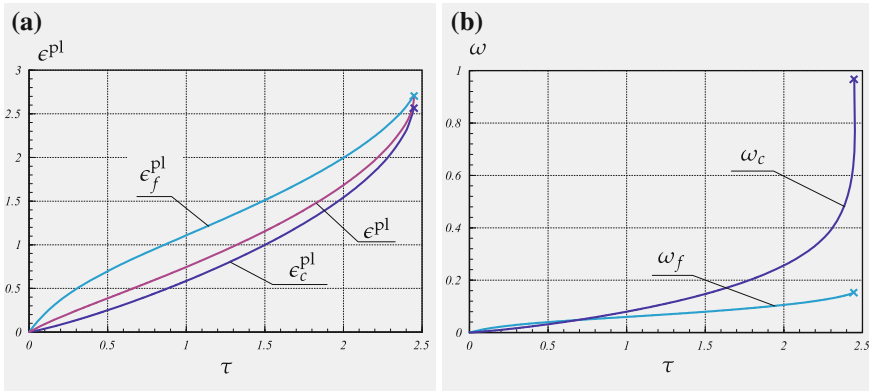


Fig. 6.16 Connection of constituents in parallel. **a** Normalized creep strains versus normalized time, **b** damage parameters versus normalized time

value for s_c is obtained from (6.3.50). The results are

$$s_{f_{\min}} = \frac{\alpha^{\frac{1}{n}}}{1 - \eta_f(1 - \alpha^{\frac{1}{n}})}, \quad s_{c_{\max}} = \frac{1}{1 - \eta_f(1 - \alpha^{\frac{1}{n}})}$$

We observe that these stress values are determined by the volume fraction of the “fine-grained” constituent η_f and the ratio of minimum creep rates α . The stress value s_c is higher than s_f after the initial stress redistribution. Therefore, the coarse-grained constituent exhibits the higher creep rate and the higher damage rate in the final stage of the creep process, Fig. 6.16. The simulation predicts the failure initiation in the coarse-grained constituent.

In the case of a connection of constituents in series (iso-stress approach) we assume

$$\sigma_0 = \sigma_f = \sigma_c, \quad \varepsilon^{\text{pl}} = \eta_f \varepsilon_f^{\text{pl}} + (1 - \eta_f) \varepsilon_c^{\text{pl}}$$

The results can be obtained by integration (6.3.48) for $s_f = s_c = 1$. The corresponding plots of normalized creep strains are presented in Fig. 6.14. The maximum creep and damage rates are now in the fine-grained constituent. The lifetime of the binary structure is determined by the lifetime of the fine-grained constituent for the given constant stress.

Figure 6.17 shows the creep curves obtained for the two considered cases of the binary structure under the same constant load. The results of the presented model provide an analogy to the creep behavior of a weld metal loaded in the longitudinal (welding) and the transverse directions. The experimental creep curves for the specimen removed from the weld metal in two directions are presented in Hyde et al. (2003a). They show, that the transverse specimens exhibit higher minimum creep rate. Furthermore, the creep curves for transverse specimens have a much shorter tertiary stage and lower values of fracture strain if compared to curves for specimens removed in the welding direction. The times to fracture for the transverse speci-

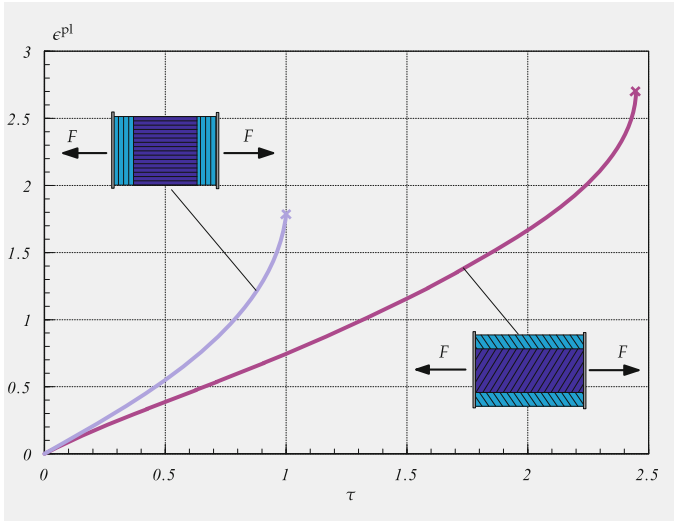


Fig. 6.17 Creep curves for the binary structure in the cases of parallel and series connections of constituents

mens are much shorter than those for the longitudinal specimens. From the results in Fig. 6.17 we observe that these effects are predicted by the mechanical model of the binary structure. Furthermore, our results for the damage evolution qualitatively agree with the results of microstructural damage observations presented in Hyde et al. (2003a). For the longitudinal specimens extensive voids and cracks were observed in columnar and coarse-grained regions along the entire specimen length. For the transverse specimens voids and cracks are localized near the fracture surface. The fracture surface has fine-grained structure and the failure propagated through the fine-grained regions of the specimen.

Based on the presented results we may conclude that among many different creep and damage mechanisms which may operate and interact during the creep process an essential role plays the stress redistribution between the creep-weak and creep-strong constituents. For longitudinal specimens this mechanism leads to a prolonged tertiary creep stage. The material behaves like a “more ductile” material, although the damage and failure occur in the “more brittle” creep-strong constituent.

In Hyde and Sun (2005), Lvov et al. (2014) micromechanical models of multi-pass weld are presented by taking into account realistic distributions of weld beads and microstructural zones. Finite element simulations of the weld metal sample are performed for different stress states including tension in welding and transverse directions as well a longitudinal and transverse shear.

6.3.2.3 Constitutive Model

For the analysis of welded structures a model which is able to reflect anisotropic creep in a weld metal under multi-axial stress states has to be developed. Three-dimensional models for mixtures are discussed within the framework of continuum mechanics, e.g. Altenbach et al. (2003). A generalization of the composite model developed in the previous section to the multi-axial stress states would however require the knowledge of creep properties of constituents under multi-axial stress states. Furthermore, creep mechanisms of interaction between constituents, like frictional sliding should be taken into account.

In what follows we assume the weld metal to be a quasi-homogeneous anisotropic material. For a description of creep we prefer the engineering creep mechanics approach, where the creep potential hypothesis, the representation of tensor functions and internal state variables are applied (see Sect. 5.4.3). The resulting constitutive equations can be utilized in standard finite element codes for structural analysis purposes.

Examples for anisotropic creep behavior and related constitutive equations are presented for a single-crystal alloy in Bertram and Olschewski (2001), a fiber-reinforced material in Robinson et al. (2003) and a forged aluminium alloy in Sect. 6.3.1. One problem of anisotropic creep modeling is that the assumed material symmetries (microstructure symmetries) are difficult to verify in creep tests due to the relatively large scatter of experimental data. Furthermore, the material may lose some or even all symmetries during the creep as a consequence of hardening and damage processes.

In our case the material symmetries can be established according to the arrangement of the weld beads in the weld metal. For the structure presented in Fig. 6.13 one can assume the reflection $\mathbf{Q}_1 = \mathbf{I} - 2\mathbf{m} \otimes \mathbf{m}$, the rotation $\mathbf{Q}_2 = 2\mathbf{l} \otimes \mathbf{l} - \mathbf{I}$ and the reflection $\mathbf{Q}_3 = \mathbf{Q}_1 \cdot \mathbf{Q}_2 = \mathbf{I} - 2\mathbf{k} \otimes \mathbf{k}$ to be the elements of the material symmetry group, where \mathbf{I} is the second rank unit tensor and \mathbf{k} , \mathbf{l} and \mathbf{m} are orthogonal unit vectors.

However, this material symmetry group is poor for the modeling of creep. Indeed, based on the model discussed in the previous section we can assume that the same creep mechanisms will operate by loading the weld metal in \mathbf{k} - or \mathbf{l} -directions. Although the experimental data presented in Hyde et al. (2003a) are available only for specimen removed in \mathbf{m} - and \mathbf{k} -directions, one may assume that the difference between the experimental creep curves by loading in \mathbf{k} - and \mathbf{l} -directions will be not essential with respect to the usual scatter of experimental data. Here we assume transversely isotropic creep, where the plane spanned on the vectors \mathbf{k} and \mathbf{l} is the quasi-isotropy plane.

The models of steady-state creep under the assumption of transverse isotropy are derived in Sects. 5.4.3.1 and 5.4.3.2. Here we apply the constitutive Eq. (5.4.139). In the equivalent stress expression (5.4.137) the α_i 's play the role of dimensionless factors. Three independent uniform stress states should be realized in order to determine α_i . The relevant stress states are

- Uni-axial tension in the direction \mathbf{m} (longitudinal tension test). In this case the stress tensor is $\boldsymbol{\sigma} = \sigma_0 \mathbf{m} \otimes \mathbf{m}$, where $\sigma_0 > 0$ is the magnitude of the applied stress. From Eqs. (5.4.137) and (5.4.139) follows

$$\begin{aligned} J_m &= \sigma_0, \quad I_{3m} = I_{4m} = 0, \quad \sigma_{\text{eq}} = \sigma_0 \sqrt{\alpha_1}, \\ \dot{\boldsymbol{\varepsilon}}^{\text{pl}} &= \sqrt{\alpha_1} \dot{\varepsilon}_{\text{eq}} \left[\mathbf{m} \otimes \mathbf{m} - \frac{1}{2} (\mathbf{I} - \mathbf{m} \otimes \mathbf{m}) \right] \end{aligned} \quad (6.3.53)$$

- Uni-axial tension in the direction \mathbf{k} (transverse tension test), i.e. $\boldsymbol{\sigma} = \sigma_0 \mathbf{k} \otimes \mathbf{k}$, $\sigma_0 > 0$. From Eqs. (5.4.137) and (5.4.139) we obtain

$$\begin{aligned} \mathbf{s}_p &= \frac{1}{2} \sigma_0 (\mathbf{k} \otimes \mathbf{k} - \mathbf{l} \otimes \mathbf{l}), \quad J_m = -\frac{1}{2} \sigma_0, \\ I_{3m} &= \frac{1}{4} \sigma_0^2, \quad I_{4m} = 0, \quad \sigma_{\text{eq}} = \frac{1}{2} \sigma_0 \sqrt{\alpha_1 + 3\alpha_2}, \\ \dot{\boldsymbol{\varepsilon}}^{\text{pl}} &= \frac{\dot{\varepsilon}_{\text{eq}}}{2\sqrt{\alpha_1 + 3\alpha_2}} [(\alpha_1 + 3\alpha_2) \mathbf{k} \otimes \mathbf{k} + (\alpha_1 - 3\alpha_2) \mathbf{l} \otimes \mathbf{l} - 2\alpha_1 \mathbf{m} \otimes \mathbf{m}] \end{aligned} \quad (6.3.54)$$

- Uniform shear in the plane spanned on \mathbf{m} and \mathbf{k} , i.e. $\boldsymbol{\sigma} = \tau_0 (\mathbf{m} \otimes \mathbf{k} + \mathbf{k} \otimes \mathbf{m})$, $\tau_0 > 0$. From Eqs. (5.4.137) and (5.4.139)

$$J_m = I_{3m} = 0, \quad I_{4m} = \tau_0^2, \quad \dot{\boldsymbol{\varepsilon}}^{\text{pl}} = \frac{\sqrt{3\alpha_3}}{2} \dot{\varepsilon}_{\text{eq}} (\mathbf{m} \otimes \mathbf{k} + \mathbf{k} \otimes \mathbf{m}) \quad (6.3.55)$$

The next step is the form of the creep potential $W(\sigma_{\text{eq}})$ or the form of the creep rate versus stress dependence in the steady-state range. The criteria for the choice of a suitable function are the type of the deformation mechanisms operating for the given stress and temperature range as well as the best fitting of the experimentally obtained strain versus time curves. Experimental data for the weld metal 9CrMoNbV are presented in Hyde et al. (2003a) for the stress range 87–100 MPa and the constant temperature 650 °C. The authors used a power law in order to fit the experimental data for secondary creep of longitudinal and transverse specimens. In this case the Norton-Bailey-Odqvist creep potential can be applied (Odqvist and Hult 1962)

$$W(\sigma_{\text{eq}}) = \frac{a}{n+1} \sigma_{\text{eq}}^{n+1}, \quad \dot{\varepsilon}_{\text{eq}} = a \sigma_{\text{eq}}^n, \quad (6.3.56)$$

where a and n are material parameters. For the longitudinal direction from Eqs. (6.3.53) and (6.3.56) it follows

$$\dot{\varepsilon}_L^{\text{pl}} \equiv \mathbf{m} \cdot \dot{\boldsymbol{\varepsilon}}^{\text{pl}} \mathbf{m} = a_L \sigma_0^n, \quad a_L \equiv a \alpha_1^{\frac{n+1}{2}} \quad (6.3.57)$$

Taking the longitudinal direction to be the “reference” direction we set in Eqs. (6.3.57) $\alpha_1 = 1$. From Eqs. (6.3.54) and (6.3.56) we obtain for the transverse direction

$$\dot{\epsilon}_T^{pl} \equiv \mathbf{k} \cdot \dot{\epsilon}^{pl} \cdot \mathbf{k} = a_T \sigma_0^n, \quad a_T \equiv a \left(\frac{1 + 3\alpha_2}{4} \right)^{\frac{n+1}{2}} \tag{6.3.58}$$

In Hyde et al. (2003a) the values for the material parameters are presented. However, the exponent n is found to be different for the longitudinal and the transverse directions. Different values for n contradict to the creep potential hypothesis employed in the previous section. Here we compute the values for a_L , a_T and n based on the following functional

$$F(\tilde{a}_L, \tilde{a}_T, n) = \sum_{i=1}^k (\tilde{a}_L + n\tilde{\sigma}_i - \tilde{\epsilon}_{L_i})^2 + \sum_{i=1}^k (\tilde{a}_T + n\tilde{\sigma}_i - \tilde{\epsilon}_{T_i})^2, \tag{6.3.59}$$

$$\tilde{a}_L \equiv \log a_L, \quad \tilde{a}_T \equiv \log a_T, \quad \tilde{\sigma} \equiv \log \sigma_0,$$

$$\tilde{\epsilon}_L \equiv \log \dot{\epsilon}_L, \quad \tilde{\epsilon}_T \equiv \log \dot{\epsilon}_T,$$

where k is the number of experimental data points. Setting the first variation of F to zero leads to the system of three algebraic equations with respect to \tilde{a}_L , \tilde{a}_T and n . As the result we obtain the following set of material constants

$$a_L = 1.377 \cdot 10^{-21} \text{ MPa}^{-n} / \text{h}, \quad a_T = 2.023 \cdot 10^{-21} \text{ MPa}^{-n} / \text{h}, \tag{6.3.60}$$

$$n = 8.12$$

Figure 6.18 shows the experimental data presented in Hyde et al. (2003a) and the numerical predictions by use of Eqs. (6.3.57), (6.3.58) and (6.3.60).

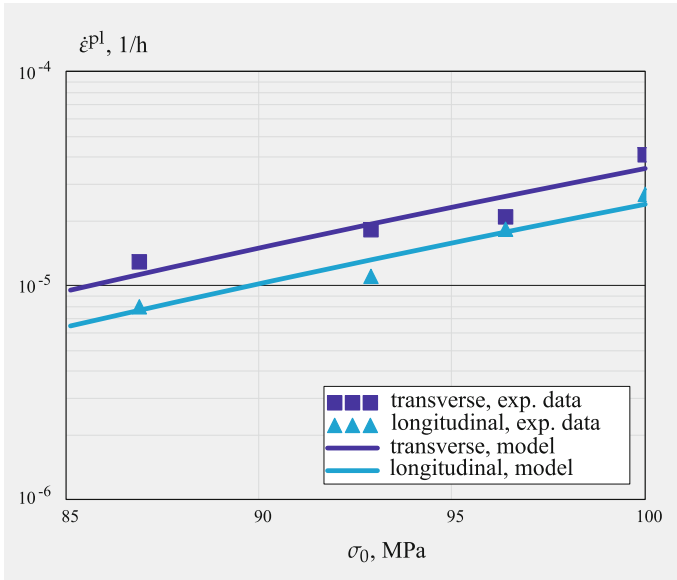


Fig. 6.18 Minimum creep rates versus stress, experimental data after Hyde et al. (2003a)

Finally let us summarize the constitutive equation for secondary creep and the set of identified material constants as follows

$$\begin{aligned} \dot{\boldsymbol{\epsilon}}^{\text{pl}} &= \frac{3}{2} a \sigma_{\text{eq}}^{n-1} \left[J_m \left(\mathbf{m} \otimes \mathbf{m} - \frac{1}{3} \mathbf{I} \right) + \alpha_2 \mathbf{s}_p + \alpha_3 (\boldsymbol{\tau}_m \otimes \mathbf{m} + \mathbf{m} \otimes \boldsymbol{\tau}_m) \right], \\ \sigma_{\text{eq}}^2 &= \left(\mathbf{m} \cdot \boldsymbol{\sigma} \cdot \mathbf{m} - \frac{1}{2} \text{tr} \boldsymbol{\sigma}_p \right)^2 + \frac{3}{2} \alpha_2 \text{tr} \mathbf{s}_p^2 + 3 \alpha_3 \tau_m^2, \\ a &= 1.377 \cdot 10^{-21} \text{ MPa}^{-n} / \text{h}, \quad n = 8.12, \quad \alpha_2 = 1.117 \end{aligned} \quad (6.3.61)$$

The weighting factor α_3 , which stands for the influence of the transverse shear stress, remains undetermined in Eqs. (6.3.61) since experimental data of creep under transverse shear stress state are not available. In Lvov et al. (2014) results of micromechanics simulations of a weld metal samples subjected to different stress states are presented. The obtained creep rates indicate that one may set $\alpha_2 \approx \alpha_3$.

Model (6.3.61) is limited only to secondary creep behavior and can be used to reproduce only the secondary part of the creep curves presented in Hyde et al. (2003a). For the description of the whole creep process including the primary and tertiary creep stages, model (6.3.61) can be modified by use of hardening, softening and damage variables.

References

- Abe F (2001) Creep rates and strengthening mechanisms in tungsten-strengthened 9Cr steels. *Mater Sci Eng A319–A321*:770–773
- Abe F (2004) Bainitic and martensitic creep-resistant steels. *Curr Opin Solid State Mater Sci* 8(3):305–311
- Altenbach H, Naumenko K (1997) Creep bending of thin-walled shells and plates by consideration of finite deflections. *Comput Mech* 19:490–495
- Altenbach H, Naumenko K (2002) Shear correction factors in creep-damage analysis of beams, plates and shells. *JSME International Journal Series A, Solid Mechanics and Material Engineering* 45:77–83
- Altenbach H, Altenbach J, Naumenko K (1997a) On the prediction of creep damage by bending of thin-walled structures. *Mech Time-Depend Mater* 1:181–193
- Altenbach H, Morachkovsky O, Naumenko K, Sychov A (1997b) Geometrically nonlinear bending of thin-walled shells and plates under creep-damage conditions. *Arch Appl Mech* 67:339–352
- Altenbach H, Kolarow G, Morachkovsky O, Naumenko K (2000) On the accuracy of creep-damage predictions in thinwalled structures using the finite element method. *Comput Mech* 25:87–98
- Altenbach H, Kushnevsky V, Naumenko K (2001) On the use of solid- and shell-type finite elements in creep-damage predictions of thinwalled structures. *Arch Appl Mech* 71:164–181
- Altenbach H, Naumenko K, Zhilin P (2003) A micro-polar theory for binary media with application to phase-transitional flow of fiber suspensions. *Continuum Mech Thermodyn* 15:539–570
- Altenbach H, Altenbach J, Kissing W (2004) *Mechanics of composite structural elements*. Springer, Berlin
- Altenbach J, Altenbach H, Naumenko K (1997c) Lebensdauerabschätzung dünnwandiger Flächentragwerke auf der Grundlage phänomenologischer Materialmodelle für Kriechen und Schädigung. *Technische Mechanik* 17(4):353–364

- Angella A, Bassani E, Gariboldi E, Ripamonti D (2008) Microstructural stability and related mechanical properties of a Al-Cu-Mg-Si alloy. In: Hirsch J, Skrotzky B, Gottstein G (eds) *Aluminium alloys*, vol 1, Wiley-VCH, pp 1092–1067
- Aurich D, Kloos KH, Lange G, Macherauch E (1999) *Eigenspannungen und Verzug durch Wärmeeinwirkung*. DFG Forschungsbericht, Wiley-VCH, Weinheim
- Bertram A, Olschewski J (2001) A phenomenological anisotropic creep model for cubic single crystals. In: Lemaître J (ed) *Handbook of materials behaviour models*. Academic Press, San Diego, pp 303–307
- Betten J (2008) *Creep Mechanics*, 3rd edn. Springer, Berlin
- Bodnar A, Chrzanowski M (1991) A non-unilateral damage in creeping plates. In: Zyczkowski M (ed) *Creep in Structures*. Springer, Berlin, Heidelberg, pp 287–293
- de Borst R (2004) Damage, material instabilities, and failure. In: Stein E, de Borst R, Hughes TJR (eds) *Encyclopedia of computational mechanics*. John Wiley & Sons, Chichester, pp 335–373
- Boyle JT, Spence J (1983) *Stress analysis for creep*. Butterworth, London
- Chawla KK (1987) *Composite materials*. Springer, New York
- Choudhary BK, Paniraj C, Rao K, Mannan SL (2001) Creep deformation behavior and kinetic aspects of 9Cr-1Mo ferritic steel. *Iron and steel institut of Japan (ISIJ)*. International 41:73–80
- Dyson BF (1996) Mechanical testing of high-temperature materials: modelling data-scatter. In: Cahn RW, Evans AG, McLean M (eds) *High-temperature structural materials*, Chapman & Hall, London, pp 160–192
- Dyson BF, McLean M (2001) Micromechanism-quantification for creep constitutive equations. In: Murakami S, Ohno N (eds) *IUTAM symposium on creep in structures*. Kluwer, Dordrecht, pp 3–16
- Eggeler G, Ramteke A, Coleman M, Chew B, Peter G, Burlibies A, Hald J, Jefferey C, Rantala J, de Witte M, Mohrmann R (1994) Analysis of creep in a welded P91 pressure vessel. *Int J Press Vessels Pip* 60:237–257
- Frost HJ, Ashby MF (1982) *Deformation-mechanism maps*. Pergamon, Oxford
- Gandy D (2006) X20CrMoV12-1 steel handbook. Technical report. Electric Power Research Institute, 1012740, Palo Ato
- Gariboldi E, Casaro F (2007) Intermediate temperature creep behaviour of a forged Al-Cu-Mg-Si-Mn alloy. *Mater Sci Eng: A* 462(1):384–388
- Gariboldi E, Conte A (2013) Effect of orientation and overaging on the creep and creep crack growth properties of 2xxx aluminium alloy forgings. In: *Advanced materials modelling for structures*. Springer, pp 165–175
- Gariboldi E, Naumenko K, Ozhoga-Maslovskaia O, Zappa E (2016) Analysis of anisotropic damage in forged Al-Cu-Mg-Si alloy based on creep tests, micrographs of fractured specimen and digital image correlations. *Mater Sci Eng: A* 652:175–185
- Hall FR, Hayhurst DR (1991) Continuum damage mechanics modelling of high temperature deformation and failure in a pipe weldment. *Proc R Soc Lond A: Math Phys Eng Sci* 433:383–403
- Hayhurst DR (1994) The use of continuum damage mechanics in creep analysis for design. *J Strain Anal Eng Des* 25(3):233–241
- Hayhurst DR (1999) Materials data bases and mechanisms-based constitutive equations for use in design. In: Altenbach H, Skrzypek J (eds) *Creep and damage in materials and structures*. Springer, Wien, New York, pp 285–348, CISM Lecture Notes No. 399
- Hayhurst DR (2001) Computational continuum damage mechanics: its use in the prediction of creep fracture in structures—past, present and future. In: Murakami S, Ohno N (eds) *IUTAM symposium on creep in structures*. Kluwer, Dordrecht, pp 175–188
- Hayhurst DR, Wong MT, Vakili-Tahami F (2002) The use of CDM analysis techniques in high temperature creep failure of welded structures. *JSME Int J Ser A, Solid Mech Mater Eng* 45:90–97
- Hoff NJ (1953) The necking and the rupture of rods subjected to constant tensile loads. *Trans of ASME J Appl Mech* 20(1):105–108
- Hyde T, Sun W, Hyde C (2013) *Applied creep mechanics*. McGraw-Hill Education

- Hyde TH, Sun W (2005) A study of anisotropic creep behaviour of a 9CrMoNbV weld metal using damage analyses with a unit cell model. *Proc Inst Mech Eng, Part L: J Mater Des Appl* 219(4):193–206
- Hyde TH, Sun W, Becker AA, Williams JA (1997) Creep continuum damage constitutive equations for the base, weld and heat-affected zone materials of a service-aged 1/2Cr1/2Mo1/4V:2 1/4Cr1Mo multipass weld at 640°C. *J Strain Anal Eng Des* 32(4):273–285
- Hyde TH, Sun W, Williams JA (1999) Creep behaviour of parent, weld and HAZ materials of new, service aged and repaired 1/2Cr1/2Mo1/4V: 21/4Cr1Mo pipe welds at 640°C. *Mater High Temp* 16(3):117–129
- Hyde TH, Sun W, Becker AA (2000) Failure prediction for multi-material creep test specimens using steady-state creep rupture stress. *Int J Mech Sci* 42:401–423
- Hyde TH, Sun W, Agyakwa PA, Shipeay PH, Williams JA (2003a) Anisotropic creep and fracture behaviour of a 9CrMoNbV weld metal at 650°C. In: Skrzypek JJ, Ganczarski AW (eds) *Anisotropic behaviour of damaged materials*. Springer, Berlin, pp 295–316
- Hyde TH, Sun W, Williams JA (2003b) Creep analysis of pressurized circumferential pipe weldments—a review. *J Strain Anal Eng Des* 38(1):1–29
- Kimura K (2006) 9Cr-1Mo-V-Nb Steel. In: Martienssen W (ed) *Creep properties of heat resistant steels and superalloys*. Springer, Berlin, pp 126–133
- Kimura K, Kushima H, Abe F, Yagi K (1997) Inherent creep strength and long term creep strength properties of ferritic steels. *Mater Sci Eng: A* 234:1079–1082
- Kimura K, Kushima H, Sawada K (2009) Long-term creep deformation properties of 9Cr-1Mo steel. *Mater Sci Eng A* 510–A511:58–63
- Kloc L, Sklenička V (2004) Confirmation of low stress creep regime in 9% chromium steel by stress change creep experiments. *Mater Sci Eng A* 387–A389:633–638
- Kloc L, Sklenička V, Ventruba J (2001) Comparison of low creep properties of ferritic and austenitic creep resistant steels. *Mater Sci Eng A* 319–A321:774–778
- Konkin VN, Morachkovskij OK (1987) Polzuchest' i dlitel'naya prochnost' legkikh splavov, proyavlyayushchikh anizotropnye svoystva (Creep and long-term strength of light alloys with anisotropic properties, in Russ.). *Probl Prochn* 5:38–42
- Kostenko E, Naumenko K (2008) Numerische zeitstandanalyse einer kraftwerkskomponente mit einem kriechschädigungs-werkstoffmodell. 31. FVW/FVHT vortragsveranstaltung, langzeitverhalten wärmefester stähle und hochtemperaturwerkstoffe, stahlinstitut VDEh, düsseldorf, pp 37–46
- Kostenko Y, Lvov G, Gorash E, Altenbach H, Naumenko K (2006) Power plant component design using creep-damage analysis. In: *Proceedings of IMECE2006*, IMECE2006-13710. ASME, Chicago, pp 1–10
- Kostenko Y, Schwass G, Naumenko K (2009a) Creep analysis of power plant components from 1%CrMoV and 10%CrMoV steels. In: Shibli IA, Holdsworth SR (eds) *Creep & fracture in high temperature components*. DEStech Publications, Lancaster, Pennsylvania, pp 797–805
- Kostenko Y, Schwass G, Naumenko K (2009b) Creep analysis of power plant components from 1%CrMoV and 10%CrMoV steels. *OMMI—Oper Maintenance Mater Issue* 6(2):1–10
- Kostenko Y, Almstedt H, Naumenko K, Linn S, Scholz A (2013) Robust methods for creep fatigue analysis of power plant components under cyclic transient thermal loading. In: *ASME turbo expo 2013: turbine technical conference and exposition*. American Society of Mechanical Engineers, pp V05BT25A040–V05BT25A040
- Kowalewski Z (1992) The role of grain size on creep of copper under uniaxial tension. *Arch Metall* 37:65–76
- Kowalewski ZL (1996) Creep rupture of copper under complex stress state at elevated temperature. Design and life assessment at high temperature. *Mechanical Engineering Publ*, London, pp 113–122
- Kowalewski ZL, Hayhurst DR, Dyson BF (1994) Mechanisms-based creep constitutive equations for an aluminium alloy. *J Strain Anal Eng Des* 29(4):309–316

- Längler F, Naumenko K, Altenbach H, Ievdokymov M (2014) A constitutive model for inelastic behavior of casting materials under thermo-mechanical loading. *J Strain Anal Eng Des* 49:421–428
- Lemaitre J (1996) A course on damage mechanics. Springer, Berlin
- Lemaitre J, Chaboche JL (1990) Mechanics of solid materials. Cambridge University Press, Cambridge
- Lin J, Liu Y, Dean TA (2005) A review on damage mechanisms, models and calibration methods under various deformation conditions. *Int J Damage Mech* 14:299–319
- Liu Y, Murakami S, Kageyama Y (1994) Mesh-dependence and stress singularity in finite element analysis of creep crack growth by continuum damage mechanics approach. *Eur J Mech A Solids* 35(3):147–158
- Lundin CD, Liu P, Prager M (2001) Creep behavior of weld heat affected zone regions for modified 9Cr-1Mo Steel. In: Proceedings of CREEP7. Japan Society of Mechanical Engineers, Tsukuba, pp 379–382
- Lvov I, Naumenko K, Altenbach H (2014) Homogenisation approach in analysis of creep behaviour in multipass weld. *Mater Sci Technol* 30(1):50–53
- Mahnken R, Stein E (1996) Parameter identification for viscoplastic models based on analytical derivatives of a least-squares functional and stability investigations. *Int J Plast* 12(4):451–479
- Mahnken R, Stein E (1997) Parameter identification for finite deformation elasto-plasticity in principal directions. *Comput Methods Appl Mech Eng* 147(1):17–39
- Maile K, Scheck R (2008) Kriechschädigungsentwicklung in 9–11%Cr Stählen. 31. FVW/FVHT Vortragsveranstaltung, Langzeitverhalten warmfester Stähle und Hochtemperaturwerkstoffe, Stahlinstitut VDEh, Düsseldorf, pp 15–26
- Malinin NN (1981) Raschet na polzuchest' konstrukcionnykh elementov (Creep calculations of structural elements, in Russ.). Mashinostroenie, Moskva
- Matsui M, Tabuchi M, Watanabe T, Kubo K, Kinugawa J, Abe F (2001) Degradation of creep strength in welded joint of 9%cr steel. *Iron Steel Inst Japan (ISIJ) Int* 41:S126–S130
- Mayer KH, Masuyama F (2008) The development of creep-resistant steels. In: Abe F, Kern TU, Viswanathan R (eds) Creep-resistant steels. Woodhead Publishing, Cambridge, pp 15–77
- Murakami S, Sanomura Y (1985) Creep and creep damage of copper under multiaxial states of stress. In: Sawczuk A, Bianchi B (eds) Plasticity today—modelling, methods and applications. Elsevier, London, New York, pp 535–551
- Naumenko K, Altenbach H (2005) A phenomenological model for anisotropic creep in a multi-pass weld metal. *Arch Appl Mech* 74:808–819
- Naumenko K, Altenbach H (2007) Modelling of creep for structural analysis. Springer, Berlin et al
- Naumenko K, Gariboldi E (2014) A phase mixture model for anisotropic creep of forged Al-Cu-Mg-Si alloy. *Mater Sci Eng: A* 618:368–376
- Naumenko K, Kostenko Y (2009) Structural analysis of a power plant component using a stress-range-dependent creep-damage constitutive model. *Mater Sci Eng A* 510–A511:169–174
- Naumenko K, Altenbach H, Gorash Y (2009) Creep analysis with a stress range dependent constitutive model. *Arch Appl Mech* 79:619–630
- Naumenko K, Altenbach H, Kutschke A (2011a) A combined model for hardening, softening and damage processes in advanced heat resistant steels at elevated temperature. *Int J Damage Mech* 20:578–597
- Naumenko K, Kutschke A, Kostenko Y, Rudolf T (2011b) Multi-axial thermo-mechanical analysis of power plant components from 9–12%Cr steels at high temperature. *Eng Fract Mech* 78:1657–1668
- Odqvist FKG (1974) Mathematical theory of creep and creep rupture. Oxford University Press, Oxford
- Odqvist FKG, Hult J (1962) Kriechfestigkeit metallischer Werkstoffe. Springer, Berlin u.a
- Orlová A, Buršík J, Kuchařová K, Sklenička V (1998) Microstructural development during high temperature creep of 9% cr steel. *Mater Sci Eng A* 245:39–48
- Penny RK, Mariott DL (1995) Design for creep. Chapman & Hall, London

- Perrin JJ, Hayhurst DR (1994) Creep constitutive equations for a 0.5Cr-0.5Mo-0.25V ferritic steel in the temperature range 600–675°C. *The. J Strain Anal Eng Des* 31(4):299–314
- Podgorny AN, Bortovoj VV, Gontarovskiy PP, Kolomak VD, Lvov GI, Matyukhin YJ, Morachkovskiy OK (1984) Polzuchest' elementov mashinostroitel'nykh konstruykij (Creep of machinery structural members, in Russ.). Naukova Dumka, Kiev
- Polcik P, Straub S, Henes D, Blum W (1998) Simulation of the creep behaviour of 9–12% CrMo-V steels on the basis of microstructural data. In: Strang A, Cawley J, Greenwood GW (eds) *Microstructural stability of creep resistant alloys for high temperature plant applications*. Cambridge University Press, Cambridge, pp 405–429
- Polcik P, Sailer T, Blum W, Straub S, Buršik J, Orlová A (1999) On the microstructural development of the tempered martensitic Cr-steel P91 during long-term creep - a comparison of data. *Mater Sci Eng A* 260:252–259
- Polmear IJ (1996) Recent developments in light alloys. *Mater Trans, Jpn Inst Met* 37(1):12–31
- Polmear IJ (2004) Aluminium alloys—a century of age hardening. *Mater Forum* 28:1–14
- Rabotnov YN (1963) O razrushenii vsledstvie polzuchesti (On fracture as a consequence of creep, in Russ.). *Prikladnaya Mekhanika I Tekhnicheskaya Fizika* 2:113–123
- Rabotnov YN (1969) Creep problems in structural members. North-Holland, Amsterdam
- Rauch M, Maile K, Seliger P, Reuter A, Tilsch H (2004) Numerische Berechnung und experimentelle Validierung der Schädigungsentwicklung in 9%-Chromstählen. 27. FVW/FVHT Vortragsveranstaltung, Langzeitverhalten warmfester Stähle und Hochtemperaturwerkstoffe, Stahlinstitut VDEh, Düsseldorf, pp 75–83
- Rieth M, Falkenstein A, Graf P, Heger S, Jäntsch U, Klimiankou M, Materna-Morris E, Zimmermann H (2004) Creep of the austenitic steel AISI 316 L(N). Experiments and models. Technical report, Forschungszentrum Karlsruhe, FZKA 7065, Karlsruhe
- Robinson DN, Binienda WK, Ruggles MB (2003) Creep of polymer matrix composites. I: Norton/Bailey Creep Law for transverse isotropy. *J Eng Mech* 129(3):310–317
- Röttger D (1997) Untersuchungen zum Wechselverformungs- und Zeitstandverhalten der Stähle X20CrMoV121 und X10CrMoVNb91. Dissertation, Universität GH Essen, Fortschr.-Ber. VDI Reihe 5, Nr. 507, Düsseldorf
- Sakane M, Tokura H (2002) Experimental study of biaxial creep damage for type 304 stainless steel. *Int J Damage Mech* 11:247–262
- Samir A, Simon A, Scholz A, Berger C (2005) Deformation and life assessment of high temperature materials under creep fatigue loading. *Materialwissenschaft und Werkstofftechnik* 36:722–730
- Segle P, Tu ST, Storesund J, Samuelson LA (1996) Some issues in life assessment of longitudinal seam welds based on creep tests with cross-weld specimens. *Int J Press Vessels Pip* 66:199–222
- Shibli IA (2002) Performance of P91 thick section welds under steady and cyclic loading conditions: power plant and research experience. *OMMI* 1(3). <http://www.ommi.co.uk>
- Simon A (2007) Zur Berechnung betriebsnah belasteter Hochtemperaturstähle mit einem konstitutiven Werkstoffmodell. Dissertation, Technische Universität Darmstadt, Berichte aus der Werkstofftechnik, Band 4/2007, Shaker Verlag Aachen
- Sklenička V, Kuchařová K, Svoboda M, Kloc L, Buršik J, Kroupa A (2003) Long-term creep behavior of 9–12% Cr power plant steels. *Mater Charact* 51(1):35–48
- Skrzypiek J, Ganczarski A (1998) Modelling of material damage and failure of structures. *Foundation of Engineering Mechanics*, Springer, Berlin
- Straub S (1995) Verformungsverhalten und Mikrostruktur warmfester martensitischer 12%-Chromstähle. Dissertation, Universität Erlangen-Nürnberg, VDI Reihe 5, Nr. 405, Düsseldorf
- Wohlfahrt H, Brinkmann D (2001) Consideration of inhomogenities in application of deformation models, describing the inelastic behaviour of welded joints. In: Steck E, Ritter R, Peil U, Ziegenbein A (eds) *Plasticity of metals: experiments, models, computation*. Final Report of the Collaborative Research Centre 319, Wiley-VCH, Weinheim, pp 361–382
- Wu R, Sandström R, Seitlsleam F (2004) Influence of extra coarse grains on the creep properties of 9 percent CrMoV (P91) steel weldment. *J Eng Mater Technol* 26:87–94

Appendix A

Basic Operations of Tensor Algebra

The tensor calculus is a powerful tool for the description of the fundamentals in continuum mechanics and the derivation of the governing equations for applied problems. In general, there are two possibilities for the representation of the tensors and the tensorial equations:

- the direct (symbolic, coordinate-free) notation and
- the index (component) notation

The direct notation operates with scalars, vectors and tensors as physical objects defined in the three-dimensional space (in this book we are limit ourselves to this case). A vector (first rank tensor) \mathbf{a} is considered as a directed line segment rather than a triple of numbers (coordinates). A second rank tensor \mathbf{A} is any finite sum of ordered vector pairs $\mathbf{A} = \mathbf{a} \otimes \mathbf{b} + \dots + \mathbf{c} \otimes \mathbf{d}$. The scalars, vectors and tensors are handled as invariant (independent from the choice of the coordinate system) quantities. This is the reason for the use of the direct notation in the modern literature of mechanics and rheology, e.g. Altenbach (2012), Antman (1995), Besseling and van der Giessen (1994), Giesekus (1994), Haupt (2002), Lurie (1990), Palmov (1998), Truesdell and Noll (1992), Zhilin (2001) among others. The basics of the direct tensor calculus are given in the classical textbooks of Wilson (1901) (founded upon the lecture notes of Gibbs) and Lagally (1962).

The index notation deals with components or coordinates of vectors and tensors. For a selected basis, e.g. $\mathbf{g}_i, i = 1, 2, 3$ one can write

$$\mathbf{a} = a^i \mathbf{g}_i, \quad \mathbf{A} = (a^i b^j + \dots + c^i d^j) \mathbf{g}_i \otimes \mathbf{g}_j$$

Here the Einstein's summation convention is used: in one expression the twice repeated indices are summed up from 1 to 3, e.g.

$$a^k \mathbf{g}_k \equiv \sum_{k=1}^3 a^k \mathbf{g}_k, \quad A^{ik} b_k \equiv \sum_{k=1}^3 A^{ik} b_k$$

In the above examples k is a so-called dummy index. Within the index notation the basic operations with tensors are defined with respect to their coordinates, e.g. the sum of two vectors is computed as the sum of their coordinates $c^i = a^i + b^i$. The introduced basis remains in the background. It must be noted that a change of the coordinate system leads to the change of the components of tensors.

In this book we prefer the direct tensor notation over the index one. When solving applied problems the tensor equations can be “translated into the language” of matrices for a specified coordinate system. The purpose of this Appendix is to give a brief guide to notations and rules of the tensor calculus applied throughout this book. For more comprehensive overviews on tensor calculus we recommend Betten (1987), de Boer (1982), Giesekus (1994), Lebedev et al. (2010), Lippmann (1993), Lurie (1990), Trostel (1993), Zhilin (2001). The calculus of matrices is presented in Bellmann (1970), Faddejew and Faddejewa (1964), Zurmühl and Falk (1992), for example. Appendix A provides a summary of basic algebraic operations with vectors and second rank tensors. Several rules from tensor analysis are given in Appendix B. Basic sets of invariants for different groups of symmetry transformation are presented in Sect. B.5, where a novel approach to find the functional basis is discussed.

A.1 Polar and Axial Vectors

A vector in the three-dimensional Euclidean space is defined as a directed line segment with specified scalar-valued magnitude and direction. The magnitude (the length) of a vector \mathbf{a} is denoted by $|\mathbf{a}|$. Two vectors \mathbf{a} and \mathbf{b} are equal if they have the same direction and the same magnitude. The zero vector $\mathbf{0}$ has a magnitude equal to zero. In mechanics two types of vectors can be introduced.

The vectors of the first type are directed line segments. These vectors are associated with translations in the three-dimensional space. Examples for polar vectors include the force, the displacement, the velocity, the acceleration, the momentum,

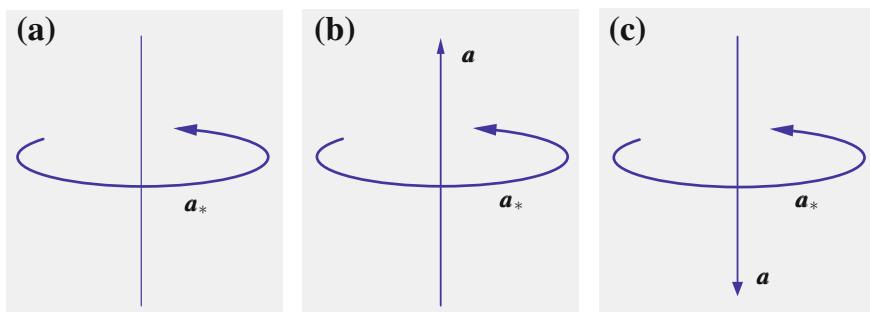


Fig. A.1 Spin vector and its representation by an axial vector. **a** Spin vector, **b** axial vector in the *right-screw* oriented reference frame, **c** axial vector in the *left-screw* oriented reference frame

etc. The second type is used to characterize spinor motions and related quantities, i.e. the moment, the angular velocity, the angular momentum, etc., Fig. A.1a shows the so-called spin vector \mathbf{a}_* which represents a rotation about the given axis. The direction of rotation is specified by the circular arrow and the “magnitude” of rotation is the corresponding length. For the given spin vector \mathbf{a}_* the directed line segment \mathbf{a} is introduced according to the following rules (Zhilin 2001):

1. the vector \mathbf{a} is placed on the axis of the spin vector,
2. the magnitude of \mathbf{a} is equal to the magnitude of \mathbf{a}_* ,
3. the vector \mathbf{a} is directed according to the right-handed screw, Fig. A.1b, or the left-handed screw, Fig. A.1c

The selection of one of the two cases in of the third item corresponds to the convention of orientation of the reference frame (Zhilin 2001). The directed line segment is called a polar vector if it does not change by changing the orientation of the reference frame. The vector is called to be axial if it changes the sign by changing the orientation of the reference frame. The above definitions are valid for scalars and tensors of any rank too. The axial vectors (and tensors) are widely used in the rigid body dynamics, e.g. Altenbach et al. (2007), Zhilin (1996), in the theories of rods, plates and shells, e.g. Altenbach and Zhilin (1988), Naumenko and Eremeyev (2014), in the asymmetric theory of elasticity, e.g. Nowacki (1986), as well as in dynamics of micro-polar media, e.g. Altenbach et al. (2003), Eringen (1999). When dealing with polar and axial vectors it should be remembered that they have different physical meanings. Therefore, a sum of a polar and an axial vector has no sense.

A.2 Operations with Vectors

A.2.1 Addition

For a given pair of vectors \mathbf{a} and \mathbf{b} of the same type the sum $\mathbf{c} = \mathbf{a} + \mathbf{b}$ is defined according to one of the rules in Fig. A.2. The sum has the following properties

- $\mathbf{a} + \mathbf{b} = \mathbf{b} + \mathbf{a}$ (commutativity),
- $(\mathbf{a} + \mathbf{b}) + \mathbf{c} = \mathbf{a} + (\mathbf{b} + \mathbf{c})$ (associativity),
- $\mathbf{a} + \mathbf{0} = \mathbf{a}$

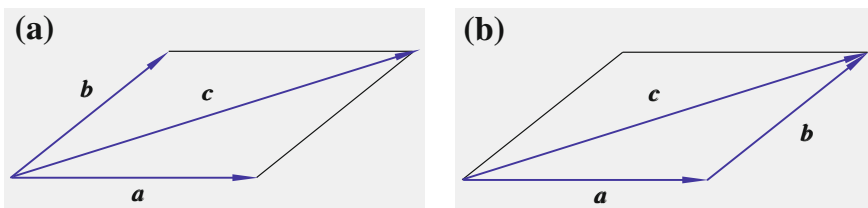


Fig. A.2 Addition of two vectors. **a** Parallelogram rule, **b** triangle rule

A.2.2 Multiplication by a Scalar

For any vector \mathbf{a} and for any scalar α a vector $\mathbf{b} = \alpha\mathbf{a}$ is defined in such a way that

- $|\mathbf{b}| = |\alpha||\mathbf{a}|$,
- for $\alpha > 0$ the direction of \mathbf{b} coincides with that of \mathbf{a} ,
- for $\alpha < 0$ the direction of \mathbf{b} is opposite to that of \mathbf{a} .

For $\alpha = 0$ the product yields the zero vector, i.e. $\mathbf{0} = 0\mathbf{a}$. It is easy to verify that

$$\begin{aligned} \alpha(\mathbf{a} + \mathbf{b}) &= \alpha\mathbf{a} + \alpha\mathbf{b}, \\ (\alpha + \beta)\mathbf{a} &= \alpha\mathbf{a} + \beta\mathbf{a} \end{aligned}$$

A.2.3 Scalar (Dot) Product of Two Vectors

For any pair of vectors \mathbf{a} and \mathbf{b} a scalar α is defined by

$$\alpha = \mathbf{a} \cdot \mathbf{b} = |\mathbf{a}||\mathbf{b}| \cos \varphi,$$

where φ is the angle between the vectors \mathbf{a} and \mathbf{b} . As φ one can use any of the two angles between the vectors, Fig. A.3a. The properties of the scalar product are

- $\mathbf{a} \cdot \mathbf{b} = \mathbf{b} \cdot \mathbf{a}$ (commutativity),
- $\mathbf{a} \cdot (\mathbf{b} + \mathbf{c}) = \mathbf{a} \cdot \mathbf{b} + \mathbf{a} \cdot \mathbf{c}$ (distributivity)

Two nonzero vectors are said to be orthogonal if their scalar product is zero. The unit vector directed along the vector \mathbf{a} is defined by (see Fig. A.3b)

$$\mathbf{n}_a = \frac{\mathbf{a}}{|\mathbf{a}|}$$

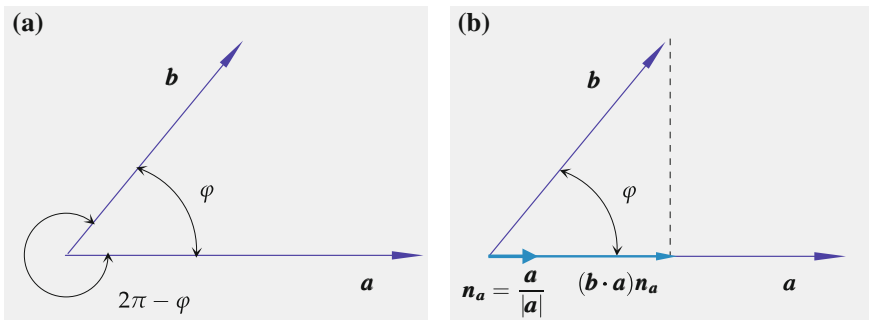


Fig. A.3 Scalar product of two vectors. **a** Angles between two vectors, **b** unit vector and projection

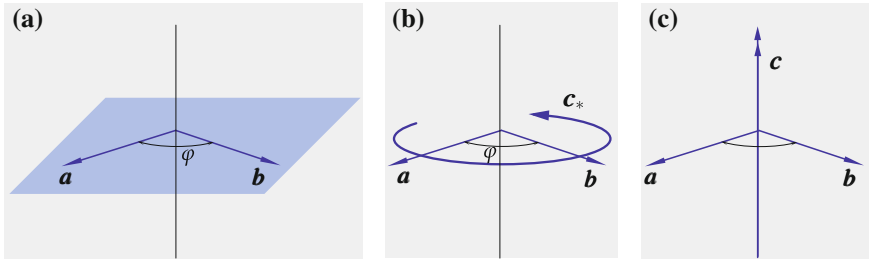


Fig. A.4 Vector product of two vectors. **a** Plane spanned on two vectors, **b** spin vector, **c** axial vector in the *right-screw* oriented reference frame

The projection of the vector \mathbf{b} onto the vector \mathbf{a} is the vector $(\mathbf{b} \cdot \mathbf{a})\mathbf{n}_a$, Fig. A.3b. The length of the projection is $|\mathbf{b}|\cos\varphi$.

A.2.4 Vector (Cross) Product of Two Vectors

For the ordered pair of vectors \mathbf{a} and \mathbf{b} the vector $\mathbf{c} = \mathbf{a} \times \mathbf{b}$ is defined in two following steps (Zhilin 2001):

- the spin vector \mathbf{c}_* is defined in such a way that
 - the axis is orthogonal to the plane spanned on \mathbf{a} and \mathbf{b} , Fig. A.4a,
 - the circular arrow shows the direction of the “shortest” rotation from \mathbf{a} to \mathbf{b} , Fig. A.4b,
 - the length is $|\mathbf{a}||\mathbf{b}|\sin\varphi$, where φ is the angle of the “shortest” rotation from \mathbf{a} to \mathbf{b} ,
- from the resulting spin vector the directed line segment \mathbf{c} is constructed according to one of the rules listed in Sect. A.1.

The properties of the vector product are

$$\begin{aligned} \mathbf{a} \times \mathbf{b} &= -\mathbf{b} \times \mathbf{a}, \\ \mathbf{a} \times (\mathbf{b} + \mathbf{c}) &= \mathbf{a} \times \mathbf{b} + \mathbf{a} \times \mathbf{c} \end{aligned}$$

The type of the vector $\mathbf{c} = \mathbf{a} \times \mathbf{b}$ can be established for the known types of the vectors \mathbf{a} and \mathbf{b} (Zhilin 2001). If \mathbf{a} and \mathbf{b} are polar vectors the result of the cross product will be the axial vector. An example is the moment of momentum for a mass point m defined by $\mathbf{r} \times (m\mathbf{v})$, where \mathbf{r} is the position of the mass point and \mathbf{v} is the velocity of the mass point. The next example is the formula for the distribution of velocities in a rigid body $\mathbf{v} = \boldsymbol{\omega} \times \mathbf{r}$. Here the cross product of the axial vector $\boldsymbol{\omega}$ (angular velocity) with the polar vector \mathbf{r} (position vector) results in the polar vector \mathbf{v} .

The mixed product of three vectors \mathbf{a} , \mathbf{b} and \mathbf{c} is defined by $(\mathbf{a} \times \mathbf{b}) \cdot \mathbf{c}$. The result is a scalar. For the mixed product the following identities are valid

$$\mathbf{a} \cdot (\mathbf{b} \times \mathbf{c}) = \mathbf{b} \cdot (\mathbf{c} \times \mathbf{a}) = \mathbf{c} \cdot (\mathbf{a} \times \mathbf{b}) \quad (\text{A.2.1})$$

If the cross product is applied twice, the first operation must be set in parentheses, e.g., $\mathbf{a} \times (\mathbf{b} \times \mathbf{c})$. The result of this operation is a vector. The following relation can be applied

$$\mathbf{a} \times (\mathbf{b} \times \mathbf{c}) = \mathbf{b}(\mathbf{a} \cdot \mathbf{c}) - \mathbf{c}(\mathbf{a} \cdot \mathbf{b}) \quad (\text{A.2.2})$$

By use of (A.2.1) and (A.2.2) one can calculate

$$\begin{aligned} (\mathbf{a} \times \mathbf{b}) \cdot (\mathbf{c} \times \mathbf{d}) &= \mathbf{a} \cdot [\mathbf{b} \times (\mathbf{c} \times \mathbf{d})] \\ &= \mathbf{a} \cdot (\mathbf{c} \mathbf{b} \cdot \mathbf{d} - \mathbf{d} \mathbf{b} \cdot \mathbf{c}) \\ &= \mathbf{a} \cdot \mathbf{c} \mathbf{b} \cdot \mathbf{d} - \mathbf{a} \cdot \mathbf{d} \mathbf{b} \cdot \mathbf{c} \end{aligned} \quad (\text{A.2.3})$$

A.3 Bases

Any triple of linear independent vectors $\mathbf{e}_1, \mathbf{e}_2, \mathbf{e}_3$ is called basis. A triple of vectors \mathbf{e}_i is linear independent if and only if $\mathbf{e}_1 \cdot (\mathbf{e}_2 \times \mathbf{e}_3) \neq 0$. For a given basis \mathbf{e}_i any vector \mathbf{a} can be represented as follows

$$\mathbf{a} = a^1 \mathbf{e}_1 + a^2 \mathbf{e}_2 + a^3 \mathbf{e}_3 \equiv a^i \mathbf{e}_i$$

The numbers a^i are called the coordinates of the vector \mathbf{a} for the basis \mathbf{e}_i . In order to compute the coordinates a^i the dual (reciprocal) basis \mathbf{e}^k is introduced in such a way that

$$\mathbf{e}^k \cdot \mathbf{e}_i = \delta_i^k = \begin{cases} 1, & k = i, \\ 0, & k \neq i \end{cases}$$

δ_i^k is the Kronecker symbol. The coordinates a^i can be found by

$$\mathbf{e}^i \cdot \mathbf{a} = \mathbf{a} \cdot \mathbf{e}^i = a^m \mathbf{e}_m \cdot \mathbf{e}^i = a^m \delta_m^i = a^i$$

For the selected basis \mathbf{e}_i the dual basis can be found from

$$\mathbf{e}^1 = \frac{\mathbf{e}_2 \times \mathbf{e}_3}{(\mathbf{e}_1 \times \mathbf{e}_2) \cdot \mathbf{e}_3}, \quad \mathbf{e}^2 = \frac{\mathbf{e}_3 \times \mathbf{e}_1}{(\mathbf{e}_1 \times \mathbf{e}_2) \cdot \mathbf{e}_3}, \quad \mathbf{e}^3 = \frac{\mathbf{e}_1 \times \mathbf{e}_2}{(\mathbf{e}_1 \times \mathbf{e}_2) \cdot \mathbf{e}_3} \quad (\text{A.3.4})$$

By use of the dual basis a vector \mathbf{a} can be represented as follows

$$\mathbf{a} = a_1\mathbf{e}^1 + a_2\mathbf{e}^2 + a_3\mathbf{e}^3 \equiv a_i\mathbf{e}^i, \quad a_m = \mathbf{a} \cdot \mathbf{e}_m, \quad a^m \neq a_m$$

In the special case of the orthonormal vectors \mathbf{e}_i , i.e. $|\mathbf{e}_i| = 1$ and $\mathbf{e}_i \cdot \mathbf{e}_k = 0$ for $i \neq k$, from (A.3.4) follows that $\mathbf{e}^k = \mathbf{e}_k$ and consequently $a_k = a^k$.

A.4 Operations with Second Rank Tensors

A second rank tensor is a finite sum of ordered vector pairs $\mathbf{A} = \mathbf{a} \otimes \mathbf{b} + \dots + \mathbf{c} \otimes \mathbf{d}$. One ordered pair of vectors is called the dyad (Wilson 1901). The symbol \otimes is called the dyadic (tensor) product of two vectors. A single dyad or a sum of two dyads are special cases of the second rank tensor. Any finite sum of more than three dyads can be reduced to a sum of three dyads. For example, let

$$\mathbf{A} = \sum_{i=1}^n \mathbf{a}_{(i)} \otimes \mathbf{b}_{(i)}$$

be a second rank tensor. Introducing a basis \mathbf{e}_k the vectors $\mathbf{a}_{(i)}$ can be represented by $\mathbf{a}_{(i)} = a_{(i)}^k \mathbf{e}_k$, where $a_{(i)}^k$ are coordinates of the vectors $\mathbf{a}_{(i)}$. Now we may write

$$\mathbf{A} = \sum_{i=1}^n a_{(i)}^k \mathbf{e}_k \otimes \mathbf{b}_{(i)} = \mathbf{e}_k \otimes \sum_{i=1}^n a_{(i)}^k \mathbf{b}_{(i)} = \mathbf{e}_k \otimes \mathbf{d}^k, \quad \mathbf{d}^k \equiv \sum_{i=1}^n a_{(i)}^k \mathbf{b}_{(i)}$$

A.4.1 Addition

The sum of two tensors is defined as the sum of the corresponding dyads. The sum has the properties of associativity and commutativity. In addition, the following operation can be introduced

$$\mathbf{a} \otimes (\mathbf{b} + \mathbf{c}) = \mathbf{a} \otimes \mathbf{b} + \mathbf{a} \otimes \mathbf{c}, \quad (\mathbf{a} + \mathbf{b}) \otimes \mathbf{c} = \mathbf{a} \otimes \mathbf{c} + \mathbf{b} \otimes \mathbf{c}$$

A.4.2 Multiplication by a Scalar

This operation is introduced first for one dyad. For any scalar α and any dyad $\mathbf{a} \otimes \mathbf{b}$

$$\begin{aligned} \alpha(\mathbf{a} \otimes \mathbf{b}) &= (\alpha\mathbf{a}) \otimes \mathbf{b} = \mathbf{a} \otimes (\alpha\mathbf{b}), \\ (\alpha + \beta)\mathbf{a} \otimes \mathbf{b} &= \alpha\mathbf{a} \otimes \mathbf{b} + \beta\mathbf{a} \otimes \mathbf{b} \end{aligned} \tag{A.4.5}$$

By setting $\alpha = 0$ in the first equation of (A.4.5) the zero dyad can be defined, i.e. $0(\mathbf{a} \otimes \mathbf{b}) = \mathbf{0} \otimes \mathbf{b} = \mathbf{a} \otimes \mathbf{0}$. The above operations can be generalized for any finite sum of dyads, i.e. for second rank tensors.

A.4.3 Inner Dot Product

For any two second rank tensors \mathbf{A} and \mathbf{B} the inner dot product is specified by $\mathbf{A} \cdot \mathbf{B}$. The rule and the result of this operation can be explained in the special case of two dyads, i.e. by setting $\mathbf{A} = \mathbf{a} \otimes \mathbf{b}$ and $\mathbf{B} = \mathbf{c} \otimes \mathbf{d}$

$$\mathbf{A} \cdot \mathbf{B} = \mathbf{a} \otimes \mathbf{b} \cdot \mathbf{c} \otimes \mathbf{d} = (\mathbf{b} \cdot \mathbf{c})\mathbf{a} \otimes \mathbf{d} = \alpha \mathbf{a} \otimes \mathbf{d}, \quad \alpha \equiv \mathbf{b} \cdot \mathbf{c}$$

Note that in general $\mathbf{A} \cdot \mathbf{B} \neq \mathbf{B} \cdot \mathbf{A}$. This can be again verified for two dyads. The operation can be generalized for two second rank tensors as follows

$$\begin{aligned} \mathbf{A} \cdot \mathbf{B} &= \sum_{i=1}^3 \mathbf{a}_{(i)} \otimes \mathbf{b}_{(i)} \cdot \sum_{k=1}^3 \mathbf{c}_{(k)} \otimes \mathbf{d}_{(k)} \\ &= \sum_{i=1}^3 \sum_{k=1}^3 (\mathbf{b}_{(i)} \cdot \mathbf{c}_{(k)}) \mathbf{a}_{(i)} \otimes \mathbf{d}_{(k)} = \sum_{i=1}^3 \sum_{k=1}^3 \alpha_{(ik)} \mathbf{a}_{(i)} \otimes \mathbf{d}_{(k)} \end{aligned}$$

with $\alpha_{(ik)} \equiv \mathbf{b}_{(i)} \cdot \mathbf{c}_{(k)}$. The result of this operation is a second rank tensor.

A.4.4 Transpose of a Second Rank Tensor

The transpose of a second rank tensor \mathbf{A} is defined as follows

$$\mathbf{A}^T = \left(\sum_{i=1}^3 \mathbf{a}_{(i)} \otimes \mathbf{b}_{(i)} \right)^T = \sum_{i=1}^3 \mathbf{b}_{(i)} \otimes \mathbf{a}_{(i)}$$

A.4.5 Double Inner Dot Product

For any two second rank tensors \mathbf{A} and \mathbf{B} the double inner dot product is specified by $\mathbf{A} \cdot\cdot \mathbf{B}$. The result of this operation is a scalar. This operation can be explained for two dyads $\mathbf{A} = \mathbf{a} \otimes \mathbf{b}$ and $\mathbf{B} = \mathbf{c} \otimes \mathbf{d}$ as follows

$$\mathbf{A} \cdot\cdot \mathbf{B} = \mathbf{a} \otimes \mathbf{b} \cdot\cdot \mathbf{c} \otimes \mathbf{d} = (\mathbf{b} \cdot \mathbf{c})(\mathbf{a} \cdot \mathbf{d})$$

By analogy to the inner dot product one can generalize this operation for two second rank tensors. It can be verified that $\mathbf{A} \cdot \cdot \mathbf{B} = \mathbf{B} \cdot \cdot \mathbf{A}$ for arbitrary second rank tensors \mathbf{A} and \mathbf{B} . For a second rank tensor \mathbf{A} and for a dyad $\mathbf{a} \otimes \mathbf{b}$ the double inner dot product yields

$$\mathbf{A} \cdot \cdot \mathbf{a} \otimes \mathbf{b} = \mathbf{b} \cdot \mathbf{A} \cdot \mathbf{a} \quad (\text{A.4.6})$$

A scalar product of two second rank tensors \mathbf{A} and \mathbf{B} is defined by

$$\alpha = \mathbf{A} \cdot \cdot \mathbf{B}^T$$

One can verify that

$$\mathbf{A} \cdot \cdot \mathbf{B}^T = \mathbf{B}^T \cdot \cdot \mathbf{A} = \mathbf{B} \cdot \cdot \mathbf{A}^T$$

A.4.6 Dot Products of a Second Rank Tensor and a Vector

The right dot product of a second rank tensor \mathbf{A} and a vector \mathbf{c} is defined by

$$\mathbf{A} \cdot \mathbf{c} = \left(\sum_{i=1}^3 \mathbf{a}_{(i)} \otimes \mathbf{b}_{(i)} \right) \cdot \mathbf{c} = \sum_{i=1}^3 (\mathbf{b}_{(i)} \cdot \mathbf{c}) \mathbf{a}_{(i)} = \sum_{i=1}^3 \alpha_{(i)} \mathbf{a}_{(i)}$$

with $\alpha_{(i)} \equiv \mathbf{b}_{(i)} \cdot \mathbf{c}$. The left dot product is defined by

$$\mathbf{c} \cdot \mathbf{A} = \mathbf{c} \cdot \left(\sum_{i=1}^3 \mathbf{a}_{(i)} \otimes \mathbf{b}_{(i)} \right) = \sum_{i=1}^3 (\mathbf{c} \cdot \mathbf{a}_{(i)}) \mathbf{b}_{(i)} = \sum_{i=1}^3 \beta_{(i)} \mathbf{b}_{(i)}$$

with $\beta_{(i)} \equiv \mathbf{c} \cdot \mathbf{a}_{(i)}$. The results of these operations are vectors. One can verify that

$$\mathbf{A} \cdot \mathbf{c} \neq \mathbf{c} \cdot \mathbf{A}, \quad \mathbf{A} \cdot \mathbf{c} = \mathbf{c} \cdot \mathbf{A}^T$$

A.4.7 Cross Products of a Second Rank Tensor and a Vector

The right cross product of a second rank tensor \mathbf{A} and a vector \mathbf{c} is defined by

$$\mathbf{A} \times \mathbf{c} = \left(\sum_{i=1}^3 \mathbf{a}_{(i)} \otimes \mathbf{b}_{(i)} \right) \times \mathbf{c} = \sum_{i=1}^3 \mathbf{a}_{(i)} \otimes (\mathbf{b}_{(i)} \times \mathbf{c}) = \sum_{i=1}^3 \mathbf{a}_{(i)} \otimes \mathbf{d}_{(i)}$$

with $\mathbf{d}_{(i)} \equiv \mathbf{b}_{(i)} \times \mathbf{c}$. The left cross product is defined by

$$\mathbf{c} \times \mathbf{A} = \mathbf{c} \times \left(\sum_{i=1}^3 \mathbf{a}_{(i)} \otimes \mathbf{b}_{(i)} \right) = \sum_{i=1}^3 (\mathbf{c} \times \mathbf{a}_{(i)}) \otimes \mathbf{b}_{(i)} = \sum_{i=1}^3 \mathbf{e}_{(i)} \otimes \mathbf{b}_{(i)}$$

with $\mathbf{e}_{(i)} \equiv \mathbf{b}_{(i)} \times \mathbf{c}$. The results of these operations are second rank tensors. It can be shown that

$$\mathbf{A} \times \mathbf{c} = -[\mathbf{c} \times \mathbf{A}^T]^T$$

A.4.8 Trace

The trace of a second rank tensor is defined by

$$\text{tr } \mathbf{A} = \text{tr} \left(\sum_{i=1}^3 \mathbf{a}_{(i)} \otimes \mathbf{b}_{(i)} \right) = \sum_{i=1}^3 \mathbf{a}_{(i)} \cdot \mathbf{b}_{(i)}$$

By taking the trace of a second rank tensor the dyadic product is replaced by the dot product. It can be shown that

$$\text{tr } \mathbf{A} = \text{tr } \mathbf{A}^T, \quad \text{tr} (\mathbf{A} \cdot \mathbf{B}) = \text{tr} (\mathbf{B} \cdot \mathbf{A}) = \text{tr} (\mathbf{A}^T \cdot \mathbf{B}^T) = \mathbf{A} \cdot \cdot \mathbf{B}$$

A.4.9 Symmetric Tensors

A second rank tensor is said to be symmetric if it satisfies the following equality

$$\mathbf{A} = \mathbf{A}^T$$

An alternative definition of the symmetric tensor can be given as follows. A second rank tensor is said to be symmetric if for any vector $\mathbf{c} \neq \mathbf{0}$ the following equality is valid

$$\mathbf{c} \cdot \mathbf{A} = \mathbf{A} \cdot \mathbf{c}$$

An important example of a symmetric tensor is the unit or identity tensor \mathbf{I} , which is defined by such a way that for any vector \mathbf{c}

$$\mathbf{c} \cdot \mathbf{I} = \mathbf{I} \cdot \mathbf{c} = \mathbf{c}$$

The representations of the identity tensor are

$$\mathbf{I} = \mathbf{e}_k \otimes \mathbf{e}^k = \mathbf{e}^k \otimes \mathbf{e}_k$$

for any basis \mathbf{e}_k and \mathbf{e}^k , $\mathbf{e}_k \cdot \mathbf{e}^m = \delta_k^m$. For three orthonormal vectors \mathbf{m} , \mathbf{n} and \mathbf{p} the identity tensor has the form

$$\mathbf{I} = \mathbf{n} \otimes \mathbf{n} + \mathbf{m} \otimes \mathbf{m} + \mathbf{p} \otimes \mathbf{p}$$

A symmetric second rank tensor \mathbf{P} satisfying the condition $\mathbf{P} \cdot \mathbf{P} = \mathbf{P}$ is called projector. Examples of projectors are

$$\mathbf{m} \otimes \mathbf{m}, \quad \mathbf{n} \otimes \mathbf{n} + \mathbf{p} \otimes \mathbf{p} = \mathbf{I} - \mathbf{m} \otimes \mathbf{m},$$

where \mathbf{m} , \mathbf{n} and \mathbf{p} are orthonormal vectors. The result of the dot product of the tensor $\mathbf{m} \otimes \mathbf{m}$ with any vector \mathbf{a} is the projection of the vector \mathbf{a} onto the line spanned on the vector \mathbf{m} , i.e. $\mathbf{m} \otimes \mathbf{m} \cdot \mathbf{a} = (\mathbf{a} \cdot \mathbf{m})\mathbf{m}$. The result of $(\mathbf{n} \otimes \mathbf{n} + \mathbf{p} \otimes \mathbf{p}) \cdot \mathbf{a}$ is the projection of the vector \mathbf{a} onto the plane spanned on the vectors \mathbf{n} and \mathbf{p} .

A.4.10 Skew-Symmetric Tensors

A second rank tensor is said to be skew-symmetric if it satisfies the following equality

$$\mathbf{A} = -\mathbf{A}^T$$

or if for any vector $\mathbf{c} \neq \mathbf{0}$

$$\mathbf{c} \cdot \mathbf{A} = -\mathbf{A} \cdot \mathbf{c}$$

Any skew-symmetric tensor \mathbf{A} can be represented by

$$\mathbf{A} = \mathbf{a} \times \mathbf{I} = \mathbf{I} \times \mathbf{a}$$

The vector \mathbf{a} is called the associated vector. Any second rank tensor can be uniquely decomposed into the symmetric and skew-symmetric parts

$$\begin{aligned} \mathbf{A} &= \frac{1}{2} (\mathbf{A} + \mathbf{A}^T) + \frac{1}{2} (\mathbf{A} - \mathbf{A}^T) = \mathbf{A}_1 + \mathbf{A}_2, \\ \mathbf{A}_1 &= \frac{1}{2} (\mathbf{A} + \mathbf{A}^T), \quad \mathbf{A}_1 = \mathbf{A}_1^T, \\ \mathbf{A}_2 &= \frac{1}{2} (\mathbf{A} - \mathbf{A}^T), \quad \mathbf{A}_2 = -\mathbf{A}_2^T \end{aligned}$$

A.4.11 Linear Transformations of Vectors

A vector valued function of a vector argument $\mathbf{f}(\mathbf{a})$ is called to be linear if $\mathbf{f}(\alpha_1\mathbf{a}_1 + \alpha_2\mathbf{a}_2) = \alpha_1\mathbf{f}(\mathbf{a}_1) + \alpha_2\mathbf{f}(\mathbf{a}_2)$ for any two vectors \mathbf{a}_1 and \mathbf{a}_2 and any two scalars α_1 and α_2 . It can be shown that any linear vector valued function can be represented by $\mathbf{f}(\mathbf{a}) = \mathbf{A} \cdot \mathbf{a}$, where \mathbf{A} is a second rank tensor. In many textbooks, e.g. Antman (1995), Smith (1993), a second rank tensor \mathbf{A} is defined to be the linear transformation of the vector space into itself.

A.4.12 Determinant and Inverse of a Second Rank Tensor

Let \mathbf{a} , \mathbf{b} and \mathbf{c} be arbitrary linearly-independent vectors. The determinant of a second rank tensor \mathbf{A} is defined by

$$\det \mathbf{A} = \frac{(\mathbf{A} \cdot \mathbf{a}) \cdot [(\mathbf{A} \cdot \mathbf{b}) \times (\mathbf{A} \cdot \mathbf{c})]}{\mathbf{a} \cdot (\mathbf{b} \times \mathbf{c})} \quad (\text{A.4.7})$$

The following identities can be verified

$$\begin{aligned} \det(\mathbf{A}^T) &= \det(\mathbf{A}), \\ \det(\mathbf{A} \cdot \mathbf{B}) &= \det(\mathbf{A}) \det(\mathbf{B}) \end{aligned}$$

The inverse of a second rank tensor \mathbf{A}^{-1} is introduced as the solution of the following equation

$$\mathbf{A}^{-1} \cdot \mathbf{A} = \mathbf{A} \cdot \mathbf{A}^{-1} = \mathbf{I}$$

\mathbf{A} is invertible if and only if $\det \mathbf{A} \neq 0$. A tensor \mathbf{A} with $\det \mathbf{A} = 0$ is called singular. Examples for singular tensors are projectors.

Applying (A.4.7) one may derive the following identities valid for a non-singular tensor \mathbf{A} and vectors \mathbf{a} and \mathbf{b} (Zhilin 2001)

$$\begin{aligned} \det \mathbf{A} \mathbf{A}^{-T} \cdot (\mathbf{a} \times \mathbf{b}) &= (\mathbf{A} \cdot \mathbf{a}) \times (\mathbf{A} \cdot \mathbf{b}), \\ \det \mathbf{A} \mathbf{A}^{-T} \cdot (\mathbf{a} \times \mathbf{I}) \cdot \mathbf{A}^{-1} &= (\mathbf{A} \cdot \mathbf{a}) \times \mathbf{I} \end{aligned} \quad (\text{A.4.8})$$

A.4.13 Principal Values and Directions of Symmetric Second Rank Tensors

Consider a dot product of a second rank tensor \mathbf{A} and a unit vector \mathbf{n} . The resulting vector $\mathbf{a} = \mathbf{A} \cdot \mathbf{n}$ differs in general from \mathbf{n} both by the length and the direction. However, one can find those unit vectors \mathbf{n} , for which $\mathbf{A} \cdot \mathbf{n}$ is collinear with \mathbf{n} , i.e.

only the length of \mathbf{n} is changed. Such vectors can be found from the equation

$$\mathbf{A} \cdot \mathbf{n} = \lambda \mathbf{n} \quad \text{or} \quad (\mathbf{A} - \lambda \mathbf{I}) \cdot \mathbf{n} = \mathbf{0} \quad (\text{A.4.9})$$

The unit vector \mathbf{n} is called the principal vector (principal direction) and the scalar λ the principal value of the tensor \mathbf{A} . The problem to find the principal values and principal directions of Eq. (A.4.9) is the eigen-value problem for \mathbf{A} . The principal values are the eigen-values, the principal directions are the eigen-directions.

Let \mathbf{A} be a symmetric tensor. In this case the principal values are real numbers and there exist at least three mutually orthogonal principal vectors. The principal values can be found as roots of the characteristic polynomial

$$\det(\mathbf{A} - \lambda \mathbf{I}) = -\lambda^3 + J_1(\mathbf{A})\lambda^2 - J_2(\mathbf{A})\lambda + J_3(\mathbf{A}) = 0 \quad (\text{A.4.10})$$

Here $J_i(\mathbf{A}) (i = 1, 2, 3)$ are the principal invariants of the tensor \mathbf{A}

$$\begin{aligned} J_1(\mathbf{A}) &= \text{tr } \mathbf{A}, \\ J_2(\mathbf{A}) &= \frac{1}{2}[(\text{tr } \mathbf{A})^2 - \text{tr } \mathbf{A}^2], \\ J_3(\mathbf{A}) &= \det \mathbf{A} = \frac{1}{6}(\text{tr } \mathbf{A})^3 - \frac{1}{2}\text{tr } \mathbf{A} \text{tr } \mathbf{A}^2 + \frac{1}{3}\text{tr } \mathbf{A}^3 \end{aligned} \quad (\text{A.4.11})$$

The principal values are specified by $\lambda_I, \lambda_{II}, \lambda_{III}$. The following three cases can be introduced

- three distinct values $\lambda_i, i = I, II, III$, i.e. $\lambda_I \neq \lambda_{II} \neq \lambda_{III}$, or
- one single value and one double solution, e.g. $\lambda_I = \lambda_{II} \neq \lambda_{III}$, or
- one triple solution $\lambda_I = \lambda_{II} = \lambda_{III}$

For a fixed solution $\lambda_i, i = I, II, III$ the eigen-directions can be found from

$$(\mathbf{A} - \lambda_i \mathbf{I}) \cdot \mathbf{n}_{(i)} = \mathbf{0} \quad (\text{A.4.12})$$

The eigen-direction is defined with respect to an arbitrary scalar multiplier.

For known principal values and principal directions the second rank tensor can be represented as follows (spectral representation)

$$\begin{aligned} \mathbf{A} &= \lambda_I \mathbf{n}_I \otimes \mathbf{n}_I + \lambda_{II} \mathbf{n}_{II} \otimes \mathbf{n}_{II} + \lambda_{III} \mathbf{n}_{III} \otimes \mathbf{n}_{III} & \text{for } \lambda_I \neq \lambda_{II} \neq \lambda_{III}, \\ \mathbf{A} &= \lambda_I (\mathbf{I} - \mathbf{n}_{III} \otimes \mathbf{n}_{III}) + \lambda_{III} \mathbf{n}_{III} \otimes \mathbf{n}_{III} & \text{for } \lambda_I = \lambda_{II} \neq \lambda_{III}, \\ \mathbf{A} &= \lambda \mathbf{I} & \text{for } \lambda_I = \lambda_{II} = \lambda_{III} = \lambda \end{aligned}$$

A.4.14 Cayley-Hamilton Theorem

Any second rank tensor satisfies the following equation

$$\mathbf{A}^3 - J_1(\mathbf{A})\mathbf{A}^2 + J_2(\mathbf{A})\mathbf{A} - J_3(\mathbf{A})\mathbf{I} = \mathbf{0}, \quad (\text{A.4.13})$$

where $\mathbf{A}^2 = \mathbf{A} \cdot \mathbf{A}$, $\mathbf{A}^3 = \mathbf{A} \cdot \mathbf{A} \cdot \mathbf{A}$. The Cayley-Hamilton theorem can be applied to compute the powers of a tensor higher than two or negative powers of a non-singular tensor. For example, the fourth power of \mathbf{A} can be computed by multiplying (A.4.13) by \mathbf{A}

$$\mathbf{A}^4 - J_1(\mathbf{A})\mathbf{A}^3 + J_2(\mathbf{A})\mathbf{A}^2 - J_3(\mathbf{A})\mathbf{A} = \mathbf{0}$$

After eliminating the third power we get

$$\mathbf{A}^4 = (J_1^2(\mathbf{A}) - J_2(\mathbf{A}))\mathbf{A}^2 + (J_3(\mathbf{A}) - J_1(\mathbf{A})J_2(\mathbf{A}))\mathbf{A} + J_1(\mathbf{A})J_3(\mathbf{A})\mathbf{I}$$

For a non-singular tensor \mathbf{A} ($\det \mathbf{A} \neq 0$) the inverse can be computed by multiplying (A.4.13) by \mathbf{A}^{-1} . As a result one obtains

$$\mathbf{A}^{-1} = [\mathbf{A}^2 - J_1(\mathbf{A})\mathbf{A} + J_2(\mathbf{A})\mathbf{I}] \frac{1}{J_3(\mathbf{A})}$$

A.4.15 Vector Invariant

The vector invariant or ‘‘Gibbsian Cross’’ of a second rank tensor \mathbf{A} is defined by

$$\mathbf{A}_\times = \left(\sum_{i=1}^3 \mathbf{a}_{(i)} \otimes \mathbf{b}_{(i)} \right)_\times = \sum_{i=1}^3 \mathbf{a}_{(i)} \times \mathbf{b}_{(i)}$$

The result of this operation is a vector. The vector invariant of a symmetric tensor is the zero vector. The following identities can be verified

$$\begin{aligned} (\mathbf{a} \times \mathbf{I})_\times &= -2\mathbf{a}, \\ \mathbf{a} \times \mathbf{I} \times \mathbf{b} &= \mathbf{b} \otimes \mathbf{a} - (\mathbf{a} \cdot \mathbf{b})\mathbf{I} \end{aligned} \quad (\text{A.4.14})$$

For any vector \mathbf{a} and any second rank tensor \mathbf{B} the following identity is valid

$$(\mathbf{a} \times \mathbf{B})_\times = \mathbf{B} \cdot \mathbf{a} - (\text{tr } \mathbf{B})\mathbf{a}, \quad (\mathbf{B} \times \mathbf{a})_\times = \mathbf{B}^T \cdot \mathbf{a} - (\text{tr } \mathbf{B})\mathbf{a} \quad (\text{A.4.15})$$

For any vector \mathbf{a} and symmetric tensors \mathbf{A}, \mathbf{B} the following identity can be established

$$\begin{aligned}
[(\mathbf{A} \times \mathbf{a}) \cdot \mathbf{B}]_{\times} &= [\mathbf{A} \cdot (\mathbf{a} \times \mathbf{B})]_{\times} = \mathbf{C} \cdot \mathbf{a}, \\
\mathbf{C} &= \sum_{i=1}^3 \lambda_i^A \hat{\mathbf{n}}_i^A \times \mathbf{B} \times \hat{\mathbf{n}}_i^A = \sum_{i=1}^3 \lambda_i^B \hat{\mathbf{n}}_i^B \times \mathbf{A} \times \hat{\mathbf{n}}_i^B \\
&= [\text{tr}(\mathbf{A} \cdot \mathbf{B}) - \text{tr} \mathbf{A} \text{tr} \mathbf{B}] \mathbf{I} + (\text{tr} \mathbf{B}) \mathbf{A} + (\text{tr} \mathbf{A}) \mathbf{B} - \mathbf{A} \cdot \mathbf{B} - \mathbf{B} \cdot \mathbf{A},
\end{aligned} \tag{A.4.16}$$

where λ_i^A and λ_i^B are principal values of the tensors \mathbf{A} and \mathbf{B} , respectively. The orthonormal vectors $\hat{\mathbf{n}}_i^A$ and $\hat{\mathbf{n}}_i^B$ are corresponding principal directions.

A.4.16 Coordinates of Second Rank Tensors

Let \mathbf{e}_i be a basis and \mathbf{e}^k the dual basis. Any two vectors \mathbf{a} and \mathbf{b} can be represented as follows

$$\mathbf{a} = a^i \mathbf{e}_i = a_j \mathbf{e}^j, \quad \mathbf{b} = b^l \mathbf{e}_l = b_m \mathbf{e}^m$$

A dyad $\mathbf{a} \otimes \mathbf{b}$ has the following representations

$$\mathbf{a} \otimes \mathbf{b} = a^i b^j \mathbf{e}_i \otimes \mathbf{e}_j = a^i b_j \mathbf{e}_i \otimes \mathbf{e}^j = a_i b_j \mathbf{e}^i \otimes \mathbf{e}^j = a_i b^j \mathbf{e}^i \otimes \mathbf{e}_j$$

For the representation of a second rank tensor \mathbf{A} one of the following four bases can be used

$$\mathbf{e}_i \otimes \mathbf{e}_j, \quad \mathbf{e}^i \otimes \mathbf{e}^j, \quad \mathbf{e}^i \otimes \mathbf{e}_j, \quad \mathbf{e}_i \otimes \mathbf{e}^j$$

With these bases one can write

$$\mathbf{A} = A^{ij} \mathbf{e}_i \otimes \mathbf{e}_j = A_{ij} \mathbf{e}^i \otimes \mathbf{e}^j = A^{i*}_j \mathbf{e}_i \otimes \mathbf{e}^j = A^{*j}_i \mathbf{e}^i \otimes \mathbf{e}_j$$

For a selected basis the coordinates of a second rank tensor can be computed as follows

$$\begin{aligned}
A^{ij} &= \mathbf{e}_i \cdot \mathbf{A} \cdot \mathbf{e}_j, \quad A_{ij} = \mathbf{e}^i \cdot \mathbf{A} \cdot \mathbf{e}^j, \\
A^{i*}_j &= \mathbf{e}_i \cdot \mathbf{A} \cdot \mathbf{e}^j, \quad A^{*j}_i = \mathbf{e}^i \cdot \mathbf{A} \cdot \mathbf{e}_j
\end{aligned}$$

A.4.17 Orthogonal Tensors

A second rank tensor \mathbf{Q} is said to be orthogonal if it satisfies the equation

$$\mathbf{Q}^T \cdot \mathbf{Q} = \mathbf{I}$$

If \mathbf{Q} operates on a vector, its length remains unchanged, i.e. let $\mathbf{b} = \mathbf{Q} \cdot \mathbf{a}$, then

$$|\mathbf{b}|^2 = \mathbf{b} \cdot \mathbf{b} = \mathbf{a} \cdot \mathbf{Q}^T \cdot \mathbf{Q} \cdot \mathbf{a} = \mathbf{a} \cdot \mathbf{a} = |\mathbf{a}|^2$$

Furthermore, the orthogonal tensor does not change the scalar product of two arbitrary vectors. For two vectors \mathbf{a} and \mathbf{b} as well as $\mathbf{a}' = \mathbf{Q} \cdot \mathbf{a}$ and $\mathbf{b}' = \mathbf{Q} \cdot \mathbf{b}$ one can calculate

$$\mathbf{a}' \cdot \mathbf{b}' = \mathbf{a} \cdot \mathbf{Q}^T \cdot \mathbf{Q} \cdot \mathbf{b} = \mathbf{a} \cdot \mathbf{b}$$

From the definition of the orthogonal tensor follows

$$\begin{aligned} \mathbf{Q}^T &= \mathbf{Q}^{-1}, & \mathbf{Q}^T \cdot \mathbf{Q} &= \mathbf{Q} \cdot \mathbf{Q}^T = \mathbf{I}, \\ \det(\mathbf{Q} \cdot \mathbf{Q}^T) &= (\det \mathbf{Q})^2 = \det \mathbf{I} = 1 & \Rightarrow & \det \mathbf{Q} = \pm 1 \end{aligned}$$

Orthogonal tensors with $\det \mathbf{Q} = 1$ are called proper orthogonal or rotation tensors. The rotation tensors are widely used in the rigid body dynamics, e.g. Zhilin (1996), and in the theories of rods, plates and shells, e.g. Altenbach and Zhilin (1988), Antman (1995).

Any orthogonal tensor is either the rotation tensor or the composition of the rotation and the tensor $-\mathbf{I}$. Let \mathbf{P} be a rotation tensor, $\det \mathbf{P} = 1$, then an orthogonal tensor \mathbf{Q} with $\det \mathbf{Q} = -1$ can be composed by

$$\mathbf{Q} = (-\mathbf{I}) \cdot \mathbf{P} = \mathbf{P} \cdot (-\mathbf{I}), \quad \det \mathbf{Q} = \det(-\mathbf{I}) \det \mathbf{P} = -1$$

For any two orthogonal tensors \mathbf{Q}_1 and \mathbf{Q}_2 the composition $\mathbf{Q}_3 = \mathbf{Q}_1 \cdot \mathbf{Q}_2$ is the orthogonal tensor, too. This property is used in the theory of symmetry and symmetry groups, e.g. Nye (1992), Zheng and Boehler (1994). Two important examples for orthogonal tensors are the

- rotation tensor about a fixed axis

$$\mathbf{Q}(\varphi \mathbf{m}) = \mathbf{m} \otimes \mathbf{m} + \cos \varphi (\mathbf{I} - \mathbf{m} \otimes \mathbf{m}) + \sin \varphi \mathbf{m} \times \mathbf{I}, \quad \det \mathbf{Q} = 1, \quad (\text{A.4.17})$$

where the unit vector \mathbf{m} represents the axis and φ is the angle of rotation,

- reflection tensor

$$\mathbf{Q} = \mathbf{I} - 2\mathbf{n} \otimes \mathbf{n}, \quad \det \mathbf{Q} = -1, \quad (\text{A.4.18})$$

where the unit vector \mathbf{n} represents the normal to the mirror plane.

One can prove the following identities (Zhilin 2001)

$$(\mathbf{Q} \cdot \mathbf{a}) \times (\mathbf{Q} \cdot \mathbf{b}) = \det \mathbf{Q} \mathbf{Q} \cdot (\mathbf{a} \times \mathbf{b}), \quad (\text{A.4.19})$$

$$\mathbf{Q} \cdot (\mathbf{a} \times \mathbf{Q}^T) = \mathbf{Q} \cdot (\mathbf{a} \times \mathbf{I}) \cdot \mathbf{Q}^T = \det \mathbf{Q} [(\mathbf{Q} \cdot \mathbf{a}) \times \mathbf{I}] \quad (\text{A.4.20})$$

A.4.18 Polar Decomposition

Any regular second rank tensor \mathbf{A} with $\det \mathbf{A} > 0$ can be represented in a unique manner as following polar decompositions of the positive-semidefinite symmetric tensors \mathbf{U} or \mathbf{V} and a rotation tensor \mathbf{R}

$$\mathbf{A} = \mathbf{R} \cdot \mathbf{U} = \mathbf{V} \cdot \mathbf{R} \quad (\text{A.4.21})$$

$\mathbf{R} \cdot \mathbf{U}$ is the right and $\mathbf{V} \cdot \mathbf{R}$ the left polar decomposition. The following statements are valid

- \mathbf{R} is the proper orthogonal tensor: $\mathbf{R} \cdot \mathbf{R}^T = \mathbf{I}$, $\det \mathbf{R} = +1$.
- \mathbf{U} and \mathbf{V} are symmetric, positive-semidefinite tensors:

$$\mathbf{U} = \mathbf{U}^T, \quad \mathbf{V} = \mathbf{V}^T, \quad (\mathbf{U} \cdot \mathbf{a}) \cdot \mathbf{a} > 0, \quad (\mathbf{V} \cdot \mathbf{b}) \cdot \mathbf{b} > 0$$

\mathbf{a}, \mathbf{b} are arbitrary non-zero vectors.

- \mathbf{U}, \mathbf{V} can be uniquely computed from \mathbf{F} .
- The eigen-values of the tensors \mathbf{U} and \mathbf{V} are the same. If $\boldsymbol{\eta}$ is an eigen-vector of \mathbf{U} , then $\mathbf{R} \cdot \boldsymbol{\eta}$ is an eigen-vector of \mathbf{V} .

The proof of the statements is elementary. For any tensor \mathbf{A} and vector $\mathbf{a} \neq \mathbf{0}$ we can write

$$(\mathbf{A} \cdot \mathbf{a}) \cdot (\mathbf{A} \cdot \mathbf{a}) = \mathbf{a} \cdot (\mathbf{A}^T \cdot \mathbf{A}) \cdot \mathbf{a} > 0$$

Hence $\mathbf{A}^T \cdot \mathbf{A}$ is a symmetric positive-semidefinite tensor. Therefore the tensors $\mathbf{U} = (\mathbf{A}^T \cdot \mathbf{A})^{1/2}$ and \mathbf{U}^{-1} are also symmetric and positive-semidefinite. The orthogonality of \mathbf{R} follows from

$$\begin{aligned} \mathbf{R} \cdot \mathbf{R}^T &= (\mathbf{A} \cdot \mathbf{U}^{-1}) \cdot (\mathbf{A} \cdot \mathbf{U}^{-1})^T = \mathbf{A} \cdot \mathbf{U}^{-2} \cdot \mathbf{A}^T = \mathbf{A} \cdot (\mathbf{U}^2)^{-1} \cdot \mathbf{A}^T \\ &= \mathbf{A} \cdot (\mathbf{A}^T \cdot \mathbf{A})^{-1} \cdot \mathbf{A}^T = \mathbf{A} \cdot \left[\mathbf{A}^{-1} \cdot (\mathbf{A}^T)^{-1} \right] \cdot \mathbf{A}^T \\ &= (\mathbf{A} \cdot \mathbf{A}^{-1}) \cdot \left[(\mathbf{A}^T)^{-1} \cdot \mathbf{A}^T \right] = \mathbf{I} \cdot \mathbf{I} = \mathbf{I} \end{aligned}$$

With $\det \mathbf{F} > 0$ we obtain $\det \mathbf{U}^{-1} > 0$ and it follows $\det \mathbf{R} = \det \mathbf{A} \det \mathbf{U}^{-1} > 0$. The orthogonality condition $\mathbf{R} \cdot \mathbf{R}^T = \mathbf{I}$ yields $\det (\mathbf{R} \cdot \mathbf{R}^T) = (\det \mathbf{R})^2 = +1$ and $\det \mathbf{R} = +1$. The proof of the uniqueness can be given as follows. From $\mathbf{A} = \mathbf{R} \cdot \mathbf{U} = \mathbf{R}_1 \cdot \mathbf{U}_1$ it follows $(\mathbf{R} \cdot \mathbf{U})^T = (\mathbf{R}_1 \cdot \mathbf{U}_1)^T$. Hence

$$\mathbf{U} = \mathbf{U}^T, \quad \mathbf{U}_1 = \mathbf{U}_1^T, \quad \mathbf{U} \cdot \mathbf{R}^T = \mathbf{U}_1 \cdot \mathbf{R}_1^T$$

Finally,

$$\begin{aligned} \mathbf{U}^2 &= \mathbf{U} \cdot (\mathbf{R}^T \cdot \mathbf{R}) \cdot \mathbf{U} = (\mathbf{U} \cdot \mathbf{R}^T) \cdot (\mathbf{R} \cdot \mathbf{U}) \\ &= (\mathbf{U}_1 \cdot \mathbf{R}_1^T) \cdot (\mathbf{R}_1 \cdot \mathbf{U}_1) = \mathbf{U}_1 \cdot (\mathbf{R}_1^T \cdot \mathbf{R}_1) \cdot \mathbf{U}_1 = \mathbf{U}_1^2, \end{aligned}$$

that means $\mathbf{U} = \mathbf{U}_1$. The proof of the second decomposition is similar. For $\mathbf{F} = \mathbf{V} \cdot \mathbf{R}$ with $\mathbf{V} = (\mathbf{F} \cdot \mathbf{F}^T)^{1/2}$ we obtain

$$\begin{aligned} \mathbf{V}^2 &= \mathbf{F} \cdot \mathbf{F}^T = (\mathbf{R} \cdot \mathbf{U}) \cdot (\mathbf{R} \cdot \mathbf{U})^T = \mathbf{R} \cdot \mathbf{U}^2 \cdot \mathbf{R}^T = (\mathbf{R} \cdot \mathbf{U}) \cdot (\mathbf{R}^T \cdot \mathbf{R}) \cdot (\mathbf{U} \cdot \mathbf{R}^T) \\ &= (\mathbf{R} \cdot \mathbf{U} \cdot \mathbf{R}^T) \cdot (\mathbf{R} \cdot \mathbf{U} \cdot \mathbf{R}^T) = (\mathbf{R} \cdot \mathbf{U} \cdot \mathbf{R}^T)^2, \\ \mathbf{V} &= \mathbf{R} \cdot \mathbf{U} \cdot \mathbf{R}^T \implies \mathbf{V} \cdot \mathbf{R} = \mathbf{R} \cdot \mathbf{U} \cdot (\mathbf{R}^T \cdot \mathbf{R}) = \mathbf{R} \cdot \mathbf{U} = \mathbf{F} \end{aligned}$$

If $\boldsymbol{\eta}$ and λ are eigen-vector and eigen-value of \mathbf{U} , then $\lambda \boldsymbol{\eta} = \mathbf{U} \cdot \boldsymbol{\eta}$ and

$$\lambda(\mathbf{R} \cdot \boldsymbol{\eta}) = (\mathbf{R} \cdot \mathbf{U}) \cdot \boldsymbol{\eta} = (\mathbf{V} \cdot \mathbf{R}) \cdot \boldsymbol{\eta} = \mathbf{V} \cdot (\mathbf{R} \cdot \boldsymbol{\eta})$$

\mathbf{U} and \mathbf{V} have the same eigen-value λ and $\boldsymbol{\eta}$ or $\mathbf{R} \cdot \boldsymbol{\eta}$ are the eigen-vectors of \mathbf{U} and \mathbf{V} , respectively.

References

- Altenbach H (2015) Kontinuumsmechanik - Einführung in die materialunabhängigen und materialabhängigen Gleichungen. Springer Vieweg, Berlin, Heidelberg
- Altenbach H, Zhilin PA (1988) Osnovnye uravneniya neklassicheskoi teorii uprugikh obolochek (Basic equations of a non-classical theory of elastic shells, in Russ.). Adv Mech 11:107–148
- Altenbach H, Naumenko K, Zhilin P (2003) A micro-polar theory for binary media with application to phase-transitional flow of fiber suspensions. Continuum Mech Thermodyn 15:539–570
- Altenbach H, Naumenko K, Pylypenko S, Renner B (2007) Influence of rotary inertia on the fiber dynamics in homogeneous creeping flows. ZAMM-J Appl Math Mech/Zeitschrift für Angewandte Mathematik und Mechanik 87(2):81–93
- Antman S (1995) Nonlinear problems of elasticity. Springer, Berlin
- Bellmann R (1970) Introduction to matrix analysis. McGraw Hill, New York
- Besseling JF, van der Giessen E (1994) Mathematical modelling of inelastic deformation. Chapman and Hall, London
- Betten J (1987) Tensorrechnung für Ingenieure. Springer, Berlin
- de Boer R (1982) Vektor und Tensorrechnung für Ingenieure. Springer, Berlin
- Eringen AC (1999) Microcontinuum field theories, vol I: Foundations and Solids. Springer, New York
- Faddejew DK, Faddejewa WN (1964) Numerische Methoden der linearen Algebra. Deutscher Verlag der Wissenschaften, Berlin
- Giesekus H (1994) Phänomenologische Rheologie. Springer, Berlin
- Haupt P (2002) Continuum mechanics and theory of materials. Springer, Berlin
- Lagally M (1962) Vorlesungen über Vektorrechnung. Geest and Portig, Leipzig
- Lebedev LP, Cloud MJ, Eremeyev VA (2010) Tensor analysis with applications in mechanics. World Scientific

- Lippmann H (1993) *Angewandte Tensorrechnung*. Springer, Berlin
- Lurie AI (1990) *Nonlinear theory of elasticity*. North-Holland, Dordrecht
- Naumenko K, Eremeyev VA (2014) A layer-wise theory for laminated glass and photovoltaic panels. *Compos Struct* 112:283–291
- Nowacki W (1986) *Theory of asymmetric elasticity*. Pergamon Press, Oxford
- Nye JF (1992) *Physical properties of crystals*. Oxford Science Publications, Oxford
- Palmov V (1998) *Vibrations in elasto-plastic bodies*. Springer, Berlin
- Smith DR (1993) *An introduction to continuum mechanics*. Kluwer, Dordrecht
- Trostel R (1993) *Mathematische Grundlagen der Technischen Mechanik*, vol I: Vektor- und Tensoralgebra. Vieweg, Braunschweig
- Truesdell C, Noll W (1992) *The non-linear field theories of mechanics*, 2nd edn. Springer, Berlin
- Wilson EB (1901) *Vector analysis, founded upon the lectures of G. W. Gibbs*. Yale University Press, New Haven
- Zheng QS, Boehler JP (1994) The description, classification and reality of material and physical symmetries. *Acta Mech* 102:73–89
- Zhilin PA (1996) A new approach to the analysis of free rotations of rigid bodies. *ZAMM-J Appl Math Mech/Zeitschrift für Angewandte Mathematik und Mechanik* 76(4):187–204
- Zhilin PA (2001) Vektory i tensory vtorogo ranga v trekhmernom prostranstve (Vectors and second rank tensors in three-dimensional space, in Russ.). Nestor, St. Petersburg
- Zurmühl R, Falk S (1992) *Matrizen und ihre Anwendungen*. Springer, Berlin

Appendix B

Elements of Tensor Analysis

B.1 Coordinate Systems

The vector \mathbf{r} characterizing the position of a point \mathbf{P} can be represented by use of the Cartesian coordinates x_i as follows, Fig. B.1,

$$\mathbf{r}(x^1, x^2, x^3) = x^1 \mathbf{e}_1 + x^2 \mathbf{e}_2 + x^3 \mathbf{e}_3 = x^i \mathbf{e}_i$$

Instead of coordinates x^i one can introduce any triple of curvilinear coordinates q^1, q^2, q^3 by means of one-to-one transformations

$$x^k = x^k(q^1, q^2, q^3) \Leftrightarrow q^k = q^k(x^1, x^2, x^3)$$

It is assumed that the above transformations are continuous and continuous differentiable as many times as necessary and for the Jacobians

$$\det \left(\frac{\partial x^k}{\partial q^i} \right) \neq 0, \quad \det \left(\frac{\partial q^i}{\partial x^k} \right) \neq 0$$

must be valid. With these assumptions the position vector can be considered as a function of curvilinear coordinates q^i , i.e. $\mathbf{r} = \mathbf{r}(q^1, q^2, q^3)$. Surfaces $q^1 = \text{const}$, $q^2 = \text{const}$, and $q^3 = \text{const}$, Fig. B.1, are called coordinate surfaces. For given fixed values $q^2 = q^2_*$ and $q^3 = q^3_*$ a curve can be obtained along which only q^1 varies. This curve is called the q^1 -coordinate line, Fig. B.1. Analogously, one can obtain the q^2 - and q^3 -coordinate lines.

The partial derivatives of the position vector with respect the to selected coordinates

$$\mathbf{r}_1 = \frac{\partial \mathbf{r}}{\partial q^1}, \quad \mathbf{r}_2 = \frac{\partial \mathbf{r}}{\partial q^2}, \quad \mathbf{r}_3 = \frac{\partial \mathbf{r}}{\partial q^3}, \quad \mathbf{r}_1 \cdot (\mathbf{r}_2 \times \mathbf{r}_3) \neq 0$$

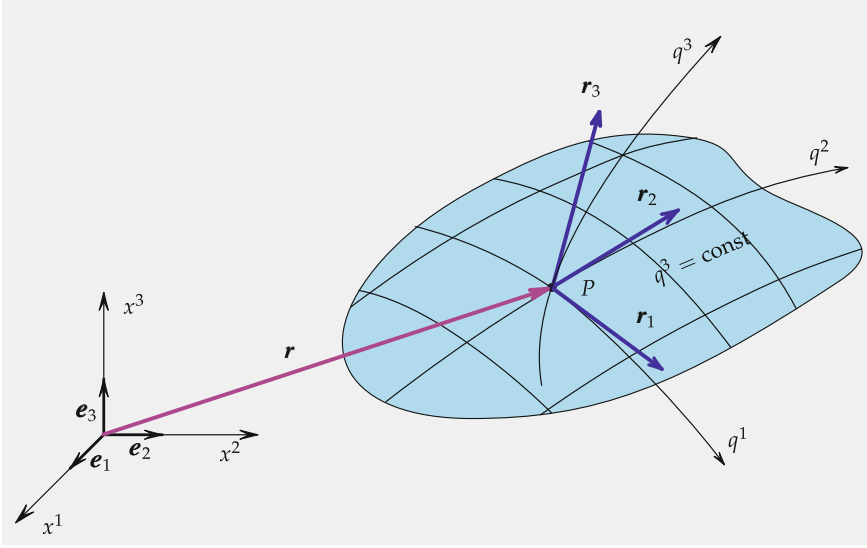


Fig. B.1 Cartesian and curvilinear coordinates

define the tangential vectors to the coordinate lines in a point P , Fig. B.1. The vectors \mathbf{r}_i are used as the local basis in the point P . By use of (A.3.4) the dual basis \mathbf{r}^k can be introduced. The vector $d\mathbf{r}$ connecting the point P with a point P' in the differential neighborhood of P is defined by

$$d\mathbf{r} = \frac{\partial \mathbf{r}}{\partial q^1} dq^1 + \frac{\partial \mathbf{r}}{\partial q^2} dq^2 + \frac{\partial \mathbf{r}}{\partial q^3} dq^3 = \mathbf{r}_k dq^k$$

The square of the arc length of the line element in the differential neighborhood of P is calculated by

$$ds^2 = d\mathbf{r} \cdot d\mathbf{r} = (\mathbf{r}_i dq^i) \cdot (\mathbf{r}_k dq^k) = g_{ik} dq^i dq^k,$$

where $g_{ik} \equiv \mathbf{r}_i \cdot \mathbf{r}_k$ are the so-called contravariant components of the metric tensor. With g_{ik} one can represent the basis vectors \mathbf{r}_i by the dual basis vectors \mathbf{r}^k as follows

$$\mathbf{r}_i = (\mathbf{r}_i \cdot \mathbf{r}_k) \mathbf{r}^k = g_{ik} \mathbf{r}^k$$

Similarly

$$\mathbf{r}^i = (\mathbf{r}^i \cdot \mathbf{r}^k) \mathbf{r}_k = g^{ik} \mathbf{r}_k, \quad g^{ik} \equiv \mathbf{r}^i \cdot \mathbf{r}^k,$$

where g^{ik} are termed covariant components of the metric tensor. For the selected bases \mathbf{r}_i and \mathbf{r}^k the second rank unit tensor has the following representations

$$\mathbf{I} = \mathbf{r}_i \otimes \mathbf{r}^i = \mathbf{r}_i \otimes g^{ik} \mathbf{r}_k = g^{ik} \mathbf{r}_i \otimes \mathbf{r}_k = g_{ik} \mathbf{r}^i \otimes \mathbf{r}^k = \mathbf{r}^i \otimes \mathbf{r}_i$$

B.2 Hamilton (Nabla) Operator

A scalar field is a function which assigns a scalar to each spatial point P for the domain of definition. Let us consider a scalar field $\varphi(\mathbf{r}) = \varphi(q^1, q^2, q^3)$. The total differential of φ by moving from a point P to a point P' in the differential neighborhood is

$$d\varphi = \frac{\partial\varphi}{\partial q^1}dq^1 + \frac{\partial\varphi}{\partial q^2}dq^2 + \frac{\partial\varphi}{\partial q^3}dq^3 = \frac{\partial\varphi}{\partial q^k}dq^k$$

Taking into account that $dq^k = d\mathbf{r} \cdot \mathbf{r}^k$

$$d\varphi = d\mathbf{r} \cdot \mathbf{r}^k \frac{\partial\varphi}{\partial q^k} = d\mathbf{r} \cdot \nabla\varphi$$

The vector $\nabla\varphi$ is called the gradient of the scalar field φ and the invariant operator ∇ (the Hamilton or nabla operator) is defined by

$$\nabla = \mathbf{r}^k \frac{\partial}{\partial q^k}$$

For a vector field $\mathbf{a}(\mathbf{r})$ one may write

$$\begin{aligned} d\mathbf{a} &= (d\mathbf{r} \cdot \mathbf{r}^k) \frac{\partial\mathbf{a}}{\partial q^k} = d\mathbf{r} \cdot \mathbf{r}^k \otimes \frac{\partial\mathbf{a}}{\partial q^k} = d\mathbf{r} \cdot \nabla \otimes \mathbf{a} = (\nabla \otimes \mathbf{a})^T \cdot d\mathbf{r}, \\ \nabla \otimes \mathbf{a} &= \mathbf{r}^k \otimes \frac{\partial\mathbf{a}}{\partial q^k} \end{aligned}$$

The gradient of a vector field is a second rank tensor. The operation ∇ can be applied to tensors of any rank. For vectors the following additional operations are defined

$$\begin{aligned} \text{div} \mathbf{a} &\equiv \nabla \cdot \mathbf{a} = \mathbf{r}^k \cdot \frac{\partial\mathbf{a}}{\partial q^k}, \\ \text{rota} \mathbf{a} &\equiv \nabla \times \mathbf{a} = \mathbf{r}^k \times \frac{\partial\mathbf{a}}{\partial q^k} \end{aligned}$$

The divergence and the rotation (curl) of tensor fields of any rank higher 1 can be calculated in a similar manner.

The following identities can be verified

$$\nabla \otimes \mathbf{r} = \mathbf{r}^k \otimes \frac{\partial\mathbf{r}}{\partial q^k} = \mathbf{r}^k \otimes \mathbf{r}_k = \mathbf{I}, \quad \nabla \cdot \mathbf{r} = 3$$

For a scalar α , a vector \mathbf{a} and for a second rank tensor \mathbf{A} the following identities are valid

$$\nabla(\alpha \mathbf{a}) = \mathbf{r}^k \otimes \frac{\partial(\alpha \mathbf{a})}{\partial q^k} = \left(\mathbf{r}^k \frac{\partial \alpha}{\partial q^k} \right) \otimes \mathbf{a} + \alpha \mathbf{r}^k \otimes \frac{\partial \mathbf{a}}{\partial q^k} = (\nabla \alpha) \otimes \mathbf{a} + \alpha \nabla \otimes \mathbf{a}, \quad (\text{B.2.1})$$

$$\begin{aligned} \nabla \cdot (\mathbf{A} \cdot \mathbf{a}) &= \mathbf{r}^k \cdot \frac{\partial(\mathbf{A} \cdot \mathbf{a})}{\partial q^k} = \mathbf{r}^k \cdot \frac{\partial \mathbf{A}}{\partial q^k} \cdot \mathbf{a} + \mathbf{r}^k \cdot \mathbf{A} \cdot \frac{\partial \mathbf{a}}{\partial q^k} \\ &= (\nabla \cdot \mathbf{A}) \cdot \mathbf{a} + \mathbf{A} \cdot \left(\frac{\partial \mathbf{a}}{\partial q^k} \otimes \mathbf{r}^k \right) \\ &= (\nabla \cdot \mathbf{A}) \cdot \mathbf{a} + \mathbf{A} \cdot (\nabla \otimes \mathbf{a})^T \end{aligned} \quad (\text{B.2.2})$$

For a second rank tensor \mathbf{A} and a position vector \mathbf{r} one can prove the following identity

$$\begin{aligned} \nabla \cdot (\mathbf{A} \times \mathbf{r}) &= \mathbf{r}^k \cdot \frac{\partial(\mathbf{A} \times \mathbf{r})}{\partial q^k} = \mathbf{r}^k \cdot \frac{\partial \mathbf{A}}{\partial q^k} \times \mathbf{r} + \mathbf{r}^k \cdot \mathbf{A} \times \frac{\partial \mathbf{r}}{\partial q^k} \\ &= (\nabla \cdot \mathbf{A}) \times \mathbf{r} + \mathbf{r}^k \cdot \mathbf{A} \times \mathbf{r}_k = (\nabla \cdot \mathbf{A}) \times \mathbf{r} - \mathbf{A} \times \end{aligned} \quad (\text{B.2.3})$$

Here we used the definition of the vector invariant as follows

$$\mathbf{A} \times = (\mathbf{r}_k \otimes \mathbf{r}^k \cdot \mathbf{A}) \times = \mathbf{r}_k \times (\mathbf{r}^k \cdot \mathbf{A}) = -\mathbf{r}^k \cdot \mathbf{A} \times \mathbf{r}_k$$

B.3 Integral Theorems

Let $\varphi(\mathbf{r})$, $\mathbf{a}(\mathbf{r})$ and $\mathbf{A}(\mathbf{r})$ be continuously differentiable scalar, vector and second rank tensor fields. Let V be the volume of a bounded domain with a regular surface $A(V)$ and \mathbf{n} be the outer unit normal to the surface at \mathbf{r} . The integral theorems can be summarized as follows

- Gradient Theorems

$$\begin{aligned} \int_V \nabla \varphi \, dV &= \int_{A(V)} \mathbf{n} \varphi \, dA, \\ \int_V \nabla \otimes \mathbf{a} \, dV &= \int_{A(V)} \mathbf{n} \otimes \mathbf{a} \, dA, \\ \int_V \nabla \otimes \mathbf{A} \, dV &= \int_{A(V)} \mathbf{n} \otimes \mathbf{A} \, dA \end{aligned} \quad (\text{B.3.4})$$

- Divergence Theorems

$$\int_V \nabla \cdot \mathbf{a} \, dV = \int_{A(V)} \mathbf{n} \cdot \mathbf{a} \, dA, \tag{B.3.5}$$

$$\int_V \nabla \cdot \mathbf{A} \, dV = \int_{A(V)} \mathbf{n} \cdot \mathbf{A} \, dA$$

• Curl Theorems

$$\int_V \nabla \times \mathbf{a} \, dV = \int_{A(V)} \mathbf{n} \times \mathbf{a} \, dA, \tag{B.3.6}$$

$$\int_V \nabla \times \mathbf{A} \, dV = \int_{A(V)} \mathbf{n} \times \mathbf{A} \, dA$$

Based on the first equation in (B.3.5) and Eq. (B.2.2) the following formula can be derived

$$\int_{A(V)} \mathbf{n} \cdot \mathbf{A} \cdot \mathbf{a} \, dA = \int_V \nabla \cdot (\mathbf{A} \cdot \mathbf{a}) \, dV = \int_V [(\nabla \cdot \mathbf{A}) \cdot \mathbf{a} + \mathbf{A} \cdot (\nabla \otimes \mathbf{a})^T] \, dV \tag{B.3.7}$$

With the second equation in (B.3.5) and Eq. (B.2.3) the following relation can be obtained

$$\begin{aligned} \int_{A(V)} \mathbf{r} \times (\mathbf{n} \cdot \mathbf{A}) \, dA &= - \int_{A(V)} \mathbf{n} \cdot \mathbf{A} \times \mathbf{r} \, dA \\ &= - \int_V \nabla \cdot (\mathbf{A} \times \mathbf{r}) \, dV \\ &= \int_V [\mathbf{r} \times (\nabla \cdot \mathbf{A}) + \mathbf{A} \times] \, dV \end{aligned} \tag{B.3.8}$$

B.4 Scalar-Valued Functions of Vectors and Second Rank Tensors

Let ψ be a scalar valued function of a vector \mathbf{a} and a second rank tensor \mathbf{A} , i.e. $\psi = \psi(\mathbf{a}, \mathbf{A})$. Introducing a basis \mathbf{e}_i the function ψ can be represented as follows

$$\psi(\mathbf{a}, \mathbf{A}) = \psi(a^i \mathbf{e}_i, A^{ij} \mathbf{e}_i \otimes \mathbf{e}_j) = \psi(a^i, A^{ij})$$

The partial derivatives of ψ with respect to \mathbf{a} and \mathbf{A} are defined according to the following rule

$$\begin{aligned} d\psi &= \frac{\partial\psi}{\partial a^i} da^i + \frac{\partial\psi}{\partial A^{ij}} dA^{ij} \\ &= d\mathbf{a} \cdot \mathbf{e}^i \frac{\partial\psi}{\partial a^i} + d\mathbf{A} \cdot \mathbf{e}^j \otimes \mathbf{e}^i \frac{\partial\psi}{\partial A^{ij}} \end{aligned} \quad (\text{B.4.9})$$

In the coordinate-free form the above rule can be rewritten as follows

$$d\psi = d\mathbf{a} \cdot \frac{\partial\psi}{\partial \mathbf{a}} + d\mathbf{A} \cdot \left(\frac{\partial\psi}{\partial \mathbf{A}} \right)^T = d\mathbf{a} \cdot \psi_{,\mathbf{a}} + d\mathbf{A} \cdot (\psi_{,\mathbf{A}})^T \quad (\text{B.4.10})$$

with

$$\psi_{,\mathbf{a}} \equiv \frac{\partial\psi}{\partial \mathbf{a}} = \frac{\partial\psi}{\partial a^i} \mathbf{e}^i, \quad \psi_{,\mathbf{A}} \equiv \frac{\partial\psi}{\partial \mathbf{A}} = \frac{\partial\psi}{\partial A^{ij}} \mathbf{e}^i \otimes \mathbf{e}^j$$

It can be verified that $\psi_{,\mathbf{a}}$ and $\psi_{,\mathbf{A}}$ are independent from the choice of the basis. As an example let us calculate the partial derivatives of the function

$$\psi(\mathbf{a}, \mathbf{b}, \mathbf{A}) = \mathbf{a} \cdot \mathbf{A} \cdot \mathbf{b}$$

with respect to \mathbf{a} , \mathbf{b} and \mathbf{A} . With

$$\begin{aligned} d\psi &= d\mathbf{a} \cdot \mathbf{A} \cdot \mathbf{b} + \mathbf{a} \cdot d\mathbf{A} \cdot \mathbf{b} + \mathbf{a} \cdot \mathbf{A} \cdot d\mathbf{b} \\ &= d\mathbf{a} \cdot \mathbf{A} \cdot \mathbf{b} + d\mathbf{A} \cdot (\mathbf{b} \otimes \mathbf{a}) + d\mathbf{b} \cdot (\mathbf{a} \cdot \mathbf{A}) \\ &= d\mathbf{a} \cdot \psi_{,\mathbf{a}} + d\mathbf{A} \cdot (\psi_{,\mathbf{A}})^T + d\mathbf{b} \cdot \psi_{,\mathbf{b}} \end{aligned}$$

we obtain

$$\psi_{,\mathbf{a}} = \mathbf{A} \cdot \mathbf{b}, \quad \psi_{,\mathbf{b}} = \mathbf{a} \cdot \mathbf{A}, \quad \psi_{,\mathbf{A}} = \mathbf{a} \otimes \mathbf{b}$$

Let us calculate the derivatives of the functions $J_1(\mathbf{A}^k) = \text{tr } \mathbf{A}^k$, $k = 1, 2, 3$ with respect to \mathbf{A} . With

$$J_1(\mathbf{A}) = \mathbf{A} \cdot \mathbf{I}, \quad J_1(\mathbf{A}^2) = \mathbf{A} \cdot \mathbf{A}, \quad J_1(\mathbf{A}^3) = \mathbf{A} \cdot (\mathbf{A} \cdot \mathbf{A})$$

we can write

$$dJ_1(\mathbf{A}) = d\mathbf{A} \cdot \mathbf{I}, \quad dJ_1(\mathbf{A}^2) = 2d\mathbf{A} \cdot \mathbf{A}, \quad dJ_1(\mathbf{A}^3) = 3d\mathbf{A} \cdot (\mathbf{A} \cdot \mathbf{A})$$

Consequently

$$J_1(\mathbf{A})_{,\mathbf{A}} = \mathbf{I}, \quad J_1(\mathbf{A}^2)_{,\mathbf{A}} = 2\mathbf{A}^T, \quad J_1(\mathbf{A}^3)_{,\mathbf{A}} = 3\mathbf{A}^{2T} \quad (\text{B.4.11})$$

With (B.4.11) the derivatives of principal invariants of a second rank tensor \mathbf{A} can be calculated as follows

$$\begin{aligned} J_1(\mathbf{A})_{,\mathbf{A}} &= \mathbf{I}, \\ J_2(\mathbf{A})_{,\mathbf{A}} &= J_1(\mathbf{A})\mathbf{I} - \mathbf{A}^T, \\ J_3(\mathbf{A})_{,\mathbf{A}} &= \mathbf{A}^{2T} - J_1(\mathbf{A})\mathbf{A}^T + J_2(\mathbf{A})\mathbf{I} = J_3(\mathbf{A})(\mathbf{A}^T)^{-1} \end{aligned} \quad (\text{B.4.12})$$

To find the derivative of the function $\psi(\mathbf{A}) = \psi(J_1(\mathbf{A}), J_2(\mathbf{A}), J_3(\mathbf{A}))$ with respect to \mathbf{A} we may write

$$d\psi = d\mathbf{A} \cdot \left[\frac{\partial\psi}{\partial J_1} \left(J_1(\mathbf{A})_{,\mathbf{A}} \right)^T + \frac{\partial\psi}{\partial J_2} \left(J_2(\mathbf{A})_{,\mathbf{A}} \right)^T + \frac{\partial\psi}{\partial J_3} \left(J_3(\mathbf{A})_{,\mathbf{A}} \right)^T \right]$$

Taking into account (B.4.12) we obtain

$$\begin{aligned} \psi \left(J_1(\mathbf{A}), J_2(\mathbf{A}), J_3(\mathbf{A}) \right)_{,\mathbf{A}} &= \left(\frac{\partial\psi}{\partial J_1} + J_1 \frac{\partial\psi}{\partial J_2} + J_2 \frac{\partial\psi}{\partial J_3} \right) \mathbf{I} \\ &\quad - \left(\frac{\partial\psi}{\partial J_2} + J_1 \frac{\partial\psi}{\partial J_3} \right) \mathbf{A}^T + \frac{\partial\psi}{\partial J_3} \mathbf{A}^{T^2} \end{aligned} \quad (\text{B.4.13})$$

B.5 Orthogonal Transformations and Orthogonal Invariants

An application of the theory of tensor functions is to find a basic set of scalar invariants for a given group of symmetry transformations, such that each invariant relative to the same group is expressible as a single-valued function of the basic set. The basic set of invariants is called functional basis. To obtain a compact representation for invariants, it is required that the functional basis is irreducible in the sense that removing any one invariant from the basis will imply that a complete representation for all the invariants is no longer possible.

Such a problem arises in the formulation of constitutive equations for a given group of material symmetries. For example, the strain energy density of an elastic non-polar material is a scalar valued function of the second rank symmetric strain tensor. In the theory of the Cosserat continuum two strain measures are introduced, where the first strain measure is a polar tensor while the second one is an axial tensor, e.g. Eringen (1999). The strain energy density of a thin elastic shell is a function of two second rank tensors and one vector, e.g. Altenbach and Zhilin (1988), Altenbach et al. (2005). In all cases the problem is to find a minimum set of functionally independent invariants for the considered tensorial arguments.

For the theory of tensor functions we refer to Boehler (1987). Representations of tensor functions are reviewed in Rychlewski and Zhang (1991), Zheng (1994). An orthogonal transformation of a scalar α , a vector \mathbf{a} and a second rank tensor \mathbf{A} is

defined by Altenbach and Zhilin (1988), Zhilin (1982)

$$\alpha' \equiv (\det \mathbf{Q})^\zeta \alpha, \quad \mathbf{a}' \equiv (\det \mathbf{Q})^\zeta \mathbf{Q} \cdot \mathbf{a}, \quad \mathbf{A}' \equiv (\det \mathbf{Q})^\zeta \mathbf{Q} \cdot \mathbf{A} \cdot \mathbf{Q}^T, \quad (\text{B.5.14})$$

where \mathbf{Q} is an orthogonal tensor, $\zeta = 0$ for absolute (polar) scalars, vectors and tensors and $\zeta = 1$ for axial ones. An example of the axial scalar is the mixed product of three polar vectors, i.e. $\alpha = \mathbf{a} \cdot (\mathbf{b} \times \mathbf{c})$. A typical example of the axial vector is the cross product of two polar vectors, i.e. $\mathbf{c} = \mathbf{a} \times \mathbf{b}$. An example of the second rank axial tensor is the skew-symmetric tensor $\mathbf{W} = \mathbf{a} \times \mathbf{I}$, where \mathbf{a} is a polar vector. Consider a group of orthogonal transformations S (e.g., the material symmetry transformations) characterized by a set of orthogonal tensors \mathbf{Q} . A scalar-valued function of a second rank tensor $f = f(\mathbf{A})$ is called to be an orthogonal invariant under the group S if

$$\forall \mathbf{Q} \in S : \quad f(\mathbf{A}') = (\det \mathbf{Q})^\eta f(\mathbf{A}), \quad (\text{B.5.15})$$

where $\eta = 0$ if values of f are absolute scalars and $\eta = 1$ if values of f are axial scalars.

Any second rank tensor \mathbf{B} can be decomposed into a symmetric and a skew-symmetric part, i.e. $\mathbf{B} = \mathbf{A} + \mathbf{a} \times \mathbf{I}$, where \mathbf{A} is a symmetric tensor and \mathbf{a} is an associated vector. Therefore $f(\mathbf{B}) = f(\mathbf{A}, \mathbf{a})$. If \mathbf{B} is a polar (axial) tensor, then \mathbf{a} is an axial (polar) vector. For the set of symmetric second rank tensors and vectors the definition of an orthogonal invariant (B.5.15) can be generalized as follows

$$\begin{aligned} \forall \mathbf{Q} \in S : \quad f(\mathbf{A}'_1, \mathbf{A}'_2, \dots, \mathbf{A}'_n, \mathbf{a}'_1, \mathbf{a}'_2, \dots, \mathbf{a}'_k) \\ = (\det \mathbf{Q})^\eta f(\mathbf{A}_1, \mathbf{A}_2, \dots, \mathbf{A}_n, \mathbf{a}_1, \mathbf{a}_2, \dots, \mathbf{a}_k) \end{aligned} \quad (\text{B.5.16})$$

B.6 Invariants for the Full Orthogonal Group

In Zhilin (2003) orthogonal invariants for different sets of second rank tensors and vectors with respect to the full orthogonal group are presented. It is shown that orthogonal invariants are integrals of a generic partial differential equation (basic equations for invariants). Let us present two following examples

- Orthogonal invariants of a symmetric second rank tensor \mathbf{A} are

$$I_k = \text{tr } \mathbf{A}^k, \quad k = 1, 2, 3$$

Instead of I_k it is possible to use the principal invariants J_k defined by (A.4.11).

- Orthogonal invariants of a symmetric second rank tensor \mathbf{A} and a vector \mathbf{a} are

$$\begin{aligned} I_k = \text{tr } \mathbf{A}^k, \quad k = 1, 2, 3, \quad I_4 = \mathbf{a} \cdot \mathbf{a}, \quad I_5 = \mathbf{a} \cdot \mathbf{A} \cdot \mathbf{a}, \\ I_6 = \mathbf{a} \cdot \mathbf{A}^2 \cdot \mathbf{a}, \quad I_7 = \mathbf{a} \cdot \mathbf{A}^2 \cdot (\mathbf{a} \times \mathbf{A} \cdot \mathbf{a}) \end{aligned} \quad (\text{B.6.17})$$

In the above set of invariants only 6 are functionally independent. The relation between the invariants (so-called syzygy) can be formulated as follows

$$I_7^2 = \begin{vmatrix} I_4 & I_5 & I_6 \\ I_5 & I_6 & \mathbf{a} \cdot \mathbf{A}^3 \cdot \mathbf{a} \\ I_6 & \mathbf{a} \cdot \mathbf{A}^3 \cdot \mathbf{a} & \mathbf{a} \cdot \mathbf{A}^4 \cdot \mathbf{a} \end{vmatrix}, \tag{B.6.18}$$

where $\mathbf{a} \cdot \mathbf{A}^3 \cdot \mathbf{a}$ and $\mathbf{a} \cdot \mathbf{A}^4 \cdot \mathbf{a}$ can be expressed by $I_l, l = 1, \dots, 6$ applying the Cayley-Hamilton theorem (A.4.13).

The set of invariants for a symmetric second rank tensor \mathbf{A} and a vector \mathbf{a} can be applied for a non-symmetric second rank tensor \mathbf{B} since it can be represented by $\mathbf{B} = \mathbf{A} + \mathbf{a} \times \mathbf{I}, \mathbf{A} = \mathbf{A}^T$.

B.7 Invariants for the Transverse Isotropy Group

Transverse isotropy is an important type of the symmetry transformation due to a variety of applications. Transverse isotropy is usually assumed in constitutive modeling of fiber reinforced materials Altenbach et al. (2003a), Kröner et al. (2009), fiber suspensions, Altenbach et al. (2003b, 2007), directionally solidified alloys, Mücke and Bernhardt (2003), deep drawing sheets, Betten (1976, 2001), forgings Naumenko and Gariboldi (2014), Gariboldi et al. (2016) and piezoelectric materials Schröder and Gross (2004). The invariants and generating sets for tensor-valued functions with respect to different cases of transverse isotropy are discussed in Bruhns et al. (1999), Xiao et al. (2000) (see also relevant references therein). In what follows we analyze the problem of a functional basis within the theory of linear first order partial differential equations rather than the algebra of polynomials. Let us discuss the approach proposed in Altenbach et al. (2006) for the invariants with respect to the group of transverse isotropy. The invariants will be found as integrals of the generic partial differential equations. Although a functional basis formed by these invariants does not include any redundant element, functional relations between them may exist. It may be therefore useful to find out simple forms of such relations. We show that the proposed approach may supply results in a direct, natural manner.

B.7.1 Invariants for a Single Second Rank Symmetric Tensor

Consider the proper orthogonal tensor which represents a rotation about a fixed axis, i.e.

$$\mathbf{Q}(\varphi\mathbf{m}) = \mathbf{m} \otimes \mathbf{m} + \cos \varphi(\mathbf{I} - \mathbf{m} \otimes \mathbf{m}) + \sin \varphi \mathbf{m} \times \mathbf{I}, \quad \det \mathbf{Q}(\varphi\mathbf{m}) = 1, \tag{B.7.19}$$

where \mathbf{m} is assumed to be a constant unit vector (axis of rotation) and φ denotes the angle of rotation about \mathbf{m} . The symmetry transformation defined by this tensor corresponds to the transverse isotropy, where five different cases are possible, e.g. Spencer (1987), Zheng and Boehler (1994). Let us find scalar-valued functions of a second rank symmetric tensor \mathbf{A} satisfying the condition

$$f(\mathbf{A}'(\varphi)) = f(\mathbf{Q}(\varphi\mathbf{m}) \cdot \mathbf{A} \cdot \mathbf{Q}^T(\varphi\mathbf{m})) = f(\mathbf{A}), \quad \mathbf{A}'(\varphi) \equiv \mathbf{Q}(\varphi\mathbf{m}) \cdot \mathbf{A} \cdot \mathbf{Q}^T(\varphi\mathbf{m}) \quad (\text{B.7.20})$$

Equation (B.7.20) must be valid for any angle of rotation φ . In (B.7.20) only the left-hand side depends on φ . Therefore its derivative with respect to φ can be set to zero, i.e.

$$\frac{df}{d\varphi} = \frac{d\mathbf{A}'}{d\varphi} \cdot \left(\frac{\partial f}{\partial \mathbf{A}'} \right)^T = 0 \quad (\text{B.7.21})$$

The derivative of \mathbf{A}' with respect to φ can be calculated by the following rules

$$\begin{aligned} d\mathbf{A}'(\varphi) &= d\mathbf{Q}(\varphi\mathbf{m}) \cdot \mathbf{A} \cdot \mathbf{Q}^T(\varphi\mathbf{m}) + \mathbf{Q}(\varphi\mathbf{m}) \cdot \mathbf{A} \cdot d\mathbf{Q}^T(\varphi\mathbf{m}), \\ d\mathbf{Q}(\varphi\mathbf{m}) &= \mathbf{m} \times \mathbf{Q}(\varphi\mathbf{m}) d\varphi \quad \Rightarrow \quad d\mathbf{Q}^T(\varphi\mathbf{m}) = -\mathbf{Q}^T(\varphi\mathbf{m}) \times \mathbf{m} d\varphi \end{aligned} \quad (\text{B.7.22})$$

By inserting the above equations into (B.7.21) we obtain

$$(\mathbf{m} \times \mathbf{A} - \mathbf{A} \times \mathbf{m}) \cdot \left(\frac{\partial f}{\partial \mathbf{A}} \right)^T = 0 \quad (\text{B.7.23})$$

Equation (B.7.23) is classified in Courant and Hilbert (1989) to be the linear homogeneous first order partial differential equation. The characteristic system of (B.7.23) is

$$\frac{d\mathbf{A}}{ds} = (\mathbf{m} \times \mathbf{A} - \mathbf{A} \times \mathbf{m}) \quad (\text{B.7.24})$$

Any system of n linear ordinary differential equations has not more than $n - 1$ functionally independent integrals (Courant and Hilbert 1989). By introducing a basis \mathbf{e}_i the tensor \mathbf{A} can be written down in the form $\mathbf{A} = A^{ij} \mathbf{e}_i \otimes \mathbf{e}_j$ and (B.7.24) is a system of six ordinary differential equations with respect to the coordinates A^{ij} . The five integrals of (B.7.24) may be written down as follows

$$g_i(\mathbf{A}) = c_i, \quad i = 1, 2, \dots, 5,$$

where c_i are integration constants. Any function of the five integrals g_i is the solution of the partial differential equation (B.7.23). Therefore the five integrals g_i represent the invariants of the symmetric tensor \mathbf{A} with respect to the symmetry transformation (B.7.19). The solutions of (B.7.24) are

$$\mathbf{A}^k(s) = \mathbf{Q}(s\mathbf{m}) \cdot \mathbf{A}_0^k \cdot \mathbf{Q}^T(s\mathbf{m}), \quad k = 1, 2, 3, \quad (\text{B.7.25})$$

where \mathbf{A}_0 plays the role of the initial condition. In order to find the integrals, the variable s must be eliminated from (B.7.25). Taking into account the following identities

$$\begin{aligned} \text{tr}(\mathbf{Q} \cdot \mathbf{A}^k \cdot \mathbf{Q}^T) &= \text{tr}(\mathbf{Q}^T \cdot \mathbf{Q} \cdot \mathbf{A}^k) = \text{tr} \mathbf{A}^k, \quad \mathbf{m} \cdot \mathbf{Q}(sm) = \mathbf{m}, \\ (\mathbf{Q} \cdot \mathbf{a}) \times (\mathbf{Q} \cdot \mathbf{b}) &= (\det \mathbf{Q}) \mathbf{Q} \cdot (\mathbf{a} \times \mathbf{b}) \end{aligned} \quad (\text{B.7.26})$$

and using the notation $\mathbf{Q}_m \equiv \mathbf{Q}(sm)$ the integrals can be found as follows

$$\begin{aligned} \text{tr}(\mathbf{A}^k) &= \text{tr}(\mathbf{A}_0^k), \quad k = 1, 2, 3, \\ \mathbf{m} \cdot \mathbf{A}^l \cdot \mathbf{m} &= \mathbf{m} \cdot \mathbf{Q}_m \cdot \mathbf{A}_0^l \cdot \mathbf{Q}_m^T \cdot \mathbf{m} \\ &= \mathbf{m} \cdot \mathbf{A}_0^l \cdot \mathbf{m}, \quad l = 1, 2, \\ \mathbf{m} \cdot \mathbf{A}^2 \cdot (\mathbf{m} \times \mathbf{A} \cdot \mathbf{m}) &= \mathbf{m} \cdot \mathbf{Q}_m \cdot \mathbf{A}_0^2 \cdot \mathbf{Q}_m^T \cdot (\mathbf{m} \times \mathbf{Q}_m \cdot \mathbf{A}_0 \cdot \mathbf{Q}_m^T \cdot \mathbf{m}) \\ &= \mathbf{m} \cdot \mathbf{A}_0^2 \cdot \mathbf{Q}_m^T \cdot [(\mathbf{Q}_m \cdot \mathbf{m}) \times (\mathbf{Q}_m \cdot \mathbf{A}_0 \cdot \mathbf{m})] \\ &= \mathbf{m} \cdot \mathbf{A}_0^2 \cdot (\mathbf{m} \times \mathbf{A}_0 \cdot \mathbf{m}) \end{aligned} \quad (\text{B.7.27})$$

As a result we can formulate the six invariants of the tensor \mathbf{A} with respect to the symmetry transformation (B.7.19) as follows

$$\begin{aligned} I_k &= \text{tr}(\mathbf{A}^k), \quad k = 1, 2, 3, \quad I_4 = \mathbf{m} \cdot \mathbf{A} \cdot \mathbf{m}, \\ I_5 &= \mathbf{m} \cdot \mathbf{A}^2 \cdot \mathbf{m}, \quad I_6 = \mathbf{m} \cdot \mathbf{A}^2 \cdot (\mathbf{m} \times \mathbf{A} \cdot \mathbf{m}) \end{aligned} \quad (\text{B.7.28})$$

The invariants with respect to various symmetry transformations are discussed in Bruhns et al. (1999). For the case of the transverse isotropy six invariants are derived in Bruhns et al. (1999) by the use of another approach. In this sense our result coincides with the result given in Bruhns et al. (1999). However, from the derivations presented here it follows that only five invariants listed in (B.7.28) are functionally independent. Taking into account that I_6 is the mixed product of vectors \mathbf{m} , $\mathbf{A} \cdot \mathbf{m}$ and $\mathbf{A}^2 \cdot \mathbf{m}$ the relation between the invariants can be written down as follows

$$I_6^2 = \det \begin{bmatrix} 1 & I_4 & I_5 \\ I_4 & I_5 & \mathbf{m} \cdot \mathbf{A}^3 \cdot \mathbf{m} \\ I_5 & \mathbf{m} \cdot \mathbf{A}^3 \cdot \mathbf{m} & \mathbf{m} \cdot \mathbf{A}^4 \cdot \mathbf{m} \end{bmatrix} \quad (\text{B.7.29})$$

One can verify that $\mathbf{m} \cdot \mathbf{A}^3 \cdot \mathbf{m}$ and $\mathbf{m} \cdot \mathbf{A}^4 \cdot \mathbf{m}$ are transversely isotropic invariants, too. However, applying the the Cayley-Hamilton theorem (A.4.13) they can be uniquely expressed by I_1, I_2, \dots, I_5 in the following way (Betten 1987)

$$\begin{aligned} \mathbf{m} \cdot \mathbf{A}^3 \cdot \mathbf{m} &= J_1 I_5 + J_2 I_4 + J_3, \\ \mathbf{m} \cdot \mathbf{A}^4 \cdot \mathbf{m} &= (J_1^2 + J_2) I_5 + (J_1 J_2 + J_3) I_4 + J_1 J_3, \end{aligned}$$

where J_1, J_2 and J_3 are the principal invariants of \mathbf{A} defined by (A.4.11). Let us note that the invariant I_6 cannot be dropped. In order to verify this, it is enough to consider two different tensors

$$\mathbf{A} \quad \text{and} \quad \mathbf{B} = \mathbf{Q}_n \cdot \mathbf{A} \cdot \mathbf{Q}_n^T,$$

where

$$\mathbf{Q}_n \equiv \mathbf{Q}(\pi\mathbf{n}) = 2\mathbf{n} \otimes \mathbf{n} - \mathbf{I}, \quad \mathbf{n} \cdot \mathbf{n} = 1, \quad \mathbf{n} \cdot \mathbf{m} = 0, \quad \det \mathbf{Q}_n = 1$$

One can prove that the tensor \mathbf{A} and the tensor \mathbf{B} have the same invariants I_1, I_2, \dots, I_5 . Taking into account that $\mathbf{m} \cdot \mathbf{Q}_n = -\mathbf{m}$ and applying the last identity in (B.7.26) we may write

$$\begin{aligned} I_6(\mathbf{B}) &= \mathbf{m} \cdot \mathbf{B}^2 \cdot (\mathbf{m} \times \mathbf{B} \cdot \mathbf{m}) = \mathbf{m} \cdot \mathbf{A}^2 \cdot \mathbf{Q}_n^T \cdot (\mathbf{m} \times \mathbf{Q}_n \cdot \mathbf{A} \cdot \mathbf{m}) \\ &= -\mathbf{m} \cdot \mathbf{A}^2 \cdot (\mathbf{m} \times \mathbf{A} \cdot \mathbf{m}) = -I_6(\mathbf{A}) \end{aligned}$$

We observe that the only difference between the two considered tensors is the sign of I_6 . Therefore, the triples of vectors $\mathbf{m}, \mathbf{A} \cdot \mathbf{m}, \mathbf{A}^2 \cdot \mathbf{m}$ and $\mathbf{m}, \mathbf{B} \cdot \mathbf{m}, \mathbf{B}^2 \cdot \mathbf{m}$ have different orientations and cannot be combined by a rotation. It should be noted that the functional relation (B.7.29) would in no way imply that the invariant I_6 should be “dependent” and hence “redundant”, namely should be removed from the basis (B.7.28). In fact, the relation (B.7.29) determines the magnitude but not the sign of I_6 .

To describe yielding and failure of oriented solids a dyad $\mathbf{M} = \mathbf{v} \otimes \mathbf{v}$ has been used in Betten (1985), Boehler and Sawczuk (1977), where the vector \mathbf{v} specifies a privileged direction. A plastic potential is assumed to be an isotropic function of the symmetric Cauchy stress tensor and the tensor generator \mathbf{M} . Applying the representation of isotropic functions the integrity basis including ten invariants was found. In the special case $\mathbf{v} = \mathbf{m}$ the number of invariants reduces to the five I_1, I_2, \dots, I_5 defined by (B.7.28). Further details of this approach and applications in continuum mechanics are given in Betten (2008), Boehler (1987). However, the problem statement to find an integrity basis of a symmetric tensor \mathbf{A} and a dyad \mathbf{M} , i.e. to find scalar valued functions $f(\mathbf{A}, \mathbf{M})$ satisfying the condition

$$\begin{aligned} f(\mathbf{Q} \cdot \mathbf{A} \cdot \mathbf{Q}^T, \mathbf{Q} \cdot \mathbf{M} \cdot \mathbf{Q}^T) &= (\det \mathbf{Q})^n f(\mathbf{A}, \mathbf{M}), \\ \forall \mathbf{Q}, \quad \mathbf{Q} \cdot \mathbf{Q}^T &= \mathbf{I}, \quad \det \mathbf{Q} = \pm 1 \end{aligned} \quad (\text{B.7.30})$$

essentially differs from the problem statement (B.7.20). In order to show this we take into account that the symmetry group of a dyad \mathbf{M} , i.e. the set of orthogonal solutions of the equation $\mathbf{Q} \cdot \mathbf{M} \cdot \mathbf{Q}^T = \mathbf{M}$ includes the following elements

$$\begin{aligned} \mathbf{Q}_{1,2} &= \pm \mathbf{I}, \\ \mathbf{Q}_3 &= \mathbf{Q}(\varphi\mathbf{m}), \quad \mathbf{m} = \frac{\mathbf{v}}{|\mathbf{v}|}, \\ \mathbf{Q}_4 &= \mathbf{Q}(\pi\mathbf{n}) = 2\mathbf{n} \otimes \mathbf{n} - \mathbf{I}, \quad \mathbf{n} \cdot \mathbf{n} = 1, \quad \mathbf{n} \cdot \mathbf{v} = 0, \end{aligned} \quad (\text{B.7.31})$$

where $\mathbf{Q}(\varphi\mathbf{m})$ is defined by (B.7.19). The solutions of the problem (B.7.30) are at the same time the solutions of the following problem

$$f(\mathbf{Q}_i \cdot \mathbf{A} \cdot \mathbf{Q}_i^T, \mathbf{M}) = (\det \mathbf{Q}_i)^n f(\mathbf{A}, \mathbf{M}), \quad i = 1, 2, 3, 4,$$

i.e. the problem to find the invariants of \mathbf{A} relative to the symmetry group (B.7.31). However, (B.7.31) includes much more symmetry elements if compared to the problem statement (B.7.20).

An alternative set of transversely isotropic invariants can be formulated by the use of the following decomposition

$$\mathbf{A} = \alpha \mathbf{m} \otimes \mathbf{m} + \beta (\mathbf{I} - \mathbf{m} \otimes \mathbf{m}) + \mathbf{A}_{pD} + \mathbf{t} \otimes \mathbf{m} + \mathbf{m} \otimes \mathbf{t}, \quad (\text{B.7.32})$$

where α , β , \mathbf{A}_{pD} and \mathbf{t} are projections of \mathbf{A} . With the projectors $\mathbf{P}_1 = \mathbf{m} \otimes \mathbf{m}$ and $\mathbf{P}_2 = \mathbf{I} - \mathbf{m} \otimes \mathbf{m}$ we may write

$$\begin{aligned} \alpha &= \mathbf{m} \cdot \mathbf{A} \cdot \mathbf{m} = \text{tr}(\mathbf{A} \cdot \mathbf{P}_1), \\ \beta &= \frac{1}{2}(\text{tr} \mathbf{A} - \mathbf{m} \cdot \mathbf{A} \cdot \mathbf{m}) = \frac{1}{2} \text{tr}(\mathbf{A} \cdot \mathbf{P}_2), \\ \mathbf{A}_{pD} &= \mathbf{P}_2 \cdot \mathbf{A} \cdot \mathbf{P}_2 - \beta \mathbf{P}_2, \\ \mathbf{t} &= \mathbf{m} \cdot \mathbf{A} \cdot \mathbf{P}_2 \end{aligned} \quad (\text{B.7.33})$$

The decomposition (B.7.32) is the analogue to the following representation of a vector \mathbf{a}

$$\mathbf{a} = \mathbf{I} \cdot \mathbf{a} = \mathbf{m} \otimes \mathbf{m} \cdot \mathbf{a} + (\mathbf{I} - \mathbf{m} \otimes \mathbf{m}) \cdot \mathbf{a} = \psi \mathbf{m} + \boldsymbol{\tau}, \quad \psi = \mathbf{a} \cdot \mathbf{m}, \quad \boldsymbol{\tau} = \mathbf{P}_2 \cdot \mathbf{a} \quad (\text{B.7.34})$$

Decompositions of the type (B.7.32) are applied in Bischoff-Beiermann and Bruhns (1994), Bruhns et al. (1999). The projections introduced in (B.7.33) have the following properties

$$\text{tr}(\mathbf{A}_{pD}) = 0, \quad \mathbf{A}_{pD} \cdot \mathbf{m} = \mathbf{m} \cdot \mathbf{A}_{pD} = \mathbf{0}, \quad \mathbf{t} \cdot \mathbf{m} = 0 \quad (\text{B.7.35})$$

With (B.7.32) and (B.7.35) the tensor equation (B.7.24) can be transformed to the following system of equations

$$\left\{ \begin{aligned} \frac{d\alpha}{ds} &= 0, \\ \frac{d\beta}{ds} &= 0, \\ \frac{d\mathbf{A}_{pD}}{ds} &= \mathbf{m} \times \mathbf{A}_{pD} - \mathbf{A}_{pD} \times \mathbf{m}, \\ \frac{d\mathbf{t}}{ds} &= \mathbf{m} \times \mathbf{t} \end{aligned} \right. \quad (\text{B.7.36})$$

From the first two equations we observe that α and β are transversely isotropic invariants. The third equation can be transformed to one scalar and one vector equation as follows

$$\frac{d\mathbf{A}_{pD}}{ds} \cdot \mathbf{A}_{pD} = 0 \quad \Rightarrow \quad \frac{d(\mathbf{A}_{pD} \cdot \mathbf{A}_{pD})}{ds} = 0, \quad \frac{d\mathbf{b}}{ds} = \mathbf{m} \times \mathbf{b}$$

with $\mathbf{b} \equiv \mathbf{A}_{pD} \cdot \mathbf{t}$. We observe that $\text{tr}(\mathbf{A}_{pD}^2) = \mathbf{A}_{pD} \cdot \mathbf{A}_{pD}$ is a transversely isotropic invariant, too. Finally, we have to find the integrals of the following system

$$\begin{cases} \frac{d\mathbf{t}}{ds} = \mathbf{t} \times \mathbf{m}, \\ \frac{d\mathbf{b}}{ds} = \mathbf{b} \times \mathbf{m} \end{cases} \quad (\text{B.7.37})$$

The solutions of (B.7.37) are

$$\mathbf{t}(s) = \mathbf{Q}(s\mathbf{m}) \cdot \mathbf{t}_0, \quad \mathbf{b}(s) = \mathbf{Q}(s\mathbf{m}) \cdot \mathbf{b}_0,$$

where \mathbf{t}_0 and \mathbf{b}_0 play the role of initial conditions. The vectors \mathbf{t} and \mathbf{b} belong to the plane of isotropy, i.e. $\mathbf{t} \cdot \mathbf{m} = 0$ and $\mathbf{b} \cdot \mathbf{m} = 0$. Therefore, one can verify the following integrals

$$\mathbf{t} \cdot \mathbf{t} = \mathbf{t}_0 \cdot \mathbf{t}_0, \quad \mathbf{b} \cdot \mathbf{b} = \mathbf{b}_0 \cdot \mathbf{b}_0, \quad \mathbf{t} \cdot \mathbf{b} = \mathbf{t}_0 \cdot \mathbf{b}_0, \quad (\mathbf{t} \times \mathbf{b}) \cdot \mathbf{m} = (\mathbf{t}_0 \times \mathbf{b}_0) \cdot \mathbf{m} \quad (\text{B.7.38})$$

We found seven integrals, but only five of them are functionally independent. In order to formulate the relation between the integrals we compute

$$\mathbf{b} \cdot \mathbf{b} = \mathbf{t} \cdot \mathbf{A}_{pD}^2 \cdot \mathbf{t}, \quad \mathbf{t} \cdot \mathbf{b} = \mathbf{t} \cdot \mathbf{A}_{pD} \cdot \mathbf{t}$$

For any plane tensor \mathbf{A}_p satisfying the equations $\mathbf{A}_p \cdot \mathbf{m} = \mathbf{m} \cdot \mathbf{A}_p = \mathbf{0}$ the Cayley-Hamilton theorem can be formulated as follows, see e.g. Boehler (1987)

$$\mathbf{A}_p^2 - (\text{tr } \mathbf{A}_p)\mathbf{A}_p + \frac{1}{2}[(\text{tr } \mathbf{A}_p)^2 - \text{tr}(\mathbf{A}_p^2)](\mathbf{I} - \mathbf{m} \otimes \mathbf{m}) = \mathbf{0}$$

Since $\text{tr } \mathbf{A}_{pD} = 0$ we have

$$2\mathbf{A}_{pD}^2 = \text{tr}(\mathbf{A}_{pD}^2)(\mathbf{I} - \mathbf{m} \otimes \mathbf{m}), \quad \mathbf{t} \cdot \mathbf{A}_{pD}^2 \cdot \mathbf{t} = \frac{1}{2}\text{tr}(\mathbf{A}_{pD}^2)(\mathbf{t} \cdot \mathbf{t})$$

Because $\text{tr}(\mathbf{A}_{pD}^2)$ and $\mathbf{t} \cdot \mathbf{t}$ are already defined, the invariant $\mathbf{b} \cdot \mathbf{b}$ can be omitted. The vector $\mathbf{t} \times \mathbf{b}$ is spanned on the axis \mathbf{m} . Therefore

$$\begin{aligned} \mathbf{t} \times \mathbf{b} &= \gamma \mathbf{m}, \quad \gamma = (\mathbf{t} \times \mathbf{b}) \cdot \mathbf{m}, \\ \gamma^2 &= (\mathbf{t} \times \mathbf{b}) \cdot (\mathbf{t} \times \mathbf{b}) = (\mathbf{t} \cdot \mathbf{t})(\mathbf{b} \cdot \mathbf{b}) - (\mathbf{t} \cdot \mathbf{b})^2 \end{aligned}$$

Now we can summarize six invariants and one relation between them as follows

$$\begin{aligned} \bar{I}_1 &= \alpha, \quad \bar{I}_2 = \beta, \quad \bar{I}_3 = \frac{1}{2} \text{tr} (\mathbf{A}_{pD}^2), \quad \bar{I}_4 = \mathbf{t} \cdot \mathbf{t} = \mathbf{t} \cdot \mathbf{A} \cdot \mathbf{m}, \\ \bar{I}_5 &= \mathbf{t} \cdot \mathbf{A}_{pD} \cdot \mathbf{t}, \quad \bar{I}_6 = (\mathbf{t} \times \mathbf{A}_{pD} \cdot \mathbf{t}) \cdot \mathbf{m}, \\ \bar{I}_6^2 &= \bar{I}_4^2 \bar{I}_3 - \bar{I}_5^2 \end{aligned} \quad (\text{B.7.39})$$

Let us assume that the symmetry transformation $\mathbf{Q}_n \equiv \mathbf{Q}(\pi \mathbf{n})$ belongs to the symmetry group of the transverse isotropy, as it was made in Betten (2008), Boehler (1987). In this case $f(\mathbf{A}') = f(\mathbf{Q}_n \cdot \mathbf{A} \cdot \mathbf{Q}_n^T) = f(\mathbf{A})$ must be valid. Taking into account that $\mathbf{Q}_n \cdot \mathbf{m} = -\mathbf{m}$ we can write

$$\alpha' = \alpha, \quad \beta' = \beta, \quad \mathbf{A}'_{pD} = \mathbf{A}_{pD}, \quad \mathbf{t}' = -\mathbf{Q}_n \cdot \mathbf{t}$$

Therefore in (B.7.39) $\bar{I}'_k = \bar{I}_k$, $k = 1, 2, \dots, 5$ and

$$\begin{aligned} \bar{I}'_6 &= (\mathbf{t}' \times \mathbf{A}'_{pD} \cdot \mathbf{t}') \cdot \mathbf{m} = ((\mathbf{Q}_n \cdot \mathbf{t}) \times \mathbf{Q}_n \cdot \mathbf{A}_{pD} \cdot \mathbf{t}) \cdot \mathbf{m} \\ &= (\mathbf{t} \times \mathbf{A}_{pD} \cdot \mathbf{t}) \cdot \mathbf{Q}_n \cdot \mathbf{m} = -(\mathbf{t} \times \mathbf{A}_{pD} \cdot \mathbf{t}) \cdot \mathbf{m} = -\bar{I}_6 \end{aligned}$$

Consequently

$$\begin{aligned} f(\mathbf{A}') &= f(\bar{I}'_1, \bar{I}'_2, \dots, \bar{I}'_5, \bar{I}'_6) = f(\bar{I}_1, \bar{I}_2, \dots, \bar{I}_5, -\bar{I}_6) \\ \Rightarrow f(\mathbf{A}) &= f(\bar{I}_1, \bar{I}_2, \dots, \bar{I}_5, \bar{I}_6^2) \end{aligned}$$

and \bar{I}_6^2 can be omitted due to the last relation in (B.7.39).

B.7.2 Invariants for a Set of Vectors and Second Rank Tensors

By setting $\mathbf{Q} = \mathbf{Q}(\varphi \mathbf{m})$ in (B.5.16) and taking the derivative of (B.5.16) with respect to φ results in the following generic partial differential equation

$$\sum_{i=1}^n \left(\frac{\partial f}{\partial \mathbf{A}_i} \right)^T \cdot (\mathbf{m} \times \mathbf{A}_i - \mathbf{A}_i \times \mathbf{m}) + \sum_{j=1}^k \frac{\partial f}{\partial \mathbf{a}_j} \cdot (\mathbf{m} \times \mathbf{a}_j) = 0 \quad (\text{B.7.40})$$

The characteristic system of (B.7.40) is

$$\left\{ \begin{aligned} \frac{d\mathbf{A}_i}{ds} &= (\mathbf{m} \times \mathbf{A}_i - \mathbf{A}_i \times \mathbf{m}), \quad i = 1, 2, \dots, n, \\ \frac{d\mathbf{a}_j}{ds} &= \mathbf{m} \times \mathbf{a}_j, \quad j = 1, 2, \dots, k \end{aligned} \right. \quad (\text{B.7.41})$$

The above system is a system of N ordinary differential equations, where $N = 6n + 3k$ is the total number of coordinates of \mathbf{A}_i and \mathbf{a}_j for a selected basis. The system (B.7.41) has not more than $N - 1$ functionally independent integrals. Therefore we can formulate:

Theorem B.1 *A set of n symmetric second rank tensors and k vectors with $N = 6n + 3k$ independent coordinates for a given basis has not more than $N - 1$ functionally independent invariants for $N > 1$ and one invariant for $N = 1$ with respect to the symmetry transformation $\mathbf{Q}(\varphi\mathbf{m})$.*

In essence, the proof of this theorem is given within the theory of linear first order partial differential equations (Courant and Hilbert 1989).

As an example let us consider the set of a symmetric second rank tensor \mathbf{A} and a vector \mathbf{a} . This set has eight independent invariants. For a visual perception it is useful to keep in mind that the considered set is equivalent to

$$\mathbf{A}, \mathbf{a}, \mathbf{A} \cdot \mathbf{a}, \mathbf{A}^2 \cdot \mathbf{a}$$

Therefore it is necessary to find the list of invariants, whose fixation determines this set as a rigid whole. The generic equation (B.7.40) takes the form

$$\left(\frac{\partial f}{\partial \mathbf{A}} \right)^T \cdot (\mathbf{m} \times \mathbf{A} - \mathbf{A} \times \mathbf{m}) + \frac{\partial f}{\partial \mathbf{a}} \cdot (\mathbf{m} \times \mathbf{a}) = 0 \quad (\text{B.7.42})$$

The characteristic system of (B.7.42) is

$$\frac{d\mathbf{A}}{ds} = \mathbf{m} \times \mathbf{A} - \mathbf{A} \times \mathbf{m}, \quad \frac{d\mathbf{a}}{ds} = \mathbf{m} \times \mathbf{a} \quad (\text{B.7.43})$$

This system of ninth order has eight independent integrals. Six of them are invariants of \mathbf{A} and \mathbf{a} with respect to the full orthogonal group. They fix the considered set as a rigid whole. The orthogonal invariants are defined by Eqs. (B.6.17) and (B.6.18).

Let us note that the invariant I_7 in (B.6.17) cannot be ignored. To verify this it is enough to consider two different sets

$$\mathbf{A}, \mathbf{a} \text{ and } \mathbf{B} = \mathbf{Q}_p \cdot \mathbf{A} \cdot \mathbf{Q}_p^T, \mathbf{a},$$

where $\mathbf{Q}_p = \mathbf{I} - 2\mathbf{p} \otimes \mathbf{p}$, $\mathbf{p} \cdot \mathbf{p} = 1$, $\mathbf{p} \cdot \mathbf{a} = 0$. One can prove that the invariants I_1, I_2, \dots, I_6 are the same for these two sets. The only difference is the invariant I_7 , i.e. $\mathbf{a} \cdot \mathbf{B}^2 \cdot (\mathbf{a} \times \mathbf{B} \cdot \mathbf{a}) = -\mathbf{a} \cdot \mathbf{A}^2 \cdot (\mathbf{a} \times \mathbf{A} \cdot \mathbf{a})$. Therefore the triples of vectors $\mathbf{a}, \mathbf{A} \cdot \mathbf{a}, \mathbf{A}^2 \cdot \mathbf{a}$ and $\mathbf{a}, \mathbf{B} \cdot \mathbf{a}, \mathbf{B}^2 \cdot \mathbf{a}$ have different orientations and cannot be combined by a rotation. In order to fix the considered set with respect to the unit vector \mathbf{m} it is enough to fix the next two invariants

$$I_8 = \mathbf{m} \cdot \mathbf{A} \cdot \mathbf{m}, \quad I_9 = \mathbf{m} \cdot \mathbf{a} \quad (\text{B.7.44})$$

The eight independent transversely isotropic invariants are (B.6.17), (B.6.18) and (B.7.44).

B.8 Invariants for the Orthotropic Symmetry Group

The orthogonal tensors

$$\mathbf{Q}_1 = 2\mathbf{n}_1 \otimes \mathbf{n}_1 - \mathbf{I}, \quad \mathbf{Q}_2 \equiv \mathbf{n}_2 \otimes \mathbf{n}_2 - \mathbf{I}, \quad \det \mathbf{Q}_1 = \det \mathbf{Q}_2 = 1$$

represent the rotations on the angle π about the axes \mathbf{n}_1 and \mathbf{n}_2 . These tensors are the symmetry elements of the orthotropic (orthorhombic) symmetry group. Let us find the scalar-valued functions of a symmetric tensor \mathbf{A} satisfying the following conditions

$$f(\mathbf{Q}_1 \cdot \mathbf{A} \cdot \mathbf{Q}_1^T) = f(\mathbf{Q}_2 \cdot \mathbf{A} \cdot \mathbf{Q}_2^T) = f(\mathbf{A}) \quad (\text{B.8.45})$$

Replacing the tensor \mathbf{A} by the tensor $\mathbf{Q}_2 \cdot \mathbf{A} \cdot \mathbf{Q}_2^T$ we find that

$$f(\mathbf{Q}_1 \cdot \mathbf{Q}_2 \cdot \mathbf{A} \cdot \mathbf{Q}_2^T \cdot \mathbf{Q}_1^T) = f(\mathbf{Q}_2 \cdot \mathbf{A} \cdot \mathbf{Q}_2^T) = f(\mathbf{A}) \quad (\text{B.8.46})$$

Consequently the tensor $\mathbf{Q}_3 = \mathbf{Q}_1 \cdot \mathbf{Q}_2 = 2\mathbf{n}_3 \otimes \mathbf{n}_3 - \mathbf{I} = \mathbf{Q}(\pi\mathbf{n}_3)$ belongs to the symmetry group, where the unit vector \mathbf{n}_3 is orthogonal to \mathbf{n}_1 and \mathbf{n}_2 . Consider three tensors \mathbf{A}'_i formed from the tensor \mathbf{A} by three symmetry transformations i.e., $\mathbf{A}'_i \equiv \mathbf{Q}_i \cdot \mathbf{A} \cdot \mathbf{Q}_i^T$. Taking into account that $\mathbf{Q}_i \cdot \mathbf{n}_i = \mathbf{n}_i$ (no summation over i) and $\mathbf{Q}_i \cdot \mathbf{n}_j = -\mathbf{n}_j, i \neq j$ we can write

$$\begin{aligned} \text{tr}(\mathbf{A}'_i{}^k) &= \text{tr}(\mathbf{A}^k), \quad k = 1, 2, 3, \quad i = 1, 2, 3, \\ \mathbf{n}_i \cdot \mathbf{A}'_i \cdot \mathbf{n}_i &= \mathbf{n}_i \cdot \mathbf{Q}_i \cdot \mathbf{A} \cdot \mathbf{Q}_i^T \cdot \mathbf{n}_i \\ &= \mathbf{n}_i \cdot \mathbf{A} \cdot \mathbf{n}_i, \quad i = 1, 2, 3, \\ \mathbf{n}_i \cdot \mathbf{A}'_i{}^2 \cdot \mathbf{n}_i &= \mathbf{n}_i \cdot \mathbf{Q}_i \cdot \mathbf{A}^2 \cdot \mathbf{Q}_i^T \cdot \mathbf{n}_i \\ &= \mathbf{n}_i \cdot \mathbf{A}^2 \cdot \mathbf{n}_i, \quad i = 1, 2, 3 \end{aligned} \quad (\text{B.8.47})$$

The above set of includes 9 scalars. The number can be reduced to 7 due to the obvious relations

$$\text{tr}(\mathbf{A}^k) = \mathbf{n}_1 \cdot \mathbf{A}^k \cdot \mathbf{n}_1 + \mathbf{n}_2 \cdot \mathbf{A}^k \cdot \mathbf{n}_2 + \mathbf{n}_3 \cdot \mathbf{A}^k \cdot \mathbf{n}_3, \quad k = 1, 2$$

Therefore the orthotropic scalar-valued function of the symmetric second rank tensor can be represented as a function of the following seven arguments

$$\begin{aligned} I_1 &= \mathbf{n}_1 \cdot \mathbf{A} \cdot \mathbf{n}_1, \quad I_2 = \mathbf{n}_2 \cdot \mathbf{A} \cdot \mathbf{n}_2, \quad I_3 = \mathbf{n}_3 \cdot \mathbf{A} \cdot \mathbf{n}_3, \\ I_4 &= \mathbf{n}_1 \cdot \mathbf{A}^2 \cdot \mathbf{n}_1, \quad I_5 = \mathbf{n}_2 \cdot \mathbf{A}^2 \cdot \mathbf{n}_2, \quad I_6 = \mathbf{n}_3 \cdot \mathbf{A}^2 \cdot \mathbf{n}_3, \quad I_7 = \text{tr} \mathbf{A}^3 \end{aligned} \quad (\text{B.8.48})$$

Instead of I_4, I_5, I_6 and I_7 in (B.8.48) one may use the following list of arguments (Lurie 1990)

$$J_1 = (\mathbf{n}_1 \cdot \mathbf{A} \cdot \mathbf{n}_2)^2, \quad J_2 = (\mathbf{n}_2 \cdot \mathbf{A} \cdot \mathbf{n}_3)^2, \quad J_3 = (\mathbf{n}_1 \cdot \mathbf{A} \cdot \mathbf{n}_3)^2, \quad (\text{B.8.49})$$

$$J_4 = (\mathbf{n}_1 \cdot \mathbf{A} \cdot \mathbf{n}_2)(\mathbf{n}_1 \cdot \mathbf{A} \cdot \mathbf{n}_3)(\mathbf{n}_2 \cdot \mathbf{A} \cdot \mathbf{n}_3)$$

The invariants J_1, J_2, J_3, J_4 can be uniquely expressed through I_1, \dots, I_7 by use of the following relations

$$I_4 = I_1^2 + J_1 + J_3, \quad I_5 = I_2^2 + J_1 + J_2, \quad I_6 = I_3^2 + J_2 + J_3, \quad (\text{B.8.50})$$

$$I_7 = 2I_1(I_4 - I_1^2) + 2I_2(I_5 - I_2^2) + 2I_3(I_6 - I_3^2) + J_4$$

Let us note that if \mathbf{A} is the polar tensor, then the lists of invariants (B.8.48) and (B.8.49) are also applicable to the class of the orthotropic symmetry characterized by the following eight symmetry elements

$$\mathbf{Q} = \pm \mathbf{n}_1 \otimes \mathbf{n}_1 \pm \mathbf{n}_2 \otimes \mathbf{n}_2 \pm \mathbf{n}_3 \otimes \mathbf{n}_3 \quad (\text{B.8.51})$$

In Sect. B.7 we derived the generic partial differential equation for the case of the transverse isotropy. Applying this approach one may find the list of functionally independent invariants among all possible invariants. Let us formulate the generic partial differential equation for the case of orthotropic symmetry. To this end let us find the scalar valued arguments of the tensor \mathbf{A} from the following condition

$$f(\mathbf{A}', \mathbf{n}'_1 \otimes \mathbf{n}'_1, \mathbf{n}'_2 \otimes \mathbf{n}'_2, \mathbf{n}'_3 \otimes \mathbf{n}'_3) = f(\mathbf{A}, \mathbf{n}_1 \otimes \mathbf{n}_1, \mathbf{n}_2 \otimes \mathbf{n}_2, \mathbf{n}_3 \otimes \mathbf{n}_3), \quad (\text{B.8.52})$$

where $\mathbf{A}' = \mathbf{Q} \cdot \mathbf{A} \cdot \mathbf{Q}^T$, $\mathbf{n}'_i = \mathbf{Q} \cdot \mathbf{n}_i$, $\forall \mathbf{Q}$, $\det \mathbf{Q} = 1$. The symmetry group of a single dyad is given by Eqs. (B.7.31). It can be shown that the symmetry group of three dyads $\mathbf{n}_i \otimes \mathbf{n}_i$ includes eight elements (B.8.51). Among all rotation tensors \mathbf{Q} the three rotations $\mathbf{Q}_1, \mathbf{Q}_2$ and \mathbf{Q}_3 belong to the symmetry group of $\mathbf{n}_i \otimes \mathbf{n}_i$. Therefore Eq. (B.8.52) is equivalent to the following three equations

$$f(\mathbf{Q}_1 \cdot \mathbf{A} \cdot \mathbf{Q}_1^T, \mathbf{n}_1 \otimes \mathbf{n}_1, \mathbf{n}_2 \otimes \mathbf{n}_2, \mathbf{n}_3 \otimes \mathbf{n}_3) = f(\mathbf{A}, \mathbf{n}_1 \otimes \mathbf{n}_1, \mathbf{n}_2 \otimes \mathbf{n}_2, \mathbf{n}_3 \otimes \mathbf{n}_3),$$

$$f(\mathbf{Q}_2 \cdot \mathbf{A} \cdot \mathbf{Q}_2^T, \mathbf{n}_1 \otimes \mathbf{n}_1, \mathbf{n}_2 \otimes \mathbf{n}_2, \mathbf{n}_3 \otimes \mathbf{n}_3) = f(\mathbf{A}, \mathbf{n}_1 \otimes \mathbf{n}_1, \mathbf{n}_2 \otimes \mathbf{n}_2, \mathbf{n}_3 \otimes \mathbf{n}_3),$$

$$f(\mathbf{Q}_3 \cdot \mathbf{A} \cdot \mathbf{Q}_3^T, \mathbf{n}_1 \otimes \mathbf{n}_1, \mathbf{n}_2 \otimes \mathbf{n}_2, \mathbf{n}_3 \otimes \mathbf{n}_3) = f(\mathbf{A}, \mathbf{n}_1 \otimes \mathbf{n}_1, \mathbf{n}_2 \otimes \mathbf{n}_2, \mathbf{n}_3 \otimes \mathbf{n}_3)$$

Consequently, the scalar-valued arguments of \mathbf{A} found from (B.8.52) satisfy three Eqs. (B.8.45) and (B.8.46). To derive the generic partial differential equation for invariants we follow the approach presented in Zhilin (2003, 2006). Let $\mathbf{Q}(\tau)$ be a continuous set of rotations depending on the real parameter τ . In this case

$$\frac{d}{d\tau} \mathbf{Q}(\tau) = \boldsymbol{\omega}(\tau) \times \mathbf{Q}(\tau) \quad \Rightarrow \quad \frac{d}{d\tau} \mathbf{Q}^T(\tau) = -\mathbf{Q}^T(\tau) \times \boldsymbol{\omega}(\tau),$$

$$\mathbf{Q}(0) = \mathbf{I}, \quad \boldsymbol{\omega}(0) = \boldsymbol{\omega}_0,$$

where the axial vector $\boldsymbol{\omega}$ has the sense of the angular velocity of rotation. Taking the derivative of Eq. (B.8.52) with respect to τ we obtain the following partial differential equation

$$\begin{aligned}
& (\boldsymbol{\omega} \times \mathbf{A}' - \mathbf{A}' \times \boldsymbol{\omega}) \cdot \left(\frac{\partial f}{\partial \mathbf{A}'} \right)^{\text{T}} \\
& + \sum_{i=1}^3 (\boldsymbol{\omega} \times \mathbf{n}'_i \otimes \mathbf{n}'_i - \mathbf{n}'_i \otimes \mathbf{n}'_i \times \boldsymbol{\omega}) \cdot \left(\frac{\partial f}{\partial \mathbf{n}'_i \otimes \mathbf{n}'_i} \right)^{\text{T}} = 0,
\end{aligned} \tag{B.8.53}$$

where $\mathbf{A}'(\tau) = \mathbf{Q}(\tau) \cdot \mathbf{A} \cdot \mathbf{Q}^{\text{T}}(\tau)$, $\mathbf{n}'_i(\tau) = \mathbf{Q}(\tau) \cdot \mathbf{n}_i$. For $\tau = 0$ Eq.(B.8.53) takes the form

$$\begin{aligned}
& (\boldsymbol{\omega}_0 \times \mathbf{A} - \mathbf{A} \times \boldsymbol{\omega}_0) \cdot \left(\frac{\partial f}{\partial \mathbf{A}} \right)^{\text{T}} \\
& + \sum_{i=1}^3 (\boldsymbol{\omega}_0 \times \mathbf{n}_i \otimes \mathbf{n}_i - \mathbf{n}_i \otimes \mathbf{n}_i \times \boldsymbol{\omega}_0) \cdot \left(\frac{\partial f}{\partial \mathbf{n}_i \otimes \mathbf{n}_i} \right)^{\text{T}} = 0
\end{aligned} \tag{B.8.54}$$

Taking into account the following identities

$$(\mathbf{a} \times \mathbf{A}) \cdot \mathbf{B} = \mathbf{a} \cdot (\mathbf{A} \cdot \mathbf{B})_{\times}, \quad \mathbf{B} \cdot (\mathbf{A} \times \mathbf{a}) = \mathbf{a} \cdot (\mathbf{B} \cdot \mathbf{A})_{\times},$$

Eq.(B.8.54) can be transformed to

$$\begin{aligned}
& \boldsymbol{\omega}_0 \cdot \left[\mathbf{A} \cdot \left(\frac{\partial f}{\partial \mathbf{A}} \right)^{\text{T}} - \left(\frac{\partial f}{\partial \mathbf{A}} \right)^{\text{T}} \cdot \mathbf{A} \right. \\
& \left. + \sum_{i=1}^3 \mathbf{n}_i \otimes \mathbf{n}_i \cdot \left(\frac{\partial f}{\partial \mathbf{n}_i \otimes \mathbf{n}_i} \right)^{\text{T}} - \sum_{i=1}^3 \left(\frac{\partial f}{\partial \mathbf{n}_i \otimes \mathbf{n}_i} \right)^{\text{T}} \cdot \mathbf{n}_i \otimes \mathbf{n}_i \right]_{\times} = 0
\end{aligned}$$

Because $\boldsymbol{\omega}_0$ is the arbitrary vector we obtain

$$\begin{aligned}
& \left[\mathbf{A} \cdot \left(\frac{\partial f}{\partial \mathbf{A}} \right)^{\text{T}} - \left(\frac{\partial f}{\partial \mathbf{A}} \right)^{\text{T}} \cdot \mathbf{A} \right. \\
& \left. + \sum_{i=1}^3 \mathbf{n}_i \otimes \mathbf{n}_i \cdot \left(\frac{\partial f}{\partial \mathbf{n}_i \otimes \mathbf{n}_i} \right)^{\text{T}} - \sum_{i=1}^3 \left(\frac{\partial f}{\partial \mathbf{n}_i \otimes \mathbf{n}_i} \right)^{\text{T}} \cdot \mathbf{n}_i \otimes \mathbf{n}_i \right]_{\times} = 0
\end{aligned} \tag{B.8.55}$$

The vector partial differential equation (B.8.55) corresponds to three scalar differential equations. The total number of scalar arguments of the function f is 9 including 6 components of the symmetric tensor \mathbf{A} and three parameters (e.g. three Euler angles) characterizing three dyads $\mathbf{n}_i \otimes \mathbf{n}_i$. Each of the scalar partial differential equations in (B.8.55) reduces the number of independent arguments by one. Therefore, the total number of independent arguments is 6. It can be shown that all seven arguments presented by Eqs.(B.8.48) or (B.8.49) satisfies (B.8.55). Because only six of them are independent, one functional relation must exist. In the case of the list (B.8.49) the functional relation is obvious. Indeed, we can write

$$J_4^2 = J_1 J_2 J_3 \quad (\text{B.8.56})$$

To derive the functional relation for the list (B.8.48) one may apply Eqs. (B.8.50) to express J_1, \dots, J_4 through I_1, \dots, I_7 . The result should be inserted into Eq. (B.8.56).

References

- Altenbach H, Zhilin PA (1988) Osnovnye uravneniya neklassicheskoi teorii uprugikh obolochek (Basic equations of a non-classical theory of elastic shells, in Russ.). *Adv Mech* 11:107–148
- Altenbach H, Naumenko K, L'vov GI, Pylypenko S (2003a) Numerical estimation of the elastic properties of thin-walled structures manufactured from short-fiber reinforced thermoplastics. *Mech Compos Mater* 39:221–234
- Altenbach H, Naumenko K, Zhilin P (2003b) A micro-polar theory for binary media with application to phase-transitional flow of fiber suspensions. *Continuum Mech Thermodyn* 15:539–570
- Altenbach H, Naumenko K, Zhilin PA (2005) A direct approach to the formulation of constitutive equations for rods and shells. In: Pietraszkiewicz W, Szymczak C (eds) *Shell structures: theory and applications*, pp 87–90. Taylor and Francis, Leiden
- Altenbach H, Naumenko K, Zhilin P (2006) A note on transversely isotropic invariants. *ZAMM-J Appl Math Mech/Zeitschrift für Angewandte Mathematik und Mechanik* 86:162–168
- Altenbach H, Naumenko K, Pylypenko S, Renner B (2007) Influence of rotary inertia on the fiber dynamics in homogeneous creeping flows. *ZAMM-J Appl Math Mech/Zeitschrift für Angewandte Mathematik und Mechanik* 87(2):81–93
- Betten J (1976) Plastic anisotropy and Bauschinger-effect - general formulation and comparison with experimental yield curves. *Acta Mech* 25(1–2):79–94
- Betten J (1985) On the representation of the plastic potential of anisotropic solids. In: Boehler J (ed) *Plastic behavior of anisotropic solids*, CNRS, Paris, pp 213–228
- Betten J (1987) *Tensorrechnung für Ingenieure*. Springer, Berlin
- Betten J (2001) *Kontinuumsmechanik*. Springer, Berlin
- Betten J (2008) *Creep mechanics*, 3rd edn. Springer, Berlin
- Bischoff-Beiermann B, Bruhns O (1994) A physically motivated set of invariants and tensor generators in the case of transverse isotropy. *Int J Eng Sci* 32:1531–1552
- Boehler JP (ed) (1987) *Application of tensor functions in solid mechanics*. CISM Lecture Notes No. 292, Springer, Wien
- Boehler JP, Sawczuk A (1977) On yielding of oriented solids. *Acta Mech* 27:185–206
- Bruhns O, Xiao H, Meyers A (1999) On representation of yield functions for crystals, quasicrystals and transversely isotropic solids. *Eur J Mech A/Solids* 18:47–67
- Courant R, Hilbert D (1989) *Methods of mathematical physics, vol 2: Partial differential equations*. Wiley Interscience Publication, New York
- Eringen AC (1999) *Microcontinuum field theories, vol I: Foundations and Solids*. Springer, New York
- Gariboldi E, Naumenko K, Ozhoga-Maslovskaja O, Zappa E (2016) Analysis of anisotropic damage in forged Al-Cu-Mg-Si alloy based on creep tests, micrographs of fractured specimen and digital image correlations. *Mater Sci Eng: A* 652:175–185
- Kröner C, Altenbach H, Naumenko K (2009) Coupling of a structural analysis and flow simulation for short-fiber-reinforced polymers: property prediction and transfer of results. *Mech Compos Mater* 45(3):249–256
- Lurie AI (1990) *Nonlinear theory of elasticity*. North-Holland, Dordrecht
- Mücke R, Bernhardt O (2003) A constitutive model for anisotropic materials based on Neuber's rule. *Comput Methods Appl Mech Eng* 192:4237–4255

- Naumenko K, Gariboldi E (2014) A phase mixture model for anisotropic creep of forged Al-Cu-Mg-Si alloy. *Mater Sci Eng: A* 618:368 – 376
- Rychlewski J, Zhang J (1991) On representation of tensor functions: a rerview. *Adv Mech* 14:75–94
- Schröder J, Gross D (2004) Invariant formulation of the electromechanical enthalpy function of transversely isotropic piezoelectric materials. *Arch Appl Mech* 73:533–552
- Spencer AJM (1987) Isotropic polynomial invariants and tensor functions. In: Boehler J (ed) *Applications of tensor functions in solid mechanics*, Springer, Wien, pp 141–169. CISM Lecture Notes No. 292
- Xiao H, Bruhns O, Meyers A (2000) Minimal generating sets for symmetric 2nd-order tensor-valued transversely isotropic functions of vectors and 2nd-order tensors. *ZAMM-J Appl Math Mech/Zeitschrift für Angewandte Mathematik und Mechanik* 80:565–569
- Zheng QS (1994) Theory of representations of tensor functions. *Appl Mech Rev* 47(11):545–587
- Zheng QS, Boehler JP (1994) The description, classification and reality of material and physical symmetries. *Acta Mech* 102:73–89
- Zhilin PA (1982) Osnovnye uravneniya neklassicheskoi teorii obolochek (basic equations of a non-classical theory of shells, in russ.). *Dinamika i prochnost' mashin, Trudy LPI* 386:29–46
- Zhilin PA (2003) Modifizirovannaya teoriya simmetrii tenzorov i tenzornykh invariantov (A modified theory of symmetry for tensors and tensor invariants, in Russ.). *Izvestiya vuzov Estestvennye Nauki* pp 176–195
- Zhilin PA (2006) Symmetries and orthogonal invariance in oriented space. In: Indeitsev D, Ivanova E, Krivtsov A (eds) *Advanced problems in mechanics*, vol 2, pp 204–226. Nestor, St. Petersburg

Index

A

- Ageing, 62, 242, 264, 300
- Aluminium alloy BS 1472, 299
- Angular velocity vector, 152, 153, 191, 232
- Anisotropy, 26, 249
 - damage induced, 27, 206, 254, 266, 271
 - deformation induced, 27, 206
 - induced, 27
 - initial, 26, 206, 271
- Annihilation, 8
- Annihilation of dislocations, 4
- Arrhenius function of the temperature, 97, 304
- Arrhenius temperature dependence, 126, 225, 243, 264

B

- Backstress, 111, 112, 243, 289, 296
- Bailey-Orowan recovery hypothesis, 244
- Balance of angular momentum, 165
- Balance of momentum, 84, 85, 159, 161, 164, 167
- Base metal, 57, 308
- Bauschinger effect, 114
- Biaxial tests, 258
- Bulk modulus, 237

C

- Cauchy formula, 163
- Cauchy-Green tensor, 147
- Cavitated area fraction, 263
- Cavitation, 264
- Cavities, 123, 124, 266
- Cayley-Hamilton theorem, 154, 233

- Clausius-Duhem inequality, 88, 169
- Clausius-Planck inequality, 87, 168
- Climb-plus-glide deformation mechanism, 226
- Coarse-grained region, 58, 308
- Coarsening, 263
 - carbide precipitates, 9
 - subgrain microstructure, 9
 - subgrains, 4
- Coble creep, 227
- Coffin-Manson equation, 21
- Columnar region, 58, 308
- Compressibility, 203
- Conjugate variable, 91, 174
- Connection in parallel, 311
- Connection in series, 313
- Conservation of mass, 83, 159
- Constituent
 - inelastic-hard, 251
 - inelastic-soft, 251
- Continuity, 124
- Continuum mechanics modeling, 62
- Continuum micromechanics, 63
- Convexity condition, 260
- Crack driving force, 134
- Creep
 - accelerated, 6
 - anisotropic, 13, 26, 266, 303, 315
 - cyclic, 13
 - dynamic, 15
 - fracture, 256
 - grain boundary, 300
 - high cyclic, 15
 - McVetty-type, 269
 - multi-axial rupture data, 265
 - power law, 124, 260

primary, 6, 240, 264, 289, 299, 300, 309
 ratcheting, 59
 recovery, 10, 247
 reduced, 6
 rupture, 301
 secondary, 6, 125, 126, 256, 269, 300, 309, 318
 stationary, 6
 steady-state, 196, 201, 248, 312
 tertiary, 6, 105, 129, 255, 288, 292, 300, 309, 314
 transient, 13, 242
 transversely isotropic, 315
 volumetric, 203, 262
 Creep condition, 195
 Creep damage, 21, 61, 129
 Kachanov-Rabotnov model, 124, 255
 mechanim-based model, 262
 micromechanically-consistent model, 260
 model based on dissipation, 265
 Creep damage evolution, 18
 Creep equation, 203
 classical, 201, 204
 non-classical, 201
 non-quadratic, 216
 tensorial non-linear, 200
 Creep failure, 257, 308
 Creep-fatigue, 18
 Creep fracture, 129, 131
 Creep history, 267
 Creep in structures, 30
 Creep potential, 195, 196, 255, 260, 315, 316
 classical, 199
 Norton-Bailey-Odqvist, 196, 255, 316
 Creep rate
 volumetric, 203
 Creep strain tensor, 285
 Creep strength, 127
 Creep test, 57, 308, 315
 biaxial, 254
 multi-axial, 256, 301
 short-term uni-axial, 60
 triaxial, 254
 uni-axial, 5, 254, 262, 265, 266
 Creep theory
 von Mises-Odqvist, 241
 Cross section shrinkage, 104, 105
 Cross-weld specimens, 57, 308
 Cubic symmetry, 215

D

Damage, 62, 123, 124, 254, 255, 287, 296, 315, 318
 activation, 271
 deactivation, 271
 elastic-brittle, 268
 Damage driving force, 134
 Damage effect tensor, 269
 Damage equivalent stress, 285, 286
 Damage evolution, 286, 308, 309
 Damage evolution equation, 127, 256
 Damage mechanism, 132
 Damage parameter, 292
 scalar-valued, 254, 269, 285
 tensor-valued, 268
 Damage process
 evolution equation, 124
 Damage rate, 124
 Damage state variable, 124
 Damage tensor, 268
 higher order, 271
 second rank, 269
 Damage variable, 124
 tensor-valued, 254
 Darboux problem, 181
 Decomposition
 polar, 339
 Deformation gradient, 81, 145, 150, 191, 206
 decomposition, 228
 multiplicative decomposition, 229
 Deformation rate tensor, 151
 Degradation function, 133, 135
 Degradation of stiffness, 132
 Diffusion creep, 226
 Diffusion equation, 93, 175
 Diffusion of vacancies, 66
 Dilatation, 203, 262
 Discrete dislocation dynamics, 65
 Dislocation creep, 226
 Dislocation density hardening, 121
 Displacement, 80, 143
 Dissipation inequality, 88, 97, 131, 169, 170, 179, 190, 229
 Dissipation power, 197, 266
 Drag stress, 62, 107, 121
 Ductile creep rupture, 105, 293
 Dyad, 329
 Dyadic product, 332

E

Effective stress, 125
 Effective stress concept, 125, 271

- Effective stress tensor, 255, 269, 271
 - Eigen-direction, 335
 - Eigen-value, 335
 - Eigen-value problem, 335
 - Elasticity tensor, 188, 190
 - Elastic range, 2
 - Elastic regime, 3
 - Elastic springback, 3
 - Elastoplasticity, 100
 - Empirical modeling, 60
 - Energy
 - free, 92, 176, 179, 184, 186, 189, 190
 - internal, 85, 166, 175
 - kinetic, 85, 166
 - total, 85, 166
 - Energy balance, 87, 93, 95, 96, 167, 168, 175, 189
 - Energy supply, 167
 - Engineering stress, 103
 - Entropy inequality, 88, 169
 - Equivalent creep rate
 - von Mises, 24
 - Equivalent creep strain, 263
 - von Mises, 24
 - Equivalent deformation rate
 - von Mises, 194
 - Equivalent stress, 200, 202, 204, 214, 257, 263, 315
 - damage, 256, 258
 - generalized, 258
 - von Mises, 22, 194, 200, 204, 243, 258, 288, 302
- F**
- Fatigue damage, 16, 21, 59, 61
 - surface induced, 52
 - Fatigue failure, 16
 - Fatigue life, 18, 19
 - Fatigue strength, 16
 - Fine-grained region, 58, 308
 - First law of dynamics, 84
 - First principal direction, 255
 - First principal stress, 286, 295
 - Flow potential, 195, 243
 - Flow rule, 195, 196, 202
 - Oddqvist, 199
 - Fluid
 - incompressible, 193
 - linear viscous, 98
 - non-linear viscous, 98, 192
 - non-Newtonian, 193
 - Fourier law of heat conduction, 92, 175
 - Fracture, 124
 - Frederick-Armstrong model, 114, 253
 - Free-surface effect, 64
 - Friction welding, 99
 - Function of temperature, 285
 - Functions of stress
 - exponential law, 224
 - hyperbolic sine, 301
 - hyperbolic sine law, 224
 - power, 301, 316
 - power law, 223
 - power law breakdown equation, 224
 - souble power law, 224
- G**
- Grain boundary cavitation, 64
 - Grain boundary sliding, 53, 64, 227
 - Grain boundary strengthening, 52
 - Grain size, 309
- H**
- Hall-Petch effect, 52
 - Hamilton operator, 144
 - Hardening, 5, 13, 53, 62, 129, 226, 250, 264, 288, 289, 315, 318
 - anisotropic, 249
 - cyclic, 16, 59, 111
 - initial, 249
 - isotropic, 242
 - kinematic, 242, 248
 - Hardening parameter, 107
 - Hardening rate, 109
 - Hardening regime, 2
 - Hardening rule, 242
 - Hardening variable, 122, 248, 300
 - Harmonic stress variation, 14
 - Heat-affected zone, 56, 57, 265, 308, 309
 - Heat capacity, 93, 175, 189
 - Heat equation, 93, 175, 189
 - Heat flow, 89, 167
 - Heat flow vector, 168
 - Heat flux, 97, 175
 - Heat flux vector, 191
 - Heat transfer equation, 96, 189
 - Helmholtz free energy, 89, 170
 - Heterogeneous structure, 309
 - High-temperature inelasticity, 64
- I**
- Identity tensor, 333
 - Independent variable, 91, 174

- Inelastic-hard constituent, 116
- Inelastic regime, 3
 - with hardening, 3
 - with necking, 3
- Inelastic strain rate, 61
- Internal state variable, 242, 300, 315
- Invariant
 - cubic, 202
 - linear, 202
 - principal, 155, 183, 185
 - quadratic, 202
- Isochronous rupture surface, 258
- Iso-strain approach, 252
- Iso-strain concept, 311
- Iso-stress approach, 99, 108, 131, 231, 313

- K**
- Kachanov-Rabotnov model, 310
- Kachanov's continuity, 124
- Kinematic hardening model, 242

- L**
- Lamé constants, 190, 237
- LCF test, 114
- Least squares method, 284
- Linear damage summation rule, 61
- Linear hardening rule, 112
- Linear stress-strain relationship, 2
- Loading
 - combined, 26
 - complex, 242
 - cyclic, 13
 - multi-axial, 254
 - multi-axial non-proportional, 271
 - non-isothermal, 51
 - non-proportional, 26, 27, 248, 254
 - proportional, 26
 - simple, 248
 - thermo-mechanical cyclic, 39
- Low cycle fatigue, 16

- M**
- Martensitic transformation, 4
- Mass, 83
- Material
 - aelotropic, 177
 - anisotropic, 177, 206
 - crystalline, 198
 - cubic symmetry, 215
 - Hencky, 231
 - isotropic, 179, 182, 190
 - poly-crystalline, 227
 - transversely-isotropic, 179, 185
- Material processing, 12
- Materials science modeling, 61
- Material symmetry, 67, 176, 177, 315
- Material symmetry group, 188, 315
- Maximum tensile stress, 255, 286
- Maxwell model, 100
- Mean dislocation density, 121
- Mean dislocation density model, 109
- Mechanical action, 160
- Mechanical power, 86, 99, 108, 110, 131, 166, 175, 190, 227
- Mechanism-based model, 262, 299
- Method of characteristics, 180
- Micromechanically-consistent model, 260
- Micromechanical modeling, 63
- Microstructural analysis, 67
- Minimum creep rate, 126, 304
- Mirror reflection, 176, 177
- Mixture model, 288
- Mixture rule, 116, 252
- Momentum, 83, 159
 - angular, 165
- Monkman-Grant relationship, 60, 129
- Motion, 80, 143
- Multi-pass weld, 56, 309

- N**
- Nabarro-Herring creep, 227
- Nabla operator, 144
- Necking, 3, 5
- Net-stress, 125
- Net-stress tensor, 269
- Neumann principle, 177
- Newton law of cooling, 93, 175
- Non-mechanical energy supply, 86, 166
- Norton-Bailey law, 248
- Norton-Bailey type potential, 201
- Notation
 - component, 323
 - coordinate-free, 323
 - direct, 173, 323
 - index, 323
 - symbolic, 323
- Notch stress effect, 64

- O**
- Offset yield point, 3, 5
- Orientation averaging, 271
- Orientation distribution function, 271
- Orientation tensor, 271

Orowan hardening, 121
 Orowan stress, 121
 Orthotropic symmetry, 211
 Overstress, 117

P

Parent material, 309
 Particle hardening, 121
 Peach-Köhler force, 65
 Permanent plastic strain, 3
 Phase mixture model, 250
 Physical symmetry, 176, 177
 Piping system, 308
 Plasticity
 rate-independent, 98, 195
 rigid, 98
 Plastic pre-strain, 249
 Poisson's ratio, 190
 Polar decomposition, 152, 231
 Position vector, 142
 Power-law function of stress, 97
 Poynting-Swift effect, 194, 200
 Prandtl model, 100
 Pre-damage, 267
 Pre-loading, 267
 Pressure vessel, 308
 Pressurized cylindrical shell, 302
 Pre-straining, 267
 Principal direction, 335
 Principal value, 335
 Principal vector, 335
 Projector, 333

R

Ratchetting, 15
 Rate of plastic strain, 111
 Recovery, 4, 8, 13, 62, 226, 288
 Redistribution, 302
 Relaxation, 10, 302
 Relaxation-fatigue, 18
 Relaxation test, 12
 Representative volume element, 64
 Requirements for the modeling, 66
 Resistance function, 133, 135
 Rigid body rotation, 186
 Rotation, 315
 infinitesimal, 150
 Rotation about a fixed axis, 176
 Rotation tensor, 148, 152, 153, 181, 191, 232
 linearized, 150
 Rupture time, 258

S

Saturation, 4
 Saturation stress, 117
 Sdobyrev criterion, 257
 Shear flow, 193
 Shear modulus, 190, 298
 Softening, 4, 5, 13, 250, 253, 287, 290, 296
 cyclic, 16, 59
 Specific dissipation work, 265
 Specimen
 circumferentially notched, 22
 cruciform, 22
 cylindrical, 5
 standard, 2
 thin-walled tube, 22
 Spectral form, 178
 Spectral representation, 148, 153
 Spin tensor, 152, 153
 left, 152
 State variables
 hidden, 62
 internal, 62
 Steady-state flow regime, 4
 Steel 13CrMo4-5, 286
 Strain, 81
 creep, 7
 cyclic, 18
 elastic, 7
 Hencky, 94
 infinitesimal, 150
 local, 81
 local normal, 146
 Strain deviator, 237
 Strain equivalence principle, 125, 256, 269, 271
 Strain hardening, 240, 242
 Strain hardening model, 240
 Strain local shear, 147
 Strain tensor
 additive split, 236
 Almansi, 148
 Biot, 148
 Cauchy-Green, 148
 left, 148
 Green-Lagrange, 149
 Hencky, 148, 156, 158, 230
 right Cauchy-Green, 181
 Strain trajectory, 26, 256
 Strengthening
 mechanism, 54
 Stress
 effective, 125
 engineering, 89

- hydrostatic, 193
 - Kirchhoff, 95
 - mean, 193
 - Stress concentration, 53
 - Stress deviator, 193
 - active, 288, 297
 - Stress function
 - hyperbolic sine, 264
 - power law, 243
 - Stress redistribution, 308, 309, 312, 314
 - Stress relaxation, 10, 12
 - Stress state effect, 25, 27, 254, 266
 - Stress state index, 265, 300
 - Stress tensor
 - active part, 243
 - additional part, 243
 - Cauchy, 163, 180, 183, 185, 190–192, 230, 232
 - deviatoric part, 22, 227, 243
 - dissipative, 227, 230, 231
 - effective part, 243
 - Piola-Kirchhoff, 164, 168, 182
 - second, 182
 - quasi-conservative, 227, 229
 - spherical part, 243
 - translation part, 243
 - Stress vector, 160
 - Stretch, 81
 - local, 81, 146
 - principal, 148, 183
 - Stretch tensor, 153
 - left, 148
 - right, 148
 - St. Venant model, 98
 - Symmetries of microstructure, 67
 - Symmetry group, 176, 187
 - physical, 230
 - Symmetry transformation, 176, 178
- T**
- Taylor hardening, 121
 - Tensile test
 - uni-axial, 2
 - Tensor
 - orthogonal, 337
 - second rank, 329
 - singular, 334
 - skew-symmetric, 333
 - symmetric, 332
 - Test
 - multi-axial, 22
 - stress controlled, 23
 - Thermal conductivity, 92, 132, 179
 - tensor, 175, 177
 - Thermal expansion
 - coefficient, 190
 - tensor, 188, 190
 - Thermal expansion coefficient, 95
 - Thermally-activated dislocation climb, 66
 - Thermodynamic force, 91, 174
 - Thermoelasticity, 101
 - Thermo-elasto-plasticity, 236
 - Thermo-mechanical fatigue, 19
 - Time hardening, 240, 242, 299
 - Time hardening function, 299
 - Time hardening model, 240
 - Time to fracture, 127
 - Transient heat transfer, 45
 - Transverse isotropy, 207
 - Transversely loaded rectangular plate, 302
 - Type 316 stainless steel, 285
- U**
- Uni-axial tension, 316
 - Unified model, 44
 - Uniform shear, 316
- V**
- Variable
 - hidden, 107
 - internal state, 107, 118, 122, 132
 - Vector
 - axial, 324
 - polar, 324
 - spin, 325
 - Velocity field, 81, 144
 - Velocity gradient, 151, 152, 190, 191, 206
 - Viscoelasticity, 100
 - Viscoplasticity, 98
 - Void, 123, 124, 254, 260, 270
 - Void growth, 64
 - Volume constancy, 23
 - Volume fraction, 252
 - Von Mises-Odqvist type inelastic flow, 237
 - Von Mises type potential, 200
 - Voronoi tessellation, 64
 - Vorticity vector, 151
- W**
- Weakening, 53
 - Weissenberg effect, 193
 - Welded joint, 308, 309
 - Weld metal, 57, 265, 283, 308, 309

Weld metal 9CrMoNbV, [308](#), [316](#)
Work hardening, [264](#)

Y

Yield condition, [195](#)

Yield limit, [3](#)

Yield point, [2](#)

 lower, [3](#)

 upper, [3](#)

Young's modulus, [190](#), [298](#)